MATHEMATICS IS FOR SOLVING PROBLEMS

SIAM PROCEEDINGS SERIES LIST

Neustadt, L. W., Proceedings of the First International Congress on Programming and Control (1966)

Hull, T. E., Studies in Optimization (1970)

Day, R. H. and Robinson, S. M., Mathematical Topics in Economic Theory and Computation (1972)

Proschan, F. and Serfling, R. J., Reliability and Biometry: Statistical Analysis of Lifelength (1974)

Barlow, R. E., Reliability & Fault Tree Analysis: Theoretical & Applied Aspects of System Reliability & Safety Assessment (1975)

Fussell, J. B. and Burdick, G. R., Nuclear Systems Reliability Engineering and Risk Assessment (1977)

Erisman, A. M., Neves, K. W., and Dwarakanath, M. H., Electric Power Problems: The Mathematical Challenge (1981)

Bednar, J. B., Redner, R., Robinson, E., and Weglein, A., Conference on Inverse Scattering: Theory and Application (1983)

Santosa, Fadil, Symes, William W., Pao, Yih-Hsing, and Holland, Charles, Inverse Problems of Acoustic and Elastic Waves (1984)

Gross, Kenneth I., Mathematical Methods in Energy Research (1984)

Babuska, I., Chandra, J., and Flaherty, J., Adaptive Computational Methods for Partial Differential Equations (1984)

Boggs, Paul T., Byrd, Richard H., and Schnabel, Robert B., Numerical Optimization 1984 (1985)

Angrand, F., Dervieux, A., Desideri, J. A., and Glowinski, R., Numerical Methods for Euler Equations of Fluid Dynamics (1985)

Wouk, Arthur, New Computing Environments: Parallel, Vector and Systolic (1986)

Fitzgibbon, William E., Mathematical and Computational Methods in Seismic Exploration and Reservoir Modeling (1986)

Drew, Donald A. and Flaherty, Joseph E., Mathematics Applied to Fluid Mechanics and Stability: Proceedings of a Conference Dedicated to R.C. DiPrima (1986)

Heath, Michael T., Hypercube Multiprocessors 1986 (1986)

Papanicolaou, George, Advances in Multiphase Flow and Related Problems (1987)

Wouk, Arthur, New Computing Environments: Microcomputers in Large-Scale Computing (1987)

Chandra, Jagdish and Srivastav, Ram, Constitutive Models of Deformation (1987)

Heath, Michael T., Hypercube Multiprocessors 1987 (1987)

Glowinski, R., Golub, G. H., Meurant, G. A., and Periaux, J., First International Conference on Domain Decomposition Methods for Partial Differential Equations (1988)

Salam, Fathi M. A. and Levi, Mark L., Dynamical Systems Approaches to Nonlinear Problems in Systems and Circuits (1988)

Datta, B., Johnson, C., Kaashoek, M., Plemmons, R., and Sontag, E., Linear Algebra in Signals, Systems and Control (1988)

Ringeisen, Richard D. and Roberts, Fred S., Applications of Discrete Mathematics (1988)

McKenna, James and Temam, Roger, ICIAM '87: Proceedings of the First International Conference on Industrial and Applied Mathematics (1988)

Rodrigue, Garry, Parallel Processing for Scientific Computing (1989)

Caflish, Russel E., Mathematical Aspects of Vortex Dynamics (1989)

Wouk, Arthur, Parallel Processing and Medium-Scale Multiprocessors (1989)

Flaherty, Joseph E., Paslow, Pamela J., Shephard, Mark S., and Vasilakis, John D., Adaptive Methods for Partial Differential Equations (1989)

Kohn, Robert V. and Milton, Graeme W., Random Media and Composites (1989)

Mandel, Jan, McCormick, S. F., Dendy, J. E., Jr., Farhat, Charbel, Lonsdale, Guy, Parter, Seymour V., Ruge, John W., and Stüben, Klaus, Proceedings of the Fourth Copper Mountain Conference on Multigrid Methods (1989)

Colton, David, Ewing, Richard, and Rundell, William, Inverse Problems in Partial Differential Equations (1990)

Chan, Tony F., Glowinski, Roland, Periaux, Jacques, and Widlund, Olof B., Third International Symposium on Domain Decomposition Methods for Partial Differential Equations (1990)

Dongarra, Jack, Messina, Paul, Sorensen, Danny C., and Voigt, Robert G., Proceedings of the Fourth SIAM Conference on Parallel Processing for Scientific Computing (1990)

Glowinski, Roland and Lichnewsky, Alain, Computing Methods in Applied Sciences and Engineering (1990)

Coleman, Thomas F. and Li, Yuying, Large-Scale Numerical Optimization (1990)

Aggarwal, Alok, Borodin, Allan, Gabow, Harold, N., Galil, Zvi, Karp, Richard M., Kleitman, Daniel J., Odlyzko, Andrew M., Pulleyblank, William R., Tardos, Éva, and Vishkin, Uzi, Proceedings of the Second Annual ACM-SIAM Symposium on Discrete Algorithms (1990)

Cohen, Gary, Halpern, Laurence, and Joly, Patrick, Mathematical and Numerical Aspects of Wave Propagation Phenomena (1991)

Gómez, S., Hennart, J. P., and Tapia, R. A., Advances in Numerical Partial Differential Equations and Optimization: Proceedings of the Fifth Mexico-United States Workshop (1991)

Glowinski, Roland, Kuznetsov, Yuri A., Meurant, Gérard, Périaux, Jacques, and Widlund, Olof B., Fourth International Symposium on Domain Decomposition Methods for Partial Differential Equations (1991)

Alavi, Y., Chung, F. R. K., Graham, R. L., and Hsu, D. F., Graph Theory, Combinatorics, Algorithms, and Applications (1991)

Wu, Julian J., Ting, T. C. T., and Barnett, David M., Modern Theory of Anisotropic Elasticity and Applications (1991)

Shearer, Michael, Viscous Profiles and Numerical Methods for Shock Waves (1991)

Griewank, Andreas and Corliss, George F., Automatic Differentiation of Algorithms: Theory, Implementation, and Application (1991)

Frederickson, Greg, Graham, Ron, Hochbaum, Dorit S., Johnson, Ellis, Kosaraju, S. Rao, Luby, Michael, Megiddo, Nimrod, Schieber, Baruch, Vaidya, Pravin, and Yao, Frances, Proceedings of the Third Annual ACM-SIAM Symposium on Discrete Algorithms (1992)

Field, David A. and Komkov, Vadim, Theoretical Aspects of Industrial Design (1992)

Field, David A. and Komkov, Vadim, Geometric Aspects of Industrial Design (1992)

Bednar, J. Bee, Lines, L. R., Stolt, R. H., and Weglein, A. B., Geophysical Inversion (1992)

O'Malley, Robert E. Jr., ICIAM 91: Proceedings of the Second International Conference on Industrial and Applied Mathematics (1992)

Keyes, David E., Chan, Tony F., Meurant, Gérard, Scroggs, Jeffrey S., and Voigt, Robert G., Fifth International Symposium on Domain Decomposition Methods for Partial Differential Equations (1992)

Dongarra, Jack, Messina, Paul, Kennedy, Ken, Sorensen, Danny C., and Voigt, Robert G., Proceedings of the Fifth SIAM Conference on Parallel Processing for Scientific Computing (1992)

Corones, James P., Kristensson, Gerhard, Nelson, Paul, and Seth, Daniel L., Invariant Imbedding and Inverse Problems (1992)

Ramachandran, Vijaya, Bentley, Jon, Cole, Richard, Cunningham, William H., Guibas, Leo, King, Valerie, Lawler, Eugene, Lenstra, Arjen, Mulmuley, Ketan, Sleator, Daniel D., and Yannakakis, Mihalis, Proceedings of the Fourth Annual ACM-SIAM Symposium on Discrete Algorithms (1993)

Kleinman, Ralph, Angell, Thomas, Colton, David, Santosa, Fadil, and Stakgold, Ivar, Second International Conference on Mathematical and Numerical Aspects of Wave Propagation (1993)

Banks, H. T., Fabiano, R. H., and Ito, K., Identification and Control in Systems Governed by Partial Differential Equations (1993)

Sleator, Daniel D., Bern, Marshall W., Clarkson, Kenneth L., Cook, William J., Karlin, Anna, Klein, Philip N., Lagarias, Jeffrey C., Lawler, Eugene L., Maggs, Bruce, Milenkovic, Victor J., and Winkler, Peter, Proceedings of the Fifth Annual ACM-SIAM Symposium on Discrete Algorithms (1994)

Lewis, John G., Proceedings of the Fifth SIAM Conference on Applied Linear Algebra (1994)

Brown, J. David, Chu, Moody T., Ellison, Donald C., and Plemmons, Robert J., Proceedings of the Cornelius Lanczos International Centenary Conference (1994)

Dongarra, Jack J. and Tourancheau, B., Proceedings of the Second Workshop on Environments and Tools for Parallel Scientific Computing (1994)

Bailey, David H., Bjørstad, Petter E., Gilbert, John R., Mascagni, Michael V., Schreiber, Robert S., Simon, Horst D., Torczon, Virginia J., and Watson, Layne T., Proceedings of the Seventh SIAM Conference on Parallel Processing for Scientific Computing (1995)

Clarkson, Kenneth, Agarwal, Pankaj K., Atallah, Mikhail, Frieze, Alan, Goldberg, Andrew, Karloff, Howard, Manber, Udi, Munro, Ian, Raghavan, Prabhakar, Schmidt, Jeanette, and Young, Moti, Proceedings of the Sixth Annual ACM-SIAM Symposium on Discrete Algorithms (1995)

Cohen, Gary, Third International Conference on Mathematical and Numerical Aspects of Wave Propagation (1995)

Engl, Heinz W., and Rundell, W., GAMM–SIAM Proceedings on Inverse Problems in Diffusion Processes (1995)

Angell, T. S., Cook, L. Pamela, Kleinman, R. E., and Olmstead, W. E., Nonlinear Problems in Applied Mathematics (1995)

Cook, L. Pamela, Roytburd, Victor, and Tulin, Marshal, Mathematics Is for Solving Problems (1996)

MATHEMATICS IS FOR SOLVING PROBLEMS

IN HONOR OF JULIAN D. COLE ON HIS 70TH BIRTHDAY

Edited by L. Pamela Cook
University of Delaware
Newark, Delaware

Victor Roytburd
Rensselaer Polytechnic Institute
Troy, New York

Marshall Tulin
University of California
Santa Barbara, California

siam.

Society for Industrial and Applied Mathematics
Philadelphia

10 9 8 7 6 5 4 3 2 1

ISBN 0-89871-371-4

Julian David Cole – A Scientific Biography

Julian David Cole was born in Brooklyn, NY on April 2, 1925, the first son of Rose and Jacob Cole. His father had flown in the Army Signal Corps in the first World War, and while maintaining his interest in flying, became a teacher and eventually principal in the New York City public schools, where Julian received his early education. Upon graduating from Erasmus High School, Julian entered Cornell with a Regents' scholarship. In 1945, while a senior in Mechanical Engineering, he applied to Caltech for admission to graduate studies in the Guggenheim Aeronautical Laboratories (GALCIT). Failing to receive a reply, he took a job at the Edo Aircraft Co. on Long Island, where he worked on aircraft structural analysis under the supervision of Korvin-Krokouvsky, the chief engineer. Upon phoning Clark Millikan, who had just succeeded von Karman as Director of GALCIT, Julian learned that his application had been lost, but was offered admission on the spot, as well as a job in the 10-foot GALCIT wind tunnel.

Julian's remarkably fruitful stay at GALCIT was to last until 1968. Upon his arrival in 1945 he had the good fortune to fall under the influence and enjoy the tutelage of Hans Liepmann, who had begun experimental studies of shock formation and shock-boundary layer interaction in 1944 after being led there by von Karman. The fruit of their growing collaboration is evident in "Experiments in Transonic Flow," by Liepmann, Ashkenas, and Cole [1a],[1] a 1948 technical report for the Air Force comprising a substantial and thorough review of transonic fundamentals, including similarity theory and viscous effects, and the presentation of experimental results on airfoil sections at zero angle of attack. There is considerable discussion of the possibility of large, shock-free, supersonic zones on transonic airfoils: the 1940 special hodograph solutions of Ringleb are noted and the authors state, "(this) demonstration that transonic potential flows could be constructed free from singularities gave rise to the hope that shock waves could be avoided by a suitable form of the boundary." It is striking to read this today, as it was directly contrary to the belief prevalent among aerodynamicists (and most mathematicians!) both then and for another 20 years. This contrary belief was dispelled only by the finite difference computations of Cole and Murman on transonic airfoils with large embedded supersonic regions [32], and the corresponding hodograph work of Garabedian and the Dutch school at a slightly earlier time; these works have had a profound influence on airfoil design since then.

Ignorance of transonic flows had caused considerable discomfort for aircraft designers during World War II, and by 1947 an assault on the so-called sound barrier had become a subject of the highest national priority; the work was being led by John Stack of the NACA Langley laboratory. But transonic flows were poorly understood from a fundamental point of view, impossible to calculate, and difficult to study experimentally; the Caltech transonic initiative was therefore most timely and important. As we know, Julian would go on from this 1948 beginning to eventually illuminate the entire field of transonics through a long sequence of research papers and the influential book *Transonic Aerodynamics* with Pam Cook. The major reason for the intractability of transonic flows was, of course, their

[1] References are found in the CV that follows. There are two lists: [x] refers to the first and [xa] to the second.

essentially nonlinear nature; thus their proper understanding required a very high degree of mathematical ability.

In 1946, at the instigation of Hans Liepmann, Paco Lagerstrom joined GALCIT from Douglas Aircraft. Around him a small group, of which Julian was a part, began in 1948 to work seriously on general analytical methods for the systematic approximation to solutions of PDEs, including what they called "perturbation theory." Their interest was initially focused on the Navier–Stokes equation, for which the linear model of Oseen was first examined, with the goal of understanding the structure of viscous layers. Weak shock structure was also studied through a nonlinear model of Navier–Stokes type; (1) $u_t + uu_x = \nu u_{xx}$, which had earlier been introduced as a model equation for turbulence by Burgers; this equation is also, in the viscous free limit, the nonlinear signal equation, leading to shock formation. Julian revealed [3] that the solution of (1) was related to any solution $\psi(x,t)$ of the one-dimensional linear heat equation through the transformation $u = -2\nu\,(log\psi)_x$. This result has since become very widely used. Then, it was shown how propagating disturbances evolve into a continuous shock of thickness $\delta = O(\nu)$ [2, 3]. This work represented the beginning of Julian's contributions to the subject of analytical approximation, which were to assume increasing and great importance for applied mathematics, and when interwoven (as it already was) with his engineering interest in transonics, hypersonics, and other physical problems were to provide results of great engineering importance.

It's a long way to transonics (Julian ca. 1930).

Upon completion of his dissertation on problems in transonic flow in 1949, Julian received an appointment first as a Research Associate and then as an Assistant Professor at Caltech. His collaboration with Paco Lagerstrom on approximations to the Navier–Stokes equations culminated in extensive work [11] on the flow about a sliding, expanding cylinder. This flow has the advantage of offering considerable complexity and multiple parameters, while at the same time being reducible to a linear description; in certain cases exact solutions are possible. By this time, the Lagerstrom group (P. Lagerstrom, J. D. Cole, L. Trilling, G. Latta, S. Kaplun) had the notion clearly in mind of arriving at approximations to differential equations through formal limit processes, and in the cylinder analysis, several limiting (or asymptotic) approximations were derived, their interrelations studied, and they were compared with exact solutions.

In the process of this work [11], the notion of "distinguished" limits leading to similarity parameters was used, and expansions appropriate in different but overlapping regions were completed by matching them in the region of overlap. A good part of the basic arsenal so widely used today in asymptotic analysis was thus already drawn up.

Julian was soon to put these tools to striking use on aerodynamic problems. In preparation he explored the general features of transonic flow: through careful analysis of experimental GALCIT data [6], by studying the limits of linearized theory including the effects of acceleration through M=1 [7], through the hodograph calculation of the high subsonic flow over a finite wedge [1], and by the review and analysis of other available experimental data and calculations, especially in the light of von Karman's transonic similarity parameter [3a]. He presented the latter review at an Industrial Associates Conference at Caltech, beginning a practice which he maintains until today of working with industry and taking pains to present useful results in a conscientious way to the engineering audience. The hodograph calculation [1] provided the very first estimate of transonic drag past a body over the entire subsonic range, and showed very good agreement with experiments of Bryson. The hodograph representation transforms the nonlinear transonic small disturbance equation into the linear Tricomi equation for the approximate streamlines: (2) $wy_{vv} + y_{ww} = 0$. As part of the wedge calculation, Julian carried out a study [4] of the fundamental solutions of (2) and its continuation into the hyperbolic region based on physical-like considerations of the flow; great mathematical dexterity and knowledge of special functions was required, and was exhibited.

This preparation was followed by important work with Art Messiter[2] [13] involving a very systematic application of expansion procedures to the steady transonic flow past suitably thin wings and bodies; in this way von Karman's 1947 similarity law was systematically derived and extended and transonic small disturbance theory and higher-order expansions were successively derived. This paper also contains at its conclusion a result which is actually a type of "area rule," since the noncircular body is compared to a body of revolution that has the same cross-sectional area everywhere. This was in the period following Whitcomb's 1952 annunciation of the area rule on experimental grounds. Eventually J. was to make a thorough theoretical study of the area rule in the transonic regime.

In these early Caltech days, J. solved non-gas dynamic problems too, a practice which has continually expanded until today. He worked on heat transfer in relation to anemometry with Ted Wu[2] [5], and with Anatol Roshko [9], then a Research Fellow in GALCIT, and on waves in solids [8, 16]. The latter work with J. Huth marked the beginning of a fruitful consultancy with the Rand Corporation, which evolved into work on magneto-hydrodynamics [17,19] and on blasts, including the generation and propagation of acoustic-gravity waves in the atmosphere with Carl Greifinger [30], and on hypersonic problems with J. Aroesty [24].

J.'s interests were to be broadened further during a 14-month period from 1955 to 1957, when he served as a Scientific Liaison Officer (Mechanics) in the London Office of Naval Research, observing first-hand fluids research, and especially aerodynamics and ship hydrodynamics, in European universities and laboratories. He also interacted with

[2] A complete list of Cole's graduate students is given at the end of the CV.

and established friendships with several British applied mathematicians, notably Keith Stewartson and L. E. Fraenkel, who were themselves to become vigorous expositors of asymptotic methods.

Hypersonic research began at NACA Langley in the mid 1940s and interest accelerated in the 1950s with focus on warhead reentry problems; the first perturbation theory had been expounded by Van Dyke, who also studied with Lagerstrom at Caltech (late 1940s). In connection with RAND, J. very systematically developed the highly useful asymptotic ($M \to \infty$; $\gamma = 1$) flow theory for slender bodies [14], which is known as Newtonian theory and had first been formulated by A. Busemann in 1933. Cole's theory allowed a description of the shock shape and of the velocity field behind it. Applications were made to a family of bodies, $r \sim x^n$, and the minimum drag shape found for $n = 2/3$. This work was extended to optimization including friction, and to the prediction of lift on slender noses [15]. In work with T. F. Zien,[2] the exact axisymmetric flow fields of [14] were also used in a novel way to predict the compression side lift on a class of three-dimensional wings of maximum lift/drag ratio [28], the so-called wave riders.

Julian Cole and Hans Liepmann.

Heating had been identified as an important reentry problem and J. applied nonlinear strip theory to the prediction of heat transfer on slender flat wings at high angles of attack. This necessitated the solution of the two-dimensional flat plate normal to a hypersonic stream [13a]; here an inner region near the body was found and matched to the outer solution behind the shock. The heat transfer predictions were in excellent agreement with NASA data.

In all of these works, the use of sophisticated mathematical analysis is always ultimately subordinated to the calculation and expression of results for engineers.

By the early 1960s, perturbation, or asymptotic, theory (the nomenclature varied) had proven itself in application to viscous flows, shock wave structure, transonics, hypersonics, hydromagnetics, and a rapidly growing, diverse group of other major subjects; it was becoming more widely known throughout the world. This process was greatly facilitated a little later by the publication of Van Dyke's *Perturbation Methods in Fluid Mechanics* in 1964 and by Cole's *Perturbation Methods in Applied Mathematics* in 1968. After this time, a knowledge of these methods became increasingly obligatory among research workers in mechanics and other fields. J.'s role in the development, application, and exposition of asymptotic theory had enormous influence on its widespread success. He has succinctly outlined the history of perturbation theory development by the Caltech group [51], where he acknowledged the early leadership of Paco Lagerstrom and the support of Hans Liepmann and Clark Millikan.

The subject of asymptotic theory had itself developed very fruitful bifurcations. One of these concerns situations where dominant phenomena occur on different time scales. The uniformly valid treatment of nonlinear problems of this type, represented by ODEs, was undertaken by J. Kevorkian[2] while he was a graduate student with J. This work led to, among other things, the development of the method of multiple scales, a formal asymptotic approach, applicable to PDEs as well, which has had a profound influence on the treatment of nonlinear dynamical systems. It has been conspicuously successful in application to the evolution of nonsteady, nonlinear water waves, where wave amplitudes modulate slowly in space and time as a result of nonlinear interactions. This branch of asymptotic theory applied to ODEs was the subject of a separate chapter in Cole's 1968 book, where the lucidity of the exposition and explicitness of the many illustrative examples are of particular note. It was continuously developed by Kevorkian, his students, and others, and was further exposed and elaborated in the 1980 successor to *Perturbation Methods* coauthored by Kevorkian and Cole. Here again, knowledge of these methods has become obligatory.

Another important bifurcation of asymptotic theory involves the appearance of similarity solutions of the asymptotic equations, as in the transonic case; these play very important roles in understanding the far field and local singularities. The quest for deeper understanding of similarity solutions of PDEs, which continues to play such a prominent role in mechanics, led to the work by G. Bluman[2] and Cole on the application of infinitesimal transformations (Lie groups) to the heat equation [29], where a very general solution was first given. It then led to further work by Bluman and to their book *Similarity Methods for Differential Equations*, which contains more widespread applications. These works literally provided the first accessible introduction to these group theoretic methods to workers outside the field of pure mathematics.

In view of the clear success of these serious applications of mathematics to nonlinear problems in gas dynamics, and the obvious general potential for the future, in the early 1960s Julian and Hans Liepmann urged the Caltech administration to create a coherent Applied Mathematics effort. Their advice was heeded in 1963, and from that date J. identified with that group, which included the newcomers G. Whitham, H. Keller, and P. Saffman, and he contributed to its early work, for example, in his collaboration with Saffman and Keller in a study of the Taylor–Reiner problem of compressible flow in a narrow gap at low Reynolds number [25]. The eventual impact of the Caltech Department of Applied Mathematics on fluids, including nonlinear water waves, is now well known.

After over 20 years, the Caltech era came to a close in 1968 when J. received a Boeing Company Faculty fellowship and went to work at the Boeing Scientific Research Laboratory. BSRL had an outstanding group of young researchers in Mechanics, including Earll Murman, working under the direction of Arnold Goldburg. At this time, the sonic barrier was 20 years in the past and a coherent quantitative picture of transonic flow fields had emerged, very much as a result of the nonlinear analyses which had been brought to bear in an ongoing effort. Although the actual numerical prediction of flows past aircraft components had not been routinely accomplished, the growing availability of computing power had encouraged the calculation of shock-free airfoil flows, utilizing the hodograph plane, notably by Nieuwland and other Dutch workers and by Garabedian and his colleagues. The subject is very well reviewed by J. in [21a] and in an expanded form [35]. These elegant methods, which confirmed the existence of lifting airfoils with large shock-free embedded regions, could not, unfortunately, be applied to truly three-dimensional flows, like wings, and needed extension to allow shocks. At Boeing, Julian, in collaboration with Earll Murman, began the development of a finite-difference, relaxation method of calculation in the physical plane based on the transonic small disturbance theory. A great advantage in using this theory was the knowledge of the far field behavior which had been gained in preceding years utilizing asymptotic methods. The idea of the relaxation calculation of compressible flows goes back at least to Howard Emmons in the 1940s, but the usual calculation fails in the supersonic regime. Cole and Murman realized that the difference scheme had to change with the flow regime; their other great achievement was the treatment of discontinuous shocks. Their first results appeared in [32], which concludes, "The modified relaxation procedure is sufficiently simple that thought can be given to doing lifting airfoils, axisymmetric bodies, and even three dimensional flows." All of this has now come about. Further results of the Murman–Cole collaboration appear in [27a], including calculations of shock losses and of wall effects on transonic performance.

At the end of the Boeing fellowship, J. returned to Los Angeles in 1969 to a position in the Mechanics and Structures Department of the School of Engineering and Applied Science at UCLA; a joint appointment with the Mathematics Department subsequently resulted. This change was soon to result in new interests and fruitful working relationships, especially one with Pam Cook in the UCLA Mathematics Department, and another with Norm Malmuth[2] of the Rockwell International Science Center. In work with Malmuth and Shankar [35a, 40], the potential of the Cole–Murman method is realized in its application to finite-span, swept-wing, and wing-body configurations; wind tunnel effects were also computed and comparisons with experiments are shown. In [40], wings of desired pressure distribution are found (inverse problem). These results comprise a very important engineering achievement: they demonstrate the ability to base transonic design on mathematical computations. It provides a measure of the distance traveled as the result of the persistent questing research since J. arrived at Caltech in 1945.

During the 1970s Julian developed four other serious interests (in addition to handicapping horse races, a hobby which emerged following a most pleasant stay of the present author at UCLA in 1974, where we developed a graduate course in marine hydrodynamics together). One of these, which began in 1979, concerned the design and operation of specialized gas ultra-centrifuges employed for the separation of isotopes; this involved complex fluid phenomena which were studied for DOE by a group including J.'s colleagues Hans Liepmann and George Carrier. (Julian spent 1963–1964 at Harvard with Carrier.) Some of his work on this appears in print, for example, [39a]. Houston Wood reveals some details of this project in his paper in this volume.

Another abiding interest was in an outstanding classical problem in physiology, the mechanism of functioning of the cochlea in the ear; the cochlea had originally been modeled by Helmholtz as a tapered thin plate in vacuo, but driven by pressure differences across it; despite much attention, the ability of the cochlea to distinguish pure tones had never been adequately explained, although a relation between frequency and position on the cochlear beam has been widely accepted since Helmholtz. This work began in collaboration with R. Chadwick (who J. had met in 1975 during his sabbatical at the Technion in Haifa), and continued with M. Holmes[2] [37, 30a, 36a, 42a, 44]. Proceeding with models of increasing complexity in each step, they were able to obtain a refined and detailed theory of the response profile of the plate, including the motion of the viscous fluid within the cochlear shell in its coupled reaction to the motion of the tapered plate. In [44] they show the existence of a single family of traveling waves, and a frequency-dependent singular point on the plate, where the wave phase velocity goes to zero; the existence of this point depends both on the existence of fluid and the plate mass. It is not clear whether a better understanding of the functioning cochlea can be reached without some new means of actual observation within it. In connection with this work on hearing, it is worth noting that Julian's brother Gerald, his only sibling, is a doctor specializing in otology. J. studied another problem in physiology: with Victor Barcilon in UCLA's Department of Mathematics and other colleagues in Physiology, Julian applied singular perturbation theory to the study of the electrical properties of nerve cells, and particularly their experimental determination [33,36]; this involved interesting problems in potential theory.

It was natural for Julian to be interested in water waves, and during a visit to Australia (University of Adelaide, 1979) he focused on the question of ships in shallow water near the critical speed (depth Froude number near one). This is an analogue, but in a dispersive medium, to the transonic problem in aerodynamics. He worked on this problem with Susan Cole,[2] who become his wife in 1983. It had been known (see Lighthill's *Waves in Fluids*) that in two dimensions, the conventional linearized theory showed that a body in shallow water (say a bump in the bottom) had a finite drag, although the wave amplitude blew up. But what actually happened? How did nonlinearities intervene? Did breaking waves emerge? In fact, nature had invented an unsteady resolution to this problem with steady boundary conditions, in which forward-moving solitons are created at the body periodically; in this way, the momentum loss corresponding to the drag is carried away. These results, published by Susan Cole, supplemented those of independent groups at Berkeley (Wehausen) and at Caltech (T. Y. Wu). Julian also published singular perturbation analyses of finite-depth water waves near the critical speed [32a] as part of an overview discussion of limit process expansions and approximate equations.

In the early 1980s, Richard DiPrima began to try to convince Julian to move to Rensselaer Polytechnic Institute in Troy, NY to join the Department of Mathematical Sciences. It was the largest mathematics group in the country doing real applied mathematics, and one where DiPrima had played an outstanding leadership role, as he had with SIAM. With the help of Bob O'Malley, another SIAM leader, DiPrima succeeded, and Julian became the Margaret Darrin Distinguished Professor of Applied Mathematics at RPI in 1982.

Again Julian established very fruitful new working relations in both mathematics and engineering and has enjoyed a broadened influence throughout the Institute. He has always taken an active part in the highly successful annual RPI-Industry Workshop, where industrial workers bring their problems for joint exposure and exploration with academic applied mathematicians; this is a format which had proven successful at Oxford, organized by Alan Tayler and John Ockendon.

As mentioned earlier, work on cochlear mechanics continued at RPI with Mark Holmes, his former graduate student, who is currently chair of their department. Of course, work in transonics also continued, much of it devoted to the aforementioned 1986 book *Transonic Aerodynamics* with Pam Cook, who is now chair of her department at the University of

Delaware; in this book transonic theories are patiently exposed and applied. They also carried out the extension of the classical lifting line theory of finite wings to the transonic regime, which was an outstanding classical problem, [31a, 38]. A further notable Cook–Cole work [56a], an extension of earlier work [23a], involves an exploration of the famous and highly useful transonic area (or equivalence) rule based on asymptotic analysis, where they showed that corrections depend only on the second spanwise moment of the cross-sectional area. Collaboration with Malmuth continues to this day. In [42, 44a, 45a, 48a], they considered the wave drag of transonic lifting configurations and their optimization, including unsteady effects in part; use was made of the fact that in the transonic range, lift produces a far field flow like an equivalent axisymmetric body. They also worked together and with others on a form of single-degree transonic flutter [43].

A large problem plaguing those few experimentalists who braved the transonic regime in earlier days concerned wall effects on the measurements, which was especially serious because of the exaggerated transverse extent of the flow field. This was only ameliorated by the introduction of slotted or porous walls. Although wall effects in subsonic flow were normally corrected in part through the use of theory, this had not been possible in the transonic regime; the nonlinear problem is very difficult. In the 1980s, however, Julian provided an asymptotic (matching) theory of solid wall interference on transonic airfoils, with Malmuth and Zeigler[2] [37a]; this was later extended to choked planar flow and to slender bodies in axisymmetric tunnels, both with Pam Cook [45, 76]. Application of these results was made by Malmuth, Julian, and others [52].

Studies of transonic bodies of revolution with Malmuth [48] resulted in the interesting discovery that the shock position was simply fixed by the local body geometry $[(Area)_{xx} = 0]$, quite unlike the airfoil case. Subsequently, in collaboration with D. Schwendeman, Julian developed and applied a numerical hodograph method for the design of shock-free slender bodies of revolution [51a]. He also returned with B. Ling[2] to the problem of airfoil design at sonic velocity, which he had began with E. Tse[2] at UCLA in 1980, and they succeeded in constructing a number of airfoils and in calculating their lift and drag at sonic speed. In a different direction, the calculation of optimum transonic critical airfoils was accomplished based on Lavrentiev's free streamline comparison theorem and related work of Gilbarg and Schiffman; this work was in collaboration with Schwendeman and Kropinski[2] [53, 56].

Interest in hypersonic flows returned again in the 1980s with a national project for a high-speed airplane. Julian returned to waveriders with B. Wagner.[2] These wings were designed based on similarity solutions for power law and exponential shock waves, and optimum (lift/drag) shapes were found for the latter [51a, 53a]; the second of these papers was presented at the First International Hypersonic Waveriders Conference, illustrating the durability of the waverider concept first studied in the late 1960s by Cole and Zien [28].

Ground signatures of supersonic aircraft (sonic booms), together with economics, have had a decisive influence on discouraging the development of commercial aircraft in that regime. Many interacting factors influence the strength of the boom and, importantly, atmospheric turbulence. In work with Zvi Rusak of RPI, this problem was formulated as an extended small-disturbance, unsteady, transonic equation of mixed type and solved using Murman–Cole finite difference techniques [58a, 58]; this theory proved useful for understanding atmospheric measurements.

In the earlier development of perturbation theory, the appearance of similarity solutions of the field equation as the dominant term in the far field played an important role; thus the number of independent variables is automatically reduced. The full determination of these solutions, including constants, is a deep and tantalizing problem that takes a variety of forms depending on the circumstances, although in general the boundary or initial conditions in the near-field must be involved; a further general question concerns the way in which the asymptotic state (dominant term) is approached. Julian's early work and book with George Bluman on Lie groups were consequences of his deep interest in this problem. He returned to it in two more recent works [49a, 55a]. In the first of these he notes at the outset that "there seems to be no general theory of (this) type of question." Nevertheless the work is extraordinarily useful for revealing the approach to a resolution in the case of several second-order nonlinear equations with two independent variables: nonlinear diffusion in time and one space dimension, and the small disturbance transonic equation in two space dimensions. The general approach depends on the realization that group theory permits a two-parameter family of variable stretchings which leaves the field equation invariant. The use of one of these variables results in a similarity variable, ξ, and a solution, $f(\xi)$, given by an ODE; this is the point reached in the earliest use of similarity solutions. What Julian teaches in [49] is the use of the other stretching parameter, through the medium of a scale factor, μ, such that any solution $F(\xi)$ generates a one-parameter (μ) family of solutions, $f(\xi) = \mu^k f(\mu\xi)$. In both of the illustrative problems, the scale factor is found through the use of a conservation (integral) law which appears; he also discusses the approach to the asymptotic state.

The other work involves the one-dimensional (x,t) heat equation where a discontinuity in the diffusion coefficient occurs along one of the characteristics, $x/\sqrt{t}$, the Barenblatt nonlinear filtration equation. In this case the form of the constant α in the asymptotic state, $t^\alpha f(x/\sqrt{t})$, must be determined. This is shown from a simple inspection of the corresponding energy dissipation law; in this respect the problem is similar to that where heat is injected at a known rate at a boundary.

Another nonlinear diffusion problem of considerable practical importance has attracted Julian's interest. With the increasing miniaturization of random access memory devices (DRAMS), interest has grown in the generation of holes and electrons in silicon as the result of ionizing radiation due to strikes of alpha particles, protons, energetic electrons, and cosmic rays. Julian has studied this problem in collaboration with J. Pimbley [50], where the concentration of holes and electrons was modeled in terms of two nonlinear diffusion-drift equations and a third coupled equation for the electrostatic potential arising from hole-electron separation. A similarity solution was found and calculations made to reveal the effect of the two governing nondimensional parameters: the initial concentration of holes and electrons and the ratio of their diffusivities. J.'s interest in the application of mathematics to these semiconductor problems has continued [54].

Another general, classic problem which has attracted Julian in the 1990s is homogenization, i.e., how to calculate the bulk properties (thermal or electrical conductivity; viscosity) of a material that is not homogeneous, but has embedded structure on a certain scale. The problem has a certain resemblance to the wind tunnel interference problem, which in the subsonic (linear) regime is solved through the use of multipole images. This is the general technique brought to bear here by Julian, but with the aid of formal and systematic limit process expansions. He demonstrated this general technique on the Rayleigh problem of determining the effective thermal conductivity of a regular cubic array of spheres of one conductivity embedded in a matrix of different conductivity. Rayleigh had found for the effective conductivity an expansion in the fraction of sphere volume, ϵ, containing terms ϵ, ϵ^2, ϵ^3, ϵ^4, $\epsilon^{13/3}$. Julian recovered Rayleigh's result and was able to explicate the very curious exponent in the last term. An interesting aspect of the Rayleigh problem is a summability difficulty of paradoxical form, which also occurs in the calculation of added mass and had earlier been considered by Theodorsen.

The significance of Julian's contributions to both aerodynamics and applied mathematics was recoggnized very early by his peers with his simultaneous election in 1976 to the National Academies of Engineering and Science, an exceptional occurrence. He has received many other awards and honors, including the von Karman Prize from SIAM in 1984. This award would seem to have special significance for a number of reasons. Foremost among these, Julian's early experience in bringing mathematics forcefully to bear on important, current engineering problems took place at GALCIT, the very laboratory where von Karman translated his own tradition in America. The heart of that tradition was a deep commitment to the scientific formulation and mathematical solution of real engineering problems, rather than to the development of mathematics for its own sake (see "Theodore von Karman and Applied Mathematics in America," Science, 222, 1300-1304, 23 December 1983). That committment would seem to spring from one's personal value system and is therefore not easily taught. Here the importance of historical and exemplary figures like Rayleigh and Kelvin in the last century and Timoshenko, Burgers, and von Karman in the first half of this century are crucial. In the second half of this century, Julian Cole certainly takes his place with his predecessors. von Karman had clearly understood and publicized the vast and mostly uncharted territory of nonlinear phenomena looming ahead in engineering, and it was the heart of this territory in aerodynamics, transonics, which Julian conquered; it is, of course, the exact place where we normally fly. What sets Julian aside from many other engineers using theory is the depth and general applicability of the mathematical tools which he has devised for the solution of problems. In this respect, his body of work is exceptional.

We have not spoken directly here of Julian's role as a teacher, but his sincere dedication to education is evident, in both the patient and meticulous preparation of lecture notes and the invention of illustrative homework problems, in exposition, in stimulative and caring guidance and supervision, and in providing his considerable wisdom to university administration. His teaching has, in fact, extended far beyond the classroom and beyond applied mathematics. In his relation to both problems and people, his patience, persistence, integrity, and caring approach serve as an example to all of us.

Julian continues his research and teaching at RPI and lives in nearby Loudonville with Susan, their daughter Amy, two children from Susan's previous marriage, and three large dogs. He enjoys close and loving contact with his four children from his first marriage and with his three grandchildren.

Marshall P. Tulin
Santa Barbara, CA

Julian D. Cole
Margaret Darrin Distinguished Professor
of Applied Mathematics
Department of Mathematical Sciences
Rensselaer Polytechnic Institute

Education

E. Cornell University, 1944 (with distinction)
. California Institute of Technology, 1949
(Summa Cum Laude)

Industrial and Government

- 1945 Engineer, EDO Aircraft Corp., LI, NY
- 1957 Scientific Liaison Officer, Office of Naval Research, London
- 1969 Boeing Company, Scientific Research Laboratory

University Experience

- 1963 Professor of Aeronautics, California Institute of Technology
- 1968 Professor of Applied Mathematics, California Institute of Technology
- 1964 Visiting Professor, Harvard University
- 1982 Professor of Engineering and Mathematics, University of California, Los Angeles
- 1973 Chairman of Mechanics and Structures Department, University of California, Los Angeles
- date Margaret Darrin Distinguished Professor of Applied Mathematics, Department of Mathematical Sciences, Rensselaer Polytechnic Institute

Honors

enheim Fellow, 1963
v, American Physical Society, 1965
ıg Company Faculty Fellowship, 1968-69
ırnia Institute of Technology Distinguished Alumni Award, 1971
v, American Academy of Arts and Sciences, 1975
Davis Fellow, Technion, Haifa, Israel, 1975
ɔer, National Academy of Sciences, 1976
ɔer, National Academy of Engineering, 1976
v, American Institute of Aeronautics and Astronautics
Laskowitz Medal, New York Academy of Sciences, 1978
ıan Fairchild Distinguished Scholar, California Institute of Technology, 1980
ır Newell Talbot Award for Research in Mechanics, University of Illinois, 1981
Karman Prize, Soc. Ind. & Applied Math, 1984
d for Meritorious Civilian Service, Department of the Air Force, 1988
Dynamics Award, The American Institute of Aeronautics and Astronautics, 1992
. Sears Distinguished Lecture, Cornell 1993
nal Academy of Sciences Award in Applied Mathematics and Numerical Analysis,

Service and Administrative Activities

Chairman, Faculty Budget and Planning Committee to the Trustees' Finance Committ (Rensselaer) 1993-1994

Restructuring Steering Committee (Rensselaer) 1993-1994

SIAM Board of Trustees, 1992 - 1994

Review Committee (University Delaware - Mathematics Department) 1992

Mathematics Visiting Committee (Lehigh University) 1992

Member of President & Provost's Committee to Assess the Computer Calculus Progra (Rensselaer) 1992

Member of the Advisory Committee for International Workshop on Computational Ele tronics, 1991-1993

Member of Board on Assessment of NBS Programs, National Research Council, 1988

SIAM Council (Governing Board) 1971-77

Publications
by
Julian D. Cole

Books, Monographs

"*Magnetohydrodynamic Waves*," in Magnetohydrodynamics of Conducting Fluids, D. Bershader, Editor, Stanford University Press, 1959.

"*Continuum Plasma Dynamics*," in Plasma Dynamics, F. Clauser, Editor, Addison Wesley, Reading, MA, Chapter 6, 1960 (with H. Liepmann).

"*Hydromagnetic Flow*," Plasma Physics in Theory and Applications, Wolf Kunkel, Editor, McGraw Hill, 1966.

"*Perturbation Methods in Applied Mathematics*," Blaisdell Publishing Company, Massachusetts, 1968.

"*Similarity Methods for Differential Equations*," Applied Mathematics, Springer, Series vol. 13, 1974 (with G. Bluman).

"*Perturbation Methods in Applied Mathematics*," Springer Verlag, New York, 1980 (with J. Kevorkian).

"*Transonic Aerodynamics*," North Holland, 1986, (with P. Cook).

"*Semiconductors Part I*," The IMA Volumes in Mathematics and Its Applications, vol. 58, W.M. Coughran, Jr., Julian Cole, Peter Lloyd and Jacob K. White, Editors, 1994.

"*Semiconductors Part II*," The IMA Volumes in Mathematics and Its Applications, vol. 59, W.M. Coughran, Jr., Julian Cole, Peter Lloyd and Jacob K. White, Editors, 1994.

Journal Articles

In refereed journals
(a) Major articles

1. "Drag of a Finite Wedge at High Subsonic Speeds," *J. of Mathematics and Physics*, **30**(2), 79-93, July 1951.
2. "Heat Conduction in a Compressible Fluid," *J. of Appl. Mech.*, **19**, 20-214, July 1951 (with T. Wu).
3. "On a Quasi-Linear Parabolic Equation Occurring in Aerodynamics," *Quarterly of Applied Mathematics*, **9**(3), 225-236, October 1951.
4. "Note on a Fundamental Solution of $wYvv+Yww=0$," *Zeitschrift fur Angewandt Mathematik und Physik*, **3** 286-297, May 1952.

5. "Anemometry of a Heated Flat Plate," *Heat Transfer and Fluid Mechanics Institute*, UCLA, 139-157, June 1952 (with T. Y. Wu).
6. "Transonic Flow Past Simple Bodies," *J. of Aeronautical Sci.*, **20**(9), 627-634, September 1953 (with Solomon and Willmarth).
7. "Note on Non-stationary Slender Body Theory," *J. of Aeronautical Sci.*, **20**(11), 798-799, November 1953.
8. "Constant-Strain Waves in Strings," *J. of Appl. Mech.*, **20**(4), 519-522, December 1953 (with Dougherty and J. Huth).
9. "Heat Transfer from Wires at Reynolds Numbers in the Oseen Range," *1954 Heat Transfer and Fluid Mechanics Institute*, Univ. of California, Berkeley, 13-23, July 1954 (with A. Roshko).
10. "Acceleration of Slender Bodies of Revolution through Sonic Velocity," *J. of Applied Physics*, **26**(3), 322-327, March 1955
11. "Examples Illustrating Expansion Procedures for Navier- Stokes Equations," *J. Math. Mech.*, **4**(6), 817-882, November 1955 (with P. Lagerstrom).
12. "Elastic Stress Waves Produced by Pressure Loads on a Spherical Shell," *J. of Appl. Mech.*, **22**(4), 473-478, December 1955 (with J. Huth).
13. "Expansion Procedures and Similarity Laws for Transonic Flow: Part I. Slender Bodies at Zero Incidence," *Z.A.M.P J. of Applied Mathematics and Physics*, **8**(8), 1-25, January 1957 (with A. Messiter).
14. "Newtonian Flow Theory for Slender Bodies," *J. of Aeronautical Sci.*, **24** (6), 448-455, June 1957.
15. "Lift of Slender Nose Shapes According to Newtonian Theory," *J. of Aeronautical Sci.*, **25**(6), 1958.
16. "Stresses Produced in a Half Plane by Moving Loads," *J. of Appl. Mech.*, **25**, 433-436, December 1958 (with J. Huth).
17. "Some Interior Problems of Hydromagnetics," *J. of Physics and Fluids*, **2** (6), November 1959 (with J. Huth).
18. "Slender Wings at High Angles of Attack in Hypersonic Flow," *Hypersonic Flow Research*, **7**, 1962 (with J. Brainerd).
19. "Similarity Solutions for Cylindrical Magnetohydrodynamic Blast Waves," *J. of Physics and Fluids*, **5**(12), December 1962 (with C. Greifinger).
20. "Uniformly Valid Asymptotic Approximation for Certain Non-linear Differential Equations," *Proceedings of International Symposium on Non-linear Differential Equations and Non-linear Mech.*, Academic Press, 113-120, 1963 (with J. Kevorkian).

21. "Slender Body Theory of Flow Around Minimum Drag Shapes," *Theory of Optimum Aerodynamic Shapes*, Academic Press, 387-404, 1965 (A. Miele, Ed.).

22. "Optimum Slender Shapes with a Variable Skin- Friction Coefficient," *Theory of Optimum Aerodynamic Shapes*, Academic Press, 233-250, 1965 (A. Miele, Ed.).

23. "Expansion of a Finite Mass of Gas into a Vacuum," *AIAA Journal*, **3**(6), 1200-1201, June 1965 (with C. Greifinger).

24. "Optimum Hypersonic Lifting Surface Close to Flat Plates," *AIAA Journal*, **3**(8), 1520-1522, August 1965 (with J. Aroesty).

25. "The Flow of a Viscous Compressible Fluid Through a Very Narrow Gap," SIAM J. Appl. Math., **15**(3), May 1967 (with H. Keller and P. Saffman).

26. "The Blowhard Problem - Inviscid Flows with Surface Injection," *International Journal of Heat Mass Transfer*, **11**, 1167-1183, 1968, Pergamon Press, New York.

27. "Asymptotic Behaviour of Certain Non-linear Boundary Value Problems," *J. of Mathematics and Physics*, **9**(11), 1915-1921, November 1968 (with J. Canosa).

28. "A Class of Three Dimensional Optimum Hypersonic Wings," *AIAA Journal*, **7**, 264-271, AIAA Paper No. 68-158, No. 2, February 1969 (with T. F. Zien).

29. "The General Similarity Solution of the Heat Equation," *J. Math. and Mechanics*, **18**(11), 1025-1042, May 1969.

30. "Acoustic Gravity Waves from an Energy Source at the Ground in an Isothermal Atmosphere," *Journal of Geophysical Research*, **74**(14), 3693-3703, July 1, 1969 (with C. Greifinger).

31. "Hypersonic Similarity Solutions for Airfoils Supporting Exponential Shock Waves," *AIAA Journal*, **8**(2), 308-315, February 1970 (with J. Aroesty).

32. "Calculation of Plane Steady Transonic Flows," *AIAA Journal*, **9**(1), 114-121, January 1971 (with E. Murman).

33. "A Singular Perturbation Analysis of Induced Electric Fields in Nerve Cells," SIAM J. Appl. Math., **21**(2), 339-354, September 1971 (with V. Barcilon and R. S. Eisenberg).

34. "An Asymptotic Solution of the Laminar Flow of Thin Film on a Rotating Disk," *J. of Appl. Mech.*, Paper No. 72-APMA-38, ASME Summer Conference, June 1972, February 1972 (with J. W. Rauscher and R. E. Kelly).

35. "Modern Developments in Transonic Flow," SIAM J. Appl. Math., **29**(4), 763-787, December 1975.

36. "Matched Asymptotic Expansions of the Green's Function for the Electric Potential in an Infinite Cylindrical Cell," SIAM J. Appl. Math., **30**(2), 222-239, March 1976 (with A. Peskoff and R. Eisenberg).

37. "An Approach to Mechanics of the Cochlea," *Zeit. Ang. Math u. Physik*, **28**(5), 785-804, 1977 (with R. S. Chadwick).

38. "Transonic Lifting Line Theory," SIAM J. Appl. Math., **35**(2), 209-228, September 1978 (with P. Cook).

39. "Studies of Upper Surface Blown Airfoils in Incompressible and Transonic Flows," *AIAA Journal*, paper no. 80-0270, 1981 (with N. Malmuth, W. Murphy, V. Shankar, E. Cumberbatch).

40. "Computational Transonic Inverse Procedure for Wing Design ," *AIAA Journal*, volume 20, **8**, August 1982, 1044-1050 (with N. Malmuth, V. Shankar).

41. "Note on the Axisymmetric Sonic Jet," SIAM J. Appl. Math., **43**(4), 944-948, August 1983.

42. "Slender-Body Theory and Optimization Procedure for Transonic Lifting Wing Bodies," AIAA Conf. Reno, Nevada 1983. AIAA paper no 83-0184. *J. of Aircraft*, **21**(4), 256-263, April 1984 (with N. Malmuth, C. C. Wu).

43. "Bending Effects on Structural Dynamic Instabilities of Transonic Wings," AIAA paper no 83-0920. Presented AIAA/ASME/ASEE/AHS 24th Structures and Materials Conference, Lake Tahoe, 1983. *J. of Aircraft*, **21**(11), 913-920, November 1984, (with N. Malmuth, S. Chakravarthy, T. Goebel).

44. "Cochlear Mechanics: Analysis for a Pure Tone," *J. Acoustic Soc. America*, **76**(3), September 1984 (with M. Holmes).

45. "Two-dimensional choked transonic flow," *Journal of App. Mathe. and Physics* (ZAMP) **38**, November 1987 (with L. P. Cook).

46. "Transonic Choking and Stabilization for Flows about Slender Bodies," Rensselaer Polytechnic Institute, CAMAC report no 87-12, 1987; *Mechanics Research Communications*, **15**(4) 1988 (with L. P. Cook).

47. "Early Transonic Ideas in the Light of Later Developments" *Lecture Notes in Physics* No. 320, Perspectives in Fluid Mechanics, D. Coles, Ed., Springer-Verlag 1988.

48. "Shock Wave Location on a Slender Transonic Body of Revolution," *Mechanics Research Communications*, **16**(6) November-December 1989 (with N. Malmuth).

49. "Scale Factors in Similarity Solutions," Proceedings of the Annual Seminar of the Canadian Mathematical Society on Lie Theory, Differential Equations and Representation Theory, Edited by V. Hussin, 1989.

50. "Charge Carrier Dynamics in Alpha Particle Tracks," submitted for publication SIAM J. Appl. Math., February 1990 (with J. Pimbley).

51. "The Development of Perturbation Theory at GALCIT," SIAM Meeting July 1992. To appear in *SIAM Review*.

52. "Asymptotic Methods Applied to Transonic Wall Interference," AIAA Paper 91-1712, presented at the AIAA 22^{nd} Fluid and Plasma Dynamics Conference, June 22-26, 1991, Honolulu, Hawaii, and *AIAA Journal* **31** (5), May 1993. (with N.D. Malmuth, H. Jafroudi, C.C. Wu, R. Mclachlan)

53. "On the construction and calculation of optimal nonlifting critical airfoils," *Z angew Math Phys* (ZAMP), 44, 1993, (co-authors M. C. Kropinski and D. Schwendeman).

54. Semiconductors. I, II. Editors, W. M. Coughran, Julian D. Cole, Peter Lloyd and Jacob White, v58,59 *IMA Volumes in Math. and Its Applications.* Springer Verlag, NY 1993.

55. "On Self-Similar Solutions of Barenblatt's Nonlinear Filtration Equation," New Jersey Institute of Technology, Research Report: CAMS-013, Fall 1993 (with B. Wagner). To appear *European Journal of Applied Mathematics*

56. "Hodograph Design of Lifting Airfoils with High Critical Mach Numbers," Rensselaer Polytechnic Institute, Dept. of Mathematical Sciences Report No. 206, December 1993. (with M.C. Kropinski and D. Schwendeman) To appear *J. of Theoretical and Computational Fluid Mechanics.*

57. "Limit Process Expansions and Homogenization," *SIAM J. Appl. Math.* **55** (2), pp. 410-424, 1995; Rensselaer Polytechnic Institute, Dept. of Mathematical Sciences Report No. 212, April 1994.

58. "Interact of a Weak Shock with Turbulence," accepted for publication *AIAA Journal* June 1994 (with Z. Rusak and T.E. Giddings).

Abstracts, letters of correspondence, book reviews, etc.

2. In non-refereed journals

(a) Major articles

1. "Experiments on Transonic Flow," *AF Technical Report*, No. 5667, February 1948, (with H. Liepmann and A. Ashkenas).
2. "Problems in the Theory of Viscous Compressible Fluids," *GALCIT Monograph*, March 1949; reproduced with Appendix by Durand Rep. Co., 1950 (with P. Lagerstrom and Trilling).
3. "Transonic Limits of Linearized Theory," *Caltech Report*, No. OSR TN 228, 1954.
4. "Expansion Procedures and Similarity Laws for Transonic Flow: Part I. Slender Bodies at Zero Incidence," *Caltech Report*, No. OSR TN 56-1, January 1957.
5. "Sweepback Theory for Shock Waves at Hypersonic Speeds," Rand Corporation, No. RM 1991, October 1957.
6. "Lift of Slender Nose Shapes According to Newtonian Theory," Rand Corporation, No. P-1270, 1958.
7. "An Approximate Theory for the Pressure Distributions and Wave Drag of Bodies of Revolution at Mach Number One," *Proceedings of the 6th Annual Midwest Conference on Fluid Mechanics*, Austin, TX, September 1959 (with W. Royce).
8. "Magnetohydrodynamic Simple Waves," *Caltech Report*, No. AFOSR, TN-59-1302, December 1959 (with Y. Lynn).
9. "One-Dimensional expansion of a Finite Mass of Gas into Vacuum," Rand Corporation, no. P-2008, June 1960 (with C. Greifinger).
10. "On Cylindrical Magnetohydrodynamic Shock Waves," *J. of Physics and Fluids*, 4(5), 1961 (with C. Greifinger).
11. "Analytic Methods and Approximations of MHD Problems," *Proceedings of AF-SWC Conference*, AFSWC TN-61-29, 1961 (with C. Greifinger).
12. "Magnetically Driven Shock Waves," *Proceedings of Symposium on Electromagnetics and Fluid Dynamics of Gaseous Plasma*, Polytechnic Institute of Brooklyn, NY April 1961 (with C. Greifinger).
13. "Slender Wings at High Angles of Attack in Hypersonic Flow," *Progress in Astronautics and Rocketry*, American Rocket Society, 1962 (with J. Brainerd).
14. "Experiments on Propagation of Weak Disturbances in Stationary Supersonic Nozzle Flow of Chemically Reacting Gas Mixtures," Proceedings of 8th Symposium on Combustion, Williams and Wilkins, Baltimore MD, 1962 (with P. Wegener).

15. "Estimate for the Pressure on Rapidly Accelerating Bodies in High Speed Flight," Rand Corporation, No. RM 4153-PR, January 1965.

16. "Optimum Slender Shapes with a Variable Skin-Friction Coefficient," *Theory of Optimum Aerodynamic Shapes*, Academic Press, 1965 (with A. Miele).

17. "Note on Prandtl-Meyer Flow for a Gas with Vorticity and Entropy Gradient," Rand Corporation, P3207, August 1965.

18. "Hydromagnetic Flow," in *Plasma Physics in Theory and Application*, McGraw-Hill (W. Kunkel, Ed.), 208-228, 1966.

19. "The Blowhard Problem - Inviscid Flows with Surface Injection," Rand Corporation, Memorandum No. RM5196, ARPA, April 1967 (with J. Aroesty).

20. "Acoustic-Gravity Waves Produces by Energy Release," Proceedings of the Symposium on Acoustic-Gravity Waves in Atmosphere, 25-43, July 1968, sponsored by the Department of Commerce, ESSA and Dept. of Defense, ARPA, Boulder CO (with C. Greifinger).

21. "Twenty Years of Transonic Flow," Boeing Company Report, No. DI-82-0878, July 1969.

22. "The New Math of Mechanics," Proceedings of 6th U.S. National Congress of Applied Mechanics, 3-10, sponsored by ASME, June 15-19, 1970.

23. "Studies in Transonic Flow I. Transonic Area Rule Bodies," UCLA-ENG-7257, August 1972.

24. "Potential Induced by a Point Source of Current in the Interior of a Spherical Cell," UCLA-ENG-7259, December 1972 (with A. Peskoff).

25. "Potential Induced by a Point Source of Current Inside an Infinite Cylindrical Cell," UCLA-ENG-7303, January 1973 (with A. Peskoff).

26. "Singular Perturbation," *Advances in Mathematics* **16**, 380-392, 1975.

27. "Studies in Transonic Flow III. Inviscid Drag at Transonic Speeds," UCLA-ENG-7603, December 1975 (with E. M. Murman).

28. "Studies in Transonic Flow IV. Unsteady Transonic Flow," UCLA-ENG-76104, October 1976 (with J. A. Krupp).

29. "A Consistent Design Procedure for Transonic Airfoils and Wings in Free Field and a Wind Tunnel," Proceedings of NASA-Langley Conference on Advanced Airfoil Technology, March 1978 (with V. Shankar and N. D. Malmuth).

30. "Modes and Waves in the Cochlea," *Mechanics Research Communications*, **6**(3), 177-184, 1979 (with R. S. Chadwick).

31. "Finite Span Wings at Sonic Speed," *Mechanics Research Communications*, **7**(4) 253-260 (with P. Cook and F. Zeigler).

32. "Limit Process Expansion," Proceedings of Advanced Seminar on Singular Perturbations and Asymptotics, Mathematics Research Center, University of Wisconsin-Madison, Academic Press, 1980.

33. "Inverse Transonic Solvers," *AIAA Journal*, accepted for publication (with N. Malmuth and V. Shankar).

34. "Computational Transonic Airfoil Design in Free Air and a Wind Tunnel, *AIAA Journal*, paper no. 78-103, January 1978 (with V. Shankar and N. Malmuth).

35. "Computational Transonic Design Procedures for Three-dimensional wings and Wing-Body Combinations" *AIAA Journal*, Paper 79-0344 1979 (with N. Malmuth and V. Shankar).

36. "Pseudo-Resonance in the Cochlea," *Mechanics Research Communications*, **9**, 205-210, 1982.

37. "An Asymptotic Theory of Solid Tunnel Wall Interface," *AIAA Journal*, Paper No. 82-093 AIAA/ASME 3rd Joint Thermophysics Fluid Conference, June 1982 (with N. Malmuth, F. Ziegler).

38. "Flow Structures Associated with Upper Surface Blown Airfoils," N. Malmuth, J. Murphy, V. Shankar, E. Cumberbatch. Invited paper at Symposium of Numerical and Physical Aspects of Aerodynamic Flows, Calif. State Univ. Long Beach, CA January 1981, Proc. Springer Verlag 1982.

39. "Numerical Treatment of Blown Boundary Layer and Wakes over Transonic Airfoils," with J. Murphy, N. Malmuth. Second International Conference on Boundary and Interim Layers Num. Anal. Group, AIAA, A. Met. Soc. Inst. Num. Comp. Irish Math Society, Dublin, June 1982 - Proceedings 1983.

40. "Asymptotic Problems in Transonic Flow," *AIAA Journal*, paper no 82-0104, AIAA 30th Aerospace Sciences Meeting, January 1982, Orlando, FL.

41. "Asymptotics and Numerics," Transactions of the First Army Conference on Applied Mathematics and Computing, 1983, Proceedings, 1984.

42. "Cochlear Mechanics: Analysis for a Pure Tone," Rensselaer Polytechnic Institute, Dept. of Mathematical Sciences Report No. 149, November 1983 (with M. Holmes).

43. "Airfoil Design at Sonic Velocity," Rensselaer Polytechnic Institute, Dept. of Mathematical Sciences Report No. 146, February 1985 (with Baoyu Ling).

44. "Slender Body Theory and Space Shuttle Transonic Aerodynamics," AIAA paper no. 85-0478 AIAA 23rd Aerospace Sciences Meeting, January 1985 Reno, Nevada (with N. Malmuth, and C. C. Wu).

45. "Transonic Wave Drag Estimation and Optimization Using the Nonlinear Area Rule," AIAA 86, AIAA 4th Applied Aerodynamics Conference, June 1986, San Diego, CA (with N. Malmuth and C. C. Wu). *J. of Aircraft* **24** 3, 203-210, March 1987.

46. "Note on Entropy and Wave Drag," Rensselaer Polytechnic Institute, CAMAC report no 87-13, 1987.

47. "Some Asymptotic Problems of Transonic Flow Theory," IUTAM Symposium Transsonicum III, Springer-Verlag 1989, J Zierep, H. Oertel (Eds.), pp 157-170 (with L. P. Cook).

48. "Wave Drag Due to Lift for Transonic Airplanes," NASA Transonic Symposium: Theory, Application, and Experiment, NASA Conference Publication 3020 - Vol 1, Part 1, pp 293-308, 1989 (with N. Malmuth).

49. "Shock Wave Location on a Slender Transonic Body of Revolution," *Mechanics Research Communications* **10**, (6), pp 353-358, November-December, 1989. Rensselaer Polytechnic Institute Math. Report No. 171, August 1989 (with N. Malmuth).

50. "Optimum Hypersonic Wings and Wave Riders," XIXth Biennial Symposium on Advanced Problems and Methods in Fluid Mechanics, Kozubnik, Poland September 1989. Appeared in Proceedings 1990.

51. "Hodograph Design of a Shock-Free Transonic Slender Body," *3rd International Conference on Hyperbolic Problems,* Uppsala, Sweden June 1990 (co-author D. Schwendeman). Appeared in Proceedings 1991.

52. "Optimum Similarity Flows and Waveriders," *1st International Hypersonic Waveriders Symposium*, University of Maryland, College Park October 1990.

53. "Asymptotic Theory in Aerodynamics," AIAA paper no. 91-0028 AIAA 29th Aerospace Sciences Meeting, January 1991 Reno, Nevada.

54. "Asymptotic Theory of the Transonic Area Rule," Dept. of Mathematics Rept. 194, Rensselaer Polytechnic Institute December 1990. Appeared in "Mathematical Approaches in Hydrodynamics" M. P. Tulin anniversary volume SIAM Publications 1991 (co-author L. P. Cook).

55. "A Study of Optimum Critical Airfoils," Dept. of Mathematics Rept. 197, Rensselaer Polytechnic Institute July 1991. Presented at *4th International Conference on Computational Fluid Dynamics*, Davis, CA, September 1991 (co-authors M. C. Kropinski and D. Schwendeman).

56. "Interaction of the sonic boom with atmospheric turbulence," *AIAA Journal*, paper no 93-2943, AIAA 24th Fluid Dynamics Conference, July 6-9, 1993, Orlando, FL.

57. "Interaction of the Sonic Boom with Atmospheric Turbulence," NASA Conference Publication 10132, Ames Research Center, Moffett Field, CA May 12-14, 1993, pp. 65-92. (with Zvi Rusak)

Ph.D. Students of Julian D. Cole

Caltech T. Y. Wu (NAE)

S. Berndt
S. Shen
W. Royce
J. Petty
K. Harstad
Y. M. Lynn
K. Grimes
W. B. Bush
J. Kevorkian
R. Schmulian
G. Bluman
A. Messiter
N. Malmuth
T. F. Zien
L. Levitt (with R. Feynman)
H. Kabakow (with R. Feynman)
A. D. MacGillivray
M. Gourdine
D. Hoult

UCLA E. Tse

C. K. Feng
K. Kusunose
M. Holmes
G. Schleiniger
S. Rimbey
F. Ziegler (with P. Cook)
F. Hendriks
S. L. Cole
J. F. Hamet

RPI J. J. Xu

V. Villamisar
B. Wagner
D. Lessen
A. Kalocsai
M.C. Kropinski (with D. Schwendeman)
R. Buckmire (with D. Schwendeman)

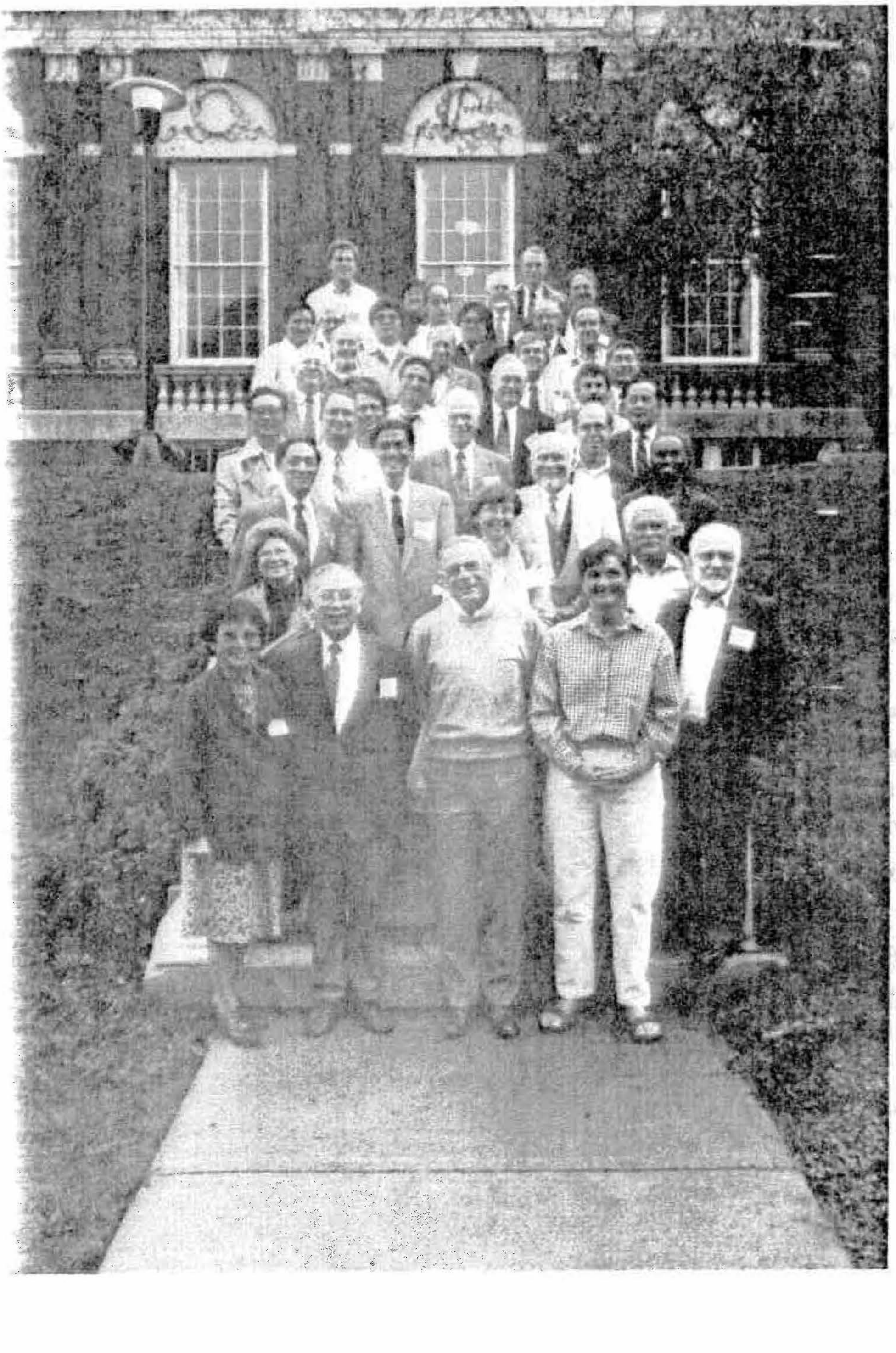

Rensselaer
"Asymptotic and Computational Methods for Applications:
A Conference in Honor of Julian D. Cole"
October 6, 1995

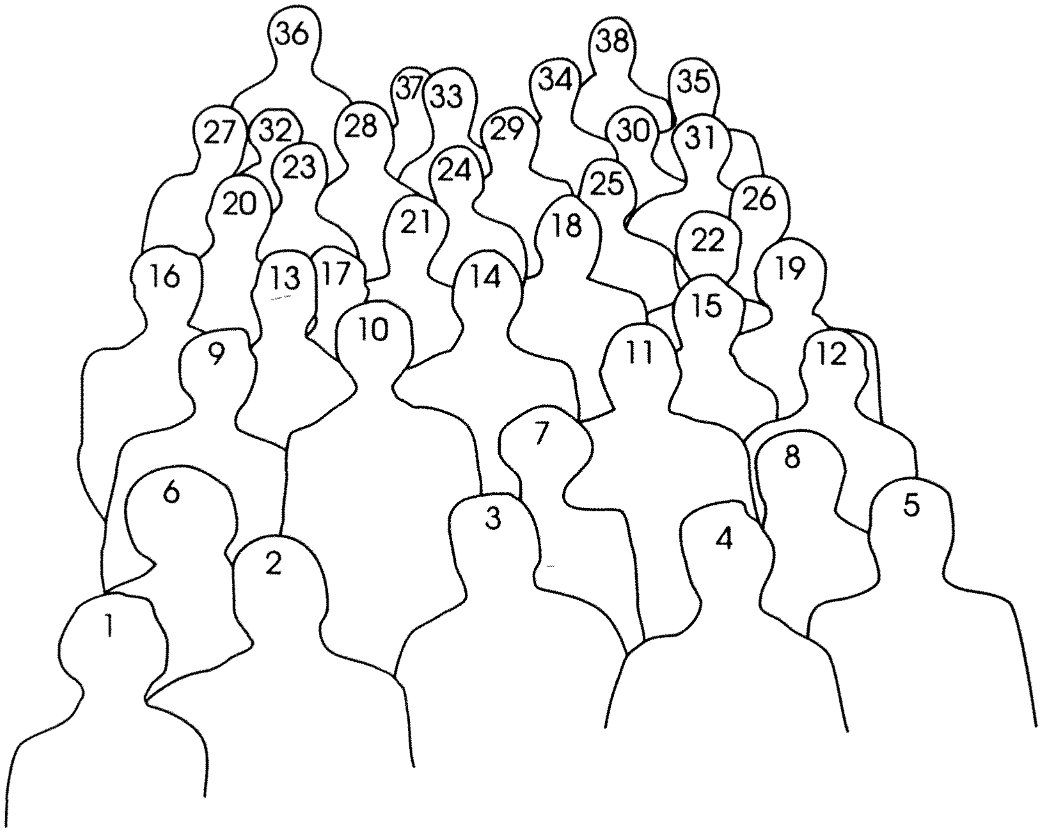

1. Annie Wu
2. Ted Wu
3. Julian D. Cole
4. Susan Cole
5. Jerry Kevorkian
6. Edith H. Luchins
7. Pam Cook
8. Joe Flaherty
9. T. F. Zien
0. C. K. Feng
11. Marshall Tulin
12. Ron Buckmire
13. George Bluman
14. Oleg Ryzhov
15. Jon Bell
16. J. J. Xu
17. S. D. Shih
18. Bob O'Malley
19. Y. M. Lynn
20. Gary Judd
21. Zvi Rusak
22. Victor Roytburd
23. Joe Keller
24. Hirsh Cohen
25. Gilberto Schleiniger
26. Kasu Kusunose
27. Scott Rimbey
28. S. Wang
29. Chjan Lim
30. Art Messiter
31. Mark Holmes
32. Jim Simmonds
33. Johan Helsing
34. Milton Van Dyke
35. Joe Haus
36. Don Schwendeman
37. Peggy Lashway
38. Houston Wood

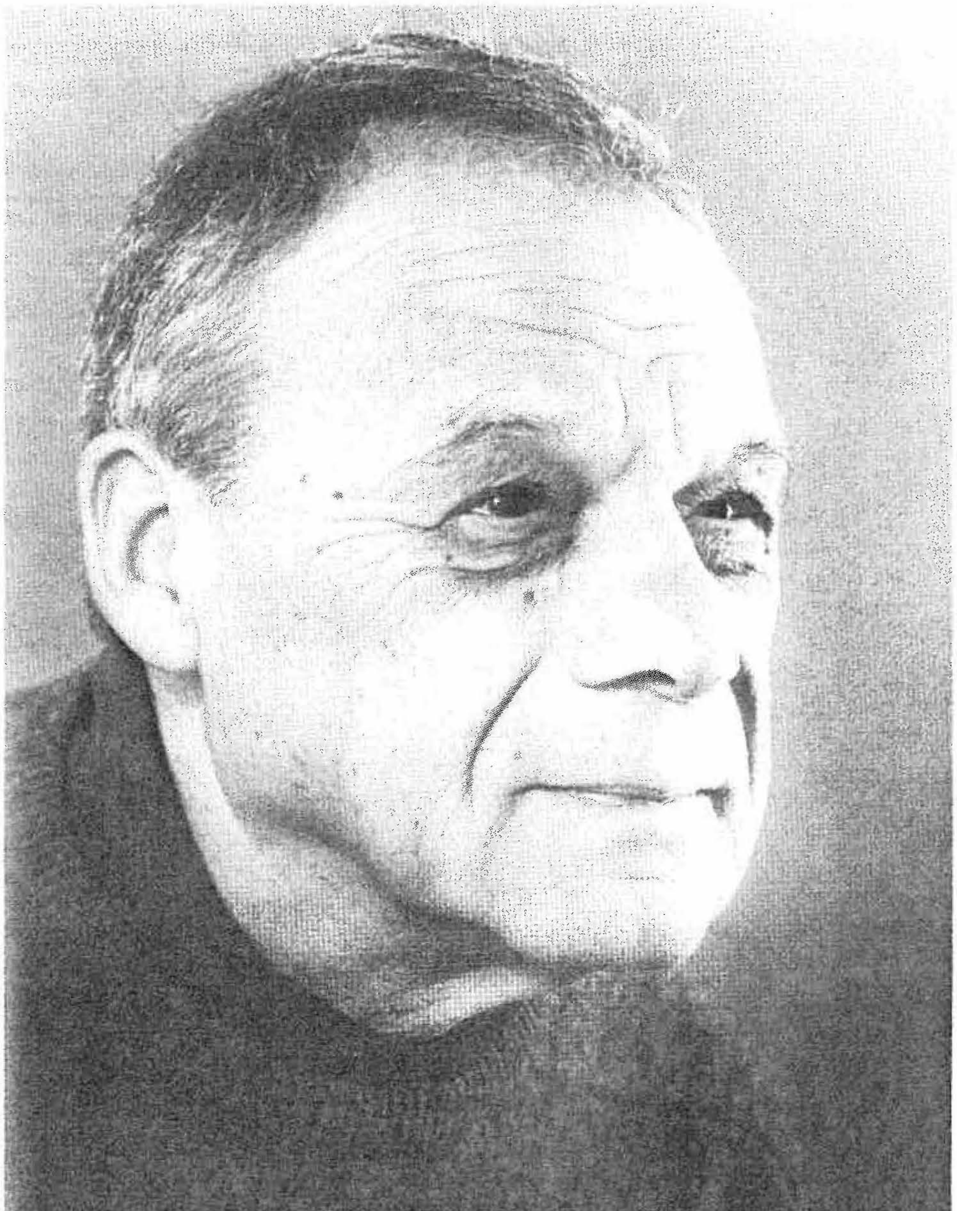

JULIAN DAVID COLE

CONTENTS

CONTRIBUTED PAPERS

A new finite-difference scheme for singular differential equations in cylindrical or spherical coordinates

by Ron Buckmire *

Mathematics Department
Occidental College
Los Angeles, CA 90041-3338, U.S.A.

December 18, 1995

It is well known that the standard finite-difference scheme for approximating the radial derivative in polar coordinates (r-derivative) in Laplace's Equation has difficulty capturing the singular (logarithmic) behavior of the solution near the origin. By choosing a non-standard finite difference scheme ("logarithmic differencing") the singular behavior can be captured with a significantly smaller local truncation error. In the almost-trivial 1-dimensional case, the singular behavior is captured *exactly*. A number of numerical examples are given which illustrate the utility of the new scheme.

1 Introduction

This paper discusses a method for computing numerical solutions to partial differential equations and ordinary differential equations written in spherical or cylindrical coordinates. It involves a new way to discretize the operator $\mathcal{R} \equiv r^p \frac{d}{dr}$, where $p = 1$ is the cylindrical coordinates case and $p = 2$ is the spherical coordinates case.

The scheme introduced in this paper was first presented in Buckmire's 1994 thesis [1], in which particular slender bodies of revolution were found to possess shock-free flows. The problem is formulated using transonic small disturbance theory found in [2], [3] and [4], among other sources. Cole & Schwendeman announced the first computation of a fore-aft symmetric shock-free transonic slender body in [6]. Computationally, the problem involves numerically solving a boundary value problem with an elliptic-hyperbolic partial differential equation (the Kármán-Guderley equation) in cylindrical coordinates, with a singular inner Neumann boundary condition at $r = 0$ and a non-singular outer Dirichlet boundary condition

*The author can be reached by electronic mail at ron@abacus.oxy.edu.

far away from $r = 0$. Namely,

$$(K - (\gamma + 1)\phi_x)\phi_{xx} + \phi_{\tilde{r}\tilde{r}} + \frac{1}{\tilde{r}}\phi_{\tilde{r}} = 0. \tag{1}$$

$$\begin{array}{ll} \phi(x, \tilde{r}) \to S(x)\log\tilde{r} + G(x), & \text{as } \tilde{r} \to 0,\ |x| \leq 1 \\ \phi(x, \tilde{r}) \text{ bounded}, & \text{for } \tilde{r} = 0,\ |x| > 1. \end{array} \tag{2}$$

$$\phi(x, \tilde{r}) \to \frac{\mathcal{D}}{4\pi}\frac{x}{(x^2 + K\tilde{r}^2)^{3/2}}, \qquad \text{as } (x^2 + \tilde{r}^2)^{1/2} \to \infty. \tag{3}$$

In (1), (2) and (3) the variable $\tilde{r}$ is a scaled cylinrdical coordinate, K is the transonic similarity parameter, $\mathcal{D}$ is the dipole strength and $\phi(x, \tilde{r})$ is a velocity disturbance potential. Both $S(x)$ and $G(x)$ are bounded functions. The main point of sketching the boundary value problem here is to emphasize that the function $G(x)$ which occurs in (2) needs to be computed very accurately, because the pressure coefficient on the body depends directly on $G'(x)$. Computing it is complicated by the fact that $\phi(x, \tilde{r})$ and $S(x)\log\tilde{r}$ are becoming singular as $\tilde{r} \to 0$, which is where the boundary condition must be evaluated. Thus a numerical scheme was needed to compute the solution accurately as $\tilde{r} \to 0$. This was the motivation for the scheme introduced in this paper.

In 1971, Murman and Cole [5] introduced a numerical scheme which was the first of its kind to be able to handle mixed-type elliptic-hyperbolic partial differential equations like the Kármán-Guderley equation. The method is now known as "Murman-Cole switching" and is a particular scheme to discretize the x-derivatives in the partial differential equation. It is fitting that the new scheme which deals with the discretization of the r-derivatives in the same PDE is presented at a gathering honoring the contributions of Julian Cole.

2 Discretizing the operator $\mathcal{R} \equiv r^p \frac{d}{dr}$

This section shall explain the discretization of $\mathcal{R}$, limited to the $p = 1$ case; the $p = 2$ discretization is derived in a similar manner. Consider the quantity $B(r)$ which is defined as

$$B(r) = \mathcal{R}u = \frac{r^p du}{dr},$$

where $u = u(r)$ is an unknown function (the solution) the operator $\mathcal{R}$ acts on.

The first step in the discretization of the operator is to choose a grid $\{r_j\}_{j=0}^{N}$ on the interval $0 \leq r \leq 1$ where

$$0 \leftarrow r_0 < r_1 < r_2 < \ldots < r_j < \ldots < r_N = 1. \tag{4}$$

On the grid defined in (4) one has discrete forms of the quantities of interest, such as $u(r_j) = u_j$ and $B_{j+1/2} = r^p \left.\frac{d}{dr}\right|_{r=r_{j+1/2}}$ where $r_{j+1/2} = \frac{r_j + r_{j+1}}{2}$.

There are two choices of discretizing $B(r)$, the standard forward-difference approximation method and the new scheme, which shall be compared with each other.

$$B^{(1)}_{j+1/2} = r_{j+12/} \frac{u_{j+1} - u_j}{r_{j+1} - r_j} \tag{5}$$

$$B^{(2)}_{j+1/2} = \frac{u_{j+1} - u_j}{\log(r_{j+1}) - \log(r_j)} = \frac{u_{j+1} - u_j}{\log(r_{j+1}/r_j)} \tag{6}$$

The standard scheme in (5) shall be referred to as Scheme$^{(1)}$ and the new scheme in (6) shall be referred to as Scheme$^{(2)}$. Scheme$^{(2)}$ can be obtained by assuming that $B(r)$ should be constant on each subinterval (r_j, r_{j+1}) of the grid. If one relates $B(r)$ back to the physical fluid mechanics problem we want to solve, it corresponds to a mass flux. The relationship between $B_{j+1/2}$ and u_j and u_{j+1} solves the simple boundary value problem

$$ru' = B_{j+1/2} = \text{constant} \tag{7}$$

$$u(r_j) = u_j \tag{8}$$

$$u(r_{j+1}) = u_{j+1}. \tag{9}$$

The solution to this is $u(r) = B_{j+1/2} \log r + C$, which, when one applies the boundary conditions (8) and (9) leads to the formula

$$B_{j+1/2} = \frac{u_{j+1} - u_j}{\log(r_{j+1}/r_j)}.$$

3 Applying the method

The question to be asked now is, how well does the new scheme given in (6) work? This question will be answered by giving an example of the new scheme being applied to a simple differential equation. The Kármán-Guderley equation (1) and the associated boundary conditions of (2) and (3) can be related to the simpler boundary value problem given below

$$\frac{1}{r}\frac{d}{dr}\left(r\frac{du}{dr}\right) + qu = 0, \qquad q \text{ constant} \tag{10}$$

$$r\frac{du}{dr}\bigg|_{r=0} = S, \tag{11}$$

$$u(1) = G. \tag{12}$$

If one linearizes and substitutes $\phi(x, r) = u(r)e^{ikx}$ into (1) one will obtain the above boundary value problem. This simple boundary value problem is used as the test problem to benchmark the new finite-difference scheme instead of the transonic small-distrurbance equation (1) one is really interested in solving, because the simpler problem has a known exact solution involving logarithms and Bessel functions, depending on the value of $q = k^2$. The exact solution can be written as

$$q > 0, \qquad u(r) = \frac{\pi}{2} S Y_0(r\sqrt{q}) + (G - S\frac{\pi}{2} Y_0(\sqrt{q}))\frac{J_0(r\sqrt{q})}{J_0(\sqrt{q})} \tag{13}$$

$$q = 0, \qquad u(r) = S \log r + G \tag{14}$$

$$q < 0, \qquad u(r) = \frac{-\pi}{2} S K_0(r\sqrt{-q}) + (G + S\frac{\pi}{2} K_0(\sqrt{-q}))\frac{I_0(r\sqrt{-q})}{I_0(\sqrt{-q})}. \tag{15}$$

First consider the $q = 0$ model problem. The differential equation in this case is simply

$$\frac{1}{r}\frac{d}{dr}\left(r\frac{du}{dr}\right) = B'(r) = 0.$$

This has the simple solution $B(r)$ = constant. Using the boundary condition at $r = 0$, $B(0) = S \Rightarrow B(r) = S$. Thus the discrete version of the model equation which is being solved is

$$B_{j+1/2} = S. \tag{16}$$

Using scheme$^{(1)}$ (the standard forward-difference approximation)

$$B_{j+1/2} = r_{j+1/2}\frac{u_{j+1} - u_j}{r_{j+1} - r_j} = S$$

$$\Rightarrow u_j = u_{j+1} - 2S\frac{r_{j+1} - r_j}{r_{j+1} + r_j} \qquad \text{with } u_N = G.$$

This is a simple marching scheme which allows one to compute all the u_j, $j = 0, \ldots, N$ starting from $u_N = G$ and "marching" down to u_0.

Using scheme$^{(2)}$ (the new scheme) the discrete equation to be solved is

$$B_{j+1/2} = \frac{u_{j+1} - u_j}{\log(r_{j+1}/r_j)} = S$$

$$\Rightarrow u_j = u_{j+1} - S\log(\frac{r_{j+1}}{r_j}), \qquad \text{with } u_N = G$$

Scheme$^{(2)}$ also leads to a marching scheme which solves the model equation exactly *by definition*. This happens because the scheme was derived assuming that $B(r)$ would be constant on each subinterval. For this model equation $B(r) = S$, so it is the same constant, namely S on each subinterval. So scheme$^{(2)}$ is exact for this model equation where $q = 0$. A similar idea of deriving a finite-difference scheme by using a discretization which solves a simple version of the differential equation one is actually interested in solving is given in Scharfetter & Gummel [8].

Compare the two schemes by looking at the difference between the numerical solution each generates, at each grid point.

$$e_j = u_j^{(1)} - u_j^{(2)} \tag{17}$$

where $u_j^{(1)}$ is the solution to the equation obtained using scheme$^{(1)}$ and $u_j^{(2)}$ is the solution to the equation obtained using scheme$^{(2)}$.

$$\begin{aligned} e_j &= u_{j+1}^{(1)} - 2S\frac{r_{j+1} - r_j}{r_{j+1} + r_j} - u_j^{(2)} + S\log(\frac{r_{j+1}}{r_j}) \\ &= e_{j+1} - 2S\delta_j + S\log\left(\frac{1 + \delta_j}{1 - \delta_j}\right) \end{aligned} \tag{18}$$

where $\delta_j = \dfrac{r_{j+1} - r_j}{r_{j+1} + r_j}$. The symbol δ_j is a characteristic of the grid disretization somewhat akin to grid separation.

If $\delta_j \ll 1$, then using a simple Taylor series expansion

$$\frac{e_j - e_{j+1}}{S} = \frac{2}{3}\delta_j^3 + \frac{2}{5}\delta_j^5 + \dots \tag{19}$$

Thus the local discretization error made by the typical difference scheme is $O(\delta_j^3)$, which implies that the global error is $O(\delta_j^2)$. However, suppose that δ_j is not small for all j. Remember that δ_j depends on the choice of $\{r_j\}_{j=0}^N$. It is a characteristic of the grid discretization. For example, suppose that the choice is to use a uniform grid. In that case,

$$r_j = jh, \qquad h = \frac{1}{N}, \quad j = 0, \dots, N.$$

In this case $\delta_j = \dfrac{r_{j+1} - r_j}{r_{j+1} + r_j} = \dfrac{h}{jh + (j+1)h} = \dfrac{1}{2j+1}$. Clearly, $\dfrac{1}{2N+1} \leq \delta_j \leq \dfrac{1}{3}$. So the parameter δ_j varies depending on what grid point it is evaluated at, but at $j = 1$, δ_1 is a constant which does not depend on N or h which means that as $h \to 0$ (or $N \to \infty$) the local discretization error, which is $O(\delta_j^3)$ does not get smaller and go to zero, but in fact the error at $j = 1$ is $O(1)$!

A uniform grid is a bad choice to pick when discretizing the domain if one is solving a differential equation with a $r^p \dfrac{d}{dr}$ operator and the domain includes the singular point $r = 0$, i.e. singular differential equations. A better grid choice is to ensure that the grid has the property that δ_j is small for all j. The easiest way to do that is to pick one value of δ for all j. The value can be chosen by looking at the definition of δ_j and re-arranging it to give a marching scheme which chooses the appropriate grid discretization $\{r_j\}_{j=0}^N$.

$$\delta_j = \frac{r_{j+1} - r_j}{r_{j+1} + r_j} \Rightarrow r_j = \left(\frac{1 - \delta_j}{1 + \delta_j}\right) r_{j+1}, \qquad \text{with } r_N = 1$$

For example, if one lets $\delta_j = 1/N$,

$$r_j = \left(\frac{1 - 1/N}{1 + 1/N}\right) r_{j+1} = \frac{N-1}{N+1} r_{j+1}$$

which implies that $r_j = \alpha^{N-j} r_N$, where $\alpha = \dfrac{1-\delta}{1+\delta} = \dfrac{N-1}{N+1} < 1$. This grid choice corresponds to an approximately exponentially stretched grid, with many points clustered near $r = 0$. This analysis supports the grid choice used by Krupp & Murman [7] to solve the Kármán-Guderley equation back in 1972.

The standard forward-difference scheme can be used to solve singular differential equations, but the grid must be chosen intelligently. Using the new scheme there is flexibility about what kind of grid to use.

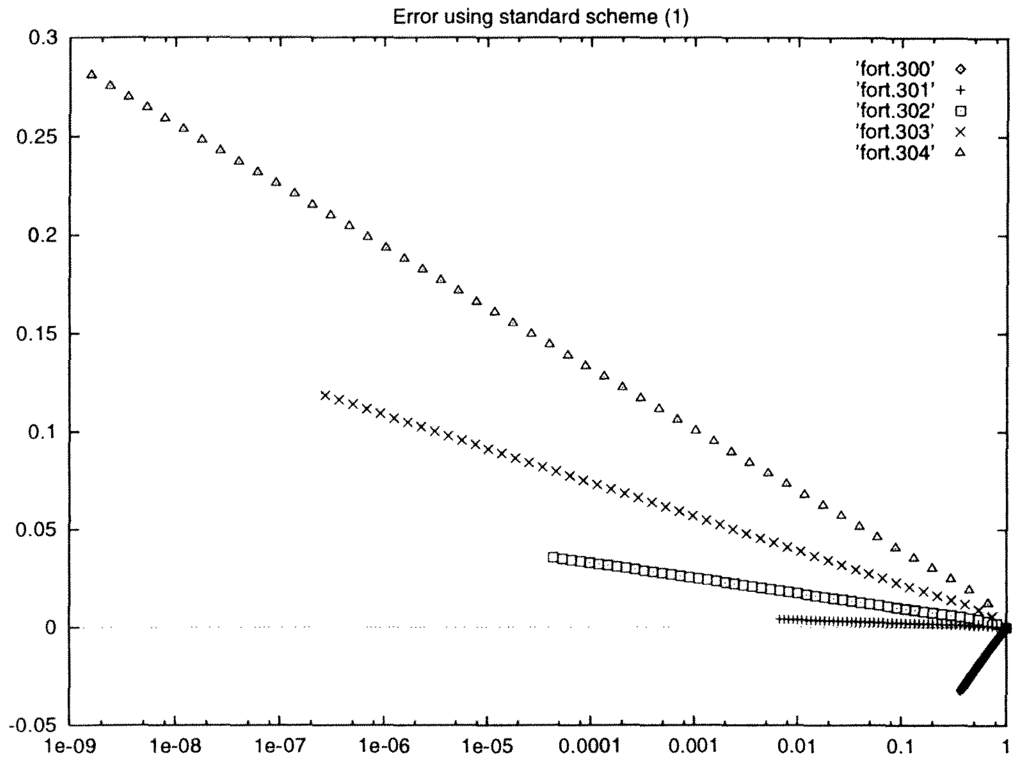

FIG. 1. *Error Due to scheme*$^{(1)}$

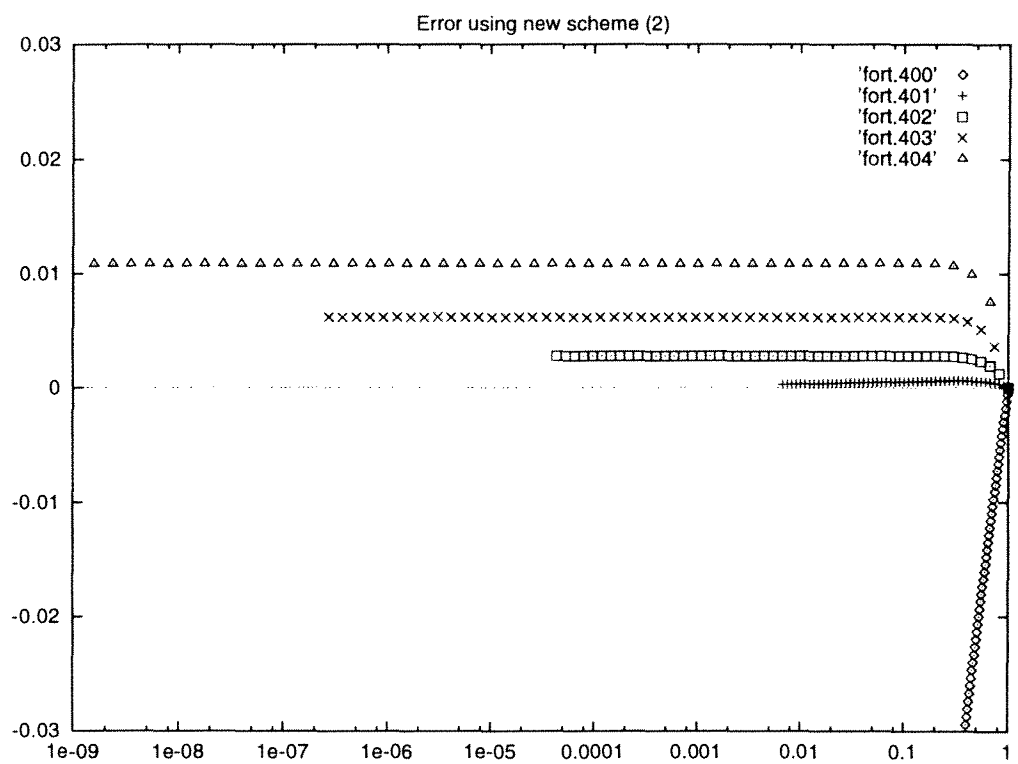

FIG. 2. *Error Due to scheme*$^{(2)}$

4 Numerical Results

Consider how the competing schemes fare when used to solve the $q \neq 0$ model problems. Exact solutions are known, so one can compare the absolute error scheme$^{(1)}$ makes in solving the problem to the absolute error scheme$^{(2)}$ makes to solve the identical problem. The numerical results are given in Figures 1 and 2. In all cases, the new scheme is more accurate than the standard scheme. Even when scheme$^{(2)}$ is used on a uniform grid but scheme$^{(1)}$ is used on an exponentially-stretched grid the new scheme fares better. Both schemes get worse errors as the point at which the inner boundary condition is evaluated approaches zero. For the numerical results given in Figures 1 and 2, a grid was chosen consisting of $N = 50$ points and then a series of computations performed solving the model problem (15) using a value of $q = \pm 1$. By choosing steadily decreasing values for α the degree to which the grid was exponentially stretched was increased, culminating in the final run with $r_0 = 10^{-9}$.

5 Conclusions

A new finite-difference scheme has been introduced to deal with differential equations in cylindrical or spherical co-ordinates. It appears to tackle singular problems more accurately and efficiently than other standard schemes. The author urges others to use this new scheme and look forward to hearing how it fares when used to solve other differential equations numerically. Future research will involve using the ideas in this paper to attempt to derive other similar finite-difference schemes.

References

[1] Buckmire R., *The Design of Shock-free Transonic Slender Bodies of Revolution*, Ph.D. thesis, Rensselaer Polytechnic Institute, Troy, NY (1994)

[2] Cole J.D., and L.P. Cook, *Transonic Aerodynamics*, North Holland, (1986).

[3] Cole J.D., and N. Malmuth, *Shock Wave Location on a Slender Transonic Body of Revolution*, Mechanics Research Communications, **16(6)**, (1989), pp. 353-357.

[4] Cole J.D., and A.F. Messiter, *Expansion Procedures and Similarity Laws for Transonic Flow*, Z.A.M.P., **8**, (1957), pp. 1-25.

[5] Cole J.D., and E.M. Murman, *Calculation of Plane Steady Transonic Flows*, AIAA Journal, Volume **9** Number 1, (January 1971), pp. 114-121.

[6] Cole J.D., and D.W. Schwendeman, *Hodograph Design of Shock-free Transonic Slender Bodies*, 3rd International Conference on Hyperbolic Problems, Editors Bjorn Engqvist and Bertil Gustafsson, Uppsala, Sweden, (June 11-15 1990).

[7] Krupp J.A., and E.M. Murman, *Computation of Transonic Flows past Lifting Airfoils and Slender Bodies*, AIAA Journal, Volume **10** Number 7, (July 1972), pp. 880-886.

[8] Scharfetter, D.L. and H.K. Gummel, *Large-Signal Analysis of a Silicon Read Diode Oscillator*, IEEE Transactions on Electron Devices, Vol. ED-16, Number 1, (January 1969) pp. 64-84.

Decay of Resonant Free Surface Waves in a Rectangular Basin*

S. L. Cole[†] T. D. Strayer[‡] A. P. Cochran[§]

This talk was given in honor of Julian Cole on the occasion of his 70th birthday with gratitude and respect for his many contributions to the field of mathematics and to my life personally. *Susan Cole*

1 Introduction

Resonant free surface waves can be generated in a rectangular basin such as depicted in Fig. 1 for small oscillation amplitudes a when the forcing frequency ω is close to a discrete set of frequencies. The fluid motion in the basin is governed by the Navier Stokes equations with appropriate boundary and free surface conditions. The two-dimensional form of these is

$$u_t + uu_x + vu_y = -\frac{P_x}{\rho} + \nu(u_{xx} + u_{yy})$$

$$v_t + uv_x + vv_y = -\frac{P_y}{\rho} + \nu(v_{xx} + v_{yy}) - g \tag{1}$$

$$u_x + v_y = 0$$

with the free surface conditions

$$\left(\frac{P}{\rho} - 2\nu u_x\right)\eta_x + \nu\left(u_y + v_x\right) = 0 \qquad \text{on} \quad y = \eta$$

$$\nu(u_y + v_x)\eta_x + \frac{P}{\rho} - 2\nu v_y = 0 \qquad \text{on} \quad y = \eta \tag{2}$$

$$v = u\eta_x + \eta_t \qquad \text{on} \quad y = \eta$$

and boundary conditions

$$u = -a\omega \sin \omega t \quad \text{and} \quad v = 0 \quad \text{along the solid boundaries} \tag{3}$$

---

* This project was supported with gratitude under the National Science Foundation grant DMS-9301163.

† Department of Mathematical Sciences, Rensselaer Polytechnic Institute, Troy, NY 12180-3590

‡ Knolls Atomic Power Laboratory, Schenectady, NY 12301-1072

§ Department of Mathematical Sciences, Rensselaer Polytechnic Institute, Troy, NY 12180-3590

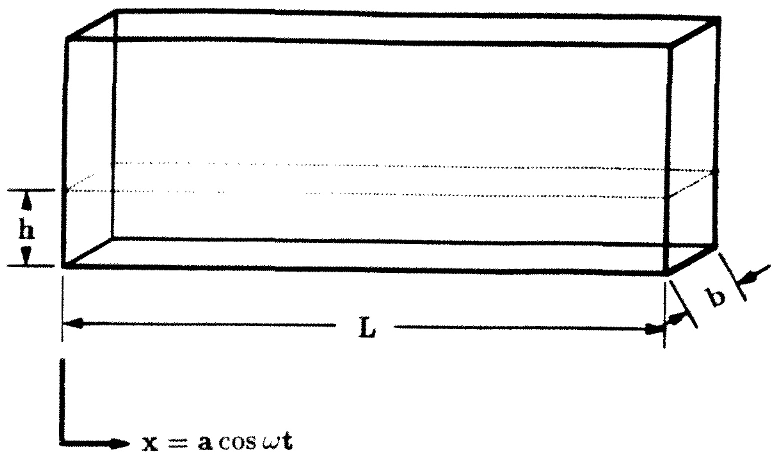

FIG. 1. *Box used to generate free surface waves.*

for forced motion and

(4) $$u = 0 \quad \text{and} \quad v = 0 \quad \text{along the solid boundaries}$$

for unforced motion. Here u is the fluid velocity in the x-direction, v is the velocity in the y-direction, η is the free surface height, P is the pressure, ρ is the density, ν is the kinematic viscosity and g is the gravitational constant of acceleration.

The problem of forced resonant motion is extremely complicated; both nonlinearity and viscosity play important roles in the shallow water near resonant case. See for example, Chester and Bones [1] or Khosropour, Cole and Strayer [2]. These papers show that a frequency sweep plot of the amplitude of the free surface waves for a given driving amplitude exhibits a complicated pattern of peaks as sequential ultraharmonics are excited. While the general pattern of predicted excitation matches experimental measurements, the theory overpredicts the peakiness of the solutions. It is shown in [2] that these peaks are very sensitive to viscous damping.

In order to better understand the role of viscous damping on resonant free surface waves, this paper investigates the related problem of the decay of unforced waves. Experimental results are presented and a simple mathematical theory is derived to model the behavior.

2 Experimental Results

Resonant waves were generated on the RPI campus in a rectangular tank with dimensions $L = 61.0$ cm, $h = 7.9$ cm and $b = 20.3$ cm using a Compumotor S83-135 motor with an S6 driver for a variety of near resonant frequencies and driving amplitudes. These runs were very sensitive to the water height even due to the effects of evaporation over a day's time, so the tank was covered to minimized evaporative losses. A small amount of Kodak Photoflo was added to the water to reduce surface tension effects. (Photoflo was added a little at a time until no discernable change in response was detected.) The forced resonant wave height was measured and then the forcing was discontinued and the wave height was measured again as the waves decayed. All wave height measurements were made 5 cm from the end wall to reduce the effects of endwall interference with the gauge. Typical response curves are presented next.

Fig. 2a shows the free surface height for the forced problem with $\omega = .65$ hz and $a = .089$

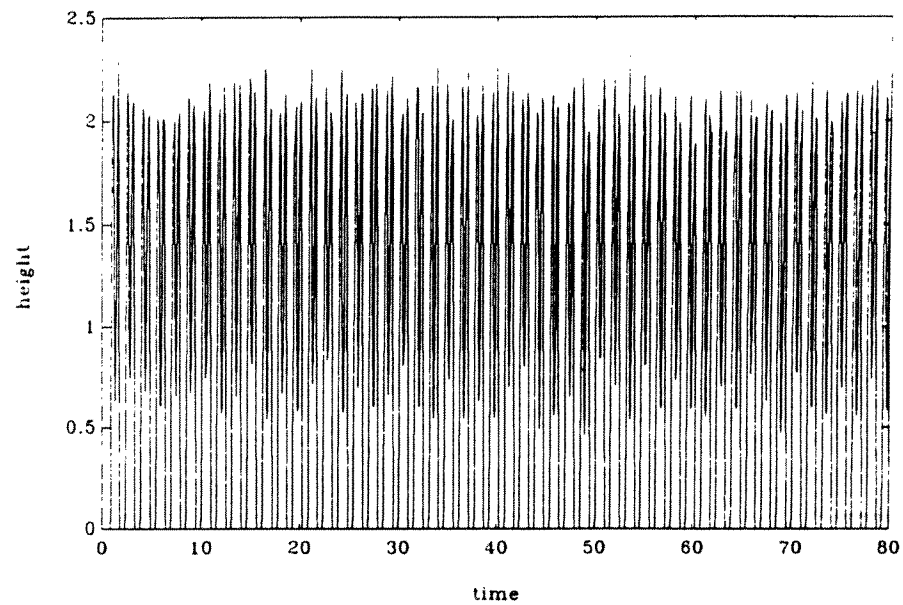

FIG. 2A. *Free surface height measured 5 cm from the end wall for ω=.65 hz and a=.089 cm.*

cm for 80 seconds of the large time flow. As a wave passes the wave gauge, water slides down the side of the gauge more slowly than it falls in the fluid nearby so the actual minimum height is lower than that measured. Because of this, only the portion of the wave above the reference height $y = 0$ is plotted. Water rises along the gauge fairly consistently with the nearby flow so the measured maximas are relatively accurate. Note that there are two local maximas of approximately the same height for each oscillation cycle (as can be traced by the lowest set of minimas). Fig. 2b shows the free surface peaks only measured for the unforced case overlaid with a plot of the function $2.75e^{-.018(t-5)}$. Note that the free surface height initially rises after the forcing is discontinued and that there are two waves (corresponding to the pair of peaks for each oscillation cycle) with the same frequency and decay rate.

Similarly, Fig. 3a shows the free surface height for the forced problem with $\omega = .72$ hz and $a = .089$ cm while Fig. 3b shows the corresponding peaks only of the decay motion overlaid with a plot of the function $2.8e^{-.02t}$. Note that there is only one set of peaks for each oscillation cycle in the forced and decay problems and that the free surface height remains fairly constant immediately following the cessation of box motion.

3 Mathematical Model

Although the details of the flow immediately following turning off the forcing depends on where the box is in relation to the forcing cycle, the pattern shown in Figs. 2b and 3b are representative for their forcing configurations. Flows for ω near but less than the first linear resonant frequency, .705 hz, corresponding to $\omega^2 = g\pi/L\tanh(\pi h/L)$ are highly nonlinear for this driving amplitude as can be seen from the two sets of peaks for every cycle in Fig. 2a. Expanding equations (1) in a perturbation expansion where each successive harmonic term is of subsequently lower order shows that the expansion breaks down for ω^2 near $g\pi/(nL)\tanh(n\pi h/L)$ where $n = 1, 2, 3, \cdots$ represents the first, second, third, etc. ultraharmonic terms. For this experimental configuration, the case $n = 2$ corresponds to

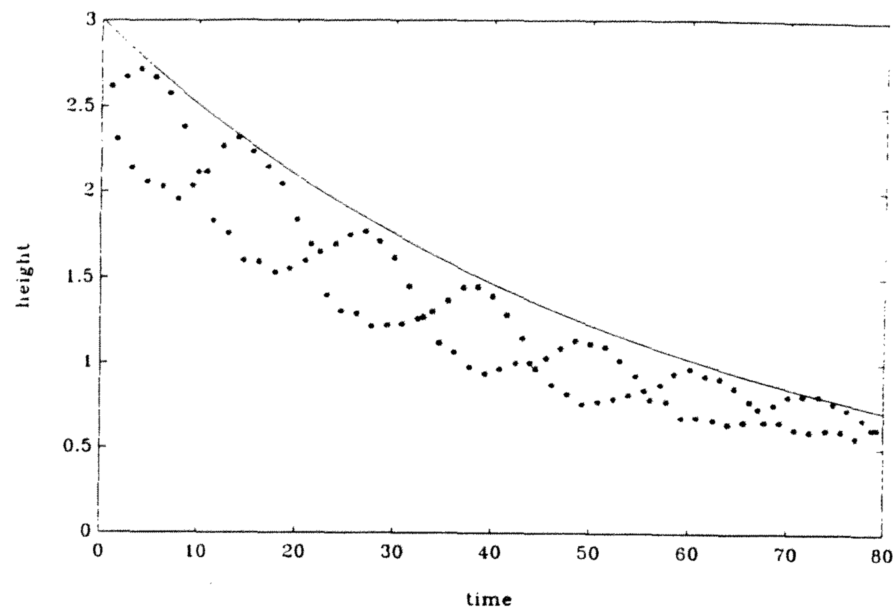

FIG. 2B. *Free surface peaks of decaying wave overlaid with the function* $2.75e^{-.018(t-5)}$.

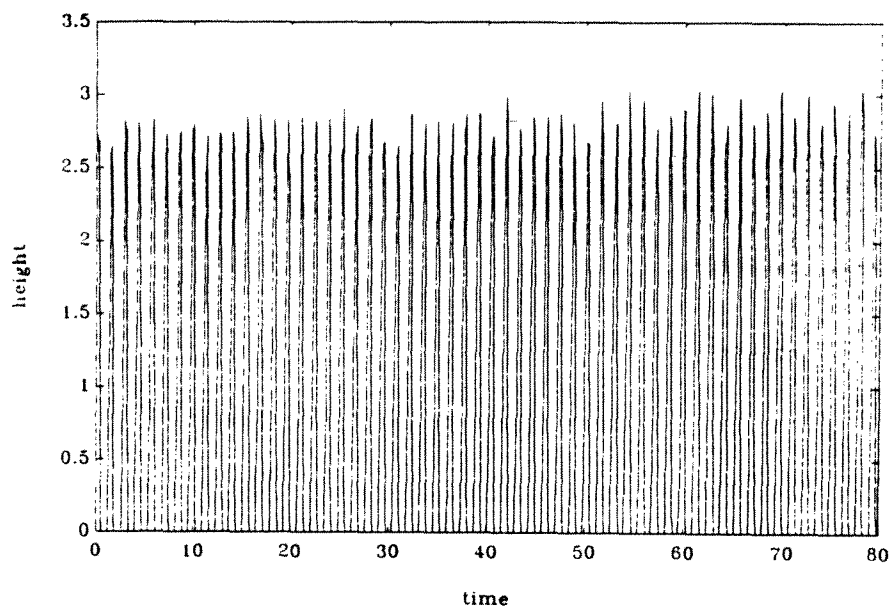

FIG. 3A. *Free surface height measured 5 cm from the end wall for* ω=.72 *hz and* a=.089 *cm.*

ω = .657 hz and ω decreases for increasing n. For ω near .657 hz, the contribution from the third and higher harmonic terms becomes more significant than for values of ω where the flow can be modeled by a regular perturbation expansion (at least for the first two modes). Flows for ω enough greater than the first resonant frequency such as in Fig. 3a are dominated by a single mode as can be seen by the single free surface peak for every forcing cycle. A regular perturbation expansion in harmonic modes converges in this frequency regime. The free surface initially rises after the forcing is turned off for highly nonlinear flows such as in Fig. 2b while it remains relatively constant for flows such as in Fig. 3b

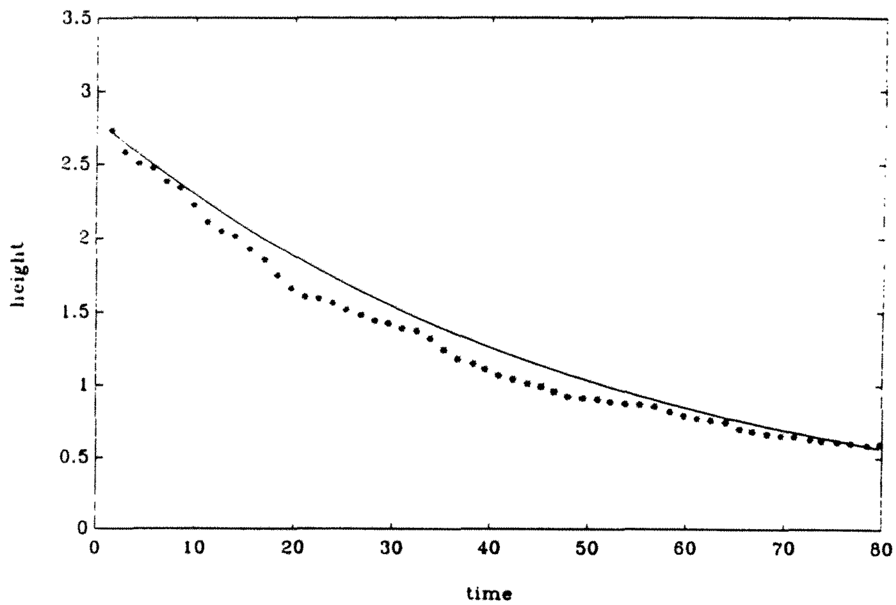

FIG. 3B. *Free surface peaks of decaying wave overlaid with the function $2.8e^{-.02t}$.*

which are dominated by the fundamental harmonic.

In order to understand this consider the integrated form of equations (1) over an interval of time small enough to ignore the viscous dissipation terms

$$\int_{x=0}^{L}\int_{y=-h}^{\eta} u\left(u_t + uu_x + vu_y\right) dy\, dx = \int_{x=0}^{L}\int_{y=-h}^{\eta} u\left(\frac{-P_x}{\rho}\right) dy\, dx \tag{5a}$$

and

$$\int_{x=0}^{L}\int_{y=-h}^{\eta} v\left(v_t + uv_x + vv_y\right) dy\, dx = \int_{x=0}^{L}\int_{y=-h}^{\eta} v\left(\frac{-P_y}{\rho} - g\right) dy\, dx\,. \tag{5b}$$

Combining these equations and simplifying yields

$$\int_{x=0}^{L}\int_{y=-h}^{\eta} \left(\frac{u^2+v^2}{2}\right) dy\, dx + \int_{x=0}^{L} g\frac{\eta^2}{2}\, dx = const. \tag{6}$$

Since energy is conserved, flows that include significant higher harmonic contributions increase in free surface height (at $x = 5$ cm) as they adapt to a simpler eigenfunction form for the decay problem while near resonant flows that are primarily of the lowest harmonic change little as they adapt to their eigenfunction form.

The linear inviscid unforced wave solution for equations (1) which is proportional to $\sin \omega t$ is

$$u = a\cos k(x - L/2)\cosh k(y+h)\sin \omega t \tag{7a}$$

with

$$v = a\sin k(x - L/2)\sinh k(y+h)\sin \omega t \tag{7b}$$

for $k = \pi/L, 3\pi/L, 5\pi/L, \cdots$ and $\omega^2 = gk\tanh kh$. For this tank geometry, this corresponds to $\omega = .705$ hz, 2.11 hz, 3.52 hz, $\cdots$. Yet, the frequency of the free waves measured in

Figs. 2b and 3b is $\approx .67$ hz after the waves have adjusted to their eigenfunction form. In order to understand the existence of a shift in frequency consider the viscous form of equations (1) for the linear problem. The linear approximation is reasonable for this case since the decaying wave is primarily of a single harmonic. (The decay and shift rates of the three-dimensional experimental situation is larger than that of this two-dimensional approximation. This simple model is used only to show the theoretical existence of a frequency shift.) Eliminating P and v from them gives

$$\Delta u_t = \nu \Delta(\Delta u). \tag{8}$$

Assuming $u = Ue^{i\Omega t}$ gives

$$c\Delta U = \Delta(\Delta U) \quad \text{for} \quad c = \frac{i\Omega}{\nu}. \tag{9}$$

Thus, U can be written as the superposition of terms U_ν and U_p which satisfy either $cU_\nu = \Delta U_\nu$ or $\Delta U_p = 0$. A similiar argument shows that v can also be written as the superposition of viscous and potential terms. Noting $|c^{1/2}|h \gg 1$ and $|c^{1/2}|L \gg 1$ and choosing

$$\begin{aligned} u = e^{i\Omega t}\Big\{ & \cos\lambda(x - L/2)\Big(a\cosh\lambda(y+h) + b\sinh\lambda(y+h) \\ & + \frac{(c+\lambda^2)^{1/2}}{\lambda} b\, e^{-(c+\lambda^2)^{1/2}(y+h)}\Big) \\ & + \frac{\lambda}{(c-\lambda^2)^{1/2}} \sin\lambda L/2 \Big(e^{-(c-\lambda^2)^{1/2}x} + e^{-(c-\lambda^2)^{1/2}(L-x)}\Big) \\ & \Big(a\cosh\lambda(y+h) + b\sinh\lambda(y+h)\Big)\Big\} \end{aligned} \tag{10}$$

and

$$\begin{aligned} v = e^{i\Omega t}\Big\{ & \sin\lambda(x - L/2)\Big(a\sinh\lambda(y+h) + b\cosh\lambda(y+h) \\ & - b\, e^{-(c+\lambda^2)^{1/2}(y+h)}\Big) \\ & + \sin\lambda L/2 \Big(e^{-(c-\lambda^2)^{1/2}x} - e^{-(c-\lambda^2)^{1/2}(L-x)}\Big) \\ & \Big(a\sinh\lambda(y+h) + b\cosh\lambda(y+h)\Big)\Big\} \end{aligned} \tag{11}$$

implies $v = 0$ is satisfied asymptotically on the solid boundaries $x = 0, L$ and $y = -h$ away from the seams and $u_x + v_y = 0$ everywhere. The remaining constants are chosen so that $u = 0$ asymptotically on the solid boundaries away from the seams and the linearized free surface boundary conditions are satisfied. This implies

$$b = \frac{-\lambda}{(c+\lambda^2)^{1/2}} a \tag{12}$$

$$\cos\lambda L/2 + \frac{\lambda}{(c-\lambda^2)^{1/2}} \sin\lambda L/2 = 0 \tag{13}$$

and

$$\Omega^2\Big(a\cosh\lambda h + b\sinh\lambda h\Big) = g\lambda\Big(a\sinh\lambda h + b\cosh\lambda h\Big). \tag{14}$$

Substituting b from equation (12) into equation (14) yields the homogeneous system of two complex equations (13,14) in the two complex unknowns λ and Ω. (a is now arbitrary since it scales out of these equations.) Thus, although the forced problem produces solutions with any driving frequency ω, the decay problem admits solutions with only discrete response frequencies Ω.

As ν tends to 0, c tends to infinity and equation (13) implies $\lambda = n\pi/L$ for $n = 1, 3, 5, \cdots$. Equation (14) then reduces to the familiar dispersion relation $\Omega^2 \cosh\lambda h = g\lambda\sinh\lambda h$. For $\nu \neq 0$ but $|\lambda/c^{1/2}| \ll 1$, λ is near the inviscid resonant wavenumbers and Ω is near the inviscid resonant frequencies. Then, equations (13) and (14) can be solved using a perturbation approach. Substituting

$$\lambda = \pi/L + \frac{2}{L}\epsilon e^{i\theta} \qquad \text{and} \qquad \Omega = \Omega_0 + \delta e^{i\sigma} \tag{15}$$

into equations (13) and (14) and retaining terms of order ϵ or δ yields

$$\Omega_0^2 \cosh\pi h/L = g\pi/L\sinh\pi h/L \tag{16a}$$

$$\epsilon = \pi/L\sqrt{\frac{\nu}{\Omega_0}} \tag{16b}$$

$$\sigma = \theta = -\pi/4 \quad \text{or} \quad 3\pi/4 \tag{16c}$$

and

$$\delta = \frac{g\pi/L\Big[(2h/L - 1) + \frac{1}{\pi}\sinh 2\pi h/L\Big]\epsilon}{2\Omega_0\cosh^2\pi h/L}. \tag{16d}$$

The root of θ must be chosen so that the wave decays; i.e., choose θ so that Im $\Omega < 0$. This implies the oscillation frequency will decrease by $\delta\cos\theta$ and the wave will decay at a rate of $\delta\sin\theta$. It also shows that instead of a pure sine wave, the decaying wave will be a combination of primarily a sine wave with a cosine component due to viscous effects as can be seen in Fig. 3b.

To estimate the rate of decay of the unforced wave after it has adjusted to its eigenfunction form, consider the three-dimensional form of equation (6) with viscous effects included. (This approach is similar to that used by Keulegan [3] following the boundary layer theory of Boussinesq.)

$$\frac{\partial}{\partial t}\left\{\int_{x=0}^{L}\int_{y=0}^{b}\int_{z=-h}^{\eta}\frac{u^2+v^2+w^2}{2}\,dz\,dy\,dx + \int_{x=0}^{L}\int_{y=0}^{b} g\frac{\eta^2}{2}\,dy\,dx\right\}$$

$$= -\nu\int_{x=0}^{L}\int_{y=0}^{b}\int_{z=-h}^{\eta}\Big(|\nabla u|^2 + |\nabla v|^2 + |\nabla w|^2\Big)\,dz\,dy\,dx. \tag{17}$$

Here u, v and w represent the velocity components in the x, y and z directions respectively with the z coordinate now measured vertically upwards and the x and y components measured horizontally along the box length and width respectively.

Approximate the terms on the left-hand side of equation (17) as the inviscid linear solution

$$u \sim a\, e^{-Rt} \sin \pi x/L \cosh \pi(z+h)/L \sin \omega t$$

$$v = 0 \tag{18}$$

$$w \sim a\, e^{-Rt} \cos \pi x/L \sinh \pi(z+h)/L \sin \omega t$$

with

$$\eta \sim \frac{a}{-\omega} e^{-Rt} \cos \pi x/L \sinh \pi h/L \cos \omega t \tag{19}$$

$R \ll \omega$ and $\omega^2 = g\pi/L \tanh \pi h/L$ and the terms on the right-hand side of equation (17) by the laminar boundary layer flow past a plate (along each solid wall but away from the seams) required to satisfy the unforced boundary conditions (4),

$$u_b \sim -a\, e^{-Rt} \sin \pi x/L\, e^{-\sqrt{\omega/2\nu}(z+h)} \sin(\omega t - \sqrt{\omega/2\nu}(z+h)) \tag{20a}$$

along the bottom,

$$w_e \sim -a\, e^{-Rt} \sinh \pi(z+h)/L\, e^{-\sqrt{\omega/2\nu}\, x} \sin(\omega t - \sqrt{\omega/2\nu}\, x) \tag{20b}$$

near $x = 0$ with a similar term for x near L,

$$u_s \sim -a\, e^{-Rt} \sin \pi x/L \cosh \pi(z+h)/L\, e^{-\sqrt{\omega/2\nu}\, y} \sin(\omega t - \sqrt{\omega/2\nu}\, y) \tag{20c}$$

near $y = 0$ with a similar term for y near b and

$$w_s \sim -a\, e^{-Rt} \cos \pi x/L \sinh \pi(z+h)/L\, e^{-\sqrt{\omega/2\nu}\, y} \sin(\omega t - \sqrt{\omega/2\nu}\, y) \tag{20d}$$

near $y = 0$ with a similar term for y near b. Then the decay rate of the first harmonic is estimated as $R \approx .016$ 1/sec. This estimate is slightly smaller than the average measured for flows with ω near .65 hz or .72 hz. The decay rate for Fig. 2b is $R \approx .018$ 1/sec and for Fig. 3b is $R \approx .02$ 1/sec. This leads to the conclusion that sources of damping other than from boundary layer flow past a plate may be significant.

4 Conclusions

Forced resonant free surface waves must adjust to an eigenfunction form when the forcing is discontinued. Flows with significant higher harmonic contributions at first rise after the motion is terminated while flows comprised of primarily the fundamental harmonic remain relatively constant in height. Viscous effects cause the decay oscillation frequency to shift relative to the inviscid eigenfunction frequency. Boundary layer theory can be used to estimate the rate of decay of the unforced free surface waves, however, the measured decay rates are slightly higher than that predicted. This suggests that other effects may be significant such as viscous damping due to the flow near the box seams.

References

[1] W. Chester and J. A. Bones, *Resonant oscillations of water waves. II. Experiment*, Proc. Roy. Soc. Lond. Ser. A. 306, (1968), pp. 23-39.

[2] R. Khosropour, S. L. Cole and T. D. Strayer, *Resonant free surface waves in a rectangular basin*, Wave Motion 22, (1995), pp. 187-199.

[3] G. H. Keulegan, *Energy dissipation in standing waves in rectangular basins*, Jour. Fluid Mech. 6, (1959), pp. 33-50.

Nonlinear Asymptotic Theory of Supersonic Corner Flow

Chao-Kang Feng*

Abstract

The exact solutions of Prandtl-Meyer flow and supersonic wedge flow are discussed. A systematic and rigorous approach for obtaining the nonlinear asymptotic theory of supersonic corner flow is exhibited. The correct first-order solutions to the boundary-value problems of centered expansion and compression waves are obtained.

Key words. centered expansion and compression waves, nonlinear theory

1 Introduction

Supersonic centered expansion and compression flows are fundamental problems to the study of gasdynamics. Due to the singularity at the corner, the supersonic linearized theory is invalid for calculating the flow field of corner flow. The aim of the present study is to re-examine the small perturbation theory of supersonic corner flow.

By using the method of strained coordinates [11], [14], a systematic and rigorous approach for obtaining the nonlinear asymptotic equation to the boundary-value problem of supersonic centered expansion and compression flow is exhibited. The supersonic nonlinear theory of corner flow gives the correct asymptotic solution. For centered expansion wave, the nonlinear result in the fan region equals the asymptotic solution from an expansion of the exact solution of the Prandtl-Meyer flow [12]. For centered compression wave, the unique solution in the compression region can be found from the jump condition, and the shock-wave position agrees well with the oblique shock wave theory [10].

2 Exact Solutions of Supersonic Corner Flow

2.1 Supersonic centered expansion wave

The supersonic centered expansion flow is the so-called Prandtl-Meyer flow [12]. For inviscid supersonic flow past a two-dimensional convex body $y = F(x;\delta) = -\tan\delta x$, the boundary-value problem of the full potential gasdynamic equations is [3]

$$(1) \qquad (a^2 - \Phi_x^2)\Phi_{xx} - 2\Phi_x\Phi_y\Phi_{xy} + (a^2 - \Phi_y^2)\Phi_{yy} = 0$$

$$\frac{a^2}{\gamma - 1} + \frac{\Phi_x^2 + \Phi_y^2}{2} = \frac{a_1^2}{\gamma - 1} + \frac{U_1^2}{2}$$

with the boundary conditions

$$(2) \qquad \Phi \longrightarrow U_1 x \quad , \quad \text{at} \quad \eta = \eta_1$$

$$(3) \qquad \frac{\Phi_y}{\Phi_x} = \frac{dF}{dx} = -\tan\delta \quad , \quad \text{at} \quad \eta = \eta_2$$

*Department of Aeronautical Engineering, College of Engineering, Tamkang University, Tamsui, Taipei, Taiwan, R. O. C.

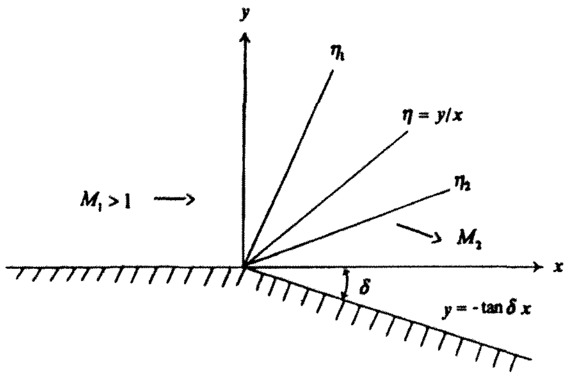

FIG. 1. *B.V.P. of supersonic centered expansion.*

where $\eta = y/x$ is the characteristic in the fan region, $\eta_1 = 1/\sqrt{M_1^2 - 1}$ is the first characteristic and η_2 the last to be determined as shown in FIG. 1. Here the free stream Mach number $M_1 = U_1/a_1 > 1$ and δ is the deflection angle.

The exact pressure coefficient in the flow field is given by [10]

$$C_p = \frac{2}{\gamma M_1^2}\left\{\left[1 + \frac{\gamma - 1}{2} M_1^2 \left(1 - \frac{\Phi_x^2 + \Phi_y^2}{U_1^2}\right)\right]^{\frac{\gamma}{\gamma - 1}} - 1\right\} \tag{4}$$

For Prandtl-Meyer flow, the velocity potential Φ in (1) has the similarity transformation

$$\Phi = U_1 x f(\eta; M_1, \gamma, \delta) \quad ; \quad \eta = \frac{y}{x} \tag{5}$$

with $f(\eta)$ satisfies the following nonlinear ordinary differential equation and boundary conditions

$$f''(\eta)\cdot\left[(1+\eta^2)f'^2 - 2\eta f f' + \frac{1}{1+\eta^2}\left(\frac{\gamma-1}{\gamma+1} + \eta^2\right) f^2 - \frac{2 + (\gamma - 1)M_1^2}{(\gamma + 1)M_1^2}\right] = 0 \tag{6}$$

$$f(\eta_1) = 1 \tag{7}$$

$$f'(\eta_2) = -\tan\delta\,[f(\eta_2) - \eta_2 f'(\eta_2)] \tag{8}$$

From (6), (7) and (8), we have two solutions.

Case (i) Linear Flow. In (6), $f''(\eta) = 0$, it gives the solution for linear flow

$$\Phi = U_1 x f(\eta) \tag{9}$$

with the exact solution

$$f(\eta) = \frac{1 - \eta\tan\delta}{1 - \eta_1 \tan\delta} \tag{10}$$

For $M_1 > 1$, $\delta \to 0$, the second-order solution of (9) is

$$\Phi = U_1\left\{x - \delta x(\eta - \eta_1) - \delta^2 x(\eta_1\eta - \eta_1^2) + \cdots\right\} \tag{11}$$

Substituting (11) into (4), we obtain the second-order pressure coefficient for convex corner

$$C_{p_b} = \frac{-2\delta}{\sqrt{M_1^2-1}} - \frac{2\delta^2}{(M_1^2-1)} + \cdots \tag{12}$$

Case (ii) Nonlinear Flow. In (6), if $f''(\eta) \neq 0$, we obtain the similarity solution for centered expansion wave

$$\Phi = U_1 x f(\eta) \tag{13}$$

and the exact solution of $f(\eta)$ is

$$f(\eta) = \sqrt{1+\frac{2}{(\gamma-1)M_1^2}}\sqrt{1+\eta^2}\sin\left(K - \sqrt{\frac{\gamma-1}{\gamma+1}}\tan^{-1}\eta\right) \tag{14}$$

with the constant

$$K = b\tan^{-1}\eta_1 + \tan^{-1}\frac{b}{\eta_1}\ , \quad b = \sqrt{\frac{\gamma-1}{\gamma+1}} \tag{15}$$

and two important relations for downstream

$$\tan(\delta + \tan^{-1}\eta_2) = b\cot(K - b\tan^{-1}\eta_2) \tag{16}$$

$$\begin{aligned}\delta = & \sqrt{\frac{\gamma+1}{\gamma-1}}\left(\tan^{-1} b\sqrt{M_2^2-1} - \tan^{-1} b\sqrt{M_1^2-1}\right) - \\ & \left(\tan^{-1}\sqrt{M_2^2-1} - \tan^{-1}\sqrt{M_1^2-1}\right)\end{aligned} \tag{17}$$

From (16) and (17), we found that

$$\eta_2 = \eta_2(M_1, \gamma, \delta) \tag{18}$$

$$M_2 = M_2(M_1, \gamma, \delta) \tag{19}$$

Substituting (13) into (4), the exact pressure coefficient in the fan region is

$$C_p(\eta) = \frac{2}{\gamma M_1^2}\left\{\left[1 + \frac{(\gamma-1)(M_1^2-1) - (2+(\gamma-1)M_1^2)\sin^2\chi(\eta)}{\gamma+1}\right]^{\frac{\gamma}{\gamma-1}} - 1\right\} \tag{20}$$

with

$$\chi(\eta) = K - b\tan^{-1}\eta \tag{21}$$

By letting $\eta = \eta_2$ in (20) and expanding it with $\delta \to 0$, we obtain the second-order pressure coefficient for a convex corner

$$C_{p_b}(\eta_2) = \frac{-2\delta}{\sqrt{M_1^2-1}} + \frac{[(\gamma+1)M_1^4 - 4(M_1^2-1)]\delta^2}{2(M_1^2-1)^2} + \cdots \tag{22}$$

the solution (22) is the well-known result of Busemann [2] for centered expansion wave.

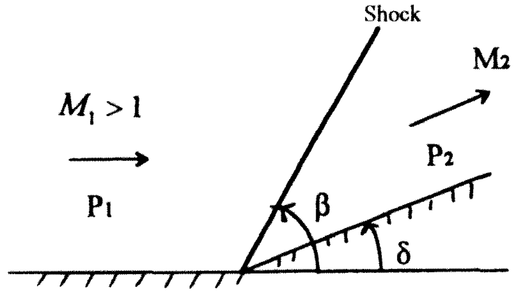

FIG. 2. *Supersonic wedge flow.*

2.2 Supersonic centered compression wave

From oblique shock wave theory [10], we have the following relations for supersonic flow past a wedge as shown in FIG. 2.

$$\frac{\tan(\beta-\delta)}{\tan\beta} = \frac{2}{\gamma+1}\frac{1}{M_1^2\sin^2\beta} + \frac{\gamma-1}{\gamma+1} \tag{23}$$

$$\frac{p_2}{p_1} = \frac{2\gamma}{\gamma+1}M_1^2\sin^2\beta - \frac{\gamma-1}{\gamma+1} \tag{24}$$

$$C_{p_b} = \frac{2}{\gamma M_1^2}\left(\frac{p_2}{p_1}-1\right) = \frac{4}{(\gamma+1)M_1^2}\left(M_1^2\sin^2\beta - 1\right) \tag{25}$$

As the free stream Mach number $M_1 > 1$ and the deflection angle $\delta \to 0$, (23) gives the second-order solution for the shock angle

$$\tan\beta = \frac{1}{\sqrt{M_1^2-1}} + \frac{\gamma+1}{4}\frac{M_1^4}{(M_1^2-1)^2}\delta + \frac{(\gamma+1)^2M_1^6(M_1^2+4)}{32(M_1^2-1)^{7/2}}\delta^2 + \cdots \tag{26}$$

and (25) gives the second-order pressure coefficient [1]

$$C_{p_b} = \frac{2\delta}{\sqrt{M_1^2-1}} + \frac{\left[(\gamma+1)M_1^4 - 4(M_1^2-1)\right]\delta^2}{2(M_1^2-1)^2} + \cdots \tag{27}$$

the solution (27) is also the result of Busemann for a wedge.

3 Supersonic Linearized Theory

For supersonic flow past a corner $y = F(x;\delta) = \pm\tan\delta x$, the positive sign is for centered compression and the negative for centered expansion. As the free stream Mach number $M_1 > 1$ and the deflection angle $\delta \to 0$ ($y = \delta F(x) = \pm\delta x$), the asymptotic expansion of Φ in (1) for linearized theory is [9]

$$\Phi(x,y;M_1,\gamma,\delta) = U_1\{x + \delta\phi^*(x,y;M_1) + O(\delta^2)\} \tag{28}$$

with the first-order perturbation potential ϕ^* satisfying the following linear equation for supersonic corner flow

$$(M_1^2-1)\phi^*_{xx} - \phi^*_{yy} = 0 \tag{29}$$

$$\phi^* \to 0 \quad , \quad \text{at upstream} \tag{30}$$

$$\phi^*_y(x,0) = \pm 1 \quad , \quad \text{at downstream} \tag{31}$$

and the first-order pressure coefficient is

$$C_p(x,y) = -2\phi_x^*(x,y)\delta \tag{32}$$

The solution of (29) gives

$$\phi^*(x,y) = \pm x(\eta - \eta_1), \quad \eta = y/x \tag{33}$$

where the first characteristic $\eta_1 = \frac{1}{\sqrt{M_1^2-1}}$.

From (33) and (32), the velocity components and the pressure coefficient are

$$u(x,y) = \phi_x^*(x,y) = \mp\eta_1 \tag{34}$$

$$v(x,y) = \phi_y^*(x,y) = \pm 1 \tag{35}$$

$$C_p(x,y) = \pm 2\eta_1\delta = \pm\frac{2\delta}{\sqrt{M_1^2-1}} \tag{36}$$

The linearized results (34) and (35) give only constant values in the flow field and we cannot find the right position of the last characteristic η_2 for corner flow. Except for the correct first-order pressure coefficient (36) on the corner surface, the supersonic linearized theory is not good for calculating the flow field of corner flow. However, Van Dyke obtained the Busemann's result of the pressure coefficient (27) for a wedge from second-order supersonic linearized theory [13].

4 Supersonic Nonlinear Asymptotic Theory

For supersonic flow past a corner with deflection angle $\delta \to 0$ ($y = \pm\delta x$) and the gage function $\alpha(\delta)$, $\beta(\delta) \to 0$ as $\delta \to 0$, the centered characteristic $\eta = y/x$ at the corner is transformed into s coordinate ($0 < s < 1$) to avoid the singularity at corner as [8]

$$\eta(s) = \eta_1 + [a_1(M_1,\gamma)\alpha(\delta) + \cdots]s \quad , \quad 0 < s < 1 \tag{37}$$

with $\eta(0) = \eta_1 = 1/\sqrt{M_1^2-1}$ and $\eta(1) = \eta_2 = \eta_1 + a_1(M_1,\gamma)\alpha(\delta)$ where $a_1(M_1,\gamma)$ is a constant to be determined.

The asymptotic expansion of Φ in (1) has the form

$$\Phi(x,y;M_1,\gamma,\delta) = U_1\{x + \beta(\delta)\phi(x,s;M_1,\gamma) + \cdots\} \tag{38}$$

Substituting (37) and (38) into (1) and b.c.'s (2) and (3), we find that $\alpha(\delta) = \delta$ and $\beta(\delta) = \delta^2$ for the distinguished limit and the asymptotic expansion in (38) is

$$\Phi(x,y;M_1,\gamma,\delta) = U_1\left\{x + \delta^2\phi(x,s;M_1,\gamma) + O(\delta^3)\right\} \tag{39}$$

$$s = \frac{\eta - \eta_1}{a_1\delta} \tag{40}$$

Then the first-order perturbation potential ϕ in (39) satisfies the following nonlinear equation for supersonic corner flow

$$\left[a_1^2 xs - \frac{\gamma+1}{2}\frac{M_1^4}{(M_1^2-1)^2}\phi_s\right]\phi_{ss} + a_1^2 x(\phi_s - x\phi_{xs}) = 0 \tag{41}$$

$$\phi(x,0) = 0 \quad , \quad \text{at} \quad \eta(0) = \eta_1 = \frac{1}{\sqrt{M_1^2-1}} \tag{42}$$

$$\phi_s(x,1) = \pm a_1 x \quad , \quad \text{at} \quad \eta(1) = \eta_2 \tag{43}$$

where the last characteristic η_2 is

$$\eta_2 = \eta_1 + a_1(M_1,\gamma)\delta + \cdots \tag{44}$$

with

$$a_1 = \pm\frac{\gamma+1}{2}\frac{M_1^4}{(M_1^2-1)^2}\left[\begin{array}{ll} (+)\text{ for comp.,} & a_1 = a_c > 0,\ \eta_2 = \eta_2^c \\ (-)\text{ for exp.,} & a_1 = a_e < 0,\ \eta_2 = \eta_2^e \end{array}\right] \tag{45}$$

and from (4), the first-order pressure coefficient is found to be

$$C_p(s) = \frac{2\phi_s(x,s)\eta_1\delta}{a_1 x} \tag{46}$$

The exact solution of (41) has the form

$$\phi(x,s) = x f_1(s) \tag{47}$$

with $f_1(s)$ satisfying the following equation

$$f_1''(s)\cdot\left[\frac{\gamma+1}{2}\frac{M_1^4}{(M_1^2-1)^2}f_1'(s) - a_1^2 s\right] = 0 \tag{48}$$

$$f_1(0) = 0 \tag{49}$$

$$f_1'(1) = \pm a_1 \tag{50}$$

4.1 Centered expansion wave

From (48), there are two solutions. In (48), $f_1''(s) = 0$ gives the linearized result (33) for convex corner flow

$$\phi^*(x,y) = \delta\phi(x,s) = -a_e xs\delta = -x(\eta-\eta_1) \tag{51}$$

and the other one in (48) gives the correct first-order solution for centered expansion wave as

$$\phi^*(x,y) = \delta\phi(x,s) = \frac{-1}{2}a_e xs^2\delta = \frac{-1}{2}\frac{x}{a_e}\frac{(\eta-\eta_1)^2}{\delta}, \quad a_e < 0 \tag{52}$$

$$\eta_2^e = \eta_1 + a_e\delta + \cdots = \eta_1 - \frac{\gamma+1}{2}\frac{M_1^4}{(M_1^2-1)^2}\delta + \cdots < \eta_1 \tag{53}$$

The centered expansion fan region is shown in FIG 3. The nonlinear results of (52) and (53) agree well asymptotically with the exact solution of the Prandtl-Meyer flow as shown in FIG. 4. and FIG. 5.

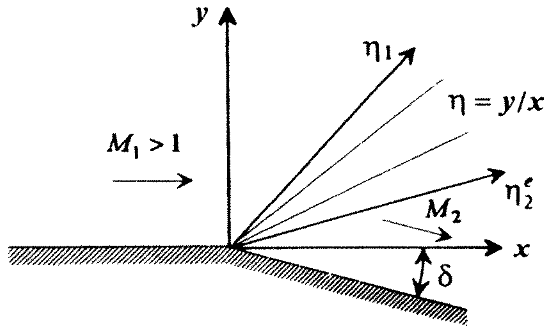

FIG. 3. *Centered expansion wave.*

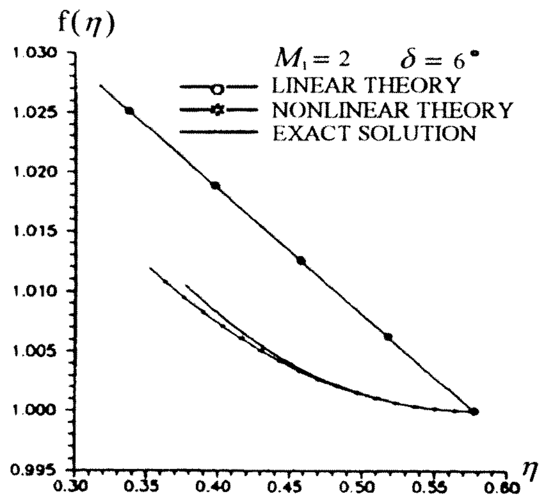

FIG. 4. *Similarity solution of Prandtl-Meyer flow.*

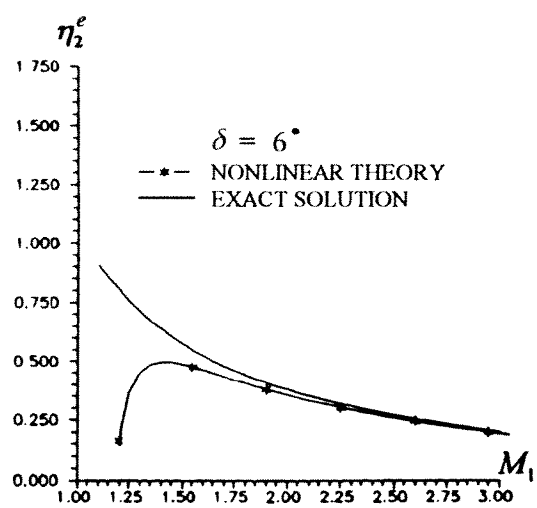

FIG. 5. η_2^e *v.s.* M_1 *curve.*

From (52) and (46), the velocity components and the pressure coefficient in the expansion fan region ($\eta_2^e < \eta < \eta_1$) are

$$u(\eta) = \phi_x^*(\eta) = (\eta^2 - \eta_1^2)/2a_e\delta \tag{54}$$

$$v(\eta) = \phi_y^*(\eta) = -(\eta - \eta_1)/a_e\delta \tag{55}$$

$$C_p(\eta) = -2\eta_1(\eta - \eta_1)/a_e \tag{56}$$

On the convex surface $\eta = \eta_2^e$, we obtain the velocity components

$$u(\eta_2^e) = \eta_1 + \frac{1}{2}a_e\delta \tag{57}$$

$$v(\eta_2^e) = -1 \tag{58}$$

From (56), the first-order pressure coefficient on the convex surface is

$$C_{p_b}(\eta_2^e) = -2\eta_1\delta = \frac{-2\delta}{\sqrt{M_1^2 - 1}} \tag{59}$$

4.2 Centered compression wave

Similar to the expansion wave, there are two solutions for (48). In (48), $f_1''(s) = 0$ gives the linearized result for concave corner flow

$$\phi^*(x, y) = \delta\phi(x, s) = a_c x s\delta = x(\eta - \eta_1) \tag{60}$$

and the other one in (48) gives

$$\phi^*(x, y) = \delta\phi(x, s) = \frac{1}{2}a_c x s^2\delta = \frac{1}{2}\frac{x}{a_c}\frac{(\eta - \eta_1)^2}{\delta}, \quad a_c > 0 \tag{61}$$

$$\eta_2^c = \eta_1 + a_c\delta + \cdots = \eta_1 + \frac{\gamma + 1}{2}\frac{M_1^4}{(M_1^2 - 1)^2}\delta + \cdots > \eta_1 \tag{62}$$

Comparing (61) with (52), the form of the solution of centered compression flow seems the same as the centered expansion flow. However, it is not the case because the last characteristic η_2^c in (62) for compression wave is different from that η_2^e in (53) for expansion wave.

From (61) and (46), the velocity components and the pressure coefficient are

$$u(\eta) = \phi_x^*(\eta) = -(\eta^2 - \eta_1^2)/2a_c\delta \tag{63}$$

$$v(\eta) = \phi_y^*(\eta) = (\eta - \eta_1)/a_c\delta \tag{64}$$

$$C_p(\eta) = 2\eta_1(\eta - \eta_1)/a_c \tag{65}$$

The solutions of (63) and (64) satisfy the irrotational equation

$$\frac{\partial v}{\partial x} - \frac{\partial u}{\partial y} = 0 \tag{66}$$

From (62), it shows that the multivalued region begins at the origin and is bounded by the characteristics $\eta_1 < \eta < \eta_2^c$. This corresponds to a centered compression wave with over-lapping characteristics and the solution is not unique.

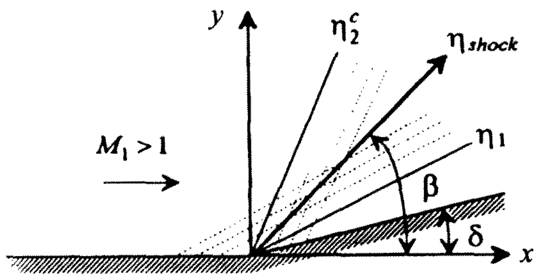

FIG. 6. *Centered compression wave.*

From the conservation form of the irrotationality (66), we have the jump condition

$$\frac{dy}{dx})_{shock} = -\frac{[u]}{[v]} \tag{67}$$

where the jump $= [\ ] = (\ )_{\eta_2^c} - (\ )_{\eta_1}$, that is the value of a quantity behind the shock less the value ahead [3].

Substituting (63) and (64) into (67), we find the correct first-order shock position for centered compression wave

$$\tan\beta = \eta_1 + \frac{1}{2}a_c\delta + \cdots = \frac{1}{\sqrt{M_1^2 - 1}} + \frac{\gamma+1}{4}\frac{M_1^4}{(M_1^2-1)^2}\delta + \cdots \tag{68}$$

where β is the shock angle as shown in FIG. 6.

The shock position ($\eta_1 < \eta_{shock} < \eta_2^c$) in (68) for the weak shock agrees well with the result (26) of the oblique shock wave theory.

Finally, the correct first-order unique solution for the centered compression wave is found to be

$$\text{Before shock} \quad : \quad u(\eta_1) = v(\eta_1) = 0 \tag{69}$$

$$\text{Shock position} \quad : \quad \eta_{shock} = \eta_1 + \frac{a_c\delta}{2} \tag{70}$$

$$\text{After shock} \quad : \quad u(\eta_2^c) = -(\eta_1 + \frac{a_c\delta}{2}) \tag{71}$$

$$v(\eta_2^c) = 1 \tag{72}$$

and from (65), the pressure coefficient on the concave surface is

$$C_{p_b}(\eta_2^c) = 2\eta_1\delta = \frac{2\delta}{\sqrt{M_1^2 - 1}} \tag{73}$$

It can be shown that the second-order nonlinear asymptotic theory will give the surface pressure coefficient of supersonic corner flow to the well-known result of Busemann.

5 Remarks

The supersonic nonlinear asymptotic theory gives the correct asymptotic solutions for corner flow. The first- and second-order solutions of the transonic and hypersonic flow past a convex corner can be obtained from a systematic expansion of the exact solution of the Prandtl-Meyer flow [4] and [5]. The similarity solution of the boundary-value problem of transonic and hypersonic corner flow with their applications are also discussed in [6] and [7].

It is worth mentioning that the asymptotic solutions of hypersonic corner flow [7] can be generated from the nonlinear results of supersonic corner flow by considering an expansion of the hypersonic similarity parameter together with the stretched coordinate.

Acknowledgement

The author would like to express sincere gratitude to Professor Julian D. Cole for his outstanding guidance and deep influence. Special thanks also go to Professor M. Van Dyke and Professor Z. Rusak for their invaluable comments in the Conference in Honor of Julian D. Cole.

References

[1] Ames Research Staff, *Equations, tables and charts for compressible flow*, NACN Rep. No. 1135, 1953.
[2] A. Busemann, *Aerodynamischer Auftrieb bei Überschallgeschwindigkeit*, Atti dei Convegni 5, R. Accad . d' Italia (1936), pp. 328–360.
[3] J. D. Cole and L. Pamela Cook, *Transonic aerodynamics*, Elsevier Publishers B. V., Amsterdam, The Netherland, 1986.
[4] C. K. Feng, *Second-order transonic solution obtained from the exact solution of the Prandtl-Meyer flow*, Proc. 30th Israel Annual Conference on Aviation & Astronautics (1989), pp. 62–67.
[5] ——, *Second-order hypersonic solution of the Prandtl-Meyer flow*, Proc. 14th National Conference on Theoretical and Applied Mechanics, Taiwan, R.O.C. (1990), pp. 1047–1056.
[6] ——, *The similarity solution of the B.V.P. of transonic corner flow with applications*, Proc. 33rd Aero. & Astro. Conf., AASRC (1991), pp. 51–62.
[7] ——, *The similarity solution of the B.V.P. of hypersonic corner flow with applications*, Proc. 34th Aero. & Astro. Conf., AASRC (1992), pp. 479–488.
[8] ——, *Nonlinear asymptotic theory of supersonic centered expansion and compression waves*, Proc. 2nd International Conference on Fluid Mechanics, Peking University Press, Beijng (1993), pp. 311–316.
[9] J. Kevorkian and J. D. Cole, *Perturbation methods in applied mathematics*, Springer-Verlag, New York, 1981.
[10] H. W. Liepmann and A. Roshko, *Elements of gasdynamics*, John Wiley and Sons, Inc., New York, 1957.
[11] M. J. Lighthill, *A technique for rendering approximate solutions to physical problems uniformly valid*, Philos. Mag., 40 (1949), pp. 1179–1201.
[12] T. Meyer, *Üeber Zweidimensionale Bewegungsvargänge in einem Gas, das mit Üeberschallgeschwindigkeit Strömt*, Ph.D. dissertation, Göttingen, 1908.
[13] M. Van Dyke, *A study of second-order supersonic flow theory*, NACA Rep. No. 1081, 1952.
[14] ——, *Perturbation methods in fluid mechanics*, The Parabolic Press, Stanford, Calif., 1975.

Electrostatics of thin bridges

Johan Helsing*

Abstract

Fast hierarchical methods for potential field evaluations have in recent years found interesting applications in physics and engineering. For example, these methods have been used together with integral equation methods for solving the electrostatic equation for materials with inclusions. A lingering obstacle on the way to constructing a general purpose algorithm for inclusion problems is the treatment of inclusion interfaces that lie very close to each other. The difficulty is to assess the need for resolution and to evaluate layer potentials close to their sources in a fast and accurate fashion. This paper presents an automated algorithm for such an assessment and evaluation. The robustness and speed of the algorithm is demonstrated through a series of examples involving thin bridges, coatings, narrow necks, corners, cusps, and random mixtures.

1 Introduction

The inclusion problem is an old and intriguing problem in linear elasticity and electrostatics. It has been addressed by hundreds of authors over time. See [1, 2, 3, 4] for lists of references. An inclusion is a piece of some homogeneous material that is embedded in a, likewise homogeneous, filler material. A filler with inclusions may be subjected to an external load or voltage. The inclusion problem concerns the estimation of fields, potentials, or effective properties of such a system.

A numerical approach to the inclusion problem is challenging in the sense that computations often take long time and do not always lead to accurate results. The most progress seems to have been made in two dimensions. Here finite element methods compete with finite difference methods, spectral methods, integral equation methods, and asymptotic methods. In my opinion integral equation methods are generally the winners. They require relatively few discretizations points since they are concerned with the interfaces only. Their chief disadvantage, which they share with finite element and finite difference methods, is that they encounter difficulties when inclusions are located close to each other. This can happen in random mixtures and in devices containing thin layers of separation. The problem here is resolution. Many degrees of freedom are needed to accurately represent the solution, if this at all is possible. In such situations, and if the geometry is simple, asymptotic methods [5, 6] may provide a viable alternative.

This paper presents a general purpose algorithm for solving two-dimensional electrostatic inclusion problems in the presence of strong inhomogeneity, thin bridges, and narrow necks. As we shall see, the algorithm also works well for corners and cusps. In seven numerical examples we will demonstrate its versatility, speed, and accuracy. Some examples, involving disks and squares, have been addressed before with special purpose algorithms. Other examples, involving complicated shapes and large "random" systems, are new.

*Department of Mathematical Sciences, Rensselaer Polytechnic Institute, Troy, New York 12180-3590

Our algorithm is automated. The only required geometric input is a parameterization of the inclusion interfaces and their unit normal vectors. The algorithm is based on an integral equation: Eq. (2) of the next section. This equation was discussed by Jaswon and Symm [7]. Hetherington and Thorpe [8] used it together with Gaussian quadrature and asymptotic analysis for a polygonal inclusion in free-space. Greengard and Moura [4] used it together with the trapezoidal quadrature rule and the Fast Multipole Method [9, 10, 11] for large collections of reasonably separated inclusions of general shapes. We use this integral equation together with Gaussian quadrature. The approach is adaptive and somewhat similar to the method of Lee and Greengard [12] for two-point boundary value problems.

This paper is a condensed version of a longer paper that has been submitted to the Journal of Computational Physics under the title *Thin bridges in isotropic electrostatics.*

2 Integral Equation and Effective Properties

The inclusions and the filler together constitute a composite material. The material's geometry is given in a unit cell which is periodically repeated as to cover the entire plane. We take the unit cell to be a square with sides of unit length and centered at the origin of a cartesian coordinate system. The conductivity of the filler is σ_1 and the conductivity of the inclusions is σ_2. The interface between the inclusions and the filler is called B.

An average electric field $\mathbf{e}$ of unit strength is applied to the composite. The potential $\mathbf{u}$ at position $\mathbf{r}$ in the composite can then be represented on the form

$$\mathbf{u}(\mathbf{r}) = \mathbf{e}\cdot\mathbf{r} - \frac{1}{2\pi}\int_B \log|\mathbf{r}-\mathbf{r}'|\rho(s')\mathrm{d}s', \tag{1}$$

where ρ is an unknown charge density and s' is arclength measured from some arbitrary origin. The charge density can be solved for from the integral equation

$$-2\mathbf{n_r}\cdot\mathbf{e} = \frac{(\sigma_2+\sigma_1)}{(\sigma_2-\sigma_1)}\rho(s) + \frac{1}{\pi}\int_B K(\mathbf{r}-\mathbf{r}',\mathbf{n_r})\rho(s')\mathrm{d}s', \tag{2}$$

where the kernel K is

$$K(\mathbf{r}-\mathbf{r}',\mathbf{n_r}) = \frac{\mathbf{n_r}\cdot(\mathbf{r}-\mathbf{r}')}{|\mathbf{r}-\mathbf{r}'|^2}, \tag{3}$$

and where $\mathbf{n_r}$ is the outward unit normal at $\mathbf{r}$ on B. Once the integral equation is solved the effective conductivity σ_{eff} in the direction $\mathbf{e}$ can be computed from

$$\sigma_{\text{eff}} = \sigma_1 - \sigma_1\int_B \mathbf{e}\cdot\mathbf{r}'\rho(s')\mathrm{d}s'. \tag{4}$$

3 An Adaptive Algorithm

In this section we first introduce polynomial approximation and Gaussian quadrature. We then develop a special quadrature for discretizing integral equations where the kernel is ill-behaved. Lastly we present an adaptive algorithm for the numerical solution of equation (2) suited for composites where the inclusion interfaces are very close to each other.

Let the points T_i, $i = 1,2,...,16$, be the nodes of the 16th Legendre polynomial $P_{16}(x)$ and call these points the Legendre points. Let $f(x)$ be a function on the interval $x \in [-1,1]$. Let $f_{15}(x)$ be the 15th degree interpolating polynomial that coincides with $f(x)$ at the Legendre points. In terms of Legendre polynomials P_n and coefficients b_n one can write

$$f_{15}(x) = \sum_{n=1}^{16} b_n P_{n-1}(x) \qquad \text{and} \qquad f_{15}(T_i) = f(T_i), \qquad i = 1,2,...,16. \tag{5}$$

Let the matrix B be the mapping from the coefficients b_n to the values $f(T_i)$ so that

$$f(T_i) = \sum_{n=1}^{16} B_{in} b_n, \qquad i = 1, 2, ..., 16. \tag{6}$$

We now turn to the discretization of Eq. (2). The interface B, between the inclusions and the filler, is divided into segments I^j. The segment I^j starts at arclength s^j and end at arclength s^{j+1}. We use Gaussian quadrature on each segment for the integral. We then solve the discretized equation for the unknown charge density $\rho(s)$. The quadrature points, called s_i^j, will appear on the segments I^j, which may be of different lengths.

After discretizing and solving Eq. (2) for $\rho(s)$ we want to estimate the error in the solution on the various segments I^j. The purpose of the error estimation is to decide where to refine. An accurate estimate is not needed. It is enough to know on which segments the error is largest. Once we know this, we subdivide these segments into subsegments and then solve Eq. (2) again. For this we define the monitor function

$$E^j = (s^{j+1} - s^j)(|b_{16}| + |b_{15}|), \tag{7}$$

where

$$b_n = \sum_{i=1}^{16} B_{ni}^{-1} \rho(s_i^j), \tag{8}$$

The monitor function E^j estimates the error in $\rho(s)$ on I^j.

When two interface segments are located very close to each other it may be that the integrand of Eq. (2) is ill-behaved. Furthermore, this ill behaviour may not stem from a rapidly varying $\rho(s)$, but from the kernel K. Thus, for solving Eq. (2) it is not sufficient to resolve the unknown $\rho(s)$. Rather, the kernel K, which we know in analytic form, must be resolved. We may be forced to use many more discretization points than is needed for the resolution of $\rho(s)$ alone. We now present a special quadrature to deal with this problem.

Upon discretization Eq. (2) assumes the form

$$c_k^m = \frac{(\sigma_2 + \sigma_1)}{(\sigma_2 - \sigma_1)} \rho(s_k^m) + \sum_{i,j} W_{ki}^{mj} \rho(s_i^j). \tag{9}$$

The matrix elements W_{ki}^{mj} give an approximation to the normal current density at point s_k^m due to a certain class of line charges on I^j and all its periodic images. One such line charge is L_i^j, the 15th degree Lagrange interpolating polynomial that assumes the value unity at the point s_i^j and the value zero at all other points on I^j.

How big is the error introduced by discretization of the kernel K? Consider the monitor function E^{jkm} given by

$$E^{jkm} = (s^{j+1} - s^j)(|b_{16}| + |b_{15}|), \tag{10}$$

where b_n now is

$$b_n = \sum_{i=1}^{16} B_{ni}^{-1} K(\mathbf{r}(s_m^k) - \mathbf{r}'(s_i^j), \mathbf{n_r}), \tag{11}$$

where points s_i^j are located on I^j or on some of its periodic images. The monitor function E^{jkm} indicates how accurately the normal current density at s_m^k due to a uniform charge distribution on I^j is estimated with 16-point Gaussian quadrature. If E^{jkm} is large we expect W_{ki}^{mj}, $i = 1, 2, ..., 16$, to be inaccurate.

When it is determined that some E^{jkm} is unacceptably large we resort to a special quadrature on the corresponding segment I^j according to the following: I^j is temporarily divided into two subsegments, I^{j1} and I^{j2} of equal length. On each of these segments 16 new Legendre points are placed. The functions $E^{(j1)km}$ and $E^{(j2)km}$ are computed according to Eq. (10). Should any of these functions still be unacceptably large, further subdivision and distribution of Legendre points takes place. This process is repeated until I^j is divided into N subsegments which each has an associated function $E^{(jn)km}$, $n = 1, 2, ..., N$, with an acceptable value. The contribution to W_{ki}^{mj} from I^j is then computed by composite Gaussian quadrature in

$$\frac{1}{\pi}\int_{I^j} K(\mathbf{r}(s_k^m) - \mathbf{r}'(s'), \mathbf{n_r}) L_i^j(s') \mathrm{d}s', \tag{12}$$

Note that the the values of K in Eq. (12) has already been computed in the process of evaluating the $E^{(jn)km}$. Once Eq. (12) has been evaluated, the location of the temporary Legendre points can be forgotten. An adaptive algorithm for solving Eq. (2) is the following:

An adaptive algorithm for Eq. (2)

1. Divide the interfaces of in the unit cell into segments I^j of equal length.
2. Distribute Legendre points on the interface segments and for each discretization point s_k^m, check if any segment I^j (or periodic image) gives rise to large errors E^{jkm}.
3. Compute the contribution to W_{ki}^{mj} for each point s_k^m and segment i^j with large E^{jkm} with special quadrature as in Eq. (12).
4. Compute all other contributions to W_{ki}^{mj} with standard evaluation.
5. Solve the discretized Eq. (2) for $\rho(s)$ using some iterative technique.
6. Compute E^j for the various interface segments by Eq. (7).
7. Subdivide segments where E^j is large into two, three, or four subsegments.
8. Merge adjacent segments where E^j is too small (should they occur).
9. Go to step 2.

4 Numerical Examples

This section presents a series of numerical examples chosen as to demonstrate the robustness, flexibility, and relative speed of our numerical algorithm. We will, for example, look at corner and cusp geometries. This is not because we think that corners and cusps are particularly important or because our code is geared towards solving such problems. No, the purpose is to demonstrate that our code is so versatile so that it can treat successfully *also* these unphysical geometries, for which other authors make special analysis.

The most efficient way to solve systems of linear equations resulting from the discretization of integral equations of the type of Eq. (2) is to use an iterative solver accelerated with some version, preferably adaptive [11], of the Fast Multipole Method [9, 10, 11]. At least this holds true for large enough systems [4]. For smaller systems it may be more efficient to do something else. Below we will mostly use straight-forward BCG [15, 16] iterations. In the last few examples, involving random disks, we will use GMRES [14] iterations together with a non-adaptive version [10] of the fast multipole method. The reason that we use BCG iterations rather than CGS [13] iterations, which are usually twice as fast [17], is that for this type of ill-conditioned problems BCG is actually more efficient.

TABLE 1

The effective conductivity σ_{eff} of a square array of disks in a filler. The filler and the disks have conductivities $\sigma_1 = 1$ and $\sigma_2 = 1000$, respectively. The disk separation parameter is $c = 1000$. 'stage' is the stage of refinement, $E^j_{\max}$ is the largest value of the monitor function of Eq. (8), 'pseg' is the number of permanent segments on the interface, 'iter' is the number of iterations needed for convergence with the BCG method, 'CPU' is the total elapsed computing time in minutes, 'mod ent' is the number of modified entries in the W^{mj}_{ki} matrix of Eq. (10), and 'S' is the computing time in seconds spent doing special quadrature at a given stage.

stage	σ_{eff}	$E^j_{\max}$	pseg	iter	CPU	mod ent	S
3	242.9	15	32	77	1 m	12,000	4 s
4	243.007	0.02	40	133	2.5 m	16,000	6 s
5	243.0059781	0.0000008	48	120	5 m	20,000	8 s
6	243.0059782	0.00000005	56	40	7 m	23,000	9 s

4.1 Square array of disks

A classic geometry containing thin bridges is the square array of disks, first addressed by Rayleigh [18]. Accurate numerical results for some systems have been produced by Perrins, McKenzie, and McPhedran [19] and for more ill-conditioned systems by myself [20], using spectral methods. McPhedran, Poladian, and Milton [5] introduced the disk separation parameter c and derived an asymptotic formula for the effective conductivity σ_{eff} .

I choose $\sigma_1 = 1$, $\sigma_2 = 1000$ and $c = 1000$. The separation to diameter ratio of the disks is then $5 \cdot 10^{-7}$ and the asymptotic formula of McPhedran, Poladian, and Milton [5] gives $\sigma_{\text{eff}} = 246$. My earlier numerical calculation gave $\sigma_{\text{eff}} = 243.005978$. Table 1 shows that the present algorithm gives the same result, thereby perhaps eliminating the need for special purpose algorithms which only work for disks.

4.2 Coated cylinders

Two-dimensional systems referred to as arrays of coated fibers are of particular interest to material scientists. One reason for this is that thin coatings can model imperfect bonding in fiber reinforced composites. Of the many papers I have found in this area only one, the paper of Nicorovici, McPhedran, and Milton [21], deals with actual computations. The authors use a spectral algorithm that only applies to circular objects.

Here I start with a square array of cylinders with radii $R = 0.49$ and $\sigma_2 = 1000$ embedded in a filler with conductivity $\sigma_1 = 1$. The effective conductivity of this material is $\sigma_{\text{eff}} = 13.49238657127$. Then I coat the cylinders with a layer of thickness 0.000001 and conductivity $\sigma_3 = 0.001$. What is the effective conductivity now? The algorithm of Nicorovici, McPhedran, and Milton [21] gives $\sigma_{\text{eff}} = 12.7907800$. Table 2 gives my results. It is noteworthy that our algorithm, which uses pointwise discretization, can resolve a layer of thickness 0.000001 in just 20 seconds. This shows the strength of our special quadrature.

4.3 Amoebas

In the unit cell there is now an amoeba parameterized by

$$(x, y) = R(1 + \epsilon \cos n\phi)(\cos\phi, \sin\phi). \tag{13}$$

I seek a difficult geometry and choose $R = 0.25$, $\epsilon = 0.999$, and $n = 4$. Figure 1 shows the geometry. The thin bridge between arms of two adjacent amoebas has thickness $5 \cdot 10^{-4}$

TABLE 2

The effective conductivity σ_{eff} of a square array of coated cylinders. The cylinders have core and coating radii of $R = 0.49$ and $R = 0.490001$, respectively. The filler, coating, and core have conductivities $\sigma_1 = 1$, $\sigma_2 = 0.001$, and $\sigma_3 = 1000$.

stage	σ_{eff}	E^J_{max}	pseg	iter	CPU	mod ent	S
1	12.7907801	4	16	30	20 s	19,000	10 s
5	12.7907800	0.00003	80	30	10 m	53,000	45 s

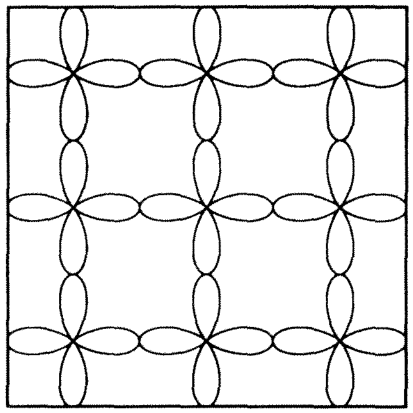

FIG. 1. *Array of amoebas parametrized as in Eq. (15), with $R = 0.25$, $\epsilon = 0.999$ and $n = 4$.*

and curvature 5. The narrow neck at the center of the amoeba has width $4 \cdot 10^{-4}$ and curvature $2 \cdot 10^7$. In this example I did not work with segments of the actual arclength s. Instead, I considered the arclength as a function of the the parameter ϕ of Eq. (13). Then I used the interval $[0, 2\pi]$ of ϕ for subdivision and quadrature. Performing the quadrature in ϕ, rather than in s, simplifies the calculations. Table 3 gives the numerical results.

The final estimate $\sigma_{\text{eff}} = 23.69271947$ was checked in two ways. A calculation with the applied field rotated 45 degrees gave $\sigma_{\text{eff}} = 23.69371936$ after nine stages of refinement. A calculation with $\sigma_1 = 1$ and $\sigma_2 = 0.001$ gave $\sigma_{\text{eff}} = 0.042207059572$, whose inverse is 23.69271895, confirming the effective conductivity to about eight digits.

4.4 Squares

A square array of squares is another classic geometry. The squares in this example are parameterized by their area fraction p_2 and oriented so that the array becomes a

TABLE 3

The effective conductivity σ_{eff} of a square array of amoebas in a filler. The filler and the amoebas have conductivities $\sigma_1 = 1$ and $\sigma_2 = 1000$, respectively.

stage	σ_{eff}	E^J_{max}	pseg	iter	CPU	mod ent	S
3	23.695	0.7	48	55	2 m	20,000	6 s
5	23.6927197	0.001	80	64	9 m	25,000	7 s
7	23.69271944	0.000005	100	61	20 m	31,000	8 s
9	23.69271947	0.0000003	108	57	33 m	38,000	8 s

TABLE 4

The effective conductivity σ_{eff} of a square array of squares in a filler. The filler and the squares have conductivities $\sigma_1 = 1$ and $\sigma_2 = 1000$, respectively. The volume fraction of squares is $p_2 = 0.499$.

stage	σ_{eff}	E^J_{max}	pseg	iter	CPU	mod ent	S
6	8.42	0.004	32	16	1.5 m	1,900	1 s
10	8.461	0.0001	48	20	5 m	1,900	1 s
14	8.46179	0.000002	64	24	11 m	1,900	1 s

TABLE 5

The effective conductivity σ_{eff} of a square array of squares with rounded corners. The squares of Table 4 have had their sharp corners replaced by quarter circles.

stage	σ_{eff}	E^J_{max}	pseg	iter	CPU	mod ent	S
5	8.4	0.02	48	20	2 m	1,900	1 s
10	8.4617	0.001	68	20	8 m	27,000	5 s
15	8.461813535	0.00000006	93	20	21 m	57,000	8 s

checkerboard for $p_2 = 0.5$. This geometry has been addressed by Milton, McPhedran, and McKenzie [22] (1981), Tao, Chen, and Sheng [23], and Bergman and Dunn [24]. The calculations of Milton, McPhedran, and McKenzie are the most accurate. The authors used a special purpose algorithm involving fractional power series. For $\sigma_1 = 1$, $\sigma_2 = 100$, $p_2 = 0.49$ they get $\sigma_{\text{eff}} = 5.15$. With 80 interface segments we get $\sigma_{\text{eff}} = 5.14729$.

A more challenging problem is $\sigma_1 = 1, \sigma_2 = 1000$, and $p_2 = 0.499$, shown in Table 4. The difficulty here is the resolution of the charge density $\rho(s)$, which diverges in the corners. When our program stops, at refinement stage 15, the error is chiefly due to insufficient resolution of $\rho(s)$ at the segment closest to each corner. This segment has a length of 10^{-9}. A calculation with $\sigma_1 = 1$, $\sigma_2 = 0.001$, and $p_2 = 0.499$ gives $\sigma_{\text{eff}} = 0.118178$, whose inverse is 8.46181, confirming the final result of Table 4 to about five digits.

4.5 Squares with rounded corners

No manufactured corner can be infinitely sharp. What happens if we round the corners of the squares in the previous example? I let the corners be substituted by quarter circles. If the square has side of length L, I let the quarter circle that replaced the corners have radius $R = L \cdot 10^{-7}$. A convergence study is given in Table 5. In this example rounded corners allowed for nine accurate digits, compared with five accurate digits for sharp corners.

4.6 Inclusions with cusps

Is it difficult to do computations for inclusions with cusps? In an example I took the star-shaped object found between four equisized and touching disks on a square lattice. This object, in turn, was placed on the lattice points of a square lattice as depicted in Figure 2. The inclusions in this arrangement would touch each other at volume fraction $p_2 \approx 0.4292$. A challenging geometry is $\sigma_1 = 1$, $\sigma_2 = 1000$, and $p_2 = 0.41$. A convergence study is presented in Table 6. A calculation with $\sigma_1 = 1$ and $\sigma_2 = 0.001$ gave $\sigma_{\text{eff}} = 0.180575725$, whose inverse is 5.5378429, confirming the effective conductivity to about seven digits.

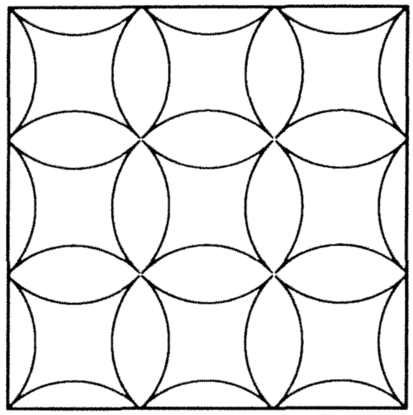

FIG. 2. *Square array of inclusions with cusps. The volume fraction of inclusions is* $p_2 = 0.41$.

TABLE 6

The effective conductivity σ_{eff} *of the geometry with cusps in Figure 2. The inclusions have volume fraction* $p_2 = 0.41$ *and conductivity* $\sigma_2 = 1000$. *The conductivity of the filler is* $\sigma_1 = 1$.

stage	σ_{eff}	E^J_{max}	pseg	iter	CPU	mod ent	S
2	5.55	0.1	24	29	0.5 m	12,000	4 s
4	5.5377	0.06	38	57	2 m	17,000	5 s
6	5.5378435	0.001	54	98	6 m	25,000	8 s
8	5.5378429	0.000004	66	97	13 m	31,000	14 s

4.7 Random disks

Sangani proposed a dense 16 "random" disk unit cell problem (personal communication 1993 and Ref. [25]) which I later solved [20] with a spectral method that only works for disk geometries. I used 8,000 spectral terms. The calculation took several hours.

The area fraction of disks in the Sangani problem is 0.7. Coordinates for the disk centers are tabulated in Ref [20]. The two disks that are closest to each other have a separation to diameter ratio of $3 \cdot 10^{-4}$. To facilitate comparison with previous results I choose $\sigma_1 = 1$ and $\sigma_2 = 100$ and let $\mathbf{e}$ be applied in the x-direction. The effective conductivity is $\sigma_{\text{eff}} = 7.44445359175$. Table 7 shows a convergence study. Here I decided to put a limit on how many iterations were allowed on certain levels. I allowed up to 20 iterations on refinement level one, up to 40 iterations on refinement level two, up to 60 iterations on refinement level three, and so on. This reduced the number of uninteresting

TABLE 7

The effective conductivity σ_{eff} *in the* x*-direction of the Sangani 16 disk configuration. The disks have volume fraction* $p_2 = 0.7$ *and conductivity* $\sigma_2 = 100$. *The conductivity of the filler is* $\sigma_1 = 1$.

stage	σ_{eff}	E^J_{max}	pseg	iter	CPU	mod ent	S
1	7.45	44	128	20	1.5m	52,000	8s
2	7.444451	0.06	176	40	5m	71,000	10s
3	7.44445359175	0.00003	224	60	11m	81,000	11s
4	7.44445359175	0.000007	266	61	22m	82,000	12s

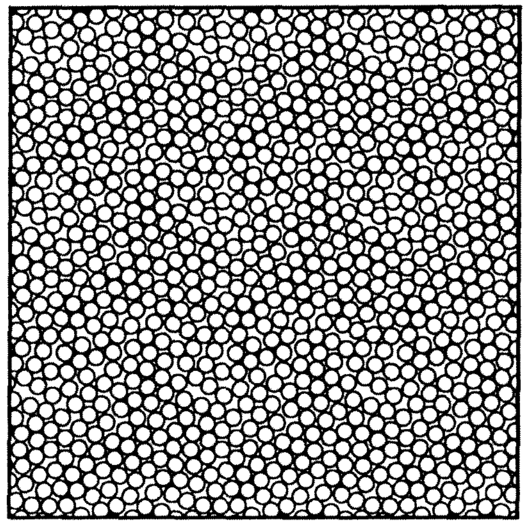

FIG. 3. *A "random" configuration generated by 1,000,000 Monte Carlo simulation steps. The unit cell with 100 disks at area fraction 0.7 is surrounded by its nearest neighbours.*

iterations for insufficiently resolved problems.

Finally, I did a computation for the "random" configuration depicted in Figure 3. The filler and disks have conductivities $\sigma_1 = 1$ and $\sigma_2 = 1000$, respectively. This configuration was generated with the Monte Carlo technique [26]. In short, this algorithm lets all disks in the unit cell be assigned a random tentative displacement. Each disk is examined in turn. If its new position does not cause disks to overlap, the move is accepted. The mean size of the random displacements is chosen so that the probability of acceptance is 0.5. When *all* disks have been examined once we say that one simulation step is completed. The unit cell in this example contains 100 disks, the disk area fraction is 0.7, and 1,000,000 simulation steps were used in the simulation. Eight segments were initially placed on each disk. In every refinement stage a total of 300 new segments were added. The field $\mathbf{e}$ was applied vertically in Figure 3. The results for σ_{eff} are, stage 1: $\sigma_{\text{eff}} = 7.987$, stage 2: $\sigma_{\text{eff}} = 7.989157$, stage 3: $\sigma_{\text{eff}} = 7.989155506$, stage 4: $\sigma_{\text{eff}} = 7.989155503$. It took 65 minutes to generate the configuration and another 97 minutes to complete the three first stages. The effective conductivity in the horizontal direction is $\sigma_{\text{eff}} = 7.927222342$.

5 Discussion

We have developed and implemented a general purpose algorithm to solve the electrostatic problem for two-dimensional composites of arbitrary geometries. Through a series of examples, involving thin bridges, narrow necks, coatings, corners, cusps, and random mixtures we demonstrated the robustness and the flexibility of the code. When comparisons were available, our algorithm often outcompeted previous investigators' algorithms incorporating special analysis.

Should we wish the algorithm to run faster, the single most important improvement is perhaps to replace the uniform fast multipole code, used here in the last example, with an adaptive fast multipole code, and then use this code for iteration in all the examples. This would pay off since the distributions of discretization points in our examples are highly non-uniform.

References

[1] S. G. Mikhlin, *Integral Equations*, Pergamon: London (1957).

[2] R. Christensen, *Mechanics of Composite Materials* (Krieger, Florida, 1979).

[3] T. Mura, *Micromechanics of Defects in Solids*, Martinus Nijhoff Publishers: Dordrecht, (1987).

[4] L. Greengard and M. Moura, *Acta Numerica 1994*, Cambridge University Press: Cambridge, (1994) pp. 379-410.

[5] R. C. McPhedran, L. Poladian and G. W. Milton (1988) *Asymptotic studies of closely spaced, highly conducting cylinders* Proc. R. Soc. Lond. A **415**, 185-196.

[6] Julian D. Cole (1995) *Limit process expansions and homogenization* Siam J. Appl. Math. **55** 410-424.

[7] M. A. Jaswon and G. T. Symm, *Integral equation methods in potential theory and elastostatics*, pp. 27-29. New York: Academic Press (1977).

[8] J. Hetherington and M. F. Thorpe (1992) *The conductivity of a sheet containing inclusions with sharp corners* Proc. R. Soc. Lond. A **438**, 591-604.

[9] V. Rokhlin (1985) *Rapid solution of integral equations of classical potential theory* J. Comput. Phys. **60** 187-207.

[10] L. Greengard and V. Rokhlin (1987) *A fast algorithm for particle simulations* J. Comput. Phys. **73**, 325-348.

[11] J. Carrier, L. Greengard and V. Rokhlin, (1988) *A fast adaptive multipole algorithm for particle simulations* SIAM J. Sci. and Stat. Comput. **9**, 669-686.

[12] J. Y. Lee and L. Greengard, (1994) *Courant Mathematics and Computing Laboratory preprint* 94-001.

[13] P. Sonneveld (1989) *CGS, A fast Lanczos-type solver for nonsymmetric linear systems* SIAM J. Sci. Statist. Comp. **10** 36-52.

[14] Y. Saad and M. H. Schultz (1986) *GMRES: A generalized minimal residual algorithm for solving nonsymmetric linear systems* SIAM J. Sci. Stat. Comput. **7**, 856-869.

[15] C. Lanczos (1952) *Solutions of systems of linear equations by minimized iterations* J. Res. Nat. Bur. Standards **49** 33-53.

[16] R. Fletcher, in *Proc. of the Dundee Biennal conference on Numerical Analysis*, edited by G. A. Watson, Springer: New York (1975).

[17] N. M. Nachtigal, S. C. Reddy, and L. N. Trefethen (1992) *How fast are nonsymmetric matrix iterations* SIAM J. Matrix Anal. Appl. **13** 778-795.

[18] Rayleigh, J. W. 1892 *On the influence of obstacles arranged in rectangular order on the properties of the medium* Phil. Mag. **34**, 481-502.

[19] Perrins, W. T., McKenzie, D. R. & McPhedran, R. C. 1979 *Transport properties of regular arrays of cylinders* Proc. R. Soc. Lond. A **369**, 207-225.

[20] J. Helsing (1994) *Fast and accurate calculations of structural parameters for suspensions* Proc. R. Soc. Lond. A. **445**, 127-140.

[21] N. A. Nicorovici, R. C. McPhedran and G. W. Milton (1993) *Transport properties of a three-phase composite material: the square array of coated cylinders* Proc. R. Soc. Lond. A **442**, 559-662.

[22] G. W. Milton, R. C. McPhedran and D. R. McKenzie (1981) *Transport Properties of Arrays of intersecting cylinders* Appl. Physics **25**, 23-30.

[23] R. Tao, Z. Chen, P. Sheng (1990) *First-principles Fourier approach for the calculation of the effective dielectric constant of periodic composites* Phys. Rev. B **41** 2417-2420.

[24] D. J. Bergman and K. Dunn (1992) *Bulk effective dielectric constant of a composite with periodic microgeometry* Phys. Rev. B **45** 13262-13271.

[25] A. S. Sangani and C. Yao (1988) *Transport properties in random arrays of cylinders. I. Thermal conduction* Phys. Fluids **31**, 2426-2434.

[26] N. Metropolis, A. W. Rosenbluth, M. N. Rosenbluth, A. N. Teller, and E. Teller (1953) *Equation of state calculations by fast computing machines* J. Chem. Phys. **21**, 1087-1092.

THE IMPORTANCE OF FLOW PHYSICS IN CFD

Kazuhiro Kusunose*

November 2, 1995

Abstract

Important physical effects which need to be taken into account for appropriate CFD simulation have been presented. To demonstrate the necessity of correct physical modelings in CFD the following three topics have been selected: grid effects; role of boundary-layer transition; and far-field boundary conditions.

1 Introduction

A successful Navier-Stokes analysis for a multi-element airfoil configuration requires a correct rendition of the complex flow physics. This includes laminar boundary layer flow, boundary layer transition, and turbulent boundary layer flow; flow separation and reattachment; as well as the interaction between wakes and boundary layers. To achieve this it is necessary to provide a physically adequate grid in the critical areas, and physically correct flow modelings in addition to the selection of a state of the art numerical algorithm.

With numerical-algorithm and turbulence-model developments getting closer to their maturities, the understanding of the flow physics becomes more important in the quest to improve the accuracy of CFD codes. To emphasize the necessity of correct physical modelings in CFD, the following three topics have been selected: the necessity of an adequate grid; importance of natural transition prediction capability; and the effects of far-field boundary conditions.

Our numerical studies are based on a Navier-Stokes analysis system [1]; which consists of the NASA Ames INS2D Navier-Stokes solver [2] with one-equation turbulence model [3], [4], and our transition prediction model [5].

2 Grid effects

To illustrate the grid effect on the flow solution, two grids were generated for a 3-element airfoil configuration. These grids are basically identical except for the the cove region of the main element. The grids shown in Figure 1 are referred to as the "old" and "new" grids. Eddy viscosity contours are plotted in Figure 2. It can be seen that the old grid, which was generated without considering the actual flow physics of shear flow, cannot resolve the detailed shear layer; and the smeared shear layer contaminates the leading edge of the flap.

Predicted lift distribution for the old grid is compared to the experimental data in Figure 3. Due to the fictitious contamination of the flap leading edge, the predicted lift level is significantly lower than the experiment. Once the new grid, which is designed to resolve the shear flow, is employed, the level of the flap leading edge contamination is

*Principal Engineer, Boeing Commercial Airplane Group, Seattle, WA 98124-2207

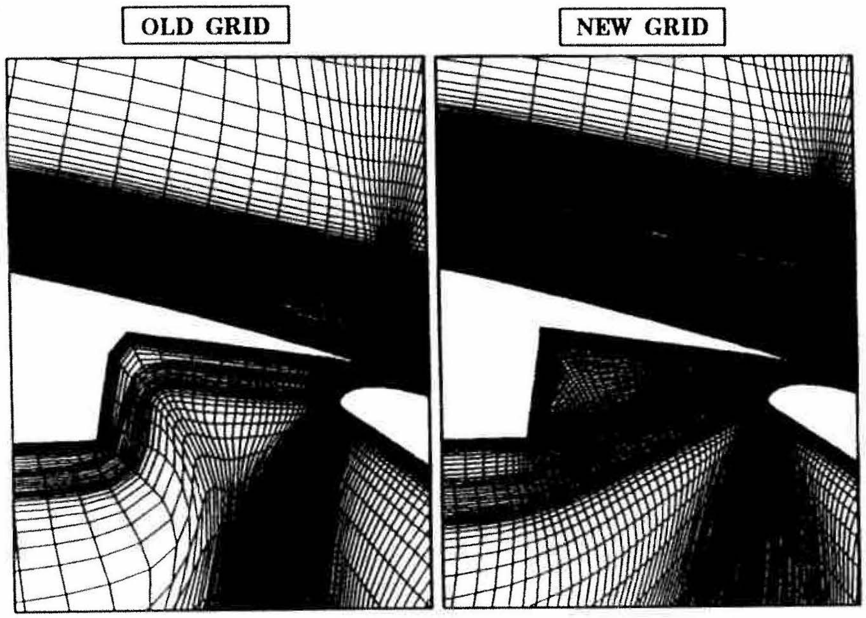

FIG. 1. *Two different grids in the cove region.*

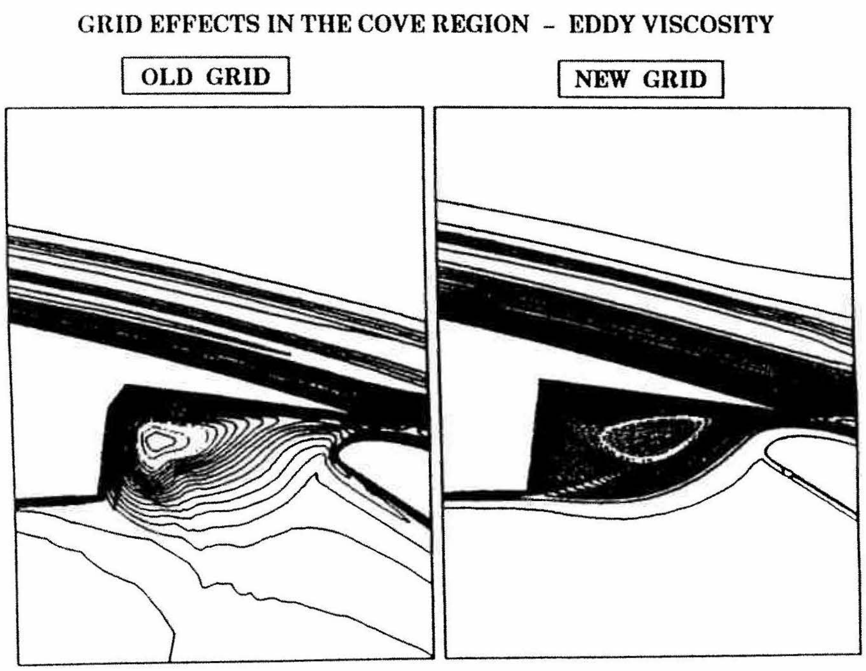

FIG. 2. *Grid effect on eddy viscosity.*

significantly reduced and the agreement between the lift curve and the experiment (shown in Figure 4) is improved. The remaining miss-match of the lift slope observed in Figure 4 will be corrected when the boundary layer transition locations are considered. (That will be discussed later.) During this grid study all of the boundary layers are treated as turbulent (fully turbulent option).

3 Role of the boundary-layer transition

Depending on the transition location (including the fully turbulent option), a range of flow solution, from attached to massively separated, can be obtained [1]. The significant effects of the boundary-layer transition location on the flow around a multi-element airfoil are clearly demonstrated in Figure 5. Here, the fully turbulent flow solution is compared to that with specified transition locations on the main element. It should be noted that the separation size on the flap is changed considerably.

Figure 6 shows two lift curves; one for the fully turbulent option (discussed in the previous grid study) and one for the specified transition locations. Once the transition locations on each element have been determined from the experimental results, the lift curve matches the experimental data very well. Since the calculated flow solutions may not be unique without specifying the boundary-layer transition locations, a boundary-layer transition-prediction capability is necessary in a Navier-Stokes code in order to obtain physically meaningful results in a predictive manner [5].

4 Far-field boundary conditions

Since multi-element airfoils carry high lifts, where the lift level is often more than 4 times larger than that of a typical single element airfoil, the locations and the treatment of the far-field boundaries become important. Here, two different types of boundary conditions are examined to demonstrate their effects on lift. One is the "typical" free stream condition and the other is the free stream condition with a point vortex model caused by a highly loaded airfoil.

The effects of far-field boundary locations on the lift (for 10, 20 and 50 chords away from the airfoil) for these two boundary conditions are plotted in Figure 7. The lifts based on the free stream boundary condition are very sensitive to the far-field boundary locations. The superiority of the model with a point vortex can be easily seen.

To study the effects of vertical location of the airfoil model in the NASA Langley Low Turbulence Pressure Tunnel (LTPT), solutions were obtained for different vertical positions: the normal (tested) position, and +/-0.5 chord [6]. The tunnel floor and ceiling are located 2 chords away from the model. As can be seen in Figure 8, the resuting flow varies significantly with vertical locations in the LTPT tunnel. Tunnel walls play a important role in the numerical simulation of a high-lift system.

5 Conclusions

The necessity of correct physical modeling in CFD has been demonstrated. It is clear that understanding and implementing flow physics into a CFD code become more important in quest to improve the accuracy of the code.

References

[1] H. V. Cao and K. Kusunose, *Grid Generation and Navier-Stokes Analysis for Multi-Element Airfoils*, AIAA-94-0748, Reno, Nevada, January 1994.

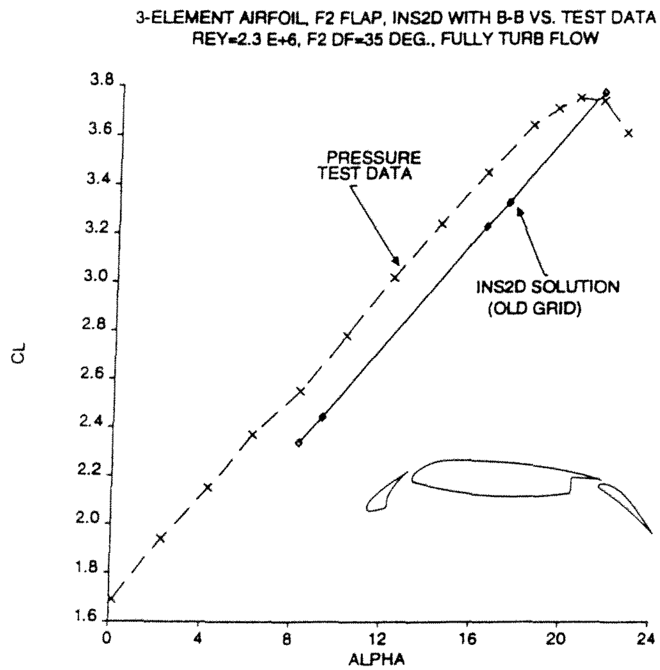

FIG. 3. *Lift distributions (old grid).*

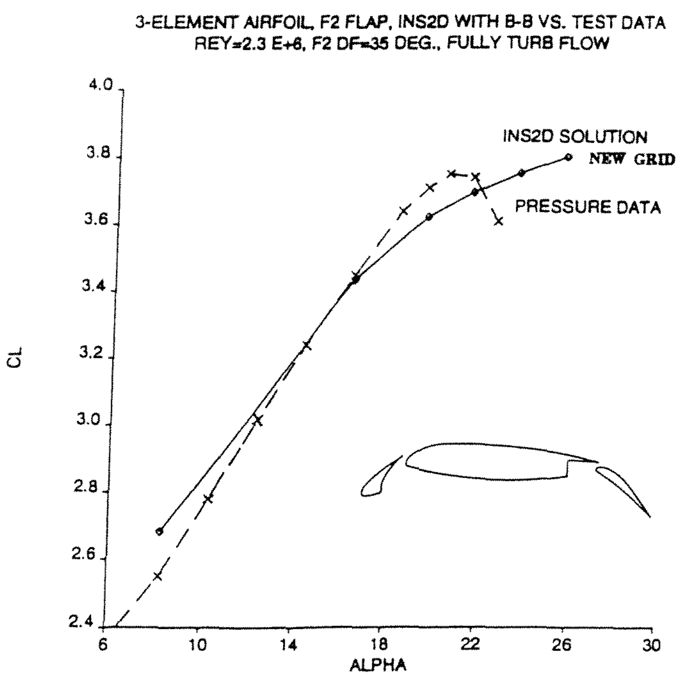

FIG. 4. *Lift distributions (new grid).*

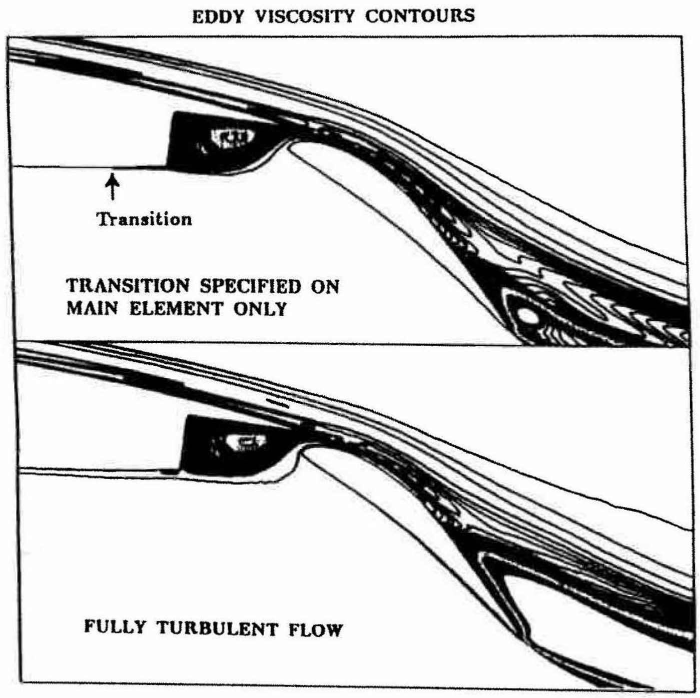

FIG. 5. *Transition effect on flap loading.*

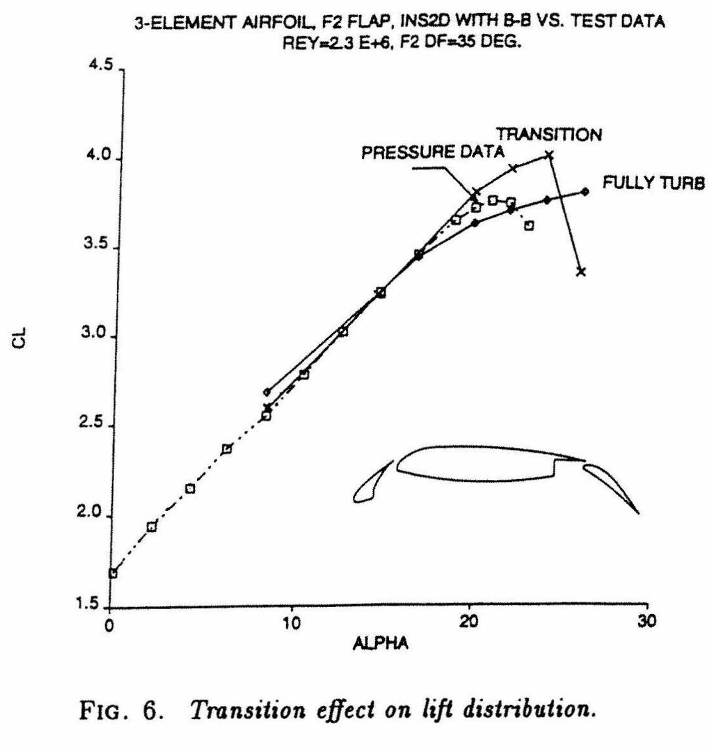

FIG. 6. *Transition effect on lift distribution.*

Free-stream condition with a point vortex

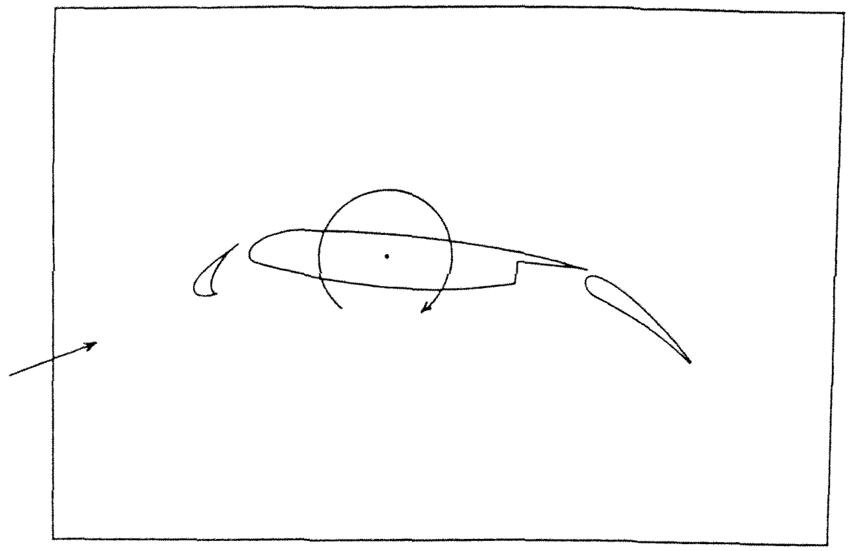

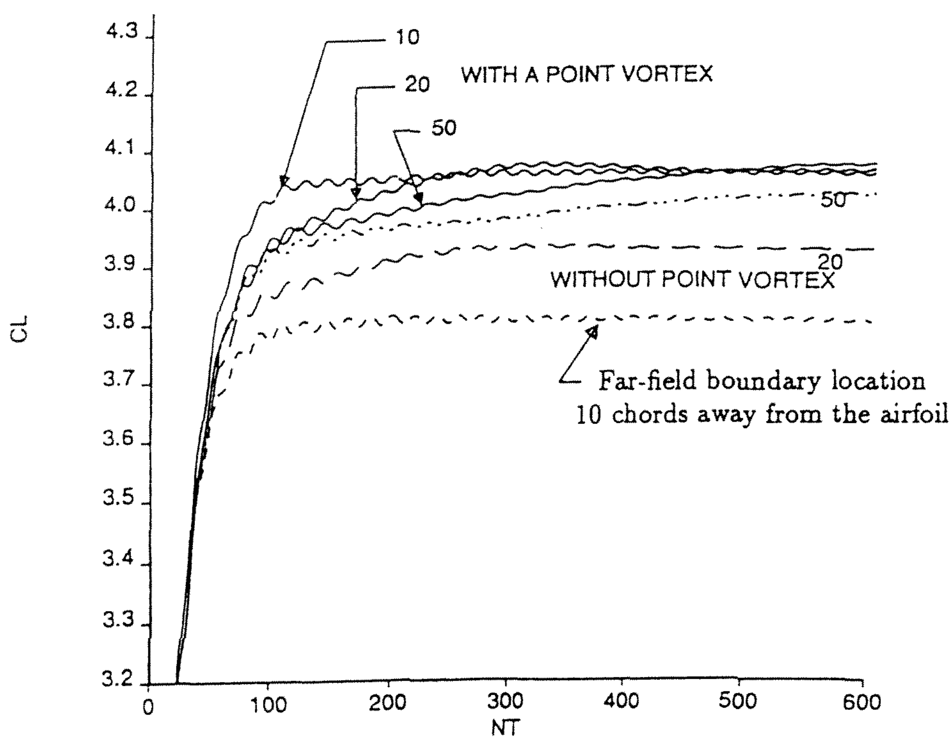

FIG. 7. *Effects of far-field boundary condition and locations on the convergence history of lift.*

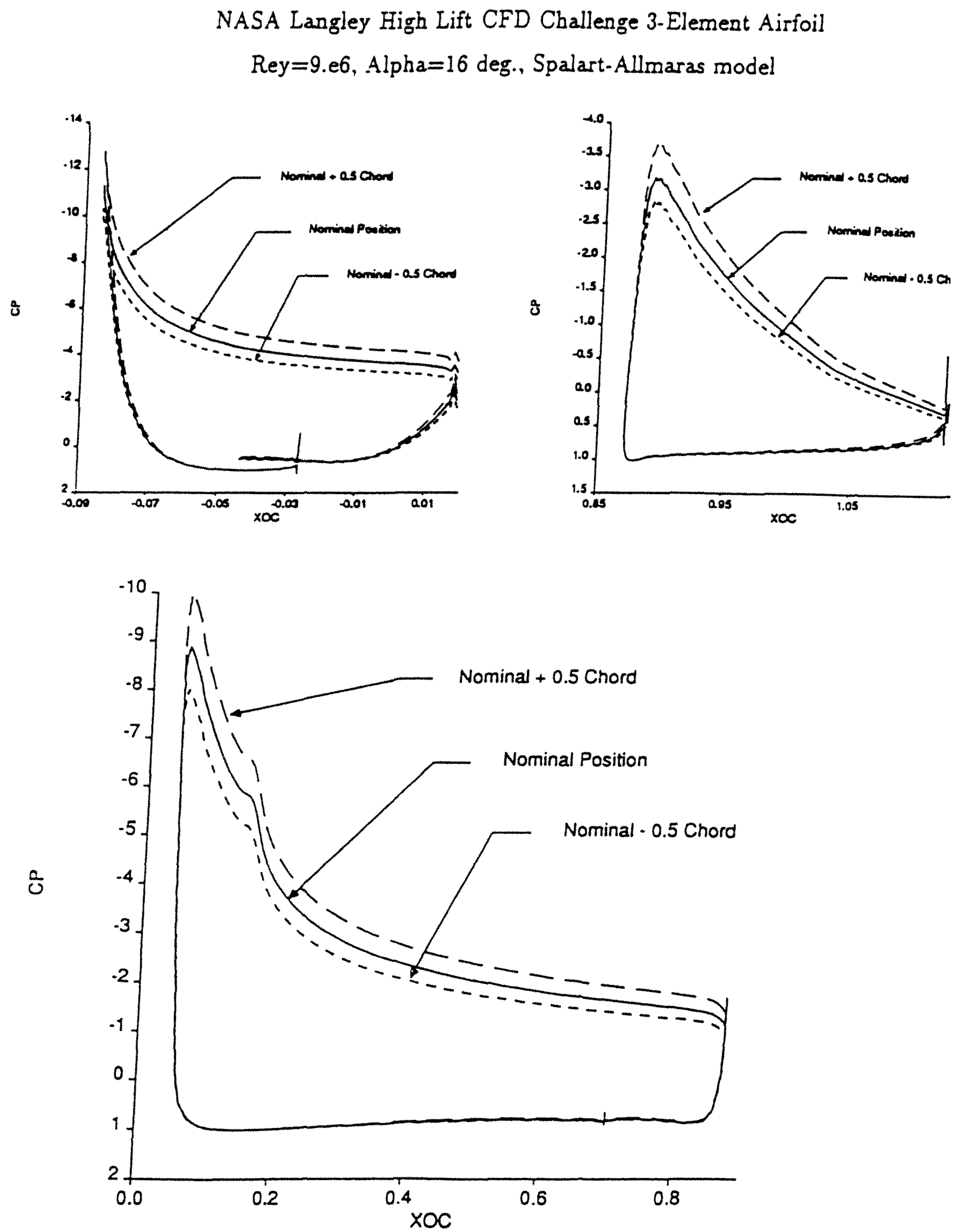

FIG. 8. *Effects of model vertical position on pressure distribution.*

[2] S. E. Rogers, N. L. Wiltberger, and D. Kwak, *Efficient Simulation of Incompressible Viscous Flow Over Single and Multi-Element Airfoils*, AIAA-92-0405,Reno,Nevada,January 1992.
[3] P. R. Spalart and S. R. Allmaras, *A One-Equation Turbulence Model for Aerodynamic Flows*, AIAA-92-0439, Reno, Nevada, January 1992.
[4] B. S. Baldwin and T. J. Barth, *A One-Equation Turbulence Transport Model for High Reynolds Number Wall-Bounded Flows*, AIAA-91-0610, Reno, Nevada, January 1991.
[5] K. Kusunose and H. V. Cao, *Prediction of Transition Location for a 2-D Navier-Stokes Solver for Multi-Element Airfoil Configurations*, AIAA-94-2376, Colorado Springs, Co, June 1994.
[6] H. V. Cao, K. Kusunose, P. R. Spalart, K, K. Ishimitsu, S. E. Rogers, and R. J. McGhee, *Study of Wind Tunnel Wall Interference for Multi-Element Airfoils Using a Navier-Stokes Code*, AIAA-94-1933, Colorado Springs, Co, June 1994.

Calculating Fluctuations in a Laminar Boundary Layer in a Turbulent Free Stream

R.E. Mayle* A. Schulz†

Abstract

A theory is presented for calculating the fluctuations in a laminar boundary layer when the free stream is turbulent. The kinetic energy equation for these fluctuations is derived and a new mechanism is revealed for their production. A methodology is presented for solving the equation using standard boundary layer computer codes. Solutions of the equation show that the fluctuations grow at first almost linearly with distance and then more slowly as viscous dissipation becomes important. Comparisons of calculated growth rates and kinetic energy profiles with data show good agreement. In addition, a hypothesis is advanced for the effective forcing frequency and free-stream turbulence level which produce these fluctuations.

1 Introduction

One of the remaining difficulties in calculating laminar-to-turbulent transition in boundary layers is predicting its onset. For natural transition, onset is usually determined using the "e^n" method developed by Smith (1956) and others. This method, which is widely used in the aircraft industry, uses the amplification rate of the most unstable Tollmien-Schlichting wave at each stream wise position to determine a disturbance-amplitude ratio. Onset is then presumed to occur at the position where this ratio attains an experimentally determined critical value related to the free-stream turbulence level (Mack, 1977). For bypass transition, which is the usual mode of transition in gas turbine engines, onset is usually determined without too much regard concerning the physics involved. In this case, empirical correlations providing the best fit to transition data are used, and these are applied either directly to the mean flow (see Mayle, 1991), or indirectly to the production of turbulent-kinetic-energy (see Sieger et al., 1993). In spite of these methods, however, predicting the onset of either natural or bypass transition is still more of an art than a science (see Sieger et al. for examples).

Transition from a practical standpoint may be considered to begin where a quantity such as the surface shear stress first deviates from its laminar value. In 1951, Emmons showed that this corresponds to the first position along the surface where isolated spots of turbulence within the boundary layer are formed. Clearly then, everything before the spots are formed happens in a completely laminar boundary layer. Measurements show this pre-transition flow is not, however, steady. For natural transition, which occurs when the free-stream turbulence level is zero or nearly so, Tollmien-Schlichting waves can be found. For bypass transition, which occurs at high free-stream turbulence levels, "turbulent-looking"

*Institut für Thermische Strömungsmaschinen Universität Karlsruhe, Karlsruhe, Germany; Professor Emeritus of Mechanical Engineering, Rensselaer Polytechnic Institute, Troy, NY, USA

†Institut für Thermische Strömungsmaschinen Universität Karlsruhe, Karlsruhe, Germany

fluctuations mimicking those in the free stream are found, and similar to the Tollmien-Schlichting waves these fluctuations also amplify to eventually form turbulent spots.

Although our eventual goal is to predict the onset of transition, our aim in this paper is to calculate the pre-transition laminar fluctuations. As will be seen, this is done by developing and solving a laminar-kinetic-energy equation for the fluctuations, but more importantly it is accomplished by recognizing a new mechanism and determining the effective frequency and turbulence level in the free stream which is responsible for both producing and amplifying them. The approach is new. It is based on Lin's (1957) analysis for unsteady laminar boundary layers and Dullenkopf and Mayle's (1995) concept of an effective frequency and turbulence level for laminar boundary layers in a turbulent free stream. Because it is easy to incorporate in any modern boundary-layer computer code, the approach is also practical.

2 Review of Lin's Analysis

Lin (1957) examined the effect of free-stream fluctuations on laminar boundary layers by decomposing the velocities and pressure into time-averaged and time-dependent components similar to Reynolds' analysis for turbulent flow, i.e., $u(x, y, t) = \bar{u}(x, y) + u'(x, y, t)$. In contrast to the usual turbulent approach, however, both the pressure and its fluctuation may be eliminated from the equations of motion by using the unsteady Euler equation and the free-stream velocity, $U(x, t) = \bar{U}(x) + U'(x, t)$.

Clearly, the time-averaged boundary-layer equations for mass and momentum are identical to those for turbulent flow, and therefore won't be presented,[1] except that now they apply to a time-averaged laminar flow. The equations for the fluctuating components of velocity can be obtained by subtracting the time-averaged equations from the equations for the instantaneous motion and, contrary to the situation for turbulent flow, can be solved once the unsteady free-stream velocity distribution is given.

Solutions for the fluctuating components are easily obtained when the frequency of the free-stream fluctuations is high enough such that $\omega \gg \nu/\delta^2$, where ω is the frequency, ν is the kinematic viscosity, and δ is the boundary layer thickness. In this case, the fluctuations occur mostly adjacent to the wall within a thickness $\delta_\omega = \sqrt{2\nu/\omega} \ll \delta$ independent of the mean flow. Since the equation for u' is linear, a solution for an arbitrary free-stream fluctuation may be obtained by superposition. For details regarding these solutions and higher order approximations, the reader is referred to Lin's original paper.

If $U'_\infty \neq \mathrm{fnc}(x)$, the normal component of the fluctuating velocity v', which is proportional to dU'_∞/dx, is zero, the apparent shear stress ($\bar{u}'\bar{v}'$) is zero, and the time-averaged velocities $\bar{u}$ and $\bar{v}$ are exactly those given by the laminar solution. Thus, for unaccelerated flow over a surface with slowly decaying free-stream turbulence, we should expect the mean flow velocity profiles to be those given by Blasius. This result is well documented by Dyban et al. (1976) and others.

3 The Laminar-Kinetic-Energy Equation

To the authors' knowledge, the energy equation for laminar fluctuations, henceforth called the "LKE" equation, has never been presented before. It can be obtained in the same way as the turbulent-kinetic-energy equation, except that the pressures $\bar{p}$ and p' can be

[1]See Lin's original paper or Schlichting (1979).

eliminated by using the time-averaged and instantaneous forms of Euler's equation. For boundary layer flows, one obtains

$$\bar{u}\frac{\partial k}{\partial x} + \bar{v}\frac{\partial k}{\partial y} = -(\ \overline{u'v'}\ )\frac{\partial \bar{u}}{\partial y} - \frac{\partial}{\partial y}\left[\overline{v'k} - \nu\frac{\partial k}{\partial y}\right] - \epsilon + \left\{\overline{u'\frac{\partial U'}{\partial t}}\right\}$$

where k is the kinetic energy of the laminar fluctuations, and ϵ is the viscous dissipation of kinetic energy defined by $\epsilon \equiv \nu\overline{(\partial u'/\partial y)^2}$. All of the terms but the last are similar to those in the TKE equation and represent the convection of laminar kinetic energy (on the left), and the production, diffusion and dissipation of laminar kinetic energy respectively (on the right). The term in curly brackets arises from taking the average of $u'(dp'/dx)$ and represents the production of laminar kinetic energy by the work of the imposed fluctuating pressure forces. This term is new. It is also the only term in the equation providing a direct link between the fluctuations in the free stream and boundary layer, and for an unaccelerated free stream, it is the only production term.

If the kinetic energy of the fluctuations is to increase, then at least one of the production terms must be larger than the dissipation term. Performing a standard boundary layer order of magnitude analysis, considering $\partial/\partial t \approx O(\omega)$, it is easy to show that only the new production term has a chance of overwhelming the dissipation term, and that this occurs when Lin's high frequency criterion is met, namely, when $\omega \gg \nu/\delta^2$. If the free-stream fluctuations result from turbulence having a broad spectrum of frequencies, this criterion will always be met. Therefore, the main effect of free-stream turbulence on a laminar boundary layer is similar to the high frequency response examined by Lin.

Using the same order of magnitude analysis, it can also be shown that the diffusion of kinetic energy by the v' component of the fluctuations can be neglected compared to the viscous diffusion. Hence, the relevant LKE equation for a laminar boundary layer with a turbulent free stream becomes

$$\bar{u}\frac{\partial k}{\partial x} + \bar{v}\frac{\partial k}{\partial y} = \overline{u'\frac{\partial U'}{\partial t}} + \nu\frac{\partial^2 k}{\partial y^2} - \epsilon$$

Hence, fluctuations in a laminar boundary layer do not arise by diffusion from the free stream, as was previously thought, but are forced.

Suitable expressions for the production and dissipation terms can be obtained from both dimensional and heuristic arguments. Without discussion, the simplest forms for these terms yield the following equation

$$\bar{u}\frac{\partial k}{\partial x} + \bar{v}\frac{\partial k}{\partial y} = C_\omega\frac{U_\infty^2}{\nu}\sqrt{kk_\infty}e^{-y^+/C^+} + \nu\frac{\partial^2 k}{\partial y^2} - -2\nu k/y^2$$

where $k \approx \bar{u}'^2/2$, U_∞ is the free-stream velocity, k_∞ is the free-stream kinetic energy, y^+ is the wall coordinate based on the local wall shear stress, and C_ω and C^+ are quantities yet to be determined. The exponential factor in the production term damps the production of kinetic energy as the free stream is approached since any fluctuation and its temporal derivative there is ninety degrees out of phase. In addition, since the dissipation and diffusion of kinetic energy are equal at the surface, the coefficient of the dissipation term must equal two.

The above equation can easily be solved by most modern boundary-layer computer codes. The boundary conditions for this equation are $k = 0$ at $y = 0$ and, for isotropic free-stream turbulence, $k \to k_\infty/3$ as $y \to \infty$. In addition, an initial kinetic energy profile must be provided. For the present calculations, Lin's kinetic energy profile was used. Calculations using other reasonable profiles had virtually no effect on the solutions. In addition, calculations were begun at $Re_x \approx 1000$ and no modifications to the equations of motion for the mean flow were made.

4 Comparisons with Experiments

Calculations for this paper were performed using the computer code called "ALFA" (Sieger et al., 1993). This is a standard boundary-layer code of the $k - \epsilon$ variety. Three of the following comparisons are made with data obtained by Rolls-Royce (1993) for free-stream turbulence levels of about 1, 3, and 6 percent. Their experiments are well documented and all necessary turbulence data are available (Roach, 1987, Roach and Brierley, 1990). In addition, these data have become standard test cases for transitional flow modeling. A comparison with data from Dyban and Epik (1985) is also made for a free-stream turbulence level of about 2 percent.

Preliminary calculations indicated that reasonably good results could be obtained by considering both C_ω and C^+ independent of x. The "best" values for C_ω and C^+ were then obtained by fitting the kinetic energy distributions in both the x and y directions by eye. With this, the best value for C^+ turned out to be virtually the same for all of the data and was consequently set equal to a constant, namely, $C^+ = 13$.

The calculated and measured maximum intensity distributions are shown in Fig. 1. Agreement is excellent, and although not shown, a good fit for the 1% data is found all the way out to $Re_x \approx 1.3(10)^6$. The values of C_ω which provide these results are presented in Table 1. Their variation will be discussed in the next section.

TABLE 1

Test Case	Tu_∞, %	C_ω
Rolls-Royce (1993)	0.9	0.00010
Dyban & Epik (1985)	1.6	0.00014
Rolls-Royce (1993)	3.0	0.00021
Rolls-Royce (1993)	6.0	0.00017

Several calculated and measured intensity profiles are shown in Figs. 2a and 2b. While on the average reasonable, the calculated profiles are not quite right. In general, the peaks of the intensity profiles are calculated closer to the wall than measured. This is particularly true for the $Tu_\infty = 1\%$ test case where just before transition (comparison not shown), the peak is predicted to be one-third of the distance from the wall than that measured. In this case, however, fluctuations at the Tollmein-Schlichting frequency were detected and the fluctuations there are suspected to be caused by a natural instability. Still, in spite of these discrepancies, the agreement between the calculated and measured intensity profiles is remarkable considering the simplicity of the model and the fact that no transitional boundary-layer code using low-Reynolds-number turbulence modeling has yet been able to calculate these data.

5 The Effective Frequency and Turbulence Level

The variation of C_ω in Table 1 can be explained by realizing that it must depend on both a frequency and turbulence level most "effective" in producing the boundary layer fluctuations. In fact, formally, it can be shown that $C_\omega \propto (\omega_{eff}\nu/U_\infty^2)(Tu_{eff}/Tu_\infty)$.

Since the boundary layer is thinnest at its beginning, the first fluctuations in the layer will be produced by turbulence in the free stream having the highest frequencies. The "highest" frequencies are not necessarily "effective," however, since fluctuations at these frequencies will be viscously dissipated. Thus, the upper frequency limit is the free-stream velocity divided by the eddy size in the free stream most affected by viscous dissipation. Assuming that the effective frequency is proportional to this, it is not too difficult to obtain $\omega_{eff} \propto \nu U_\infty/\nu$ where ν is Kolmogorov's velocity scale (Hinze, 1975).

According to Dullenkopf and Mayle (1995), a laminar boundary layer will only respond to the energy contained within a relatively small band of frequencies near its effective frequency. If the energy spectral distribution near ω_{eff} is that given by Kolmogorov, and only the energy contained within a band near this frequency is important, it is again not too difficult to show that $Tu_{eff} \propto Tu_\infty[(\nu/U_\infty)Re_\Lambda]^{-1/3}$ where Re_Λ is the Reynolds number based on the integral length scale of turbulence.

These expressions provide $C_\omega = C(\nu/U_\infty)^{2/3}Re_\Lambda^{-1/3}$, where C is expected to be a constant. The quantities ν/U_∞ and Re_Λ can be determined directly from the turbulence energy density spectrum. Since ν is related to the dissipation of turbulence, it can also be determined from the decay of turbulence, namely $(\nu/U_\infty)^4 = -(3/2)[d(Tu_\infty^2)/dRe_x]$. Estimating Re_Λ from the dissipation length scale is not recommended, however, since comparisons between these estimates and measurements usually show poor agreement.

The 1, 3, and 6% data of Rolls-Royce were obtained using three very different turbulence grids. Since the turbulence field generated by these grids is well documented by Roach (1987), however, one can easily determine the values of ν/U_∞ and Re_Λ. These values are listed in Table 2. For Dyban and Epik's test case, ν/U_∞ was evaluated from the decay of turbulence. No data on length scale, however, was reported.

TABLE 2

Test Case	ν/U_∞	Re_Λ	C
Rolls-Royce (1%)	0.0035	4740	0.073
Dyban & Epik (2%)	0.0080	-	-
Rolls-Royce (3%)	0.0098	3590	0.070
Rolls-Royce (6%)	0.0117	9830	0.071

The values for C in the last column of Table 2 were obtained using $C = C_\omega(\nu/U_\infty)^{-2/3}Re_\Lambda^{1/3}$ and the values for C_ω given in Table 1. The fact that C is virtually identical for all three cases, in spite of the large variations in Tu_∞, ν/U_∞, and Re_Λ, is truly remarkable, and nicely supports our hypotheses for an effective frequency and turbulence level.

6 Conclusions

The main idea proposed in this paper is that, for a turbulent free stream, the laminar fluctuations preceding transition are primarily caused by the work of the imposed fluctuating free-stream pressure forces on the flow in the boundary layer. Based on this thought, we presented a theory for calculating these fluctuations using the laminar-kinetic-energy equation which, after some modeling, assumes the form

$$\bar{u}\frac{\partial k}{\partial x} + \bar{v}\frac{\partial k}{\partial y} = C_\omega \frac{U_\infty^2}{\nu}\sqrt{kk_\infty}e^{-y^+/C^+} + \nu\frac{\partial^2 k}{\partial y^2} - 2\nu k/y^2$$

where $C^+ \approx 13$.

Additional ideas concerning the frequency which drives the fluctuations were also proposed. These ideas permitted us to relate the coefficient C_ω in the above equation to the free-stream turbulence-energy-density spectrum according to

$$C_\omega = C\left(\frac{\nu}{U_\infty}\right)^{2/3} Re_\Lambda^{-1/3}$$

where $C \approx 0.07$.

These ideas are new and, we believe, clear the path to predicting the onset of transition. Yet some work still needs to be done. One obvious area which remains to be investigated is the effect of free-stream acceleration.

7 Acknowledgments

The lead author wishes to express his gratitude to Professor S. Wittig for his support during the author's visits to the Institut für Thermische Strömungsmaschinen as a Visiting Professor. The work presented herein was conducted during several visits beginning January 1994 when this author was on sabbatical. The same author is also grateful to Rensselaer Polytechnic Institute for granting him the sabbatical and to the German Sonderforschungsbereichs 167 which partially funded the work.

The authors also wish to thank their good friend and colleague Dr.-Ing. K. Dullenkopf for his input during our many discussions of this work.

References

[1] K. Dullenkopf, and R. E. Mayle, *An Account of Free-Stream-Turbulence Length Scale on Laminar Heat Transfer*, ASME Journal of Turbomachinery, 117, (1995), pp. 401–406.

[2] E. Dyban, E. Epik, and T. T. Suprun, *Characteristics of the Laminar Boundary Layer in the Presence of Elevated Free-Stream Turbulence*, Fluid Mech.-Soviet Res., 5, (1976), pp. 30–36.

[3] E. Dyban, E., and E. Epik, *Thermal/Mass Transport and Hydrodynamics of Turbulent Flows*, Kiev (in Russian) 1985.

[4] H. W. Emmons, *The Laminar-Turbulent Transition in a Boundary Layer Part I* J. Aero. Sci., Vol. 18, (1951), pp. 490–498.

[5] J. O. Hinze, *Turbulence*, McGraw-Hill, 1975.

[6] C. C. Lin, *Motion in the Boundary Layer with a Rapidly Oscillating External Flow*, Proc. 9th Int. Congress Appl. Mech., Brussels, 4, (1957), pp. 155–167.

[7] L. M. Mack *Transition Prediction and Linear Stability Theory*, AGARD CP 224, (1977), pp. 1-1 to 1-22.

[8] R. E. Mayle, *The Role of Laminar-Turbulent Transition in Gas Turbine Engines*, 1991 ASME International Gas Turbine Institute Scholar Award Paper, ASME Journal of Turbomachinery, 113,(1991), pp. 509–537.

[9] P. E. Roach, *The Generation of Nearly Isotropic Turbulence by Means of Grids*, Int. J. Heat & Fluid Flow, 8, (1987), pp. 82–92.

[10] P. E. Roach, and D. H. Brierley, *The Influence of a Turbulent Free-Stream on Zero Pressure Gradient Transitional Boundary Layer Development Including the T3A & T3B Test Case Conditions*, Proc. 1st ERCOFTAC Workshop on Numerical Simulation of Unsteady Flows, Transition to Turbulence and Combustion, Lausanne, 1990.

[11] Rolls-Royce, Transmittal by J. Coupland of data from the Rolls-Royce Applied Science Laboratory 1993.

[12] H. Schlichting, *Boundary-Layer Theory*, McGraw-Hill, New York, 1979.

[13] K. Sieger, A. Schulz, S. Wittig, and M. E. Crawford, 1993, *An Evaluation of Low-Reynolds Number k-e Turbulence Models for Predicting Transition Under the Influence of Free-Stream Turbulence and Pressure Gradient*, Proc. 2nd Int. Sym. Engng. Turb. Modeling & Measurements, Florence, Italy, pp. 593–602.

[14] Smith , A.M.O., *Transition, Pressure Gradient and Stability Theory*, IX Int. Congr. Appl. Mech., Brussels, 1956.

Figures

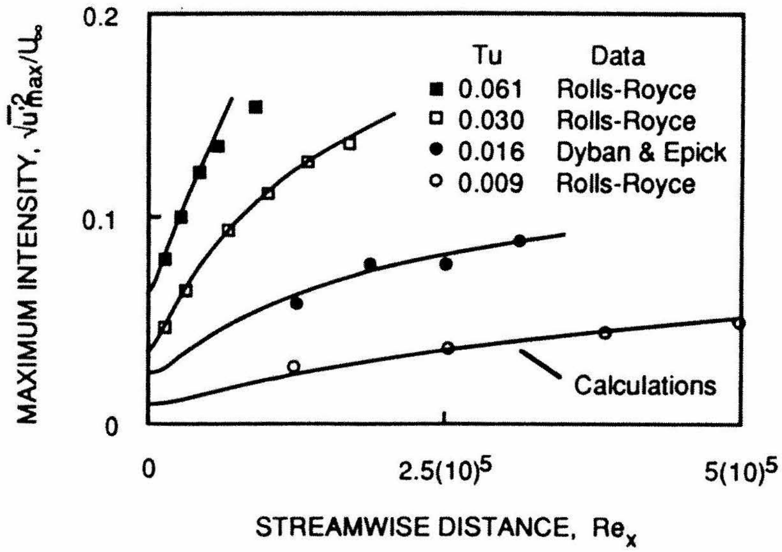

Fig. 1. A comparison of the calculations with measurements.

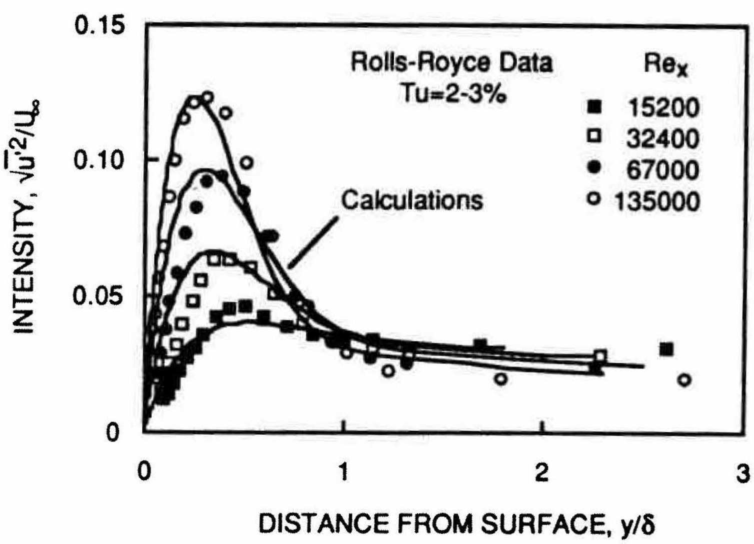

Fig. 2a. Calculated and measured intensity profiles for one set of free-stream conditions.

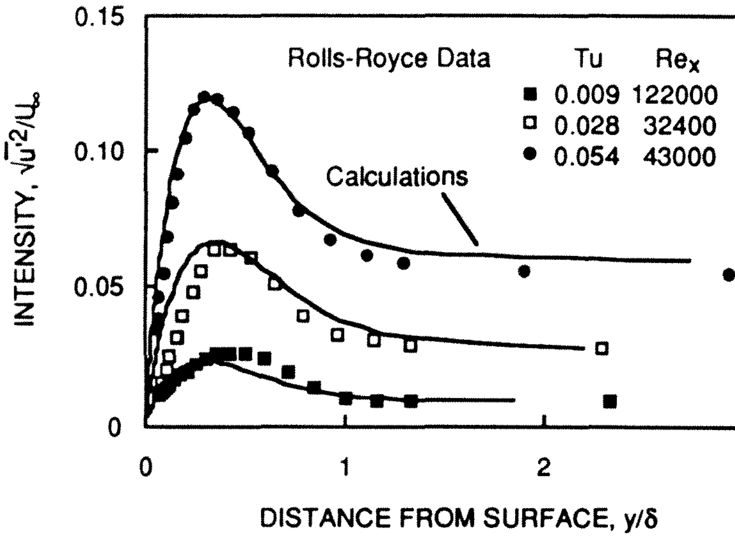

Fig. 2b. Calculated and measured intensity profiles for three different sets of free-stream conditions.

Two-Dimensional Transonic Jet Flow: Small Disturbance Theory

Scott E. Rimbey*

Dedicated to Julian Cole on the occasion of his seventieth birthday.

Abstract

A study is made of transonic flow of a gas through a two-dimensional nozzle. Of particular interest are the shape of the sonic line and the conditions at which the maximal mass flux (choking) occurs. The angle of the nozzle wall to the horizontal is assumed to be small so that transonic small disturbance theory is used. Boundary value problems for the stream function are established in the hodograph (velocity) plane and then type-sensitive finite difference versions of the partial differential equations are solved numerically by the method of line relaxation. The resulting technique is also applicable to axisymmetric jet flow and to other problems in transonic flow.

1 Introduction

The flow of a compressible gas through converging plane walls which are open at one end is studied. The gas is at rest far upstream and the flow smoothly accelerates toward the opening. Symmetry with respect to the axis is assumed and therefore only the upper half of the flow need be considered. The situation is as shown in Figure 1. A typical streamline is shown with the arrows indicating the direction of flow.

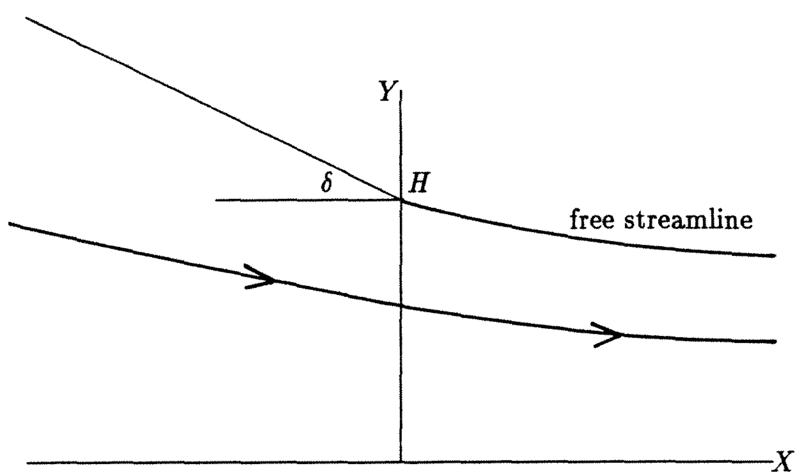

FIG. 1. *Jet Flow*

As the gas exits from the opening into the still atmosphere, it forms a jet whose boundary is a free streamline. If steady motion is assumed, the pressure is constant on this slipstream. Bernoulli's equation then implies the velocity is also constant on the

*University of Delaware, Dept. of Mathematical Sciences, Newark, DE 19716

slipstream. Different values of this velocity are obtained by altering the pressure in the surrounding atmosphere. Specifically, lowering the pressure increases the velocity. Thus, corresponding to the free streamline velocity, the jet can be classified as subsonic, sonic, or supersonic. Since the flow is stagnant far upstream, the supersonic jet is actually a transonic flow problem and is of primary interest here.

The shape of the free streamline is unknown. It is therefore very difficult to solve this problem in the physical plane. This obstacle is overcome, however, by using the velocity, or hodograph, plane. Since the velocity along the slipstream is a known constant, the unknown boundary in the physical plane maps to a known curve in the hodograph. A second difficulty in dealing with the physical plane is the inherent nonlinearity of the governing partial differential equations. The hodograph plane is again of significant value in this regard since the equations become linear.

The wall angle δ in Figure 1 is assumed small, thus allowing the use of transonic small disturbance (TSD) theory. The reasons for this assumption are two-fold. First, the equations of TSD two-dimensional theory are simpler than those of exact two-dimensional theory, but retain all the essential features of the flow. The results here can therefore serve as a guide when computing the exact case [10]. Second, one of the goals of this research is to study the axisymmetric transonic jet. Little work has been done on this problem, primarily because the governing equations remain nonlinear in the hodograph. The TSD framework will again be used for initial investigations of the axisymmetric case and the TSD two-dimensional results will provide a useful benchmark.

In the following the equations of TSD theory are developed and applied to the supersonic jet problem. The boundary value problem in the hodograph plane is established and then solved using finite differences. Results are compared to values resulting from an eigenfunction expansion. Comparisons of supersonic jets with different exit velocities concentrate on the shape of the sonic line and the amount of mass flowing through the opening. To facilitate the latter, the discharge coefficient C_d is defined as the actual mass flux divided by the mass flux of an ideal (one-dimensional) nozzle having the same throat area and operating with the same gas at the same pressure ratio. Thus,

$$C_d = \frac{\text{actual mass flux}}{2\rho^* a^* H}, \tag{1}$$

where H is the nozzle half-width and ρ^* and a^* are the density and speed of sound, respectively, at sonic conditions.

2 Equations of Transonic Small Disturbance Theory

The flow is assumed to be steady, irrotational, inviscid, and isentropic. Under these conditions a velocity potential Φ can be introduced such that $\Phi_X = u$ and $\Phi_Y = v$, where u and v are the X and Y components of velocity. The potential Φ satisfies the system of equations (cf. [4]):

$$\left\{ \begin{array}{c} \dfrac{\Phi_X^2 + \Phi_Y^2}{2} + \dfrac{a^2}{\gamma - 1} = \dfrac{\gamma + 1}{\gamma - 1}\dfrac{a^{*2}}{2} \\[2ex] (a^2 - \Phi_X^2)\Phi_{XX} - 2\Phi_X\Phi_Y\Phi_{XY} + (a^2 - \Phi_Y^2)\Phi_{YY} = 0. \end{array} \right\} \tag{2}$$

In these equations a is the local speed of sound and a^* is the speed of sound when the Mach number is equal to one. Also, γ is the ratio of specific heats ($\gamma = 1.4$ for air).

The equations of transonic small disturbance (TSD) theory are now developed; these are based on the assumption of a small wall angle δ. For the supersonic jet, discussed in Section 1, most of the action occurs near the wall opening, where the flow accelerates through sonic conditions. It is therefore desirable to introduce a variable x which "stretches out" the axial flow near the jet exit [3]. The dimensionless variables x and y are defined as

$$x = \frac{1}{\delta^{1/3}(\gamma+1)^{1/3}}\frac{X}{H} \quad \text{and} \quad y = \frac{Y}{H}.$$

Note that the lines $y =$ constant yield the streamlines (to leading order in TSD theory).

The flow velocity in these coordinates remains near a^* and therefore a perturbation potential ϕ is defined as

$$\Phi(X,Y) = a^*(X + \delta H \phi(x,y) + \cdots). \tag{3}$$

Insertion of (3) into the system (2) yields the second-order nonlinear equation for ϕ :

$$-\phi_x\phi_{xx} + \phi_{yy} = 0. \tag{4}$$

Defining the variables $w = \phi_x$ and $\vartheta = \phi_y$, equation (4) can be written as the pair of equations

$$\left\{ \begin{array}{c} -ww_x + \vartheta_y = 0 \\ \\ w_y - \vartheta_x = 0. \end{array} \right\} \tag{5}$$

The discussion has been limited so far to the physical plane, with x and y as independent variables and w and ϑ as dependent variables. Reversing these roles leads to the hodograph plane. The following relations hold:

$$\left\{ \begin{array}{ll} x_w = \frac{1}{j}\vartheta_y, & y_w = -\frac{1}{j}\vartheta_x \\ \\ x_\vartheta = -\frac{1}{j}w_y, & y_\vartheta = -\frac{1}{j}w_x, \end{array} \right\} \tag{6}$$

where $j = \dfrac{\partial(w,\vartheta)}{\partial(x,y)} = w_x\vartheta_y - \vartheta_x w_y$ is the jacobian. Substitution of (6) into (5) yields

$$\left\{ \begin{array}{c} -wy_\vartheta + x_w = 0 \\ \\ y_w - x_\vartheta = 0. \end{array} \right\} \tag{7}$$

Combining equations (7) produces Tricomi's equation for y:

$$wy_{\vartheta\vartheta} - y_{ww} = 0, \tag{8}$$

which is linear!

Equation (8) is elliptic for $w < 0$ (subsonic flow), parabolic for $w = 0$ (sonic flow), and hyperbolic for $w > 0$ (supersonic flow). The variable w thus measures the perturbation from sonic.

By standard methods [4], equations (7) are written in characteristic form as

$$\left\{ \begin{array}{l} \vartheta_\alpha - (\frac{2}{3}w^{3/2})_\alpha = 0 \\ \\ \vartheta_\beta + (\frac{2}{3}w^{3/2})_\beta = 0 \end{array} \right\} \tag{9}$$

$$\left\{ \begin{array}{l} x_\alpha - \sqrt{w}y_\alpha = 0 \\ \\ x_\beta + \sqrt{w}y_\beta = 0, \end{array} \right\} \tag{10}$$

where α and β are the characteristic coordinates. It is easily seen that real characteristics occur only in supersonic flow ($w > 0$). Equations (9) can be explicitly integrated to show the characteristics are members of two families of semi-cubic curves. The characteristic coordinates are chosen as

$$\alpha = \vartheta + \frac{2}{3}w^{3/2} \quad \text{and} \quad \beta = \vartheta - \frac{2}{3}w^{3/2}. \tag{11}$$

Combining equations (9) then gives

$$8w^{3/2}y_{\alpha\beta} - y_\alpha + y_\beta = 0. \tag{12}$$

3 Boundary Value Problem for the Supersonic Jet

The jet flow depicted in Figure 1 has several inherent boundary conditions. These boundary conditions are given first in terms of the full velocity potential Φ and then translated to the perturbation potential ϕ. To do so, note from (3):

$$\Phi_X = a^*(1 + \frac{\delta^{2/3}}{(\gamma+1)^{1/3}}\phi_x + \cdots) \quad \text{and} \quad \Phi_Y = a^*(\delta\phi_y + \cdots).$$

Also, recall the definitions $w = \phi_x$ and $\vartheta = \phi_y$.

The first boundary condition is that the flow is stagnant far upstream. Thus, $\sqrt{u^2+v^2} = \sqrt{\Phi_X^2 + \Phi_Y^2} = 0$ as $X \to -\infty$. In terms of ϕ this requires $w = \phi_x \to -\infty$ as $x \to -\infty$. Second, no mass flows across the X axis. Hence, $v = \Phi_Y = 0$ on $Y = 0$. The implication for TSD variables is $\vartheta = \phi_y = 0$ on $y = 0$. Third, the flow is tangent on the wall: $v/u = \Phi_y/\Phi_X = -\tan\delta$ on $Y = H - (\tan\delta)X$ ($X < 0$) and, fourth, the velocity is constant on the free streamline. These translate respectively to $\vartheta = \phi_y = -1$ on $y = 1$ ($x < 0$) and $w = \phi_x =$ constant on $y = 1$ ($x > 0$). The last boundary condition to be satisfied is that the wall and the slipstream form one streamline. This condition has already been satisfied in TSD coordinates by the above prescription on $y = 1$, since the streamlines are given by $y =$ constant.

The nature of the boundary value problem changes considerably depending on the value chosen for w on the free streamline, w_{fs}. As discussed in Section 1 this value can be varied by changing the pressure in the external atmosphere. Since w equals zero at sonic, the jet is subsonic (supersonic) if w_{fs} is less than (greater than) zero. The supersonic jet is of interest here since the problem is then transonic. The supersonic jets to be considered are bounded by two limiting cases, given in terms of lower and upper bounds for the range of w_{fs}. At the low end is the sonic jet where w_{fs} equals zero. At the high end is the choked jet, which will be discussed shortly.

When the pressure in the surrounding atmosphere is low enough to make the jet supersonic, the flow must turn from subsonic along the vessel wall to a supersonic velocity w_{fs} along the free streamline. This turn is made by a simple wave, or Prandtl-Meyer expansion.

The picture in the physical plane for the supersonic non-choked jet is shown in Figure 2. A fan of expansion waves (shown as dashed lines) emanates from point b. These are reflected from the sonic line bx_s as compression waves (shown as solid lines), which in turn are reflected from the free streamline bd as expansion waves. The waves are actually characteristics and carry information about the presence of the free streamline to the sonic line and thus to the entire subsonic (elliptic) domain. The last expansion wave dx_s which hits the sonic line is called the limit characteristic. The flow upstream of the limit characteristic must be solved as one transonic flow problem. However, the flow downstream of dx_s is wholly supersonic and can be determined separately (once the upstream flow is calculated) by the method of characteristics. This flow has no bearing on either the shape of the sonic line or the mass flux and is not calculated here.

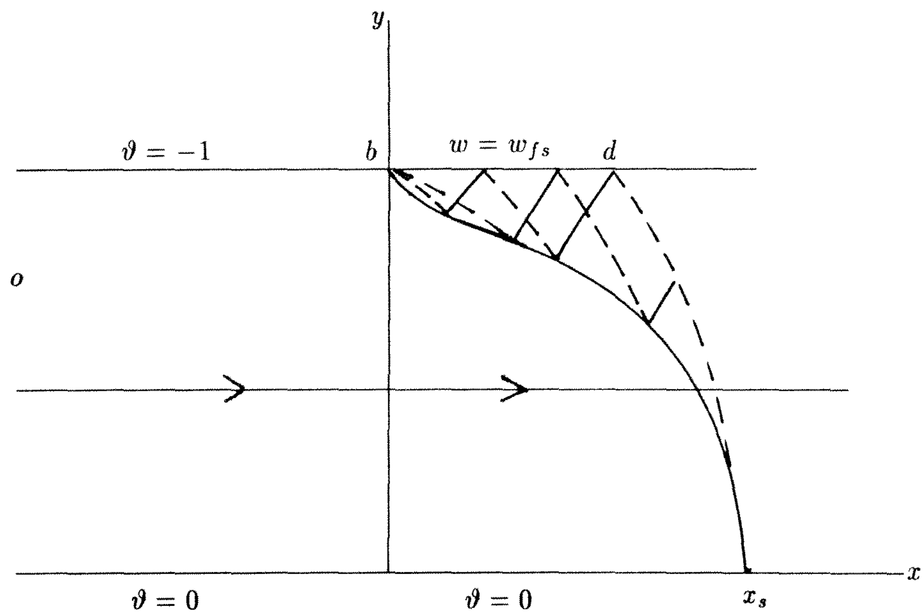

FIG. 2. *Supersonic Jet (Physical Plane)*

The boundary value problem for w and ϑ in the (x, y) physical plane is now cast into a boundary value problem for the approximate stream function y in the (w, ϑ) hodograph plane. Mapping the flow in Figure 2 into the hodograph plane requires two well-known facts [4]. First, characteristics in the physical plane map to characteristics in the hodograph plane. Second, a simple wave is mapped to an arc of a characteristic in the hodograph.

The supersonic jet maps to the hodograph plane as shown in Figure 3. The unprimed points map to primed points. The Prandtl-Meyer expansion at b maps to the arc $b'b''$. Also, all streamlines flow into the limit characteristic $d'x'_s$. This infers a time-like direction for the flow, with time increasing in the direction of the arrows. This is important for numerical calculations.

To complete the specification of the boundary value problem, the function $y_u(\vartheta)$ must be determined. This function represents the far field behavior of the streamlines at upstream infinity (stagnation) and is found by integrating Tricomi's equation (8): $y \to y_u(\vartheta) = -\vartheta$ as $w \to -\infty$.

3.1 Sonic Jet

Lowering the velocity w_{fs} to zero gives rise to the sonic jet. In this case the free streamline and the sonic line are the same. The Prandtl-Meyer expansion is no longer needed to turn the flow from subsonic to supersonic velocities. However, Ovsiannikov [8] has proven an interesting phenomenon occurs: a uniform sonic state is achieved inside the exact two-dimensional jet at a finite distance from the opening, $x = x_s$. A corresponding result for the TSD two-dimensional jet is shown in Cole and Cook [3].

In the hodograph plane the points b' and b'' now coincide, as do x'_s and d'. Since all the streamlines reach the uniform sonic state, the mapped streamlines all flow into the origin in the hodograph plane. This singularity is sufficiently benign to require no special treatment in the numerical procedure.

3.2 Choked Jet

If the velocity w_{fs} is increased sufficiently, the points b and d in Figure 2 coincide. Equivalently, points b'' and d' in Figure 3 are the same. In this case characteristics from the free streamline no longer reach the sonic line and thus further increase of w_{fs} no longer has any effect on the shape of the sonic line or the mass flux. The value of the discharge coefficient C_d, defined by equation 1, stays at this, its maximal, value. This situation is known as choked flow.

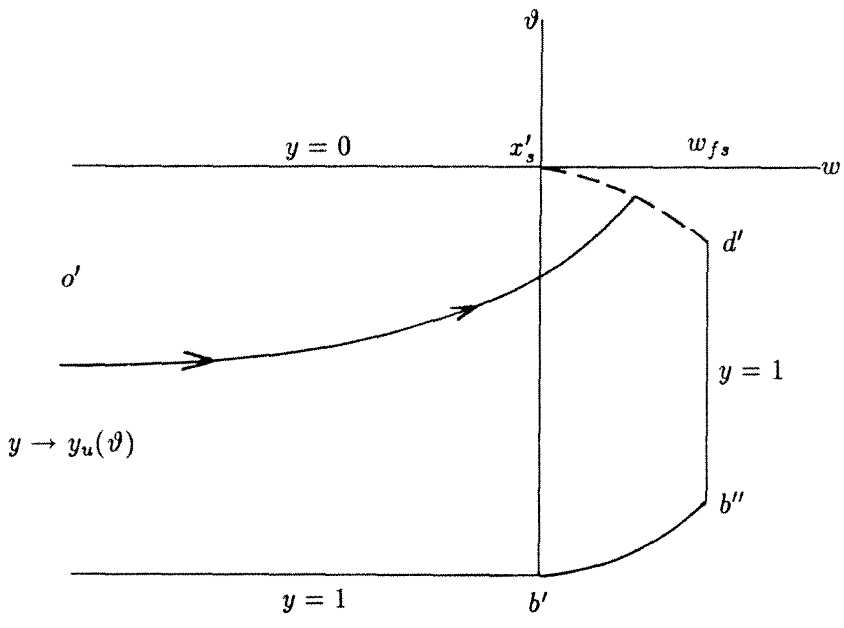

FIG. 3. *Supersonic Jet (Hodograph Plane)*

4 Finite Difference Calculations

To solve the boundary value problem, finite differences are employed and a mesh is established as in Figure 4. Relaxation by lines is used to converge to the answer. Each line consists of a segment ϑ = constant in the elliptic region ($w < 0$) and a characteristic arc β = constant in the hyperbolic region ($w > 0$). The relaxation starts at the bottom and marches upward toward the limit characteristic.

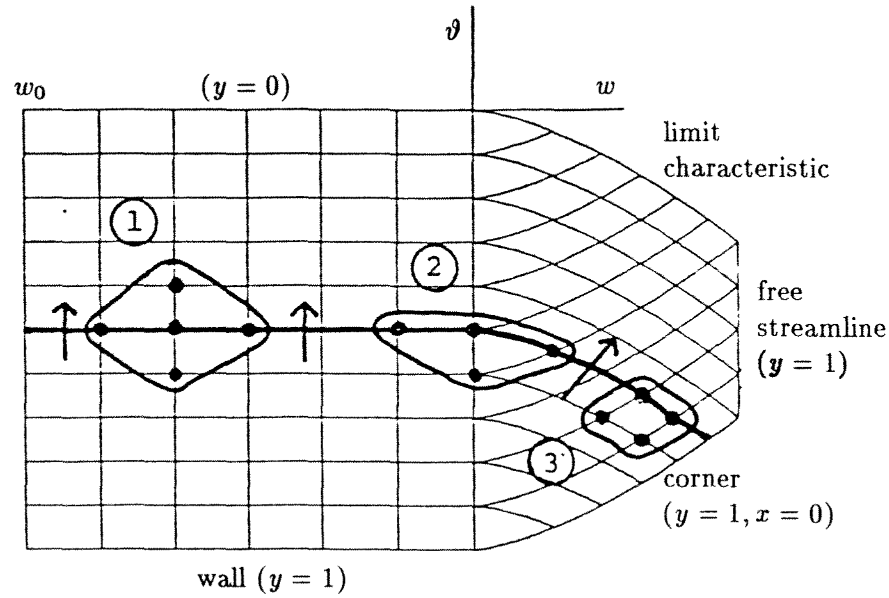

FIG. 4. *Finite Difference Grid*

There are, in general, three different difference schemes on a line (see Figure 4). Scheme (1) is a standard 5-point difference operator used for elliptic points. The centered nature of the scheme models the behavior of elliptic equations, where a disturbance at any point can influence all the neighboring points. Scheme (3) is a 4-point difference operator used for hyperbolic points. The scheme is not centered since disturbances in hyperbolic regions propagate along the characteristics. In other words, downstream points must be prohibited from influencing upstream points. The orientation of upstream and downstream is determined by the flow direction, which was discussed in Section 3. Finally, scheme (2) is used for sonic points. This type-sensitive finite differencing is in the spirit of the technique pioneered by Murman and Cole [6] for transonic flow calculations in the physical plane (where the sonic line location is unknown). The present method is less demanding since the location of the sonic line is known in the hodograph plane.

Tricomi's equation (8) is differenced for subsonic points and equation (12) is differenced for supersonic points. For sonic points ($w = 0$), Tricomi's equation reduces to $y_{ww} = 0$. Differencing this equation involves three points on a line ϑ = constant, as shown in Figure 5. However, the region of influence of point C does not include point B and therefore point C should not be used when calculating values at the sonic point B. Failure to avoid this leads to an unstable numerical scheme. Therefore, the value of y at C is replaced by an equivalent relation (derived from Taylor series) depending on the values of y at points D and E. These points include point B in their region of influence. The four points A, B, D, and E lead to scheme (2) in Figure 4.

Initially, y is set equal to $y_u(\vartheta)$ at all the grid points. The whole grid is then iterated line by line until the difference between successive y values at a point is less than some set tolerance ϵ. Good results require $\epsilon = 0.00001$. Along each line schemes (1)–(3) are linked together to form an implicit scheme, which requires solving a tridiagonal system. The solution provides new values for y at each point along the line. The number of iterations of the whole grid drops dramatically if point overrelaxation is used to update y at each elliptic point on the line and point underrelaxation is used at each hyperbolic point. By experimentation an overrelaxation factor of 1.8 and an underrelaxation factor of 0.85 were found to give the best results. Typically 100 steps are used in each direction of the subsonic portion to partition the grid; convergence is obtained in a few hundred iterations. The domain of the grid, which should extend to $w = -\infty$, must be truncated at some finite negative value w_0. Satisfactory results are obtained for $w_0 = -3$ and the function $y_u(\vartheta)$, defined above, is then prescribed at w_0 instead of $-\infty$ (see Figure 4).

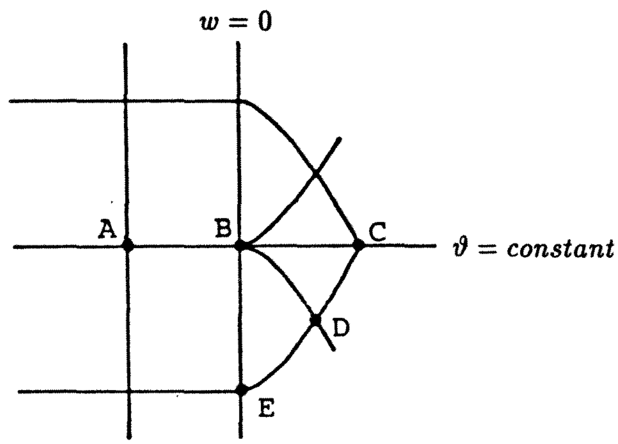

FIG. 5. *Finite Difference Scheme for Sonic Points*

The above discussion and figures are for the supersonic jet. The sonic jet and choked jet are limiting cases and the restrictions imposed should be obvious.

After converging to the values for the stream function y, other calculations of interest are made. The y-coordinates along the sonic line $w = 0$ are at hand and the corresponding x-coordinates are found by integrating equations (7) with the trapezoidal rule. The x-coordinates in the supersonic region are obtained by integrating equations (10). The trapezoidal rule is again employed and the initial values are along the sonic line.

Results for the sonic line for the sonic jet ($w_{f_s} = 0$), several supersonic jets and the choked jet ($w_{f_s} = 0.8255$) are shown in Figure 6. The figure shows there is a continuous deformation of the sonic line from the sonic jet through choked jet cases. Also, the sonic line becomes more vertical as w_{f_s} increases. This is to be expected since C_d is approaching the one-dimensional value of 1 and therefore the sonic line should approach the one-dimensional result of a vertical line lying along the x-axis.

The discharge coefficient C_d defined by (1) is also calculated. In the context of TSD theory, the formula for C_d is

$$C_d = 1 - \delta^{4/3}(\gamma + 1)^{1/3} I, \quad \text{where} \quad I = \int_{-1}^{0} x^* d\vartheta. \tag{13}$$

The values of x^* are the x-coordinates on the sonic line ($w = 0$).

The calculations for the sonic line and the integral I are independent of γ and δ. However, as equation (13) indicates, these parameters must be specified to find C_d. Typical values of C_d using $\gamma = 1.4$ and $\delta = 10°$ are shown in Table 1 in the next section. The value of C_d increases from the sonic through the choked jet cases. A further increase of w_{fs} past choked flow does not change C_d, since the mass flow is then at its maximum. In the case of the sonic jet, the discharge coefficient C_d has a further significance. It can be shown [9] that the value of C_d is equal to that of the contraction coefficient C_c of the sonic jet. The contraction coefficient is defined as the ratio of the y-coordinate when the final asymptotic (sonic) state is reached to the y-coordinate at the nozzle exit.

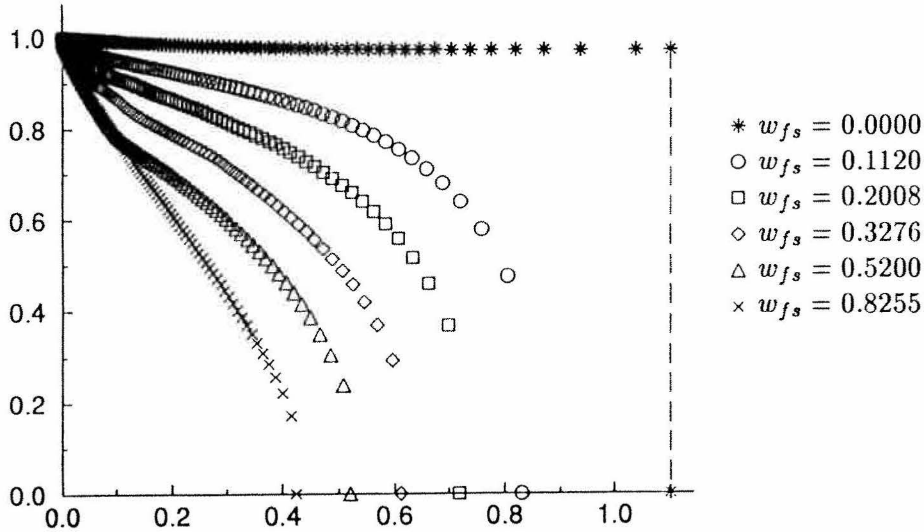

FIG. 6. *Sonic Line for different choices of* w_{fs}

5 Eigenfunction Expansion

Since Tricomi's equation is linear, an eigenfunction expansion for the solution to the jet flow problem can be found [3]. This provides a useful means of checking the results from the finite difference scheme. The series is obtained by the usual means of separation of variables and is given by

$$y(w, \vartheta) = -\vartheta + \sum_{m=1}^{\infty} a_m \sin(m\pi\vartheta) Ai(-(m\pi)^{2/3} w), \tag{14}$$

where $Ai(z)$ is Airy's function. This solution satisfies the boundary conditions on the axis and the wall and the condition at upstream infinity.

For the sonic jet the coefficients a_m can be explicitly determined by satisfying the condition $y = 1$ on the free streamline $b's'$ in Figure 3. The result is

$$a_m = -\frac{2}{m\pi Ai(0)}.$$

For the supersonic jet the boundary condition $y = 1$ is imposed at K points along the characteristic arc $b'b''$ and the line segment $b''d'$ in Figure 3. The coefficients a_m are then calculated by the method of least squares. The series (14) will thus satisfy the conditions at the corner and on the free streamline.

Setting $w = 0$ in (14) produces the y-coordinates of the sonic line. To obtain the corresponding x-coordinates, equations (7) are integrated. Results for the discharge coefficient for the sonic jet, a typical supersonic jet, and the choked jet are shown in Table 1.

For the sonic jet, 100 terms in (14) were taken. For the supersonic cases, 20 terms in (14) were used and $K = 100$. The corresponding values using the method of finite differences are also shown. The correlation between the two methods is quite good.

w_{fs}	finite differences	series
0.0000 (sonic)	0.96926	0.96931
0.5200 (supersonic)	0.98096	0.98105
0.8255 (choked)	0.98233	0.98242

TABLE 1

Values of Discharge Coefficient (for $\gamma = 1.4$ and $\delta = 10°$)

6 Conclusions And Future Work

The method of type-sensitive line relaxation in the hodograph plane gives accurate results for two-dimensional TSD transonic jet flow. The method can also be applied to the equations of exact two-dimensional flow [10]. The approach is to again use the hodograph plane and establish a boundary value problem for the stream function Ψ. This is directly analogous to the TSD formulation since in that context the stream function is given to leading order by y.

Other work on the exact two-dimensional transonic jet has proceeded along the same two lines shown in this paper: eigenfunction expansions and finite differences (both in the hodograph plane). Chaplygin [2] and Frankl [5] used an eigenfunction expansion analogous to that in Section 5 to study the sonic and choked jets, respectively. These series results provide a useful check of the finite difference results, but will be unavailable for the nonlinear axisymmetric case.

Norwood [7] and Alder [1] used finite differences to study the problem. Norwood used an equivalent mesh to that shown in Figure 4, but his method of iteration was different. A guess was made of the Ψ distribution on the sonic line and the subsonic and supersonic portions of the grid were solved separately. Accuracy was then measured by the difference in values of the normal derivative of Ψ at sonic calculated from subsonic and supersonic iterates. The process was repeated until this difference was acceptably small. Alder also made a guess of the Ψ distribution on the sonic line, but then solved for elliptic points in the hodograph plane by nonlinear overrelaxation and for hyperbolic points in the physical plane by the method of characteristics. Accuracy was measured by the deviation of the results from the known lip and free streamline conditions. The process was repeated until this difference was exceptably small. Both of these methods yield results in agreement with [10]. However, the method of line relaxation seems preferable since it solves for the subsonic and supersonic portions at the same time.

The method has also been successfully applied [9] to the sonic and choked cases for the axisymmetric transonic small disturbance jet. Current work is underway to obtain results for the intermediate supersonic axisymmetric TSD jets. The approach still uses the hodograph plane, but is complicated by the nonlinearity of the axisymmetric hodograph equations. Ultimately, it is hoped the exact axisymmetric transonic jet can be treated. The only known work on this problem is that of Alder [1].

References

[1] G. M. Alder, *The Numerical Solution of Choked and Supercritical Ideal Gas Flow through Orifices and Convergent Conical Nozzles*, J. Mech. Eng. Sci., 21 (1979), pp. 197–203.

[2] S. A. Chaplygin, *Gas Jets*, NACA TM 1063, 1944.

[3] J. D. Cole and L. P. Cook, *Transonic Aerodynamics*, North-Holland, Amsterdam, 1986.

[4] R. Courant and K. O. Friedrichs, *Supersonic Flow and Shock Waves*, Interscience, New York, 1948.

[5] F. I. Frankl, *The Flow of a Supersonic Jet from a Vessel with Plane Walls*, Tech. Report F-TS-1213-IA, Headquarters Air Materiel Command, 1947.

[6] E. M. Murman and J. D. Cole, *Calculation of Plane Steady Transonic Flows*, AIAA Journal, 9 (1971), pp. 114–121.

[7] R. E. Norwood, *Two-Dimensional Transonic Gas Jets*, Proc. 4th U.S. National Cong. Appl. Mech., 2 (1962), pp. 1359–1367.

[8] L. V. Ovsiannikov, *Gas Flow with Straight Transition Line*, NACA TM 1295, 1951.

[9] S. E. Rimbey, *Transonic Jets: A Numerical Approach in the Hodograph Plane*, Ph.D. Dissertation, Department of Mathematics, UCLA, 1984.

[10] S. E. Rimbey, *Two-Dimensional Transonic Jet Flow*, To be submitted.

Theoretical Study of The Axisymmetric Vortex Breakdown Phenomenon

Z. Rusak and S. Wang *

Abstract

We summarize in this paper a recent theory of the nearly axisymmetric vortex breakdown in a pipe. The theory is built of global analysis of the steady state solutions to the Euler equations that describe the motion of an axisymmetric and inviscid swirling flow in a pipe and of linear stability analysis of the various steady state solutions under certain boundary conditions that may reflect the physical situation. The theory unifies the major previous theoretical approaches and provides for the first time a consistent explanation of the physical mechanism leading to the vortex breakdown phenomenon as well as the conditions for its occurrence.

1 Introduction

Vortex breakdown is a remarkable phenomenon in fluid dynamics which is referred to as the abrupt change in structure that may occur in high Reynolds number vortex flows with an axial flow component and where the level of swirl is high. It is usually characterized by a sudden deceleration of the axial flow over a relatively short distance and the formation of a free stagnation point in the flow, followed by a large separation zone and turbulence behind it. Several breakdown patterns have been observed, ranging from highly asymmetric spiral waves to almost axisymmetric bubble type disturbances. The vortex breakdown phenomena may have applications in the technologies of high angles of attack aerodynamics, combustion chambers, hydrocyclone separators and are common in atmospheric vortices such as tornados. Several review papers on this subject have been presented, including the reports by [6], [10], [11] and [5]. Those papers show that previous efforts to explain vortex breakdown are based on local analyses and therefore mask important information on the possible development of swirling flows. Vortex breakdown is considered today as a basic scientific problem that is yet unexplained with a variety of technological applications.

This paper concentrates on the axisymmetric vortex breakdown phenomenon. Numerical simulations of the Navier-Stokes equations of axisymmetric swirling flows in a pipe have recently been able to present solutions that may describe vortex breakdown [3],[2],[13]. The numerical results show that there exists a range of swirl ratios ω (ratio of the circumferential speed to axial speed) where multiple solutions are found (see Figure 1). There exists one branch of almost columnar flow solutions that is connected at a limit swirl ratio to another branch of solutions, that may describe a localized bubble in the swirling flow.

*Department of Mechanical Engineering, Aeronautical Engineering and Mechanics, Rensselaer Polytechnic Institute, Troy, New York 12180-3590

Also, there exists another limit swirl ratio where the branch of localized bubble solutions turns into a branch of solutions describing a large separation zone in the flow. The stability of those branches of solutions have been tested numerically and it has been found that the almost columnar flow solutions and the large separation zone solutions are stable to axisymmetric perturbations, whereas the connecting branch of localized bubble solutions is unstable. This unique behavior of solutions to Navier-Stokes equations is not fully understood and a theoretical study to explain it may shed light on the development of breakdown phenomena in swirling flows.

The theoretical analyses of the vortex breakdown phenomena have suggested several different classes of explanations:

1. Hall[6] showed that the quasi-cylindrical approximation to the Navier-Stokes equations fails to describe swirling flow solutions above a certain level of swirl in analogy to boundary layer separation.

2. Benjamin[1] showed that swirling flows are characterized by a critical state where $\omega = \omega_1$ that is related to the ability of the flow to sustain standing, axisymmetric small disturbance waves. Supercritical vortex flows have low swirl ratios, where $\omega < \omega_1$, and are unable to support such waves, while subcritical flows have high swirl ratios, where $\omega > \omega_1$, and are able to sustain standing waves.

3. Leibovich and Kribus[12] showed that the critical state is a singular transcritical bifurcation point of steady solutions to the Euler equations and stationary axisymmetric solitary waves may bifurcate at this state and can exist only in a supercritical swirling flow. They numerically continued this branch of solutions for any $\omega < \omega_1$ and down to almost zero swirl ratio where large nonrealistic separation zones were found.

4. In another approach, Keller and Egli[9] described the axisymmetric vortex breakdown in a pipe as a transition around a stagnation zone of free boundaries. Their solution matches between given inlet columnar flow conditions and another outlet columnar flow solution that has the same "flow force". However, this solution is limited only to a specific value of the swirl, defined as ω_0, where $\omega_0 < \omega_1$.

5. Stability analyses of swirling flows [14], [7], [8] show that as ω is increased the flow is usually neutrally stable to axisymmetric perturbations and no relation with the critical swirl was found. As was pointed out by Leibovich [11], breakdown can occur in a vortex flow with just a little sign of instability and a vortex flow can become unstable without any breakdown phenomenon. However, all of the known stability analyses are based on an axial Fourier modeof disturbance and such a mode can not reflect the physical situation where the inlet conditions have a strong influence on the flow.

The bifurcation diagram in Figure 1 summarizes the state of art at 1995 of solutions to the vortex breakdown phenomenon. Here the minimum of axial speed w along the pipe centerline is chosen as the parameter to characterize a solution. When $w < 0$ a stagnation point and a separation zone appear in the flow. This figure demonstrates the greate confusion in the theoretical explanation of vortex breakdown. There is no clear relation between the solutions of Leibovich and Kribus[12] and Keller and Egli [9] as well as no correlation between inviscid steady solutions and the numerical simulations of viscous swirling flows. Also, stability analyses do not reflect the change of stability around the limit points as was found in the numerical studies of Beran [2] and Lopez [13] and show no relation with vortex breakdown phenomenon.

We summarize in this paper a recent theory of the nearly axisymmetric vortex breakdown in a pipe. The theory is built of two major steps: a) Global analysis of all the steady state solutions to the Euler equations that describe the motion of an axisymmetric

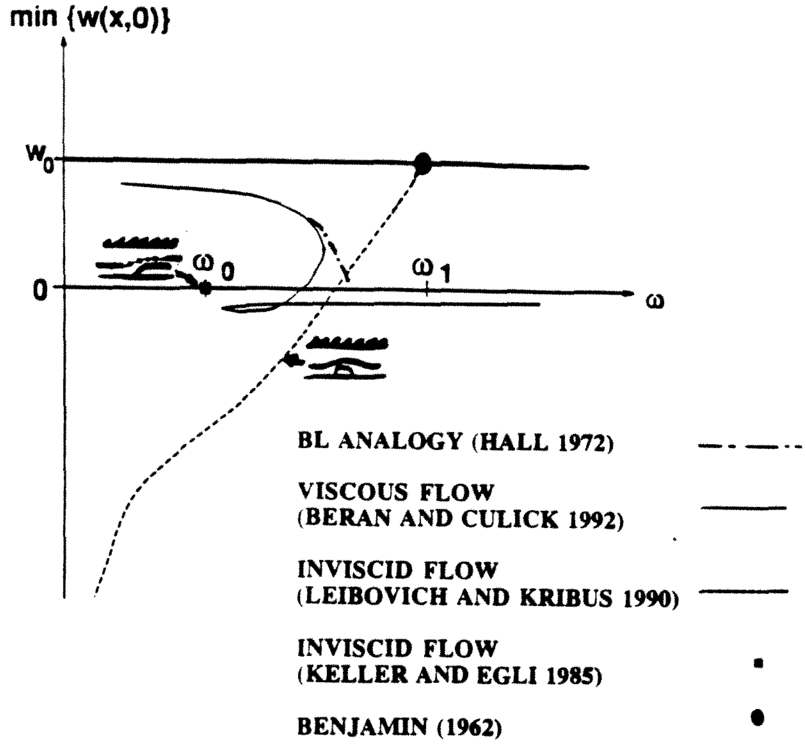

Figure 1: bifurcation diagram

and inviscid swirling flow in a pipe; b) Linear stability analysis of the various steady state solutions under certain boundary conditions that may reflect the physical situation. The theory unifies the major previous theoretical approaches, shows the relations between them, nicely correlates with the numerical simulations and provides for the first time a consistent explanation of the physical mechanism leading to the vortex breakdown phenomenon as well as the conditions for its occurrence. For the detailed mathematical analysis of the phenomenon see the recent papers by Wang and Rusak [16], [17],[18].

2 Mathematical Model

An axisymmetric, incompressible and inviscid flow with swirl is considered in a finite length pipe of a unit radius, the centerline of which is the x-axis and where $0 \leq x \leq x_0$. The axial and radial distances are rescaled with the radius of the pipe. By virtue of the axisymmetry, a stream function $\psi(x,r,t)$ can be defined where the radial component of velocity $u = -\psi_x/r$, and the axial component of velocity $w = \psi_r/r$. Let $y = r^2/2$, then the azimuthal vorticity is given by $\chi = -(\psi_{yy} + \psi_{xx}/2y)$. The circulation function K is defined as $K = rv$ where v is the circumferential velocity. The equations which connect the development in time (t) of the stream function ψ, azimuthal vorticity χ and the circulation function K may be given by

$$K_t + \{\psi, K\} = 0,$$

$$\chi_t + \{\psi, \chi\} = \frac{1}{4y^2}(K^2)_x. \qquad (1)$$

Here the brackets $\{\psi, K\}$ and $\{\psi, \chi\}$ are defined by

$$\begin{aligned} \{\psi, K\} &= \psi_y K_x - \psi_x K_y, \\ \{\psi, \chi\} &= \psi_y \chi_x - \psi_x \chi_y. \end{aligned} \tag{2}$$

We study the development of the flow in the pipe with certain conditions posed on the boundaries. For any time t we set $\psi(x,0,t) = 0$ to satisfy the axisymmetry along the pipe centerline, and $\psi(x, 1/2, t) = w_0$ to describe the total mass flux across the pipe. Also, for any time t we set along the inlet $x = 0$

$$\psi(0,y,t) = \psi_0(y), \quad K(0,y,t) = \omega K_0(y), \quad \psi_{xx}(0,y,t) = 0, \quad \chi(0,y,t) = -\psi_{0yy} \tag{3}$$

and along the pipe outlet $x = x_0$

$$\psi_x(x_0, y, t) = 0. \tag{4}$$

Similar boundary conditions have been considered by Beran and Culick [3] and Lopez [13] in their numerical simulations and may also reflect the physical situation as reported in Bruecker and Althaus's [4] experiments. The problem defined by equations (1) through (4) is well posed and describes the evolution of a swirling flow in a finite length pipe.

3 Study of Steady State Solutions

When the flow is steady equations (1)-(4) may be reduced to the Squire-Long equation (SLE)

$$\psi_{yy} + \frac{\psi_{xx}}{2y} = H'(\psi) - \frac{I'(\psi)}{2y} \quad \text{on} \quad 0 \le x \le x_0, \quad 0 \le y \le 1/2 \tag{5}$$

with boundary conditions

$$\psi(0,y) = \psi_0(y), \quad K(0,y) = \omega K_0(y), \quad \psi_{xx}(0,y) = 0, \quad \psi_x(x_0,y) = 0 \tag{6}$$

Here, H is the total head function of the flow, $H = p/\rho + (u^2 + w^2 + v^2)/2$, and $I = K^2/2$ is the extended circulation function. H and I are functions of ψ only due to the conservation of mechanical energy and angular momentum of inviscid flows. Also, from the inlet conditions those are fixed functions for given profiles $\psi_0(y)$, $K_0(y)$ and the swirl ratio ω. For relevant inlet flows such as the Rankine vortex model or the "Q-vortex" model it can be shown that both H and I are nonlinear functions of ψ; H is approximately a linear function of ψ and I is approximately a quadratic function of ψ when ψ is small, and both functions are constant when ψ is near w_0. This nonlinearity may give rise to multiple solutions of Eqs. (5) and (6) for a fixed value of the swirl ratio ω.

The approach presented here is a global variational approach and is summarized in Wang and Rusak [15]. Solutions of the SLE correspond to the stationary points of the following functional

$$\mathbf{E}(\psi) = \int_0^{x_0} \int_0^1 \left(\frac{\psi_y^2}{2} + \frac{\psi_x^2}{4y} + H(\psi) - \frac{I(\psi)}{2y}\right) dy\,dx. \tag{7}$$

We study the properties of $\mathbf{E}(\psi)$. We first rigorously prove that for any given swirl ω when $H(\psi)$ and $I(\psi)$ are bounded and piecewise smooth non-negative functions with bounded first derivatives and when $I(\psi) \leq c|\psi|^p$ (where p is a fixed number, $1 < p \leq 2$, and $c > 0$), the global minimizer $\min_{\psi \in W_b^{1,p}(\Omega, \frac{1}{y})} \mathbf{E}(\psi)$ exists and is denoted by $\psi_g(x,y)$. Here, Ω is the domain $0 \leq x \leq x_0, 0 \leq y \leq 1/2$ and $W_b^{1,p}(\Omega, \frac{1}{y})$ is the closure of the smooth functions satisfying the boundary conditions in the weighted Sobolev space with the norm

$$||f||_{W^{1,p}(\Omega,\frac{1}{y})} = \left(\int_0^{x_0}\int_0^1 (|f_y|^p + \frac{|f_x|^p}{y} + |f|^p)dydx\right)^{\frac{1}{p}}. \tag{8}$$

Then, we prove the relation between $\psi_g(x,y)$ and the minimizer of the columnar problem of (5) (the x-independent problem) with the same functions $H(\psi)$ and $I(\psi)$ which is denoted by $\psi_s(y)$. We show that as the length of the pipe x_0 is increased $\psi_g(x_0,y)$ tends to $\psi_s(y)$. This means that the global minimizer of the PDE (5) is strongly controlled by the minimizer of the x-independent problem (ODE) resulting from (5) and actually describes a transition along the pipe from state $\psi_0(y)$ along the inlet to state $\psi_s(y)$ along the outlet.

Now, by studying the behavior of the columnar functional resulting from (7) we are able to show that as ω is increased there exists a certain swirl ratio, ω_0, that was actually found by Keller and Egli [9], across which the minimizer of the columnar functional abruptly changes its nature. When $\omega < \omega_0$ we find that $\psi_s(y) = \psi_0(y)$ and when $\omega > \omega_0$ the minimizer $\psi_s(y)$ is a different state that must have a stagnation zone along a finite range $0 \leq y \leq y_s$. Therefore, we can show that when $\omega < \omega_0$ the global minimizer of $\mathbf{E}(\psi)$ describes a columnar flow all along the pipe, $\psi_g(x,y) = \psi_0(y)$. However, when $\omega > \omega_0$ the global minimizer of $\mathbf{E}(\psi)$ describes a noncolumnar flow with a separation zone which may describe an axisymmetric vortex breakdown solution.

We can also show that there exists a critical level of swirl $\omega = \omega_1$ where for $\omega < \omega_1$ the columnar flow solution $\psi(x,y) = \psi_0(y)$ is a local minimizer of $\mathbf{E}(\psi)$ and when $\omega > \omega_1$ it is a min-max point of $\mathbf{E}(\psi)$. The critical swirl is calculated by the eigenvalue problem

$$\begin{gathered}\psi_{1yy} + \frac{\psi_{1xx}}{2y} - (H''(\psi_0;\omega_1) - \omega_1^2\frac{\tilde{I}''(\psi_0)}{2y})\psi_1 = 0,\\ \psi_1(x,0) = \psi_1(x,1/2) = 0 \text{ for every } 0 \leq x \leq x_0,\\ \psi_1(0,y) = \psi_{1x}(x_0,y) = 0 \text{ for every } 0 \leq y \leq 1/2\end{gathered} \tag{9}$$

which is the linearized SLE. Here, $\tilde{I} = K_0^2(y)/2$. We can show that

$$\psi_1(x,y) = \Phi(y)sin(\frac{\pi}{2x_0}x). \tag{10}$$

Here Φ is the eigenfunction that corresponds to the critical swirl ω_1. Both Φ and ω_1 are determined by the eigenvalue problem

$$\begin{gathered}\Phi_{yy} - (\frac{\pi^2/4x_0^2}{2y} + H''(\psi_0;\omega_1) - \frac{\omega_1^2\tilde{I}''(\psi_0)}{2y})\Phi = 0,\\ \Phi(0) = 0, \quad \Phi(1/2) = 0.\end{gathered} \tag{11}$$

When x_0 tends to infinity ω_1 tends to the critical swirl ratio of Benjamin [1].

We rigorously prove the existence of a branch of min-max solutions of (7) for any swirl ratio $\omega_0 < \omega < \omega_1$ which connects the solution of Keller and Egli [9] at $\omega = \omega_0$ with the critical state at $\omega = \omega_1$. The proof uses the "Mountain-Pass Theorem" from nonlinear analysis. The min-max solution describes a swirling flow in a pipe that may have a localized

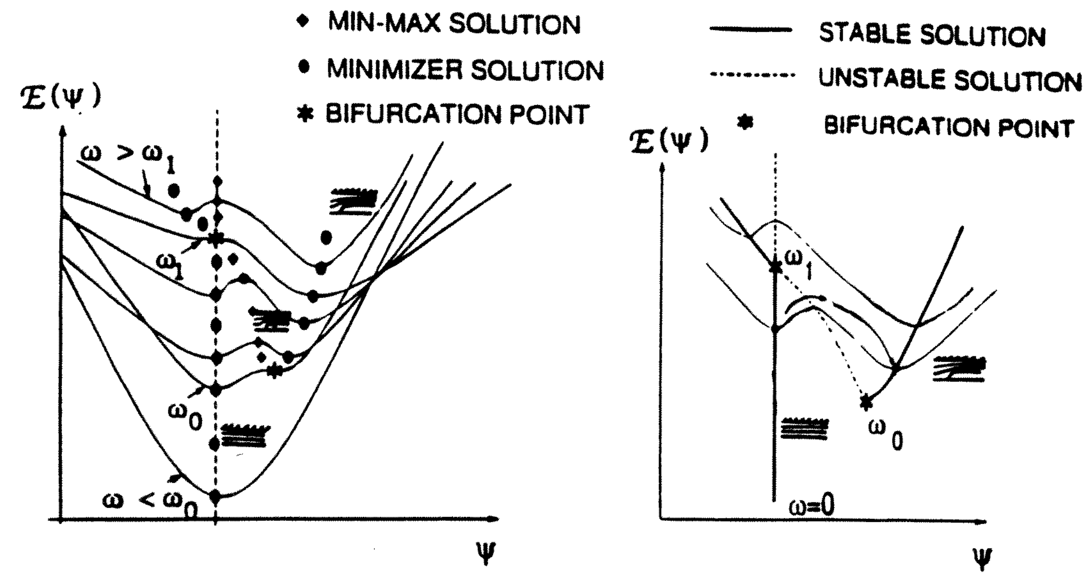

Figure 2: bifurcation diagram

separation zone. It can be shown that for a long pipe this branch of solutions is actually Leibovich and Kribus's [12] solitary wave solutions near the critical state.

The above results can be summarized in the bifurcation diagrams in Figures 2 and 3. We find that for $\omega < \omega_1$ the inlet flow $\psi_0(y)$ develops as a columnar flow all along the pipe and is a global minimizer of $\mathbf{E}(\psi)$ and a unique solution of (1). When ω is larger than the threshold value ω_0 we find for relatively long pipes three possible solutions of the SLE. One is the trivial columnar solution $\psi_0(y)$ that develops all along the pipe and is a local minimizer of $\mathbf{E}(\psi)$. The two other solutions bifurcate at about ω_0 from a certain state which is a large disturbance to the columnar solution. One is the global minimizer of $\mathbf{E}(\psi)$ which describes a strong open separation zone. The global minimizer solution is the extension of Keller and Egli [9] solution for $\omega > \omega_0$. The second solution is the min-max point of $\mathbf{E}(\psi)$ which describes a closed bubble in the swirling flow. The family of min-max points of $\mathbf{E}(\psi)$ also bifurcates at ω_0. As the swirl is increased toward ω_1 we find that the family of min-max solutions tends toward the critical state of the inlet flow and bifurcates from this state.

As swirl is increased a little above the critical level ω_1 the columnar flow solution becomes a min-max point of $\mathbf{E}(\psi)$ and a new branch of local minimizer solutions bifurcates at ω_1 and may describe a non-columnar flow where the rotating flow is intensified along the pipe and has a smaller vortical core. The third possible solution when $\omega > \omega_1$ is the global minimizer solution described above, where now it can be shown that the separation zone becomes much larger and moves toward the inlet. The results also show that the critical swirl is actually a transcritical bifurcation point from which various branches of local minimizer solutions and min-max solutions may develop.

Figure 3 shows our results in terms of the bifurcation diagram described in Figure 1. We

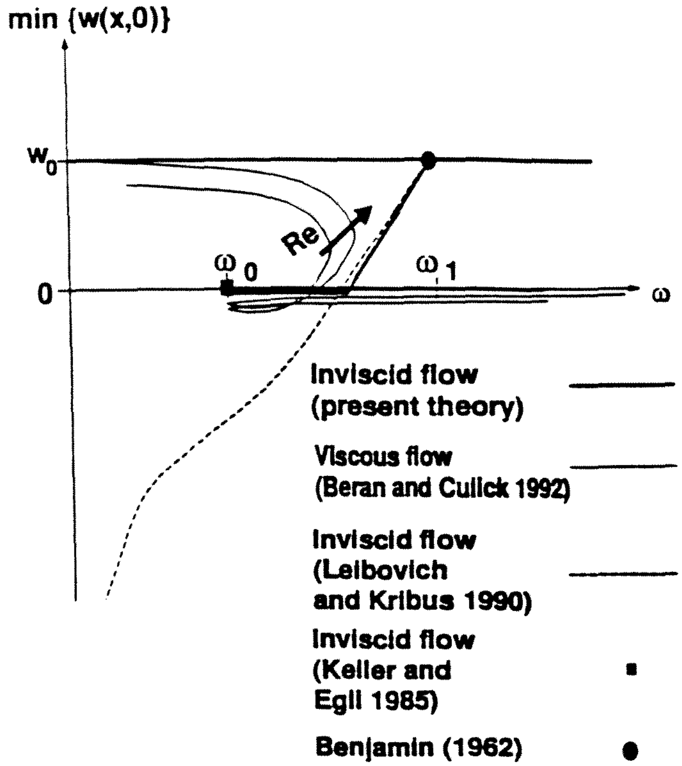

Figure 3: bifurcation diagram

can see that the bifurcation picture of the SLE (steady Euler equations) unifies between the theories of Benjamin [1], Leibovich and Kribus [12] and the special solution of Keller and Egli [9] and provides for the first time the relations between the various solutions as well as fills the gap between them. It is also evident that the bifurcation picture of the SLE is similar to the bifurcation picture resulting from numerical simulations of the Navier-Stokes equations and strongly dominates it.

4 Study of Linear Stability of Steady State Solutions

In this section we show the relation between the critical state at the swirl level ω_1 and the stability of the vortex flow. We study the linear stability of the various branches of solutions bifurcating at the critical state. From the theory of dynamical systems it is strongly expected that the critical level of swirl is also a point of exchange of stability. The stability analyses are summarized in Wang and Rusak [17],[18]. The analysis is based on studying the development of a general mode of disturbance (which is not an axial Fourier mode) and its interaction with the inlet conditions.

4.1 Stability of Columnar Swirling Flows

We consider first a steady, swirling and columnar flow where $\psi = \psi_0(y)$ and $K = \omega K_0(y)$. This base flow is a steady state solution of (1) through (4). It is also a solution of the Squire - Long equation (5) with boundary conditions (6). To study the stability of this base flow we let

(12) $\psi(x,y,t) = \psi_0(y) + \epsilon_1\psi_1(x,y,t) + \dots, \quad K(x,y,t) = \omega K_0(y) + \epsilon_1 K_1(x,y,t) + \dots$

where ψ_1 is the disturbance stream function and K_1 is the circulation disturbance. On substituting these expressions into (1) and neglecting second order terms, we obtain the linearized equations of motion of the swirling flow

$$\begin{aligned} &K_{1t} + \psi_{0y}K_{1x} - K_{0y}\psi_{1x} = 0, \\ &-\frac{K_0}{2y^2}K_{1x} + \chi_{1t} + \psi_{0y}\chi_{1x} - \chi_{0y}\psi_{1x} = 0. \end{aligned} \tag{13}$$

Here $\chi_1 = -(\psi_{1yy} + \psi_{1xx}/2y)$ is the disturbance of the azimuthal vorticity. From boundary conditions (3) and (4) we find that the solution to the system (13) must satisfy

$$\begin{aligned} &\psi_1(x,0,t) = 0, \quad \psi_1(x,1/2,t) = 0, \quad \text{for every } (0 \le x \le x_0, t), \\ &\psi_1(0,y,t) = 0, \quad \psi_{1xx}(0,y,t) = 0, \quad K_1(0,y,t) = 0 \quad \text{for every } (0 \le y \le 1/2, t), \\ &\psi_{1x}(x_0,y,t) = 0 \quad \text{for every } (0 \le y \le 1/2, t). \end{aligned} \tag{14}$$

We can also show from (14) that $\chi_1(0,y,t) = 0$. This means that no azimuthal vorticity disturbance is introduced along the inlet.

A suitable mode analysis of (13) and (14) is considered

$$\psi_1 = \phi(x,y)e^{\sigma t}, \quad K_1 = k(x,y)e^{\sigma t} \tag{15}$$

where in the general case the growth rate σ may be a complex number and $\phi(x,y)$ and $k(x,y)$ are complex functions. We obtain

$$\begin{aligned} &(\phi_{yy} + \frac{\phi_{xx}}{2y} - (H''(\psi_0;\omega) - \frac{\omega^2 \tilde{I}''(\psi_0)}{2y})\phi)_{xx} \\ &+\frac{\sigma\chi_{0y}}{\psi_{0y}^2}\phi_x + \frac{2\sigma}{\psi_{0y}}(\phi_{yy} + \frac{\phi_{xx}}{2y})_x + \frac{\sigma^2}{\psi_{0y}^2}(\phi_{yy} + \frac{\phi_{xx}}{2y}) = 0, \end{aligned} \tag{16}$$

with boundary conditions

$$\begin{aligned} &\phi(x,0) = 0, \quad \phi(x,1/2) = 0, \quad \text{for every } 0 \le x \le x_0, \\ &\phi(0,y) = 0, \quad \phi_{xx}(0,y) = 0, \\ &\phi_{yyx}(0,y) + \frac{\phi_{xxx}(0,y)}{2y} - (H''(\psi_0;\omega) - \frac{\omega^2\tilde{I}''(\psi_0)}{2y})\phi_x(0,y) = 0 \\ &\phi_x(x_0,y) = 0 \quad \text{for every } 0 \le y \le 1/2. \end{aligned} \tag{17}$$

Equation (16) with boundary conditions (17) is an eigenvalue problem for the solution of the growth rate σ as function of the swirl level ω.

It can be noticed that when $\sigma = 0$ the eigenvalue problem reduces to (9). Therefore, there exists a neutrally stable mode of disturbance at the specific critical swirl ω_1 and it is given by (10). Moreover, when the swirl changes around the critical swirl it is expected that σ may change its sign and so the critical state is a state of exchange of stability.

To demonstrate this idea we first studied the special case of a solid body rotation with a uniform axial speed where $w = w_0, v = \omega r, u = 0$ or $\psi_0 = w_0 y$, $K_0 = 2y$. In this case the eigenvalue problem (16) - (17) can be solved using the method of separation of variables. Results show that when the flow is supercritical an asymptotically stable mode is found and when the flow is subcritical an unstable mode is found. This result is strongly related with the boundary conditions (16) - (17) and is rather surprising. It is very different from Rayleigh's[14] criterion that predicts the stability of solid body rotation with a uniform axial flow to any axial Fourier mode of disturbance.

For the case of a general swirling flow in a pipe we use asymptotic techniques in the limit ω tends to ω_1 and σ tends to zero and find asymptotic solutions to the eigenvalue problem (16) - (17). We find that for the columnar flow solutions

$$\frac{\sigma_R}{\omega^2-\omega_1^2} = \frac{\pi^2}{4x_0} \frac{\int_0^{1/2} \frac{\bar{I}'(\psi_0)}{2y^2\psi_{0y}} \Phi^2(y)dy}{\int_0^{1/2} [\omega_1^2 \frac{\bar{I}'(\psi_0)}{y^2\psi_{0y}^2} + \frac{\psi_{0yyy}}{\psi_{0y}^2}]\Phi^2(y)dy} > 0. \tag{18}$$

Here σ_R is the real part of the growth rate σ and $\Phi(y)$ is the solution of (11). Equation (18) shows that the transcritical point of bifurcation at ω_1 is also a point of exchange of stability of the columnar flow $\psi = \psi_0(y)$ and $K = \omega K_0(y)$. When the columnar flow is subcritical it is linearly unstable.

4.2 Stability of Noncolumnar Swirling Flows

The stability analysis of the noncolumnar flow solutions bifurcating from the critical state is more involved. We consider a base, steady and non-columnar swirling flow where $\psi = \Psi_0(x,y)$ and $K = K_*(x,y)$. This base flow is a steady state solution of (1) through (4) for which $K_* = K_*(\Psi_0)$ and $\Psi_0(x,y)$ is a solution of the Squire-Long equation (5).

To study the stability of this base flow we let

$$\psi(x,y,t) = \Psi_0(x,y) + \epsilon_1\psi_1(x,y,t) + \ldots, \quad K(x,y,t) = K_*(x,y) + \epsilon_1 K_1(x,y,t) + \ldots \tag{19}$$

On substituting these expressions into (1) and neglecting second order terms, we then obtain the linearized equations of motion of the swirling flow

$$\begin{aligned} &K_{1t} + \Psi_{0y}K_{1x} - K_{*y}\psi_{1x} + K_{*x}\psi_{1y} - \Psi_{0x}K_{1y} = 0, \\ &\chi_{1t} + \Psi_{0y}\chi_{1x} - \chi_{0y}\psi_{1x} + \chi_{0x}\psi_{1y} - \Psi_{0x}\chi_{1y} = \frac{(K_*K_1)_x}{2y^2}. \end{aligned} \tag{20}$$

Here, $\chi_0 = -(\Psi_{0yy} + \Psi_{0xx}/2y)$. Using the mode of disturbance given by (15) we get an integro-differential equation for solving ϕ

$$\begin{aligned} &\sigma^2\int_0^x \bar{\chi}_1 dx - \sigma\int_0^x [\Psi_{0y}(\mathbf{L}(\phi))_x - \Psi_{0x}(\mathbf{L}(\phi))_y]dx + \sigma\frac{I'(\Psi_0)}{2y^2}\phi + \sigma\Psi_{0y}\bar{\chi}_1 \\ &-\Psi_{0y}[\Psi_{0y}(\mathbf{L}(\phi))_x - \Psi_{0x}(\mathbf{L}(\phi))_y] - \frac{\Psi_{0x}}{y^2}[y^2\int_0^x (\sigma\bar{\chi}_1 - \Psi_{0y}(\mathbf{L}(\phi))_x + \Psi_{0x}(\mathbf{L}(\phi))_y)dx]_y = 0 \end{aligned} \tag{21}$$

where $\bar{\chi}_1 = -(\phi_{yy} + \phi_{xx}/2y)$ and $\mathbf{L}(\psi_1) = \psi_{1yy} + \frac{\psi_{1xx}}{2y} - (H''(\Psi_0) - \frac{I''(\Psi_0)}{2y})\psi_1$. Equation (21) with boundary conditions (17) (where ψ_0 should be replaced with Ψ_0) form a complicated eigenvalue problem for determining the the growth rate σ as function of ω. However, in the limit ω tend to ω_1 we can show that

$$\Psi_0(x,y;\omega) = \psi_0(y) + (\omega^2 - \omega_1^2)\kappa_0\psi_1(x,y) + \ldots,$$

$$\kappa_0 = -2\frac{\int_0^{1/2}\int_0^{x_0} \frac{\tilde{I}'(\psi_0)}{2y^2\psi_{0y}}\psi_1^2 dx dy}{\int_0^{1/2}\int_0^{x_0}(\omega_1^2\frac{\tilde{I}'''(\psi_0)}{2y} - H'''(\psi_0;\omega_1^2))\psi_1^3 dx dy} \tag{22}$$

where $\psi_1(x,y)$ is the given by (10). Using asymptotic techniques in the limit ω tends to ω_1 and σ tends to zero we can find asymptotic solution to this problem and show that for the noncolumnar branch of solutions bifurcating at the critical state

$$\frac{\sigma_R}{\omega^2 - \omega_1^2} = -\frac{\pi^2}{4x_0}\frac{\int_0^{1/2}\frac{\tilde{I}'(\psi_0)}{2y^2\psi_{0y}}\Phi^2(y)dy}{\int_0^{1/2}[\omega_1^2\frac{\tilde{I}'(\psi_0)}{y^2\psi_{0y}^2} + \frac{\psi_{0yyy}}{\psi_{0y}^2}]\Phi^2(y)dy} < 0. \tag{23}$$

We find again that the transcritical point of bifurcation at ω_1 is a point of exchange of stability of the branches of the non-columnar solutions bifurcating at ω_1.

4.3 Summary of Stability Analyses

Results of the stability analyses are also summarized in Figure 2. We can see that the branches of local minimizer solutions have an asymptotically stable mode of disturbance whereas the branches of min-max solutions are linearly unstable. Specifically, the branch of columnar flows along the pipe is asymptotically stable for $\omega < \omega_1$ and becomes unstable when $\omega > \omega_1$.

5 Conclusions

The above results shed light on the physical mechanism leading to the axisymmetric vortex breakdown phenomenon. As the swirl along the inlet of the pipe is increased toward the critical level, the base columnar vortex flow tends to lose its stability margin and definitely above the critical level it is linearly unstable (see Figure 2). Therefore, near the critical swirl ω_1, any finite perturbation that is large enough will induce a transition from the columnar state to another possible state. It is clear that the min-max solution is linearly unstable and, therefore, is not a final steady state. Moreover, the only other steady state that is possible is the global minimizer solution of the Squire-Long equation. As discussed above, the global minimizer solution exists and above a certain threshold level of swirl ω_0, it describes a swirling flow with a big separation zone that resembles the breakdown zone. Although we have not yet shown that the global minimizer solution is stable, there are strong reasons to believe that it is so. In this way, the mechanism of the axisymmetric vortex breakdown phenomenon is explained as a transition, that may occur when $\omega > \omega_0$, and definitely for the first time when $\omega < \omega_1$, from an equilibrium state of a columnar vortex flow that loses its stability and develops in a dynamical process into another completely different steady and stable equilibrium state which is the global minimizer solution for the same boundary conditions and that can be thought as a strong attractor.

Acknowledgement This research was carried out with the support of the National Science Foundation under Grant CTS-9310181, monitored by Dr. R. Powell and Dr. D.S. Ahluwalia.

References

[1] Benjamin, *T.B.* 1962 "Theory of the Vortex Breakdown Phenomenon", *Journal of Fluid Mechanics,* **14**, 593-629.

[2] Beran, P.S. 1994 "The Time-Asymptotic Behavior of Vortex Breakdown in Tubes", *Computers Fluids*, **23**, 7, 913-937.

[3] Beran, P.S. and Culick, *F.E.C.* 1992 "The Role of Non-uniqueness in the Development of Vortex Breakdown in Tubes", *Journal of Fluid Mechanics,* **242**, 491-527.

[4] Bruecker, Ch. and Althaus, W. 1995 "Study of Vortex Breakdown by Particle Tracking Velocimetry (PTV), Part 3: Time-Dependent Structure and Development of breakdown Modes," *Experiments in Fluids*, **18**, 174-186.

[5] Escudier, *M*. 1988 "Vortex Breakdown: Observations and Explanations", *Progress in Aerospace Sciences*, **25**, 189-229.

[6] Hall, M.G., 1972 "Vortex Breakdown", *Annual Review of Fluid Mechanics,* **4**, 195-217.

[7] Howard, L. N. and Gupta, A. S., 1962 " On the Hydrodynamic and Hydromagnetic Stability of Swirling Flows," *Journal of Fluid Mechanics,* **14**, 463-476.

[8] Lessen, H., Singh, P.J. and Paillet, *F.* 1974 "The Stability of a Trailing Line Vortex, Part 1: Inviscid Theory", *Journal of Fluid Mechanics,* **63**, 753-763.

[9] Keller, *J.J.* and Egli, *W.* 1985 "Force- and Loss-Free Transitions Between Flow States", Journal of Applied Mathematics and Physics (ZAMP), **36**, 854-889.

[10] Leibovich, *S*. 1978 "The Structure of Vortex Breakdown", *Annual Review of Fluid Mechanics,* **10**, 221-246.

[11] Leibovich, *S*. 1984 "Vortex Stability and Breakdown: Survey and Extension", *AIAA Journal,* **22**, 1192-1206.

[12] Leibovich, S. and Kribus, A. 1990 "Large Amplitude Wavetrains and Solitary Waves in Vortices", *Journal of Fluid Mechanics,* **216**, 459-504.

[13] Lopez, J.M. 1994 "On the Bifurcation Structure of Axisymmetric Vortex Breakdown in a Constricted Pipe", *Physics of Fluids*, **6**, 11, 3683-3693.

[14] Rayleigh, Lord, 1916 " On the Dynamics of Revolving Fluids," *Proceedings of the Royal Society of London,* **a93**, 148-154.

[15] Wang, S. and Rusak, Z. 1995a "A Theory of the Axisymmetric Vortex Breakdown in a Pipe," R.P.I. Aeronautical Engineering Report 107 (submitted to the Journal of Fluid Mechanics).

[16] Wang, S. and Rusak, Z. 1995b "On the Stability of an Axisymmetric Rotating Flow in a Pipe," R.P.I. Aeronautical Engineering Report 108 (submitted to the Physics of Fluids).

[17] Wang, S. and Rusak, Z. 1995c "On the Stability of Non-Columnar Swirling Flows," R.P.I. Aeronautical Engineering Report 109 (submitted to the Physics of Fluids).

Solution of Burgers' Equation in the Quarter Plane and Phase Shift of its Viscous Shock

Shagi-Di Shih*

Abstract

The solution of Burgers' equation defined in the quarter plane subject to an initial condition and a Dirichlet boundary condition is given in closed form by virtue of solving in closed form a linear Volterra integral equation of the second kind having a weakly singular kernel of Abel type. The phase shift of its traveling wave solution is also stated explicitly in terms of input data.

1 Introduction

In studying motion of a viscous flow in the vanishing viscosity limit, Bateman [3] considered the equation

$$\frac{\partial u}{\partial t} + u\,\frac{\partial u}{\partial x} = \epsilon\,\frac{\partial^2 u}{\partial x^2} \tag{1}$$

as an illustrative example in 1915. By assuming $u(x,t) = f(\xi)$ with $\xi = x - ct$, he reduced (1) to an ordinary differential equation

$$-c\,f'(\xi) + f(\xi)\,f'(\xi) = \epsilon\,f''(\xi),$$

from which the traveling wave solution (or the viscous shock) is found to be

$$u(x,t) = \frac{u_\ell + u_r}{2} - \frac{u_\ell - u_r}{2}\,\tanh\left\{\frac{u_\ell - u_r}{4}\,[x - ct + x_0]\right\}, \tag{2}$$

where two constants u_ℓ, u_r are related by $u_\ell > u_r$ so that u_ℓ is the left state and u_r is the right state in the sense that

$$\lim_{x \downarrow -\infty} u(x,t) = u_\ell \quad \text{and} \quad \lim_{x \uparrow \infty} u(x,t) = u_r \qquad \text{hold.}$$

Moreover, the wave speed c and two states are related by $c = [u_\ell + u_r]/2$. The remaining constant x_0 is not specified by Bateman.

As one system of equations to describe mathematical models of turbulence, Burgers [6] had two equations

$$\begin{cases} \dfrac{dV}{dt} &=& P - \epsilon\,V - \displaystyle\int_0^1 u^2 dx, \\[2ex] \dfrac{\partial u}{\partial t} &=& V u + \epsilon\,\dfrac{\partial^2 u}{\partial x^2} - \dfrac{\partial}{\partial x}(u^2). \end{cases}$$

*Department of Mathematics, University of Wyoming, Laramie, WY 82071-3036.

To make this system more tractable, Burgers chose $V = 0$ to obtain the equation

$$\frac{\partial u}{\partial t} + 2u\frac{\partial u}{\partial x} = \epsilon\frac{\partial^2 u}{\partial x^2} \tag{3}$$

in some subsequent papers [7], [8]. In a series of papers [9], [10], [11] on the formation of vortex sheets between 1950 and 1954, Burgers considered (1) instead of (3) due to a slight difference in some of the formulae. In addition to a discontinuity propagation with a velocity $c = u_\ell + u_r$ for $u_\ell > u_r$ by neglecting the term $\epsilon\,\partial^2 u/\partial x^2$ for small ϵ, Burgers had also been interested in a solution of the form $v(\rho)/\sqrt{t-t_0}$ with $\rho = (x - x_0)/\sqrt{t-t_0}$. Such solution may be called a *self-similar solution* in the terminology of Barenblatt and Zel'dovich [1], [2], or *viscous triangular wave solution* as in Whitham [41].

In the context of gas dynamics, Lagerstrom, Cole, and Trilling [28] introduced (1) independently as an equation approximately valid for the time-dependent development of a weak transonic shock wave. After using a substitution in (3) introduced by Burgers in papers [7], [8], Hopf [21] studied (1) by converting it to the heat equation. Cole [16] also obtained the heat equation from (1). More precisely, the transformation

$$u(x,t) = -\frac{2\epsilon}{\psi}\frac{\partial\psi}{\partial x} \tag{4}$$

had been applied by both Hopf and Cole independently to (1) defined in the half plane $-\infty < x < \infty, t > 0$ subject to the initial condition

$$u(x,0) = u_0(x), \qquad -\infty < x < \infty; \tag{5}$$

so that the function $\psi(x,t)$, which is the solution of the heat equation

$$\frac{\partial\psi}{\partial t} = \epsilon\frac{\partial^2\psi}{\partial x^2} \tag{6}$$

defined in $-\infty < x < \infty, t > 0$ subject to the initial condition

$$\psi(x,0) = \exp\left[\frac{-1}{2\epsilon}\int_0^x u_0(s)\,ds\right] \tag{7}$$

for $-\infty < x < \infty$, can be found readily to be of the form

$$\psi(x,t) = \int_{-\infty}^{\infty} K(x-\eta,t)\exp\left[\frac{-1}{2\epsilon}\int_0^\eta u_0(\sigma)\,d\sigma\right]\,d\eta, \tag{8}$$

where $K(x,t)$ is the fundamental solution of the heat operator $\partial/\partial t - \epsilon\,\partial^2/\partial x^2$ defined by

$$K(x,t) = \frac{1}{2\sqrt{\pi t\epsilon}}\exp\left(-\frac{x^2}{4t\epsilon}\right). \tag{9}$$

Based on this analytical expression given by (4), (8), Hopf proved that the solution of the Cauchy problem (1), (5) converges as $t \uparrow \infty$ to the function

$$u_{ss}(x,t) = 2\sqrt{\frac{\epsilon}{\pi t}}\,\frac{\exp\left(-\frac{x^2}{4t\epsilon}\right)}{2\left[\exp\left(\frac{M}{2\epsilon}\right)-1\right]^{-1} + \operatorname{erfc}\left(\frac{x}{2\sqrt{t\epsilon}}\right)},$$

where erfc is the complementary error function defined by

$$\operatorname{erfc}(x) = \frac{2}{\sqrt{\pi}} \int_x^\infty \exp(-s^2)\, ds,$$

if the integral

$$\int_{-\infty}^{\infty} u_0(x)\, dx = M$$

exists as a sum of two improper integrals: $\int_{-\infty}^{0} + \int_0^\infty$. Such number M is called the moment (at the time $t = 0$) of the velocity distribution by Burgers.

As far as we know in the literature, the only work of giving the phase shift x_0 of the viscous shock (2) is Lagerstrom [26], who cited L.N. Howard's result of finding the value $x_0 = (2\epsilon/u_\ell)\log(2)$ when (1) is defined in $x > 0, t > 0$ subject to the homogeneous initial condition and the constant Dirichlet boundary data $u_\ell > 0$. Lagerstrom [27] called such problem as a piston problem in fluid dynamics.

Kevorkian and Cole [25], and Kevorkian [24] studied the asymptotic behavior of the signaling problem, (1) defined in the quarter plane $x > 0, t > 0$ subject to a constant initial condition and a constant Dirichlet boundary condition, for small viscosity.

The purpose of this work is to announce an explicit formula for the solution of (1) defined in the quarter plane $x > 0, t > 0$ subject to an initial condition $u(x,0)$ and a Dirichlet boundary condition $u(0,t)$ as well as an explicit formula for the phase shift x_0 of its viscous shock (2), which is a limiting function of the exact solution as time tends to infinity.

From the historical viewpoint, one might be curious who and when named (1) after Johannes Martinus Burgers. It is interesting to know that H. Bateman reviewed Burgers' two papers [6], [7] in the Mathematical Reviews (MR), 1 (1940) #186. Moreover, C.C. Lin reviewed Burgers' papers [8], [9], [10], [11], and Hopf's paper [21] in MR 10 (1949) #270, MR 11 (1950) #752, MR 12 (1951) #648, MR 15 (1954) #961, MR 13 (1952) #846, respectively; while R. Gerber reviewed in French two Cole's works [28] and [16] in MR 12 (1951) #873, MR 13 (1952) #178, respectively. In reviewing [12], M.J. Lighthill stated that (1) has become known as "Burgers's equation," see MR 16 (1955) #969. On the other hand, Burgers [13] was aware of the fact that Bateman studied (1) in 1915.

We conclude the introduction by providing some biographical facts about Burgers. He was born in Arnhem, Netherlands, in 1895 and died of pneumonia at the Sligo Gardens Nursing Home in Takoma Park, Maryland, in 1981. He earned in 1918 a doctorate in mathematics and physics at the University of Leiden, where he studied with the world-renowned Dutch physicists H.A. Lorentz and Heike Kamerlingh Onnes. That year, he was appointed professor of aerodynamics and hydrodynamics in the Department of Mechanical Engineering and Shipping at the Technical University of Delft. In 1955, he resigned at the Technical University of Delft to become research professor at the Institute for Fluid Dynamics and Applied Mathematics (now the Institute for Physical Science and Technology), the University of Maryland, College Park. He was named professor emeritus when he retired ten years later.

2 Singular integral equation

We are interested in obtaining in closed form a solution of the Volterra integral equation of the second kind having a weakly singular kernel of Abel type

$$\gamma(t) = \phi(t) + \int_0^t \frac{\psi(\tau)}{\sqrt{t-\tau}}\gamma(\tau)\,d\tau, \qquad 0 \le t \le T; \tag{10}$$

for two given functions ϕ, ψ and a given constant T. The existence and uniqueness for a solution $\gamma(t)$ of the singular integral equation (10) is furnished by Cannon [15] with the use of the Picard iteration procedure in a Banach space of continuous functions on $0 \le t \le T$ equipped with the maximum norm. In this work, this equation is motivated by determining Robin's function of the heat operator defined in the quarter plane $x > 0, t > 0$ subject to the time-dependent Robin boundary operator, and then finding in closed form the solution of Burgers' equation defined in the quarter plane subject to a time-dependent Dirichlet boundary data. In addition, Satoh [37] derived the equation (10) having

$$\phi(t) = c, \qquad \psi(t) = \frac{-h(t)}{\sqrt{\pi}};$$

in the study of heat conduction problem for a given constant c and a given function $h(t)$. Next, Delahay [17] obtained the equation

$$\gamma(t) = \exp(t-a) - \exp(t-a)\int_0^t \frac{\gamma(\tau)}{\sqrt{t-\tau}}\,d\tau, \tag{11}$$

from the theory of stationary electrode polarography in electroanalytical chemistry; while Ghez and Lew [19] analyzed the equation

$$\gamma(t) = a\exp(-bt)\left\{1 - \exp(-t) - \int_0^t \frac{\gamma(\tau)}{\sqrt{\pi(t-\tau)}}\,d\tau\right\}, \tag{12}$$

in the study of crystal growth for given parameters a, b. Both (11) and (12) can be reduced to the form (10) with a substitution. Moreover, exact solution of equation (10) is known for some selected functions ϕ, ψ in the course of its analytical and numerical investigations since 1950 as shown in the following table.

Table 1. Known Solutions to $\gamma(t) = \phi(t) + \int_0^t \frac{\psi(\tau)}{\sqrt{t-\tau}}\gamma(\tau)\,d\tau$ for given ϕ, ψ

$\phi(t)$	$\psi(t)$	$\gamma(t)$	References
1	$-c/\sqrt{\pi}$	$\exp(c^2 t)\mathrm{erfc}(c\sqrt{t})$	Satoh [37]
$2c\sqrt{t/\pi}$	$-c/\sqrt{\pi}$	$2c\sqrt{t/\pi} - c^2 \times \int_0^t \exp(c^2 s)\mathrm{erfc}(c\sqrt{s})ds$	Mann and Wolf [31]
1	-1	$E_{1/2}(-\sqrt{\pi t})$	Friedman [18]
$2\sqrt{t/\pi}$	$-1/\sqrt{\pi}$	$\sum_{k=1}^{\infty} \frac{(-1)^{k-1} t^{k/2}}{\Gamma(k/2+1)}$	Oulés [33]
$1 + 2\sqrt{t}$	-1	1	Miller and Feldstein [32]
1	-1	$\exp(\pi t)\,\mathrm{erfc}(\sqrt{\pi t})$	Miller and Feldstein [32]
$(1+t)^{-1/2} + \pi/8$ $-\frac{1}{4}\arcsin(\frac{1-t}{1+t})$	$-1/4$	$(1+t)^{-1/2}$	Linz [29]
$c\{1 - \exp(-t)\}$	$-c/\sqrt{\pi}$	$\frac{c}{1+c^2}\{\exp(c^2 t)\,\mathrm{erfc}(c\sqrt{t}) - \exp(-t) + \frac{2c}{\sqrt{\pi}}F(\sqrt{t})\}$	Ghez and Lew [19]
$2\sqrt{t}$	-1	$1 - \exp(\pi t)\,\mathrm{erfc}(\sqrt{\pi t})$	Logan [30]
$\sqrt{t} - \pi t/2$	1	$\sqrt{t}$	Logan [30]
$\sqrt{t}\,\exp(-ct) + \frac{\pi t}{2}\times$ $\exp(-\frac{ct}{2})\{I_0(-\frac{ct}{2})$ $+I_1(-\frac{ct}{2})\}$	-1	$\sqrt{t}\,\exp(-ct)$	Logan [30]
$\exp(-t)+$ $2\sqrt{t}\,M(1;3/2;-t)$	-1	$\exp(-t)$	Brunner and Nørsett [5]
$\sqrt{t} + \pi t/2$	-1	$\sqrt{t}$	te Riele [35]
$t + \frac{4}{3}t^{3/2}$	-1	t	te Riele [35]
$t^{3/2} + \frac{3}{8}\pi t^2$	-1	$t^{3/2}$	te Riele [35]
$t^2 + \frac{16}{15}t^{5/2}$	-1	t^2	te Riele [35]
1	$c/\sqrt{\pi}$	$E_{1/2}(c\sqrt{t})$	Kershaw [23]
d	c	$dE_{1/2}(c\sqrt{\pi t})$	Brunner [4]
$2c\sqrt{t/\pi}$	$-c/\sqrt{\pi}$	$1 - E_{1/2}(-c\sqrt{t})$	Gorenflo and Vessella [20]

c and d are constants.

$\Gamma(x) = \int_0^\infty s^{x-1}\exp(-s)\,ds$ is the Gamma function.

$F(t) = \exp(-t^2)\int_0^t \exp(s^2)\,ds$ is the Dawson integral.

I_ν is a modified Bessel function.

M is the Kummer's function.

$E_\beta(t) = \sum_{n=0}^{\infty} \frac{t^n}{\Gamma(1+n\beta)}$ is the Mittag-Leffler function.

THEOREM 2.1. *Equation* (10) *has the solution of the form*

$$\gamma(t) = G(t) + \pi \int_0^t \psi^2(\tau)G(\tau) \exp\left[\pi \int_\tau^t \psi^2(s)\,ds\right] d\tau, \tag{13}$$

with

$$G(t) = \phi(t) + \int_0^t \frac{\psi(s)\phi(s)}{\sqrt{t-s}}\,ds, \tag{14}$$

if the integral

$$\int_\tau^t \frac{\psi(s)}{\sqrt{(t-s)(s-\tau)}}\,ds \tag{15}$$

is independent of t.

Proof. Equation (10) can be shown by using the Abel inversion method to be equivalent to an initial value problem for a linear first order differential equation

$$\gamma'(t) - \pi\psi^2(t)\gamma(t) = G'(t), \qquad 0 < t < T;$$

with G defined by (14), subject to the initial condition $\gamma(0) = \phi(0)$, from which the solution to (10) is determined easily. □

Note that the condition on (15) includes the case of ψ being a constant. A more general singular integral equation than (10) is investigated in [40].

3 Explicit formulae

Consider Burgers' equation (1) defined in the quarter plane $x > 0$, $t > 0$ subject to the initial condition

$$u(x,0) = u_0(x), \qquad x > 0; \tag{16}$$

and the Dirichlet boundary condition

$$u(0,t) = u_1(t), \qquad t > 0; \tag{17}$$

for two given functions u_0, u_1. The Cole-Hopf transformation (4) converts the problem (1), (16), (17) to the heat equation (6) defined in the quarter plane $x > 0$, $t > 0$ subject to the initial condition (7) for $x > 0$, and the Robin boundary condition

$$u_1(t)\,\psi(0,t) + 2\,\epsilon\,\frac{\partial\psi}{\partial x}(0,t) = 0, \qquad t > 0. \tag{18}$$

The problem of determining the unique solution of the initial boundary value problem (6), (16), (17) is equivalent to the problem of determining the unique solution of the integral equation (10) with

$$\phi(t) = \frac{1}{\sqrt{\pi t\epsilon}} \int_0^\infty \exp\left[-\frac{\eta^2}{4t\epsilon} - \frac{1}{2\epsilon}\int_0^\eta u_0(s)\,ds\right] d\eta, \qquad \psi(t) = \frac{u_1(t)}{2\sqrt{\pi\epsilon}}.$$

The necessity of solving a singular integral equation in the study of Burgers' equation defined in the quarter plane is known, see Rodin [36], Calogero and De Lillo [14], Kevorkian

[24], and Ranasinghe and Chang [34] among others. We are not aware of any work in the literature that presents a solution of the resultant singular integral equation in closed form when the quarter plane problem is subject to the time-dependent Dirichlet boundary data.

THEOREM 3.1. *Suppose that*

$$\int_\tau^t \frac{u_1(s)}{\sqrt{(t-s)(s-\tau)}}\, ds$$

is independent of t. Then the solution of the quarter plane problem (6), (7), (18) *is given by*

$$\psi(x,t) = \int_0^\infty R(x,\eta,t) \exp\left[\frac{-1}{2\epsilon}\int_0^\eta u_0(s)\, ds\right] d\eta, \tag{19}$$

where $R(x,\eta,t)$ is Robin's function of the heat operator $\partial/\partial t - \epsilon\, \partial^2/\partial x^2$ in the quarter plane $x>0$, $t>0$ subject to the Robin boundary operator $u_1(t) + 2\epsilon\, \partial/\partial x$ at $x=0$ defined by

$$R(x,\eta,t) = N(x,\eta,t) + \int_0^t u_1(\tau)\, K(x,t-\tau)\, \Gamma(\tau,\eta)\, d\tau. \tag{20}$$

Here $N(x,\eta,t)$ is Neumann's function of the heat operator $\partial/\partial t - \epsilon\, \partial^2/\partial x^2$ in the quarter plane $x>0$, $t>0$ given by

$$N(x,\eta,t) = K(x-\eta,t) + K(x+\eta,t), \tag{21}$$

with $K(x,t)$ defined by (9), *and Γ defined by*

$$\begin{aligned}
\Gamma(t,\eta) &= g(t,\eta) + \frac{1}{4\epsilon}\int_0^t u_1^2(\tau) g(\tau,\eta) \exp\left[\frac{1}{4\epsilon}\int_\tau^t u_1^2(s)\, ds\right] d\tau, \\
g(t,\eta) &= \frac{1}{\sqrt{\pi t\epsilon}} \exp\left(-\frac{\eta^2}{4t\epsilon}\right) + \frac{1}{2\pi\epsilon}\int_0^t \frac{u_1(s)}{\sqrt{s(t-s)}} \exp\left(-\frac{\eta^2}{4s\epsilon}\right) ds.
\end{aligned}$$

In particular, when $u_1(t) = u_\ell$ is a constant, then $R(x,\eta,t)$ is defined by

$$R(x,\eta,t) = N(x,\eta,t) + \frac{u_\ell}{2\,\epsilon} \exp\left(\frac{u_\ell^2 t - 2u_\ell(x+\eta)}{4\,\epsilon}\right) \operatorname{erfc}\left(\frac{x+\eta-u_\ell t}{2\sqrt{t\epsilon}}\right). \tag{22}$$

Moreover, the solution of the quarter plane problem (1), (16), (17) *is obtained via* (4) *and* (19).

A complete proof is provided in [38]. Note that Joseph [22] has the following expression for Robin's function of the initial boundary value problem (6), (7), (18)

$$R(x,\eta,t) = N(x,\eta,t) + \frac{u_\ell}{2\epsilon\sqrt{\pi t\epsilon}} \int_\eta^\infty \exp\left[-\frac{u_\ell}{2\epsilon}(\eta - z) - \frac{(x+z)^2}{4t\epsilon}\right] dz \tag{23}$$

when $u_1(t) = u_\ell$ is independent of the time. The form (23) can be reduced to (22) through integration.

As an application, one can employ (19) and (4) to study the asymptotic behavior of the initial boundary value problem (1), (16), (17) as $\epsilon \downarrow 0$, or $t \uparrow \infty$.

Finally, we have the following explicit form of the phase shift x_0 of the viscous shock (2) for the quarter plane problem (1), (16), (17). The value of the phase shift appearing in the traveling-wave solution (2) is important in the study of its asymptotic stability for large time.

THEOREM 3.2. *Suppose that*

$$\int_\tau^t \frac{u_1(s)}{\sqrt{(t-s)(s-\tau)}}\, ds$$

is independent of t. We further assume that there exist two constants u_ℓ, u_r such that

$$\lim_{t\uparrow\infty} u_1(t) = u_\ell, \qquad \lim_{x\uparrow\infty} u_0(x) = u_r, \qquad u_\ell > |u_r|;$$

and the improper integrals

$$\int_0^\infty [u_0(x) - u_r]\, dx \quad \text{and} \quad \int_0^\infty [u_1^2(t) - u_\ell^2]\, dt \qquad \text{exist.}$$

Then the solution of the quarter plane problem (1), (16), (17) *converges as $t \uparrow \infty$ to the viscous shock* (2) *where the phase shift is given by*

$$x_0 = \frac{1}{u_\ell - u_r}\left\{\int_0^\infty [u_0(x) - u_r]\, dx + 2\epsilon \log\left[\int_0^\infty H(\eta)\exp\left(-\frac{1}{2\epsilon}\int_0^\eta u_0(s)\, ds\right) d\eta\right]\right\},$$

with

$$\begin{aligned} H(\eta) \;=\; & \int_0^\infty \left\{\frac{1}{4\sqrt{\pi\tau\epsilon^3}}\exp(-\frac{\eta^2}{4\tau\epsilon}) + \frac{1}{8\pi\epsilon^2}\int_0^\tau \frac{u_1(\sigma)}{\sqrt{\sigma(\tau-\sigma)}}\exp(-\frac{\eta^2}{4\sigma\epsilon})\, d\sigma\right\} \times \\ & u_1^2(\tau)\exp\left[-\frac{u_\ell^2\tau}{4\epsilon} + \frac{1}{4\epsilon}\int_\tau^\infty [u_1^2(s) - u_\ell^2]\, ds\right] d\tau. \end{aligned}$$

In particular, H can be reduced to

$$H(\eta) = \frac{u_\ell}{\epsilon}\exp(-\frac{u_\ell\eta}{2\epsilon}),$$

when $u_1(x) = u_\ell$.

A complete proof will appear in another paper [39].

References

[1] G.I. Barenblatt, *Similarity, Self-Similarity, and Intermediate Asymptotics*, Consultants Bureau, New York, 1979.

[2] G.I. Barenblatt and Y.B. Zel'dovich, *Self-similar solutions as intermediate asymptotics*, Ann. Rev. Fluid Mech., 4 (1972), pp. 285-312.

[3] H. Bateman, *Some recent researches on the motion of fluids*, Monthly Weather Review, 43 (1915), pp. 163-170.

[4] H. Brunner, *Nonpolynomial spline collocation for Volterra equations with weakly singular kernels*, SIAM J. Numer. Anal., 20 (1983), pp. 1106-1119.

[5] H. Brunner and S.P. Nørsett, *Superconvergence of collocation methods for Volterra and Abel integral equations of the second kind*, Numer. Math., 36 (1981), pp. 347-358.

[6] J.M. Burgers, *Mathematical examples illustrating relations occurring in the theory of turbulent fluid motion*, Verh. Nederl. Akad. Wetensch. Afd. Natuurk. Sect. 1. 17 (1939), pp. 1-53.

[7] J.M. Burgers, *Applications of a model system to illustrate some points of the statistical theory of the free turbulence*, Nederl. Akad. Wetensch., Proc., 43 (1940), pp. 2-12.

[8] J.M. Burgers, *A mathematical model illustrating the theory of turbulence*, in Advances in Applied Mechanics, R. von Mises and T. von Kármán ed., 1, Academic Press, New York, 1948, pp. 171-199.

[9] J.M. Burgers, *Correlation problems in a one-dimensional model of turbulence. I, II, III, IV*, Nederl. Akad. Wetensch., Proc., 53 (1950), pp. 247-260, pp. 393-406, pp. 718-731, pp. 732-742.

[10] J.M. Burgers, *On the coalescence of wave like solutions of a simple non-linear partial differential equation. I, II, III*, Nederl. Akad. Wetensch., Proc., Ser. B, 57 (1954), pp. 45-56, pp. 57-66, pp. 67-72.

[11] J.M. Burgers, *Further statistical problems connected with the solutions of a simple non-linear partial differential equation*, Nederl. Akad. Wetensch., Proc., Ser. B, 57 (1954), pp. 159-169.

[12] J.M. Burgers, *A model for one-dimensional compressible turbulence with two sets of characteristics. I, II.* Nederl. Akad. Wetensch., Proc., Ser. B, 58 (1955), pp. 1-8, pp. 9-18.

[13] J.M. Burgers, *The Nonlinear Diffusion Equation, Asymptotic Solutions and Statistical Problems*, D. Reidel Publishing Company, Dordrecht, 1974.

[14] F. Calogero and S. De Lillo, *The Burgers equation on the semi-infinite and finite intervals*, Nonlinearity, 2 (1989), pp. 37-43.

[15] J.R. Cannon, *The One-Dimensional Heat Equation*, Addison-Wesley Publishing Company, Menlo Park, California, 1984.

[16] J.D. Cole, *On a quasi-linear parabolic equation occurring in aerodynamics*, Quart. Appl. Math., 9 (1951), pp. 225-236.

[17] P. Delahay, *Theory of irreversible waves in oscillographic polarography*, J. Am. Chem. Soc., 75 (1953), pp. 1190-1196.

[18] A. Friedman, *On integral equation of Volterra type*, J. Analyse Math., 11 (1963), pp. 381-413.

[19] R. Ghez and J.S. Lew, *Interface kinetics and crystal growth under conditions of constant cooling rate*, Journal of Crystal Growth, 20 (1973), pp. 273-282.

[20] R. Gorenflo and S. Vessella, *Abel Integral Equations: Analysis and Applications*, Lecture Notes in Mathematics, No. 1461, Springer-Verlag, New York, 1991.

[21] E. Hopf, *The partial differential equation* $u_t + uu_x = \mu\, u_{xx}$, Comm. Pure Appl. Math., 3 (1950), pp. 201-230 [Title misprinted as $u_t + uu_x = \mu_{xx}$].

[22] K.T. Joseph, *Burgers' equation in the quarter plane, a formula for the weak limit*, Comm. Pure Appl. Math., 41 (1988), pp. 133-149.

[23] D. Kershaw, *Some results for Abel-Volterra integral equations of the second kind*, in Treatment of Integral Equations by Numerical Methods, based on the Proceedings of Symposium held in Durham from 19-29 July, 1982, C.T.H. Baker and G.F. Miller, ed., Academic Press, New York, 1982, pp. 273-282.

[24] J. Kevorkian, *Partial Differential Equations: Analytical Solution Techniques*, Wadsworth & Brooks/Cole, Pacific Grove, CA, 1990.

[25] J. Kevorkian and J.D. Cole, *Perturbation Methods in Applied Mathematics*, Springer-Verlag, New York, 1981.

[26] P.A. Lagerstrom, *Laminar flow theory*, in High Speed Aerodynamics and Jet Propulsion, Volume IV: Theory of Laminar Flows, F.K. Moore ed., Princeton University Press, Princeton, New Jersey, 1964, pp. 20-285.

[27] P.A. Lagerstrom, *Matched Asymptotic Expansions: Ideas and Techniques*, Springer-Verlag, New York, 1988.

[28] P.A. Lagerstrom, J.D. Cole, and L. Trilling, *Problems in Theory of Viscous Compressible Fluids*, Monograph, California Institute of Technology, Pasadena, California, 1949.

[29] P. Linz, *Numerical methods for Volterra integral equations with singular kernels*, SIAM J. Numer. Anal., 6 (1969), pp. 365-374.

[30] J.E. Logan, *The Approximate Solution of Volterra Integral Equations of the Second Kind*, Doctoral thesis, University of Iowa, Iowa City, 1976.

[31] W.R. Mann and F. Wolf, *Heat transfer between solids and gases under nonlinear boundary conditions*, Quart. Appl. Math., 9 (1951), pp. 163-184.

[32] R.K. Miller and A. Feldstein, *Smoothness of solutions of Volterra equations with weakly singular kernels*, SIAM J. Math. Anal., 2 (1971), pp. 242-258.

[33] H. Oulés, *Résolution numérique d'une intégrale singulière*, Rev. Française Traitement Information Chiffres, 7 (1964), pp. 117-124.

[34] A.I. Ranasinghe and M.H. Chang, *Solution of the Burgers equation on semifinite and finite intervals via a stream function*, Appl. Math. Comput., 41 (1991), pp. 145-158.

[35] H.J.J. te Riele, *Collocation methods for weakly singular second-kind Volterra integral equations with non-smooth solution*, IMA J. Numer. Anal., 2 (1982), pp. 437-449.

[36] E.Y. Rodin, *On some approximate and exact solutions of boundary value problems for Burgers' equation*, J. Math. Anal. Appl., **30** (1970), 401-414.

[37] T. Satoh, *On the mathematical analysis of the problem of the conduction of heat when emissivity is variable*, J. Phys. Soc. Japan, 5 (1950), pp. 253-254.

[38] S.-D. Shih, *Explicit formula for Burgers' equation in the quarter plane with general Dirichlet boundary data*, submitted to SIAM J. Math. Anal.

[39] S.-D. Shih, *Phase shift for viscous shocks of Burgers' equation*, in preparation.

[40] S.-D. Shih, *On linear second-kind Volterra integral equations having weakly singular kernels of Abel type*, in preparation.

[41] G.B. Whitham, *Linear and Nonlinear Waves*, John Wiley, New York, 1974.

A Brief History of Gas Centrifuge Theory

Houston G. Wood III*

Abstract

The gas centrifuge process is used for the separation of isotopes and the efficient operation of these centrifuges requires accurate models of the internal flow field. In the United States, a group of scientists and engineers were engaged in developing such models; but the need for classification has delayed the reporting of many of these activities. In this paper, a brief history of the development of gas centrifuge theory in the United States is presented.

1. Introduction

Our honoree, Julian Cole, is well known for his many contributions to asymptotic analysis and to applications such as transonic flows. An area in which he has made important contributions, but with much less renown, is in the development of models of compressible flows in rapidly rotating gas centrifuges. In this paper, I will present a history of some of the efforts involved in developing such models and indicate some of Julian's contributions to the theory. For readers unfamiliar with how a gas centrifuge functions, a description is given in the Appendix.

2. History of Flow Theory

The first successful application of a gas centrifuge to separate isotopes was conducted at the University of Virginia by Beams [1] who used chlorine as the process gas. During World War II, interest turned toward separating the isotopes of uranium to produce material enriched in the fissionable isotope ^{235}U for the production of nuclear weapons. Hence, much of the work has been kept under the umbrella of classification which has made these important contributions relatively unknown.

Practitioners recognized very early the importance of understanding how to control this countercurrent flow, and one of the early attempts was by Nobel laureate P. A. M. Dirac in an unpublished report (1942, The motion in a self- fractionating centrifuge.) He considered end driven flows in the high speed approximation at uniform temperature and solved a sixth order eigenvalue problem in the perturbed angular velocity. He computed the minimum eigenvalue which corresponds to motion extending the greatest distance from the end of the cylinder.

In the late 1950's, the U.S. Atomic Energy Commission realized the need for better understanding of the internal flow field, and a group of scientists was recruited to lead this effort. Lars Onsager, a Nobel laureate from Yale, was chosen to be the chair of the group. Other members and their affiliations were George Carrier (Harvard), Sterling Colgate (Los Alamos National Laboratory), Wendell DeMarcus (University of Kentucky), Carl Eckart (Scripps Oceanographic Institute), Harold Grad (New York University), and

*Department of Mechanical, Aerospace and Nuclear Engineering, University of Virginia, Charlottesville, VA 22903

Stephen Maslen (Martin Marietta). In 1962, Carrier and Maslen [2] reported an analysis of the Ekman layers along the horizontal surfaces. Another of the results of the committee was an unpublished manuscript in 1965 by Lars Onsager entitled "Approximate solutions of the linearized flow equations." In this paper, he used a minimum principle to obtain the appropriate equations and introduced a "master potential" χ which allowed the equations to be collapsed into a single sixth order partial differential equation

$$(e^x(e^x\chi_{xx})_{xx})_{xx} + B^2\chi_{zz} = 0 \tag{1}$$

where x is the dimensionless radial variable measured in density scale heights, z is the dimensionless axial variable, and B contains the process gas information. In the high speed approximation curvature was neglected due to the "atmosphere being as flat as a pancake;" Onsager referred to this as the "pancake model" for the flow along the vertical side wall. After this, the committee felt that their work was done, and it was left for someone to implement this theory in a computer program. The committee became less active with only Onsager, DeMarcus and Maslen continuing to be involved at infrequent meetings.

In 1969, Jeffrey Morton, at the University of Virginia, and I, at the Oak Ridge Gaseous Diffusion Plant (ORGDP), began the task of implementing the theory laid out by Onsager, Carrier and Maslen. Our work was first described in the open literature in 1980 [3]. In this work, Onsager's pancake model was matched to the Ekman layers on the horizontal surfaces using the analysis due to Carrier and Maslen. The pancake equation was solved by separation of variables which gives an eigenvalue problem for the radial eigenfunctions. This provided a very accurate and efficient solution to the flow field. In 1971, complementary efforts to model the flow field by direct numerical solutions using finite difference methods to approximate forms of the Navier Stokes equations were initiated by R. A. Gentry at Los Alamos National Laboratory and J. A. Viecelli at Lawrence Livermore National Laboratory.

Onsager died in 1976, and the committee was reformed in 1979 and named the Gas Centrifuge Theory Group (GCTG) with George Carrier as chair and DeMarcus and Maslen remaining as active members. The new members of the GCTG were Julian Cole (UCLA/RPI), Stephen Crandall (MIT), J. P. den Hartog (MIT), Howard Emmons (Harvard), Harvey Greenspan (MIT), Hans Liepmann (Cal Tech), and John Miles (UCSD). I was a full time centrifuge person (FTCP) and served as liaison to the GCTG. I retained this role after I joined the faculty at the University of Virginia in 1981 until the termination of the project in 1985. The committee would be briefed several times a year by the centrifuge contractors (FTCPers.) The primary contracts with the Department of Energy were held by the University of Virginia, Union Carbide Corporation Nuclear Division (Oak Ridge, Tennessee), and AirResearch Corporation (Torrence, California.) Besides the briefings, the committee would meet as a whole for two weeks each summer to attack specific problems. These meetings were held for several years at Los Alamos; but after a few years, the committee wanted a change of restaurants. The meetings were held at EG & G in Santa Barbara for the next few years until the U. S. Gas Centrifuge project was terminated by the Department of Energy in 1985.

During the time of the GCTG's activities, all of the models were axisymmetric, but it was clear that non-symmetries existed in the flow due to such geometrical effects as the withdrawal scoops and the feed (see Figure 1.) Julian Cole undertook the effort to develop an asymptotic theory that would capture the non-axisymmetric features of the flows. This effort resulted in a dissertation by Schleiniger [4] and a proceedings publication by Schleiniger and Cole [5].

A particular non-axisymmetric flow was analyzed by Matsuda and Nakagawa [6] who considered a pie-shaped section rotating about its axis (see Figure 2.) They considered the case of a cylinder of infinite length with relatively slow rotation. This work revealed

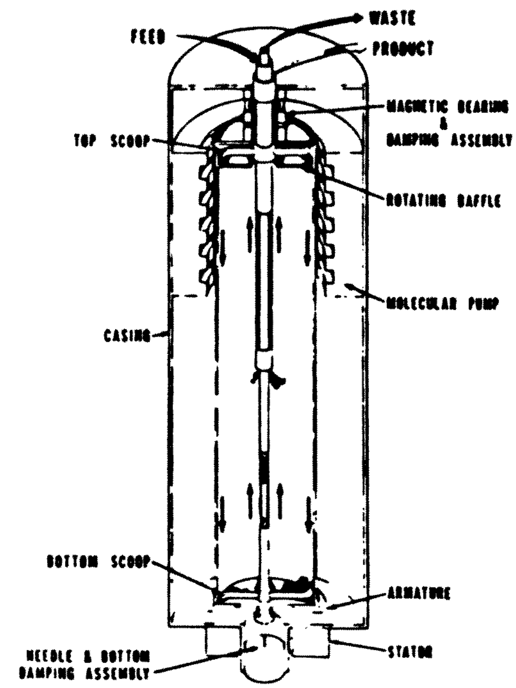

Fig. 1. Early Model Gas Centrifuge

boundary layers they called buoyancy layers that exist on the radial walls. Using the asymptotic theory of Cole and Schleiniger, Babarsky [7] solved the flow in a pie-shaped cylinder of finite length in the limit of high speed rotation. This research produced a number of interesting results that were published. The latest publication by Wood and Babarsky [8] contains these references.

Following the same approach as Wood and Morton [3], the analogous pancake equation for the pie-shaped sector is

$$(e^x(e^x\chi_{xx})_{xx})_{xx} + 2R^2G\chi_{\theta\theta} + 2R^2(2+G)\chi_{zz} - 2Re^x\chi_{xx\theta} = 0 \tag{2}$$

where θ is the azimuthal variable and R and G are similarity parameters. This equation was also derived by Maslen [9]. This equation is solved by separation of variables and by seeking a solution in terms of the eigenfunctions for the symmetric equation (1). It is matched with the Ekman layers and the buoyancy layers using the asymptotic methods of Cole and Schleiniger.

3. Current Centrifuge Applications

In recent years, the plateau of construction of new nuclear power reactors in the United States and the end of the cold war reducing the demand for nuclear weapons, a world wide glut of enriched ^{235}U exists. However, a new market has developed for stable isotopes in medicine and physics research [10]. Much of this new demand is for elements which have more than two isotopes. For production of these isotopes in large quantities (e.g. tens of Kgs per year), the gas centrifuge method is the most economical process. However, this requires a new theory for the isotope transport equations. For isotopic mixtures, the fluid parameters vary only slightly which means the flow model can be the same. However, the operating conditions of the centrifuge are quite different. For example, the feed flow rate, the temperature, the gas content in the centrifuge, and the scoop drive can be quite different than in the binary uranium case.

A recent paper by Wood, et.al.[11] has addressed this problem by using the pancake equation (1) for the flow field, and then solving N diffusion equations for the concentration distribution of the N isotopes. In [11], a model is presented for the flow and isotope transport which is coupled with an algorithm for optimizing the performance of the centrifuge. Applications are presented where the isotopic mixture is spent reactor fuel with 5 isotopes of uranium and a case of chromium with 4 isotopes.

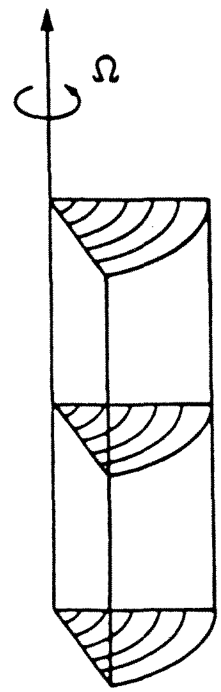

Fig. 2. Pie Shaped Cylinder Rotating About Its Vertex

The countries with existing centrifuge capabilities such as China, Russia, Germany, Great Britain and The Netherlands are very interested in developing this market for stable isotopes.

4. Conclusions

The gas centrifuge has been the source of much research and development activity around the world for over fifty years. The problems of calculating and measuring the flow field have presented great challenges, but significant progress has been accomplished. A group of scientists in this country has been involved in attacking and solving these problems, and this is true for all of the countries involved.

For those interested in this field, international meetings on this subject, called Workshops on Gases in Strong Rotation, were started in Sweden in 1975 and continued every other year until 1985 when the name was changed to Workshops on Separation Phenomena in Liquids and Gases. The next meeting is scheduled for Brazil in 1996. So it appears that the new interest in multi-component separation of stable isotopes is sure to continue to produce new challenging problems for many more years.

Appendix

A gas centrifuge is a device used for separating isotopes with the element in a gaseous compound. The centrifuge is a right circular cylinder which is spun at very high rotational speeds and is contained inside a casing with a high vacuum in order to reduce the drag on the rotating cylinder. This high rotation produces centrifugal forces that can be on the order of 10^6 times that of earth's gravity. Therefore, analogous to the earth's atmosphere, a gradient of isotopic concentration is produced in the radial direction of the centrifuge. In the case of a process gas with two isotopes (a binary mixture) the heavier isotope is concentrated near the outer wall and the lighter isotope is concentrated near the axis. This separation is small, but it can be enhanced many times by a countercurrent flow as shown in Figure 1. The flow near the wall is enriched in heavy isotope as it moves axially downward in this convective flow field, and the flow near the axis is enriched in the light isotope as it moves axially upward. As shown in Figure 1, the centrifuge is inside a casing in which a high vacuum is maintained in order to minimize drag on the rotating cylinder.

In a high speed centrifuge, the strong centrifugal field produces a steep radial gradient in the density and pressure. Hence, most of the gas is near the outer wall and a vacuum exists near the axis. This stratified gas behaves in an analogous way with the earth's atmosphere. For example, heating at the wall causes the gas to move toward the axis or "rise" in this setting; and, cooling the gas at the wall causes the gas to "fall" towards the wall. If the bottom of the centrifuge is heated and the top cooled, the gas that "rises" at the bottom moves upward near the axis until it is cooled and "falls" to the wall. The cooler gas moves downward along the wall to replenish the "rising" gas. In this manner, a counter-current convective flow is established which can enhance the separation of the isotopes.

The introduction and removal of gas also act as methods for driving counter-current flows. The process gas is fed into the centrifuge from a pipe at the axis and removed by non-rotating pipes called scoops. As shown in Figure 1, the top scoop is shielded by a baffle which rotates with the outer wall. If this scoop were not shielded by the baffle, it would produce a flow that would cancel the flow produced by the unshielded bottom scoop. For a given geometry, rotational speed and process gas, the performance of the gas centrifuge can be optimized by adjusting the wall temperature gradient, the friction drag of the bottom scoop, the feed rate and the percent of feed removed from the top or "cut." In order to determine the optimal operating conditions, it is necessary to have mathematical models of the flow field and transport equations.

References

[1] J. W. Beams and F. B. Haynes, The separation of isotopes by centrifuging. *Phys. Rev.*, **50**, (1936), pp. 491-492.

[2] G. F. Carrier and S. H. Maslen, Flow phenomena in rapidly rotating systems. USAEC Report TID-18065, (1962).

[3] H. G. Wood and J. B. Morton, Onsager's pancake approximation for the fluid dynamics of a gas centrifuge. *J. Fluid Mech.*, **101**, (1980), pp. 1-31.

[4] G. F. Schleiniger, Study of non-axisymmetric flows in a gas centrifuge. Ph.D. Thesis, UCLA, (1982).

[5] G. F. Schleiniger and J. D. Cole, An asymptotic study of pancake theory. *Proc. 4th Workshop on Gases in Strong Rotation*, Oxford, (ed. E. Ratz), pp. 678-688, (1982), Frankenforster Strasse 21, Begisch Gladbach 1, Germany.

[6] T. Matsuda and K. Nakagawa, A new type of boundary layer in a rapidly rotating gas, *J. Fluid Mech.*, **126**, (1983), pp. 431-442.

[7] R. J. Babarsky, Compressible flow in a pie-shaped cylinder rotating about the vertex, Ph.D. Dissertation, University of Virginia, (1986).

[8] H. G. Wood and R. Babarsky, Analysis of a rapidly rotating gas in a pie-shaped cylinder, *J. Fluid Mech.*, **239**, (1992), pp. 249-271.

[9] S. H. Maslen, Unsymmetrical flow in a centrifuge, School of Engineering and Applied Science, University of Virginia, Rep. No. UVA-ER-953-84U, (1984).

[10] A. Tikhomirov, Modern tendencies in the enrichment ofstable isotopes and their applications in the USSR and elsewhere, it Nuc. Instr. and Meth. in Physics Res., **B70**, (1992), pp. 1-4.

[11] H. G. Wood, T. C. Mason and Soubbaramayer, Multi-isotope separation in a gas centrifuge using Onsager's pancake model, *Separation Science and Technology*, in press.

Interfacial Instability Theory Of Hele-Shaw Flow

Jian-Jun Xu *

Abstract

Formation of viscous fingers in Hele-Shaw cells has been a phenomenon of considerable interest for almost half a century ([1-10]). The basic problem involved in this subject has been the selection of the interfacial patterns at the later stage of its evolution. In order to solve this problem, the understanding of the instability mechanism of the system plays a central role. By using a unified asymptotic approach, we found two different types of instability mechanisms for slowly time-evolving finger solutions.

(1). The global trapped wave (GTW) instability, induced by perturbations with a high frequency, $|\omega| = O(1)$ and

(2). The zero-frequency (Null-f) instability, induced by perturbations with a low frequency, $\omega \leq O(\varepsilon)$.

On the basis of these instability mechanisms, the selection of viscous finger formation is clarified.

1 Mathematical Formulation Of Problem

Consider the evolution of a finger developing in a Hele-Shaw cell in the positive y direction in a moving $\{x, y\}$ coordinate system fixed at the finger's tip. The flow velocity at the upstream far field is set to be a constant U_∞, but the tip velocity, in general, will change with time. We utilize one-half of the width of the cell W as the length scale and use the flow velocity U_∞ at far field up-stream as the velocity scale; the product $U_\infty W$ is used as the scale of the potential function $\phi(x, y, t)$ of the absolute velocity field $\mathbf{u}(x, y, t)$. With these scales, $U(t)$ denotes the non-dimensional tip velocity, while $y_s(x, t)$ describes the interfacial shape. The total length of the finger is $y_T(t)$ and the effective width of the finger is defined as $\lambda(t) = 1/U(t)$.

It is well known that for the special case of zero surface tension ($\varepsilon = 0$), the system allows an exact steady finger solution with constant $U = U_0 = 1/\lambda_0, (0 < \lambda_0 < 1)$ and $y_T = \infty$. This is the so-called Zhuravlev-Saffman-Taylor (ZST) solution ([1-2]). Assume $\phi_*(x, y)$ and $\psi_*(x, y)$ are respectively the potential function and stream function of the ZST solution and define

$$(1) \qquad \xi = -\psi_*, \quad \eta = \phi_*, \quad \zeta = \xi + i\eta, \quad Z = x + iy.$$

The ZST solution can be written in the form

$$(2) \qquad Z = x + iy = Z(\zeta) = \lambda_0 \zeta + i\frac{2(1-\lambda_0)}{\pi} \ln \cos\left(\frac{\pi\zeta}{2}\right).$$

On the basis of the ZST solution, we introduce a new orthogonal curvilinear coordinate system in the (x, y)-plane (see Figure 1):

$$(3) \qquad x = X(\xi, \eta), \quad y = Y(\xi, \eta)$$

*Department of Mathematics and Statistics, McGill University, Montreal, Quebec, Canada H3A 2K6.

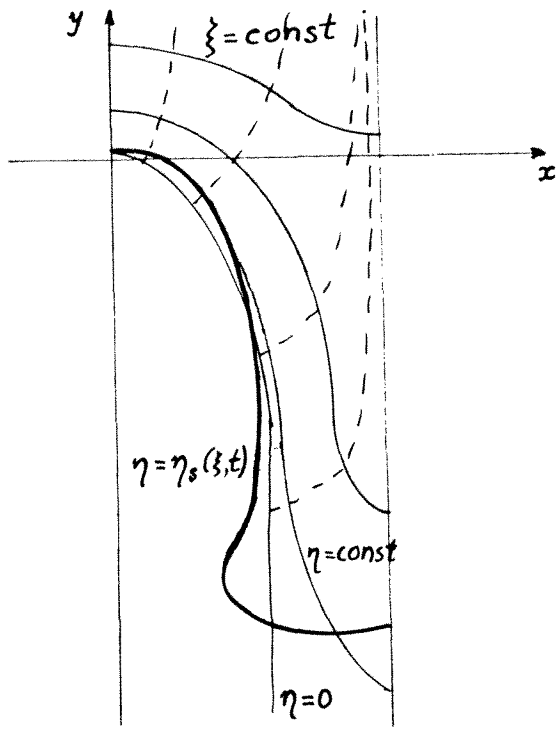

FIG. 1. *The sketch of the orthogonal curvilinear coordinate system* (ξ,η) *based on the ZST zero surface tension steady state solutions.*

The Lame coefficients $\mathcal{G}_1$ and $\mathcal{G}_2$ along two coordinate curves of (3)

$$\mathcal{G}_1 = \mathcal{G}_2 = \mathcal{G} = |Z'(\zeta)| = \sqrt{X_\xi^2 + Y_\xi^2}. \tag{4}$$

can be calculated from (2) and we obtain:

$$\mathcal{G}_0 = \mathcal{G}(\xi, 0) = \sqrt{\lambda_0^2 + (1-\lambda_0)^2 \tan^2\left(\frac{\pi\xi}{2}\right)}. \tag{5}$$

The general unsteady fingering formation problem can then be formulated in this coordinate system (ξ,η). Let the potential function of the flow be $\phi = \phi(\xi,\eta,t)$ and the interface's shape function be $\eta = \eta_s(\xi,t)$. The governing equation is

$$\left(\frac{\partial^2\phi}{\partial\xi^2} + \frac{\partial^2\phi}{\partial\eta^2}\right) = 0, \tag{6}$$

the boundary conditions are

$$\text{the upstream condition:} \quad \frac{\partial\phi}{\partial\eta} = 1, \quad \text{as } \eta \to \infty; \tag{7}$$

$$\text{the side-wall slip condition :} \quad \frac{\partial\phi}{\partial\xi} = 0, \quad \text{at } \xi = \pm 1; \tag{8}$$

the interface condition: at $\eta = \eta_s(\xi,t)$,

$$\phi = \varepsilon^2 \mathcal{K}\{\eta_s(\xi,t)\} \tag{9}$$

$$\left(\frac{\partial\phi}{\partial\eta} - \eta_s'\frac{\partial\phi}{\partial\xi}\right) = U_0(Y_\eta - \eta_s' Y_\xi) + \mathcal{G}^2\left(\frac{\partial\eta_s}{\partial t}\right). \tag{10}$$

In the above, the prime represents a derivative with respect to ξ, $U_0 = 1/\lambda_0$ is the tip velocity for the ZST solution observed in the laboratory frame; the surface tension parameter ε is defined as

$$\varepsilon^2 = \frac{b^2\gamma}{12\mu U_\infty W^2} \tag{11}$$

where γ is the surface tension, b is the thickness of the cell; and $\mathcal{K}\{\eta_s(\xi,t)\}$ is the curvature operator.

(12) the downstream condition: $\dfrac{\partial\phi}{\partial\eta} = \dfrac{\partial\phi}{\partial\xi} = 0$, at $\xi = \pm 1; \eta = \eta_T(t) \approx e^{\frac{\pi y_T}{1-\lambda_0}}$;

(13) the smooth tip condition: $\dfrac{\partial\eta_s}{\partial\xi} = 0$, at $\xi = 0$.

The above system is highly non-linear. Obviously, the ZST solution satisfies the above system at $\varepsilon = 0$. Hereby, we are interested in studying the slowly evolving finger solution at $t \gg 1$ with $\varepsilon \neq 0$. Thus, we define

$$\bar{t} = \varepsilon(t - t_0); \quad (t_0 \gg 1). \tag{14}$$

By using the slow variable $\bar{t}$, the tip velocity $U(t)$ is written as $U(t) = U(\bar{t},\varepsilon)$. Accordingly, the location of the triple point T is expressed as

$$\bar{y}_T(\bar{t},\varepsilon) = y_T(t) = -\frac{1}{\varepsilon}\left(L + \int_0^{\bar{t}} U(\bar{t},\varepsilon)d\bar{t}\right) = \bar{y}_T(\bar{t},\varepsilon)/\varepsilon, \quad \text{where } (L \gg 1). \tag{15}$$

Thus, in the coordinate system (ξ,η) at the triple point T, we have $\xi = \pm 1$; $\eta = \bar{\eta}_T \approx e^{\frac{\pi \bar{y}_T}{\varepsilon(1-\lambda_0)}} \ll 1$. Moreover, the kinematic interface condition (10) is changed to

$$\left(\frac{\partial\phi_B}{\partial\eta} - \eta_B'\frac{\partial\phi_B}{\partial\xi}\right) = U_0(Y_\eta - \eta_s'Y_\xi) + \varepsilon\mathcal{G}^2\left(\frac{\partial\eta_B}{\partial\bar{t}}\right). \tag{16}$$

Finding the slowly evolving solutions $q_B =: \{\phi_B;\eta_B\}(\xi,\eta,\bar{t},\varepsilon)$ for the above system with $0 < \varepsilon \ll 1$ is a singular perturbation problem. Letting $\varepsilon \to 0$, the uniformly valid asymptotic solution for q_B is expected to have the following structure:

$$q_B \approx q_* + (R_N) + (S_N). \tag{17}$$

Here, the first part q_* is the ZST solution, (R_N) is the partial summation of the time independent, regular perturbation expansion (RPE), whereas S_N is the singular perturbation expansion (SPE) part, which contains the slow time variable $\bar{t}$. For any given $\bar{t} > 0$, as $\varepsilon \to 0$, the singular perturbation solution S_N is an exponentially small correction term to the (RPE) part. In this sense, we call these slowly time evolving solutions 'the generalized steady finger solutions' and define them as the basic state solutions. We shall not derive the precise form of these slowly evolving finger solutions. The goal of the present paper is simply to explore the stability of these solutions. For this purpose, the only information we need is that these solutions exist and for fixed $0 < \bar{t} < \infty$, in the region away from the triple point, they are close to the ZST solutions, namely,

$$\{\phi_B(\xi,\eta,\bar{t},\varepsilon);\eta_B(\xi,\bar{t},\varepsilon);\bar{U}(\bar{t},\varepsilon);\lambda(\bar{t},\varepsilon)\} = \{\phi_*(\eta);0;U_0;\lambda_0\} + O(\varepsilon^2). \tag{18}$$

2 The Linear Perturbed System Around The Basic State And The Outer Solutions

We consider the following infinitesimal perturbations around the basic state. Let

$$\begin{cases} \phi(\xi,\eta,t) = \phi_B + \tilde{\phi}(\xi,\eta,t), \\ \eta_s(\xi,t) = \eta_B + \tilde{h}(\xi,t). \end{cases} \tag{19}$$

From (6)-(13), the linear perturbed system is derived:

$$\nabla^2\tilde{\phi} = \Big(\frac{\partial^2\tilde{\phi}}{\partial\xi^2} + \frac{\partial^2\tilde{\phi}}{\partial\eta^2}\Big) = 0, \tag{20}$$

with the boundary conditions

$$\tfrac{\partial\tilde{\phi}}{\partial\eta} = \tfrac{\partial\tilde{\phi}}{\partial\xi} = 0, \quad \text{as } \eta \to \infty; \tag{21}$$

$$\tfrac{\partial\tilde{\phi}}{\partial\xi} = 0, \quad \text{at } \xi = \pm 1; \tag{22}$$

$$\tilde{\phi} + \tilde{h} = -\tfrac{\varepsilon^2}{\hat{\mathcal{G}}(\xi)}\Big\{\tfrac{\partial^2\tilde{h}}{\partial\xi^2} - \tfrac{\hat{\Pi}_1(\xi)}{\hat{\mathcal{G}}^2(\xi)}\tfrac{\partial\tilde{h}}{\partial\xi_+} + \tfrac{\partial\hat{\Pi}_0(\xi)}{\partial\eta}\tfrac{\tilde{h}}{\hat{\mathcal{G}}^2(\xi)}\Big\} \tag{23}$$

$$\text{and} \qquad \tfrac{\partial\tilde{\phi}}{\partial\eta} + U_0\hat{Y}_\xi(\xi)\tfrac{\partial\tilde{h}}{\partial\xi} - \hat{\mathcal{G}}^2(\xi)\tfrac{\partial\tilde{h}}{\partial t} - U_0\hat{Y}_{\eta\eta}(\xi)\tilde{h} = 0, \tag{24}$$

at $\eta = \eta_B$, where $\hat{\mathcal{G}}(\xi), \hat{Y}_\xi(\xi), \hat{Y}_{\eta\eta}(\xi), \hat{\Pi}_0(\xi), \hat{\Pi}_1(\xi)$ are deterined by the transformation functions $X(\xi,\eta), Y(\xi,\eta)$ and the shape function $\eta_B(\xi)$.

$$\tilde{h} = 0; \quad \tfrac{\partial\tilde{\phi}}{\partial\xi} = \tfrac{\partial\tilde{\phi}}{\partial\eta} = 0, \quad \text{at } \xi = \pm 1, \eta = \eta_T; \tag{25}$$

$$\tfrac{\partial\tilde{h}}{\partial\xi} = 0; \quad \tilde{h} = O(1), \qquad \text{for symmetric modes (S-modes)}; \tag{26}$$

$$\text{and} \quad \tfrac{\partial\tilde{h}}{\partial\xi} = O(1); \quad \tilde{h} = 0, \qquad \text{for anti-symmetric modes (A-modes)}, \tag{27}$$

at $\xi = 0$. The above system contains two parameters ε, and λ_0. It leads to a linear eigenvalue problem, when one looks for solutions of the type $\tilde{q} = \hat{q}e^{\sigma t}$. The eigenvalue σ must be a function of (λ_0, ε). We shall solve this eigenvalue problem in two steps. We first solve the system (20)-(25) for any given $(\sigma, \lambda_0, \varepsilon)$. In doing so, we shall apply the multiple variable expansion (MVE) method to look for a uniformly valid asymptotic solution in the limit $\varepsilon \to 0$. The solution should satisfy all boundary conditions except the tip condition. Then, we apply the tip condition (26) or (27). Thus, the parameter σ must be chosen as a function of λ_0 and ε.

In order to find the asymptotic solutions $\tilde{q}(\xi,\eta,t,\varepsilon)$ for the system (20)-(25), we introduce a set of stretched fast variables $\{\xi_+, \eta_+, t_+\}$:

$$\xi_+ = \frac{1}{\varepsilon}\int k(\xi,\bar{t},\varepsilon)d\xi, \quad \eta_+ = \frac{g(\xi,\bar{t},\varepsilon)}{\varepsilon}\eta, \quad t_+ = t/\varepsilon\,. \tag{28}$$

In terms of the multiple scale variables $(\xi,\eta,\bar{t},\xi_+,\eta_+,t_+)$, we can make the following MVE for the perturbed state:

$$\begin{cases} \tilde{\phi} = \Big\{\tilde{\phi}_0(\xi,\eta,\bar{t},\xi_+,\eta_+) + \varepsilon\tilde{\phi}_1(\xi,\eta,\bar{t},\xi_+,\eta_+) + \cdots\Big\}e^{\sigma t_+}\,, \\ \tilde{h} = \Big\{\tilde{h}_0(\xi,\bar{t},\xi_+) + \varepsilon\tilde{h}_1(\xi,\bar{t},\xi_+) + \cdots\Big\}e^{\sigma t_+}\,, \\ k(\xi,\bar{t},\varepsilon) = k_0 + \varepsilon k_1 + \cdots, \quad g(\xi,\bar{t},\varepsilon) = k_0 + \varepsilon g_1 + \cdots, \\ \sigma(\bar{t},\varepsilon) = \sigma_0 + \varepsilon\sigma_1 + \varepsilon^2\sigma_2\cdots. \end{cases} \tag{29}$$

In the above, $\sigma = \sigma_R - i\omega, \omega \geq 0$ is a given parameter, whereas the fast variables and slow variables $(\xi, \eta, \bar{t}, \xi_+, \eta_+, t_+)$ in the solution are treated formally as independent variables. One can convert the linear system into a system with the multiple variables and successively derive each order approximation.

As the zero-th order approximation, we obtain the mode solutions:

$$\left\{ \begin{array}{l} \tilde{\phi}_0 = A_0(\xi, \eta) \ \exp\{i\ \xi_+ - \eta_+\} \\ \tilde{h}_0 = \hat{D}_0 \ \exp\{i\ \xi_+\}\ . \end{array} \right. \tag{30}$$

The coefficient $\hat{D}_0$ in the zero-th order approximation is taken as a constant. In order to satisfy the interface condition at $\eta = 0$, the wave number function $k_0(\xi)$ is made subject to the local dispersion formula

$$\mathcal{G}_0^2 \sigma_0 = i k_0 U_0 Y_{\xi,0}(\xi) + k_0 \left(1 + \frac{k_0^2}{\mathcal{G}_0}\right). \tag{31}$$

Later, for convenience, we shall often employ a new variable ρ defined by

$$\rho = -\frac{Y_{\xi,0}(\xi)}{\lambda_0} = \left(\frac{1-\lambda_0}{\lambda_0}\right) \tan\left(\frac{\pi\xi}{2}\right) \tag{32}$$

to replace ξ. The variable ρ is connected with the arc length $\ell(\xi)$ measured along the interface of the basic state starting from the tip. Thus, we have $\xi = \int_0^\rho \frac{d\rho_1}{G(\rho_1)}$, $G(\rho) = \frac{\pi}{2a}\frac{\lambda_0}{1-\lambda_0}\left[\rho^2 + a^2\right]$, $\mathcal{G}_0(\xi) = \lambda_0 S(\rho)$, $a = \frac{(1-\lambda_0)}{\lambda_0}$ and $S(\rho) = \sqrt{1+\rho^2}$. Moreover, in terms of the variable ρ, the normal mode solution is expressed in the form

$$\tilde{h}_0 = \tilde{h}_0(\rho) = D_0 \exp\left\{\frac{i}{\varepsilon}\int_0^\rho \tilde{k}_0 d\rho\right\}, \tag{33}$$

where $\tilde{k}_0(\rho) = \frac{k_0(\xi)}{G(\rho)}$. The corresponding local dispersion formula will be

$$\sigma_0 = \Sigma_*(\rho, \tilde{k}_0) = \frac{G(\rho)\tilde{k}_0}{\lambda_0^2 S(\rho)^2}\left[(1 - i\rho) - \frac{G^2(\rho)\tilde{k}_0^2}{\lambda_0 S(\rho)}\right]. \tag{34}$$

For any given constant σ_0, one can find three roots from (34): $\{\tilde{k}_0^{(1)}; \tilde{k}_0^{(2)}; \tilde{k}_0^{(3)}\}$, where $\Re\{\tilde{k}_0^{(1)}\} > \Re\{\tilde{k}_0^{(3)}\} > 0$ and $\Re\{\tilde{k}_0^{(2)}\} < 0$. Accordingly, the system has three fundamental solutions, $H_i(\rho), (i = 1, 2, 3)$, corresponding to each wave number functions $\tilde{k}_0^{(i)}$. In order for the potential $\tilde{\phi}_0$ to satisfy the boundary condition (21), the requirement $\mathrm{Re}\{\tilde{k}_0\} > 0$ is necessary. Consequently, only $\{H_1(\rho),\ H_3(\rho)\}$ are meaningful, which correspond to the short wave branch and long wave branch, respectively. Thus, the general solution must be a linear combination

$$\tilde{h} = D_1 H_1(\rho) + D_3 H_3(\rho) = D_1 \exp\left\{\tfrac{i}{\varepsilon}\textstyle\int_0^\rho \tilde{k}_0^{(1)} d\rho_1\right\} + D_3 \exp\left\{\tfrac{i}{\varepsilon}\textstyle\int_0^\rho \tilde{k}_0^{(3)} d\rho_1\right\}. \tag{35}$$

The constants D_1 and D_3 are to be determined by the root condition (25) and the tip condition.

However, the MVE solution (29) is not uniformly valid in the whole complex ρ (or ξ) plane (refer to [7-8]). The first order approximate solution has a singularity at the point ρ_c (or ξ_c) in the complex ρ (or ξ) plane, which is the the root of the equation

$$\frac{\partial \Sigma_*(\rho, \tilde{k}_0)}{\partial \tilde{k}_0} = 0, \quad \text{or} \quad \sigma_0 = e^{-i\frac{3\pi}{4}}\sqrt{\frac{4}{27\lambda_0^3}}\left(\frac{\rho_c + i}{\rho_c - i}\right)^{3/4}. \tag{36}$$

To obtain a uniformly valid solution for our problem, in general, the coefficients $\{D_1, D_3\}$ in (35) must be different constants in different sectors. These sectors are divided by the Stokes lines emanating from this singular point. This is the so-called Stokes phenomenon. The so-called Stokes line is defined as

$$\Re\Big\{\int_{\rho_c}^{\rho}\Big(\tilde{k}_0^{(1)}-\tilde{k}_0^{(3)}\Big)d\rho_1\Big\}=0. \tag{37}$$

It can be shown that one Stokes curve (L_2) divides the whole complex ρ (or ξ)-plane into a sector (S_1) and a sector (S_2) . The root point $\rho=\rho_T$ belongs to sector (S_2), while the tip point $\rho=0$ belongs to sector (S_1). We denote the coefficients of the solution (35) by $\{D_1, D_3\}$ in (S_1), while by $\{D_1', D_3'\}$ in (S_2).

In order to determine these four constants to obtain the uniformly valid asymptotic solution, one must divide the whole complex ρ (or ξ)-plane into two regions: the inner region near the singular point ρ_c (or ξ_c) and the outer region away from ρ_c (or ξ_c). The solution (35) is only valid in the outer region. One also needs to find the inner solution in the inner region, and then match the inner solution with the outer solution. This will be done in the next section.

We can now apply the root condition (25) to the outer solution (35). This leads to $D_1'=0$. So to leading order, the root condition is replaced by the radiation condition:

$$\tilde{h}_0 \sim D_3' H_3, \tag{38}$$

where the constant D_3' is a constant proportional to the characteristic amplitude of the initial perturbation.

3 The Inner Equation Near The Singular Point ξ_c.

In the inner region $|\xi-\xi_c|\ll 1,\ |\eta-1|\ll 1$, we introduce the inner variables:

$$\xi_*=\frac{\xi-\xi_c}{\varepsilon^{\alpha}}\qquad \eta_*=\frac{\eta}{\varepsilon^{\alpha}}, \tag{39}$$

and denote the inner solution as

$$\tilde{h}(\xi,t)=\varepsilon^{\alpha}\hat{h}(\xi_*,t);\quad \tilde{\phi}(\xi,\eta,t)=\varepsilon^{\alpha}\hat{\phi}(\xi_*,\eta_*,t), \tag{40}$$

where α is to be determined.

We look for the mode solutions of the inner expansions:

$$\begin{cases} \hat{\phi}(\xi_*,\eta_*,t)=\{\nu_0(\varepsilon)\hat{\phi}_0(\xi_*,\eta_*)+\nu_1(\varepsilon)\hat{\phi}_1(\xi_*,\eta_*)+\dots\}e^{\frac{\sigma t}{\varepsilon\eta_0^2}} \\ \hat{h}=\{\nu_0(\varepsilon)\hat{h}_0+\nu_1(\varepsilon)\hat{h}_1+\cdots\}e^{\frac{\sigma t}{\varepsilon\eta_0^2}}. \end{cases} \tag{41}$$

Letting $\varepsilon\to 0$, the perturbed system in the inner region can be simplified into a third order O.D.E for the interface perturbation $\hat{h}$. With the new inner variable $\rho_*=\varepsilon^{\alpha}\rho$, it can be written in the form:

$$i\frac{\varepsilon^{3-3\alpha}G^3}{\lambda_0 S}\frac{d^3\hat{h}}{d\rho_*^3}\ +\ \varepsilon^{1-\alpha}G(\rho+i)\frac{d\hat{h}}{d\rho_*}+\lambda_0^2S^2\sigma_0\hat{h}=O(\text{H.O.T.})\ . \tag{42}$$

To further simplify the problem, we use the transformation introduced by Xu (refer to [8]):

$$\tilde{h}=W(\xi)\ \exp\Big\{\tfrac{i}{\varepsilon}\ \textstyle\int_0^{\rho_c}\ \tilde{k}_c(\rho_1)\ d\rho_1\Big\}\ \text{ and }\ \hat{h}=\hat{W}(\rho_*)\ \exp\Big\{\tfrac{i}{\varepsilon}\ \textstyle\int_{\xi_c}^{\rho}\ \tilde{k}_c(\rho_1)\ d\rho_1\Big\}, \tag{43}$$

with a properly choosing function $k_c(\xi)$. It is found that besides the simple turning point ρ_c, the singular points $\rho = (-i, -ia)$ may enter the inner region of ρ_c, and influence the behavior of the inner solution. Two cases are found to be significant. In both cases, at the far field of the inner region, as $\rho_* \gg 1$, the inner equation can be approximately written in the form:

$$\frac{d^2\hat{W}_0}{d\hat{\rho}_*^2} + \hat{\rho}_*^{p_0}\hat{W}_0 = 0, \tag{44}$$

where

$$\hat{\rho}_* = \frac{B}{\varepsilon^{\alpha}}(\rho - \rho_c), \quad B = O(1). \tag{45}$$

By matching the inner solution with the outer solution in the sector (S_1), we derive

$$\left(\frac{D_1}{D_3}\right)\exp\left\{\frac{i}{\varepsilon}\int_0^{\rho_c}\left[\tilde{k}_0^{(1)} - \tilde{k}_0^{(3)}\right]d\rho\right\} = i2\cos(\nu\pi). \tag{46}$$

For case (I), $|\sigma_0| \geq O(\varepsilon^{1/2})$: $\alpha = 2/3$, $p_0 = 1$ and $\nu = 1/3$;

For case (II), $|\sigma_0| \leq O(\varepsilon^{3/5}), |\lambda_0 - 1/2|^{3/4} = O(\sigma_0)$: $\alpha = 4/5, p_0 = 3/4$ and $\nu = 4/11$. So far, we obtain the asymptotic solution in the limit $\varepsilon \to 0$, for any parameters σ_0, λ_0. We have not applied the tip condition yet. As the second step, we shall require the solution to satisfy the tip condition. Thus, the parameter σ_0 must be chosen as a function of λ_0 and ε. We found two different types of spectra of eigenvalues: (1) The complex spectrum: $\sigma_0 = (\sigma_R - i\omega)$; $\omega > 0$; (2) The real spectrum: $\sigma_0 = \sigma_R$. Consequently, the system is subject to two different types of instability mechanisms: The global trapped wave (GTW) instability, induced by perturbations with a high frequency, $|\omega| = O(1)$ and the Zero-Frequency (Null-f) instability mechanism, induced by perturbations with low frequency, $\omega \leq O(\varepsilon)$.

4 The Spectra Of Eigenvalues And Instability Mechanisms

4.1 The complex spectrum of eigenvalues and GTW instability:

With the complex eigenvalue σ_0, the physical solution in the outer region is

$$\Re\left\{\tilde{h}_0(\xi, t)\right\} = \Re\left\{\left(D_1H_1 + D_3H_3\right)e^{\frac{\sigma_0 t}{\varepsilon\eta_0^2}}\right\}. \tag{47}$$

For a smooth tip solution, the coefficients D_1, D_3 must be subject to the following conditions:

$$D_3/D_1 = -\tilde{k}_0^{(1)}(0)/\tilde{k}_0^{(3)}(0), \quad \text{for the S-modes ,} \tag{48}$$

$$D_1 = -D_3, \quad \text{for the A-modes .} \tag{49}$$

Combining (46) with (48), or (49), one obtains the following quantization conditions:

$$\chi = (2n + 1 + 1/2 + \theta_0)\pi - i[\ln\alpha_0 + \ln(2\cos(\nu\pi))] \quad n = (0, \pm1, \pm2, \pm3, \cdots), \tag{50}$$

where

$$\chi = \tfrac{1}{\varepsilon}\textstyle\int_0^{\rho_c}\left(\tilde{k}_0^{(1)} - \tilde{k}_0^{(3)}\right)d\xi \;\text{ and }\; \begin{cases} \alpha_0 e^{i\theta_0\pi} = \tilde{k}_0^{(1)}(0)\big/\tilde{k}_0^{(3)}(0), & \text{(for S-modes);} \\ \alpha_0 = 1;\ \theta_0 = 0, & \text{(for A-modes).} \end{cases} \tag{51}$$

The system allows only the complex eigenvalues with $|\sigma_0| = O(1)$ corresponding to the case (I) with $\nu = 1/3$. This spectrum contains two discrete sets of complex eigenvalues for S-modes and A-modes, respectively, given by the quantization conditions (50) as

$$\sigma_0^{(n)}, (n = 0, \pm 1, \pm 2, \cdots) \sim (\varepsilon, \lambda_0).$$

These eigenmodes are all traveling waves propagating along the interface. The numerical results for these eigen modes have been given in previous work [8] and it has been found that the neutral A-mode are more stable than the neutral S-mode.

4.2 The real spectrum of eigenvalues and Null-f instability:

In this case, the physical solution becomes

$$\Re\left\{\tilde{h}_0(\xi, t)\right\} = \Re\left\{D_1 H_1 + D_3 H_3\right\} \; e^{\frac{\sigma_0 t}{\varepsilon \eta_0^2}}. \tag{52}$$

Without losing generality, we can assume D_1 to be a positive real number. We denote

$$D_3 = |D_3| e^{i\chi_0 \pi} \tag{53}$$

In this case, the tip conditions can be written as follows:

$$\text{For the S-modes:} \quad \frac{D_1}{D_3} = \left|\frac{D_1}{D_3}\right| e^{-i\chi_0\pi}, \quad (\chi_0 = 0 \ \text{ or } \ 1). \tag{54}$$

$$\text{For the A-modes:} \quad \left|\frac{D_1}{D_3}\right| = -\cos(\chi_0 \pi). \tag{55}$$

With these tip conditions combining (46), we obtain the quantization condition:

$$\Re\left\{\frac{1}{\varepsilon}\int_0^{\rho_c} [\tilde{k}_0^{(1)} - \tilde{k}_0^{(3)}] d\rho\right\} = (2n + 1/2 + \chi_0)\pi \quad (n = 0, \pm 1, \pm 2, \cdots) \tag{56}$$

$$\left|\frac{D_1}{D_3}\right| = 2\cos(\nu\pi) e^{\Im\{\chi\}} \tag{57}$$

where

$$\chi_0 = \begin{cases} (0 \ \text{ or } \ 1), & \text{(for S- modes);} \\ 1 + \dfrac{\cos^{-1}\left|\frac{D_1}{D_3}\right|}{\pi}, & \text{(for A- modes).} \end{cases} \tag{58}$$

The quantization condition (56) determines the eigenvalues $\sigma_0^{(n)}$, while formula (57) determines the corresponding eigenfunction. We only found the real eigenvalues with $|\sigma_0| \ll 1$, which corresponds to the case (II) with $\sigma_0 \leq O(\varepsilon^{3/5}); 0 < (\lambda_0 - 1/2)^{3/4} = O(\sigma_0)$. With the assumption $|\sigma_0| \ll 1$, from the local dispersion formula (34) we derive that as $\sigma_0 \to 0$,

$$\left(\tilde{k}_0^{(1)} - \tilde{k}_0^{(3)}\right) = \frac{2(1-\lambda_0)}{\pi\lambda_0^{1/2}}\left\{\frac{(1+i\rho)^{3/4}(1-i\rho)^{1/4}}{(\rho-ia)(\rho+ia)} - \frac{3\sigma_0}{2}\lambda_0^{3/2}\frac{(1+i\rho)}{(\rho-ia)(\rho+ia)}\right\} + O(\sigma_0^2). \tag{59}$$

As $1/2 \leq \lambda_0 < 1$, we calculate

$$\chi = \frac{1}{\varepsilon}\left\{\frac{(2\lambda_0 - 1)^{3/4}}{\lambda_0^{1/2}} - i\hat{B}_1\frac{1-\lambda_0}{\lambda_0^{1/2}} - \sigma_0\left[\frac{3\lambda_0}{2} - i\lambda_0(1-\lambda_0)\hat{B}_2\right]\right\} \tag{60}$$

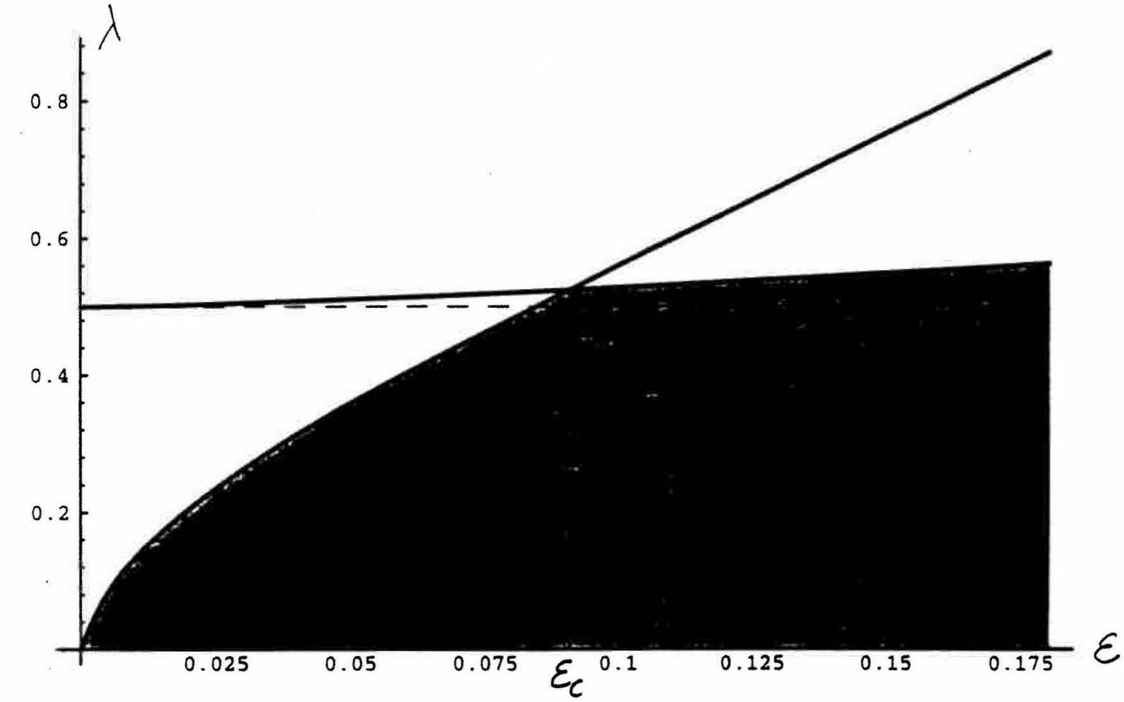

FIG. 2. *The stability diagram of viscous fingering.*

where we denote $\hat{B}_1 = \frac{2}{\pi}\int_0^1 \frac{(1-x)^{3/4}(1+x)^{1/4}}{(a-x)(a+x)}dx$; $\hat{B}_2 = \frac{3}{\pi}\int_0^1 \frac{(1-x)}{(a-x)(a+x)}dx$. Therefore,

$$\Re\{\chi\} = \frac{1}{\varepsilon}\left\{\frac{(2\lambda_0-1)^{3/4}}{\lambda_0^{1/2}} - \frac{3\lambda_0}{2}\sigma_0\right\}, \quad \Im\{\chi\} = \frac{1}{\varepsilon}\left\{-\hat{B}_1\frac{1-\lambda_0}{\lambda_0^{1/2}} + \sigma_0\hat{B}_2\lambda_0(1-\lambda_0)\right\} \tag{61}$$

By using these results, we obtain the following simplified quantization condition:

(62) For the S-modes:
$$\frac{3}{2}\lambda_0\sigma_0 = \frac{(2\lambda_0-1)^{3/4}}{\lambda_0^{1/2}} - \varepsilon(n+1/2)\pi \tag{62}$$

(63) For the A-modes:
$$\begin{cases} \frac{3}{2}\lambda_0\sigma_0 = \frac{(2\lambda_0-1)^{3/4}}{\lambda_0^{1/2}} - \varepsilon(2n+1/2+\chi_0)\pi \\ \cos(\chi_0\pi) = -2\cos(4\pi/11)e^{\Im\{x\}} \end{cases} \tag{63}$$

Given $\varepsilon > 0$, the system allows a discrete set of neutral modes with the width parameters $\lambda_0 = \lambda_0^{(n)}$, or the tip velocity $U_0 = U_0^{(n)}$. The neutral S-modes are determined by the formula:

$$\frac{(2\lambda_0^{(n)}-1)^{3/4}}{\sqrt{\lambda_0^{(n)}}} = \varepsilon(n+1/2)\pi, \tag{64}$$

which is found to be more stable than the corresponding neutral A-modes.

The above neutral modes are steady finger solutions that coincide with the classic steady finger solutions discovered numerically by Vanden Broeck (1983) and by some other investigators analytically in terms of the so-called microscopic solvability condition (MSC) theory (refer to [9]). The null-f instability was first discovered numerically by Kessler and Levine (1986). It was also studied by Bensimon Pelce and Shraiman in terms of a different approach (1987).

5 The Selection Condition Of Finger Solutions

Based on the understanding of the instability mechanisms, a selection criteria for finger solutions can be naturally derived. In Figure 2, in the parameter (ε, λ) plane we plot the two neutral curves, $\{\gamma_0\}$ and $\{C_0\}$, which represent A-modes (n=0) of branch (A) of the GTW mechanism and S-modes (n=0) of the null-f mechanism, respectively. These two curves intersect with each other at a critical number $\varepsilon_c = 0.0908$. For a given operating condition, ε is fixed, but $\lambda(\bar{t})$ may vary. Hence, the state point of the system slowly moves in the (ε, λ) phase plane.

On the basis of our stability analysis, it can be concluded that

(1). as $\bar{t} \to \infty$, if the basic finger solution approaches a steady solution, the state point of the limiting steady solution must be on the neutral curve $\{C_0\}$, and it occurs only when $\varepsilon \geq \varepsilon_c$;

(2). as $\bar{t} \to \infty$, if the basic finger solution approaches a time-periodic solution, the state point of the limiting oscillatory solution must be a neutral mode on the neutral curve $\{\gamma_0\}$, and it occurs only when $\varepsilon \leq \varepsilon_c$; Of course, such a time periodic oscillatory finger solution on the neutral curve $\{\gamma_0\}$ is not necessarily always observable, if the non-linear instability of the system is invoked.

(3). as $\bar{t} \to \infty$, if the basic finger solution has no limiting solution and displays a chaotic pattern with many short time scales, the state point of the solution must fall into the unstable region.

Apparently, the conclusion made by Tanveer and others (refer to [6],[9]) that the steady finger solution is linearly stable in the whole range of $0 < \varepsilon \ll 1$ is incorrect, and the selection criteria for steady smooth finger formation given by the MSC theory is not applicable as $\varepsilon < \varepsilon_c$.

References

[1] Zhuravlev, PA, Zap Leningr. Com. Inst. Vol. 33, p. 54-61 (1956).
[2] P.G. Saffman and G.I. Taylor, Proc.R. Soc. London Ser. A. **245**, p. 312, (1958).
[3] Jean-Marc Vanden-Broeck, Phys. Fluids, Vol. 26, No:8, p. 2033, (1983).
[4] D.A. Kessler and H. Levine, Phys. Rev. A, **32**, p. 1930, (1985); Phys. Rev. A, **33**, p. 2632, (1986).
[5] D. Bensimon, P. Pelce and B.I. Shraiman, J. Physique **48**, p. 2081, (1987).
[6] S. Tanveer, Phys. Fluid **30**, (8), p. 1589, (1987).
[7] J.J. Xu, Physical Review A 15., Vol. 43, No: 2, p. 930-947, (1991).
[8] J.J. Xu, European Journal of Applied Mathematics, Vol. 2, p. 105-132, (1991).
[9] 'Asymptotics Beyond All Orders', NATO ASI Series, Series B: Physics Vol. 284, edited by H. Segur, S. Tanveer and H. Levine, Plenum Press, New York, (1991).
[10] J.J. Xu, No: 94-01, Report from the Department of Mathematics and Statistics, ISSN 0824-4944, (1994).

INVITED PAPERS

Developments in Similarity Methods Related to Pioneering Work of Julian Cole

George W. Bluman*   Vladimir Shtelen*

Dedicated to Julian Cole: Mentor, Friend, and Pioneer in Similarity Methods

Abstract

Julian Cole's 1951 paper on relating Burgers' equation to the heat equation (Cole-Hopf transformation) [1], and his co-authored 1969 paper which introduced the nonclassical method for finding solutions of PDEs [2], have inspired the development of significant algorithms to find explicit solutions of PDEs. In the present paper we review these developments and exhibit new algorithms which further extend the nonclassical method.

1 Two Papers of Julian Cole Influencing the Development of Similarity Methods

Two of Julian Cole's most cited papers (cf. [1] and [2]) have played fundamental roles in advancing methods in applied mathematics. Julian Cole and these papers have aged well. Both papers have been cited increasingly over time as illustrated by the following table which gives the number of citations for each paper over each indicated five year interval:

	1965-69	1970-74	1975-79	1980-84	1985-89	1990-94
Paper [1] (1951)	27	49	39	54	55	64
Paper [2] (1969)		9	12	5	18	58

The peak citation year for each paper is 1994!

In [1], Cole established the remarkable relationship between solutions of Burgers' equation

(1.1) $$u_t + uu_x = u_{xx},$$

and solutions of the heat equation

(1.2) $$\theta_t = \theta_{xx}.$$

In particular, he showed that if $\theta(x,t)$ solves (1.2), then

(1.3) $$u = -2\frac{\theta_x}{\theta}$$

*Department of Mathematics, University of British Columbia, Vancouver, BC, Canada V6T 1Z2.
Supported by NSERC grant 5-87157.

solves (1.1). The transformation (1.3) is known as the *Cole-Hopf transformation*. In [1], Cole discovered this transformation as follows:

In (1.1), let $u=\phi_x$. Then (1.1) becomes

$$\frac{\partial}{\partial x}\left(\phi_t+\tfrac{1}{2}\phi_x^{\,2}\right)=\frac{\partial}{\partial x}(\phi_{xx}), \tag{1.4}$$

and hence, after integration, one has

$$\phi_t+\tfrac{1}{2}\phi_x^{\,2}=\phi_{xx}+A(t), \tag{1.5}$$

for arbitrary $A(t)$. Setting $A(t)\equiv 0$, one obtains the integrated Burgers' equation

$$\phi_t+\tfrac{1}{2}\phi_x^{\,2}=\phi_{xx}. \tag{1.6}$$

Observe that the heat equation (1.2) and the integrated Burgers' equation (1.6) are both invariant under scalings $x\to ax, t\to a^2t$. This suggests looking for solutions of (1.6) of the form

$$\phi(x,t)=\Phi(\theta(x,t)), \tag{1.7}$$

where $\theta(x,t)$ solves the heat equation (1.2). Substitution of (1.7) into (1.6) leads to the equation

$$\Phi'\left[\theta_t-\theta_{xx}\right]=\left[\Phi''-\tfrac{1}{2}(\Phi')^2\right]\theta_x^{\,2}. \tag{1.8}$$

If $\Phi(\theta)=-2\log\theta$, then $\Phi''-\frac{1}{2}(\Phi')^2=0$. Consequently one obtains the Cole-Hopf transformation (1.3).

Conversely, Hopf [3] showed that each solution of Burgers' equation (1.1) yields a solution of the heat equation (1.2) as follows:

Suppose $u(x,t)$ is a solution of Burgers' equation (1.1). Let $u=-2\dfrac{\psi_x}{\psi}$. Then

$$\frac{\partial}{\partial x}\left(\frac{\psi_t-\psi_{xx}}{\psi}\right)=0, \tag{1.9}$$

i.e.,

$$\psi_t-\psi_{xx}=\lambda(t)\psi, \tag{1.10}$$

for some $\lambda(t)$. Now set

$$\theta(x,t)=\psi(x,t)e^{-\int^t\lambda(t')\,dt'}. \tag{1.11}$$

Then $\theta(x,t)$, given by (1.11), solves the heat equation (1.2).

Hence there is a one-to-one correspondence between *solutions* of the nonlinear Burgers' equation (1.1) and those of the linear heat equation (1.2).

The Cole-Hopf transformation sparked the development of systematic methods for finding transformations relating nonlinear PDEs to linear PDEs (cf. [4]-[8]). In particular, the Cole-Hopf transformation is systematically found in [7].

In [2], two methods were presented for finding explicit solutions of scalar PDEs with two independent variables. The heat equation

$$u_{xx} = u_t \tag{1.12}$$

was used as a prototypical example.

1.1 Method I: The "Classical" Lie Method

This method is due to Sophus Lie [9]: Suppose a one-parameter Lie group of point transformations (point symmetry), characterized by an infinitesimal generator of the form

$$\mathbf{X} = \xi(x,t,u)\frac{\partial}{\partial x} + \tau(x,t,u)\frac{\partial}{\partial t} + \eta(x,t,u)\frac{\partial}{\partial u}, \tag{1.13}$$

leaves invariant an nth order scalar PDE

$$H\left(x,t,u,\underset{1}{u},\ldots,\underset{n}{u}\right) = 0. \tag{1.14}$$

In (1.14) the coordinates of $\underset{k}{u}$ are the kth order partial derivatives of u. A consequence of the invariance criterion is that any solution $u=\theta(x,t)$ of (1.14) is mapped into solutions of (1.14). In particular, let

$$\begin{aligned} U(x,t,u;\delta) &= e^{\delta \mathbf{X}}u, \\ X(x,t,u;\delta) &= e^{\delta \mathbf{X}}x, \\ T(x,t,u;\delta) &= e^{\delta \mathbf{X}}t. \end{aligned} \tag{1.15}$$

Then, under the point symmetry (1.13), a solution $u=\theta(x,t)$ of (1.14) is mapped into solutions $u=\theta(x,t;\varepsilon)$ of (1.14) where $u=\theta(x,t;\varepsilon)$ implicitly satisfies the equation

$$u = U(e^{\varepsilon \mathbf{X}}x, e^{\varepsilon \mathbf{X}}t, \theta(e^{\varepsilon \mathbf{X}}x, e^{\varepsilon \mathbf{X}}t); -\varepsilon). \tag{1.16}$$

The implicit relationship (1.16) is explicit if $\xi_u = \tau_u = \eta_{uu} \equiv 0$.

Solutions which map into themselves are called *invariant solutions* (*similarity solutions*). Such similarity solutions $u=\theta(x,t)$ of (1.14), related to its invariance under point symmetry (1.13), satisfy the system of PDEs consisting of the original PDE (1.14) augmented by the *invariant surface condition*

$$[\mathbf{X}(u-\theta(x,t))]_{u=\theta(x,t)} = 0, \tag{1.17}$$

i.e.,

$$\xi(x,t,u)u_x + \tau(x,t,u)u_t = \eta(x,t,u). \tag{1.18}$$

The general solution of (1.18) can be represented in the form

$$z(x,t,u) = \text{ const } = c_1, \ (\textit{similarity variable}) \tag{1.19a}$$

$$W(x,t,u) = \text{ const } = c_2 = w(z), \tag{1.19b}$$

yielding an *ansatz*

$$u = \Phi(x,t,w(z(x,t,u))) \tag{1.20}$$

for solutions of (1.14), after solving (1.19b) in terms of u. For a given point symmetry (1.13), the dependence of Φ on x, t, and $w(z)$ is explicit in (1.20); $w(z)$ is an arbitrary function of the similarity variable z. The substitution of (1.20) into (1.14) leads to a reduced ODE of order at most n with independent variable z and dependent variable w.

If $\xi_u = \tau_u \equiv 0$, then $z(x,t,u) \equiv z(x,t)$, and hence the ansatz (1.20) reduces to the form

$$u = \Phi(x,t,w(z(x,t))). \tag{1.21}$$

If $\xi_u = \tau_u = \eta_{uu} \equiv 0$, then the ansatz (1.20) further reduces to the form

$$u = A(x,t) + B(x,t)w(z(x,t)), \tag{1.22}$$

for some explicit functions $A(x,t)$ and $B(x,t)$.

Most importantly, in [9], Lie gave an algorithm to find all point symmetries (1.13) admitted by a given (linear or nonlinear) PDE (1.14). Lie's algorithm does not depend on the order of (1.14) and is also applicable to finding all point symmetries of systems of PDEs. Suppose (1.14) is a second order PDE in solved form:

$$u_{xx} = F(x,t,u,u_x,u_t,u_{xt},u_{tt}). \tag{1.23}$$

An infinitesimal generator $\mathbf{X}$ can be naturally extended (prolonged) to

$$\mathbf{X}^{(2)} = \mathbf{X} + \eta^x \frac{\partial}{\partial u_x} + \eta^t \frac{\partial}{\partial u_t} + \eta^{xt} \frac{\partial}{\partial u_{xt}} + \eta^{tt} \frac{\partial}{\partial u_{tt}} + \eta^{xx} \frac{\partial}{\partial u_{xx}}, \tag{1.24}$$

with

$$\begin{aligned}
\eta^x &= \frac{D\eta}{Dx} - \frac{D\xi}{Dx}u_x - \frac{D\tau}{Dx}u_t, \quad \eta^t = \frac{D\eta}{Dt} - \frac{D\xi}{Dt}u_x - \frac{D\tau}{Dt}u_t,\\
\eta^{xt} &= \frac{D\eta^t}{Dx} - \frac{D\xi}{Dx}u_{xt} - \frac{D\tau}{Dx}u_{tt} = \frac{D\eta^x}{Dt} - \frac{D\xi}{Dt}u_{xx} - \frac{D\tau}{Dt}u_{xt},\\
\eta^{tt} &= \frac{D\eta^t}{Dt} - \frac{D\xi}{Dt}u_{xt} - \frac{D\tau}{Dt}u_{tt}, \quad \eta^{xx} = \frac{D\eta^x}{Dx} - \frac{D\xi}{Dx}u_{xx} - \frac{D\tau}{Dx}u_{xt},
\end{aligned} \tag{1.25}$$

where $\dfrac{D}{Dx}$ and $\dfrac{D}{Dt}$ are total derivative operators given by

$$\begin{aligned}
\frac{D}{Dx} &= \frac{\partial}{\partial x} + u_x\frac{\partial}{\partial u} + u_{xx}\frac{\partial}{\partial u_x} + u_{xt}\frac{\partial}{\partial u_t} + \cdots,\\
\frac{D}{Dt} &= \frac{\partial}{\partial t} + u_t\frac{\partial}{\partial u} + u_{xt}\frac{\partial}{\partial u_x} + u_{tt}\frac{\partial}{\partial u_t} + \cdots.
\end{aligned} \tag{1.26}$$

Then $(\xi(x,t,u), \tau(x,t,u), \eta(x,t,u))$ satisfies

$$\left[\eta^{xx} - \xi F_x - \tau F_t - \eta F_u - \eta^t F_{u_t} - \eta^{xt} F_{u_{xt}} - \eta^{tt} F_{u_{tt}}\right]\Big|_{u_{xx}=F} = 0. \tag{1.27}$$

Since equation (1.27) must be satisfied for *any* solution $u=\theta(x,t)$ of (1.23), one obtains an overdetermined system of ***linear PDEs*** (***determining equations***) satisfied by (ξ,τ,η). For the heat equation (1.12), equation (1.27) becomes

$$(1.28)\qquad \begin{aligned}&\tau_{uu}u_x{}^2u_t+\xi_{uu}u_x{}^3+2\tau_u u_{xt}u_x+2(\tau_{xu}+\xi_u)u_xu_t+(2\xi_{xu}-\eta_{uu})u_x{}^2+2\tau_x u_{xt}\\&+(\tau_{xx}-\tau_t+2\xi_x)u_t+(\xi_{xx}-\xi_t-2\eta_{xu})u_x+(\eta_t-\eta_{xx})=0.\end{aligned}$$

Equation (1.28) is a polynomial form in the derivatives of u. The resulting nine determining equations arise from equating to zero the coefficients of this polynomial form. The general solution of (1.28) is given by

$$(1.29)\qquad \begin{aligned}&\xi(x,t,u)=\xi(x,t)=\alpha_1+\alpha_2x+\alpha_3t+\alpha_4xt,\\&\tau(x,t,u)=\tau(t)=2\alpha_2t+\alpha_4t^2+\alpha_5,\\&\eta(x,t,u)=\left[-\tfrac{1}{2}\alpha_3x-\alpha_4(\tfrac{1}{4}x^2+\tfrac{1}{2}t)+\alpha_6\right]u+g(x,t),\end{aligned}$$

where $\alpha_1,\alpha_2,\alpha_3,\alpha_4,\alpha_5$, and α_6 are arbitrary constants, and, due to the linearity of (1.12), $g(x,t)$ is an arbitrary solution of the heat equation $g_{xx}-g_t=0$.

Some of the similarity solutions of the heat equation (1.12) arising from its point symmetries, presented in [2], yielded novel solutions of the heat equation. Since 1962 several books have given prominence to Lie's work (cf. [8], [10]-[14]).

1.2 Method II: The "Nonclassical" Method

The algorithmic nonclassical method, introduced in [2], generalizes and includes Lie's classical method *for obtaining solutions of PDEs*. Here one seeks all functions $(\xi(x,t,u),\tau(x,t,u),\eta(x,t,u))$ so that (1.13) is a symmetry (*nonclassical symmetry*)) which leaves invariant the *augmented system* consisting of (1.14), (1.18), and differential consequences of (1.18). From the above discussion, it follows that the set of all invariant solutions $u=\theta(x,t)$, arising from the nonclassical symmetries of this augmented system, is equivalent to the set of *all* solutions of (1.14) of the form $u=\Phi(x,t,w(z(x,t,u)))$ where $w(z)$ satisfies a reduced ODE. From the nature of the invariant surface condition (1.18), without loss of generality, two cases arise: $\tau\equiv1;\tau\equiv0,\xi\equiv1$. Equation (1.18), and its differential consequences, introduce additional relationships between the derivatives of u. For *any* choice of (ξ,τ,η),(1.13) leaves invariant (1.18) itself (cf. [15]). Consequently, the invariant solutions of (1.14), arising from the solutions of the determining equations (which are now nonlinear in (ξ,τ,η)) for the nonclassical symmetries of the augmented system, include all invariant solutions of (1.14) arising from the point symmetries of (1.14) obtained through Lie's algorithm. One can show that the compatibility of the *completely augmented system* consisting of the given PDE (1.14), the invariant surface condition (1.18), and the differential consequences of *both* (1.14) and (1.18), leads to $(\xi(x,t,u),\tau(x,t,u),\eta(x,t,u))$ satisfying the determining equations of the nonclassical method (when applied to the completely augmented system).

Now we apply the nonclassical method to the heat equation (1.12).

Case 1: $\tau\equiv1$

If $u=\theta(x,t)$ satisfies the augmented system, consisting of the heat equation (1.12), the invariant surface condition (1.18), and differential consequences of (1.18), it follows that all t-derivatives of u and higher order x-derivatives of u can be expressed as polynomial forms in terms of u_x. In particular, one obtains

$$(1.30)\qquad u_{xt}=(\eta_x-\xi\eta)+(\eta_u-\xi_x+\xi^2)u_x-\xi_u u_x{}^2.$$

Consequently, (1.28) collapses to the following polynomial form in u_x:

$$\xi_{uu}u_x^3 + (2\xi_{xu} - \eta_{uu} - 2\xi\xi_u)u_x^2 + (\xi_{xx} - \xi_t - 2\eta_{xu} - 2\xi\xi_x + 2\eta\xi_u)u_x + (\eta_t - \eta_{xx} + 2\eta\xi_x) = 0. \tag{1.31}$$

The solution of the resulting four nonlinear determining equations is given by

$$\begin{aligned} &\xi = \xi(x,t), \\ &\eta = C(x,t)u + D(x,t), \end{aligned} \tag{1.32a}$$

where $(\xi(x,t), C(x,t), D(x,t))$ is any solution of the nonlinear system

$$\begin{aligned} &\xi_t - \xi_{xx} + 2\xi\xi_x = -2C_x, \\ &C_t - C_{xx} + 2\xi_x C = 0, \\ &D_t - D_{xx} + 2\xi_x D = 0. \end{aligned} \tag{1.32b}$$

Case 2: $\tau \equiv 0, \xi \equiv 1$
Here it is easy to show that (1.28) collapses to the single determining equation

$$\eta^2\eta_{uu} + 2\eta\eta_{xu} + \eta_{xx} - \eta_t = 0. \tag{1.33}$$

Note that

$$\eta = -\tfrac{1}{2}\sigma(x,t)u \tag{1.34}$$

solves (1.33) if $\sigma(x,t)$ is any solution of Burgers' equation

$$\sigma_t + \sigma\sigma_x = \sigma_{xx}. \tag{1.35}$$

Since in this case $\eta = u_x$, from (1.34) we obtain the Cole-Hopf transformation

$$\sigma = -2\frac{u_x}{u}$$

through the nonclassical method! This case was first considered in [16] (see also Appendix 7 in [17]).

The nonclassical method essentially lay dormant for many years. The first significant discussion of it appeared in the papers of Olver and Rosenau (cf. [18] and [19]). The real interest in the nonclassical method was ignited by the remarkable paper of Clarkson and Kruskal [20], in which they exhibited similarity solutions of the Boussinesq equation

$$u_{tt} + uu_{xx} + u_x^2 + u_{xxxx} = 0, \tag{1.36}$$

not obtainable by Lie's method. In this paper the Direct Method was introduced to find solutions of scalar PDEs based on the ansatz of the form (1.21). In a "tour de force" Clarkson and Kruskal found all such solutions for the Boussinesq equation (1.36). For example, their solution of (1.36), given by

$$u(x,t) = t^2w(z) - t^{-2}(x + \lambda t^5)^2, \quad z = xt + \tfrac{1}{6}\lambda t^6, \quad \lambda = \text{const}, \tag{1.37}$$

with $w(z)$ satisfying the reduced ODE

$$(w''' + ww' + 5\lambda w - 50\lambda^2 z)' = 0, \tag{1.38}$$

is not obtainable by Lie's method.

Our previous discussion demonstrates that *all* solutions arising from the Direct Method must arise from the nonclassical method. In a seminal paper [15], Levi and Winternitz showed the usefulness of the nonclassical method in using it to obtain all the Clarkson and Kruskal solutions of the Boussinesq equation (1.36). In [21], Nucci and Clarkson used the nonclassical method to obtain solutions of the Fitzhugh-Nagumo equation

$$u_t = u_{xx} + u(1-u)(u-a),\ a = \text{const}, \tag{1.39}$$

which could not be found by either Lie's method or the Direct Method. These solutions fit the ansatz (1.20) but not the ansatz (1.21) of the Direct Method. As with Lie's method, the nonclassical method (unlike the Direct Method) can be used for clasification problems. In [22], Clarkson and Mansfield applied the nonclassical method to the nonlinear heat equation

$$u_t = u_{xx} + f(u), \tag{1.40}$$

to find forms of the reaction term $f(u)$ and solutions of the corresponding PDEs (1.40) which are not obtainable by Lie's method.

2 Extensions of the Nonclassical Method

If a given PDE (1.14) can be expressed as an equivalent conservation law (cf. [23]), then (1.14) can be embedded in an auxiliary potential system. A point symmetry of the potential system, obtained through Lie's algorithm, could yield a nonlocal symmetry of (1.14). A similarity solution of a potential system, arising from such a point symmetry, could yield a solution of (1.14) which cannot be obtained by a *direct* application of the nonclassical method to (1.14).

Without loss of generality, suppose (1.14) is a second order PDE (1.23) written as a conservation law

$$\frac{D}{Dx} f^1(x,t,u,u_x,u_t) - \frac{D}{Dt} f^2(x,t,u,u_x,u_t) = 0. \tag{2.1}$$

Through (2.1) one can introduce an auxiliary potential variable v and form the auxiliary potential system

$$\begin{aligned} v_t &= f^1(x,t,u,u_x,u_t), \\ v_x &= f^2(x,t,u,u_x,u_t). \end{aligned} \tag{2.2}$$

The integrability condition of (2.2) shows that any solution $(u(x,t), v(x,t))$ of (2.2) yields a solution $u(x,t)$ of (2.1) and that conversely, for any solution $u(x,t)$ of (2.1), there corresponds a solution $(u(x,t), v(x,t))$ of (2.2). Most importantly, if $(u(x,t), v(x,t))$ solves (2.2), then so does $(u(x,t), v(x,t)+C)$ for any constant C. Consequently, from this non-invertible relationship between solutions of (2.1) and (2.2), a point symmetry of (2.2) could yield a nonlocal symmetry of (2.1). In particular, suppose

$$\mathrm{X} = \xi(x,t,u,v)\frac{\partial}{\partial x} + \tau(x,t,u,v)\frac{\partial}{\partial t} + \eta(x,t,u,v)\frac{\partial}{\partial u} + \zeta(x,t,u,v)\frac{\partial}{\partial v} \tag{2.3}$$

is the infinitesimal generator of a point symmetry admitted by (2.2). Then (2.3) yields a nonlocal symmetry of (2.1) if and only if $(\xi(x,t,u,v), \tau(x,t,u,v), \eta(x,t,u,v))$ depends essentially on v. (Otherwise (2.3) yields a point symmetry of (2.1).) The similarity solutions $(u,v) = (\theta^1(x,t), \theta^2(x,t))$ of (2.2), arising from (2.3), satisfy the invariant surface condition

$$\begin{aligned} &\mathbf{X}(u-\theta^1(x,t))\Big|_{(u,v)=(\theta^1(x,t),\theta^2(x,t))}=0, \\ &\mathbf{X}(u-\theta^2(x,t))\Big|_{(u,v)=(\theta^1(x,t),\theta^2(x,t))}=0, \end{aligned} \tag{2.4}$$

i.e.,

$$\begin{aligned} &\xi(x,t,u,v)u_x+\tau(x,t,u,v)u_t=\eta(x,t,u,v), \\ &\xi(x,t,u,v)v_x+\tau(x,t,u,v)v_t=\zeta(x,t,u,v). \end{aligned} \tag{2.5}$$

The general solution of the characteristic equations

$$\frac{dx}{\xi}=\frac{dt}{\tau}=\frac{du}{\eta}=\frac{dv}{\zeta}, \tag{2.6}$$

corresponding to (2.5), can be represented in the form

(2.7a) $z(x,t,u,v)=$ const $=c_1$, *(similarity variable)*

(2.7b) $W_1(x,t,u,v)=$ const $=c_2=w_1(z)$,

(2.7c) $W_2(x,t,u,v)=$ const $=c_3=w_2(z)$,

yielding an ansatz

$$u=\Phi(x,t,w_1(z),w_2(z)), \tag{2.8a}$$

$$v=\Psi(x,t,w_1(z),w_2(z)), \tag{2.8b}$$

for solutions of potential system (2.2), after solving (2.7b,c) in terms of u and v. The dependence of Φ and Ψ on x, t, $w_1(z)$, and $w_2(z)$ in (2.8a,b) is explicit; $w_1(z)$ and $w_2(z)$ are arbitrary functions of the similarity variable z. The substitution of (2.8a,b) into (2.2) leads to a reduced system of ODEs with independent variable z and dependent variables $w_1(z)$ and $w_2(z)$. Clearly (2.8a,b) represents a different ansatz for obtaining solutions of (2.1) than the ansatz (1.20) corresponding to the nonclassical method. When (2.3) yields a nonlocal symmetry of (2.1) with $\dfrac{\xi}{\tau}$ independent of v, then the similarity variable z is independent of v, and hence one can substitute (2.8a) directly into (2.1) to obtain solutions of (2.1) without further use of the corresponding potential system (2.2). Here the substitution of (2.8a) into (2.1) leads both to a system of ODEs which yields all solutions of (2.1) obtained through substitution of (2.8a,b) into the potential system (2.2) and possibly even more solutions of (2.1) (cf. [24]). If $\xi_u=\xi_v=\tau_u=\tau_v=\eta_{uu}=\eta_{uv}=\eta_{vv}=\zeta_{uu}=\zeta_{uv}=\zeta_{vv}\equiv 0$, then the ansatz (2.8a) simplifies to

$$u=A(x,t)+B_1(x,t)w_1(z(x,t))+B_2(x,t)w_2(z(x,t)), \tag{2.9}$$

for some specific functions $A(x,t)$, $B_1(x,t)$, $B_2(x,t)$.

The use of potential systems to obtain nonlocal symmetries of a given PDE originated in [25] and [26]. In these papers new solutions of the wave equation

$$u_{tt}-c^2(x)u_{xx}=0, \tag{2.10}$$

corresponding to the ansatz (2.9), were found for various forms of the wave speed $c(x)$. These solutions cannot be obtained by a direct application of either Lie's method or the nonclassical method to (2.10). See [8] and references in [23] for more details on, and examples of, potential systems and nonlocal symmetries for both linear and nonlinear PDEs.

2.1 Extension of the Nonclassical Method to Potential Systems

We now introduce an algorithm which incorporates the nonclassical method to potential systems. This allows one to find wider classes of solutions of a scalar PDE of the form (2.8). We seek all $(\xi(x,t,u,v), \tau(x,t,u,v), \eta(x,t,u,v), \zeta(x,t,u,v))$ so that (2.3) is a symmetry which leaves invariant the augmented system consisting of the potential system (2.2), the invariant surface condition (2.5), and differential consequences of (2.5). System (2.5), and its differential consequences, introduce additional relationships between the derivatives of u and v beyond those used to find the point symmetries of potential system (2.2). For any choice of (ξ, τ, η, ζ), (2.3) leaves invariant (2.5). Consequently, the invariant solutions of potential system (2.2), arising from solutions of the determining equations for the nonclassical symmetries of the augmented system, include all invariant solutions of (2.2) which arise from the point symmetries of (2.2) obtained through Lie's algorithm. One can show that the compatibility of the completely augmented system consisting of (2.2), (2.5), and differential consequences of *both* (2.2) and (2.5), leads to $(\xi(x,t,u,v), \tau(x,t,u,v), \eta(x,t,u,v), \zeta(x,t,u,v))$ satisfying the determining equations of the nonclassical method (when applied to this completely augmented system).

As a prototypical example, consider the nonlinear heat equation

$$u_t = \big(K(u)u_x\big)_x. \tag{2.11}$$

For any conductivity $K(u)$, one has the potential system

$$\begin{aligned} v_x &= u, \\ v_t &= K(u)u_x. \end{aligned} \tag{2.12}$$

The point symmetries of (2.11) arise from solving nine linear determining equations in three unknowns whereas the point symmetries of its potential system (2.12) arise from solving seven linear determining equations in four unknowns. On the other hand, the nonclassical method applied directly to the scalar PDE (2.11) involves four nonlinear determining equations in two unknowns (ξ, η) when $\tau \equiv 1$. (See [8] for the solution of the classification problem of (2.11) with respect to point symmetries and nonlocal symmetries arising from potential system (2.12).)

For any $K(u)$, when applying the nonclassical method to potential system (2.2) with $\tau \equiv 1$, one arrives at the following two nonlinear determining equations involving three unknowns (ξ, η, ζ):

$$\zeta_u u_x + \zeta_v v_x - \xi_u u_x v_x - \xi_v {v_x}^2 = \eta - \zeta_x, \tag{2.13a}$$

$$\begin{aligned} &\zeta_u u_t + \zeta_v v_t - (K(u)\eta_v + \xi_t)v_x - \xi_u u_t v_x - \xi_v v_t v_x - (K'(u)\eta + K(u)\eta_u)u_x \\ &+K(u)\xi_v u_x v_x + K(u)\xi_u {u_x}^2 = K(u)\eta_x - \zeta_t, \end{aligned} \tag{2.13b}$$

where in (2.13a,b)

$$v_x = u,$$
$$v_t = \zeta - u\xi,$$
$$(2.14)\qquad u_x = \frac{1}{K(u)}(\zeta - u\xi),$$
$$u_t = \eta - \frac{1}{K(u)}(\zeta - u\xi)\xi.$$

Further details for this example will appear in a forthcoming paper [27].

2.2 A Further Extension of the Nonclassical Method

Suppose any of the following three sets of PDEs

$$(2.15)\qquad \begin{aligned} \hat{\eta} &= u_t + \xi_1(x,t,u,v)u_x - \eta(x,t,u,v) = 0, \\ \hat{\zeta} &= v_t + \xi_2(x,t,u,v)v_x - \zeta(x,t,u,v) = 0, \end{aligned}$$

with $\xi_2 \not\equiv \xi_1$,

$$(2.16)\qquad \begin{aligned} \hat{\eta} &= u_t + \xi(x,t,u,v)u_x - \eta(x,t,u,v) = 0, \\ \hat{\zeta} &= v_x - \zeta(x,t,u,v) = 0, \end{aligned}$$

with $\xi \not\equiv 0$, or

$$(2.17)\qquad \begin{aligned} \hat{\eta} &= u_x - \eta(x,t,u,v) = 0, \\ \hat{\zeta} &= v_t + \xi(x,t,u,v)v_x - \zeta(x,t,u,v) = 0, \end{aligned}$$

with $\xi \not\equiv 0$, is compatible with the potential system (2.2). Any such situation produces an ansatz for solutions of (2.2) which is not of the form (2.8a,b). Now we give algorithms to determine such compatibility sets and corresponding reductions to ODEs for a potential system (2.2).

2.2.1 Reductions

We are unable to give a functional representation for the solution of any of the systems of PDEs (2.15)-(2.17). Nonetheless, for each of these systems one is able to reduce the potential system (2.2) to a system of ODEs as follows:

For the set (2.15), the use of (2.15) and its differential consequences allows one to replace all t-derivatives of u and v in (2.2) by expressions involving x, t, u, v, and x-derivatives of u and v. Consequently (2.2) reduces to a system of ODEs with independent variable x and dependent variables u and v. The constants of integration, arising in the general solution of this reduced system of ODEs, are arbitrary functions of t. These functions of t are then determined by substituting this general solution into the set (2.15).

For sets (2.16) and (2.17), one proceeds in a similar fashion with the roles of x and t interchanged.

Note that this method of reduction is also useful and necessary when one is unable to integrate the characteristic equations corresponding to either of the invariant surface conditions (1.18) or (2.5).

2.2.2 Determination of the Compatibility Sets

One can extend Lie's algorithm to find infinitesimal generators (2.3) admitted by (2.2) with (ξ,τ,η,ζ) allowed to depend on derivatives of u and v. Here one seeks infinitesimal generators admitted by (2.2), *and its differential consequences*, of the form

$$\mathbf{X}=\hat{\eta}\left(x,t,u,v,\underset{1}{u},\underset{1}{v},\ldots,\underset{k}{u},\underset{k}{v}\right)\frac{\partial}{\partial u}+\hat{\zeta}\left(x,t,u,v,\underset{1}{u},\underset{1}{v},\ldots,\underset{k}{u},\underset{k}{v}\right)\frac{\partial}{\partial v}, \tag{2.18}$$

$k=1,2,\ldots$. Such symmetries are called *Lie-Bäcklund* (*higher order, generalized*) *symmetries*, which include all point symmetries as a special case. For details, see [8], [13], or [14]. One can show that the compatibility of any one of the sets (2.15)-(2.17) with the potential system (2.2) is equivalent to the determination of when the corresponding *nonclassical Lie-Bäcklund symmetry* is admitted by the completely augmented system consisting of the potential system (2.2), the system

$$\begin{aligned}\hat{\eta}&=0,\\ \hat{\zeta}&=0,\end{aligned} \tag{2.19}$$

arising from any one of the sets (2.15)-(2.17), and all their differential consequences Then one proceeds in the same manner as in § 2.1 to determine the coefficients of $\hat{\eta}$ and $\hat{\zeta}$. In particular, let the matrix operator $\mathcal{L}[u,v]$ be the Fréchet derivative of (2.2) (cf. [14] or [23]). Then each solution of the determining equations, defined by the matrix system

$$\mathcal{L}[u,v]\begin{bmatrix}\hat{\eta}\\ \hat{\zeta}\end{bmatrix}=0, \tag{2.20}$$

in which $(u(x,t),v(x,t))$ is any solution of the completely augmented system of PDEs consisting of (2.2), (2.19), and their differential consequences, yields a compatibility set. (Note that if in (2.15), $\xi_1\equiv\xi_2$, then one obtains the same determining equations as in § 2.1.)

3 Concluding Remarks

(1) In [5] (see also [6], [8]), it was shown that if a nonlinear system of PDEs admits an infinite-parameter group of point symmetries characterized by infinitesimal generators whose coefficients satisfy certain criteria, then one can algorithmically find an invertible transformation which maps the nonlinear system to a linear system. This algorithm was extended to non-invertible mappings (eg, the Cole-Hopf transformation) in [7] (see also [8]). More recently, it has been shown that the linearization of a system of PDEs is connected with the determination and characterization of the factors which yield the system's conservation laws (cf. [24]).

(2) Further ansätze for solutions can be obtained if one is able to find potential systems of potential systems, leading to further "generations" of potential systems. An mth generation potential system would have dependent potential variables $v^1,v^2,\ldots,v^m$. The corresponding ansatz for solutions of an mth generation potential system, arising from its invariance under point symmetries or, more generally, from applying the extension of the nonclassical method described in § 2.1, would be of the form

$$\begin{aligned}u&=\Phi(x,t,w_1(z),w_2(z),\cdots,w_m(z)),\\ v^1&=\Psi^1(x,t,w_1(z),w_2(z),\cdots,w_m(z)),\\ &\ \vdots\\ v^m&=\Psi^m(x,t,w_1(z),w_2(z),\cdots,w_m(z)),\end{aligned} \tag{3.1}$$

with similarity variable $z=z(x,t,u.v^1,\ldots,v^m)$.

Other ansätze for solutions of an mth generation potential system arise from the further extension of the nonclassical method described in § 2.2.

(3) After applying Lie's algorithm to find the point symmetries (2.3) admitted by a potential system (2.2), it can happen that one will not obtain, as a subset, all point symmetries of (2.1). (See [8] for examples illustrating this.) As mentioned previously, the application of the nonclassical method to a scalar PDE yields *all* solutions satisfying an ansatz of the form (1.20). However, when applying the extension of the nonclassical method, described in § 2.1, to a potential system (2.2) with $\xi_v = \tau_v \equiv 0$, one may not obtain all solutions of (2.1) which satisfy an ansatz of the form (2.8a). In particular, different potential systems of a given scalar PDE could yield different solutions of the scalar PDE which satisfy an ansatz of the form (2.8a) when $\xi_v = \tau_v \equiv 0$.

(4) A point symmetry admitted by a scalar PDE is not necessarily a nonclassical symmetry of the same PDE. As an example, consider the PDE

$$u_t u_{xx} + u_t + 1 = 0. \tag{3.2}$$

Clearly (3.2) is invariant under translations in t, and hence admits the point symmetry corresponding to the infinitesimal generator

$$\mathbf{X} = \frac{\partial}{\partial t}. \tag{3.3}$$

The corresponding invariant surface condition is given by the PDE

$$u_t = 0. \tag{3.4}$$

The substitution of (3.4) into (3.2) yields a contradiction

$$1 = 0, \tag{3.5}$$

and hence (3.3) is not a nonclassical symmetry of the augmented system (3.2), (3.4). (Compatibility between the invariant surface condition and a given PDE *is built into* the nonclassical method, unlike the case when one is seeking similarity solutions by the classical method of Lie.)

(5) In recent years several symbolic manipulation programs have been developed which perform one or more of the following functions automatically and/or interactively: Set up determining equations, find the dimension (if finite) of their solution space, and solve them explicitly. For the presentation of algorithms performing such functions for the nonclassical method, see [28] and references therein. Particular attention is drawn to the work of Reid et al. (cf. [29]-[31]).

(6) May Julian Cole age well for many more years!

References

[1] J. D. Cole, *On a quasilinear parabolic equation occurring in aerodynamics*, Quart. Appl. Math., 9 (1951), pp. 225-236.

[2] G. W. Bluman and J. D. Cole, *The general similarity solution of the heat equation*, J. Math. Mech., 18 (1969), pp. 1025-1042.

[3] E. Hopf, *The partial differential equation* $u_t + uu_x = \mu u_{xx}$, Comm. Pure Appl. Math., (3) (1950), pp. 201-230.

[4] G. W. Bluman, *Use of group methods for relating linear and nonlinear partial differential equations*, in Proceedings of Symposium on Symmetry, Similarity and Group Theoretic Methods in Mechanics, Calgary, (1974), pp. 203-218.

[5] S. Kumei and G. W. Bluman, *When nonlinear differential equations are equivalent to linear differential equations*, SIAM J. Appl. Math., 42 (1982), pp. 1157-1173.

[6] G. W. Bluman and S. Kumei, *Symmetry-based algorithms to relate partial differential*

equations: I. *Local symmetries*, Europ. J. Appl. Math., 1 (1990), pp. 189-216.

[7] ————, *Symmetry-based algorithms to relate partial differential equations*: II. *Linearization by nonlocal symmetries*, Europ. J. Appl. Math., 1 (1990), pp. 217-223.

[8] ————, *Symmetries and Differential Equations*, Springer-Verlag, New York, 1989.

[9] S. Lie, *Über die Integration durch bestimmte Integrale von einer Klasser linearer partieller Differentialgleichungen*, Arch. for Math., 6 (1881), pp. 328-368; also Gesammelte Abhandlungen, Vol III, B. G. Teubner, Leipzig, 1922, pp. 492-523.

[10] L. V. Ovsiannikov, *Group Properties of Differential Equations*, Novosibirsk, 1962 (in Russian).

[11] G. W. Bluman and J. D. Cole, *Similarity Methods for Differential Equations*, Springer-Verlag, New York, 1974.

[12] L. V. Ovsiannikov, *Group Analysis of Differential Equations*, Academic Press, New York, 1982.

[13] N. H. Ibragimov, *Transformation Groups Applied to Mathematical Physics*, Reidel, Boston, 1985.

[14] P. J. Olver, *Applications of Lie Groups to Differential Equations*, Springer-Verlag, New York, 1986; 2nd edition, 1993.

[15] D. Levi and P. Winternitz, *Non-classical symmetry reduction*: *example of the Boussinesq equation*, J. Phys A, 22 (1989), pp. 2915-2924.

[16] W. I. Fushchich, V. M. Shtelen, N. I. Serov, and R. Popowych, *Conditional symmetries of the linear heat equation*, Dokl. Ukr. Acad. Nauk A 12 (1992), pp. 20-26.

[17] W. I. Fushchich, V. M. Shtelen, and N. I. Serov, *Symmetry Analysis and Exact Solutions of Equations of Nonlinear Mathematical Physics*, Kluwer, Dordrecht, 1993.

[18] P. J. Olver and P. Rosenau, *The construction of special solutions to partial differential equations*, Phys. Lett. A, 114 (1986), pp. 107-112.

[19] ————, *Group-invariant solutions of differential equations*, SIAM J. Appl. Math., 47 (1987), pp. 263-278.

[20] P. A. Clarkson and M. D. Kruskal, *New similarity solutions of the Bousinnesq equation*, J. Math. Phys., 30 (1989), pp. 2201-2213.

[21] M. C. Nucci and P. A. Clarkson, *The nonclassical method is more general than the direct method for symmetry reductions. An example of the Fitzhugh-Nagumo equation*, Phys. Lett. A, 164 (1992), pp. 49-56.

[22] P. A. Clarkson and E. L. Mansfield, *Symmetry reductions and exact solutions of a class of nonlinear heat equations*, Physica D, 70 (1994), pp. 250-288.

[23] G. W. Bluman and P. Doran-Wu, *The use of factors to discover potential systems or linearizations*, Acta Appl. Math., 41 (1995), pp. 21-43.

[24] E. Pucci and G. Saccomandi, *Potential symmetries and solutions by reduction of partial differential equations*, J. Phys. A, 26 (1993), pp. 681-690.

[25] G. W. Bluman and S. Kumei, *On invariance properties of the wave equation*, J. Math. Phys., 28 (1987), pp. 307-318.

[26] ————, *Exact solutions for wave equations of two-layered media with smooth transition*, J. Math. Phys., 29 (1988), pp. 86-96.

[27] G. W. Bluman and D. Levi, *Nonclassical nonlocal solutions of PDEs*, in preparation.

[28] P. A. Clarkson and E. L. Mansfield, *Algorithms for the nonclassical method of symmetry reductions*, SIAM J. Appl. Math., 54 (1994), pp. 1693-1719.

[29] G. J. Reid, *A triangularization algorithm which determines the Lie symmetry algebra of any system of PDEs*, J. Phys. A, 23 (1990), pp. L853-L859.

[30] ————, *Algorithms for reducing a system of PDEs to standard form, determining the dimension of its solution space and calculating its Taylor series solution*, Europ. J. Appl. Math., 2 (1991), pp. 293-318.

[31] G. J. Reid and A. Wittkopf, *A Differential Algebra Package for* MAPLE, ftp 137.82.36.23 login: anonymous, password: your email address, directory: pub/standardform (1993).

Forced Soliton-Like Disturbances in Boundary Layers of Different Kinds*

Elena V. Bogdanova-Ryzhova† Oleg S. Ryzhov‡

December 18, 1995

Abstract

Properties of forced nonlinear disturbances in two classic soliton-bearing BDA and KdV models appearing in an asymptotic analysis of two- and three- dimensional boundary layers are discussed and compared. One more, recently derived and less studied, nonlinear model is investigated. It is shown that the compound equation, featuring an integro-differential term typical of the BDA equation and a third-order differential term typical of the KdV equation, possesses its own peculiar solitary eigenmodes which can be evoked by an external forcing.

1 Introduction

It is widely recognized now that a great variety of wave phenomena in fluids can be described by mathematical models based on nonlinear equations allowing of soliton solutions. The famous Benjamin-Davis-Acrivos (BDA) equation

$$\frac{\partial \tilde{A}}{\partial t} + \tilde{A}\frac{\partial \tilde{A}}{\partial x} = \frac{1}{\pi}\int_{-\infty}^{\infty} \frac{\partial^2 \tilde{A}/\partial X^2}{X - x}\, dX \tag{1}$$

and the Korteweg-de Vries (KdV) equation

$$\frac{\partial \tilde{A}}{\partial t} + \tilde{A}\frac{\partial \tilde{A}}{\partial x} = \frac{\partial^3 \tilde{A}}{\partial x^3} \tag{2}$$

naturally occur in theoretical approaches to numerous atmospheric and oceanic problems, such as generation of atmospheric waves over the mountains or ocean tidal flows over the sills. Recent developments in general boundary-layer theory based on the Prandtl equations with self-induced pressure proved that incompressible boundary layer belongs to the vast multitude of soliton-bearing systems and features solitons as free internal waves, whose type (BDA or KdV) is defined by the specific type of the boundary-layer flow itself.

Zhuk & Ryzhov [1] and Smith & Burggraf [2] showed on the basis of the asymptotic analysis that two-dimensional incompressible boundary layer must be able to generate and sustain free streamwise disturbances with amplitudes larger and lengths shorter than those of the classic Tollmien-Schlichting waves. These particular disturbances are nonlinear and are governed by the homogeneous BDA equation (1). The theoretical prediction received

*This study was supported under grant AFOSR F49620-93-1-002LDEF (O.S.R.).

†Visiting Scientist, Rensselaer Polytechnic Institute, Troy, NY.

‡Visiting Professor, Rensselaer Polytechnic Institute, Troy, NY.

a convincing experimental evidence for its validity in a series of innovative experiments by Borodulin & Kachanov [3] and Kachanov [4], who claimed the soliton-like nature of sharp spikes observed on the velocity oscilloscope traces in two-dimensional incompressible boundary layer. These distinctive negative peaks move away from the wall during their formation and exist afterwards in a rather conservative shape in the external part of the boundary layer while moving downstream for some time, before a strong three-dimensionalization of the flow sets in. After Ryzhov [5],[6] had identified those stable structures observed by the experimentalists as the BDA solitons, there was no more doubt left that the BDA solitons are, indeed, the nonlinear eigenmodes of the triple-deck system of equations for two-dimensional boundary layer in a limit when nonlinear effects exceed viscous effects. The detailed comparison of the experimental data and theoretical predictions can be found in [7].

According to [1],[2], a related problem on two-dimensional viscous flow past a plate, placed vertically in the gravity field and heated, involves the KDV equation (2), which controls the development of free nonlinear waves peculiar to the case.

Most recently, Ryzhov & Terent'ev [8],[9] suggested an asymptotic model for three-dimensional boundary layer with crossflow. The KdV equation (2) appears in their elaborated analysis as a governing equation for nonlinear distubances that have amplitudes large enough and propagate in a crossflow direction. This result means a possibility for the KdV solitons to occur as free internal waves in thee-dimensional boundary layer with crossflow. Though this last theoretical finding has not been supported yet by experiments, it, nevertheless, widens general understanding of incompressible boundary layers and opens new perspective on the phenomena of boundary-layer stability and transition.

Besides the BDA and KdV equations, there is one more nonlinear equation, which might deserve interest of applied fluid dynamysists. This equation was derived independently by Ryzhov [10],[12] and Benjamin [11] for description of entirely different physical environments. It contains an integro-differential term typical of the BDA equation as well as a third-order differential term typical of the KdV equation, and, therefore, it makes a specific combination of the both classic equations.

Benjamin [11] derived the compound equation for the description of unidirectional propagation of the long waves in a two-fluid system where the lower fluid with greater density is infinitely deep and there are the effects of capillarity at the interface. In the Benjamin's model

$$\frac{\partial u}{\partial t} + \frac{\partial u}{\partial x} + 2u\frac{\partial u}{\partial x} = -\alpha\frac{1}{\pi}\int_{-\infty}^{\infty}\frac{\partial^2 u/\partial X^2}{X-x}\,dX + \beta\frac{\partial^3 u}{\partial x^3}, \qquad 0<\alpha\ll\beta, \tag{3}$$

the integro-differential term is small as compared to the third-order differential term.

Ryzhov in [10],[12] derived his version of the compound equation whithin a framework of an asymptotic model of subsonic boundary layer by taking into account the secondary influence of the streamline's curvature on the flow parameters. Though the centrifugal forces are of second order, they may become comparable to the leading term in an asymptotic expansion for pressure distribution, when the disturbance wavelength becomes small enough. In spite of the fact, that the procedure of retaining only some of the second-order terms is not a strictly rational asymptotic approach, the model, nevertheless, may point to new important processes featuring nonlinear oscillations that are triggered by the normal pressure gradient. According to [10],[12], the compound equation for the boundary layer

$$\frac{\partial \tilde{A}}{\partial t} + \tilde{A}\frac{\partial \tilde{A}}{\partial x} = \frac{1}{\pi}\int_{-\infty}^{\infty} \frac{\partial^2 \tilde{A}/\partial X^2}{X - x}\, dX - \Delta_0 \frac{\partial^3 \tilde{A}}{\partial x^3}, \qquad 0 < \Delta_0 \ll 1 \tag{4}$$

contains the third-order differential term with a small parameter Δ_0 as a multiplier. Both equations (3) and (4) are reducible to one another by means of a transform

$$u \to -\frac{\alpha \Delta_0^2}{2\beta}(\tilde{A} - \frac{1}{2}), \qquad t \to -\frac{\beta^2}{\alpha^3 \Delta_0^2} t, \qquad x \to \frac{\beta}{\alpha \Delta_0} x.$$

Unlike (1) and (2), equation (4) is practically unstudied. It is not even proved to fall into a familly of fully integrable equations. As was shown in [11],[12], equation (4) possesses three conservation laws. Though the explicit form of its solitary wave solutions was not found, some hints at solution properties were still made. According to [11],[12], these solutions should have a propagation speed greater than the maximum speed of infinitesimal harmonic waves and should have oscillatory outskirts in the shape of short-scaled wiggles, which decay exponentially.

However, we can point out one particular explicit soliton solution of (4):

$$\tilde{A}_s(t,x) = \frac{-(24/5)\Delta_0 \gamma_0}{\Delta_0^2(\gamma_0 - 5)^2 + (x + \frac{1}{\Delta_0 \gamma_0} t)^2} + \frac{48 \Delta_0^3 (\gamma_0 - 5)^2}{[\Delta_0^2(\gamma_0 - 5)^2 + (x + \frac{1}{\Delta_0 \gamma_0} t)^2]^2}. \tag{5}$$

The constant γ_0 is a real root of a cubic equation

$$\gamma^3 - 15\gamma^2 + 625 = 0$$

and equals $\gamma_0 \approx -5.519017$. Solution (5) exists for any positive or negative value of the parameter $\Delta_0 \neq 0$. 'Mass' of this solution

$$\tilde{M}_s = \int_{-\infty}^{\infty} \tilde{A}_s(t,x)dx = \frac{24}{5}\pi$$

does not depend upon the parameter Δ_0.

To verify existence and stability of this unique soliton mode, equation (4) was solved numerically with the initial distribution of the desired function $\tilde{A} = \tilde{A}_s$ given by (5) at the moment $t = -250$ and with the value of the parameter Δ_0 fixed at 0.6. At moments $t = 0$ and $t = 250$ the numerical solution was compared with the same analytic representation (5) and both shapes remained virtually indistinguishable, as may be seen in Figure 1.

Soliton (5) has no oscillatory wings and its phase velocity is uniquely defined by a value of the parameter Δ_0 rather than belongs to the continuous spectrum. This solution is of a very special kind and its existence does not eliminate the question of whether the class of waves predicted in [11],[12] does exist.

Though the theory of the homogeneous BDA and KdV equations is well developed now, this knowledge appears to be insufficient to explain how and which solitary waves are brought to life by a specific external forcing. Meanwhile, these questions are the most important ones for many practical problems. The lack of an adequate theory explains the fact that forced oscillations governed by the inhomogeneous BDA as well as KdV models are scarcely studied so far, in spite of the achievements by Grimshaw & Smyth [13], Wu [14], Mitsudera & Grimshaw [15], Camassa & Wu [16],[17], in their inquiries into upstream radiated solitons provoked by external forcing agencies.

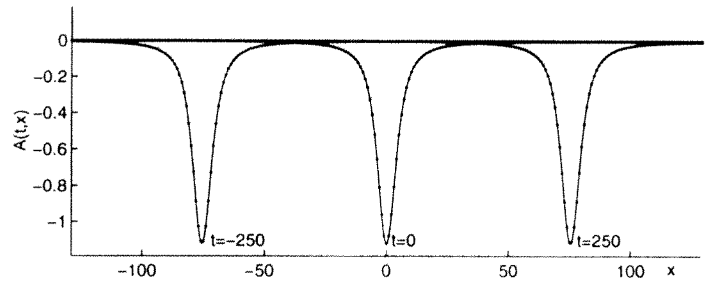

FIG. 1. *Numerical solution (solid line), computed from the initial distribution given by (5) at $t = -250$ and $\Delta_0 = 0.6$, as compared to the same analytic representation (dotted line) at $t = 0$ and $t = 250$. Here $A(t,x) = -\tilde{A}$ is a boundary-layer instantaneous displacement thickness.*

Knowledge on forced generation of nonlinear disturbances in boundary layers is crucial for problems of boundary-layer receptivity and transition. It is hoped that the following detailed consideration of the forced nonlinear waves will help to shed some light on general principles of their occurence and evolution. The present paper is not intended to make any immediate far-going conclusions about the physical interpretation of the mathematical phenomena found, leaving this difficult task for future endeavors.

2 Statement of the problem

As a rule, the forced equations of the BDA or KdV type, arising in the physics of the atmosphere or in the physics of the ocean, include, besides a forcing term, some additional terms responsible for the relevant physical processes, such as wave dissipation, detuning, radiation damping, etc. In what follows, the fBDA, fKdV and forced compound equations, respectively, are taken exactly as they appear in the boundary-layer theory, with none of the additional terms, mentioned above, present:

$$\frac{\partial \tilde{A}}{\partial t} + \tilde{A}\frac{\partial \tilde{A}}{\partial x} = \frac{1}{\pi}\int_{-\infty}^{\infty} \frac{\partial^2 \tilde{A}/\partial X^2}{X - x}\,dX - \frac{1}{\pi}\int_{-\infty}^{\infty} \frac{\partial^2 f/\partial X^2}{X - x}\,dX, \tag{6}$$

$$\frac{\partial \tilde{A}}{\partial t} + \tilde{A}\frac{\partial \tilde{A}}{\partial x} = \frac{\partial^3 \tilde{A}}{\partial x^3} - \frac{\partial^3 f}{\partial x^3}, \tag{7}$$

$$\frac{\partial \tilde{A}}{\partial t} + \tilde{A}\frac{\partial \tilde{A}}{\partial x} = \frac{1}{\pi}\int_{-\infty}^{\infty} \frac{\partial^2 \tilde{A}/\partial X^2}{X - x}\,dX - \Delta_0\frac{\partial^3 \tilde{A}}{\partial x^3} - \frac{1}{\pi}\int_{-\infty}^{\infty} \frac{\partial^2 f/\partial X^2}{X - x}\,dX + \Delta_0\frac{\partial^3 f}{\partial x^3}. \tag{8}$$

Here $\tilde{A}(t,x) = -A(t,x) + f(t,x)$ is a combination of an instantaneous displacement-thickness function A and the outer forcing f. Boundary and initial conditions are

$$\tilde{A}(t,x) \to 0, \quad x \to \pm\infty; \qquad \tilde{A}(0,x) = 0. \tag{9}$$

We consider the forcing to emerge gradually in a finite region on a flat surface and, upon obtaining its steady shape at some time, to remain unchanged thereafter.

It is worth mentioning here that an external agency is incorporated into equations very differently for boundary-layer disturbances and for atmospheric or oceanic waves. Thus, certain caution is required in attempts to establish correspondence between solutions describing different physical phenomena, even if the latter are governed by equations of actually the same type.

In what follows, the obstacle on the otherwise flat surface is chosen as

$$f(t,x) = \sigma g(t)h(x), \tag{10}$$

with

$$g(t) = \begin{cases} t/t_0, & 0 < t \le t_0 \\ 1, & t > t_0 \end{cases}, \tag{11}$$

and

$$h(x) = \begin{cases} \sigma \cos^2 \pi x/2b, & |x| \le b \\ 0, & |x| > b \end{cases}, \tag{12}$$

where $b = 3.5$, $t_0 = 1$. All computations are carried out by means of the pseudo-spectral method of Burggraf & Duck [20], based on applying a fast Fourier transform to (6)-(9).

Within a framework of any particular problem, there is always a correspondence between solutions produced by similar obstacles of different size, if some similarity parameter, characteristic of the problem, has the same value.

Consider equation (7) supplemented with conditions (9)-(12). A group of known affine transformations for the KdV equation

$$x \to \beta x', \quad t \to \beta^3 t', \quad \tilde{A} \to \beta^{-2} A'$$

reduces (7) to the following

$$\frac{\partial A'}{\partial t'} + A'\frac{\partial A'}{\partial x'} = \frac{\partial^3 A'}{\partial x'^3} - \sigma\beta^2 g(\beta^3\frac{t'}{t_0})\frac{d^3}{dx^3}h(\beta\frac{x'}{b}).$$

If $\beta = b$, $t_0 = \beta^3 t'_0$, then each value of a parameter

$$S = \sigma b^2,$$

proportional to the 'moment of mass' of the obstacle, defines a set of similar wave patterns generated by obstacles of different amplitudes σ and characteristic lengths b. According to [18],[19], the similarity parameter for the fBDA equation with the same external forcing (10)-(12) is

$$Q = \sigma b$$

and is proportinal to the area ('mass') of the obstacle. There is also a group of affine transformations

$$x \to \beta x', \qquad t \to \beta^2 t', \qquad \tilde{A} \to \beta^{-1} A',$$

which reduces the forced compound equation (8) to

$$\begin{aligned} \frac{\partial A'}{\partial t'} + A'\frac{\partial A'}{\partial x'} &= \frac{1}{\pi}\int_{-\infty}^{\infty} \frac{\partial^2 A'/\partial X'^2}{X' - x'} dX' - \frac{\Delta_0}{\beta}\frac{\partial^3 A'}{\partial x'^3} \\ &-\frac{\sigma\beta}{\pi} g(\frac{\beta^2 t'}{t_0}) \int_{-\infty}^{\infty} \frac{\partial^2 h/\partial X'^2}{X' - x'} dX' + \Delta_0 \sigma g(\frac{\beta^2 t'}{t_0})\frac{\partial^3}{\partial x'^3} h(\frac{\beta x'}{b}). \end{aligned}$$

Thus, if $\beta = b$, $t_0 = \beta^2 t'_0$, then two characteristic parameters

$$R = \frac{\Delta_0}{b}, \qquad Q = \sigma b,$$

instead of three Δ_0, σ, b, are responsible for the type of a wave pattern produced by the obstacle (10)-(12). It is always necessary to bear in mind, that alternative similarity laws may come into play for the same equation, if it is used to describe different physical environments.

Results of a systematic numerical examination of the fKdV equation (7) depending upon the similarity parameter S are presented in this paper in parallel with the results for the fBDA equation (6), that were reported recently in [18],[19]. Some of the solutions of the forced compound equation (8), featuring solitary waves, most probably of the kind predicted in [11],[12], are also discussed.

3 Properties of Forced Disturbances

The major achievement in early studies of forced soliton equations is the discovery of the remarkable phenomenon of time-periodic generation of soliton-like waves on the site of the stationary forcing and their radiation upstream and downstream, as it is well documented in [13]-[15] for both the fBDA and fKdV systems. The forced KdV equation, however, proved to have also some stable stationary solutions [16]-[17], counterparts of which were never found for the fBDA equation.

New approach to investigation of the disturbance-radiation process arises, once the similarity parameter is incorporated into a model. It appears natural to inquire into specifics of wave systems produced by obstacles with different values of the corresponding similarity parameter. Such approach was recently implemented by authors [18],[19] in their study of the fBDA equation and is used here with regard to analysis of the fKdV equation. The results obtained disclose certain similarities and distinctions inherent in the two forced models, which are to be discussed in detail.

3.1 The fBDA Model

While analyzing the process of accumulation of the solution 'mass' upstream of the obstacle

$$M_{-b}(t) = \int_{-\infty}^{-b} A(t,x)\,dx,$$

the phenomenon of bifurcations of solutions, when the similarity parameter Q reaches some threshold values, was discovered. Two bifurcations of the fBDA-equation solutions can be seen in Figure 2, where logarithm of function $M_{-b}(t)$ vs. logarithm of time is shown. The conspicuous branching of solutions is observed for two threshold values of the similarity parameter Q: $3.92 < Q_1^* < 3.93$ and $51.48 < Q_2^* < 51.49$. The wave patterns in the subcritical regime I ($Q < Q_1^*$) are characterized by slow generation of solitons in both directions, for example, see Figure 3. As can be seen from Figure 4, the situation changes drastically in supercritical regime II ($Q > Q_1^*$), when an intensive wave activity develops on the site of the obstacle and results in generation of fast solitons upstream and downstream. The first bifurcation in the fBDA system brings about specific nearly limit-cycle-type oscillations over the crest of the hump. These peculiar oscillations are due to the almost periodic back-and-force motion of a wave confined to the obstacle boundaries. The wave starts moving from left to right with a rather small amplitude. At some point on the leeward side of the hump it turns back, growing essentially in amplitude. When it reaches its most left position, a soliton emerges and starts moving upstream, while the wave goes into the next cycle. The numerous pictures of this process with detailed discussion can be found in [19]. Thus, fast solitons, discharged by a wave motion over the obstacle, are

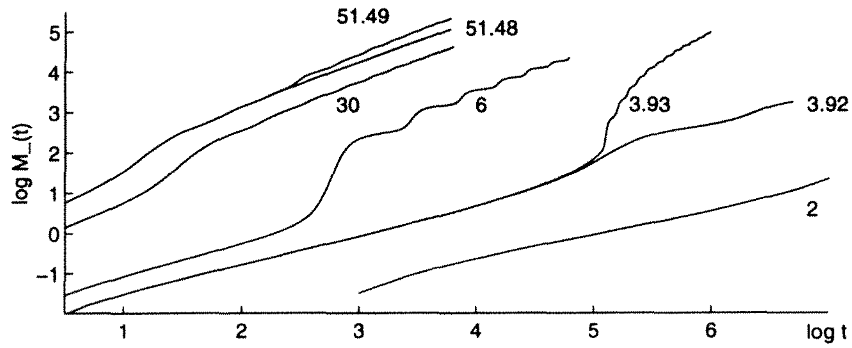

FIG. 2. *Forced BDA system: $\log M_{-b}(t)$ vs. $\log(t)$ for some values of the similarity parameter Q.*

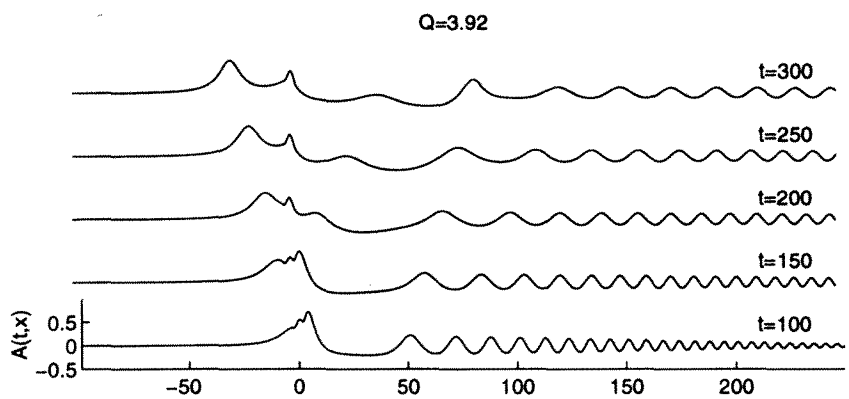

FIG. 3. *Forced BDA system: wave pattern for $Q = 3.92 < Q_1^*$ (subcritical regime I).*

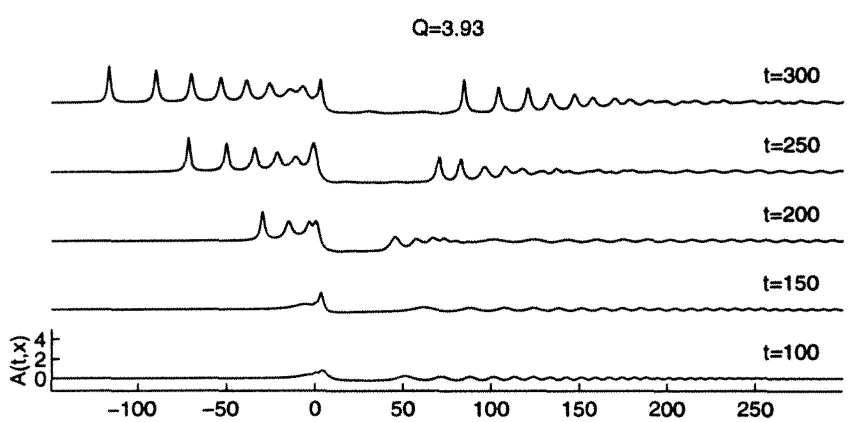

FIG. 4. *Forced BDA system: wave pattern for $Q = 3.93 > Q_1^*$ (supercritical regime II).*

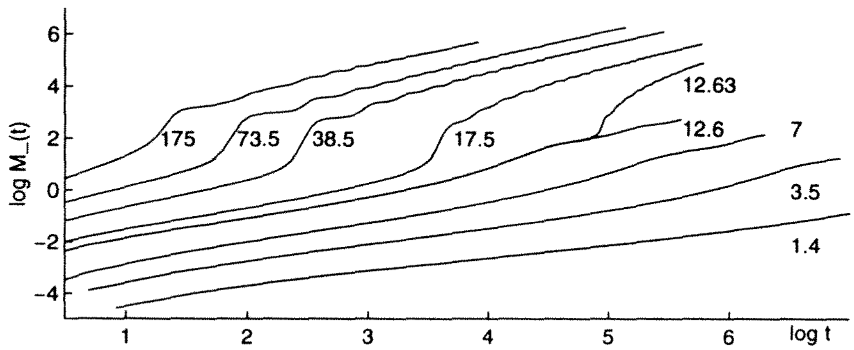

FIG. 5. *Forced KdV system: $logM_{-b}(t)$ vs. $log(t)$ for some values of the similarity parameter S.*

the most conspicuous feature of the supercritical regime II, which continuously turns into subcritical regime III on the threshold of the second bifurcation. Upon passing through the second bifurcation, the nearly periodic regime collapses, because of a second localized wave establishing itself along with the first one. The second wave is much less organized as compared to the first one, and elements of erratic behavior come into play as both waves impact on each other and produce solitons with varying amplitudes and reference times. This erratic behavior becomes a pronounced feature of the supercritical regime IV, as $Q > Q_2^*$.

3.2 The fKdV Model

Remarkably enough, many features outlined above for the fBDA-equation solutions appear to be pertinent to the fKdV-equation solutions as well. However, close resemblance of the fBDA and fKdV solutions does not go beyond the first bifurcation. The wave motion. which is considered to be responsible for the fast soliton emission and is localized on the obstacle site, looks and evolves differently for both equations: in the fBDA model it eventually develops towards the second bifurcation, while in the fKdV model the second bifurcation is not found (at least in the range of S studied).

Indeed, as can be seen in Figure 5, featuring $\log M_{-b}$ vs. $\log t$ for several positive values of S, a very distinctive bifurcation of the solutions exists for $S = S^*$, $12.60 < S^* < 12.63$.

Figure 6 and Figure 7 show wave patterns for the subcritical ($S < S^*$) and supercritical ($S > S^*$) values of the similarity parameter S. The comparison of both pictures reveals that:

(a) Prior to the bifurcation, solution consists of comparatively slow solitary waves emitted upstream and downstream; The disturbance localized over the obstacle is aproximately of the same magnitude as the solitary waves radiated upstream.

(b) After the first bifurcation, a vigorous wave process sets in at the location of the obstacle. It produces solitons, which are much faster than those pertinent to the subcritical regime I. Moreover, the amplitude of this peculiar localized wave motion is higher than the amplitudes of the solitons emitted upstream as well as downstream.

Both of these features follow closely the description of the first bifurcation of the solutions of the fBDA equation. Figure 8 illustrates the drastic change in the behavior of the instantaneous displacement function $A(t, x)$ at the point $x = 0$ due to the first bifurcation for the fBDA equation and for the fKdV equation. In both cases, slow oscillations near some mean value abruptly give place to vigorous pulsations, when the relevant similarity

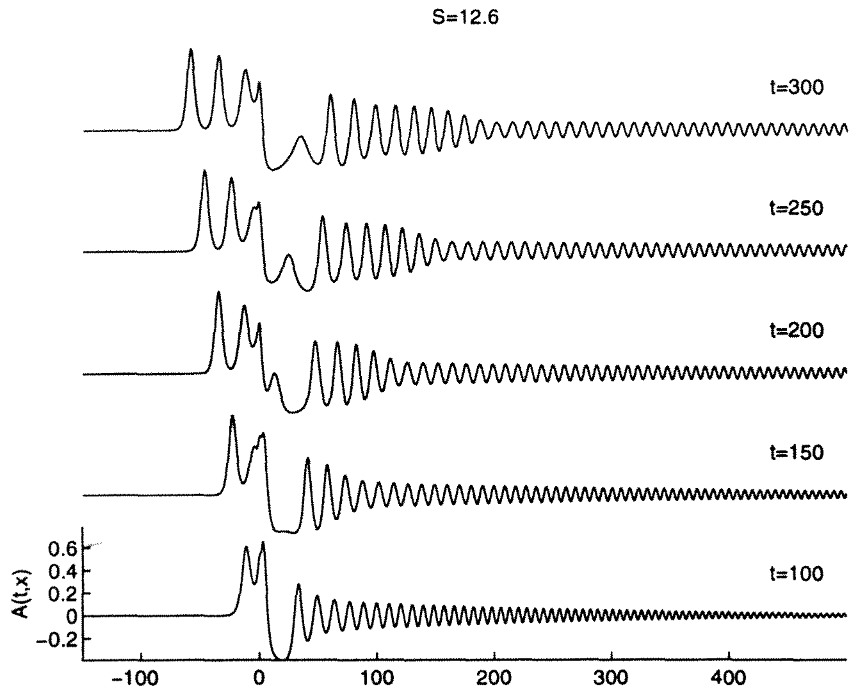

FIG. 6. *Forced KdV system: wave pattern for* $S = 12.6 < S^*$ *(subcritical regime I).*

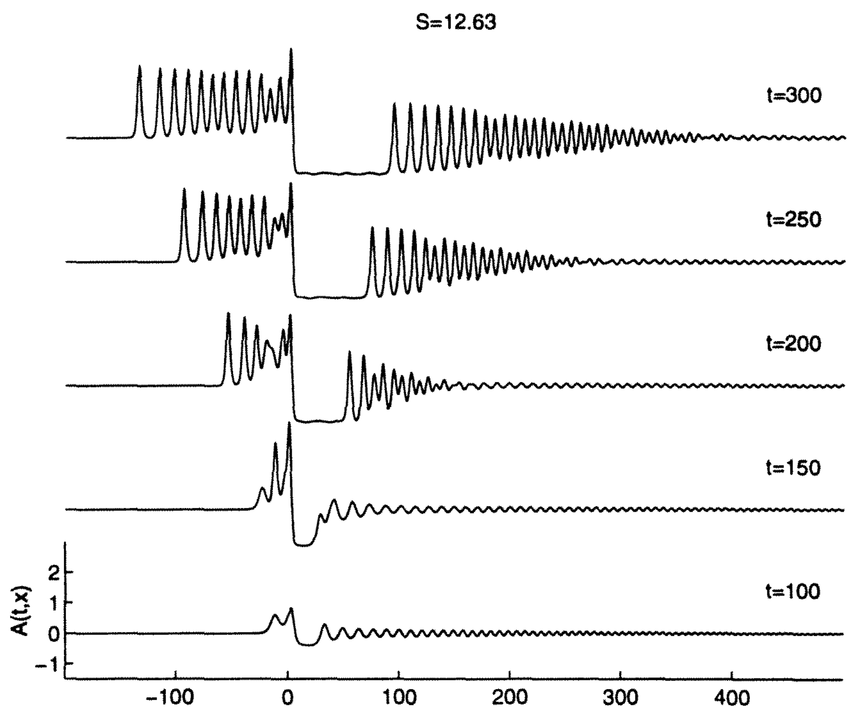

FIG. 7. *Forced KdV system: wave pattern for* $S = 12.63 > S^*$ *(supercritical regime II).*

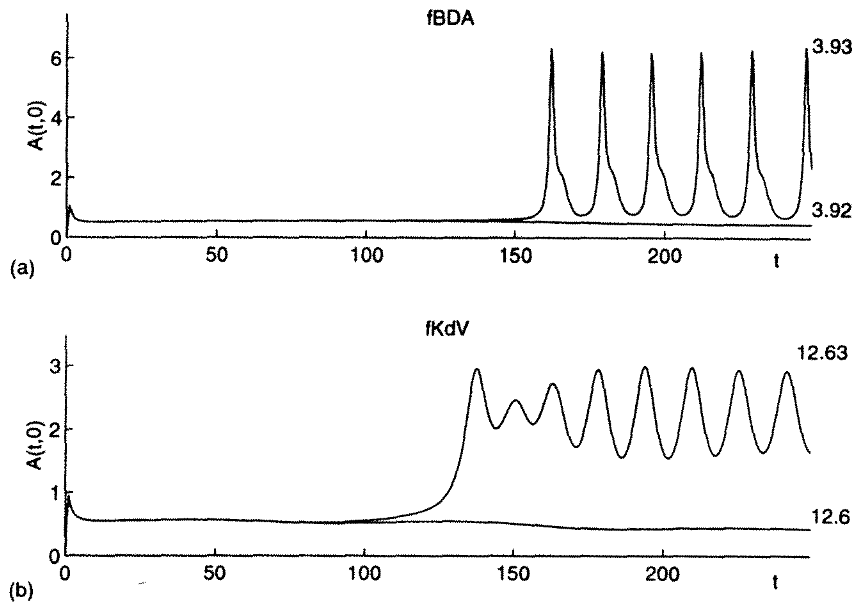

FIG. 8. *Abrupt change in behavior of function $A(t,0)$ because of the bifurcation in (a) fBDA system and (b) fKdV system. Slow variations near some medium level give place to intensive oscillations in both cases.*

parameter exceeds its threshold value.

Figure 9 shows gradual evolution of phase portraits of the function $A(t,0)$ when the similarity parameter S gradually increases beyond its critical value S^*. All of the portraits exibit trajectories, which approach a limit cycle with time. Limit-cycle-type oscillations are seen distinctively against a number of coils related to an initial transient period, that may be fairly long for some values of S. Presence of the limit-cycle-type motion above the obstacle in the fKdV system also has its parallel in the fBDA system [19].

Let us consider behavior of the intensive wave process, typical of the supercritical regime II ($S > S^*$) and located over the hump, in the fKdV model. The traces left by the moving maximum of the localized wave in hand are shown in Figure 10 for different values of S. As can be seen, the highest amplitude of this wave, which is responsible for soliton generation, is not necessarily achieved at the point $x = 0$. The wave first develops on the leeward slope of the hump and gradually moves towards the hump crest for bigger S. The motion of the wave maximum around some center tends to follow almost circle trajectories. The occurence of the second wave similar to the one that emerges in the fBDA system after the second bifurcation, was not found for the values of S as large as $S = 175$.

3.3 The Forced Compound Model

As was mentioned above, only scarce information is available on the solutions of the homogeneous compound equation (4). In a numerical search for solitary waves predicted in [11],[12], the most promising approach may be the indirect one: to investigate the forced compound model (8)-(9). It involves two similarity parameters R and Q rather than one, as it takes place for the fBDA and fKdV models, and this circumstance makes a scrutiny of the problem very time-consuming. Nevertheless, if nonlinear eigenmodes of equation (4) do exist, they must eventually get evoked by an appropriate external forcing, in much the

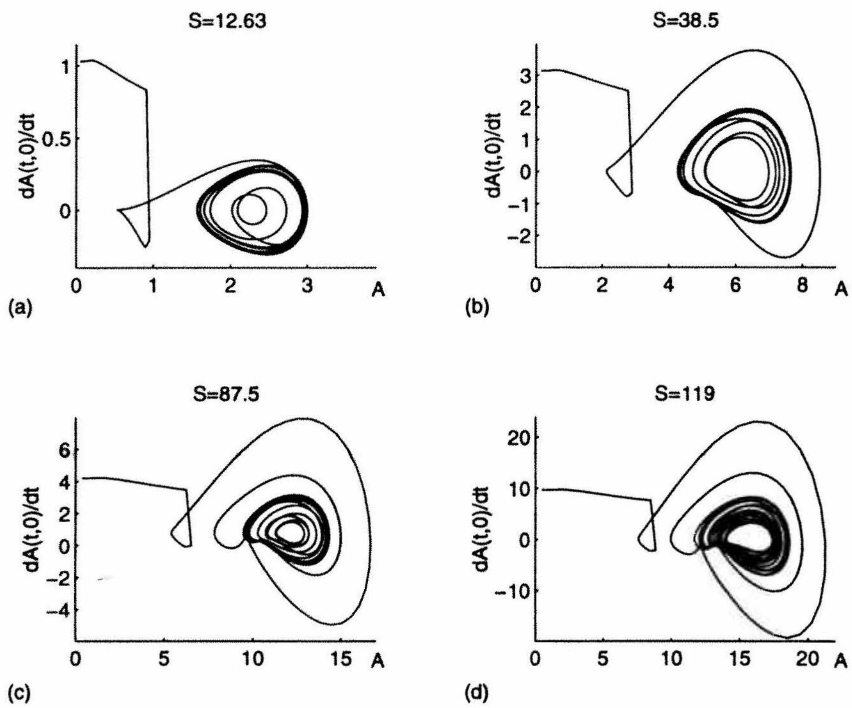

FIG. 9. *Forced KdV system: evolution of phase portraits of function $A(t,0)$ depending upon the increase in value of the similarity parameter S.*

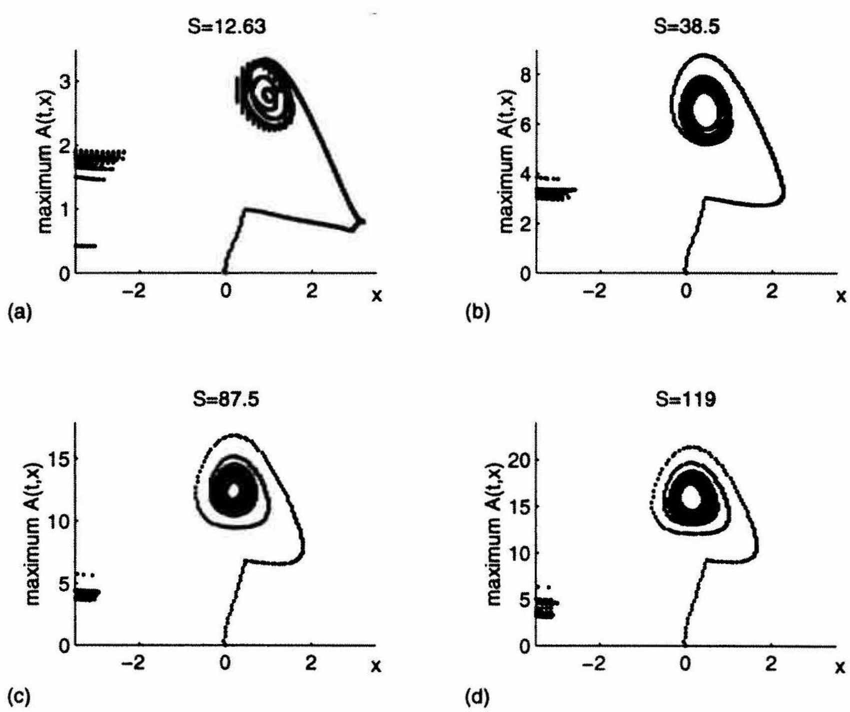

FIG. 10. *Forced KdV system: traces left by the maximum of the wave localized over the hump for different values of the similarity parameter S. Traces near the left boundary of the hump are left by peaks of solitons outgoing in upstream direction.*

same way as the classic solitons are gotten excited by forcings in the fBDA or fKdV models, respectively.

With this idea in mind, we introduce function $g(t)$ as follows

$$g(t) = \begin{cases} t/t_0, & 0 < t \leq t_0 \\ 1, & t_0 < t \leq t_1 - t_0 \\ (t_1 - t)/t_0, & t_1 - t_0 < t < t_1 \\ 0, & t \geq t_1 \end{cases},$$

so, that the obstacle disappears at time $t = t_1$ (in computations $t_1 = 80$). Figure 11 and Figure 12 demonstrate two wave patterns, which develop downstream of the hump in the forced compound system with $R = 0.2$ and two values $Q = 5.5$ and $Q = 10$, respectively. Patterns presented are strikingly different from everything we became familiar with in our studies of the fBDA and fKdV systems.

Classic solitary waves of the BDA and KdV type can propagate downstream only against some negative background, which is provided in forced models by an external agency and has a form of a finite depression zone, adjacent to the obstacle and slowly weakening while transforming into the linear oscillatory tongue that spreads downstream. Wherever the depression zone becomes too weak to support the downstream solitary waves, the latter degrade into nonlinear pulsations separating the orderly solitary structures from the linear oscillatory tail of the solution. Solitary waves themselves, regardless of the direction they propagate in, are always the waves of compression.

In the forced compound model we observe fully developed solitary waves of depression sweeping downstream so fast, that they eventually leave behind all the other disturbances and travel freely against zero background. In both wave patterns presented, the faster soliton can be seen to pass through the slower one with neither of them changing their own speed or amplitude. We strongly believe that these objects belong to the class of solitary waves predicted in [11],[12]. Figure 13 gives the close-ups of the fully developed soliton #1, soliton #2 and developing solitons #3 and #4 from Figure 12 at time $t = 700$. The visual absence of wiggles on the outskirts of soliton #1 and only a hint at weak oscillations on the outskirts of the soliton #2 have a quite rational explanation. The phase velocities of the solitons in hand are $c_1 \approx 0.91$ and $c_2 \approx 0.54$, respectively. According to the formulae derived in [12], spacing between soliton-wing zeroes is $l_z = 2\pi\Delta_0$, while the exponential decay of the corresponding amplitude goes at a rate

$$d = \frac{(4c\Delta_0 - 1)^{\frac{1}{2}}}{2\Delta_0},$$

where c is the phase velocity of a soliton.

So, in case of the soliton #1, its amplitude decreases approximately 50 times between two consecutive zeroes, while the amplitude of the soliton #2 decreases approximately 10 times beween two zeroes. Therefore, the wiggles are to be much better noticeable for slower solitons (e.g. $c < 0.4$).

4 Conclusions

Close comparison of forced solutions of the BDA and KdV equations gives evidence of very important common features of both systems:

1) An external localized agency (a) creates a distinctive background, positive upstream, negative downstream and vanishing as $x \to \pm\infty$, (b) excites a part of the continuous

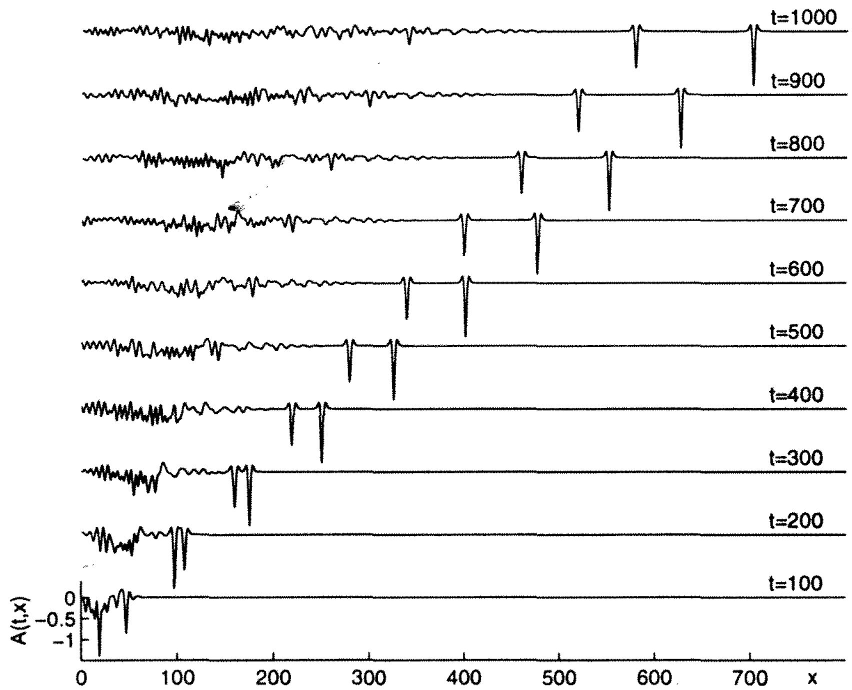

FIG. 11. *Forced compound system: wave pattern downstream of the obstacle with* $Q = 5.5$ *and* $R = 0.2$.

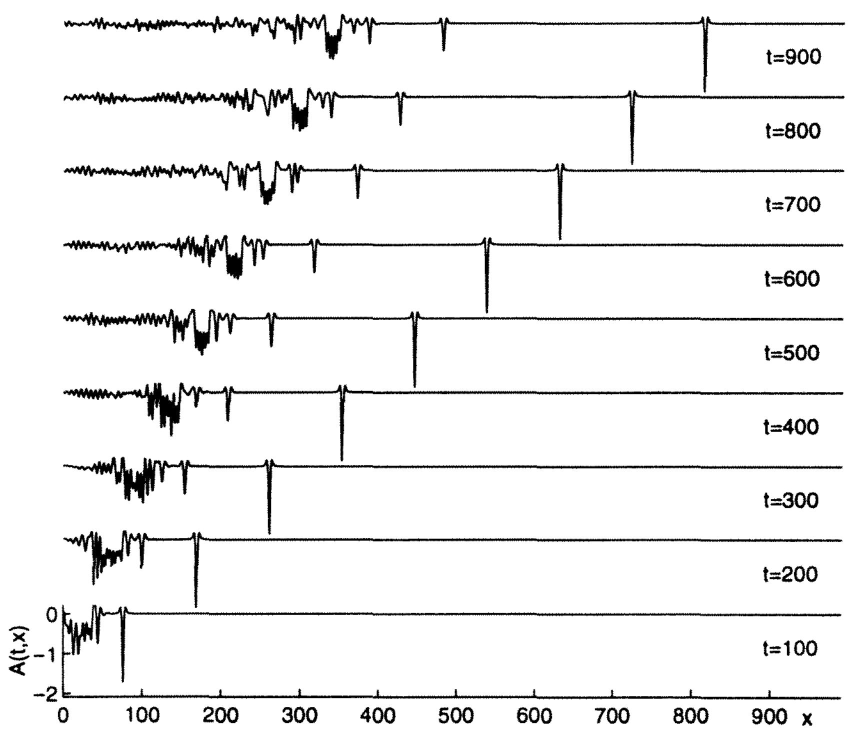

FIG. 12. *Forced compound system: wave pattern downstream of the obstacle with* $Q = 10$ *and* $R = 0.2$.

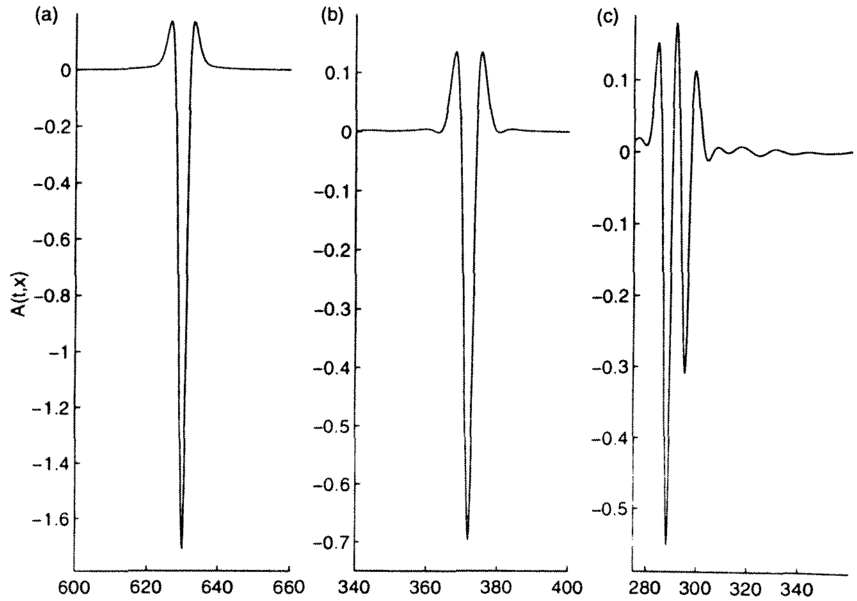

FIG. 13. *Forced compound system: solitons seen in Figure 12 at $t=700$.*

spectrum of the nonlinear eigenmodes (solitons) including a number of those, that are able to emerge, exist and travel only against the 'depression-zone' part of the background, adjacent to the leeward edge of the forcing and spreading downstream.

2) Small and moderate forcings evoke only slow eigenmodes, and no peculiar activity is present at the forcing location.

3) When size of a forcing reaches a particular threshold magnitude, suddenly an intense unstationary process establishes itself within the forcing's boundaries and starts to generate substantially faster solitons in both directions.

4) The process in hand is of a limit-cycle type.

Inquiry into the forced compound equation shows that:

1) It is, indeed, a soliton-bearing equation, because its nonlinear eigenmodes (solitons) do exist.

2) These nonlinear eigenmodes exhibit the properties predicted in [11],[12]. They propagate in the opposite direction and are of the opposite sign, as compared to their classic counterparts.

It is a great honor for both authors to present this paper as a token of their high esteem of Prof. J. D. Cole's scientific activities. The authors would like also to express their gratitude to Prof. J. D. Cole for his most genuine interest in the subject of this study, as well as for his permanent encouragement and support, without which this work would have not been possible.

References

[1] V. I. Zhuk and O. S. Ryzhov, *Locally inviscid perturbations in a boundary layer with self-induced pressure* , Dokl. Acad. Nauk. SSSR, 263 (1982), pp. 56–59 (in Russian); English transl.: Sov. Phys. Dokl., 27(3) (1982), pp. 177–179.

[2] F. T. Smith, O. R. Burggraf, *On the development of large-sized short-scaled disturbances in boundary layers*, Proc. R. Soc. Lond., A399 (1985), pp. 25–55.

[3] V. I. Borodulin and Y. S. Kachanov, *Role of the mechanism of local secondary instability in K-breakdown of boundary layer*, Proc. Siberian Div. USSR Acad. Sci. Tech. Sci., 18(1988), pp. 65–77 (in Russian); English transl.: Sov. J. Appl. Phys., 3(2)(1989), pp. 70–81.

[4] Y. S. Kachanov, *Secondary and cascade resonant instabilities of boundary layers, wave-resonant concept of breakdown and its substantiation* , In Laminar-Turbulent Transition (ed. D. Arnal and R. Michel), (1990), pp. 65–80.

[5] O. S. Ryzhov, *On the formation of ordered vortex structures from unstable oscillations in a boundary layer*, J. Comput. Maths. Math. Phys., 29(1990), pp.1804–1814 (in Russian); English transl. USSR Comput. Maths. Math. Phys., 30(1990), pp. 146–154.

[6] ——, *Formation of ordered vortex structures in a boundary layer*, In Problems of Applied Mathematics and Information Theory. Part I, Mechanics and Mathematical Physics. Russian Acad. Sci., (1992), pp. 67–89 (in Russian).

[7] Y. S. Kachanov, O. S. Ryzhov, and F. T. Smith, *Formation of solitons in transitional boundary layers: theory and experiment*, J. Fluid Mech., 251(1993), pp. 273–297.

[8] O. S. Ryzhov and E. D. Terent'ev, *Nonlinear waves in a three-dimensional boundary layer*, In Proc. IUTAM Symp. on Nonlinear Instability and Transition in 3D Boundary Layers, (1995), (to be published).

[9] ——, *A uniformly valid asymptotic model for the wave motion in a steady three-dimensional subsonic boundary layer*, (submitted to J. Fluid Mech.).

[10] O. S. Ryzhov, *Boundary-layer stability and paths to transition: theoretical concepts and experimental evidence*, In 1st European Fluid Mechanics Conf., Cambridge,UK (1991).

[11] T. B. Benjamin, *A new kind of a solitary wave*, J. Fluid Mech., 245(1992), pp. 401–411.

[12] O. S. Ryzhov, *The development of nonlinear oscillations in a boundary layer and the onset of random disturbances*, In Nonlinear Instability of Nonparallel Flows (Eds. S. P. Lin et al), Springer-Verlag,(1993), pp. 52–68.

[13] R. Grimshaw and N. Smyth, *Resonant flow of a stratified fluid over topography*, J. Fluid Mech., 169(1986), pp. 429–464.

[14] T. Y. Wu, *Generation of upstream advancing solitons by moving disturbances*, J. Fluid Mech., 184(1987), pp. 75–99.

[15] H. Mitsudera and R. Grimshaw, *Effects of radiative damping on resonantly generated internal gravity waves*, Studies Appl. Math., 84(1991), pp. 183–206.

[16] R. Camassa and T. Y. Wu, *Stability of forced solitary waves*, Phil. Trans. R. Soc. Lond., A337(1991), pp. 429–466.

[17] ——, *Stability of some stationary solutions for the forced KdV equation*, Physica D, 51(1991), pp. 295–307.

[18] E. V. Bogdanova-Ryzhova and O. S. Ryzhov, *Solitary-like waves in boundary-layer flows and their randomization*, Phil. Trans. R. Soc. Lond., A352(1995), pp. 389–404.

[19] ——, *Forced nonlinear disturbances in incompressible boundary layers*, Phys. Fluids, (1996), (to be published).

[20] O. R. Burggraf and P. W. Duck, *Spectral computation of triple-deck flows* , in Proc. Symp. on Numerical and Physical Aspects of Aerodynamic Flows, ed. Cebeci, Springer (1982) pp. 145–158.

Transonic Flow About a Suddenly Deflected Wedge *

J. D. Cole[†] L. Pamela Cook[‡] G. Schleiniger[‡] M. Sinha[§]

The second and third authors are indebted to Julian for many years of encouragement, support and collaboration.

Abstract

Unsteady transonic flows are important for the understanding of maneuvering and accelerating flight near the speed of sound. In this paper asymptotic methods are used to develop the approximate unsteady transonic small disturbance formulation. The particular problem of a suddenly deflected two-dimensional wedge is investigated. Numerical calculations are shown giving the development of shock patterns and the approach to steady state for subsonic and exactly sonic flow.

1 Introduction

The flow about a suddenly deflected wedge in a uniform stream with upstream Mach number M_∞ less than or equal to one is studied. Asymptotic methods are used to develop the approximate unsteady transonic small disturbance formulation on which numerical computation is carried out. The development of the shock patterns and the approach to steady state is shown. Also, the results are compared to those obtained previously for exactly sonic flow [2].

Consider a uniform steady flow in the x^* direction for $t^* < 0$ (and, for $t^* > 0$ at upstream infinity) with speed $U \leq a_\infty$, where a_∞ is the speed of sound in the undisturbed gas. Thus, the Mach number is $M_\infty = U/a_\infty \leq 1$ everywhere for $t^* < 0$, and at upstream infinity for all t^*. At $t^* = 0$ a wedge, originally the line $x^* > 0$, $y^* = 0$, opens to an angle $\delta \ll 1$ so that for $t^* > 0$ the wedge is located at $y^* = \pm\delta x^*$, $x^* > 0$. Since the problem is symmetric about $y^* = 0$ we consider only $y^* \geq 0$ henceforth, and the vertical velocity at $y^* = 0$ is zero for $x^* < 0$.

To study this problem we note that, since the shocks are weak, the flow is isentropic with small corrections so that a potential, $\Phi(x^*, y^*, t^*)$, describes the primary flow. The full two-dimensional potential formulation is [1]

$$(1) \qquad \begin{aligned} &(a^2 - \Phi_{x^*}^2)\Phi_{x^*x^*} - 2\Phi_{x^*}\Phi_{y^*}\Phi_{x^*y^*} + (a^2 - \Phi_{y^*}^2)\Phi_{y^*y^*} \\ &\qquad -2\Phi_{x^*}\Phi_{x^*t^*} - 2\Phi_{y^*}\Phi_{y^*t^*} - \Phi_{t^*t^*} = 0 \end{aligned}$$

where a, the local speed of sound, is given by

$$(2) \qquad \Phi_{t^*} + \frac{a^2}{\gamma - 1} + \frac{\Phi_{x^*}^2 + \Phi_{y^*}^2}{2} = \frac{a_\infty^2}{\gamma - 1} + \frac{U^2}{2}.$$

*The work of the first author was partially supported by AFOSR grant #F49620-93-1-0022DEF. The work of the second and third authors was supported by NSF grant #DMS-9210467

[†]Rensselaer Polytechnic Institute, Dept. of Mathematical Sciences, Troy, NY

[‡]University of Delaware, Dept. of Mathematical Sciences, Newark, DE

[§]Visiting Undergraduate Student Scholar, Imperial College, London, England

The boundary conditions are (H is the Heaviside function):

$$H(\zeta) = \begin{cases} 1 & \text{if } \zeta \geq 0 \\ 0 & \text{if } \zeta < 0 \end{cases}$$

$$\Phi \to Ux^* \quad \text{as} \quad x^* \to -\infty, \tag{3}$$

$$\Phi_{y^*}(x^*, 0) = 0 \quad \text{if} \quad x^* < 0, \tag{4}$$

$$\Phi_{y^*}(x^*, \delta x^*) = \delta \Phi_{x^*}(x^*, \delta x^*) H(t^*) \quad \text{if} \quad x^* > 0. \tag{5}$$

We first study the predictions of linear theory to find where and how it breaks down. That information then guides the development and description of the nonlinear theory.

2 Linear Theory

Linear theory results, after non-dimensionalization with $t^* = (\ell/U)t$, $x^* = \ell x$, $y^* = \ell y$ (where ℓ is a length scale), from an asymptotic expansion in terms of $\delta \ll 1$

$$\Phi(x^*, y^*, t^*) = U\ell \{x + \delta\phi(x, y, t) + \delta^2\phi_2(x, y, t) + \cdots\}. \tag{6}$$

Substitution into (1)–(5), collection of terms of corresponding orders, and a change of coordinates to $x' = x - t$, and $\bar{t} = t/M_\infty$, gives to order δ the following problem, namely the wave equation

$$\phi_{x'x'} + \phi_{yy} - \phi_{\bar{t}\,\bar{t}} = 0$$

with

$$\phi_y|_{y=0} = H(x' + M_\infty \bar{t})H(\bar{t})$$

and

$$\phi_x \sim 0 \quad \text{as} \quad x \to -\infty,$$

(see Figure 1). The solution to this problem is

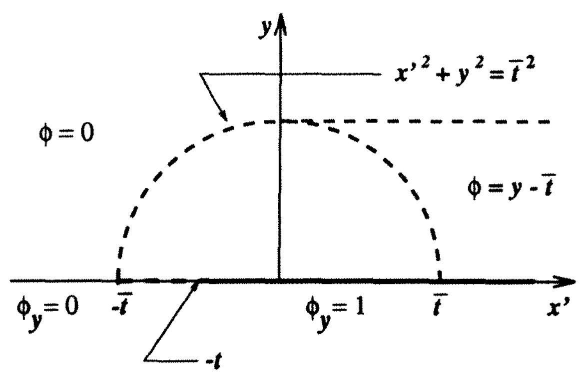

FIG. 1.

$$\begin{aligned} \phi &= (y - \bar{t})H(x')H(\bar{t} - y), \quad \text{for} \quad x'^2 + y^2 \geq \bar{t}^2 \\ \phi &= \frac{-1}{\pi} \iint_{\mathcal{D}} \frac{H(\xi + M_\infty \tau)}{\sqrt{(\bar{t} - \tau)^2 - (x' - \xi)^2 - y^2}} \, d\xi d\tau, \quad \text{for} \quad x'^2 + y^2 < \bar{t}^2. \end{aligned}$$

Note that the domain of integration $\mathcal{D}$ is the region bounded by the wedge, the $y = 0$ axis and the retrograde Mach cone. This can be integrated out directly to give, for $x'^2 + y^2 < \bar{t}^2$, (in $x, t, \bar{t}$ variables)

$$(7) \qquad -\pi\phi = \bar{t}\left[\sin^{-1}\left(\frac{x-t}{\sqrt{\bar{t}^2-y^2}}\right)+\frac{\pi}{2}\right] - y\left[\sin^{-1}\left(\frac{\bar{t}(x+\bar{t}-t)-y^2}{(x+\bar{t}-t)\sqrt{\bar{t}^2-y^2}}\right)+\frac{\pi}{2}\right]$$
$$-y\left[\sin^{-1}\left(\frac{(1-M_\infty)y^2+x(x+\bar{t}-t)}{(x+\bar{t}-t)\sqrt{x^2+(1-M_\infty^2)y^2}}\right)-\frac{\pi}{2}\right]$$
$$+\frac{x}{\sqrt{1-M_\infty^2}}\left\{\ln\left|\sqrt{(M_\infty^2-1)\left[(x-t)^2+y^2-\bar{t}^2\right]}+M_\infty(x-t)+\bar{t}\right|\right.$$
$$\left.-\ln\sqrt{x^2+(1-M_\infty^2)y^2}\right\}.$$

As expected the solution is well behaved except near the nose of the wedge ($x' = -t$ or $x = 0$, $y = 0$) when $M_\infty \to 1$. Note that for x, y, t fixed, $M_\infty \to 1$, this expression reduces to precisely that obtained in [2], namely

$$-\pi\phi = \sqrt{t^2-x'^2-y^2}+t\left(\frac{\pi}{2}+\sin^{-1}\frac{x'}{\sqrt{t^2-y^2}}\right)-y\left(\frac{\pi}{2}+\sin^{-1}\frac{t(t+x')-y^2}{(t+x')\sqrt{t^2-y^2}}\right).$$

The breakdown for $M_\infty \approx 1$ is to be expected since, in $x', \bar{t}$ coordinates, the wedge is flying at Mach one so that disturbances pile up at the nose giving a singularity in the pressure as obtained by linear theory. Nonlinear theory must be used to correctly represent the interactions at this point in recognition of the fact that disturbances in the flow direction are of much larger order than those occurring transversely.

3 Nonlinear Theory

In the nonlinear theory we look for $\mu(\delta)$, $\nu(\delta)$, $\epsilon(\delta)$, $\sigma(\delta)$, so that

$$\Phi(x^*, y^*, t^*) = U\ell\left\{x + \epsilon(\delta)\varphi(\tilde{x}, \tilde{y}, t; K) + \cdots\right\},$$

where $\tilde{x}, \tilde{y}$ are stretched coordinates, $\tilde{x} = x/\mu(\delta)$, $\tilde{y} = y/\nu(\delta)$ and $K = (1-M_\infty^2)/\sigma(\delta)$. Determination of ϵ, μ, ν and σ is made by insisting that the boundary condition be retained ($\Phi_{y^*}|_{y^*=0} = U(\epsilon/\nu)\varphi_{\tilde{y}} = O(\delta)$), that the nonlinear term in the flow direction be preserved as well as the subsonic nature of the equation, and that the unsteady nature of the problem be maintained. Hence $\nu = \delta^{1/3}$, $\mu = \delta^{2/3}$, $\epsilon = \delta^{4/3}$, $\sigma = \delta^{2/3}$, so that

$$\Phi = U\ell\left\{x + \delta^{4/3}\varphi(\tilde{x}, \tilde{y}, t; K) + \cdots\right\},$$

where

$$K = \frac{1-M_\infty^2}{\delta^{2/3}}, \quad \tilde{x} = \frac{x}{\delta^{2/3}}, \quad \tilde{y} = \frac{y}{\delta^{1/3}},$$

and φ is governed by the unsteady transonic small disturbance equation,

$$(8) \qquad (K - (\gamma+1)\varphi_{\tilde{x}})\varphi_{\tilde{x}\tilde{x}} + \varphi_{\tilde{y}\tilde{y}} - 2\varphi_{\tilde{x}\bar{t}} = 0,$$

with

$$(9) \qquad \varphi_{\tilde{y}}|_{\tilde{y}=0} = H(\tilde{x})H(\bar{t}),$$

and

$$
\begin{aligned}
(10) \qquad -\pi\varphi \;\sim\;& \sqrt{2t\tilde{x}+Kt^2-\tilde{y}^2} \\
& -\tilde{y}\left[\sin^{-1}\left(\frac{\tilde{x}(2\tilde{x}+Kt)+K\tilde{y}^2}{(2\tilde{x}+Kt)\sqrt{\tilde{x}^2+K\tilde{y}^2}}\right)+\sin^{-1}\left(1-\frac{2\tilde{y}^2}{t(2\tilde{x}+Kt)}\right)\right] \\
& +\frac{\tilde{x}}{\sqrt{K}}\left[\ln\left|\sqrt{K(2\tilde{x}t+Kt^2-\tilde{y}^2)}+\tilde{x}+Kt\right|-\ln\sqrt{\tilde{x}^2+K\tilde{y}^2}\right], \\
& \quad \text{for} \quad \tilde{y}^2<2\tilde{x}t+Kt^2; \\
\sim\;& 0, \quad \text{for} \quad \tilde{y}^2>2\tilde{x}t+Kt^2.
\end{aligned}
$$

The far field condition was obtained by matching with the near field linear solution obtained from (7).

Note that $\delta\phi(x,y,t)\sim\delta^{4/3}\varphi(\tilde{x},\tilde{y},t)$. Note also that this matching does in fact determine the scale of the nonlinear stretching. Instead of the conditions we used to determine ϵ,μ,ν,σ we could have used those necessary for matching. Thus from (7) we would have required $\delta\sqrt{\mu(\delta)}=\delta\nu(\delta)=\epsilon(\delta)$ giving $\mu=\nu^2$. Since $\epsilon=\nu\delta$ (from the boundary condition on the wedge), ϵ,μ,ν,σ are determined with only one other condition, namely that (8) be a distinguished limit of (1),(2). Note also that although the transonic correction to the uniform flow is $O(\delta^{4/3})$, the transonic correction to the pressure is in fact $O(\delta^{2/3})$.

4 Conical Coordinates

The nonlinear problem (8)–(10), to be solved numerically in order to determine the nonlinear effects, involves three independent variables. This boundary value problem has conical symmetry. We could thus use the conical coordinates $X=\tilde{x}/t$, $Y=\tilde{y}/t$, $\varphi(\tilde{x},\tilde{y},t)=t\psi(X,Y)$ to study the problem. But in fact it is useful to make yet one more change of variables (as used in [2], [3]), namely to let $R=X-Y^2/2+K/2$ and $\vartheta=Y$. In these coordinates the mixed derivative term disappears from the equation. Thus we get

$$(11) \qquad [(\gamma+1)\psi_R-2R]\psi_{RR}-\psi_{\vartheta\vartheta}+\psi_R=0\,,$$

with

$$(12) \qquad \psi_\vartheta|_{\vartheta=0}=H(R-K/2)\,,$$

and (see Figure 2)

$$
\begin{aligned}
(13) \qquad \psi\sim\frac{-1}{\pi}H(R)\Bigg\{&\sqrt{2R}+\frac{2R+\vartheta^2-K}{2\sqrt{K}}\Bigg[\ln\left|2\sqrt{2KR}+2R+\vartheta^2+K\right| \\
&-\ln\sqrt{(2R+\vartheta^2-K)^2+4K\vartheta^2}\Bigg]-\vartheta\Bigg[\sin^{-1}\left(\frac{2R-\vartheta^2}{2R+\vartheta^2}\right) \\
&+\sin^{-1}\left(\frac{(2R+\vartheta^2)^2-K(2R-\vartheta^2)}{(2R+\vartheta^2)\sqrt{(2R+\vartheta^2-K)^2+4K\vartheta^2}}\right)\Bigg]\Bigg\}.
\end{aligned}
$$

In these coordinates one finds the slopes of the characteristics and shocks as

$$
\begin{aligned}
\left(\frac{dR}{d\vartheta}\right)_{\text{characteristic}} &= \pm\sqrt{(\gamma+1)\psi_R-2R}\,, \\
\left(\frac{dR}{d\vartheta}\right)_{\text{shock}} &= \pm\sqrt{(\gamma+1)\langle\psi_R\rangle-2R}\,,
\end{aligned}
$$

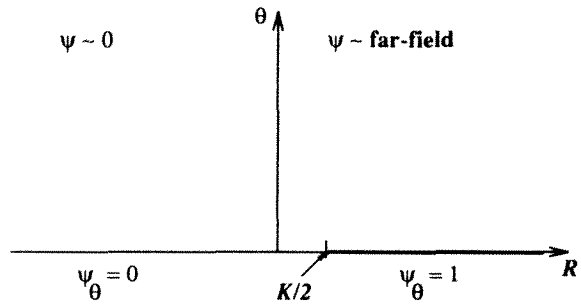

FIG. 2.

where $\langle\ \rangle$ denotes the average across the shock. The latter came from the shock jump conditions which are

$$[\![\psi]\!] = 0$$

and

$$[\![(\gamma+1)\psi_R^2/2 - 2R\psi_R]\!]d\vartheta + [\![\psi_\vartheta]\!]dR = 0.$$

Here $[\![\ ]\!]$ denotes the jump across the shock. Thus the shock polar is

$$\{(\gamma+1)\langle\psi_R\rangle - 2R\}[\![\psi_R]\!] = [\![\psi_\vartheta]\!]^2.$$

5 Numerical Results

The numerical solution of (11)–(13), coupled with the shock jump conditions, was found using a type-sensitive, conservative finite-difference scheme. The pressure coefficient plots, Figures 3–17, show the shock development. These plots also show the stagnation point singularity at the nose of the wedge and show how the shock forms ahead of the nose.

Figures 3–5 show the pressure coefficient, c_p, at each point in R, ϑ space for $K = 1.5, 1, 0$, respectively (note that the nose of the wedge, $x = y = 0$, corresponds to $R = K/2, \vartheta = 0$). The shock appears further in front of the wedge for each (x, y, t) as K increases, that is as the Mach number decreases. The shock forms initially near the nose and, as time passes, moves to upstream infinity. This is easily seen in Figures 6–9 where the pressure is plotted in physical $\tilde{x}, \tilde{y}$ coordinates, for a sequence of increasing times. The strength of the shock increases as K decreases, as can be seen more clearly from Figures 10–12 which show the pressure coefficient on the surface ($\vartheta = 0$). The shock itself, for a fixed value of K, not only moves upstream as t increases, but also straightens (see Figures 13–17). This is expected since for a fixed t the shock asymptotes the parabola $\tilde{y}^2 = 2\tilde{x}t + Kt^2$ for large values of $\tilde{y}$.

We are currently completing similar analysis for $M_\infty > 1$.

References

[1] J. D. Cole and L. P. Cook, *Transonic Aerodynamics*, North-Holland, New York, 1986.

[2] J. D. Cole, L. P. Cook, and G. Schleiniger, *An unsteady transonic flow*, ZAMM, (1995). To appear.

[3] G. Schleiniger, *Quasi-transonic flow past delta wings*, Quarterly of Applied Mathematics, 45 (1987), pp. 265–277.

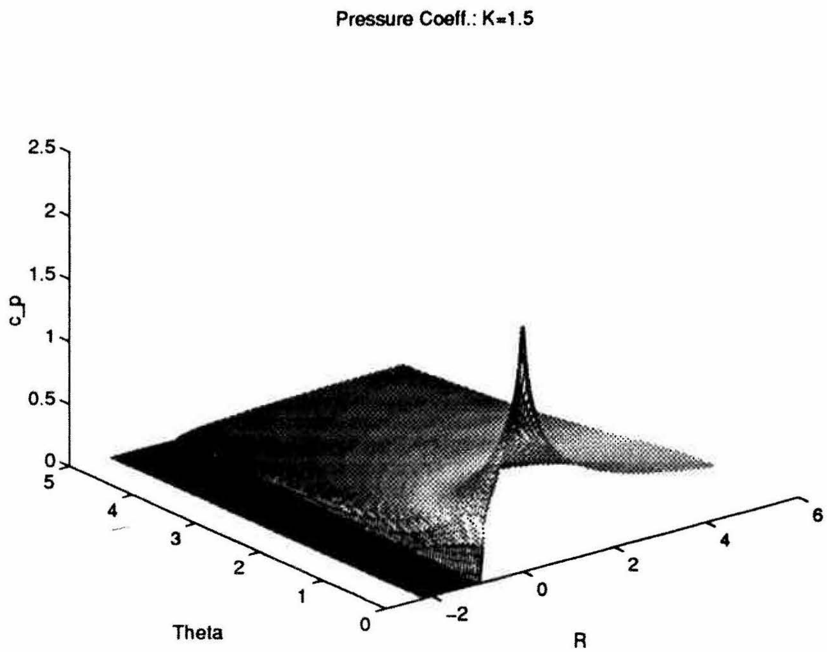
Pressure Coeff.: K=1.5
2.5
2
1.5
c_p
1
0.5
0
5
4
3
2
1
0
Theta
-2
0
2
4
6
R

FIG. 3.

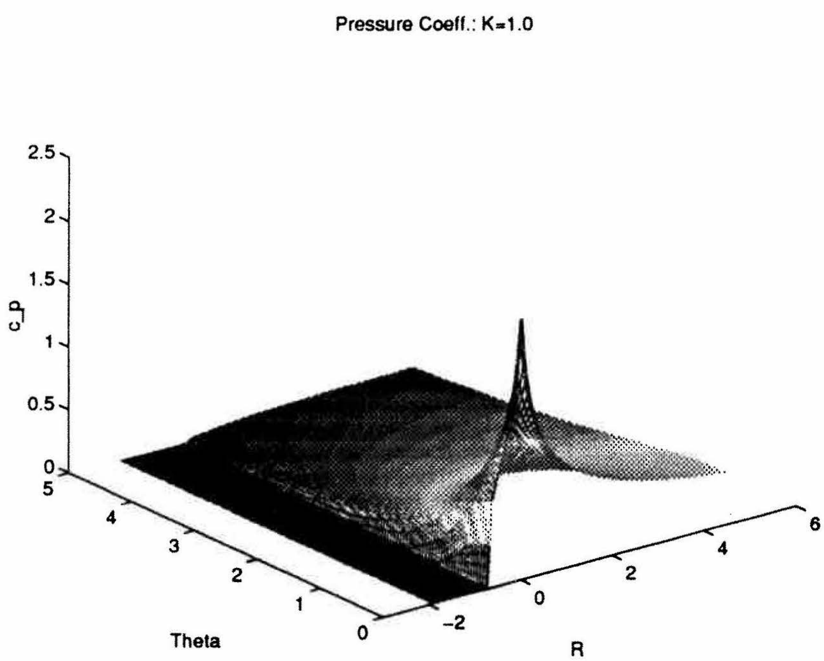
Pressure Coeff.: K=1.0
2.5
2
1.5
c_p
1
0.5
0
5
4
3
2
1
0
Theta
-2
0
2
4
6
R

FIG. 4.

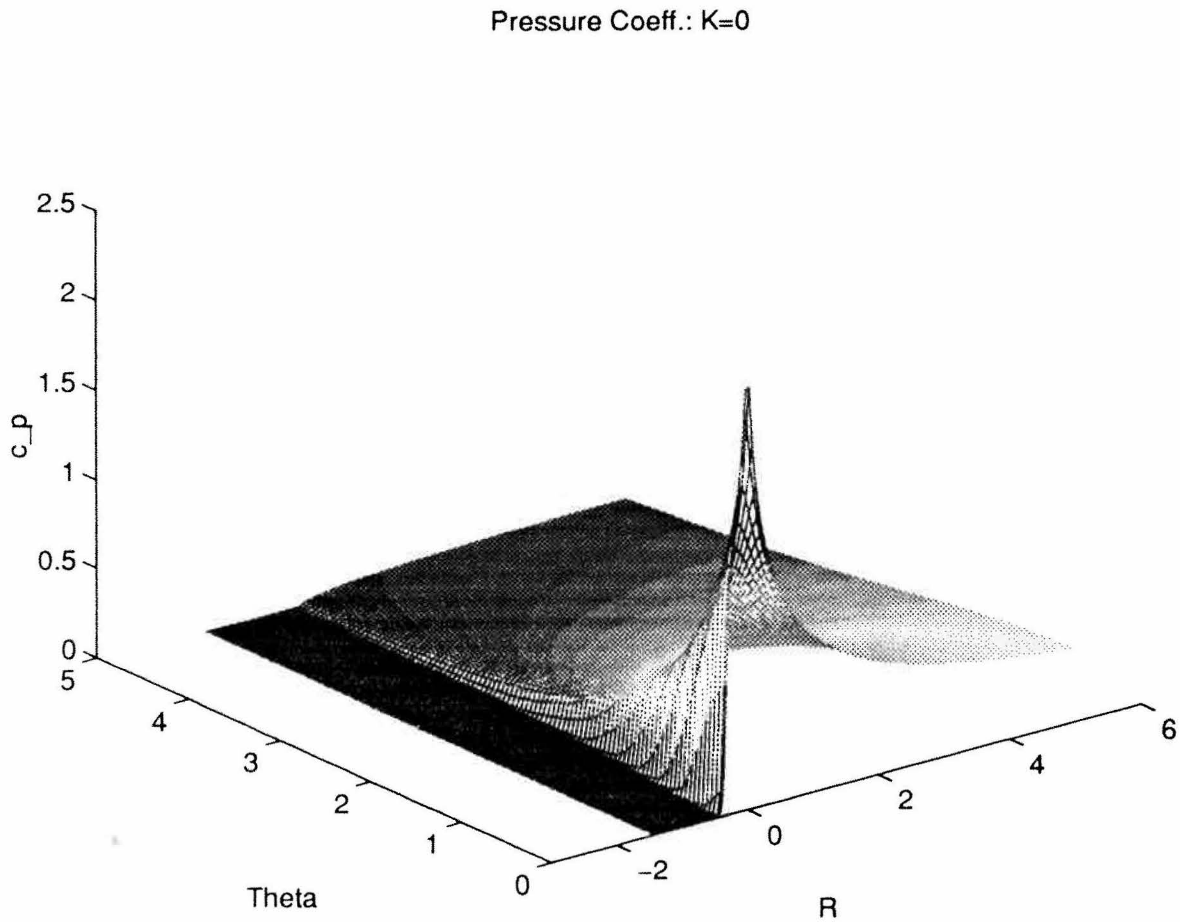

FIG. 5.

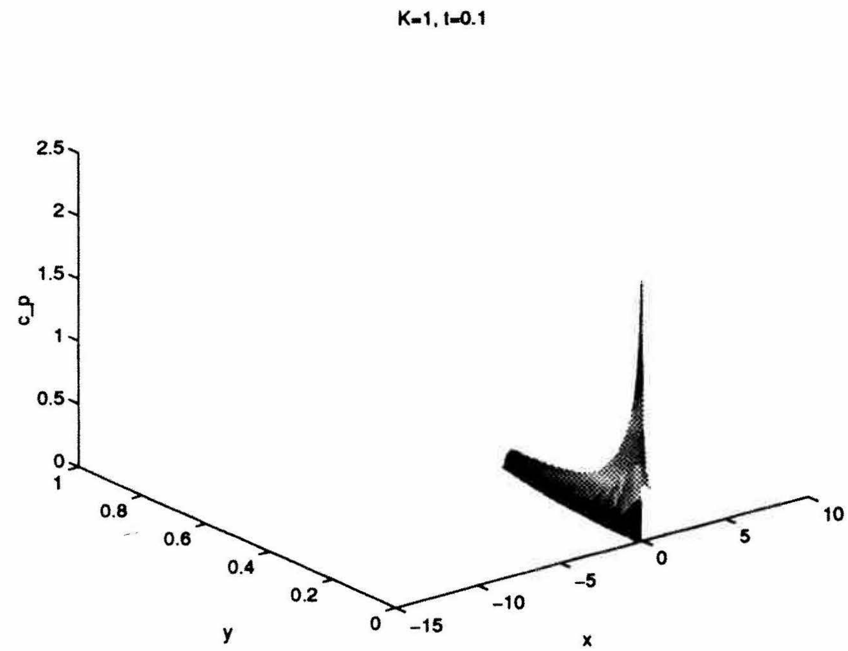
K=1, t=0.1
2.5
2
1.5
1
0.5
0
c_p
1
0.8
0.6
0.4
0.2
0
y
-15
-10
-5
0
5
10
x

FIG. 6.

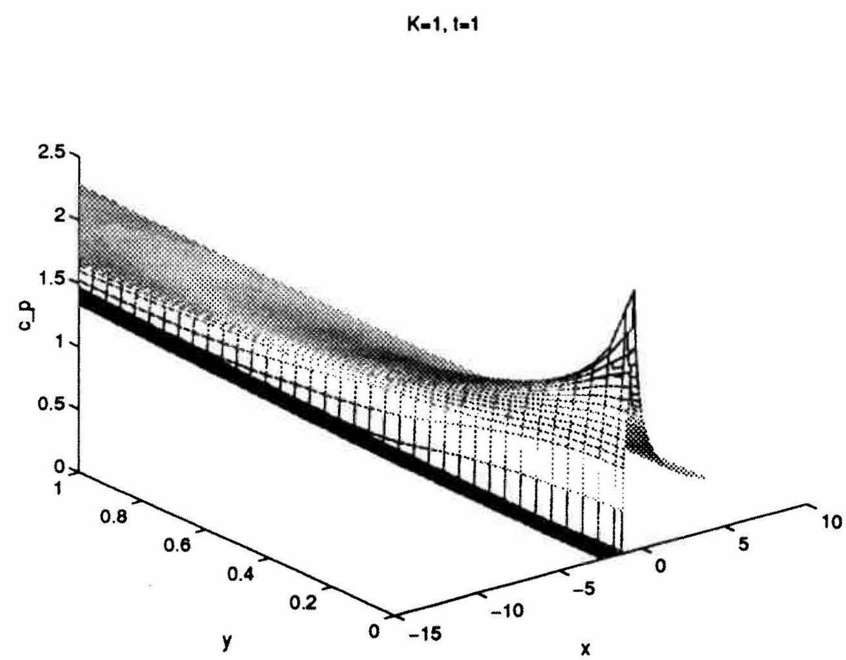
K=1, t=1
2.5
2
1.5
1
0.5
0
c_p
1
0.8
0.6
0.4
0.2
0
y
-15
-10
-5
0
5
10
x

FIG. 7.

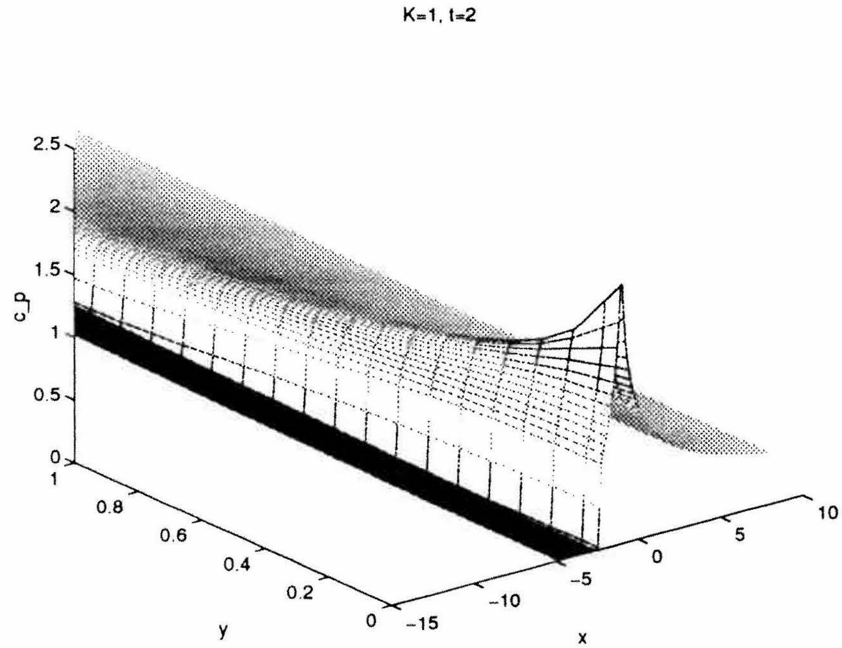
K=1, t=2
c_p
y
x
2.5
2
1.5
1
0.5
0
1
0.8
0.6
0.4
0.2
0
-15
-10
-5
0
5
10

FIG. 8.

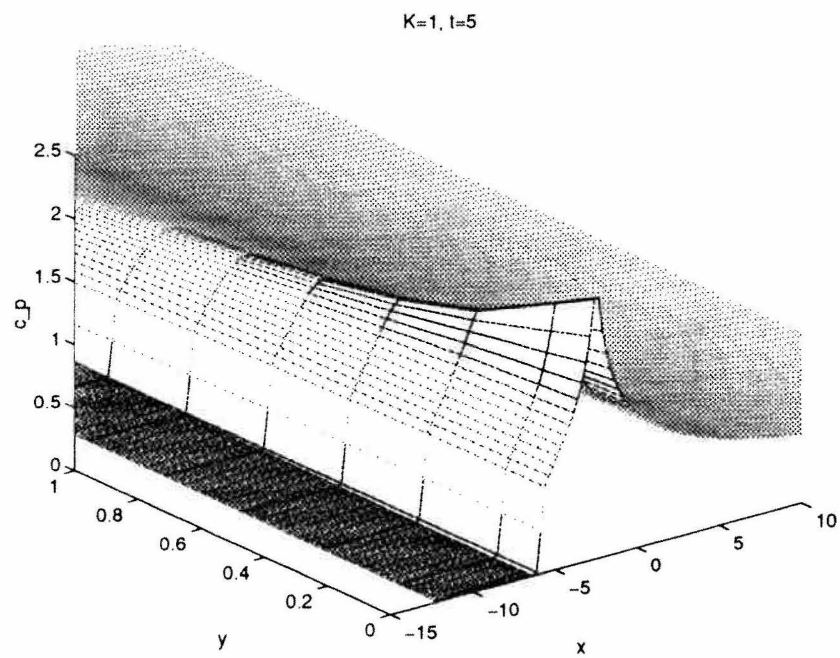
K=1, t=5
c_p
y
x
2.5
2
1.5
1
0.5
0
1
0.8
0.6
0.4
0.2
0
-15
-10
-5
0
5
10

FIG. 9.

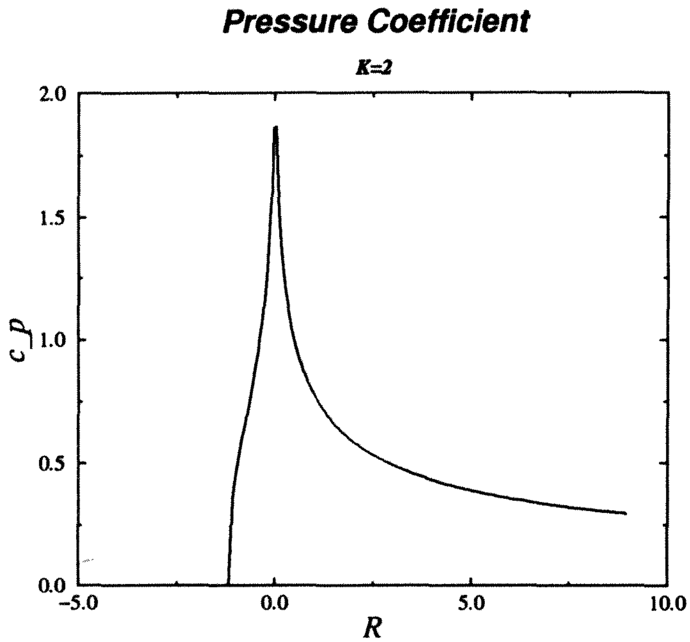
Pressure Coefficient
K=2
2.0
1.5
1.0
0.5
0.0
c_p
-5.0
0.0
5.0
10.0
R

FIG. 10.

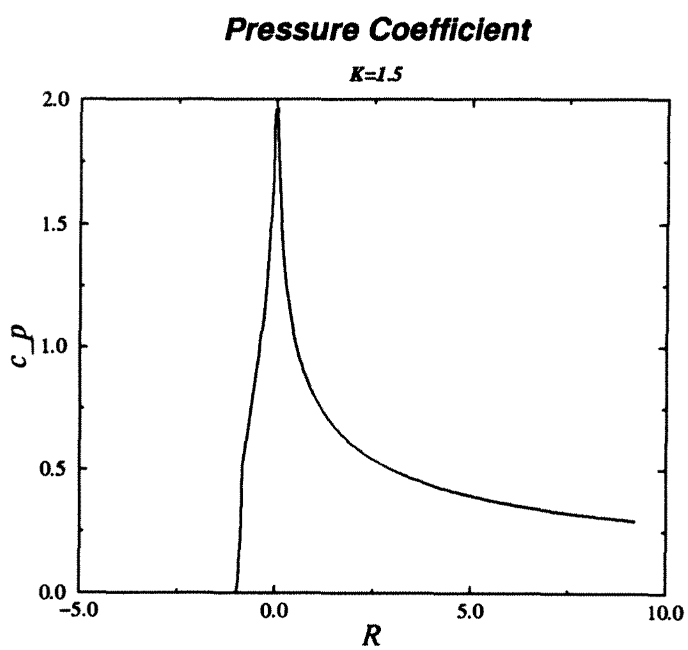
Pressure Coefficient
K=1.5
2.0
1.5
1.0
0.5
0.0
c_p
-5.0
0.0
5.0
10.0
R

FIG. 11.

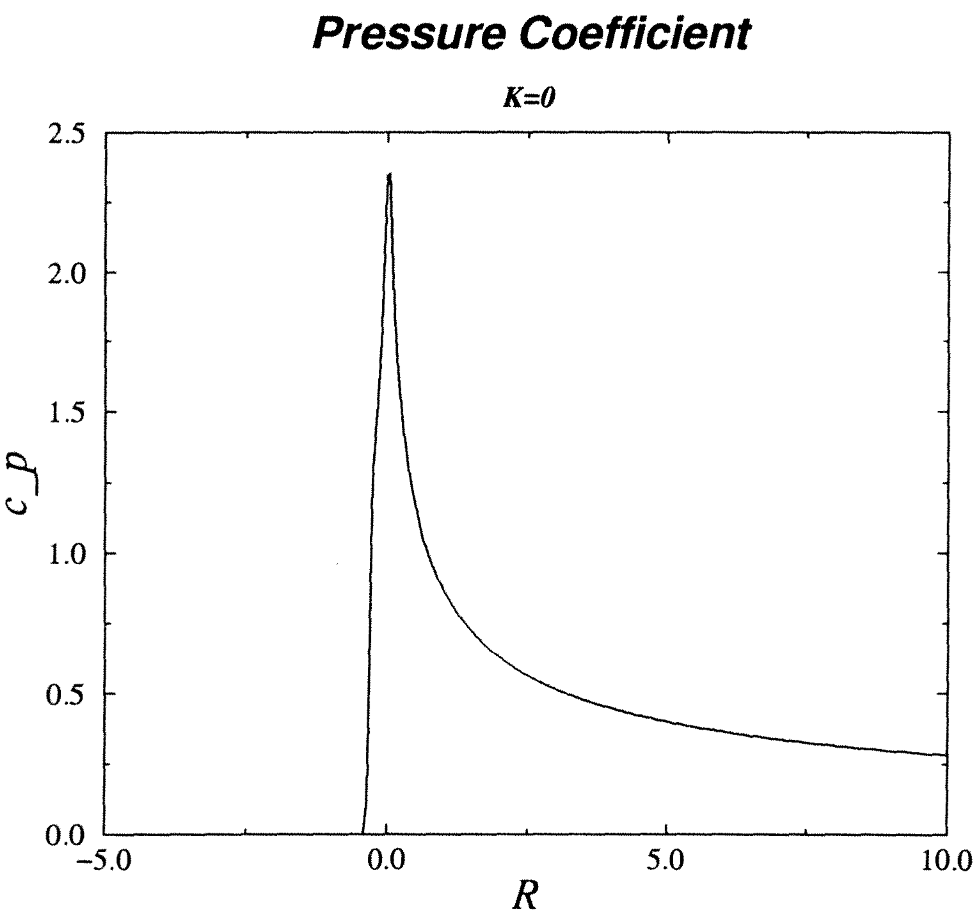

FIG. 12.

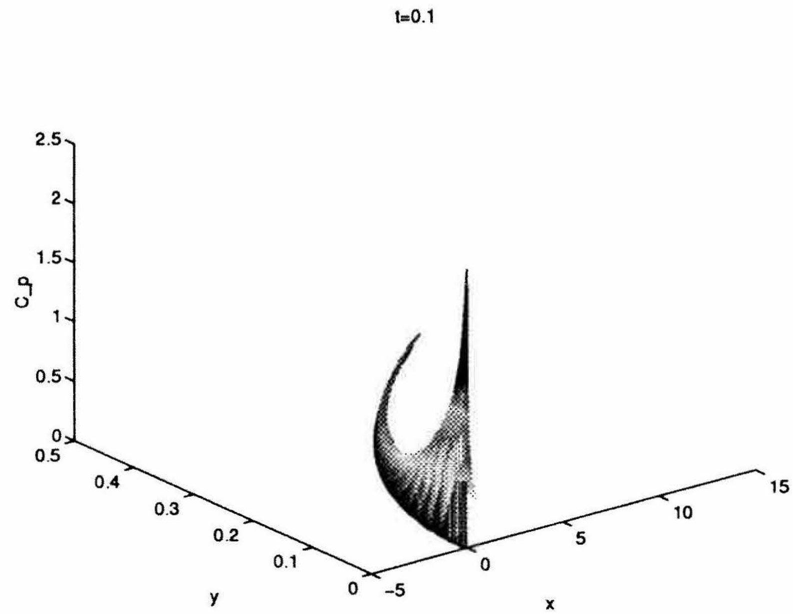
t=0.1
C_p
2.5
2
1.5
1
0.5
0
0.5
0.4
0.3
0.2
0.1
0
y
-5
0
5
10
15
x

FIG. 13.

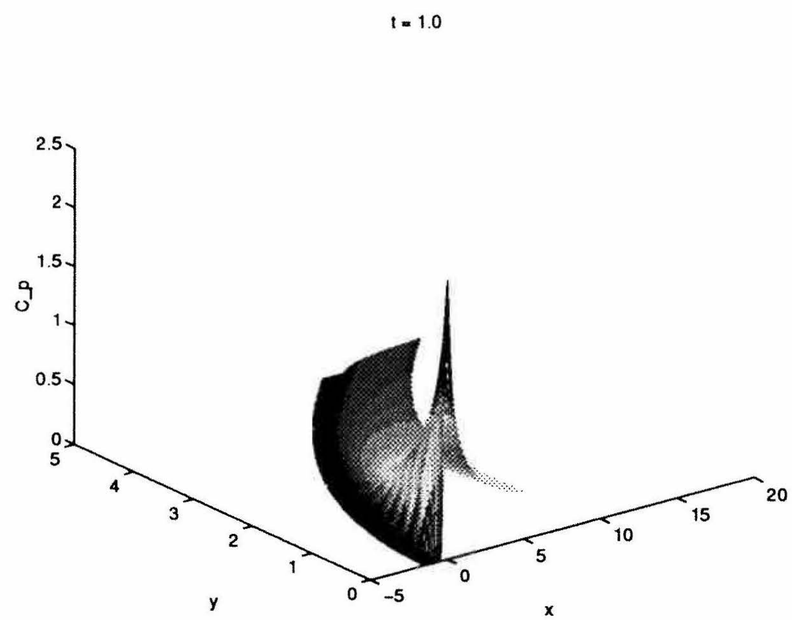
t = 1.0
C_p
2.5
2
1.5
1
0.5
0
5
4
3
2
1
0
y
-5
0
5
10
15
20
x

FIG. 14.

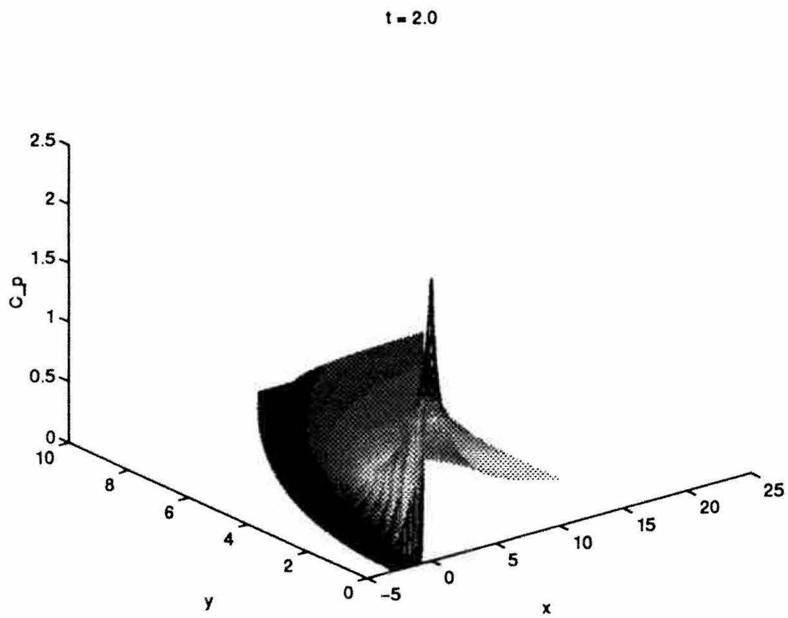
t = 2.0
2.5
2
1.5
1
0.5
0
C_p
10
8
6
4
2
0
y
-5
0
5
10
15
20
25
x

FIG. 15.

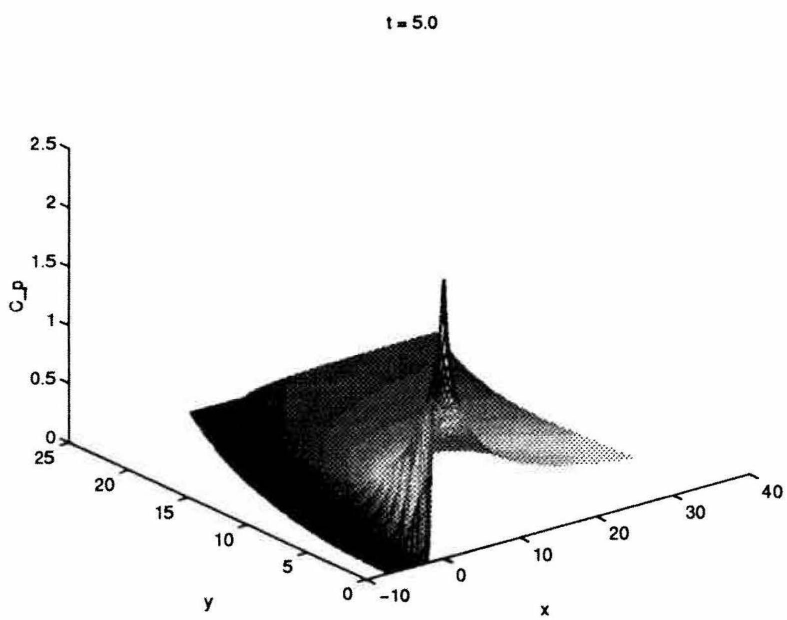
t = 5.0
2.5
2
1.5
1
0.5
0
C_p
25
20
15
10
5
0
y
-10
0
10
20
30
40
x

FIG. 16.

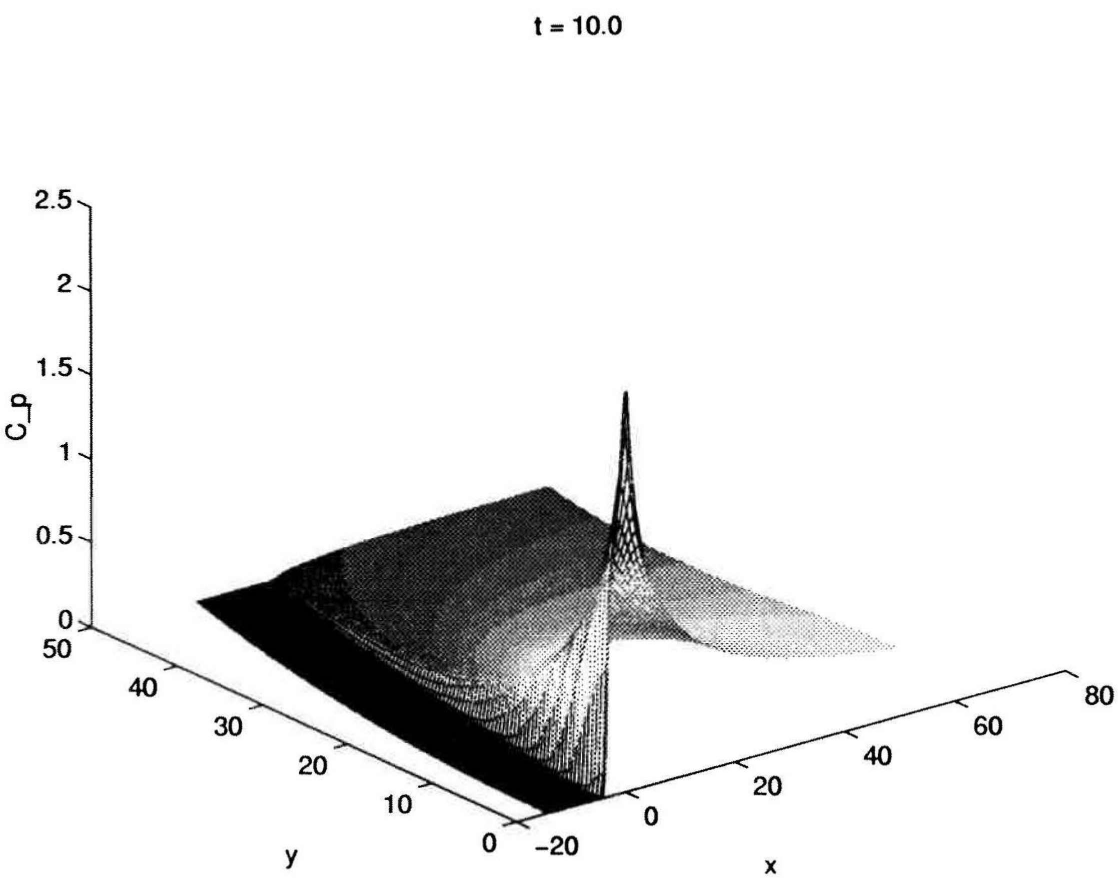

FIG. 17.

The Mechanics of a Tactile Receptor*

Mark H. Holmes†

Abstract

The Pacinian corpuscle (PC) is a tactile receptor which resides in the skin. Its function is to transduce deformations of the skin into neural signals. During the transduction process the signal is filtered considerably by the outer capsule of the PC. Exactly how or why it does this is an open question and the subject of this paper. Structurally the PC has the shape of a bulb, made up of concentric membranes that are each separated by a fluid layer. In this paper a continuum model of the bulb is reduced using homogenization. The result is a system of two partial differential equations for the homogenized pressure field and radial displacement of the bulb. From the solution an expression for the hoop strain in the receptor membrane is obtained. The latter is the input stimulus for the nerve. Numerical results of the transient behavior of the strain and receptor potential are presented.

1 Introduction

The sense of touch shares with the auditory system the task of transforming mechanical stimuli into electrical signals for the brain. However, the receptors for touch are not understood as well as those for the ear. In humans there are four principal tactile receptors: the Pacinian corpuscles, the Merkel discs, the Meissner's corpuscles, and the Ruffini end-organs (see Fig. 1). Exactly why there are four receptor types is not known, although they may be responding to different components of the deformation field in the skin (e.g., one may transduce shear stress while another picks up compressive stresses). A general discussion of their structure and possible functions can be found in [1].

The most studied tactile receptor is the Pacinian corpuscle (PC) and this is due in part to its size and prominence in various tissues. At the present time the PCs associated

* This work was partially supported by the National Science Foundation, grant DMS-9404517

† Department of Mathematical Sciences, Rensselaer Polytechnic Institute, Troy, NY 12180

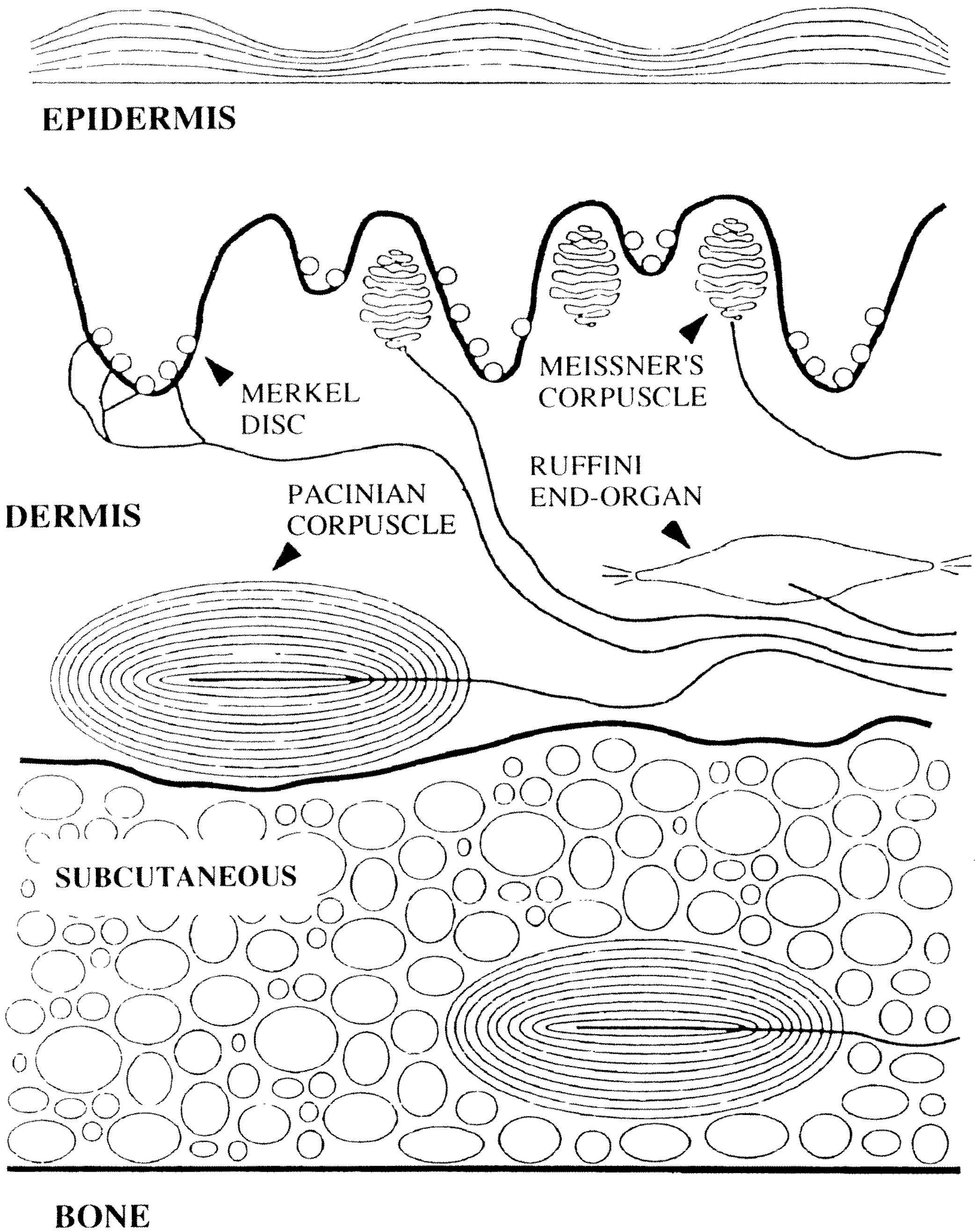

Fig. 1. Schematic diagram illustrating the four tactile receptors found in glabrous skin of the hand. Their position, density, and structure suggest that each type is responsible for different components of the tactile signal. For example, the Pacinian corpuscle is most responsive to frequencies from 100 to 1000 Hz, while the Ruffini ending operates best from 15 to 400 Hz. Why there are four receptor types, and what their roles are in the somatosensory system, are not know.

with the skin are thought to be responsible for the transduction of relatively high frequency mechanical vibrations (from 100 to about 1000 Hz). The basic structure of a PC is a dendritic ending that is encapsulated with a bulb formed from thin concentric layers of cells (Fig. 2). There are fluid spaces separating these cellular layers, and this gives the capsule the structure of a layered composite. There are 30-60 such fluid-elastic layers, and they are more or less annular in a transverse cross-section of the PC. The dendrite in the PC is comprised of a myelinated segment that enters the capsule at its proximal pole and an unmyelinated segment, known as the terminal region, extending most of the length of the capsule. The terminal region is responsible for generating the receptor current. It is thought that at the molecular level of the membrane covering the terminal region, the induced strain from the deformation of the capsule furnishes gating energy to open ionic (transduction) channels [2]. Thus, receptor potential is altered and this in turn initiates neural impulse activity. A review of the PC and its function can be found in [3].

Experimental works on PCs beyond anatomical studies have mainly been concerned with quantifying their electrical response to mechanical stimuli. Typically in these experiments the PC is compressed between two rigid plates using either a simple ramp-and-hold displacement, or a periodic displacement where the amplitude and frequency of the displacement are controlled. These experiments have made it clear that the capsule acts as a mechanical filter of the signal. For example, the PC is considered to be a

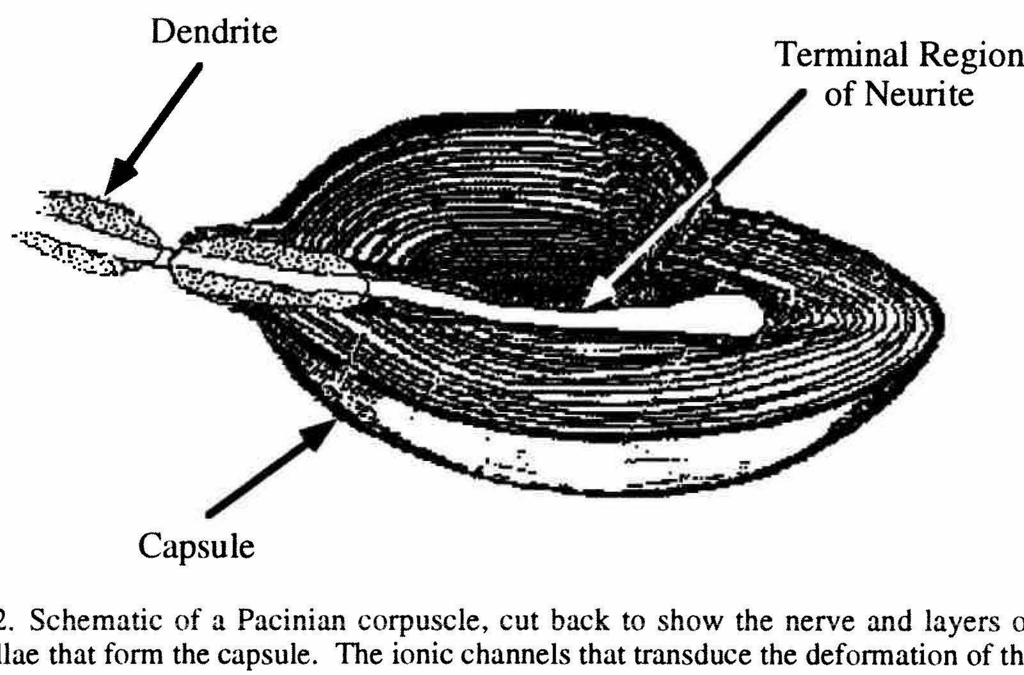

Fig. 2. Schematic of a Pacinian corpuscle, cut back to show the nerve and layers of lamellae that form the capsule. The ionic channels that transduce the deformation of the capsule are located along the neurite in the terminal region.

rapid adapting mechanoreceptor because in response to a moderate ramp compression it will typically produce only a single action potential. Interestingly, even if the compression is held for long periods of time there is usually no additional neural response, yet when the compression is removed the PC will again produce another action potential.

The model for mechanotransduction in the PC can be divided into two general components, one for the mechanics of the capsule and one for the electrophysiology of the nerve fiber. The capsule and dendrite are coupled through the hoop strain. Below, the model for the capsule is presented and formulas for the hoop strain are derived.

2 Model formulation

In terms of its mechanical behavior the capsule is assumed to be formed from concentric elastic membranes that are separated by fluid layers. The fluid in these layers, as far as its mechanical properties are concerned, is water at body temperature. Because of the collagen fibers and the way they are oriented in the PC, the membranes are modeled as thin orthotropic elastic shells. Also, because of the thinness, bending is not included in the formulation of the model considered here. The shell equations are obtained from Flügge's theory for the case of small strains about an equilibrium position. In the analysis below the capsule is considered to be two dimensional, which can be thought of as a limiting (slender body) approximation to the full PC capsule. This is a reasonable approximation because of the orientation of the fibers, as well as the local nature of the excitation of the dendrite.

Our starting point is the linearized momentum and continuity equations for the fluid along with linear shell equations for each lamella. Thus, for the fluid in the ith layer, where $r_{i-1} < r < r_i$, the nondimensional equations of motion are

$$(\partial_t - \delta^2\nabla^2)\mathbf{v} = -\frac{1}{\varepsilon^2}\nabla p \tag{1}$$

$$\nabla\cdot\mathbf{v} = 0 \ . \tag{2}$$

The scaled equations for the ith membrane, where $r = r_i$, are

$$\partial_\theta(\partial_\theta u_i - v_i) - \xi_i(u_i + \partial_\theta v_i) - \mu\xi_i r_i^2 \partial_t^2 u_i = \alpha_i r_i^2 [\![p]\!]_i \tag{3}$$

$$\partial_\theta(u_i + \partial_\theta v_i) - \mu r_i^2 \partial_t^2 v_i = -\varepsilon\zeta r_i^2 [\![\partial_r v_\theta]\!]_i \tag{4}$$

There is also a kinematic condition at the fluid-lamella interface. For the ith membrane this is given by

$$\mathbf{v}\,\Big|_{r=r_i} = \partial_t(u_i, v_i) \tag{5}$$

The notation used here is standard. The variables r,θ are the radial and angular coordinates. The vector $\mathbf{v} = (v_r, v_\theta)$ is the fluid velocity with components in the radial and circumferential directions. Also, p is the fluid pressure, and u_i , v_i represent the normal and circumferential displacement of the i<u>th</u> lamella membrane. The notation $[\![\,\cdot\,]\!]_i$ designates the jump of the quantity across the i<u>th</u> lamella, and so,

$$[\![\,p\,]\!]_i \equiv p\,\Big|_{r=r_i+} - \;p\,\Big|_{r=r_i-} \;.$$

The quantity $r_i \equiv a_i/a$ is the normalized radius of the i<u>th</u> membrane, where a is the radius of the PC and a_i is the radius of the i<u>th</u> membrane (the latter two are dimemsional). It's assumed that the radial distance, h , between the shells is constant, so, $a_i = a_{i-1} + h$. Therefore, $r_{i+1} = r_i + \varepsilon$, where

$$\varepsilon = \frac{h}{a} \;. \tag{6}$$

The other parameters are

$$\delta^2 = \frac{\nu_f t_c}{a^2} \;, \qquad \xi_i = \frac{J}{J_i} \;, \qquad \mu = \frac{\rho h_0 a^2}{J t_c^{\,2}} \;,$$

$$\alpha_i = \frac{\rho a^3}{J_i t_c^{\,2} \varepsilon^2} \;, \qquad \zeta = \frac{\mu_f a^2}{J t_c h} \;.$$

The material parameters appearing here include the kinematic viscosity ν_f , the shear viscosity μ_f , and the density ρ of the fluid; the elastic stiffness coefficients J_i , J of the shell; and the thickness h_0 and the radius a_i of the i<u>th</u> shell. Some appropriate representative physical values of various parameters are given in Table 1. It is also assumed that $J = Eh_0/(1 - \nu^2)$, where E is a Young's modulus and ν is a Poisson ratio, and $J_i = \varepsilon_i J$ where $\varepsilon_i = r_i/10$.

It is instructive to consider the relative order of magnitude of the terms in the above equations for typical parameter values. Using the values in Table 1, and taking $\varepsilon = 1/50$ and $t_c = 2 \times 10^{-3}$ sec , then $\alpha_i \approx 3\mathrm{x}10^4/\,r_i$, $\xi_i = 10/\,r_i$, $\zeta \approx 3/4$, and $\mu \approx 3\mathrm{x}10^{-4}$. Thus, we see that the inertia in the shell equations can be ignored. Note, however, that inertia is still in the system, namely, in the fluid (in Eq. (1)). The parameter of most interest is ε, which represents the ratio of the radial thickness of the fluid layer to the radius of the PC. The fact that the membranes are close together (so, $\varepsilon \ll 1$) can be used to reduce the problem. This is a singular limit and it is the basis of the homogenization procedure used in the next section (an introduction to the method of homogenization is given in [6]).

3 Homogenization Approximation

It's possible to reduce the model by taking advantage of the thinness of the fluid layers in comparison to the overall dimensions of the PC. The expansion, therefore, will be based on the fact that ε in (1)-(5) is small. There are (at least) two spatial scales in the PC. One of these is associated with the overall radial dimension r. The other is the scale associated with individual layers, which is $O(\varepsilon)$. To account for this we introduce the microscale variable

$$R = \frac{r - \bar{r}}{\varepsilon} . \tag{7}$$

This variable is centered about an arbitrary radial position $r = \bar{r}$ in the capsule, where $0 < \bar{r} < 1$. Using multiple scales the radial derivative transforms as $\partial_r \rightarrow \partial_r + \frac{1}{\varepsilon}\partial_R$, and the system in (1)-(5) becomes

Table 1: Model Parameters for PC Capsule

Parameter	**Name**	**Value (cgs)**
a	PC radius	4×10^{-2}
r_t	Radius of receptor membrane	4×10^{-4}
h	Thickness of fluid layer	10^{-4}
ρ	Fluid density	1
ν_f	Kinematic viscosity of fluid	10^{-2}
h_0	Elastic thickness of lamellae	10^{-5}
E	Young's modulus	10^6
ν	Poisson's ratio	0.5

$$[\,\varepsilon^3(\,\partial_t - \delta(\Delta - \frac{1}{r^2})) - \varepsilon^2\delta^2(2\partial_r + \frac{1}{r})\partial_R - \varepsilon\delta^2\partial_R{}^2]v_r + 2\,\frac{\varepsilon^3\delta^2}{r^2}\,\partial_\theta v_\theta = -\,(\partial_R + \varepsilon\partial_r)p \quad (8)$$

$$[\,\varepsilon^2(\,\partial_t - \delta(\Delta - \frac{1}{r^2})) - \varepsilon\delta^2(2\partial_r + \frac{1}{r})\partial_R - \delta^2\partial_R{}^2]v_\theta - 2\,\frac{\varepsilon^2\delta^2}{r^2}\,\partial_\theta v_r \;=\; -\frac{1}{r}\,\partial_\theta p \quad (9)$$

$$(\partial_R + \varepsilon\partial_r)v_r + \frac{\varepsilon}{r}(v_r + \partial_\theta v_\theta) \;=0 \quad , \quad (10)$$

and

$$\partial_\theta(\partial_\theta u_i - v_i) - \xi(u_i + \partial_\theta v_i) \;=\; \alpha[r + O(i\varepsilon) + O(\varepsilon)]^2[\![\,p\,]\!]_i \quad , \quad (11)$$

$$\partial_\theta(u_i \;+ \partial_\theta v_i) \;\;=\;\; -\,\zeta[r + O(i\varepsilon) + O(\varepsilon)]^2[\![\,(\partial_R + \varepsilon\partial_r)v_\theta\,]\!]_i \quad , \quad (12)$$

where

$$\mathbf{v}|_i \;=\; \partial_t(u_i\,,v_i) \quad . \quad (13)$$

The subscript i in the above equations refers to the layer number measured from the point about which the expansion is centered. For this reason the r_i that appears in (3) and (4) has been written in (11) and (12) as $r + O(i\varepsilon) + O(\varepsilon)$. Also, since the stiffness J_i is a function of r_i we now write $J(r_i)$. Thus, the parameters $\xi_i\,,\alpha_i$ in (3),(4) are written in (11),(12) as $\xi = \xi[r + O(i\varepsilon) + O(\varepsilon)]$ and $\alpha = \alpha[r + O(i\varepsilon) + O(\varepsilon)]$.

The appropriate expansions for small ε are

$$v \sim v_0 + \varepsilon v_1 + \dots\,, \qquad\qquad p \sim p_0 + \varepsilon p_1 + \dots\,, \quad (14)$$

and

$$(u_i\,,v_i) \sim (u_{i0}\,,v_{i0}) + \varepsilon(u_{i1}\,,v_{i1}) + \dots \quad . \quad (15)$$

Substituting these into (8)-(10) and equating the O(1) terms, the fluid equations for the i<u>th</u> layer are (note $i - 1 < R < i$)

$$\partial_R p_0 = 0 \quad , \quad \delta^2\partial_R{}^2 v_{\theta 0} = \frac{1}{r}\,\partial_\theta p_0 \quad , \quad \partial_R v_{r0} = 0 \;. \quad (16)$$

Also, from Eqs. (11) and (12), the equations for the membranes bounding the i<u>th</u> layer are (note, $j = i - 1\,,\,i$)

$$\alpha\, r^2[\![\,p_0\,]\!]_j \;=\; (\partial_\theta{}^2 - \xi)u_{j0} \;-\; (1 + \xi)\partial_\theta v_{j0}\,, \quad (17)$$

$$\partial_\theta(u_{j0}+\partial_\theta v_{j0}) = -\zeta r^2 [\![\partial_R v_{\theta 0}]\!]_j \ , \tag{18}$$

and the kinematic boundary conditions are

$$(v_{r0}, v_{\theta 0})\Big|_j = \partial_t(u_{j0}, v_{j0}) \ . \tag{19}$$

In (17) and (18), $\alpha = \alpha(r)$ and $\xi = \xi(r)$.

Equations (19) and (16c) imply

$$u_{i0} = u_0(r,\theta,t) \ , \quad v_{r0} = \partial_t u_0(r,\theta,t) \ , \tag{20}$$

that is, these quantities do not depend on the layer. The pressure in the ith layer, from (16a), is independent of R but can depend on i, so we write $p_{0i} = p_{0i}(r, \theta, t)$. With this result (17) gives

$$p_{0,i+1} = p_{0i} + \frac{1}{\alpha r^2}[(\partial_\theta{}^2 - \xi)u_0 - (1+\xi)\partial_\theta v_{i0}] \ . \tag{21}$$

Iterating backward to the first layer (where $R = 0$) yields

$$p_{0,i+1} = p_{01} + \frac{i}{\alpha r^2}\{ (\partial_\theta{}^2 - \xi)u_0 - (1+\xi)\partial_\theta [\, \frac{1}{i}\sum_{i}^{i} v_{j0}] \, \} \tag{22}$$

The remaining fluid variable to solve for is the circumferential velocity. From (16b), and given that $v_{\theta 0}\Big|_{R=i} = \partial_t v_{i0}$ and $v_{\theta 0}\Big|_{R=i-1} = \partial_t v_{i-1,0}$, we have that

$$v_{\theta 0} = \frac{1}{2r\delta^2}(R-i)(R-i+1)\partial_\theta p_{0i} + \partial_t[v_{i0} + (R-i)(v_{i0} - v_{i-1,0})] \ . \tag{23}$$

In this case

$$\partial_R v_{\theta 0} = \begin{cases} \dfrac{1}{2r\delta^2}\partial_\theta p_{0i} + \partial_t(v_{i0} - v_{i-1,0}) & \text{if } R = i \\[2ex] -\dfrac{1}{2r\delta^2}\partial_\theta p_{0i} + \partial_t(v_{i0} - v_{i-1,0}) & \text{if } R = i-1 \end{cases} \ . \tag{24}$$

Substituting this into (18) one finds that

$$\partial_\theta(u_0 + \partial_\theta v_{i0}) = \zeta r^2 [\, \frac{1}{2r\delta^2}\partial_\theta(p_{0,i+1} + p_{0i}) - \partial_t(v_{i+1,0} - 2v_{i0} + v_{i-1,0})] \tag{25}$$

The only equation that we need to consider for the $O(\varepsilon)$ terms comes from the continuity equation, and it is

$$r(\partial_r v_{r0} + \partial_R v_{r1}) + v_{r0} + \partial_\theta v_{\theta 0} = 0 \ , \tag{26}$$

where $v_{r1}\big|_j = \partial_t u_{j1}$ for $j = i, i-1$. Using the results in (20) and (23), Eq. (26) can be written as

$$\partial_R v_{r1} = -(\partial_r + \frac{1}{r})\partial_t u_0 - \frac{1}{2r\delta^2}(R-i)(R-i+1)\partial_\theta{}^2 p_{0i}$$
$$- \frac{1}{r}\partial_\theta\partial_t[v_{i0} + (R-i)(v_{i0} - v_{i-1,0})] \ .$$

Integrating this and using the boundary condition (19) at $j = i$ yields

$$v_{r1} = \partial_t u_{i1} - (R-i)(\partial_r + \frac{1}{r})\partial_t u_0 - \frac{1}{r}\partial_\theta\partial_t \{ (R-i)\, v_{i0} + \frac{1}{2}(R-i)^2(v_{i0} - v_{i-1,0}) \}$$
$$- \frac{1}{2r\delta^2}\partial_\theta{}^2 p_{0i}\,[\tfrac{1}{3}R^3 - \tfrac{1}{2}(2i-1)R^2 + i(i-1)R - \tfrac{1}{3}i^3 + \tfrac{1}{2}(2i-1)i^2 - i^2(i-1)]$$

The kinematic boundary condition in (19) at $j = i-1$ must also be satisfied, so,

$$\partial_t u_{i1} = \partial_t u_{i-1,1} - (\partial_r + \frac{1}{r})\partial_t u_0 - \frac{1}{2r}\partial_\theta\partial_t(v_{i0} + v_{i-1,0}) + \frac{1}{12r^2\delta^2}\partial_\theta{}^2 p_{0i} \ .$$

Iterating back to the layer where $R = 0$ produces the following result

$$\partial_t u_{i1} = \partial_t u_{01} + \frac{1}{2r}\partial_\theta\partial_t(v_{i0} - v_{00})$$
$$+ i \{ -(\partial_r + \frac{1}{r})\,\partial_t u_0 + \frac{1}{12r^2\delta^2}\frac{1}{i}\sum_{1\le j\le i}\partial_\theta{}^2 p_{0j} - \frac{1}{r}\partial_\theta\partial_t[\frac{1}{i}\sum_{1\le j\le i} v_{j0}] \} \tag{27}$$

Equations (20), (22), (27) are now going to be used to find equations for the homogenized versions of the dependent variables. To do so we assume v_{i0}, p_{0i}, and u_{i1} are bounded as functions of i. We also introduce an averaging operator $\langle \cdot \rangle$ defined as

$$\langle f \rangle \equiv \lim_{i\to\pm\infty} \frac{1}{i}\sum_{i}^{i} f_j \ . \tag{28}$$

With this let

$$\langle v_0\rangle = \frac{1}{i}\sum_1^i v_{j0} + V_i \quad , \qquad \langle p_0\rangle = \frac{1}{i}\sum_1^i p_{0j} + P_i \quad , \tag{29}$$

where $V_i = o(1)$ and $P_i = o(1)$ as $i \to \pm\infty$. From the above remarks (21) becomes

$$p_{0,i+1} = p_{01} + \frac{i}{\alpha r^2}\{ (\partial_\theta{}^2 - \xi)u_0 - (1+\xi)\partial_\theta[\langle v_0\rangle - V_i]\} . \tag{30}$$

Thus, to have boundedness as $i \to \pm\infty$, we must have

$$(\partial_\theta{}^2 - \xi)u_0 - (1+\xi)\partial_\theta\langle v_0\rangle = 0 \ , \tag{31}$$

and $V_i = O(\frac{1}{i})$ and $P_i = O(\frac{1}{i})$ as $i \to \pm\infty$. As a consequence of (30)

$$p_{0,i+1} = p_{01} + (1+\xi)\frac{i}{\alpha r^2}\partial_\theta V_i \quad .$$

Also, from (27) we have

$$\begin{aligned}\partial_t u_{i1} &= \partial_t u_{01} + \frac{1}{2r}\partial_\theta\partial_t(v_{i0} - v_{00}) \\ &\quad + i\{-(\partial_r + \frac{1}{r})\partial_t u_0 + \frac{1}{12r^2\delta^2}\partial_\theta{}^2(\langle p_0\rangle - P_i) - \frac{1}{r}\partial_\theta\partial_t(\langle v_0\rangle - V_i)\} \ .\end{aligned}$$

and so, for $\partial_t u_{i1}$ to be bounded we must have

$$(\partial_r + \frac{1}{r})\partial_t u_0 + \frac{1}{r}\partial_t\partial_\theta\langle v_0\rangle = \frac{1}{12r^2\delta^2}\partial_\theta{}^2\langle p_0\rangle \ . \tag{32}$$

There is one remaining homogenized equation and this comes from (27). Summing from $j = 1$ to i, dividing by i, and then taking the limits $i \to \pm\infty$ we obtain

$$u_0 + \partial_\theta\langle v_0\rangle = \frac{\zeta r}{\delta^2}[\langle p_0\rangle - \bar{p}_0] . \tag{33}$$

The constant $\bar{p}_0$ is determined from the 2π periodicity of $\langle v_0\rangle$ and the fact that the circumferential average of u_0 is zero. The result is that $\bar{p}_0$ is the circumferential average of $\langle p_0\rangle$, that is,

$$\bar{p}_0 = \frac{1}{2\pi}\int_0^{2\pi}\langle p_0\rangle\, d\theta \ .$$

The number of homogenized equations can be reduced by solving (33) for $\partial_\theta\langle v_0\rangle$ and then substituting the result into (31) and (32). Setting $p_0 = \langle p_0 \rangle - \bar{p}_0$, the result is

$$\partial_\theta{}^2 u + u = \frac{\zeta\, r(1+\xi)}{\delta^2}\, p \ , \tag{34}$$

$$\partial_\theta{}^2 p - 12\zeta r^2 \partial_t p = 12\delta^2 r^2 \partial_t \partial_r u \tag{35}$$

To simplify the presentation, the subscripts on the pressure (p) and the radial displacement (u) have been dropped. System (34)-(35) constitutes the homogenized approximation to the cross-sectional dynamics of the capsule. Eq. (34) is essentially the law of Laplace since it originates from (33). The second equation, (35), contains the viscous effects, namely the shear stress on the membranes (the middle term) and the viscous dissipation in the fluid (the last term).

There is one last result that is needed before the homogenized problem is complete, and that is the appropriate boundary condition at $r = 1$. It's assumed that on this boundary there is a prescribed pressure $\tilde{p}$ and shear stress $\tilde{\sigma}_{r\theta}$. After carrying out a boundary layer analysis one finds that at $r = 1$ the following must hold [4]

$$\partial_\theta(\partial_\theta{}^2 u + u + \alpha\, r_2\, \tilde{p}) = \zeta(1+\xi)\, r^2 \tilde{\sigma}_{r\theta} + [\alpha r^2 + \frac{\zeta r(1+\xi)}{2\delta^2}]\, \partial_\theta p \, . \tag{36}$$

This boundary condition is simply the requirement that the total stress is continuous across the boundary.

The variable of particular interest for the gating of the channels in the receptor membrane is the (scaled) hoop strain $\varepsilon_{\theta\theta} = \varepsilon_{\theta\theta}(r_t, \theta, t)$, where $r = r_t$ is the radial coordinate of the receptor membrane. This is the strain in the circumferential direction, that is, if a circumferential segment of initial length ds_0 is stretched to a length ds_1, then the hoop strain is defined to be $(ds_1 - ds_0)/ds_0$. By expressing this ratio in terms of the displacements, and linearizing the result, it is found that

$$\varepsilon_{\theta\theta} = \frac{\partial_\theta{}^2 u + u}{1 + \xi(r)} \ . \tag{37}$$

This is actually the scaled strain and this is all that is needed here; for the exact scaling, see [4].

4 Indentation Problem

In investigating the neural response of the PC it is typical that the capsule is compressed between two rigid plates, or indenters [3]. We assume that there is no shear stress imposed by the plates. In this case, on $r = 1$ we take

$$u = -\, f(t)g(\theta)\,, \ \text{for} \ \theta_0 < \theta \le \frac{\pi}{2}\,, \tag{38}$$

and

$$\tilde{p} \ = \tilde{\sigma}_{r\theta} = 0\,, \ \text{for} \ 0 \le \theta \le \theta_0\ . \tag{39}$$

The conditions over the remainder of the boundary are obtained through symmetry. It is possible to rewrite (38) in terms of p. From (34) one finds that (38) can be expressed as

$$p(1,\theta,t) = -\frac{\delta^2}{(1+\xi_1)\zeta} f(t)(\partial_\theta{}^2 + 1)g(\theta)\,, \ \text{for} \ \theta_0 < \theta \le \frac{\pi}{2}\ . \tag{40}$$

As for (39), since there is no imposed shear stress, one finds from (36) that

$$p(1,\theta,t) = -\ \frac{\delta^2 f(t)}{\theta_0(1+\xi_1)\zeta}\left[\ g'(\ \theta_0\ ) - \int_{\theta_0}^{\pi/2} g(\theta)d\theta\ \right]\,, \ \text{for} \ 0 \le \theta \le \theta_0\ . \tag{41}$$

To guarantee that $p(r,\theta,t)$ is continuous on the outer boundary it is assumed that

$$(\partial_\theta{}^2 + 1)\ g(\theta) = \ \frac{1}{\theta_0}\left[\ g'(\ \theta_0\ ) - \int_{\theta_0}^{\pi/2} g(\theta)d\theta\ \right],\ \text{for} \ \theta = \theta_0\ . \tag{42}$$

Boundary conditions (40) and (41) can be combined into the single expression

$$p(1,\theta,t) = -\ f(t)\ B(\theta)\,, \tag{43}$$

where

$$B(\theta) \ = \begin{cases} \bar{b}(\theta) & \text{for} \quad \theta_0 < \theta \le \pi/2 \\ \bar{b}(\theta_0) & \text{for} \quad 0 \le \theta \le \theta_0 \end{cases}\ , \tag{44}$$

for

$$\bar{b}(\theta) = \frac{\delta^2}{(1+\xi_1)\zeta}\,(\partial_\theta{}^2 + 1)g(\theta) \ ,$$

and the function $g(\theta)$ satisfies (42).

The solution of the homogenized problem can be obtained using modal expansions, and so, assume

$$B(\theta) = \sum_{\substack{n \geq 2 \\ \text{even}}} b_n \cos(n\theta) \ . \tag{45}$$

Only the positive even integers are included in this summation because of the symmetry assumed in the problem. With (45), let

$$p = \sum_{\substack{n \geq 2 \\ \text{even}}} q_n(r,t)\cos(n\theta) \ , \ \text{and} \quad u = \sum_{\substack{n \geq 2 \\ \text{even}}} w_n(r,t)\cos(n\theta) \ . \tag{46}$$

Taking the Laplace transform of (34),(35),(43) in t and substituting the transforms of (46) into the resulting equations, we obtain (for $n = 2, 4, 6, \ldots$)

$$(1 - n^2)W_n = \frac{(1+\xi)\zeta\, r}{\delta^2} Q_n \ , \quad (n^2 + 12sr^2\zeta)Q_n = 12\delta^2 r^2 s\partial_r W_n \ , \tag{47}$$

with

$$Q_n(1,s) = -\,b_n F(s) \ , \quad \text{at } r = 1 \ . \tag{48}$$

The capital letters in (47),(48)) denote the transforms of the variables, for example, $W_n(r,s) = \mathcal{L}(w_n)$. Reducing (47a,b) yields

$$2s\zeta(\xi_1 + r)\partial_r W_n - (n^2 - 1)(n^2 + 12\zeta sr^2)r^{-2}W_n = 0 \ .$$

The general solution of this is $W_n(r,s) = A_n(s)\overline{W}_n(r,s)$, where

$$\overline{W}_n(r,s) = G_n(r)\exp\{-\frac{\chi_n(r)}{s}\} \ ,$$

for

$$G_n(r) = \left(\frac{\xi_1 + r}{\xi_1 + 1}\right)^{n^2-1} , \ \text{and} \quad \chi_n(r) = \frac{n^2(n^2-1)}{12\xi_1{}^2\zeta}\left[\ln\left(\frac{(\xi_1+1)r}{\xi_1 + r}\right) + \frac{\xi_1(1-r)}{r}\right] .$$

From (47a),

$$Q_n(r,s) = -\frac{(n^2-1)\delta^2}{r\zeta(\xi(r)+1)} A_n(s)\overline{W}_n(r,s) \ . \tag{49}$$

Upon substituting (49) into (48), we obtain for the coefficients A_n (for n = 2, 4, 6, ...)

$$A_n(s) = \frac{\zeta(\xi_1+1)b_n}{\delta^2(n^2-1)} F(s) \ . \tag{50}$$

Therefore, the Laplace transforms of the radial displacement $u(r,\theta,t)$ is

$$\mathscr{L}(u) = \frac{\zeta(\xi_1+1)}{\delta^2} F(s) \sum_{\substack{n\geq 2 \\ \text{even}}} b_n \overline{W}_n(r,s)\frac{\cos(n\theta)}{n^2-1} \ .$$

and, from (37), the transform of the hoop strain is

$$\mathscr{L}(\varepsilon_{\theta\theta}) = -\bar{\beta} F(s) \sum_{\substack{n\geq 2 \\ \text{even}}} b_n \overline{W}_n(r_t,s)\cos(n\theta) \ , \tag{51}$$

where

$$\bar{\beta} = \frac{\zeta\varepsilon_c(\xi_1+1)}{\delta^2(\xi(r_t)+1)} \ . \tag{52}$$

Here ε_c is the maximum strain imposed. It is possible to invert this last expression for general $F(s)$ and obtain the hoop strain in the form of a convolution. This is not done here as we are interested in a specific forcing function used in experimental testing.

The forcing function we consider is a ramp-and-hold function of the form

$$f(t) = \begin{cases} \dfrac{t}{t_0} & \text{for } 0 \leq t \leq t_0 \\ 1 & \text{for } t_0 \leq t \end{cases} \ . \tag{53}$$

In this case the inverse of (51) is

$$\varepsilon_{\theta\theta} = \bar{\beta} \sum_{\substack{n \geq 2 \\ \text{even}}} b_n G_n(r_t) R_n(t) \cos(n\theta) \ , \tag{54}$$

where

$$R_n(t) = \frac{J(t,n) - J(t - t_0, n)}{t_0} \ , \tag{55}$$

and

$$J(t, n) = \begin{cases} \sqrt{\dfrac{t}{\chi_n(r_t)}} \ J_1[2\sqrt{\chi_n(r_t)\, t}\ ] & \text{if } 0 \leq t \\ 0 & \text{otherwise} \end{cases} \ . \tag{56}$$

The short-time behavior for each mode is easy to obtain by using the Taylor series expansion for J_1 in (56). In this case the n<u>th</u> term in (54) for small t is

$$\bar{\beta}\, b_n\, G_n(r_t)\, (t/t_0)[1 - \chi_n(r_t)\, t/2 + O(t^2)]\cos(n\theta) \ .$$

This result shows that the initial contribution of each mode increases linearly with t, and the smaller the mode number the longer this holds (since χ_n is a strictly increasing function of n). In general, since $r_t < 1$ then the affect of the higher modes at the receptor membrane decreases exponentially with the mode number. In other words, the higher modes are effectively damped out before reaching the receptor membrane. They also decay algebraically in time but oscillate as they do so. One consequence of this is that the hoop strain returns to its initial equilibrium value, in this case zero. This is a form of adaptation and this happens for any compression that approaches a steady state as $t \rightarrow \infty$. Another observation that can be made from (54) is that the maximum response of the PC, for a given imposed strain ε_c, can be increased by decreasing the time interval t_0 . There is an upper limit, however, and that is obtained when a step function forcing is used. In this case the n<u>th</u> mode in the initial moments expands as $\bar{\beta} b_n G_n(r_t)\{1 - \chi_n(r_t)\, t + O(t^2)\}\cos(n\theta)$. Thus the strain has an instantaneous jump at $t = 0$, and one can show that it then decays to zero in an oscillatory fashion similar to what occurs in (56).

In the calculations considered here we assume the function $g(\theta)$ in (38) is defined as follows

$$g(\theta) = \begin{cases} 1 & \text{for } \theta_1 \le \theta \le \pi/2 \\ 1 + K(\theta - \theta_1)^3 & \text{for } \theta_0 \le \theta < \theta_1 \end{cases} ,$$

where K is determined from (42) and is given as

$$K = \frac{2\pi}{(\lambda - 1)\theta_0{}^2[(\lambda - 1)^2(\lambda + 3)\theta_0{}^2 + 12(\lambda + 1)]} ,$$

for $\lambda = \theta_1 / \theta_0 > 1$. This particular function is used because it approximates the experimental condition of compressing the capsule between two plates and it guarantees that the displacement is smooth for $\theta_0 < \theta \le \pi/2$. In this case, from (44),

$$\bar{b}(\theta) = \frac{\delta^2}{(1 + \xi_1)\zeta} \begin{cases} 1 & \text{for } \theta_1 \le \theta \le \pi/2 \\ 1 + 6K(\theta - \theta_1) + K(\theta - \theta_1)^3 & \text{for } \theta_0 \le \theta < \theta_1 \end{cases} .$$

The coefficients in (54) are not hard to find, although tedious, and one obtains

$$b_n = -\frac{\delta^2}{(1 + \xi_1)\zeta} [\, c_1 \sin(n\theta_0) + c_2 \cos(n\theta_1) + c_3 \cos(n\theta_0) \,] .$$

where

$$c_1 = \frac{24K}{\pi n^3} (\theta_1 - \theta_0) , \quad c_2 = \frac{-24K}{\pi n^2} (1 - \frac{1}{n^2}) , \text{ and } c_3 = \frac{24K}{\pi n^2} (1 - \frac{1}{n^2} + \frac{(\theta - \theta_0)^2}{2}) .$$

5 Qualitative Properties of the Solution

As discussed in the introduction, it is thought that the capsule is largely responsible for the adaptive behavior observed in the neural response of the PC. Its exact role is not known since it is difficult to experimentally analyze the capsule independently of the rest of the corpuscle. Through the modeling above, and the subsequent determination of the model's solution, we now investigate the possibility of how adaptation may take place.

Historically, most of the early experiments into the neural response of the PC involved a ramp-and-hold compression of the capsule. It is from these tests that the PC became to be known as a rapid adapting receptor. The reason for this is that for small to moderate strains it is typical that the PC only produces a single neural spike in response to a ramp compression and, depending on the compression and time held, will produce

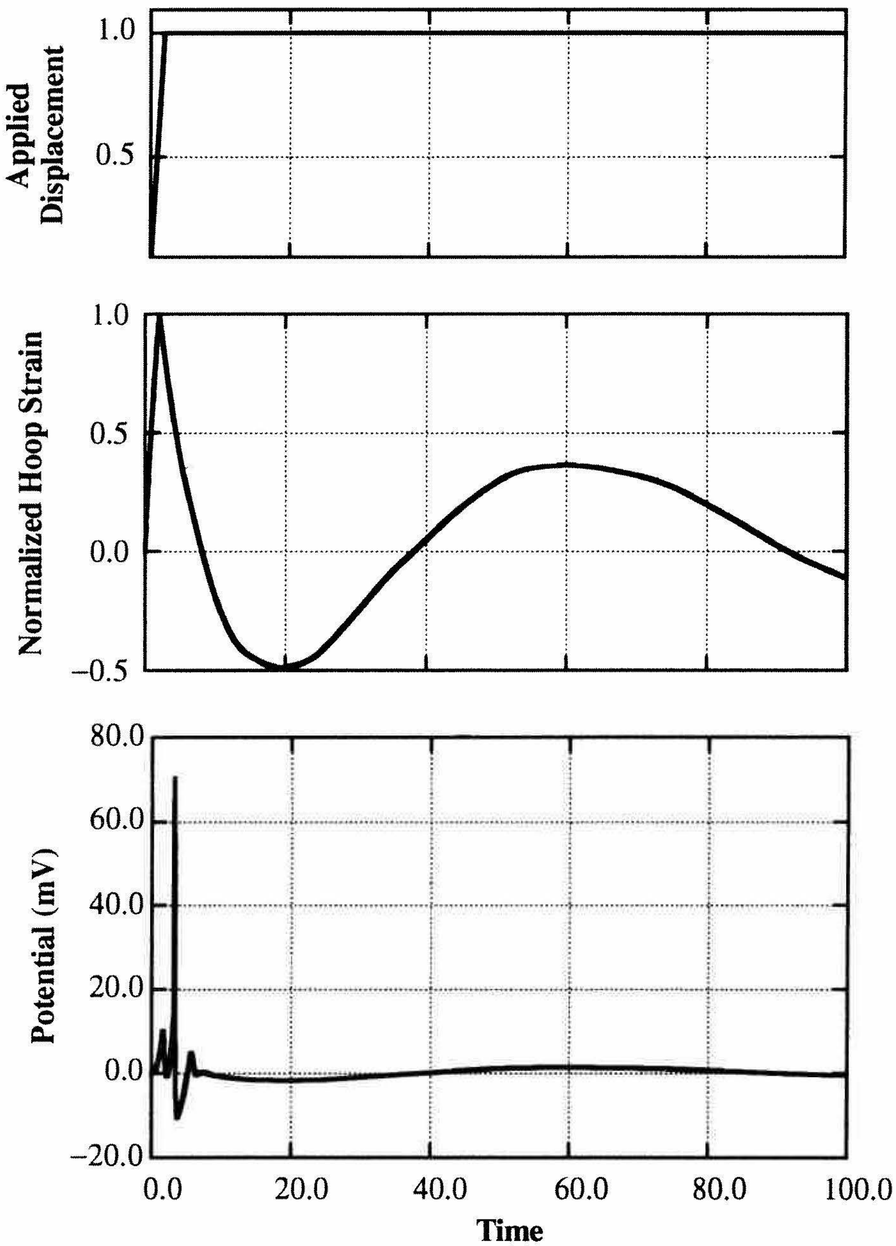

Fig. 3. Response of the model PC in response to a ramp-and-hold displacement. The stimulus is shown in (a) and the hoop strain in the receptor membrane as determined from (54) is shown in (b). The resulting dendritic membrane potential, determined using the model given in [5], is shown in (c). The ramp in (a) is 2 msec in duration and the hold phase lasts 98 msec. This single spike responses shows clearly the behavior of the PC as a rapidly adapting mechanoreceptor and the ability of the model to reproduce this type of response.

another spike when the load is removed. To investigate this in the present model we consider the test described in the previous section where the PC is compressed between two flat plates. The parameter values to be used are given in Table 1 and the determination of the neural response from the hoop strain is done using the model described in [5].

The values obtained from the model, for a ramp lasting 2 msec, are shown in Fig. 3. In addition to the forcing function, the hoop strain and receptor potential are shown. The hoop strain is obtained from (54) and it is evaluated at the location of the receptor membrane at the site of the ionic channels (so, $r = r_t$ and $\theta = 0$). The graphs demonstrate that a single voltage spike occurs in response to the ramp-up, and then produces no others even though the capsule is under compression. Therefore, the model displays the same rapidly adapting response as a PC.

As seen in Fig. 3, the response of the hoop strain consists of a sharp increase during the ramp stage but it reverses quickly once $t = t_0$, where the hold stage begins. Once the maximum stimulus has been reached at $t = t_0$, the strain oscillates and decays to zero as described by expressions (54)-(56). It is of interest to note that the sharp peak in the hoop strain can be increased by decreasing t_0, and it can be removed by making t_0 sufficiently large. For example, it disappears almost completely if $t_0 = 10$ msec.

The oscillatory response in the hoop strain can affect the neural response. For example, Fig. 4 gives the number of neural spikes obtained as a function of the amplitude of the forcing function. A ramp-and-hold forcing is used here with a ramp time of 2 msec. So, for small amplitudes there is no response but as the forcing increases the number of spikes increase. This increase is due to the oscillatory nature of the hoop strain (i.e., the subsequent peaks in the strain are initiating a spike). The maximum number of spikes is about 4 or 5 because to achieve any more the capsule would almost have to be crushed.

For the ramp-and-hold experiment the exact mechanisms for activating the neural spike are not known, but it is generally believed that strain imposed on the receptor membrane plays a key part in activating ionic channels responsible for initiation of the impulse. This is the basis of the neural model developed in [5]. Consequently, if there is a threshold level of strain which initiates a nonlinear response in the excitable membrane then the peak value of the strain is important to the transducer. If the loading is applied sufficiently slowly then, no matter what the eventual equilibrium strain imposed on the capsule, the strain in the receptor membrane does not attain sufficient magnitude during its time course to trigger a spike. This is a form of adaptation imposed on the neural response by the capsule. Reversing this, suppose the loading is applied with t_0 short enough to generate a spike. Because of the inherent refractory period of the receptor membrane following the onset of the spike, it is possible the oscillating strain has damped sufficiently during the refractory period that only one spike is initiated by the ramp loading. This appears to be a reasonable expectation and, from Fig. 3, we see that the same behavior is seen in the hoop strain.

The model provides the transient behavior of the resulting strain as a damped oscillatory function. The strain initially responds in a monotone manner to the loading but it eventually starts to oscillate. This oscillation is due to the inertia, which originates from the fluid, and the elastic elements that comes from the shells. The decay is due to the viscosity of the fluid, both from the shear stress on the membranes as well as the viscous dissipation in the fluid. This damping is not capable of producing an overdamped response, at least for the type of loading considered here. Although it is easy to find mechanical systems which exhibit both under- and over-damped responses by changing the material parameters the absence of this property is not unusual. What is more interesting is the dependence of the strain on viscosity. In the expression for the hoop strain given in (54). At a fixed time, if the viscosity is made to be very large the amplitude of each mode in the series for the strain decreases (to zero). The same dependence is obtained for the reverse limit, that is, if the viscosity is allowed to decrease to zero. In other words, there is a value of the viscosity that produces a maximum strain for each mode, and

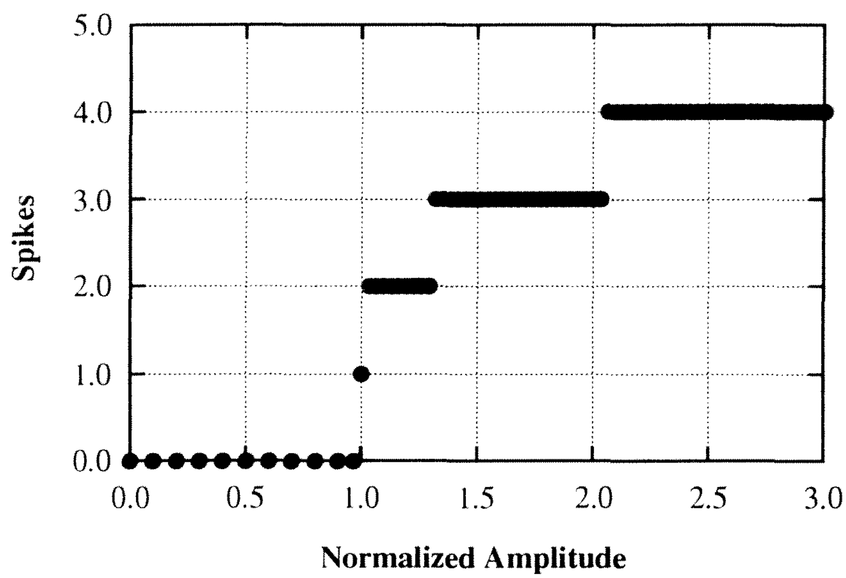

Fig. 4. Number of neural spikes generated by the model PC in response to a ramp-and-hold displacement as a function of the amplitude of the forcing function. The ramp time is 2 msec.

this value depends on the value of t that has been fixed. This dependence can be interpreted in terms of the fluid-elastic layers that form the original capsule. The behavior for large viscosity is typical of most mechanical systems so it needs little explanation. In the limit of zero viscosity, so the fluid is inviscid, the inner membranes do not move when the capsule is compressed and therefore the hoop strain is zero. So, there are competing affects associated with the viscosity, one that is responsible for transmitting the stimulus through the capsule (where a larger viscosity produces a greater strain) and another associated with standard damping (so an increase in the viscosity increases the damping).

Based on the parameter values for the PC the dominant mode in (54) is the first (where $n = 2$). The dependence on viscosity means that it is possible to "tune" the system, that is, it is possible for the system to be designed to produce a maximum response at a particular time (for the first mode). This is significant as the PC is known to be tuned, like the hair cells in the ear, and respond best for driving frequencies of about 400 Hz. More study is needed before a definite connection can be made between this tuning and the viscoelastic properties of the model but the solution of the model does provide possible insights into why experimentally the PC typically only fires a single impulse during a ramp stimulus, even for steep ramps. It may not be so much a mechanism associated with the excitable dynamics of the receptor membrane, but rather the adaptive behavior of the capsule.

References

1. McIntyre, A. K., *Overview: Receptor function,* in *Information processing in mammalian auditory and tactile systems.,* M. Rowe and L. Aitkin, Editor. 1990, Wiley-Liss: New York. p. 1 - 6.

2. Bell, J. and M. H. Holmes, *A note on modeling mechano-chemical transduction with an application to a skin receptor.* J Math Biol, 1994. **32**: p. 275-285.

3. Bell, J., S. J. Bolanowski, and M. H. Holmes, *The structure and function of Pacinian corpuscles: a review.* Prog Neurobiology, 1994. **42**: p. 79-128.

4. Holmes, M. H. and J. Bell, *A model of a sensory mechanoreceptor derived from homogenization.* SIAM J. Appl. Math., 1990. **50**: p. 147-166.

5. Bell, J. and M. Holmes, *Model of the dynamics of receptor potential in a mechanoreceptor.* J Biosci, 1992. **110**: p. 139-174.

6. Holmes, M. H., **Introduction to Perturbation Methods**. Springer-Verlag, New York, 1995.

Weakly Nonlinear Conservation Laws with Source Terms*

J. Kevorkian†

This paper is dedicated to Julian D. Cole on the occasion of his 70th birthday

ABSTRACT

We consider three general hyperbolic conservation laws with source terms and study two classes of problems for which the linearized solutions are neutrally stable and may be derived recursively in explicit form. This paper generalizes recent work, [10], on the corresponding problem for two conservation laws. We use multiple scale expansions to derive evolution equations governing the leading approximation of the weakly nonlinear problem. The principal goal is to determine the influence of source terms on the behavior of solutions. In particular, we show that if one of the waves is damped to leading order, weak nonlinearities do not produce resonant interactions; the two undamped waves satisfy decoupled evolution equations each of which is qualitatively similar to the corresponding two-wave case. If, however, source terms do not damp any of the waves to leading order, the evolution equations that describe the leading nonlinear effects are coupled via resonant interaction terms when the intial data is periodic and the characteristic speeds satisfy certain resonance conditions.

1 Introduction and summary of previous work

We consider a system of $n = 3$ strictly hyperbolic conservation laws with source terms and generalize the derivation given in [10] for the case $n = 2$ to obtain the following standard form when the solution is perturbed about a uniform state and when characteristic dependent variables are introduced

$$\frac{\partial U_i}{\partial t} + \lambda_i(\mu)\frac{\partial U_i}{\partial x} + \sum_{j=1}^{n} C_{ij}(\mu)U_j = \epsilon\phi_i, \quad i = 1,\ldots,n; \quad \lambda_1 > \lambda_2 > \ldots > \lambda_n. \tag{1.1}$$

Here ϵ is a dimensionless small parameter that measures the deviation of the initial data from a constant state, the U_i are the components of the perturbation vector in terms of a characteristic basis, the λ_i are the constant characteristic speeds, and the C_{ij} are constants that arise from linearizing the source terms. Typically, the C_{ij} and λ_i depend on a parameter μ that determines the stability of the linear problem. The leading nonlinear terms are embodied in the ϕ_i which have the form

$$\phi_i = \sum_{j=1}^{n}\sum_{k=1}^{n}[F_{ijk}(\mu)U_j\frac{\partial U_k}{\partial x} + G_{ijk}(\mu)U_jU_k], \quad i = 1,\ldots,n. \tag{1.2}$$

The constants F_{ijk} are contributed by the flux terms whereas the G_{ijk} arise from the source terms in the conservation laws. In particular, for conservation laws with no source terms,

* This research was supported by the National Science Foundation under grant DMS 9525905.

† Department of Applied Mathematics, University of Washington, Seattle, Washington 98195.

the C_{ij} and G_{ijk} all vanish identically. The relation linking the physical variables $u_i(x,t)$ to the U_i has the form

$$u_i = v_i + \epsilon \sum_{j=1}^{n} W_{ij} U_j, \tag{1.3}$$

where the v_i are the constant components of the uniform state (some or all of the v_i may equal zero) and the W_{ij} are the constant matrix components of the transformation to the form (1.1). This transformation is discussed in detail in Secs. 4.5.3 and 7.2.1 of [6].

In this paper we study the asymptotic solution of the system (1.1) to leading order for $0 < \epsilon \ll 1$ using a multiple scale expansion in terms of the characteristic fast scales $\xi_i = x - \lambda_i t$, and the slow time $\tilde{t} = \epsilon t$. The use of multiple scale expansions for solving weakly nonlinear partial differential equations is relatively recent. One of the first treatments of an initial/boundary value problem for a dispersive wave equation was given in [5] using modal expansions to represent the leading order solution. Shortly thereafter, evolution equations that give the asymptotic approximation of the solution in a form that remains uniformly valid in the far field were derived in [1] for weakly nonlinear wave equations that are non-dispersive in the absence of small perturbations.

The vast majority of problems that have been studied in the literature are restricted to the special case where the C_{ij} and G_{ijk} vanish identically and $n = 2$. For this special class of problems the leading term in the expansion for the U_i is $U_i = f_i(\xi_i, \tilde{t}) + O(\epsilon)$. Consistency conditions on the solution to $O(\epsilon)$ then lead to evolution equations for the $f_i(\xi_i, \tilde{t})$ that are decoupled inviscid Burgers equations of the form

$$\frac{\partial f_i}{\partial \tilde{t}} - F_{iii} f_i \frac{\partial f_i}{\partial \xi_i} = 0, \quad i = 1,2. \tag{1.4}$$

Equation (1.4) predicts that the initial profile $f_i(\xi_i, 0)$ propagates along the characteristics $\xi_i =$ constant and is slowly modulated in $\tilde{t}$. If characteristics converge the solution becomes multi-valued and a shock must be introduced. The correct shock conditions for the f_i follow from the exact shock conditions associated with the original system of conservation laws. This question was first discussed in Sec. 5.2 of [2] (see also Sec. 5.1 of [7]) for an example in acoustics; other examples for problems in shallow water flow are given in [6], [9] and [13].

The system (1.1) may be generalized to include the effects of weak dissipation or weak dispersion. The effect of weak dissipation is to introduce second-derivative terms, $\sum_{j=1}^{2} D_{ij} \partial^2 U_j / \partial x^2$, $D_{ii} > 0$, on the right hand side of (1.2). The evolution equations for the f_i now become the viscous Burgers equations

$$\frac{\partial f_i}{\partial \tilde{t}} - F_{iii} f_i \frac{\partial f_i}{\partial \xi_i} = D_{ii} \frac{\partial^2 f_i}{\partial \xi_i^2}, \quad i = 1,2. \tag{1.5}$$

The qualitative effect of the second derivative term on the right-hand side of (1.5) is to smooth out the shocks that occur. In some applications third derivative terms also arise in (1.1). For example, in the Boussinesq approximation for shallow water flow, the leading dispersive effect is exhibited by a third-derivative term in the momentum conservation equation. This leads to decoupled Korteweg-deVries equations for the f_i. See Sec. 5.2 of [7] for a detailed derivation, and [4] for further examples of pairs of conservation laws without source terms having both dissipative and dispersive terms. For simplicity we do not include such terms in the present analysis; their contributions are easily taken into account in any given application.

For $n > 2$, the perturbation analysis for the source-free problem differs from the above only to the extent that one must select two of the n characteristic coordinates as fast scales; the remaining $n-2$ coordinates are then expressed in terms of the two selected ones. If the initial data is of compact support one then obtains the *same* evolution equations (1.4) or (1.5) as for the case $n = 2$. For any n, the physical variables u_i are given by (1.3) to $O(\epsilon)$ in terms of the f_i; in general, each u_i involves *all* the f_i. However, if the initial conditions are further restricted such that only one of the f_i, say f_1, is non-zero, the evolution equation for f_1 may be transformed using (1.3) to an equation governing each of the physical variables as a function of (x, t) to leading order. If we denote $(u_i - v_i)/W_{i1} = \rho_i$ and $\epsilon D_{ii} = \nu_i$, (1.5) transforms to

$$\frac{\partial \rho_i}{\partial t} + (\lambda_1 - F_{iii}\rho_i)\frac{\partial \rho_i}{\partial x} = \nu_i \frac{\partial^2 \rho_i}{\partial x^2}, \quad i = 1, \ldots, n \tag{1.6a}$$

for $f_2 = f_3 = \ldots = f_n = 0$. The details are given in Sec. 6.2 of [8], where the example of gas dynamics ($n = 3$) is used to illustrate ideas. In particular, the velocity u obeys Burgers equation

$$\frac{\partial u}{\partial t} + \left(1 + \frac{\gamma + 1}{2}u\right)\frac{\partial u}{\partial x} = \frac{1 + 3\gamma}{6Re}\frac{\partial^2 u}{\partial x^2}, \tag{1.6b}$$

where γ is the gas constant and Re is the Reynolds number. This result was first worked out directly (without the use of multiple scales) as an approximation of the Navier-Stokes equations in [11]. Another example for $n = 2$ occurs for unidirectional dispersive shallow water flow. Setting one of the two $f_i = 0$ leads to the Korteweg-deVries equation for the free surface height or the flow speed. (For example, see Sec. 8.4.4 of [6]).

An interesting feature of the problem for $n > 2$ is that resonant interactions between the f_i are possible for periodic initial conditions if the characteristic speeds belong to a class of resonant values. For example, consider the case $n = 3$ and choose ξ_1 and ξ_2 as the two fast scales. Thus,

$$\xi_3 = \alpha_1\xi_1 + \alpha_2\xi_2, \quad \alpha_1 = \frac{\lambda_3 - \lambda_2}{\lambda_1 - \lambda_2}, \quad \alpha_2 = \frac{\lambda_1 - \lambda_3}{\lambda_1 - \lambda_2}. \tag{1.7}$$

Now, the evolution equations that correspond to (1.5) for the f_i are

$$\frac{\partial f_i}{\partial \tilde{t}} - F_{iii}f_i\frac{\partial f_i}{\partial \xi_i} - F_{ijk}\langle f_j \frac{\partial f_k}{\partial \xi_k}\rangle(\xi_i, \tilde{t}) - F_{ijk}\langle f_k \frac{\partial f_j}{\partial \xi_j}\rangle(\xi_i, \tilde{t}) = D_{ii}\frac{\partial^2 f_i}{\partial \xi_i^2}, \quad i = 1, 2, 3. \tag{1.8}$$

Here, the resonant interaction terms in the ith equation are averages of products of functions of $(\xi_j, \tilde{t})$ and $(\xi_k, \tilde{t})$, where $i \neq j \neq k$. In particular, if the period of the initial data is 2ℓ, the interaction terms in the equation for $i = 1$ are of the form

$$\langle S_2 S_3\rangle(\xi_1, \tilde{t}) = \frac{1}{2\ell}\int_{-\ell}^{\ell} S_2(\xi_2, \tilde{t})S_3(\alpha_1\xi_1 + \alpha_2\xi_2, \tilde{t})d\xi_2, \tag{1.9}$$

and are functions of $(\xi_1, \tilde{t})$, etc. The average terms for $i = 1$ and $i = 2$ are nonzero if the resonance conditions

$$m\alpha_2 + r = 0 \tag{1.10a}$$

$$m\alpha_1 + r = 0 \tag{1.10b}$$

are satisfied respectively for positive or negative integers m and r. In this case the resonance condition that ensures the nonvanishing of the average terms in the equation for $i = 3$, $m\alpha_1 + r\alpha_2 = 0$, is automatically satisfied. This phenomenon of resonant interactions that couples all three equations was discussed for the case of nonisentropic one-dimensional inviscid compressible flow in [12]. A detailed discussion of the general problem is given in Sec. 6.2 of [8]. Numerical and analytical studies of the solutions of the system (1.8) appear in the literature subsequent to [12] that we do not cite.

The effect of source terms is discussed for the particular example of channel flow in [13], and in the general setting (1.1) for the case $n = 2$ in [10]. As shown in [10] the necessary conditions for solutions of the linear ($\epsilon = 0$) problem (1.1) to decay are

$$C_{11} > 0; \quad C_{22} > 0; \quad \Delta \equiv C_{11}C_{22} - C_{12}C_{21} > 0. \tag{1.11}$$

The first two conditions ensure that short waves decay, and the third condition follows for the stability of long waves. We therefore distinguish the following three classes of linear problems that are consistent with the perturbation assumption (1.3) (neither U_1 nor U_2 become unbounded as $t \to \infty$) and interesting (both U_i do not decay as $t \to \infty$):

Type I$_2$: (a) $C_{11} = 0,\ C_{22} > 0,\ \Delta = 0 \Longrightarrow C_{12} = 0$ or $C_{21} = 0$ or $C_{12} = C_{21} = 0$

(b) $C_{11} > 0,\ C_{22} = 0,\ \Delta = 0 \Longrightarrow C_{12} = 0$ or $C_{21} = 0$ or $C_{12} = C_{21} = 0$

One wave decays and the other is neutrally stable.

Type II$_2$: $C_{11} = C_{22} = \Delta = 0 \Longrightarrow C_{12} = 0$ or $C_{21} = 0$ or $C_{12} = C_{21} = 0$

Both waves are neutrally stable and decoupled.

Type III$_2$: $C_{11} > 0,\ C_{22} > 0,\ \Delta = 0 \Longrightarrow C_{12} \neq 0$ and $C_{21} \neq 0$

Both waves are neutrally stable and essentially coupled.

For $\epsilon \neq 0$, we are interested in determining the effect of the small nonlinear terms upon a neutrally stable linear solution. Thus, we expand the C_{ij}, which depend on a parameter μ, around the critical value $\mu = \mu_0$ for neutral stability. Weakly nonlinear solutions for problems of type I$_2$ and II$_2$ are discussed in [10] for general values of all the nonzero constants appearing in (1.1); the results in [13] are for a special case of type I$_2$. The linear problem for type III$_2$ has the U_i essentially coupled; as shown in [10], the U_i are given in integral form involving a Bessel function. Because of the complicated structure of the linear solution, the weakly nonlinear problem is significantly more difficult to analyse and has not yet been worked out.

The main distinguishing feature for solutions of type I$_2$ is that one of the U_i decays in t even for $\epsilon > 0$, as long as ϵ is small. The other U_j has a component that decays plus one that survives. This latter obeys a nonlocal evolution equation that we do not list for brevity (see Equation (5.7) of [10]). Thus, the solution is basically defined in terms of this single evolution equation. It is shown in [10] that for certain parameter values periodic initial disturbances evolve into periodic travelling waves consisting of piecewise continuous profiles joined by one or more shocks per period; this generalizes the roll waves first discussed in [3] for channel flow. For type II$_2$ problems disturbances survive along both characteristic directions. It is shown in [10] that these disturbances are governed by coupled evolution equations, and a special case for which these equations decouple is studied in detail.

In this paper we extend the solutions for type I$_2$ and type II$_2$ problems to $n = 3$. We show that type I$_3$ problems do not admit resonant interactions between waves and that, to leading order, each U_i obeys a decoupled nonlocal evolution equation that generalizes the corresponding equation for $n = 2$. For type II_3 problems we do find resonant interaction terms analogous to those in (1.7). For both solution types we use the evolution equations to derive necessary conditions for stability of the weakly nonlinear problem. Numerical results will be reported in future work.

2 Solutions of type I_3

We are interested in the class of problems where, for $\epsilon = 0$, one of the waves, say U_2, decays as $t \to \infty$, and the other two waves are coupled to U_2 in such a way that the linear problem may be calculated recursively. This generalizes the situation for $n = 2$ discussed in Sec. 3 of [10]. We assume the following form for the C_{ij}

$$\begin{aligned} &C_{11} = \epsilon C_{11}^{(1)} + O(\epsilon^2); \quad C_{12} = C_{12}^{(0)} + \epsilon C_{12}^{(1)} + O(\epsilon^2); \quad C_{13} = \epsilon C_{13}^{(1)} + O(\epsilon^2) \\ &C_{21} = \epsilon C_{21}^{(1)} + O(\epsilon^2); \quad C_{22} = C_{22}^{(0)} + \epsilon C_{22}^{(1)} + O(\epsilon^2); \quad C_{23} = \epsilon C_{23}^{(1)} + O(\epsilon^2) \\ &C_{31} = C_{31}^{(0)} + \epsilon C_{31}^{(1)} + O(\epsilon^2); \quad C_{32} = C_{32}^{(0)} + \epsilon C_{32}^{(1)} + O(\epsilon^2); \quad C_{33} = \epsilon C_{33}^{(1)} + O(\epsilon^2), \end{aligned} \tag{2.1}$$

where we restrict $C_{22}^{(0)} > 0$ to ensure the decay of U_2, but do not restrict any of the other constants. Typically, with the C_{ij} depending on a dimensionless parameter μ, the expansions (2.1) arise by setting $\mu = \mu_0 + \epsilon\mu_1$, where μ_0 is a critical value of μ. Then

$$C_{ij}(\mu) = C_{ij}(\mu_0) + \epsilon\mu_1 C_{ij}'(\mu_0) + O(\epsilon^2), \tag{2.2}$$

and we have denoted $C_{ij}(\mu_0) \equiv C_{ij}^{(0)}$, $\mu_1 C_{ij}'(\mu_0) \equiv C_{ij}^{(1)}$. Thus, the form (2.1) assumes that $C_{11}^{(0)} = C_{13}^{(0)} = C_{21}^{(0)} = C_{23}^{(0)} = C_{33}^{(0)} = 0$, that $C_{22}^{(0)}$ is a positive $O(1)$ constant independent of ϵ, and that all the remaining $C_{ij}^{(0)}$ and $C_{ij}^{(1)}$ are arbitrary $O(1)$ constants. Special cases would correspond to some of the latter vanishing. In general the characteristic speeds λ_i are also functions of μ and we expand these as in (2.2)

$$\begin{aligned} \lambda_i(\mu) &= \lambda_i(\mu_0) + \epsilon\lambda_i'(\mu_0)\mu_1 + O(\epsilon^2) \\ &= \lambda_i^{(0)} + \epsilon\lambda_i^{(1)} + O(\epsilon^2), \quad i = 1, 2, 3. \end{aligned} \tag{2.3}$$

With the C_{ij} and λ_i defined by (2.1), (2.3), the system (1.1) reduces to the following form correct to $O(\epsilon)$.

$$\frac{\partial U_1}{\partial t} + \lambda_1^{(0)}\frac{\partial U_1}{\partial x} + C_{12}^{(0)}U_2 = \epsilon\left(-\lambda_1^{(1)}\frac{\partial U_1}{\partial x} - \sum_{j=1}^{3} C_{1j}^{(1)}U_j + \phi_1^{(0)}\right) + O(\epsilon^2) \tag{2.4a}$$

$$\frac{\partial U_2}{\partial t} + \lambda_2^{(0)}\frac{\partial U_2}{\partial x} + C_{22}^{(0)}U_2 = \epsilon\left(-\lambda_2^{(1)}\frac{\partial U_2}{\partial x} - \sum_{j=1}^{3} C_{2j}^{(1)}U_j + \phi_2^{(0)}\right) + O(\epsilon^2) \tag{2.4b}$$

$$\frac{\partial U_3}{\partial t} + \lambda_3^{(0)}\frac{\partial U_3}{\partial x} + C_{31}^{(0)}U_1 + C_{32}^{(0)}U_2 = \epsilon\left(-\lambda_3^{(1)}\frac{\partial U_3}{\partial x} - \sum_{j=1}^{3} C_{3j}^{(1)}U_j + \phi_3^{(0)}\right) + O(\epsilon^2), \tag{2.4c}$$

where $\phi_i^{(0)}$ is given by (1.2) with the F_{ijk} and G_{ijk} evaluated at $\mu = \mu_0$.

Note that for $\epsilon = 0$, (2.4b) decouples and gives a decaying wave if $C_{22}^{(0)} > 0$. Once U_2 is known, we can solve (2.4a) for U_1. Finally, given U_1 and U_2 we can solve (2.4c) for U_3. Actually, this recursive solution procedure is still possible with $C_{33}^{(0)} \neq 0$; we would need to choose $C_{33}^{(0)} > 0$ to ensure that U_3 remains bounded. We have assumed $C_{33}^{(0)} = 0$ for simplicity.

We expand the U_i in the multiple scale form

$$U_i(x,t;\epsilon) = U_{i0}(\xi_1,\xi_2,\tilde{t}) + \epsilon U_{i1}(\xi_1,\xi_2,\tilde{t}) + O(\epsilon^2), \quad i = 1,2,3, \tag{2.5}$$

where

$$\xi_i = x - \lambda_i^{(0)} t; \quad \tilde{t} = \epsilon t. \tag{2.6}$$

Thus,

$$\xi_3 = \alpha_1\xi_1 + \alpha_2\xi_2; \quad \alpha_1 = \frac{\lambda_3^{(0)} - \lambda_2^{(0)}}{\lambda_1^{(0)} - \lambda_2^{(0)}}; \quad \alpha_2 = \frac{\lambda_1^{(0)} - \lambda_3^{(0)}}{\lambda_1^{(0)} - \lambda_2^{(0)}}, \tag{2.7}$$

Derivatives transform as follows

$$\frac{\partial}{\partial x} = \frac{\partial}{\partial \xi_1} + \frac{\partial}{\partial \xi_2}; \quad \frac{\partial}{\partial t} = -\lambda_1^{(0)}\frac{\partial}{\partial \xi_1} - \lambda_2^{(0)}\frac{\partial}{\partial \xi_2} + \epsilon\frac{\partial}{\partial \tilde{t}}, \tag{2.8}$$

and (2.4) leads to the following systems for the U_{i0} and U_{i1}.

$$(\lambda_1^{(0)} - \lambda_2^{(0)})\frac{\partial U_{10}}{\partial \xi_2} + C_{12}^{(0)} U_{20} = 0 \tag{2.9a}$$

$$(\lambda_2^{(0)} - \lambda_1^{(0)})\frac{\partial U_{20}}{\partial \xi_1} + C_{22}^{(0)} U_{20} = 0 \tag{2.9b}$$

$$(\lambda_3^{(0)} - \lambda_1^{(0)})\frac{\partial U_{30}}{\partial \xi_1} + (\lambda_3^{(0)} - \lambda_2^{(0)})\frac{\partial U_{30}}{\partial \xi_2} + C_{31}^{(0)} U_{10} + C_{32}^{(0)} U_{20} = 0 \tag{2.9c}$$

$$\begin{aligned}(\lambda_1^{(0)} - \lambda_2^{(0)})\frac{\partial U_{11}}{\partial \xi_2} + C_{12}^{(0)} U_{21} &= -\frac{\partial U_{10}}{\partial \tilde{t}} - \lambda_1^{(1)}\left(\frac{\partial U_{10}}{\partial \xi_1} + \frac{\partial U_{10}}{\partial \xi_2}\right) \\ &\quad - \sum_{j=1}^{3} C_{1j}^{(1)} U_{j0} + \phi_{10}^{(0)}\end{aligned} \tag{2.10a}$$

$$\begin{aligned}(\lambda_2^{(1)} - \lambda_1^{(0)})\frac{\partial U_{21}}{\partial \xi_1} + C_{22}^{(0)} U_{21} &= -\frac{\partial U_{20}}{\partial \tilde{t}} - \lambda_2^{(1)}\left(\frac{\partial U_{20}}{\partial \xi_1} + \frac{\partial U_{20}}{\partial \xi_2}\right) \\ &\quad - \sum_{j=1}^{3} C_{2j}^{(1)} U_{j0} + \phi_{20}^{(0)}\end{aligned} \tag{2.10b}$$

$$\begin{aligned}(\lambda_3^{(0)} - \lambda_1^{(0)})\frac{\partial U_{31}}{\partial \xi_1} + (\lambda_3^{(0)} - \lambda_2^{(0)})\frac{\partial U_{31}}{\partial \xi_2} + C_{31}^{(0)} U_{11} + C_{32}^{(0)} U_{21} &= -\frac{\partial U_{30}}{\partial \tilde{t}} \\ - \lambda_3^{(1)}\left(\frac{\partial U_{30}}{\partial \xi_1} + \frac{\partial U_{30}}{\partial \xi_2}\right) - \sum_{j=1}^{3} C_{3j}^{(1)} U_{j0} + \phi_{30}^{(0)}.\end{aligned} \tag{2.10c}$$

In (2.10) the $\phi_{i0}^{(0)}$ are now given by

$$\phi_{i0}^{(0)} = \sum_{j=1}^{3}\sum_{k=1}^{3}\left\{F_{ijk}(\mu_0)\left[U_{j0}\left(\frac{\partial U_{k0}}{\partial \xi_1} + \frac{\partial U_{k0}}{\partial \xi_2}\right)\right] + G_{ijk}(\mu_0) U_{j0} U_{k0}\right\}. \tag{2.11}$$

The solution of (2.9) is

$$U_{10} = f_1(\xi_1, \tilde{t}) - \tilde{C}_{12} F_2(\xi_2, \tilde{t}) E(\xi_1) \tag{2.12a}$$

$$U_{20} = f_2(\xi_2, \tilde{t}) E(\xi_1) \tag{2.12b}$$

$$U_{30} = f_3(\xi_3, \tilde{t}) + \frac{\tilde{C}_{31}}{\alpha_2} F_1(\xi_1, \tilde{t}) + P_2(\xi_2, \tilde{t}) E(\xi_1), \tag{2.12c}$$

where we have introduced the notation

$$\tilde{C}_{ij} = \frac{C_{ij}^{(0)}}{\lambda_1^{(0)} - \lambda_2^{(0)}}, \quad E(\xi_1) = \exp(\tilde{C}_{22}\xi_1) \tag{2.13a}$$

$$F_i(\xi_i, \tilde{t}) = \int^{\xi_i} f_i(s, \tilde{t}) ds; \quad i = 1, 2, 3 \tag{2.13b}$$

$$P_2(\xi_2, \tilde{t}) = \exp\left(\frac{\tilde{C}_{22}\alpha_2}{\alpha_1}\xi_2\right) \int^{\xi_2} \left[\frac{\tilde{C}_{31}}{\alpha_1} F_2(s, \tilde{t}) - \frac{\tilde{C}_{32}}{\alpha_2} f_2(s, \tilde{t})\right] \exp\left(-\frac{\tilde{C}_{22}\alpha_2}{\alpha_1} s\right) ds. \tag{2.13c}$$

At this stage the three functions $f_i(\xi_i, \tilde{t})$, $i = 1, 2, 3$ are unknown; only their initial values are given in terms of the initial values for the U_i. In this paper, as in [10], we restrict attention to the case where the U_i have 2ℓ-periodic initial values with zero average. To determine the f_i we consider the solution of (2.10).

We multiply (2.10b) by $1/(\lambda_2^{(0)} - \lambda_1^{(0)})E$ and use the expressions in (2.12) to evaluate the right-hand side and find

$$\begin{aligned} \frac{\partial}{\partial \xi_1}\left(\frac{U_{21}}{E}\right) = {} & \frac{1}{(\lambda_1^{(0)} - \lambda_2^{(0)})} \Bigg\{ \Bigg[\frac{\partial f_2}{\partial \tilde{t}} + (C_{22}^{(1)} + \lambda_2^{(1)} \tilde{C}_{22}) f_2 + \lambda_2^{(1)} \frac{\partial f_2}{\partial \xi_2} - C_{21}^{(1)} \tilde{C}_{12} F_2 \\ & + C_{23}^{(1)} P_2 \Bigg] + \frac{1}{E} \Bigg[C_{21}^{(1)} f_1 - \frac{F_{211}}{2} \frac{\partial}{\partial \xi_1}(f_1^2) - \left(F_{213} \frac{\tilde{C}_{31}}{\alpha_2} + G_{211}\right) f_1^2 - F_{231} \frac{\tilde{C}_{31}}{\alpha_2} \frac{\partial f_1}{\partial \xi_1} F_1 \\ & + C_{23}^{(1)} \frac{\tilde{C}_{31}}{\alpha_2} F_1 - G_{233} \frac{\tilde{C}_{31}^2}{\alpha_2^2} F_1^2 - (G_{213} + G_{231}) \frac{\tilde{C}_{31}}{2\alpha_2} \frac{\partial}{\partial \xi_1}(F_1^2) - G_{233} \langle f_3^2 \rangle (\tilde{t}) \Bigg] \\ & + \frac{1}{E} \left[C_{23}^{(1)} f_3 - \frac{F_{233}}{2} \frac{\partial}{\partial \xi_3}(f_3^2) - G_{233} \left(f_3^2 - \langle f_3^2 \rangle (\tilde{t})\right) \right] + \ldots \Bigg\}. \end{aligned} \tag{2.14}$$

In the right-hand side of (2.14) the first set of bracketed terms consists of functions that depend only $(\xi_2, \tilde{t})$; upon integration these terms will introduce an inconsistent contribution to U_{21} proportional to $\xi_1 E(\xi_1)$. Removal of these terms gives the evolution equation for f_2

$$\frac{\partial f_2}{\partial \tilde{t}} + (C_{22}^{(1)} + \lambda_2^{(1)} \tilde{C}_{22}) f_2 + \lambda_2^{(1)} \frac{\partial f_2}{\partial \xi_2} - C_{21}^{(1)} \tilde{C}_{12} F_2 + C_{23}^{(1)} P_2 = 0. \tag{2.15}$$

This differs from the corresponding equation for the case $n = 2$ only by the last term $C_{23}^{(1)} P_2$, (cf. (3.17) of [10]). As in the case $n = 2$, we note that, because U_{20} is initially periodic, it follows from (2.12b) that the initial value of f_2 is the product of $\exp(-\tilde{C}_{22}\xi_2)$ with a Fourier series in ξ_2. This implies that $f_2(\xi_2, \tilde{t})$ has the form $\exp(-\tilde{C}_{22}\xi_2)$ times a Fourier series in ξ_2 with $\tilde{t}$-dependent coefficients that may be explicitly calculated (cf. (3.25) of [10]). It then follows that U_{20} equals $\exp(-C_{22}^{(0)} t)$ multiplied by a periodic function of ξ_2, and U_{20} therefore decays as $t \to \infty$.

The second and third sets of bracketed terms on the right-hand side of (2.14) are functions of $(\xi_1, \tilde{t})$ and $(\xi_3, \tilde{t})$ respectively. Although these terms have perfectly consistent contributions to U_{21}, they must be taken into account in the solutions of (2.10a) for U_{11} and (2.10c) for U_{31}, respectively, because they introduce inconsistencies there. Other terms, indicated by ... in (2.14), are products of functions of $(\xi_j, \tilde{t})$ with functions of $(\xi_k, \tilde{t})$ with $j = 1,2,3$; $k = 1,2,3$; $j \neq k$. Such terms lead to no inconsistencies and have been omitted from (2.14).

We use the second group of bracketed terms in the right-hand side of (2.14) to derive the contributions to $C_{12}^{(0)} U_{21}$ that depend only on $(\xi_1, \tilde{t})$. We then move $C_{12}^{(0)} U_{21}$ to the right-hand of (2.10a) and combine this with all the other terms on the right-hand side of (2.10a) that are functions of $(\xi_1, \tilde{t})$ only to find the following evolution equation for f_1.

$$
\begin{aligned}
(2.16)\quad & \frac{\partial f_1}{\partial \tilde{t}} + (\lambda_1^{(1)} - F_{111} f_1)\frac{\partial f_1}{\partial \xi_1} + C_{11}^{(1)} f_1 - (G_{111} + \frac{F_{211}}{2}\tilde{C}_{12} + \frac{F_{113}}{\alpha_2}\tilde{C}_{31}) f_1^2 \\
& + \tilde{C}_{12} C_{21}^{(1)} E \int^{\xi_1} \frac{f_1(s,\tilde{t})}{E(s)} ds - \tilde{C}_{12}(G_{211} + \frac{F_{211}}{2}\tilde{C}_{22} + 2F_{213} - 2F_{231}) E \int^{\xi_1} \frac{f_1^2(s,\tilde{t})}{E(s)} ds \\
& + K_1(\tilde{t}) E + \frac{\tilde{C}_{31}}{\alpha_2}\left[C_{13}^{(1)} - F_{131}\frac{\partial f_1}{\partial \xi_1} - (G_{113} + G_{131}) f_1 \right] F_1 \\
& - \frac{\tilde{C}_{31}\tilde{C}_{12}}{2\alpha_2}\left[G_{213} + G_{231} + F_{213}\tilde{C}_{22} \right] F_1^2 - \frac{F_{231}}{2\alpha_2}\tilde{C}_{12}\tilde{C}_{31}\frac{\partial}{\partial \xi_1}(F_1^2) \\
& + \frac{C_{23}^{(1)}}{\alpha_2}\tilde{C}_{31}\tilde{C}_{12} E \int^{\xi_1} \frac{F_1(s,\tilde{t})}{E(s)} ds - \frac{\tilde{C}_{12}\tilde{C}_{31}}{2\alpha_2}\left[F_{213}\tilde{C}_{22}^2 + 2G_{233}\frac{\tilde{C}_{31}}{\alpha_2} \right. \\
& \left. + (G_{213} + G_{231})\tilde{C}_{22} \right] E \int^{\xi_1} \frac{F_1^2(s,\tilde{t})}{E(s)} ds + (G_{233}\frac{\tilde{C}_{12}}{\tilde{C}_{22}} - G_{133})\langle f_3^2 \rangle(\tilde{t}) = 0.
\end{aligned}
$$

Equation (2.16) generalizes (3.19) of [10], and the function $K_1(\tilde{t})$ can be evaluated as in (3.34) of [10] using periodicity. One can also convert (2.16) to a second order equation by dividing by E, taking the derivative of the result with respect to ξ_1, and cancelling out the E. Using this expression, or proceeding directly from (2.16), we can derive an equation for $\langle f_1 \rangle(\tilde{t})$, the average part of f_1 (cf. (3.39) of [10]). By requiring $\langle f_1 \rangle(\tilde{t})$ to vanish if $\langle f_1 \rangle(0) = 0$, we obtain the following necessary conditions on the various parameters

$$
\begin{aligned}
(2.17a)\quad & \tilde{C}_{22}(G_{111} + \frac{F_{211}}{2}\tilde{C}_{12} + \frac{F_{113}}{\alpha_2}\tilde{C}_{31}) - \tilde{C}_{12}(G_{211} + \frac{F_{211}}{2}\tilde{C}_{22} + F_{213} - F_{231}) = 0 \\
(2.17b)\quad & G_{233}\tilde{C}_{12} - G_{133}\tilde{C}_{22} = 0 \\
(2.17c)\quad & F_{131}\tilde{C}_{31} = 0 \\
(2.17d)\quad & \tilde{C}_{12}\tilde{C}_{31}^2 G_{233} = 0.
\end{aligned}
$$

Equation (2.17a) generalizes (3.37) of [10], whereas (2.17b)-(2.17d) only occur if $n = 3$. Using the conditions (2.17) in (2.16) simplifies the latter to

$$
\begin{aligned}
(2.18)\quad & \frac{\partial f_1}{\partial \tilde{t}} + (\lambda_1^{(1)} - F_{111} f_1)\frac{\partial f_1}{\partial \xi_1} + C_{11}^{(1)} f_1 - (G_{111} + \frac{F_{211}}{2}\tilde{C}_{12} + \frac{F_{113}}{\alpha_2}\tilde{C}_{31})\left[f_1^2 + \tilde{C}_{22} E \int^{\xi_1} \frac{f_1^2(s,\tilde{t})}{E(s)} ds \right] \\
& + \tilde{C}_{12} C_{21}^{(1)} E \int^{\xi_1} \frac{f_1(s,\tilde{t})}{E(s)} ds + K_1(\tilde{t}) E + \frac{\tilde{C}_{31}}{\alpha_2}[C_{13}^{(1)} - (G_{113} + G_{131}) f_1] F_1 \\
& - \frac{\tilde{C}_{31}\tilde{C}_{12}}{2\alpha_2}[G_{213} + G_{231} + F_{213}\tilde{C}_{22}]\left[F_1^2 + \tilde{C}_{22} E \int^{\xi_1} \frac{F_1^2(s,\tilde{t})}{E(s)} ds \right] \\
& - \frac{F_{231}}{2\alpha_2}\tilde{C}_{12}\tilde{C}_{31}\frac{\partial}{\partial \xi_1}(F_1^2) + \frac{C_{23}^{(1)}}{\alpha_2}\tilde{C}_{31}\tilde{C}_{12} E \int^{\xi_1} \frac{F_1(s,\tilde{t})}{E(s)} ds = 0.
\end{aligned}
$$

In view of (2.17b) the term proportional to $\langle f_3^2\rangle(\tilde{t})$ is absent from (2.18) and this evolution equation involves f_1 (and integrals depending on f_1) only.

The evolution equation for f_3 is obtained by isolating the contributions involving terms that depend only on $(\xi_3,\tilde{t})$ from both $C_{31}^{(0)}U_{21}$ and $C_{32}^{(0)}U_{11}$, and combining these with all the other terms on the right-hand side of (2.10c) that depend on $(\xi_3,\tilde{t})$. The result is

$$\begin{aligned}\frac{\partial f_3}{\partial\tilde{t}} &+ (\lambda_3^{(1)} - F_{333}f_3)\frac{\partial f_3}{\partial\xi_3} + C_{33}^{(1)}f_3 - (G_{333} - \frac{F_{133}}{\alpha_2}\tilde{C}_{31})f_3^2 \\ &+ \tilde{C}_{31}\frac{C_{13}^{(1)}}{\alpha_2}F_3 + \frac{\tilde{C}_{31}}{\alpha_2}G_{133}(f_3^2 - \langle f_3^2\rangle(\tilde{t})) \\ &- \frac{\tilde{C}_{31}\tilde{C}_{12}}{\alpha_2}\int^{\xi_3} H_3(s,\tilde{t})ds + \tilde{C}_{32}H_3(\xi_3,\tilde{t}) = 0,\end{aligned} \tag{2.19}$$

where

$$\begin{aligned}H_3(\xi_3,\tilde{t}) = \frac{E(\xi_1)}{\alpha_1}\int^{\xi_3}\frac{1}{E(\frac{s}{\alpha_1}-\frac{\alpha_2}{\alpha_1}\xi_2)}&\left[C_{23}^{(1)}f_3(s,\tilde{t}) - \frac{F_{233}}{2}\frac{\partial}{\partial\xi_3}(f_3^2(s,\tilde{t}))\right.\\ &\left.- G_{233}(f_3^2(s,\tilde{t}) - \langle f_3^2\rangle(\tilde{t}))\right] ds.\end{aligned} \tag{2.20}$$

In (2.20), note that the expression in square brackets is 2ℓ-periodic in ξ_3 with zero average. Therefore, the $E(\xi_1)$ in the numerator cancels out the factor $E(\xi_3/\alpha_1 - \alpha_2\xi_2/\alpha_1) = E(\xi_1)$ that will result in the denominator after integration, making H_3 a 2ℓ-periodic function of ξ_3 with zero average.

The necessary condition that $\langle f_3\rangle(\tilde{t}) = 0$ if $\langle f_3\rangle(0) = 0$ is

$$G_{333} - \frac{F_{133}}{\alpha_2}\tilde{C}_{31} = 0. \tag{2.21}$$

Thus, the term proportional to f_3^2 must be absent from (2.19) for bounded solutons.

In summary, we see that for problems of type I_3, we find decoupled non-local evolution equations for the f_i. These generalize the corresponding equations given in [10] for problems of type I_2. In particular, no resonant interaction terms occur in this case. This outcome is to be expected since it is necessary to have *at least* three waves that are periodic in the ξ_i to generate resonant interactions, and we see that U_2 is not periodic if $\tilde{C}_{22} \neq 0$. With this observation we turn our attention to problems of type II_3 where all three waves have a periodic component.

3 Solutions of Type II_3

In order to have a periodic component in all three waves we must require $C_{ii} = O(\epsilon)$, $i = 1,2,3$. With this choice, the most general problem (aside from two essentially identical cases obtained by permuting indices) that is recursively solvable for $\epsilon = 0$ has $C_{12} = O(1)$, $C_{13} = O(\epsilon)$, $C_{21} = O(\epsilon)$, $C_{23} = O(\epsilon)$, $C_{31} = O(1)$ and $C_{32} = O(1)$, i.e., (1.1) has the form

$$\frac{\partial U_1}{\partial t} + \lambda_1^{(0)}\frac{\partial U_1}{\partial x} + C_{12}^{(0)}U_2 = \epsilon\left(-\lambda_1^{(1)}\frac{\partial U_1}{\partial x} - \sum_{j=1}^{3}C_{1j}^{(1)}U_j + \phi_1^{(0)}\right) + O(\epsilon^2) \tag{3.1a}$$

$$\frac{\partial U_2}{\partial t} + \lambda_2^{(0)}\frac{\partial U_2}{\partial x} = \epsilon\left(-\lambda_2^{(1)}\frac{\partial U_2}{\partial x} - \sum_{j=1}^{3}C_{2j}^{(1)}U_j + \phi_2^{(0)}\right) + O(\epsilon^2) \tag{3.1b}$$

$$\frac{\partial U_3}{\partial t} + \lambda_3^{(0)}\frac{\partial U_3}{\partial x} + C_{31}^{(0)}U_1 + C_{32}^{(0)}U_2 = \epsilon\left(-\lambda_3^{(1)}\frac{\partial U_3}{\partial x} - \sum_{j=1}^{3}C_{3j}^{(1)}U_j + \phi_3^{(0)}\right) + O(\epsilon^2). \tag{3.1c}$$

Now, the leading terms in the multiple scale expansions (2.5) for the U_i are given by

(3.2a) $$U_{10} = f_1(\xi_1, \tilde{t}) - \tilde{C}_{12}F_2(\xi_2, \tilde{t})$$

(3.2b) $$U_{20} = f_2(\xi_2, \tilde{t})$$

(3.2c) $$U_{30} = f_3(\xi_3, \tilde{t}) + \frac{\tilde{C}_{31}}{\alpha_2}F_1(\xi_1, \tilde{t}) - \frac{\tilde{C}_{31}\tilde{C}_{12}}{\alpha_2}\int^{\xi_2} F_2(s)ds - \frac{\tilde{C}_{32}}{\alpha_1}F_2(\xi_2, \tilde{t}),$$

where F_1 and F_2 are defined in (2.13b).

For simplicity, we only discuss the special case $\tilde{C}_{31} = 0$ for which

(3.2d) $$U_{30} = f_3(\xi_3, \tilde{t}) - \frac{\tilde{C}_{32}}{\alpha_1}F_2(\xi_2, \tilde{t}).$$

The $U_{i1}(\xi_1, \xi_2, \tilde{t})$ are governed by

(3.3a) $$(\lambda_1^{(0)} - \lambda_2^{(0)})\frac{\partial U_{11}}{\partial \xi_2} = -C_{12}^{(0)}U_{21} - \frac{\partial U_{10}}{\partial \tilde{t}} - \lambda_1^{(1)}\left(\frac{\partial U_{10}}{\partial \xi_1} + \frac{\partial U_{10}}{\partial \xi_2}\right) - \sum_{j=1}^{3} C_{1j}^{(1)}U_{j0} + \phi_{10}^{(0)}$$

(3.3b) $$(\lambda_2^{(0)} - \lambda_1^{(0)})\frac{\partial U_{21}}{\partial \xi_1} = -\frac{\partial U_{20}}{\partial \tilde{t}} - \lambda_2^{(1)}\left(\frac{\partial U_{20}}{\partial \xi_1} + \frac{\partial U_{20}}{\partial \xi_2}\right) - \sum_{j=1}^{3} C_{2j}^{(1)}U_{j0} + \phi_{20}^{(0)}$$

(3.3c) $$(\lambda_3^{(0)} - \lambda_1^{(0)})\frac{\partial U_{31}}{\partial \xi_1} + (\lambda_3^{(0)} - \lambda_2^{(0)})\frac{\partial U_{31}}{\partial \xi_2} = -C_{32}^{(0)}U_{21} - \frac{\partial U_{30}}{\partial \tilde{t}} - \lambda_3^{(1)}\left(\frac{\partial U_{30}}{\partial \xi_1} + \frac{\partial U_{30}}{\partial \xi_2}\right)$$
$$- \sum_{j=1}^{3} C_{3j}^{(1)}U_{j0} + \phi_{30}^{(0)}.$$

We note that the permutation of indices $1 \to 3$, $2 \to 2$, $3 \to 1$ leaves (3.1b) invariant and transforms (3.1a) to (3.1c) and vice-versa. Therefore, we need only study the first two equations; the evolution equation for f_3 follows by symmetry.

We use the expressions (3.2a), (3.2b) and (3.2d) for U_{10}, U_{20} and U_{30} respectively in (3.3b) and remove inconsistent terms proportional to ξ_1 from U_{21} to obtain the following evolution equation for f_2

(3.4) $$\frac{\partial f_2}{\partial \tilde{t}} + (\lambda_2^{(1)} - F_{222}f_2)\frac{\partial f_2}{\partial \xi_2} + C_{22}^{(1)}f_2 - F_{213}\langle f_1\frac{\partial f_3}{\partial \xi_3}\rangle(\xi_2, \tilde{t}) - F_{231}\langle f_3\frac{\partial f_1}{\partial \xi_1}\rangle(\xi_2, \tilde{t})$$

$$-(C_{21}^{(1)}\tilde{C}_{12}+C_{23}^{(1)}\tilde{C}_{32}/\alpha_1)F_2-[F_{211}\tilde{C}_{12}^2+(F_{231}+F_{213})\tilde{C}_{12}\tilde{C}_{32}/\alpha_1-F_{233}\tilde{C}_{32}^2/\alpha_1^2+(G_{212}+G_{221})\tilde{C}_{12}]f_2F_2$$

$$-(G_{213} + G_{231})\langle f_1 f_3\rangle(\xi_2, \tilde{t}) = 0.$$

The average terms vanish unless the resonance condition (1.10a) holds. In deriving (3.4) we have already imposed the following conditions that are necessary for $\langle f_2\rangle(\tilde{t}) = 0$ if $\langle f_2\rangle(0) = 0$.

(3.5) $$F_{212}\tilde{C}_{12} + F_{232}\tilde{C}_{32}/\alpha_1 = 0; \quad F_{221}\tilde{C}_{12} + F_{223}\tilde{C}_{32}/\alpha_1 = 0$$

$$G_{211} = G_{233} = 0; \quad \tilde{C}_{12}\tilde{C}_{32}(G_{213} + G_{231}) = 0.$$

The first line in (3.4) is just (1.8) for $i = 2$ and the special case $\lambda_2^{(1)} = C_{22}^{(1)} = D_{22} = 0$; the rest of the terms in (3.4) are contributed by the source terms in (1.1).

The terms in U_{21} that depend only on $(\xi_1, \tilde{t})$ also need to be isolated because when substituted in the right-hand side of (3.3a), they give rise to inconsistent terms proportional to ξ_2. We find the following terms in U_{21} that depend on $(\xi_1, \tilde{t})$

$$
\begin{aligned}
(3.6) \qquad U_{21} = \frac{1}{\lambda_1^{(0)} - \lambda_2^{(0)}} \Bigg\{ & C_{21}^{(1)} F_1 - \frac{F_{211}}{2} f_1^2 - G_{211} \int^{\xi_1} [f_1^2(s, \tilde{t}) - \langle f_1^2 \rangle(\tilde{t})] ds \\
& + \frac{F_{213}}{\alpha_1} \tilde{C}_{12} \langle F_2 f_3 \rangle(\xi_1, \tilde{t}) - \frac{F_{223}}{\alpha_1} \langle f_2 f_3 \rangle(\xi_1, \tilde{t}) \\
& + [F_{231} \tilde{C}_{12} + F_{233} \frac{\tilde{C}_{32}}{\alpha_1} - (G_{223} + G_{232})] \frac{1}{\alpha_1} \langle f_2 F_3 \rangle(\xi_1, \tilde{t}) - \frac{F_{232}}{\alpha_1} \langle F_3 \frac{\partial f_2}{\partial \xi_1} \rangle(\xi_1, \tilde{t}) \\
& + [2G_{233} \frac{\tilde{C}_{32}}{\alpha_1} + (G_{213} + G_{231}) \tilde{C}_{12}] \frac{1}{\alpha_1} \langle F_2 F_3 \rangle(\xi_1, \tilde{t}) + \dots \Bigg\}
\end{aligned}
$$

We use (3.6) for U_{21} in (3.3a) and collect all terms that depend only on $(\xi_1, \tilde{t})$ to obtain the following evolution equation for f_1.

$$
\begin{aligned}
(3.7) \qquad & \frac{\partial f_1}{\partial \tilde{t}} + (\lambda_1^{(1)} - F_{111} f_1) \frac{\partial f_1}{\partial \xi_1} + C_{11}^{(1)} f_1 - F_{123} \langle f_2 \frac{\partial f_3}{\partial \xi_3} \rangle(\xi_1, \tilde{t}) - F_{132} \langle f_3 \frac{\partial f_2}{\partial \xi_2} \rangle(\xi_1, \tilde{t}) \\
& + \tilde{C}_{12} C_{21}^{(1)} F_1 - G_{211} \tilde{C}_{12} \int^{\xi_1} [f_1^2(s, \tilde{t}) - \langle f_1^2 \rangle(\tilde{t})] ds \\
& + [F_{213} \tilde{C}_{12}^2 / \alpha_1 + 2G_{133} \tilde{C}_{32} / \alpha_1 + \tilde{C}_{12}(G_{113} + G_{131})] \langle f_3 F_2 \rangle(\xi_1, \tilde{t}) \\
& + [\tilde{C}_{12} F_{131} - F_{223} \tilde{C}_{12} / \alpha_1 + F_{133} \tilde{C}_{32} / \tilde{\alpha}_1 - (G_{123} + G_{132})] \langle f_2 f_3 \rangle(\xi_1, \tilde{t}) \\
& + \frac{\tilde{C}_{12}}{\alpha_1} [F_{231} \tilde{C}_{12} + F_{233} \tilde{C}_{32} / \alpha_1 - (G_{223} + G_{232})] \langle f_2 F_3 \rangle(\xi_1, \tilde{t}) - F_{232} \frac{\tilde{C}_{12}}{\alpha_1} \langle F_3 \frac{\partial f_2}{\partial \xi_2} \rangle(\xi_1, \tilde{t}) \\
& + \frac{\tilde{C}_{12}}{\alpha_1} [2G_{233} \tilde{C}_{32} / \alpha_1 + \tilde{C}_{12}(G_{213} + G_{231})] \langle F_2 F_3 \rangle(\xi_1, \tilde{t}) \\
& + [\tilde{C}_{12} F_{113} + F_{133} \tilde{C}_{32} / \alpha_1] \langle F_2 \frac{\partial f_3}{\partial \xi_3} \rangle(\xi_1, \tilde{t}) = 0.
\end{aligned}
$$

The average terms in (3.7) vanish unless the resonance condition (1.10b) holds. In deriving (3.7) we have set

$$
(3.8) \qquad F_{211} \tilde{C}_{12} + 2G_{211} = 0.
$$

This condition is necessary for $\langle f_1 \rangle(\tilde{t}) = 0$ if $\langle f_1 \rangle(0) = 0$.

Equation (3.7) reduces to (1.8) for $i = 1$ if all source terms are absent, $D_{11} = 0$, and we set $\lambda_1^{(1)} = 0$. We note that the effect of source terms is to contribute certain nonlocal terms as well as additional resonant interaction terms in the evolution equations (3.4) and (3.7). The evolution equation for f_3 follows from (3.7) by the appropriate permutation of indices.

References

[1] S.C. Chikwendu and J. Kevorkian, *A perturbation method for hyperbolic equations with small nonlinearities*, SIAM J. on Appl. Math., **22** (1972), pp. 235-258.

[2] J.D. Cole, *Perturbation Methods in Applied Mathematics*, Blaisdell, Waltham, MA, 1968.

[3] R.F. Dressler, *Mathematical solution of the problem of roll-waves in inclined open channels*, Comm. Pure Appl. Math., **2** (1949), pp. 149-194.

[4] C.L. Frenzen and J. Kevorkian, *A review of the multiple scale and reductive perturbation methods for deriving uncoupled nonlinear evolution equations*, Wave Motion, **7** (1985), pp. 25-42.

[5] J. B. Keller and S. Kogelman, *Asymptotic solution of initial value problems for nonlinear partial differential equations*, SIAM J. on Appl. Math., **18** (1970), pp. 748-758.

[6] J. Kevorkian, *Partial Differential Equations: Analytical Solution Techniques*, Chapman and Hall, New York, NY, 1990, 1993.

[7] J. Kevorkian and J.D. Cole, *Perturbation Methods in Applied Mathematics*, Springer-Verlag, New York, NY, 1981.

[8] J. Kevorkian and J.D. Cole, *Multiple Scale and Singular Perturbation Methods*, Springer-Verlag, New York, NY, 1996.

[9] J. Kevorkian and J. Yu, *Passage through the critical Froude number for shallow water waves over a variable bottom*, J. Fluid Mech., **204** (1989), pp. 31-56.

[10] J. Kevorkian, J. Yu and L. Wang, *Weakly nonlinear waves for a class of linearly unstable hyperbolic conservation laws with source terms*, SIAM J. on Appl. Math., **55** (1995), pp. 446-484.

[11] P.A. Lagerstrom, J.D. Cole and L. Trilling, *Problems in the theory of viscous compressible fluids*, Office of Naval Research, Caltech GALCIT Report, 1949.

[12] A. Majda and R. Rosales, *Resonantly interacting weakly nonlinear hyperbolic waves*, I. A single space variable, Stud. Appl. Math., **71** (1986), pp. 149-179.

[13] J. Yu and J. Kevorkian, *Nonlinear evolution of small disturbances into roll waves in an inclined open channel*, J. Fluid Mech., **243** (1992), pp. 575-594.

SPECIAL LIMITS IN SOME FLOW PROBLEMS WITH TWO OR MORE SMALL PARAMETERS

A. F. Messiter[†]

Dedicated, with thanks, to Julian D. Cole

Abstract. To obtain asymptotic solutions of problems in which two or more nondimensional parameters approach zero, it is usually desirable, and might be considered necessary, to consider the relative smallness of the parameters, or the path of approach to the origin in the parameter space. Often there is just one limit process with the property that the limiting form of the equations contains more information than is obtained with any other limit process. In other cases, two or more special (or "distinguished") limits have this property. These limits are not always easily recognized. Some preliminary examples where the special limits can be identified in a relatively straightforward manner are mentioned briefly. The determination of special limits is then discussed in greater detail for three other examples that might seem more subtle.

1. Introduction. Although singular-perturbation methods can probably be said to have originated in the nineteenth century, it was not until the 1950's that the ideas were explained in a systematic way. The procedure that has since become known as the method of matched asymptotic expansions, implied [1] in work of Laplace, Kirchhoff, Rayleigh, Prandtl, et al., was developed in detail at Caltech by Lagerstrom, Cole, and Kaplun [2]. The basic ideas underlying two-time or, more generally, multivariable methods were also explored at this time.

In problems of boundary-layer type, outer and inner limit-process expansions are obtained, respectively, by holding outer and inner variables fixed as a small parameter approaches zero. Asymptotic matching then requires term-by-term agreement between the inner expansion evaluated as the inner variable becomes large and the outer expansion evaluated as the outer variable becomes small, provided there are overlapping domains of validity. If two or more small parameters are present, the limiting forms of the equations may also depend on the combinations of these parameters chosen to be held fixed in the limit, and the concept of matching can be broadened to include matching with respect to parameters as well as coordinates.

Among the many issues related to limit-process expansions is the identification of the important special limits in specific problems. In the simplest case with two small parameters ϵ_1 and ϵ_2, one might consider various limits as $\epsilon_1 \to 0$ and $\epsilon_2 \to 0$, finding that the resulting equations depend on the ratio ϵ_2/ϵ_1; this ratio then would play the role of a similarity parameter. That is, in this situation, if ϵ_2/ϵ_1 is held fixed as $\epsilon_1 \to 0$ and $\epsilon_2 \to 0$, it is found that the limiting form of the equations contains more information than if $\epsilon_2/\epsilon_1 \to 0$ or $\epsilon_2/\epsilon_1 \to \infty$. One would then often choose to study the special or "distinguished" case with ϵ_2/ϵ_1 held fixed, in which the limiting form of the equations is "richer" than for any neighboring limit. This terminology extends the idea of a distinguished limit as given in

[†] Department of Aerospace Engineering, The University of Michigan, Ann Arbor, MI 48109-2118.

[3], where a definition is given in terms of the coordinate(s) held fixed as some parameter approaches zero.

In some examples an important limiting case might easily be overlooked, and might perhaps be recognized only after one notices a lack of overlap between two cases that are more easily identified. For example, as is well known, in a particular problem it might be observed that one result is obtained if first $\epsilon_1 \to 0$ and later $\epsilon_2 \to 0$, while a different result follows if first $\epsilon_2 \to 0$ and later $\epsilon_1 \to 0$. It can then be said that these solutions do not match with each other, but that each should match with the solution found in some limit such that both ϵ_1 and ϵ_2 approach zero, say with the ratio ϵ_2/ϵ_1 held fixed. In such a case the important similarity parameter would be ϵ_2/ϵ_1. Or, perhaps two similarity parameters $K_A(\epsilon_1, \epsilon_2)$ and $K_B(\epsilon_1, \epsilon_2)$ have been identified, where, for the range of interest, $K_B/K_A \to 0$ as $\epsilon_1, \epsilon_2 \to 0$. Then the solution obtained with K_A held fixed and evaluated as $K_A \to \infty$ should agree with the solution found for K_B fixed and evaluated as $K_B \to 0$, if the domains of validity overlap in a K_A, K_B (or ϵ_1, ϵ_2) plane. Thus a "matching" in terms of parameters should be possible, analogous to the usual matching in terms of coordinates. But, as already suggested, there are other cases in which solutions obtained in different limits do not appear to approach each other when suitable intermediate limits are taken, and it turns out that an intervening special limit allows matching with solutions for the other limits.

For an example where a direct matching is in fact possible, one can consider supersonic flow past a thin airfoil with representative surface inclination δ at supersonic Mach numbers M_∞ ranging from transonic to hypersonic. In a somewhat unconventional view of the transonic and hypersonic small-disturbance theories, the two small parameters can be taken as $\epsilon_1 = \delta$ and $\epsilon_2 = \delta/(M_\infty^2 - 1)^{1/2}$, with the usual similarity parameters rewritten as $K_A = (M_\infty^2 - 1)/\delta^{2/3} = \epsilon_1^{4/3}/\epsilon_2^2, K_B = (M_\infty^2 - 1)^{1/2}\delta = \epsilon_1^2/\epsilon_2$. Linear supersonic theory is recovered if $\epsilon_1, \epsilon_2 \to 0$ with $\epsilon_1/\epsilon_2 = (M_\infty^2 - 1)^{1/2}$ held fixed, but this particular limit does not seem to play a special role for a first approximation, since linear equations are obtained in any intermediate limit $K_A \to \infty, K_B \to 0$. An additional feature in both the transonic and hypersonic limits is the modification of the transverse coordinate by a factor $O(\epsilon_1/\epsilon_2)$. In the limit with the transonic parameter K_A held fixed, it follows that for wings of finite span the reciprocal A^{-1} of the aspect ratio is a third small parameter, and an additional similarity parameter is $(M_\infty^2 - 1)^{1/2}A$, or $\delta^{1/3}A$; further details about transonic limit processes are given in [4].

If three parameters $\epsilon_1, \epsilon_2, \epsilon_3$ all approach zero, a distinguished case might correspond to similarity parameters in the form ϵ_2/ϵ_1^a and ϵ_3/ϵ_1^b, so that in the limit the origin is approached along curves where these parameters are constant. An alternative view allows a reduction to two parameters, by taking logarithms of ϵ_2, ϵ_3 and dividing by $\ln \epsilon_1$. The new parameters are then $\epsilon_2^* = \ln \epsilon_2/\ln \epsilon_1, \epsilon_3^* = \ln \epsilon_3/\ln \epsilon_1$ and the distinguished limit corresponds to a point in the $\epsilon_2^*, \epsilon_3^*$ plane with coordinates (a, b).

On the occasion of this volume in honor of Julian Cole, I thought it might be appropriate to review a few examples in which this issue that was formalized in the 1950's has arisen since that time in somewhat obscure ways in a variety of problems. The next section lists a few examples where a distinguished limit is in some sense obvious, typically because of a reasonably clear physical interpretation. Each of the subsequent three sections is concerned with an example where the situation was not so easily recognizable and an important limiting case was initially overlooked. Some summary remarks are made in a concluding section.

2. Some preliminary examples. Often a distinguished limit can be recognized on physical grounds. This might perhaps be said, for example, of the transonic and hypersonic small-disturbance theories mentioned above, where the important special case arises when one component of the velocity perturbation is no longer small in a suitable sense. Three other examples of this kind are identified in the following paragraphs.

The compression side of a slender wing having triangular planform and flying at an angle of attack at high Mach number can be studied in the "Newtonian" limit, where the shock wave is considered to coincide with the wing surface in the limit [5]. In the thin shock layer, the density is then very high, so in this limit the small parameters are $1/M_\infty^2$ and $\gamma - 1$, where M_∞ is the flight Mach number and γ is the ratio of specific heats, and the angle of attack is held fixed. Then $\gamma - 1$ and $1/M_\infty^2$ are taken to be of the same order since they appear together in the expression for the density ratio across a very strong shock wave. If also the aspect ratio is small, the similarity parameter to be held constant in the limit is the ratio of the wing vertex half-angle to the Mach angle in the flow behind the shock. If this quantity is called Ω, there is a specific value Ω_d such that the shock is attached along the leading edges when $\Omega > \Omega_d$ but detached when $\Omega < \Omega_d$. Flow perturbations then depend on suitably scaled coordinates and on Ω. In the notation suggested in the preceding section, the three small parameters might be denoted by $\epsilon_1 = 1/M_\infty, \epsilon_2 = \gamma - 1, \epsilon_3 = A$, where A is again the aspect ratio; then it is found that ϵ_2/ϵ_1^2 and ϵ_3/ϵ_1 are to be held fixed in the limit, where ϵ_3/ϵ_1 is proportional to Ω. Interestingly, it is not clear that the two-dimensional cross-flow problem [6] is recovered in the limit as $\Omega \to 0$; there may be still another limiting case. This is the kind of question that is addressed in the following sections.

The mean flow in a constant-pressure turbulent boundary layer is often represented in terms of a velocity defect law and a law of the wall, which have been interpreted as providing an asymptotic description of the flow. The velocity change across most of the layer is of order u_τ, where u_τ is the friction velocity made nondimensional with the external-flow velocity. This is regarded as a small parameter that approaches zero as the Reynolds number approaches infinity. The same idea is used to characterize compressible as well as incompressible flows. In particular, if the Mach number M_∞ in the external flow is slightly greater than one, there is another small parameter, say $M_\infty^2 - 1$, which is proportional to the difference between the external-flow velocity and sound speed. For a thin airfoil traveling at high subsonic speed, the local flow velocity at the upper surface can exceed the local sound speed, in which case a weak nearly normal shock wave typically is present. This shock penetrates the boundary layer to a location close to the undisturbed sonic line. At the sonic line the mean flow velocity is smaller than the external-flow value by an amount proportional to $M_\infty^2 - 1$. Thus, if $\epsilon_1 = u_\tau$ and $\epsilon_2 = M_\infty^2 - 1$, the similarity parameter is seen to be $\epsilon_2/\epsilon_1 = (M_\infty^2 - 1)/u_\tau$: for small or large values of this parameter, respectively, the sonic line is near the outer edge or the bottom of the boundary layer. If this ratio is held fixed in the limit as $u_\tau \to 0$ and $M_\infty^2 - 1 \to 0$, the appropriate small-disturbance equation is the transonic small-disturbance equation modified to include a weak shear [7]. Numerical solutions are functions of suitable scaled coordinates and the similarity parameter.

A more difficult example concerns the "marginal" separation that can occur near the rounded leading edge of a thin airfoil at small angle of attack α [8,9]. On the upper surface a pressure minimum appears, downstream of which the pressure gradient is adverse and causes separation of the laminar boundary layer at a value $\alpha = \alpha_S$. For a small range of angles

$\alpha > \alpha_S$, the separated free shear layer reattaches at a very short distance further downstream, so that a short separation bubble is present. It has been found possible to obtain an analytical description of the bubble when the shear layer remains laminar through reattachment, for large values of the Reynolds number Re and for a range $(\alpha - \alpha_S)/\alpha_S = O(Re^{-2/5})$, where the reference length is the leading-edge radius, with the nondimensional length of the bubble obtained as $O(Re^{-1/5})$. The flow has a three-layer asymptotic structure. The external flow has nearly constant adverse pressure gradient, while the main part of the boundary layer has the local undisturbed velocity profile, with zero wall shear. In a sublayer close to the surface, the third approximation leads to an integrodifferential equation, for which a solution is found to exist within a limited range of the parameter $Re^{2/5}(\alpha - \alpha_S)/\alpha_S$. This, then, is another example in which a specific choice for the relative orders of small parameters $\epsilon_1 = (\alpha - \alpha_S)/\alpha_S$ and $\epsilon_2 = Re^{-2/5}$ corresponds to a particular physical feature, in this case the presence of a short bubble. That such a relationship might exist is perhaps to be anticipated; the exact form of the similarity parameter requires considerable analysis and is not at all obvious.

The example of marginal separation is included here because it appears to be an important example, not because it is a simple one. It is worth noting that a more typical kind of separation is not described in the same way [10]. For laminar separation from a bluff body such as a circular cylinder, as the Reynolds number Re tends to infinity, the limiting external flow on the scale of the body is a free-streamline flow, with the separation point shifted downstream from the point which allows continuous streamline curvature, through a distance that approaches zero with increasing Re. The adverse pressure gradient is present only on a small scale, and is large in terms of Re. The local flow has a three-layer, or "triple-deck," structure, with the main part of the boundary layer now having nonzero shear in the limit as the sublayer is approached; only in the case of "marginal" separation does the adverse pressure gradient remain nearly constant with the shear approaching zero at the bottom of the main part of the layer.

3. Flutter of a thin plate at high Mach number. If a thin plate with clamped edges is exposed to a uniform supersonic flow, under some circumstances an aeroelastic instability called panel flutter can occur. The plate is taken to lie along the x-axis, with an external flow above the plate in the positive x-direction, while below the plate the air is at rest; the motion is considered to be two-dimensional. In nondimensional form the equation of motion for the plate can be written in the form

$$\epsilon_E^3 \frac{\partial^4 w}{\partial \xi^4} - \epsilon_\sigma \frac{\partial^2 w}{\partial \xi^2} + \frac{\partial w}{\partial \xi} + \kappa \frac{\partial w}{\partial \tau} + \frac{\partial^2 w}{\partial \tau^2} = 0, \qquad 0 < \xi < 1 \tag{1}$$

$$\epsilon_E^3 = M \frac{E}{12(1-\mu^2)\rho U^2} \frac{h^3}{L^3}, \quad \epsilon_\sigma = M \frac{\sigma}{\rho U^2} \frac{h}{L}, \qquad \frac{1}{\kappa^2} = M \frac{\rho_S}{\rho} \frac{h}{L} \tag{2}$$

where $w(\xi, \tau)$ is the vertical displacement of a point on the plate; $\xi = x/L$, $\tau = \kappa U t/L$; E and μ are the Young's modulus and the Poisson ratio; h, L, and ρ_S are the thickness, length, and density of the plate; σ is the tension stress in the plate; U, M, ρ are the velocity, Mach number, and density of the air flowing over the plate. The first two terms in (1) represent the effects of bending and tension stresses. The next two terms represent the aerodynamic force, obtained from linear supersonic theory approximated for large Mach number, a result sometimes referred to as linear piston theory. The last term is proportional to the vertical acceleration of the plate. For boundary conditions, the edges are considered to be clamped, so that the deflection and slope are zero at each edge.

The three nondimensional parameters are $\epsilon_E, \epsilon_\sigma$, and κ. For the full problem no further approximation would be made, but one may also ask what limiting cases might be of interest. Two rather obvious possibilities are limits as $\epsilon_E \to 0$ with ϵ_σ and κ held fixed or $\epsilon_\sigma \to 0$ with ϵ_E and κ held fixed. Prior to the work of [11], results were known for these two cases, but they were probably not interpreted as limiting cases in the present sense. In the former case, the membrane is recovered and a solution by separation of variables shows that there is no instability; boundary layers having width $O(\epsilon_E^{3/2})$ are present at the edges to allow the zero-slope boundary conditions to be satisfied. In the latter case, it is found that for each κ there is a critical value of ϵ_E, say $(\epsilon_E)_{cr}$, such that no instabilities are present when $\epsilon_E > (\epsilon_E)_{cr}$ but flutter does occur when $\epsilon_E < (\epsilon_E)_{cr}$. Thus in the $\epsilon_\sigma, \epsilon_E$ plane there is no instability on the ϵ_σ axis, but on the ϵ_E axis flutter occurs when ϵ_E is small enough; the result obtained when first $\epsilon_E \to 0$ and later $\epsilon_\sigma \to 0$ differs from that found if first $\epsilon_\sigma \to 0$ and later $\epsilon_E \to 0$. That is, the former solution evaluated as $\epsilon_\sigma \to 0$ does not "match" with the latter solution evaluated as $\epsilon_E \to 0$.

When the situation is viewed in this way, it seems clear that one should examine the limit as the origin is approached along different paths, say along radial lines at different angles. Thus we might consider limits $\epsilon_\sigma, \epsilon_E \to 0$ such that $\epsilon_\sigma/\epsilon_E$ is held fixed. (The parameter κ is of subordinate interest; the primary issues concern ϵ_σ and ϵ_E.) The difficulty in this problem was in determining that $\epsilon_\sigma/\epsilon_E$ is in fact the correct similarity parameter; if memory serves, the work of [11] involved some trial and error. If also ξ were held fixed, the effects of bending stresses and tension would both disappear from the differential equation, and we would conclude that $w = 0$ in the first approximation. However, boundary layers might be anticipated at the edges. If exponential growth is to be avoided as the interior part of the plate is approached from the edge regions, there can be a boundary layer only at the trailing edge. Setting $\bar{\xi} = (1-\xi)/\epsilon_E$ and $\bar{\tau} = \tau/\epsilon_E^{1/2}$, we have

$$\frac{\partial^4 w}{\partial \bar{\xi}^4} - \frac{\epsilon_\sigma}{\epsilon_E}\frac{\partial^2 w}{\partial \bar{\xi}^2} - \frac{\partial w}{\partial \bar{\xi}} + \kappa \epsilon_E^{1/2}\frac{\partial w}{\partial \bar{\tau}} + \frac{\partial^2 w}{\partial \bar{\tau}^2} = 0 \tag{3}$$

where we would also take the quantity $\kappa\epsilon_E^{1/2}$ to be fixed. The scalings in (3) differ from those in [11] by factors that are held constant in the limit.

The boundary-layer equation (3) implies a dependence only on $\bar{\xi}$ and thus is not sufficient, since boundary conditions at both edges must still be satisfied, and the solution should therefore be expected to depend on both ξ and $\bar{\xi}$. One method of solution recognizes from the membrane result that an exponential factor in $\bar{\xi}$ should be anticipated; if this is removed, the remaining part of the solution depends on ξ. Or, a two-variable expansion can be introduced. The results [11] show a branching of the solution as $\epsilon_\sigma/\epsilon_E$ increases to a specific numerical value; if $\kappa = 0$, this value is $\epsilon_\sigma/\epsilon_E = 3/2$. Thus, for each κ a stability boundary exists, starting at the origin with known slope and ending at the point $\epsilon_E = (\epsilon_E)_{cr}, \epsilon_\sigma = 0$. Inside this curve, flutter occurs; outside, the motion is stable. In [11], the branching was shown in a plane with coordinates $(\epsilon_E/\epsilon_\sigma)^{3/2}$ and $(\epsilon_E^3/\epsilon_\sigma)^{1/2}$. The present formulation, in terms of ϵ_σ and ϵ_E, illustrates the situation in another way, possibly somewhat more clearly.

4. Weakly nonlinear instability of a thin shear layer in incompressible flow. A thin shear layer between uniform streams of fluid at different speeds experiences a spatially growing instability at sufficiently large distances downstream from the origin of the shear layer. The initial growth of a small disturbance is described by linear theory, but in a subsequent stage a weakly nonlinear flow description is required. For two-dimensional disturbances, results were given in [12]. If the transverse length scale is taken to be some measure, say δ, of the shear-layer thickness, the appropriate y-coordinate is $\tilde{y} = y/\delta$. The solutions for small disturbances have a singular behavior at a still thinner "critical layer" within which the flow velocity is nearly equal to the propagation speed of the disturbance; the coordinates can be chosen such that $\tilde{y} \to 0$ as the critical layer is approached. Here effects of nonlinearity and/or viscosity enter the vorticity equation. If Re is the Reynolds number based on δ and on some reference external-flow velocity, and ϵ is a disturbance amplitude made nondimensional with δ, nonlinearity is the dominant effect when $\epsilon^{3/2}Re >> 1$, whereas viscosity dominates if $\epsilon^{3/2}Re << 1$. The appropriate critical-layer coordinate is $\hat{y} = \tilde{y}/\epsilon^{1/2}$ in the former case and $\hat{y} = \tilde{y}Re^{1/3}$ in the latter. The former case is considered here; the formulation in the (distinguished) limit with $\epsilon^{3/2}Re$ fixed is given in [13]. Matching of the solution found for the critical layer with the solution outside the critical layer leads to the condition that the velocity jump calculated from the critical-layer solution must agree with that obtained from the solution in the main part of the shear layer. This is possible only if a slow growth is allowed, on a spatial scale larger than the period by a factor $O(\epsilon^{-1/2})$. The appropriate slow variable is then $\bar{x} = \epsilon^{1/2}x$. If the amplitude of the disturbance is ϵA, the result is an evolution equation that expresses $dA/d\bar{x}$ in terms of an integral across the critical layer and integrals across the main part of the layer.

In a three-dimensional case where the amplitude is assumed to have a periodic variation in the spanwise direction as well, a quite different kind of evolution equation is obtained in [14], in the form of a nonlinear integrodifferential equation. It might be hoped that the two-dimensional result would be recovered if the spanwise wavenumber were allowed to approach zero in the solution of [14]. That is, if the spanwise period made nondimensional with the shear-layer thickness is L, then the solution in terms of L might be expected to approach the two-dimensional solution when L^{-1} approaches zero. This, however, is not the case. It might then be anticipated that there is another special limit corresponding to a large spanwise period of some specific order with respect to ϵ. To understand this, one idea would be to assume that the two-dimensional results remain correct for a very slow spanwise variation, i. e., for very large L. This conclusion would be a consequence of Kaplun's extension theorem. As the spanwise period L is gradually reduced, we can then ask when a new feature first appears in one or more of the differential equations. By considering the vorticity equation and the spanwise component of the momentum equation in the critical layer, one sees rather easily that a term representing vortex stretching first appears in the vorticity equation when $L = O(\epsilon^{-1/2})$. In a limit with $z^* = \epsilon^{1/2}z/\delta$ held fixed, the problem requires solution of the coupled vorticity and spanwise momentum equations in the variables $\hat{y}, z^*$, and $\bar{x}$, with the usual requirement that solutions for each of the flow variables match as $\hat{y} \to \pm\infty$ with the corresponding solutions in the main part of the shear layer evaluated as $\tilde{y} \to 0$. The evolution equation should have the same general form as in the two-dimensional case, although the details, not yet completely worked out, will be different. It now appears that the full three-dimensional formulation does approach the new formulation as the spanwise wavenumber is decreased, since the solution as $L^{-1} \to 0$ matches with the new formulation as $L^{-1}/\epsilon^{1/2} \to \infty$, i. e., when L^{-1} is small but not as small as $\epsilon^{1/2}$.

In this example, then, we can define two small parameters as $\epsilon_1 = \epsilon^{1/2}$ and $\epsilon_2 = L^{-1}$. As in the preceding example, the difficulty is first observed when it is recognized that in a plane with coordinates $\epsilon^{1/2}$ and L^{-1} different solutions are obtained if the origin is approached along the two coordinate axes. That is, these two solutions do not match; rather, each matches with a solution found in terms of the ratio $\epsilon_2/\epsilon_1 = L^{-1}/\epsilon^{1/2}$. Again it was not recognized initially that this additional special limit exists.

5. Long-wave instability of a supersonic shear layer. If the thickness of a free shear layer is taken to be zero, the flow reduces to that over a vortex sheet. Stability calculations are then carried out under the conditions that the pressure is constant across the sheet and kinematic conditions are satisfied at the sheet. In the linear approximation, it is known that the flow is neutrally stable if the Mach number is large enough. For example, if the velocities are equal and opposite above and below the sheet, and the temperatures are the same above and below, neutral stability is found when the Mach number of each outer flow is greater than $\sqrt{2}$. If a second approximation is calculated, a slow distortion of the sheet is observed. The motion is somewhat like that for steady flow past a wavy wall, but now the wall is free to undergo a slow deformation. Thus not only is there a wave steepening in the outer flow, but the sheet also undergoes a steepening. The weak shock waves that form at large distances will move toward the sheet on one side and away on the other side, until shocks reach the sheet and corners form on the sheet. The analysis resembles that for the far field in a steady supersonic flow, with a nonsecularity condition imposed in the second approximation.

If the thickness of the shear layer is not zero and a disturbance has spatial period large in comparison with the thickness, a linear theory again gives neutral stability in a first approximation, but a slow growth in amplitude is also predicted. A weakly nonlinear description of spatial instability is given in [15], for a limiting case when the amplitude of the shear-layer displacement becomes of the same order as the thickness of the critical layer. If ϵ and δ are the displacement amplitude and shear-layer thickness, both nondimensional with the spatial period (these definitions differ from those of the preceding section), it can be shown that in the case considered $\epsilon = O(\delta^2)$. In this limit the external flow remains linear, but the critical layer is described by vorticity and temperature equations that are nonlinear because of the transverse displacement. The relation between Reynolds number and nondimensional amplitude is chosen such that diffusion effects also appear in these equations. This choice is found to give the relation $\epsilon = O(Re^{-2/5})$, where the Reynolds number Re is based on the spatial period and a reference flow velocity such as the velocity in the upper stream. Matching with the solution obtained in the main part of the shear layer leads to an amplitude evolution equation that relates the slow rate of change to integrals across the critical layer and across the main part of the shear layer [15].

It might be hoped that the vortex-sheet limit would be recovered as the ratio of amplitude to spatial period increases, but this is not the case. Once more it is expected that still another limiting case is needed. It seems reasonable to expect that an important limit corresponds to a disturbance amplitude of the same order as the shear-layer thickness, such that $\epsilon = O(\delta)$ [16]. In this limit it is found that nonlinearity appears in the external flow as well as in the critical-layer equations. One way of thinking of this limit is as the limit which adds the effect of nonzero shear-layer thickness to the formulation for a vortex sheet. The external-flow description now has the same form as for the vortex sheet, but the pressure and kinematic conditions are replaced by matching conditions. In a coordinate system moving with the disturbance, the flow is nearly steady and one can speak of approximate streamlines. These streamlines show a cat's-eye pattern in the critical layer. Here the first approximation states that the temperature is constant along a streamline, and the vorticity changes as a result of a baroclinic torque. The orders of the Reynolds number and nondimensional amplitude are chosen such that the second approximation includes both nonlinear and diffusion effects; terms representing distortion on a slow spatial scale also appear. In this case the amplitude and Reynolds number are related by $\epsilon = O(Re^{-1/4})$. A periodicity condition is imposed for streamlines outside the cat's eyes and a singlevaluedness condition inside. The result [16] is a pair of coupled nonlinear integrodifferential equations for the first approximation to the vorticity and temperature; the amplitude appears in these equations in a nonlinear way. Matching again leads to an amplitude evolution equation which contains integrals across the critical layer and across the main part of the shear layer.

The situation is clearly more complicated than in the previous examples because now there are three small parameters, namely Re^{-1}, δ, and ϵ. In the limit of [15] $\epsilon = O(\delta^2)$ and $\epsilon = O(Re^{-2/5})$, whereas in the new limit $\epsilon = O(\delta)$ and $\epsilon = O(Re^{-1/4})$. For an alternative that might be more convenient, we can introduce the length L of the shear layer, nondimensional with the spatial period. If a self-similar solution is assumed for the undisturbed shear layer, it follows that $\delta = O(L^{1/2} Re^{-1/2})$. Thus we can replace δ in terms of L^{-1} and choose the small parameters $\epsilon_1, \epsilon_2, \epsilon_3$ as $Re^{-1}, L^{-1}, \epsilon$ instead of $Re^{-1}, \delta, \epsilon$. We can then consider different paths of approach to the origin $(Re^{-1}, L^{-1}, \epsilon) = (0,0,0)$. In the limit of [15], $L = O(Re^{3/5})$ and $\epsilon = O(L^{-2/3})$, whereas in the limit of [16], $L = O(Re^{1/2})$ and $\epsilon = O(L^{-1/2})$. Each limit process corresponds to a family of curves through the origin. (It might be noted briefly that if $Re^{-1} = 0$, we have a vortex sheet with zero thickness; if $\epsilon = 0$, there is no disturbance, or we might say that if ϵ is smaller than any power of the other small parameters, the disturbance is described by linear theory; and if $L^{-1} = 0, \delta$ is no longer small, as has been assumed here.) In terms of the earlier notation, the similarity parameters may be taken as ϵ_2/ϵ_1^a and ϵ_3/ϵ_1^b, with $a = 3/5, b = 2/5$ or $a = 1/2, b = 1/4$.

Another way of picturing the relationship between the two distinguished limits requires reducing the number of parameters from three to two, which is possible if we think of L and $1/\epsilon$ as approaching infinity in proportion to different powers of the Reynolds number. If we take logarithms and define new parameters $L^* = (\ln\ L)/(\ln Re)$ and $\epsilon^* = (\ln\ \epsilon^{-1})/(\ln\ Re)$, then each point in the L^*, ϵ^* plane corresponds to a family of curves in the coordinates $Re^{-1}, L^{-1}, \epsilon$. The two distinguished limits of [15] and [16] are located at points $(L^*, \epsilon^*) = (3/5, 2/5)$ and $(1/2, 1/4)$ respectively. There does also appear to be a third distinguished limit $(3/7, 2/7)$ corresponding to an amplitude of the same order as the shear-layer thickness, but a smaller L than in [16], so that ϵ is also smaller, and diffusion effects enter the critical-layer equations in the first approximation. The solutions obtained in the three distinguished limits should then match along straight lines joining the corresponding points in the L^*, ϵ^* plane.

The formulation of [16] does not answer the question posed. For a given large Re, this limiting case corresponds to a disturbance introduced further upstream and with an amplitude larger than that of [15]. Since it corresponds to a smaller L, the new formulation [16] does not represent a later stage of the previous formulation [15]. According to the present arguments, the result of [15] should be expected to show a growth in amplitude as the appropriate slow variable increases, but at a value of L larger than that in [16], until the amplitude is no longer small in comparison with the shear-layer thickness and nonlinearity in the external flow becomes important; the scale of the slow variable indicates that the disturbance growth occurs within a distance much shorter than the length of the shear layer. Although one would in fact expect the description of this change to be simpler than the formulation of [16], the analytical details have still not been worked out. The point of this example, then, is just that there are three special limits, any of which might be regarded as difficult to identify.

6. Concluding remarks. The preceding sections have reviewed a few examples of flow problems with two or three small parameters where the important limiting cases were initially not at all obvious. An attempt was made here to indicate the difficulties encountered in recognizing these special limits. If the asymptotic representations are to be obtained in the form of limit-process expansions, the general principle, of course, is that various sets of limiting equations can be found, and each represents a different limit of the full equations. Thus it might be said that one simply has to identify all of these limiting equations. But in the examples cited, it seems that a complete list of possibilities is not always self-evident. A clue that some special limit has not been recognized may be the failure of two known results to "match" in terms of certain similarity parameters, in the same sense as for matching in terms of coordinates. For problems with only two small parameters, this observation can be a first step toward finding a missing distinguished limit.

In the above example of an incompressible shear layer, one can just think of gradually increasing a small parameter from zero until some new feature appears in the equations. But in the panel-flutter example the new limit described has the additional feature that a coordinate stretching is required as well. Moreover, neither of these problems has solutions that are strictly limit-process expansions, because each involves both a "fast" and a "slow" variable. In the example of a supersonic shear layer, the presence of three small parameters leads to the added complication that in any of the important limits the origin is approached along a three-dimensional, rather than two-dimensional, curve. In this particular example, there was a way to reduce the number of parameters to two, through taking logarithms and dividing by the logarithm of the Reynolds number. As a consequence, each special limit corresponds to a point in a certain plane, each point representing a family of three-dimensional curves in the original parameter space. This procedure seems to help toward understanding the relationships among the special limits, and might perhaps also be of use in other problems.

Thus, the question of identifying limit processes in problems with more than one small parameter has continued to arise in subtle forms. Although the issue was explored by Julian Cole and others at Caltech in the 1950's, the recognition of important distinguished limits can, at least occasionally, still present quite a challenge.

References

[1] M. D. Van Dyke, *Nineteenth-century roots of the boundary-layer idea*, SIAM Rev., 36 (1994), pp. 415-424.

[2] J. D. Cole, *The development of perturbation theory at GALCIT*, SIAM Rev., 36 (1994), pp. 425-430.

[3] J. Kevorkian and J. D. Cole, *Perturbation Methods in Applied Mathematics*, Springer, New York, 1981.

[4] J. D. Cole and L. P. Cook, *Transonic Aerodynamics*, North-Holland, Amsterdam, 1986.

[5] A. F. Messiter, *Lift of slender delta wings according to Newtonian theory*, AIAA J., 1 (1963), pp. 794-802.

[6] J. D. Cole and J. J. Brainerd, *Slender wings at high angles of attack in hypersonic flows,* in *Hypersonic Flow Research*, ed. F. R. Riddell, Academic, New York, 1962, pp. 321-343.

[7] R. E. Melnik and B. Grossman, *Analysis of the interaction of a weak normal shock wave with a turbulent boundary layer*, AIAA Paper No. 74-598, 1974.

[8] A. I. Ruban, *Asymptotic theory of short separation regions on the leading edge of a thin airfoil*, Fluid Dynamics, 17 (1982), pp. 33-41.

[9] K. Stewartson, F. T. Smith, and K. Kaups, *Marginal separation*, Stud. Appl. Math., 67 (1982), pp. 45-61.

[10] V. V. Sychev, *Laminar separation*, Fluid Dyn., 7 (1972), pp. 407-417.

[11] J. H. Spriggs, A. F. Messiter, and W. J. Anderson, *Membrane flutter paradox - an explanation by singular perturbation methods*, AIAA J., 7 (1969), pp. 1704-1709.

[12] M. E. Goldstein and S. J. Leib, *Nonlinear roll-up of externally excited free shear layers*, J. Fluid Mech., 191 (1988), pp. 481-515.

[13] M. E. Goldstein and L. S. Hultgren, *Nonlinear spatial evolution of an externally excited instability wave in a free shear layer*, J. Fluid Mech., 197 (1988), pp. 295-330.

[14] M. E. Goldstein and S.-W. Choi, *Nonlinear evolution of interacting oblique waves on two-dimensional shear layers*, J. Fluid Mech., 207 (1989), pp. 97-120; 216 (1989), pp. 659-663.

[15] T. F. Balsa, *The stability of a supersonic mixing layer: two-dimensional modes with nonlinear critical layers*, in preparation; an earlier version was presented at the Am. Phys. Soc. Div. Fluid Dyn. Meeting, 1990.

[16] A. F. Messiter, *Large-amplitude long-wave instability of a supersonic shear layer*, ICOMP 95-14, 1995; to appear in Stud. Appl. Math.

Exponential Asymptotics, Boundary Layer Resonance, and Dynamic Metastability

Robert E. O'Malley, Jr,* Michael J. Ward†

To Julian Cole—Gentleman, Scholar, and Pioneer in Applied Asymptotics

Abstract

This paper considers the linear convection–diffusion equation $u_t = \epsilon u_{xx} - xu_x$, and certain natural generalizations, on fixed bounded spatial domains including the turning point $x = 0$. For constant boundary values and consistent initial values, asymptotic solutions as $\epsilon \to 0^+$ converge to steady states over asymptotically exponentially-long time intervals. The occurrence of an asymptotically exponentially-small eigenvalue is the reason for such metastability, as well as for the sensitivity of the long-time behavior to small perturbations. The utility of these asymptotic results is illustrated through numerical computations done with only moderately small ϵ values.

1 Introduction

There has been much recent work on the asymptotic solution of exponentially ill-conditioned boundary value problems for nonlinear singularly perturbed parabolic partial differential equations. Examples of such problems include Burgers equation and the Ginzburg-Landau equation on bounded spatial domains (cf. [2], [4], [8], [10], [16] and the references therein). The solutions to these problems typically involve an extremely sluggish approach to a steady state (i.e., *dynamic metastability*). Moreover, the steady state itself is often extremely *sensitive* to perturbations of the boundary values and the coefficients in the differential operator. Both phenomena relate to the appropriate linearized problem having an asymptotically exponentially-small eigenvalue. The significance of such eigenvalues was already recognized for certain much-studied linear two-point problems involving boundary layer resonance (cf. [1], [5], [9], [11], [14], [20], among much additional literature). Some of these linear problems arise in the asymptotic determination of exit times for stochastic differential equations in one or more space dimensions (cf. [12], [13], [15], and [17]).

In this paper, we examine a class of linear time-dependent convection-diffusion equations exhibiting the phenomenon of dynamic metastability. The corresponding equilibrium problem is exponentially ill-conditioned and is associated with boundary layer resonance. In §2, we use a straightforward eigenfunction expansion to study a simple example in detail. In §3, we generalize the analysis to treat a class of convection-diffusion problems and examine the extreme sensitivity of their solutions to some small perturbations. Finally, in §4, we

*Department of Applied Mathematics, University of Washington, Seattle, Washington 98195. The support of the U.S. National Science Foundation is gratefully acknowledged.

†Department of Mathematics, University of British Columbia, Vancouver, BC, Canada V6T 1Z2. Supported by NSERC grant 5-81541.

compare the results of the asymptotic analysis with numerical computations for specific examples.

2 A Simple Example

We begin by considering the following initial-boundary value problem for $u = u(x,t)$:

$$
\begin{aligned}
(1)\qquad u_t &= \epsilon u_{xx} - x u_x\,, \qquad -1 < x < 1\,, \quad t > 0\,,\\
(2)\qquad u(-1,t) &= \alpha\,, \qquad u(1,t) = \beta\,,\\
(3)\qquad u(x,0) &= u_0(x)\,.
\end{aligned}
$$

Here $\epsilon \to 0^+$, α and β are constants, and $u_0(x)$ is smooth with $u_0(-1) = \alpha$ and $u_0(1) = \beta$. The exact steady-state solution $U(x;\epsilon)$ corresponding to (1)-(3) is given by

$$
(4)\qquad U(x;\epsilon) = \frac{1}{2}(\alpha+\beta) + \frac{1}{2}(\beta-\alpha)\left[\frac{\int_0^x e^{s^2/2\epsilon}ds}{\int_0^1 e^{s^2/2\epsilon}ds}\right].
$$

The dominant contributions to the integrals in (4) arise from s values near the upper endpoints, i.e. $\int_0^x e^{s^2/2\epsilon}ds \sim \epsilon x^{-1}e^{x^2/2\epsilon}$ provided that $x^2 \gg \epsilon$. This implies that the ratio of the two integrals behaves like $x^{-1}e^{(x^2-1)/2\epsilon}$ away from $x = 0$. Thus, for $\epsilon \to 0$,

$$
(5)\qquad U(x;\epsilon) \sim \frac{1}{2}(\alpha+\beta) + \frac{1}{2}(\alpha-\beta)\left(e^{-(1+x)/\epsilon} - e^{-(1-x)/\epsilon}\right),
$$

i. e., the steady state tends to the average $(\alpha+\beta)/2$, except in $O(\epsilon)$ boundary layer regions near each endpoint. Nothing special happens near the turning point $x = 0$.

The solution to (1)-(3) can be represented in terms of an eigenfunction expansion as

$$
(6)\qquad u(x,t) = U(x;\epsilon) + \sum_{k=0}^{\infty} c_k\phi_k(x)e^{-\lambda_k t}
$$

(cf. [6] which also takes this approach). Here, the coefficients $c_k(\epsilon)$ are uniquely given by

$$
(7)\qquad c_k = \int_{-1}^{1}[u_0(x) - U(x;\epsilon)]\phi_k w\,dx \Big/ \int_{-1}^{1}\phi_k^2 w\,dx\,,
$$

for the weight $w(x) \equiv e^{-x^2/2\epsilon}$, while the eigenpairs $(\lambda_k(\epsilon), \phi_k(x;\epsilon))$ satisfy the eigenvalue problem

$$
(8)\qquad \epsilon\phi'' - x\phi' + \lambda\phi = 0\,, \qquad -1 < x < 1\,, \qquad \phi(\pm 1) = 0\,,
$$

for real λ_k's which increase with k. To solve (8), we invoke the classical Liouville transformation $\hat{\phi} = e^{-x^2/4\epsilon}\phi$ and find that $\hat{\phi}$ must satisfy Weber's equation, which is solvable in terms of Whittaker's form of the *parabolic cylinder function* $D_\nu(z)$ (cf. [21]). Thus, the eigenfunctions ϕ must have the form

$$
(9)\qquad \phi(x) = e^{x^2/4\epsilon}[b_1 D_{-1-\lambda}(ix/\sqrt{\epsilon}) + b_2 D_\lambda(-x/\sqrt{\epsilon})]\,,
$$

for some (ϵ-dependent) constants b_1 and b_2. Since $\phi(\pm 1) = 0$, the ratio b_1/b_2 becomes specified and the eigenfunctions are proportional to

$$
(10)\qquad \phi(x) = e^{x^2/4\epsilon}[D_{-1-\lambda}(ix/\sqrt{\epsilon})D_\lambda(-1/\sqrt{\epsilon}) - D_\lambda(-x/\sqrt{\epsilon})D_{-1-\lambda}(i/\sqrt{\epsilon})]\,,
$$

while the eigenvalues λ must satisfy the transcendental eigenvalue relation

$$D_\lambda(-1/\sqrt{\epsilon}) = D_\lambda(1/\sqrt{\epsilon})\frac{D_{-1-\lambda}(i/\sqrt{\epsilon})}{D_{-1-\lambda}(-i/\sqrt{\epsilon})}\,. \tag{11}$$

To study the asymptotic behavior of the eigenpairs as $\epsilon \to 0$, we shall use the leading-order approximations

$$D_\nu(z) = \begin{cases} e^{-z^2/4}z^\nu[1+O(z^{-2})]\,, & |\arg z| < 3\pi/4 \\ e^{-z^2/4}z^\nu[1+O(z^{-2})] - \frac{\sqrt{2\pi}}{\Gamma(-\nu)}\frac{e^{z^2/4-\nu\pi i}}{z^{\nu+1}}[1+O(z^{-2})]\,, & \frac{\pi}{4} < \arg z < \frac{5\pi}{4} \end{cases} \tag{12}$$

as $|z| \to \infty$ for complex arguments z. It is critical to note that the decaying nature of $D_\nu(z)$ for large positive z becomes growing for large negative values of z, unless ν happens to be (near) zero or a positive integer, since then $1/\Gamma(-\nu)$ is (near) zero. (This reflects the Stokes phenomenon for Weber's equation and the fact that $D_\nu(z)$ for a non-negative integer ν reduces to the product of a Hermite polynomial and an exponential function which decays as $z \to \pm\infty$.) A careful use of the approximations (12) in the eigenvalue relation (11) reduces it to the limiting form

$$\frac{\epsilon^\lambda}{\Gamma(-\lambda)} \sim -\sqrt{\frac{2}{\pi\epsilon}}e^{-1/2\epsilon}\,. \tag{13}$$

Thus, for $\epsilon \to 0$, the principal eigenvalue λ_0 satisfies

$$\lambda_0 \sim \sqrt{\frac{2}{\pi\epsilon}}e^{-1/2\epsilon}\,, \tag{14}$$

while the remaining sequence of eigenvalues satisfies

$$\lambda_k \sim k \qquad \text{for } k = 1,2,3,\ldots\,. \tag{15}$$

The (un-normalized) eigenfunction corresponding to λ_0 is given asymptotically by

$$\phi_0(x) \sim 1 - e^{-(1+x)/\epsilon} - e^{-(1-x)/\epsilon}\,, \tag{16}$$

while

$$\phi_k(x) \sim x^k - (-1)^k e^{-(1+x)/\epsilon} - e^{-(1-x)/\epsilon} \qquad \text{for } k = 1,2,3,\ldots\,. \tag{17}$$

Thus, for large t, the higher terms in (6) are insignificant and the *quasi-steady state*

$$u(x,t) \sim U(x;\epsilon) + c_0\phi_0(x)e^{-\lambda_0 t} \tag{18}$$

is attained. The coefficient c_0 is obtained asymptotically by substituting (16) into (7) with $k = 0$. Since the weighting function w is localized near $x = 0$, the integrals in (7) can be evaluated for $\epsilon \to 0$ (cf. [23]) to yield $c_0 \sim u_0(0) - U(0;\epsilon)$. Thus, (18) reduces to

$$u(x,t) \sim A_0(t) + (\alpha - A_0(t))e^{-(1+x)/\epsilon} + (\beta - A_0(t))e^{-(1-x)/\epsilon} \tag{19}$$

where the level

$$A_0(t) \equiv \frac{1}{2}(\alpha+\beta) + [u_0(0) - \frac{1}{2}(\alpha+\beta)]e^{-\lambda_0 t} \tag{20}$$

is the outer limit within $-1 < x < 1$ and where λ_0 is the negligible principal eigenvalue given by (14). This significant result describes the exponentially-slow evolution of $u(x,t)$

toward the steady state $U(x;\epsilon)$. Higher-order approximations than (19) would result from using higher-order approximations than (12) in (6) and (11).

To illustrate the big effect a small perturbation can produce, consider the equation

$$u_t = \epsilon u_{xx} - x u_x - \delta u \,, \tag{21}$$

where δ is a small, but fixed, positive constant, subject to the boundary and initial conditions (2) and (3). We can again obtain a solution of the form (6), with the eigenpairs now satisfying

$$\epsilon\phi'' - x\phi' + (\lambda - \delta)\phi = 0\,, \quad \phi(\pm 1) = 0\,. \tag{22}$$

Thus, the resulting limiting eigenvalue condition $\frac{\epsilon^{\lambda-\delta}}{\Gamma(\delta-\lambda)} \sim -\sqrt{\frac{2}{\pi\epsilon}}e^{-1/2\epsilon}$ implies a sequence

$$\lambda_k \sim \delta + k \tag{23}$$

of positive eigenvalues for $k = 0, 1, 2, \ldots$. Because no eigenvalue remains asymptotically exponentially-negligible, solutions of the perturbed initial-boundary value problem will decay to the steady state in finite time (i.e., the earlier metastability is eliminated). Moreover, corresponding to the original notion of a resonant equilibrium problem having the trivial limit within $-1 < x < 1$ except for nonpositive integer values of δ, the steady state will now be trivial except in endpoint boundary layer regions. Indeed, the solution u will uniformly satisfy

$$u(x,t) \sim \alpha e^{-(1+x)/\epsilon} + \beta e^{-(1-x)/\epsilon} + O(e^{-\delta t}) \tag{24}$$

as $\epsilon \to 0$ (thereby agreeing in form with the long-time limit (19) for $\delta = 0$, but with $A_0(t) \equiv 0$). This big change between the solution with $\delta = 0$ and with any small $\delta > 0$ was called *super-sensitivity* in [10]. If we, instead, allowed $\delta(\epsilon)$ to be of the same asymptotically exponentially-small order as the eigenvalue λ_0 for $\delta = 0$, the solution u will again have a nontrivial outer limit, with metastable decay to a nontrivial steady state over an exponentially-long time interval. On the other hand, if we let δ be negative, the equilibrium solution will lose its stability.

2.1 An Alternative Metastability Analysis

The preceding analysis relied heavily on explicit analytical expressions for the eigenpairs (λ_k, ϕ_k) of (8) and their representations in terms of parabolic cylinder functions. We now present a more direct asymptotic method to study the metastable behavior for (1)-(3) in a manner which does not require such an explicit knowledge of the spectrum.

To begin, recall that the traditional method of matched asymptotic expansions fails to uniquely determine the asymptotic solution to the equilibrium problem

$$L_\epsilon U \equiv \epsilon U_{xx} - x U_x = 0\,, \qquad U(-1;\epsilon) = \alpha\,, \quad U(1;\epsilon) = \beta\,. \tag{25}$$

For $\epsilon \to 0$, a straightforward leading-order boundary layer analysis shows that

$$U(x;\epsilon) \sim \tilde{u}^\epsilon[x; A_{0e}] \equiv A_{0e} + (\alpha - A_{0e})\, e^{-(1+x)/\epsilon} + (\beta - A_{0e})\, e^{-(1-x)/\epsilon}\,, \tag{26}$$

uniformly in $-1 \le x \le 1$. Note that the form of $\tilde{u}^\epsilon$ is that already found for the long-time limit in (19). Here A_{0e} is a constant to be determined, which we naturally identify as the limit of $U(0;\epsilon)$. Note that the limiting equilibrium profile $\tilde{u}^\epsilon$ satisfies the boundary conditions of (25) to within asymptotically exponentially-small terms. In addition,

$$L_\epsilon \tilde{u}^\epsilon = \frac{1}{\epsilon}[(1+x)e^{-(1+x)/\epsilon}(\alpha - A_{0e}) + (1-x)e^{-(1-x)/\epsilon}(\beta - A_{0e})] \tag{27}$$

is asymptotically negligible away from the boundary layer regions near $x = \pm 1$ for any choice of A_{0e}. This indeterminacy in the matched asymptotic expansion persists even after one attempts to construct higher order boundary layer approximations near the endpoints. Yet, it is clear by symmetry that the correct value to select is $A_{0e} = (\alpha+\beta)/2$. The variational principle of [7] provides one analytical method for obtaining this value.

Next, we shall look for a solution to the time-dependent problem (1)-(3) in the form

$$u(x,t) = \tilde{u}^\epsilon[x; A(t;\epsilon)] + v(x,t)\,. \tag{28}$$

We insist that v remains asymptotically uniformly small for all moderately large $t > 0$, so that the translating profile $\tilde{u}^\epsilon[x; A(t;\epsilon)]$ continues to describe the limiting solution, uniformly in space, as time evolves. We define the outer solution $A(t;\epsilon)$ by

$$u(0,t) = \tilde{u}^\epsilon[0; A(t;\epsilon)]\,, \tag{29}$$

so $v(0,t) = 0$. Substituting (28) into (1)-(2), we obtain

$$\begin{aligned}
L_\epsilon v &= f(x,t) + v_t \quad -1 < x < 1\,, \quad t > 0\,, && (30)\\
v(-1,t) &= (A(t;\epsilon) - \alpha)e^{-2/\epsilon}\,, \qquad v(1,t) = (A(t;\epsilon) - \beta)e^{-2/\epsilon}\,. && (31)\\
v(0,t) &= 0\,. && (32)
\end{aligned}$$

Here, we have used the linear operator L_ϵ of (25) and defined $f(x,t)$ by

$$f(x,t) \equiv \frac{\partial \tilde{u}^\epsilon}{\partial A}\frac{dA}{dt} - L_\epsilon \tilde{u}^\epsilon\,, \tag{33}$$

where $L_\epsilon \tilde{u}^\epsilon$ given by (27). Note that (26) implies that $\partial \tilde{u}^\epsilon / \partial t$ is independent of A while (16) implies that $\partial \tilde{u}^\epsilon / \partial A \sim \phi_0$ as $\epsilon \to 0$. Integrating (30) with respect to x and setting $v(0,t) = 0$ shows that v satisfies the integral equation

$$v(x,t) = M\int_0^x e^{r^2/2\epsilon}\,dr + \int_0^x \int_0^r K(r,s)[f(s,t) + v_t(s,t)]\,ds\,dr\,, \tag{34}$$

where the constant of integration $M(t;\epsilon)$ is to be determined and the kernel is $K(r,s) \equiv \epsilon^{-1}e^{(r^2-s^2)/2\epsilon}$. Using symmetry, the boundary conditions (31) at $x = \pm 1$ yield

$$(A-\alpha)e^{-2/\epsilon} = -M\int_0^1 e^{r^2/2\epsilon}\,dr + \int_0^1 \int_0^r K(r,s)[f(-s,t) + v_t(-s,t)]\,ds\,dr\,, \tag{35}$$

and

$$(A-\beta)e^{-2/\epsilon} = M\int_0^1 e^{r^2/2\epsilon}\,dr + \int_0^1 \int_0^r K(r,s)[f(s,t) + v_t(s,t)]\,ds\,dr\,. \tag{36}$$

By adding and subtracting (35) and (36), we can eliminate M to find the relation

$$\begin{aligned}
&\frac{dA}{dt}\left(\int_0^1 \int_0^r K(r,s)\frac{\partial \tilde{u}^\epsilon(s;A)}{\partial A}\,ds\,dr\right) \\
&= \left(A - \frac{1}{2}(\alpha+\beta)\right)\left(\epsilon^2 \int_0^1 \int_0^r K(r,s)\frac{\partial}{\partial \epsilon}\left(\frac{\partial \tilde{u}^\epsilon(s;A)}{\partial A}\right)ds\,dr + e^{-2/\epsilon}\right) \\
&\quad + \frac{1}{2}\int_0^1 \int_0^r K(r,s)\,(v_t(s,t) + v_t(-s,t))\,ds\,dr\,.
\end{aligned} \tag{37}$$

We propose solving (34)-(36) (or, equivalently, (34) with M eliminated and (37)) by successive approximations with the first iterate v_0 resulting from setting $v_t \equiv 0$. Then (37) becomes the ordinary differential equation

$$
\begin{aligned}
(38) \qquad & \frac{dA_0}{dt}\left(\int_0^1 \int_0^r K(r,s)\frac{\partial \tilde{u}^\epsilon(s;A)}{\partial A}\, ds\, dr\right) \\
& = \left(A_0 - \frac{1}{2}(\alpha+\beta)\right)\left(\epsilon^2 \int_0^1 \int_0^r K(r,s)\frac{\partial}{\partial \epsilon}\left(\frac{\partial \tilde{u}^\epsilon(s;A)}{\partial A}\right) ds\, dr + e^{-2/\epsilon}\right)
\end{aligned}
$$

for A_0, which describes the corresponding motion of the limiting solution $\tilde{u}^\epsilon[x; A_0(t)]$. By asymptotically approximating the integrals in (38), we find that A_0 satisfies the limiting differential equation

$$
(39) \qquad \frac{dA_0}{dt} \sim -\sqrt{\frac{2}{\pi\epsilon}}e^{-1/2\epsilon}\left(A_0 - \frac{1}{2}(\alpha+\beta)\right) \quad \text{as } \epsilon \to 0\,.
$$

To determine an appropriate initial condition $A_0(0)$ (which will determine $A_0(t)$ for all $t \geq 0$), note that the solution U^0 of the reduced equation $U^0_t = -xU^0_x$, corresponding to (1), will be constant on its characteristics, defined by a fixed value for xe^{-t}, which spread out from the origin as t increases. Thus, to leading order, it is natural to take $A_0(0) \sim u_0(0)$, the center value of the initial data. The limiting outer solution $A_0(t)$ thereby obtained coincides precisely with the limit (20) previously found for the long time limit, and yields the anticipated steady state $A_{0e} = (\alpha+\beta)/2$. Finding higher-order approximations for the initial value $A_0(0;\epsilon)$ as $\epsilon \to 0$ would, of course, be desirable. Knowing $A_0(t)$ provides us the corresponding constant M_0 and the limiting initial iterate v_0 as a correction to the approximate asymptotic profile $\tilde{u}^\epsilon[x; A_0(t)]$. It is easy to check that v_0 is uniformly asymptotically negligible in $-1 \leq x \leq 1$ for $t \geq 0$. For consistency, we can also check that the neglected v_{0t} terms in (34)-(36) are asymptotically much smaller than the terms retained.

2.2 A Related Shock Layer Problem

We now contrast the metastable behavior of the solution to (1)-(3) with that of the modified problem

$$
(40) \qquad u_t = \epsilon u_{xx} + xu_x\,, \qquad -1 < x < 1\,, \quad t > 0\,,
$$

together with the boundary and initial conditions (2) and (3). The only difference between (40) and (1) is the sign of the xu_x term. The equilibrium solution to this problem is

$$
(41) \qquad U(x;\epsilon) = \frac{1}{2}(\alpha+\beta) + \frac{1}{2}(\beta-\alpha)\left[\frac{\int_0^x e^{-s^2/2\epsilon}ds}{\int_0^1 e^{-s^2/2\epsilon}ds}\right].
$$

For $\epsilon \to 0$, the dominant contributions to the integrals in (41) occur near $s = 0$. By evaluating these integrals asymptotically, we readily observe that the ratio of the two integrals switches from the asymptotic limit -1 for $x < 0$ to $+1$ for $x > 0$ in an $O(\sqrt{\epsilon})$ neighborhood of the *turning point* $x = 0$. Thus, as $\epsilon \to 0$, we have

$$
(42) \qquad U(x;\epsilon) \to \begin{cases} \alpha & \text{for } x < 0 \\ \frac{1}{2}(\alpha+\beta) & \text{for } x = 0 \\ \beta & \text{for } x > 0 \end{cases},
$$

with nonuniform convergence in the thin shock or transition layer about $x = 0$.

To solve the time-dependent equation (40), we expand $u(x,t)$ in an eigenfunction expansion as in (6). In place of (8), the relevant eigenvalue problem is

$$\epsilon\phi'' + x\phi' + \lambda\phi = 0\,, \qquad -1 < x < 1\,; \qquad \phi(\pm 1) = 0\,. \tag{43}$$

The solution ϕ to the differential equation with $\phi(1) = 0$ is proportional to

$$\phi(x) = e^{-x^2/4\epsilon}[D_{-\lambda}(ix/\sqrt{\epsilon})D_{\lambda-1}(-1/\sqrt{\epsilon}) - D_{\lambda-1}(-x/\sqrt{\epsilon})D_{-\lambda}(i/\sqrt{\epsilon})]\,. \tag{44}$$

By enforcing $\phi(-1) = 0$, we find that the eigenvalues λ must satisfy

$$D_{\lambda-1}(-1/\sqrt{\epsilon}) = D_{\lambda-1}(1/\sqrt{\epsilon})\frac{D_{-\lambda}(i/\sqrt{\epsilon})}{D_{-\lambda}(-i/\sqrt{\epsilon})}\,. \tag{45}$$

By using the asymptotic approximations (12), we reduce (45) when $\epsilon \to 0$ to

$$\frac{\epsilon^{\lambda-1}}{\Gamma(1-\lambda)} \sim -\sqrt{\frac{2}{\pi\epsilon}}e^{-1/2\epsilon}\,. \tag{46}$$

Thus, for $\epsilon \to 0$, the (increasing) eigenvalues λ_k satisfy

$$\lambda_k \sim k + 1 + O\left(\epsilon^{-k-1/2}e^{-1/2\epsilon}\right) \quad \text{for } \ k = 0, 1, 2, \ldots\,. \tag{47}$$

From (47) we see that the principal eigenvalue λ_0 for this modified problem is *not exponentially small.* Since λ_0 is positive and bounded away from zero, the solution to the modified problem (40)-(2)-(3) decays to the equilibrium shock-layer solution (41) on an $O(1)$ time scale. Thus, in contrast to the solution of (1)-(3), this convection-diffusion equation has a shock layer solution which does not exhibit dynamic metastability.

However, as was shown in [8], [10], and [16], metastable behavior can occur for certain *nonlinear* convection-diffusion equations with shock-layer solutions. To illustrate qualitatively how this can occur, consider Burgers equation

$$u_t \;=\; \epsilon u_{xx} - uu_x\,, \qquad -1 < x < 1\,, \quad t > 0 \tag{48}$$

with

$$u(-1,t) \;=\; 1\,, \qquad u(1,t) = -1\,, \qquad \text{and} \qquad u(x,0) = u_0(x)\,. \tag{49}$$

The unique equilibrium solution $U(x;\epsilon)$ for this problem is given asymptotically by $U(x;\epsilon) \sim -\tanh[x/2\epsilon]$ for $\epsilon \to 0$.

We shall determine the stability of this equilibrium solution by linearizing (48) about U. Substituting $u(x,t) = U(x;\epsilon) + \nu e^{-\lambda t}\Phi(x)$, where $\nu \ll 1$, into (48) and (49), we collect terms of $O(\nu)$ to find that Φ satisfies the eigenvalue problem

$$\epsilon\Phi_{xx} - (U\Phi)_x + \lambda\Phi = 0\,, \qquad -1 < x < 1\,; \qquad \Phi(\pm 1) = 0\,. \tag{50}$$

Equivalently, $\phi \equiv \exp[-\epsilon^{-1}\int_0^x U(s;\epsilon)ds]\Phi$ satisfies

$$\epsilon\phi_{xx} + U\phi_x + \lambda\phi = 0\,, \qquad -1 < x < 1\,; \qquad \phi(\pm 1) = 0\,. \tag{51}$$

Because U is monotonically decreasing in x and zero at the turning point $x = 0$, the nature of the turning point for (51) is very closely related to that for the eigenvalue problem (8), which has an exponentially small eigenvalue. In [8], it was shown that (51) has an asymptotically exponentially-small principal eigenvalue and an asymptotic formula for this eigenvalue was obtained in [10] and [16] to determine the limiting metastable behavior of the Burgers solution.

3 A More General Convection-Diffusion Equation

In the limit $\epsilon \to 0^+$, we now consider the following convection-diffusion equation for $u = u(x,t)$:

$$
\begin{aligned}
(52)\qquad u_t &= \epsilon u_{xx} - x^{2m+1} p(x) u_x + \epsilon^\nu g(x) e^{-a/\epsilon} u\,, \quad -1 < x < b\,, \quad t > 0\,,\\
(53)\qquad u(-1,t) &= \alpha\,, \qquad u(b,t) = \beta\,,\\
(54)\qquad u(x,0) &= u_0(x)\,.
\end{aligned}
$$

Here a and b are fixed positive constants, m is a non-negative integer, and α and β are constants with $u_0(-1) = \alpha$ and $u_0(b) = \beta$. In addition, $p(x) > 0$, $g(x)$, and $u_0(x)$ are smooth functions. Under these conditions, we again anticipate having boundary layer behavior at both endpoints. The final asymptotically negligible perturbation term on the right side of (52) is added to determine its effect on long-time behavior.

For $\epsilon \to 0$, a leading order boundary layer approximation for the equilibrium solution $U(x;\epsilon)$ corresponding to (52)-(53) has the form

$$
(55)\qquad U(x;\epsilon) \sim \tilde{u}^\epsilon[x; A_{0e}] \equiv A_{0e} + (\alpha - A_{0e})\, e^{-\xi_l (x+1)/\epsilon} + (\beta - A_{0e})\, e^{-\xi_r (b-x)/\epsilon}\,.
$$

Here the outer limit $A_{0e} = A_{0e}(\epsilon)$ is a constant to be determined and the decay constants are $\xi_l \equiv p(-1)$ and $\xi_r \equiv b^{2m+1} p(b)$. In the region away from the endpoint boundary layers, $L_\epsilon \tilde{u}^\epsilon \equiv \epsilon \tilde{u}^\epsilon_{xx} - x^{2m+1} p(x) \tilde{u}^\epsilon_x$ is asymptotically exponentially-small for any choice of A_{0e}. Thus, as for the simple problem of §2, A_{0e} can only be determined by somehow incorporating the effect of asymptotically exponentially-small terms into the analysis. Various methods to calculate A_{0e} are given in [7], [11], and [19].

The difficulty in determining A_{0e} using standard asymptotic methods results from the fact that the equilibrium problem is exponentially ill-conditioned as $\epsilon \to 0$ (see [5], [9], and [11]). More specifically, as shown in [11], the principal eigenvalue λ_0 for the eigenvalue problem

$$
(56)\qquad L_\epsilon \phi \equiv \epsilon \phi_{xx} - x^{2m+1} p(x) \phi_x = -\lambda \phi\,, \quad -1 < x < b\,; \qquad \phi(-1) = \phi(b) = 0
$$

is positive, but exponentially small as $\epsilon \to 0$ (see (76) below for the precise estimate). The corresponding (un-normalized) eigenfunction ϕ_0 is in the boundary layer form

$$
(57)\qquad \phi_0 \sim 1 + B_l[(1+x)/\epsilon;\epsilon]\, e^{-\xi_l (1+x)/\epsilon} + B_r[(b-x)/\epsilon;\epsilon]\, e^{-\xi_r (b-x)/\epsilon}\,,
$$

where $B_l(z;\epsilon)$ and $B_r(z;\epsilon)$ behave like polynomials in z. The exponentially small eigenvalue implies that the equilibrium solution for (52)-(54) will be very sensitive to the exponentially small perturbation term $\epsilon^\nu g(x) e^{-a/\epsilon} u$. Such sensitivity of the equilibrium solution to changes in either a or the endpoint location b was studied in [11], [18], [19], and [22].

Since $\lambda_0 > 0$, it follows that if a is sufficiently large, the equilibrium solution for (52) – (54) will remain asymptotically stable. However, because λ_0 is exponentially small, the approach to the equilibrium will occur over an asymptotically exponentially-long time scale. We shall study this slow motion asymptotically by using the projection method developed in [16] to treat related nonlinear problems. This method, which yields a higher order asymptotic theory than that given in §2.1, relies to a significant extent on the equilibrium theory of [11].

3.1 The Metastability Analysis

Following (28), we seek a solution to (52)-(54) in the form

$$u(x,t) = \tilde{u}^{\epsilon}[x; A(t;\epsilon)] + v(x,t)\,, \tag{58}$$

where $\tilde{u}^{\epsilon}$ is defined in (55). Using the projection method, we will, as in (39), derive a differential equation for A and obtain its steady-state limit A_e, provided a is large enough. For large values of t, the differential equation will capture the metastable dynamics of $u(x,t)$, since then $v \ll \tilde{u}^{\epsilon}$. The projection method differs somewhat from the method of §2.1 in that we exploit the occurrence of the exponentially small eigenvalue to directly enforce a limiting solvability condition on the correction term v, rather than explicitly obtaining an integral equation for v like (34).

Substituting (58) into (52)-(54), we obtain

$$\begin{aligned}
&(59) \quad & L_{\epsilon} v &= \tilde{u}^{\epsilon}_t + v_t - L_{\epsilon}\tilde{u}^{\epsilon} - \epsilon^{\nu} g(x) e^{-a/\epsilon}\left(\tilde{u}^{\epsilon} + v\right)\,, \quad -1 < x < b\,, \quad t > 0\,,\\
&(60) \quad & v(-1,t) &= \alpha - \tilde{u}^{\epsilon}[-1; A(t;\epsilon)]\,, \qquad v(b,t) = \beta - \tilde{u}^{\epsilon}[b; A(t;\epsilon)]\,,\\
&(61) \quad & v(x,0) &= u_0(x) - \tilde{u}^{\epsilon}[x; A(0;\epsilon)]\,.
\end{aligned}$$

Now let $\phi_k(x)$ and λ_k, for $k = 0, 1, \ldots$, be the normalized eigenfunctions and eigenvalues of (56). The λ_k are real and the ϕ_k satisfy the orthogonality relations

$$(\phi_j, \phi_k)_w \equiv \int_{-1}^{b} \phi_j \phi_k w\, dx = \delta_{jk} \qquad \text{for} \qquad w \equiv \exp[-\epsilon^{-1} \int_0^x t^{2m+1} p(t)\, dt]\,. \tag{62}$$

We then expand $v(x,t)$ in terms of the ϕ_k as

$$v(x,t) = \sum_{k=0}^{\infty} h_k(t;\epsilon)\phi_k(x)\,. \tag{63}$$

Substituting (63) into (59)-(61), orthogonality implies that the h_k will satisfy the differential equation

$$h_k' + \lambda_k h_k = -\epsilon w v \phi_{kx} \Big|_{-1}^{b} - \left(\phi_k, \tilde{u}^{\epsilon}_t\right)_w + \left(\phi_k, L_{\epsilon}\tilde{u}^{\epsilon}\right)_w + \epsilon^{\nu} e^{-a/\epsilon}\left(g\phi_k, \tilde{u}^{\epsilon} + v\right)_w\,, \tag{64}$$

together with the initial value

$$h_k(0;\epsilon) = \int_{-1}^{b} \left(u_0(x) - \tilde{u}^{\epsilon}[x; A(0;\epsilon)]\right) \phi_k w\, dx\,. \tag{65}$$

Since λ_0 is asymptotically exponentially small and the λ_k for $k \geq 1$ are bounded away from zero, to ensure that $v \ll \tilde{u}^{\epsilon}$ over exponentially-long time intervals requires $h_0(t) \equiv 0$. Thus, the right sides of (64) and (65) must vanish when $k = 0$. Then, using $v \ll \tilde{u}^{\epsilon}$ to simplify the last term on the right of (64), we obtain

$$\left(\phi_0, \tilde{u}^{\epsilon}_t\right)_w \sim -\epsilon w v \phi_{0x} \Big|_{-1}^{b} + \left(\phi_0, L_{\epsilon}\tilde{u}^{\epsilon}\right)_w + \epsilon^{\nu} e^{-a/\epsilon}\left(g\phi_0, \tilde{u}^{\epsilon}\right)_w \tag{66}$$

and

$$\int_{-1}^{b} \tilde{u}^{\epsilon}[x; A(0;\epsilon)]\phi_0 w\, dx = \int_{-1}^{b} u_0(x)\phi_0 w\, dx\,. \tag{67}$$

Equation (66) will provide a differential equation for A and (67) will determine its initial value.

To obtain an *explicit* differential equation for A, we evaluate the terms of (66), as in [11]. Upon integrating by parts, we can show that

$$(\phi_0, L_\epsilon \tilde{u}^\epsilon)_w \sim \epsilon\,(\alpha - A_0)\, w(-1)\phi_{0x}(-1) - \epsilon\,(\beta - A_0)\, w(b)\phi_{0x}(b)\,. \tag{68}$$

Since v is exponentially small at the endpoints, (68) dominates the first term on the right side of (66). From (56), the identity

$$-\lambda_0\,(1, \phi_0)_w = \epsilon w \phi_{0x}\Big|_{-1}^{b} \tag{69}$$

follows. Next, (55) implies

$$(\phi_0, \tilde{u}_t^\epsilon)_w \sim \frac{dA}{dt}\,(\phi_0, 1)_w \qquad \text{and} \qquad (g\phi_0, \tilde{u}^\epsilon)_w \sim A\,(g\phi_0, 1)_w\,. \tag{70}$$

Substituting (69) and (70) into (66) and neglecting the insignificant term yields

$$\frac{dA}{dt} \sim \left(-\lambda_0 + \epsilon^\nu e^{-a/\epsilon}\frac{(g\phi_0, 1)_w}{(\phi_0, 1)_w}\right) A + \frac{\epsilon}{(\phi_0, 1)_w}\left(\alpha w(-1)\phi_{0x}(-1) - \beta w(b)\phi_{0x}(b)\right)\,. \tag{71}$$

For convenience, we re-normalize ϕ_0 so $\phi_0(0) = 1$. Then, using a boundary layer analysis to calculate the terms B_l and B_r in (57), as in [11], we obtain

$$\phi_{0x}(b) \;=\; -\frac{1}{\epsilon}\xi_r\gamma_r(\epsilon) \quad \text{for} \quad \gamma_r(\epsilon) = 1 - \frac{\epsilon}{\xi_r}\left(\frac{p'(b)}{p(b)} + \frac{(2m+1)}{b}\right) + O(\epsilon^2)\,, \tag{72}$$

$$\phi_{0x}(-1) \;=\; \frac{1}{\epsilon}\xi_l\gamma_l(\epsilon) \quad \text{for} \quad \gamma_l(\epsilon) = 1 + \frac{\epsilon}{\xi_l}\left(\frac{p'(-1)}{p(-1)} - (2m+1)\right) + O(\epsilon^2)\,. \tag{73}$$

Higher-order coefficients in γ_l and γ_r can also be obtained. Next, since the difference $\phi_0 - 1$ is exponentially small near $x = 0$, we can calculate $(g\phi_0, 1)_w$ and $(\phi_0, 1)_w$ asymptotically by Laplace's method, as in [11]. This yields

$$(\phi_0, 1)_w \;=\; \epsilon^{1/(2m+2)}\theta_\epsilon \quad \text{for} \quad \theta_\epsilon = \frac{r^{1/(2m+2)}}{(m+1)}\Gamma\left(\frac{1}{2m+2}\right) + O(\epsilon^{1/(m+1)})\,, \tag{74}$$

$$(g\phi_0, 1)_w \;=\; \epsilon^{1/(2m+2)}g_\epsilon \quad \text{for} \quad g_\epsilon = \frac{r^{1/(2m+2)}}{(m+1)}g(0)\Gamma\left(\frac{1}{2m+2}\right) + O(\epsilon^{1/(m+1)})\,, \tag{75}$$

where $r \equiv 2(m+1)/p(0)$. Explicit formulas for some higher-order correction terms in θ_ϵ and g_ϵ are given in (3.9*b*) and (3.17*b*) of [11]. Substituting (71)–(73) into (69), we obtain the explicit asymptotic estimate

$$\lambda_0 \sim \epsilon^{-1/(2m+2)}\,\theta_\epsilon^{-1}\,[b^{2m+1}p(b)\gamma_r(\epsilon)e^{-\omega_r/\epsilon} + p(-1)\gamma_l(\epsilon)e^{-\omega_l/\epsilon}]\,, \tag{76}$$

where $\omega_l \equiv \int_0^{-1} t^{2m+1}p(t)\,dt$ and $\omega_r \equiv \int_0^b t^{2m+1}p(t)\,dt$.

Finally, by substituting (72)-(75) into (71), we obtain the explicit differential equation

$$\frac{dA}{dt} \sim \left(-\lambda_0 + \epsilon^\nu e^{-a/\epsilon}\frac{g_\epsilon}{\theta_\epsilon}\right) A + \frac{1}{\theta_\epsilon}\epsilon^{-1/(2m+2)}\left(\alpha\xi_l\gamma_l(\epsilon)e^{-\omega_l/\epsilon} + \beta\xi_r\gamma_r(\epsilon)e^{-\omega_r/\epsilon}\right)\,. \tag{77}$$

By using Laplace's method to evaluate (67), we obtain $A(0;\epsilon)\,(\phi_0, 1)_w \sim (\phi_0 u_0, 1)_w$, so

$$A(0;\epsilon) \sim \frac{1}{\theta_\epsilon}\epsilon^{-1/(2m+2)}\,(\phi_0 u_0, 1)_w\,. \tag{78}$$

TABLE 1

Comparison of numerical and asymptotic values for the principal eigenvalue for Example 1 at different values of ϵ.

ϵ	λ_0 (numerical)	λ_0 (1-term) (14)	λ_0 (2-term) (82)
0.100	0.15304×10^{-1}	0.17001×10^{-1}	0.15301×10^{-1}
0.075	0.33891×10^{-2}	0.37078×10^{-2}	0.34297×10^{-2}
0.050	0.15280×10^{-3}	0.16200×10^{-3}	0.15390×10^{-3}
0.025	0.10126×10^{-7}	0.10401×10^{-7}	0.10141×10^{-7}
0.020	0.76709×10^{-10}	0.78354×10^{-10}	0.76787×10^{-10}
0.0175	0.227×10^{-11}	0.23551×10^{-11}	0.23139×10^{-11}

The asymptotic evaluation of the integral $(\phi_0 u_0, 1)_w$ results from replacing $g(x)$ with $u_0(x)$ in (75). To leading order, we have $A(0;\epsilon) = u_0(0) + O(\epsilon^{1/(m+1)})$. Higher-order correction terms for $A(0;\epsilon)$ are obtained explicitly in §4 for a specific example.

In summary, the main result of this section is an explicit asymptotic description of the metastable dynamics for (52)-(54), valid away from an initial time layer, namely

$$(79)\quad u(x,t) \sim \tilde{u}^\epsilon[x; A(t;\epsilon)] \equiv A(t;\epsilon) + [\alpha - A(t;\epsilon)]e^{-\xi_l(x+1)/\epsilon} + [\beta - A(t;\epsilon)]e^{-\xi_r(b-x)/\epsilon}$$

where A satisfies (77) and the initial value (78). If a is large enough, it is clear from (77) that $A(t;\epsilon)$ tends to its equilibrium value A_e, which is defined by setting the right side of (77) to zero. This equilibrium result was obtained in [11].

4 Some Examples of the Theory

Example 1: Consider the perturbed problem

$$(80)\qquad u_t = \epsilon u_{xx} - x u_x + s\sqrt{\frac{2}{\pi\epsilon}}\left(1 + x^2 + x^4\right) e^{-1/2\epsilon} u\,, \qquad -1 < x < 1\,,$$

$$(81)\qquad u(-1,t) = 2\,, \qquad u(1,t) = 1/2\,, \qquad u(x,0) = 1/2 + 3(x-1)^2/8\,,$$

where s is a constant.

We first obtain a high order estimate for the principal eigenvalue λ_0 of (56). Since $p(x) = 1$, $m = 0$ and $b = 1$ in (56), (72)-(74) imply that $\gamma_l(\epsilon) = \gamma_r(\epsilon) = 1 - \epsilon + O(\epsilon^2)$ and $\theta_\epsilon = \sqrt{2\pi} + o(\epsilon^k)$ for any $k > 0$. Thus, (76) yields the estimate:

$$(82)\qquad \lambda_0 = \sqrt{\frac{2}{\pi\epsilon}}\,[1 - \epsilon + O(\epsilon^2)]\, e^{-1/2\epsilon}\,.$$

Here we give two terms in the pre-exponential factor rather than only one term, as in (14). To compare with this asymptotic result, we compute λ_0 numerically for various values of ϵ using the boundary value solver COLSYS [3]. From Table 1, it is clear that the two-term result (82) provides a significantly better determination of λ_0 than the one-term result.

Now let $s = 0$ in (80) so the asymptotically negligible term is dropped. Then, the equation (77) for $A(t;\epsilon)$ reduces to $dA/dt \sim -\lambda_0(A - 5/4)$. Substituting $u_0(x)$ into (78) and evaluating the resulting integral asymptotically gives the two-term expansion $A(0;\epsilon) \sim 7/8 + 3\epsilon/8$ for the initial condition. Thus, for $t > 0$

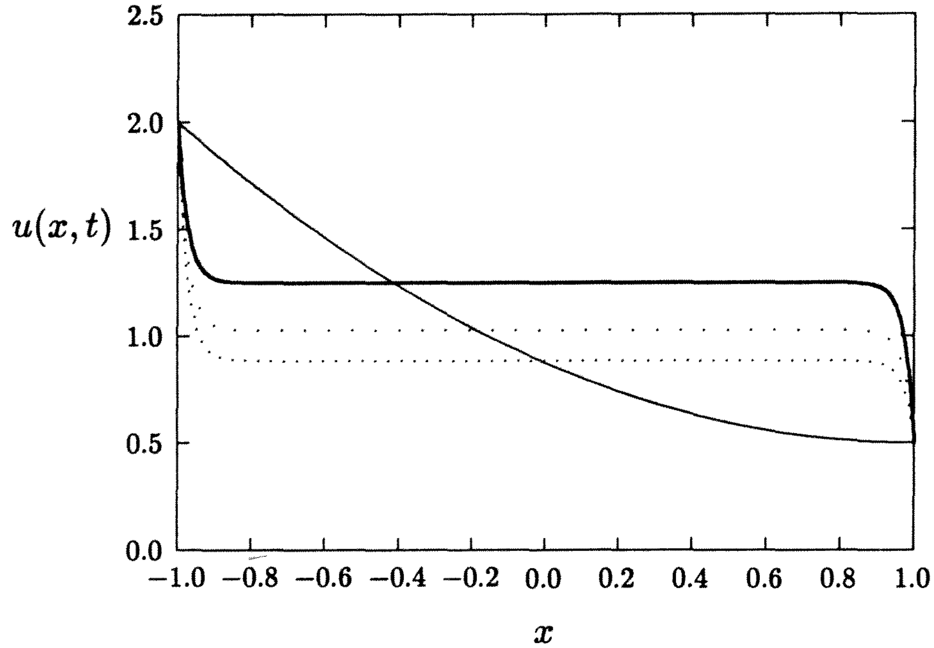

FIG. 1. *Plot of $u(x,t)$ versus x for Example 1 at the four different times, $t_0 = 0.0$ (light solid curve), $t_1 = 20.2$ (closely spaced dots), $t_2 = 4.90 \times 10^8$ (widely spaced dots) and $t_3 = 8.64 \times 10^9$ (heavy solid line). The parameter values are $s = 0$ and $\epsilon = 0.025$.*

$$A(t;\epsilon) \sim 5/4 - \frac{3}{8}(1-\epsilon)\, e^{-\lambda_0 t}. \tag{83}$$

To compare with (83), we use the routine D03PAF of the NAG software library to numerically compute the solution $u(x,t)$ to (80)-(81) when $s = 0$. From this numerical solution attains, we output the value of $u(0,t)$, which gives the numerical prediction for $A(t;\epsilon)$. In Fig. 1 we plot the numerical solution $u(x,t)$ versus x at different times for the moderately small $\epsilon = 0.025$. Notice that the numerical solution the boundary layer form predicted by (79). In Fig. 2, we plot $\log_{10}(t)$ versus A for the asymptotic result (83) and the numerically-computed result. The two curves are virtually indistinguishable and $A(t;\epsilon)$ remains constant over a time interval $t \approx 10^7$.

Now suppose that $s \neq 0$ in (80). Then, from (72)-(77), $A(t;\epsilon)$ satisfies

$$\frac{dA}{dt} \sim \lambda_0\,(5/4 - A) + s\sqrt{\frac{2}{\pi\epsilon}}\, e^{-1/2\epsilon}\,(1+\epsilon)\,A. \tag{84}$$

Note that when s is a constant independent of ϵ, the perturbing term in (84) has the same asymptotic order as λ_0 when $\epsilon \to 0$. The initial condition for (84) is $A(0;\epsilon) \sim 7/8 + 3\epsilon/8$ and the equilibrium value A_e for A, obtained by setting dA/dt to zero, is

$$A_e = \frac{5}{4}\left(\frac{1-\epsilon}{(1-s) - \epsilon(s+1)}\right). \tag{85}$$

This result clearly shows the *super-sensitivity* of the equilibrium solution to the asymptotically exponentially small term in (80) since by varying s on the range $0 < s < 1$, A_e changes

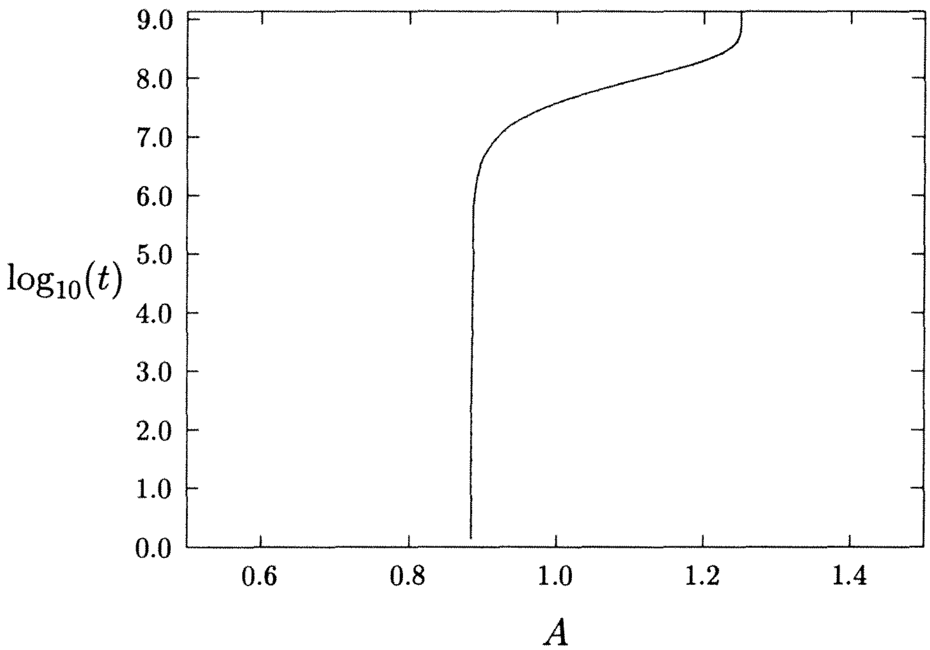

FIG. 2. *Plots of* $\log_{10}(t)$ *versus* A *for Example 1 from the full numerical solution (solid line) and from the asymptotic approximation (dotted line) when* $s = 0$ *and* $\epsilon = 0.025$.

by $O(1)$. In Fig. 3, we show the very close agreement between the asymptotic result (84) for $A(t;\epsilon)$ and the corresponding numerically-computed result when $s = 0.5$ and $\epsilon = 0.025$. For these parameter values, $A_e \approx 2.635$.

Example 2: Next, consider the perturbed problem

$$u_t = \epsilon u_{xx} - x^3 u_x + s\epsilon^{-1/4}\left(1 + x^2 + x^4\right) e^{-1/4\epsilon} u\,, \qquad -1 < x < b\,, \tag{86}$$

$$u(-1,t) = 2\,, \qquad u(b,t) = \frac{1}{2}\,, \qquad u(x,0) = \frac{1}{2} + \frac{3}{2}\left(\frac{x-b}{1+b}\right)^2, \tag{87}$$

where $b > 0$ and s is a constant. The main difference between this and the previous example is that we now have a higher-order turning point and the interval is $-1 < x < b$.

We first obtain a higher-order estimate for λ_0. From (72)-(74), $\gamma_l(\epsilon) \sim 1 - 3\epsilon$, $\gamma_r(\epsilon) \sim 1 - 3\epsilon/b^4$, and $\theta_\epsilon = \Gamma(1/4)/\sqrt{2} + o(\epsilon^k)$ for any $k > 0$. Thus, from (76),

$$\lambda_0 \sim \left(\frac{1}{4\epsilon}\right)^{1/4} \frac{2}{\Gamma(1/4)}\left[b^3\left(1 - 3\epsilon/b^4\right) e^{-b^4/4\epsilon} + (1 - 3\epsilon)\, e^{-1/4\epsilon}\right]. \tag{88}$$

For this example, (72)-(77) imply the differential equation

$$\begin{aligned}\frac{dA}{dt} \sim\ & \left[-\lambda_0 + s\epsilon^{-1/4}\left(1 + 2\epsilon^{1/2}\Gamma(3/4)/\Gamma(1/4)\right) e^{-1/4\epsilon}\right] \\ & + \left(\frac{1}{4\epsilon}\right)^{1/4} \frac{2}{\Gamma(1/4)}\left[\frac{b^3}{2}\left(1 - 3\epsilon/b^4\right) e^{-b^4/4\epsilon} + 2\,(1 - 3\epsilon)\, e^{-1/4\epsilon}\right].\end{aligned} \tag{89}$$

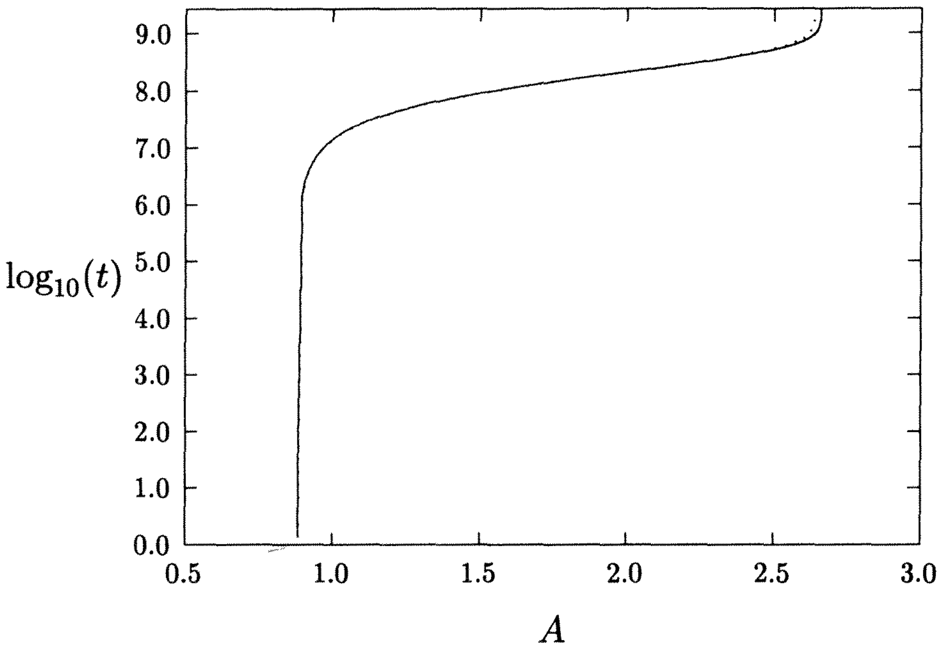

FIG. 3. *Plots of* $\log_{10}(t)$ *versus* A *for Example 1 from the full numerical solution (solid line) and from the asymptotic approximation (dotted line) when* $s = 0.5$ *and* $\epsilon = 0.025$.

From (78), the initial condition is

$$A(0;\epsilon) \sim \frac{1}{2}\left[1 + 3\frac{b^2}{(1+b)^2}\right] + \frac{3\epsilon^{1/2}}{(1+b)^2}\frac{\Gamma(3/4)}{\Gamma(1/4)} \tag{90}$$

when $\epsilon \to 0$. Comparing (89) with corresponding numerical results yields similar agreement as for Example 1.

Finally, we illustrate the *super-sensitivity* of the solution with respect to changes in the endpoint location b, by determining the equilibrium value A_e when $b > 1$ and $b = 1$. A simple calculation shows that

$$A_e = \frac{5}{4}\left(1 - \frac{s\sqrt{2}\mu\,\Gamma(1/4)}{4(1-3\epsilon)}\right)^{-1} \quad \text{for} \quad b = 1, \tag{91}$$

$$A_e = 2\left(1 - \frac{s\sqrt{2}\mu\,\Gamma(1/4)}{2(1-3\epsilon)}\right)^{-1} \quad \text{for} \quad b > 1, \tag{92}$$

with $\mu \equiv 1 + 2\epsilon^{1/2}\Gamma(3/4)/\Gamma(1/4)$. From (89) it is clear that A_e varies by an $O(1)$ amount as b is varied in an $O(\epsilon)$ region near $b = 1$.

References

[1] R. C. Ackerberg and R. E. O'Malley, Jr., *Boundary layer problems exhibiting resonance*, Studies in Applied Math. 49, (1970), pp. 277–295.

[2] N. D. Alikakos, G. Fusco, and V. Stefanopoulis, *Critical spectrum and stability of interfaces for a class of reaction-diffusion equations*, J. Differential Equations, to appear.

[3] U. Ascher, R. Christiansen, and R. Russell, *Collocation software for boundary value ODE's*, Math. Comp. 33, (1979), pp. 659–679.

[4] J. Carr and R. Pego, *Metastable patterns in solutions of $u_t = \epsilon^2 u_{xx} - f(u)$*, Comm. Pure Appl. Math. 42, (1989), pp. 523–576.

[5] P. P. N. deGroen, *The nature of resonance in a singular perturbation problem of turning point type*, SIAM J. Math. Anal. 11, (1980), pp. 1–22.

[6] P. P. N. deGroen, *Exponentially slow decay in parabolic turning point problems*, (1995), personal communication.

[7] J. Grasman and B.J. Matkowsky, *A variational approach to singularly perturbed boundary value problems for ordinary and partial differential equations with turning points*, SIAM J. Appl. Math. 32, (1977), pp. 588–597.

[8] G. Kreiss and H.-O. Kreiss, *Convergence to steady state of solutions of Burgers' equation*, Appl. Numer. Math. 2, (1986), pp. 161–179.

[9] H.-O. Kreiss, *Resonance for singular perturbation problems*, SIAM J. Appl. Math. 41, (1981), pp. 331–344.

[10] J. G. L. Laforgue and R. E. O'Malley, Jr. *Shock layer movement for Burgers' equation*, SIAM J. Appl. Math. 55, (1995), pp. 332–347.

[11] J.-Y. Lee and M. J. Ward, *On the asymptotic and numerical analyses of exponentially ill-conditioned singularly perturbed boundary value problems*, Studies in Applied Math. 94, (1995), pp. 271–326.

[12] D. Ludwig, *Persistence of dynamical systems under random perturbations*, SIAM Review 17, (1975), pp. 605–640.

[13] R. S. Maier and D. L. Stein, *Asymptotic exit location distributions in the stochastic exit problem*, to appear.

[14] B. J. Matkowsky, *On boundary layer problems exhibiting resonance*, SIAM Review 17, (1975), pp. 82–100.

[15] B. J. Matkowsky, *Singular perturbations, stochastic differential equations, and applications,* in 'Singular Perturbations and Asymptotics' (R.E. Meyer and S.V. Parter, editors), Academic Press, New York, (1980), pp. 109–147.

[16] L. G. Reyna and M. J. Ward, *On the exponentially slow motion of a viscous shock*, Comm. Pure Appl. Math. 48, (1995), pp. 79–120.

[17] Z. Schuss, *Singular perturbation methods in stochastic differential equations of mathematical physics*, *SIAM Review* 22, (1980), pp. 119–155.

[18] L. A. Skinner, *Uniform solutions of boundary value problems exhibiting resonance*, SIAM J. Appl. Math. 47, (1987), pp. 225–231.

[19] R. Srinivasan, *A variational principle for the Ackerberg-O'Malley resonance problem*, Studies in Applied Math. 79, (1988), pp. 271–289.

[20] W. Wasow, *Linear Turning Point Theory*, Springer-Verlag, New York, (1984).

[21] E. T. Whittaker and G. N. Watson, *A Course of Modern Analysis*, Cambridge University Press, London, (1952).

[22] M. Williams, *Another look at Ackerberg-O'Malley resonance*, SIAM J. Appl. Math. 41, (1981), pp. 288–293.

[23] R. Wong, *Asymptotic Approximation of Integrals*, Academic Press, San Diego, (1989).

Hodograph Design in Transonic Flow*

Donald W. Schwendeman[†]

Abstract

The use of hodograph methods to design airfoils and axisymmetric bodies in steady, transonic flow is discussed. For planar flow, hodograph methods are used to construct nonlifting and lifting airfoils with high critical free-stream Mach numbers. In the nonlifting case, boundary-value problems are formulated in the hodograph whose solutions lead to airfoils that possess the highest free-stream Mach number for a given set of geometrical constraints such that the flow is nowhere supersonic. These optimal critical airfoils possess long arcs of sonic velocity. For the lifting case, boundary-value problems are formulated in the hodograph whose solutions lead to lifting airfoils with long arcs of sonic velocity and thus high critical free-stream Mach numbers. Numerical methods are used to solve the various boundary-value problems and several example airfoils are presented.

For axisymmetric flow, we use a hodograph method to design a body of revolution that possesses a flow at a particular free-stream Mach number that has a supersonic region adjacent to the body and is free of shocks. The design problem is formulated using transonic small-disturbance theory. The boundary-value problem is mapped to the hodograph plane and relevant the partial differential equations are solved using a finite difference scheme. A method of iteration is used to adjust the boundary data to obtain a solution whose Jacobian is of one sign and thus represents a smooth, shock-free flow in the physical plane. Several example bodies are calculated. A method of calculation in the physical plane is used to study the shock formation at off-design conditions.

1 Introduction

The use of hodograph methods to study compressible flows has been around since the turn of the century. Some of the earliest work dates back to Chaplygin [8] and notable contributions have been made by Tollmien [36], Ringleb [32], von Karman [19], Tsien [37], Lighthill *et al.* [14, 22, 23], Cherry [5, 6, 7], and Nieuwland [28], among others. The book by von Mises [27] summaries much of this work and provides more references. The thrust of these investigations was to obtain analytical representations for compressible fluid flows, the hodograph transformation being attractive because for planar flow the governing equations become linear.

With the recent availability of high-speed computers and reliable numerical methods for the calculation of compressible fluid flows, analytical investigations using hodograph methods have diminished. There remains, however, some notable exceptions in which hodograph methods in conjunction with numerical methods provide an effective tool to

*This work was supported by the National Science Foundation and the Air Force Office of Scientific Research.

[†]Department of Mathematical Sciences, Rensselaer Polytechnic Institute, Troy, NY 12180.

study specific problems in theoretical aerodynamics. Two such problems, the hodograph design of optimal critical airfoils and the hodograph design of shock-free slender bodies, will be discussed in this article. The common theme in these two problems is that the hodograph transformation gives a useful framework in which to formulate the relevant boundary-value problems and solve the equations numerically.

In an interesting paper, Gilbarg and Shiffman [13] studied a special class of optimal airfoils. They proved a comparison theorem and then used it to construct a family of nonlifting airfoil shapes whose critical free-stream Mach number is the highest amongst all other airfoils with the same thickness ratio (or area) and tail angle. These optimal critical airfoils consisted of straight segments at the nose and tail connected by an arc on which the flow velocity is exactly sonic. (See Figure 1.) The flow is similar to the incompressible cavity flow studied by Riabouchinsky [31]. A boundary-value problem can be posed in the hodograph plane whose solution leads to an optimal critical airfoil shape for a given free-stream Mach number. This boundary-value problem appeared in [13] but no solutions were worked out.

Numerical solutions of the hodograph boundary-value problem were reported by Fisher [12] and analytical and numerical results for this problem were obtained by Schwendeman *et al.* [34]. In the latter work, an exact solution of the boundary-value problem was found in transonic small-disturbance theory (TSDT) and its corresponding optimal airfoil shape was given. Solutions within the full inviscid theory were found numerically and the performance of the optimal critical airfoils were compared with some standard airfoils. A significant improvement in the critical free-stream Mach number was reported.

For lifting airfoils, Gilbarg and Shiffman's comparison theorem does not apply. A conjecture is that a critical airfoil is optimal if it has the longest possible arc of sonic velocity. Using this conjecture, a hodograph boundary-value problem was formulate in Kropinski *et al.* [20] whose solution gives a lifting critical airfoil with long arcs of sonic velocity. The boundary-value problem was formulated on two Riemann sheets in the TSDT hodograph plane and solutions were found numerically for various choices of the parameters. The recent work by Kropinski [21] considered the boundary-value problem in the full inviscid theory. In both [20] and [21], comparisons were made with some standard lifting airfoils and good performance was found.

The discussion in §2 outlines some of the earlier results for nonlifting airfoils and discusses some of the recent results for lifting airfoils. Much of the work here follows that in [34], [20], and [21] and more detailed discussions can be found there.

The hodograph design of shock-free slender bodies is considered in §3. The main problem is to design a body shape that possesses a smooth, shock-free supercritical flow for a given free-stream Mach number. The first shock-free design was reported in Cole and Schwendeman [11]. In this paper, the TSDT hodograph was used to construct a shock-free flow about a slender body of revolution with fore-aft symmetry for a given value of the transonic similarity parameter $K = (1 - M_\infty^2)/\delta^2$, where δ is the thickness ratio of the body and M_∞ is the free-stream Mach number. The extension to slender bodies without fore-aft symmetry was considered by Buckmire [4]. In the hodograph, a boundary-value problem is formulated and a solution is sought whose Jacobian is of one sign everywhere so that the hodograph solution maps to a smooth flow in the physical plane. Solutions to the boundary-value problem are found numerically and a method of iteration is used to obtain shock-free flows.

The transonic area rule discussed in Cole and Cook [9] states that the flow about a body with a given distribution of cross-sectional area is related to the flow about a body of revolution with the same distribution. Thus, the work in [11] and [4] on shock-free bodies of revolution has a wider applicability.

Investigations of shock-free (supercritical) flows prior to the work in Cole and Schwendeman [11] and Buckmire [4] on axisymmetric flows considered planar flows. The first theoretical investigation was carried out by Ringleb [32] who constructed a shock-free nozzle flow. Experimental work by Pearcey [30] and by Whitcomb and Clark [38] confirmed the existence of the shock-free flows. In a series of articles, Bauer, Garabedian, and Korn [1, 2, 3] presented several shock-free airfoils obtained using a method of calculation in the hodograph plane. Their work was motivated in part by the earlier work of Nieuwland [28]. The airfoils designed by Bauer, Garabedian, and Korn were tested experimentally by Kacprzynski *et al.* [16, 17, 18] and found to possess shock-free flows (after some slight adjustment of the airfoil shapes presumably to account for wind tunnel-wall effects).

The local existence of shock-free planar flows was studied by Morawetz [24, 25, 26]. A mathematical argument was presented that suggests that a shock-free flow about an airfoil would be isolated in that the flow about a perturbed airfoil shape would possess a shock. This is an interesting result but it does not provide a complete description of the flow at off-design conditions nor does it indicate whether the flow about a shock-free airfoil would possess a shock at a perturbed free-stream Mach number. A method of calculation in the TSDT physical plane was used by Buckmire [4] to investigate the off-design flow about shock-free slender bodies. It was found that at most a weak shock formed when the value of K was perturbed indicating that the designed bodies possess a range of free-stream Mach numbers where good performance can be expected.

2 Hodograph design of optimal critical airfoils

The first portion of this section discusses the hodograph formulation and analytical and numerical results for nonlifting airfoils based on the Gilbarg and Shiffman construction. This provides useful background for the extension to the lifting case which is considered in the latter portion of this section.

2.1 Nonlifting airfoils

For the nonlifting case, the optimal critical airfoil deduced by Gilbarg and Shiffman consists of a flat vertical segment at the nose along which the flow accelerates from stagnation to sonic, a sonic arc, and a tail segment inclined at an angle θ_T from the axis of symmetry along which the flow decelerates from sonic to stagnation. The whole flow being nowhere supersonic means that the flow over the upper surface of the airfoil can be mapped to the wedge $0 \le q \le c_*$, $-\theta_T \le \theta \le \pi/2$ in the hodograph (q, θ), where q is the flow speed (made nondimensional with the limit speed), $c_* = \sqrt{(\gamma-1)/(\gamma+1)}$ is sonic speed, and θ is the flow deflection angle. (The flow under the lower surface is found by symmetry.) The optimal airfoil and the mapping of the flow about it are shown in Figure 1. The free stream maps to a square-root singularity at $(U, 0)$ in the hodograph, where U is the free-stream speed.

A boundary-value problem corresponding to the flow about an optimal critical airfoil can be formulated in the hodograph for the stream function $\psi(q, \theta)$. The equation governing the flow is Chaplygin's equation

(1) $$\left(\frac{q}{\rho}\psi_q\right)_q + \frac{1}{\rho q}\left(1 - \frac{q^2}{c^2}\right)\psi_{\theta\theta} = 0,$$

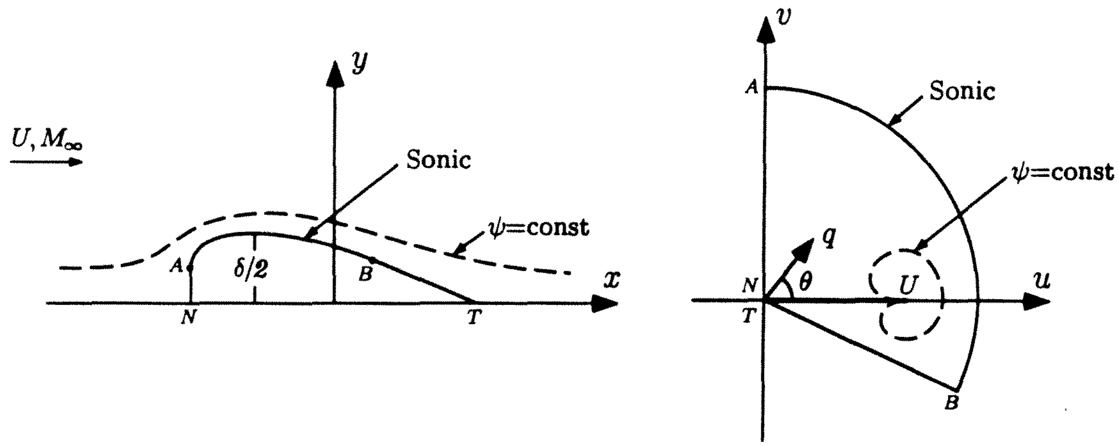

FIG. 1. *Optimal nonlifting airfoil and the mapping of the flow about it to the hodograph plane.*

where ρ and c are the (dimensionless) density and sound speed, respectively, given by

$$\rho = (1-q^2)^{1/(\gamma-1)} \qquad \text{and} \qquad c^2 = \frac{\gamma-1}{2}(1-q^2).$$

Chaplygin's equation is to be solved with $\psi = 0$ on the boundary of the wedge, which corresponds to the airfoil surface, and

$$\psi \sim \operatorname{Im}\left(\frac{1}{\sqrt{U - \hat{q}\exp(-i\hat{\theta})}}\right), \qquad \hat{q}\exp(-i\hat{\theta}) = q\cos\theta - \frac{iq\sin\theta}{\sqrt{1-M_\infty^2}},$$

near the free stream, where $(\hat{q}, \hat{\theta})$ are the flow speed and deflection with a Prandtl-Glauert correction. Once the solution is found, the position $z = x + iy$ of the airfoil surface is obtained from ψ by integrating the differential forms

$$z_q = \frac{ie^{i\theta}}{\rho q^2}\left[q\psi_q + i\left(1 - \frac{q^2}{c^2}\right)\psi_\theta\right], \qquad z_\theta = \frac{e^{i\theta}}{\rho q}[q\psi_q + i\psi_\theta] \tag{2}$$

around the boundary of the wedge in the hodograph.

The boundary-value problem for $\psi(q,\theta)$ requires a numerical solution. A second-order accurate finite difference formulation is discussed in [34]. For a given M_∞ and θ_T a numerical solution is found and a numerical integration of the differential forms in (2) around the boundary in the hodograph leads to an optimal airfoil shape and value for δ. Figure 2 shows the behavior of δ for varying M_∞ and θ_T (solid curves). The data points in Figure 2 give the critical conditions for some NACA00-series airfoils and Karman-Trefftz airfoils. This data is obtained from a numerical calculation of these airfoils in the physical plane. It is noted that the optimal critical airfoils show a significant increase in M_∞ for the same δ and θ_T. Representative optimal critical airfoil shapes are shown in Figure 3.

The hodograph boundary-value problem can be considered in TSDT ($M_\infty \to 1$, $\delta \to 0$) and it is interesting to note that there is an exact solution to the equations for the case corresponding to $\theta_T = \pi/2$. In TSDT, (1) reduces to Tricomi's equation

$$w\tilde{y}_{\vartheta\vartheta} - \tilde{y}_{ww} = 0, \tag{3}$$

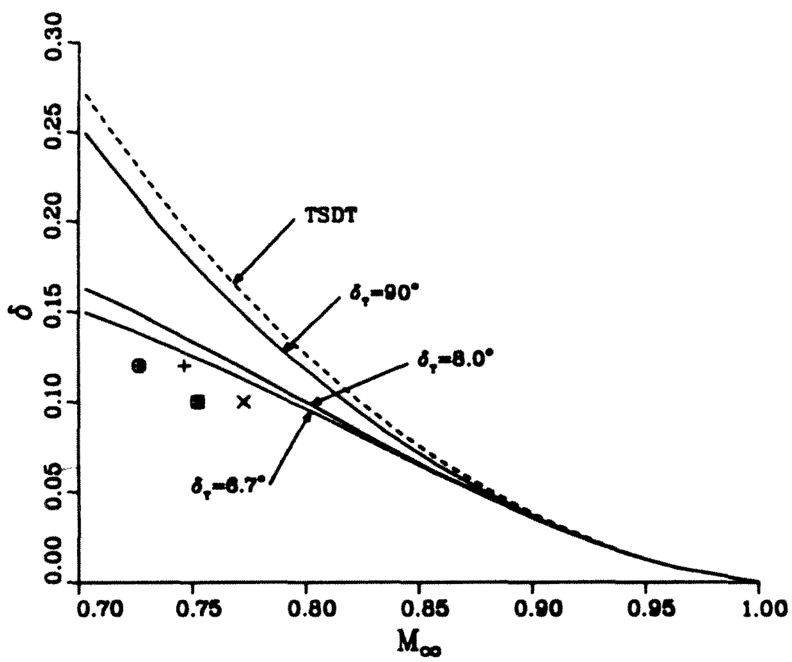

FIG. 2. *Thickness versus critical Mach number for various airfoils. Solid curves are from optimal critical airfoils with various θ_T and the dashed curve is from the TSDT optimal critical airfoil. Marks indicate critical conditions for + Karman-Trefftz with $\theta_T = 8.0°$, $\oplus$ NACA0012, $\times$ Karman-Trefftz with $\theta_T = 6.7°$, $\otimes$ NACA0010.*

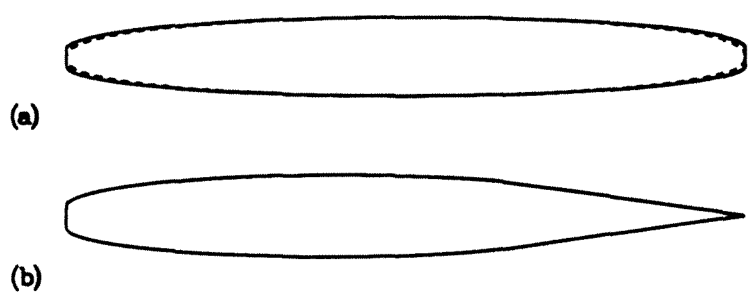

FIG. 3. *Optimal critical airfoil shapes: (a) $M_\infty = .802$, $\delta = .116$, $\theta_T = 90°$ (dashed curve is the corresponding TSDT shape); (b) $M_\infty = .768$, $\delta = .122$, $\theta_T = 8°$.*

where w is a scaled perturbation from sonic and ϑ is a scaled flow deflection (cf. [9] and [34]). The streamlines ψ = constant reduce to $\tilde{y}$ = constant, where $\tilde{y} = \delta^{1/3} M_\infty^{2/3} y$. The sonic line $w = 0$ becomes the whole airfoil surface and the flow about it maps to the half plane $w < 0$. The free stream maps to $w = -K$, where $K = (1 - M_\infty^2) M_\infty^{-4/3} \delta^{-2/3}$ is the transonic similarity parameter.

A solution to (3) can be found that has $\tilde{y} = 0$ on $w = 0$ and the correct singular behavior at $w = -K$:

$$\tilde{y} = A\sqrt{\frac{\pi}{2}} \tau_\infty^{5/6} \tau^{1/3} \int_0^\infty e^{-\lambda\vartheta} J_{1/3}(\lambda\tau) J_{5/6}(\lambda\tau_\infty) \lambda^{1/2}\, d\lambda, \qquad \tau = \frac{2}{3}(-w)^{3/2}, \qquad \vartheta > 0,$$

where $\tau_\infty = (2/3)K^{3/2}$ and $J_{1/3}$ and $J_{5/6}$ are Bessel functions. This integral was also used by Helliwell and Mackie [15] to study the flow past a pointed airfoil with a sonic arc. A reduced form of (2) determines x corresponding to the solution for $\tilde{y}$, and the constant A can be chosen to make the length of the airfoil equal to one. If the airfoil shape is given by $y = \delta F(x)$, $-1/2 \le x \le 1/2$, then the normalization $\max F = 1/2$ determines a value for K (cf. [34]). It is found that

$$K = \left(\frac{3}{2}\tau_\infty\right)^{2/3} = \left(\sqrt{\pi}\,\frac{\gamma+1}{2}\,\frac{\Gamma(5/6)}{\Gamma(4/3)}\right)^{2/3} = 1.934, \qquad \text{for } \gamma = 1.4.$$

This value determines a relationship between M_∞ and δ for optimal critical airfoils in the limit $M_\infty \to 1$, $\delta \to 0$ and this is the dashed curve in Figure 2. The corresponding airfoil shape is given parametrically by

$$\left.\begin{array}{rcl} F(\vartheta^*) &=& \dfrac{1}{2}\dfrac{1}{(1+\vartheta^{*2})^{1/3}} \\ x(\vartheta^*) &=& -\dfrac{1}{\sqrt{\pi}}\dfrac{\Gamma(4/3)}{\Gamma(5/6)}\displaystyle\int_0^{\vartheta^*} \frac{d\vartheta}{(1+\vartheta^2)^{4/3}} \end{array}\right\} \qquad -\infty < \vartheta^* = \frac{\vartheta}{\tau_\infty} < \infty,$$

and this is the dashed airfoil shape in Figure 3(a).

It is noted in [34] that near the nose of the TSDT airfoil shape $F \sim \vartheta^{*-2/3}$ and $x + 1/2 \sim \vartheta^{*-5/3}$ so that

$$F(x) \sim \left(x + \frac{1}{2}\right)^{2/5} \qquad \text{as } x \to -\frac{1}{2}.$$

The behavior of F near the nose is the same as that of the sonic half-body investigated first by Nonweiler[29] and more recently by Rusak[33].

2.2 Lifting airfoils

The flow about a lifting airfoil with small circulation maps to two Riemann sheets in the hodograph plane that are connected across a branch cut. The free stream singularity is dominated by a dipole at $(U, 0)$ on one of the sheets. A branch point with a square-root behavior lies close to the free-stream singularity. A qualitative picture of the mapping is shown in Figure 4. A streamline on which $\psi = 0$ emerges from the free stream at $(U, 0)$ on the lower sheet. It crosses the branch cut and moves to the stagnation point at N. From the nose, the flow accelerates to sonic along the arc from N to A. The sonic arc along the upper surface of the airfoil maps to the sonic circle between points A and C, and the branch cut is crossed again at B. The flow decelerates along the straight path from C to

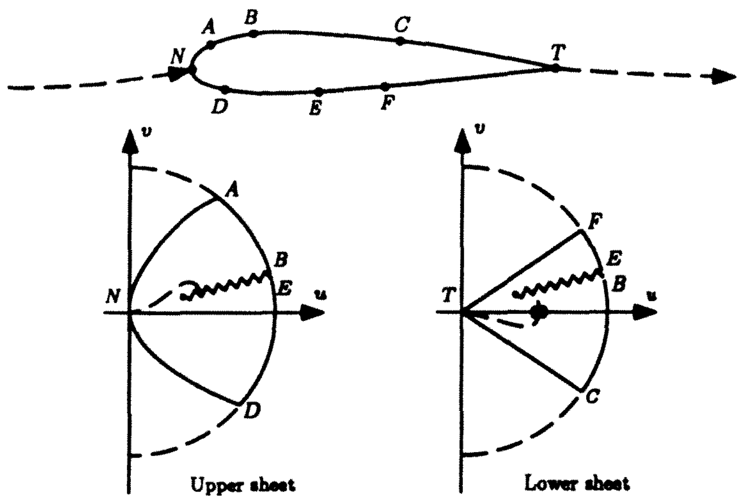

FIG. 4. *Hodograph mapping of a lifting critical airfoil with long sonic arcs.*

T, and then returns to the free stream. The mapping of the lower surface of the airfoil is similar.

A boundary-value problem in the hodograph for the calculation of a lifting critical airfoil consists of (1) subject to $\psi = 0$ on the boundary in Figure 4 and subject to a prescribed singular behavior near the free stream and branch point.

The singular behavior of ψ near the free stream and branch point is determined by an asymptotic analysis of the flow in the far field of the physical plane. At a far distance, the airfoil reduces to a dipole and a point vortex in a uniform stream governed by the complex potential

$$\Phi = U\hat{z} + \frac{D}{2\pi\hat{z}} + \frac{i\Gamma}{2\pi}\log\hat{z}, \qquad \hat{z} = x + i\beta y, \qquad \beta = \sqrt{1 - M_\infty^2}, \tag{4}$$

where D is the complex dipole strength, Γ is the circulation, and $\hat{z}$ includes a Prandtl-Glauert correction factor. The real part of D is related to the area of the airfoil and the imaginary part is related to the pitching moment of the airfoil (cf. [20]). A complex velocity $\hat{w} = \hat{w}(\hat{z})$ can be calculated from (4) and then inverted to give

$$\hat{z} = \frac{i\Gamma}{4\pi U}\frac{1}{\hat{w} - 1}\left(1 \pm \left|\frac{\hat{w} - \hat{w}_b}{1 - \hat{w}_b}\right|^{1/2} e^{i(\hat{\theta} - \hat{\theta}_b)/2}\right), \qquad \hat{w} = \frac{1}{U}\left(u - i\frac{v}{\beta}\right), \tag{5}$$

where $\hat{\theta} = \arg(\hat{w} - \hat{w}_b)$, $\hat{\theta}_b = \arg(1 - \hat{w}_b) = -\arg D$, and where

$$\hat{w}_b = 1 - \frac{\Gamma^2}{8\pi U D}$$

gives the location of the branch point in the hodograph plane. The plus sign in (5) is taken for the upper sheet and the minus sign for the lower sheet. The free-stream singularity at $\hat{w} = 1$ sits on one of the sheets depending on the sign of the imaginary part of D, and the

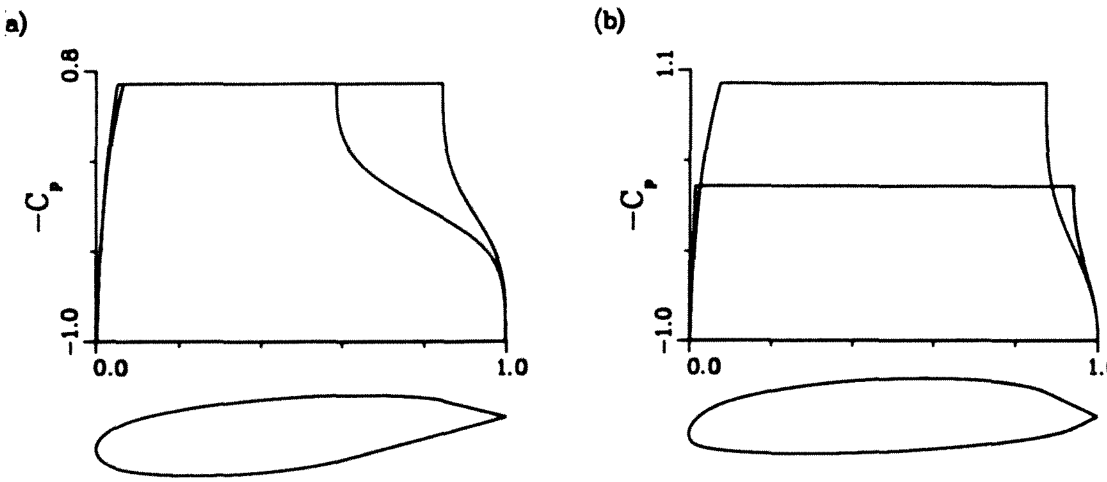

FIG. 5. *Lifting airfoils with long sonic arcs: (a)* $M_\infty = .716$, $A = .130$, $C_l = .199$; *(b)* $M_\infty = .652$, $A = .140$, $C_l = .638$.

branch point at $\hat{w}_b$ is close to 1 when Γ is small. Thus, the singular behavior of ψ near the free stream and branch point, $|\hat{z}| \gg 1$, is given by

$$\psi = \operatorname{Im} \Phi \sim U \operatorname{Im} \hat{z} + \frac{\Gamma}{2\pi} \ln |\hat{z}|,$$

where $\hat{z}$ is taken from (5). Further details of the derivation of this singular form can be found in [21].

A choice is needed for the boundary of the domain in the hodograph connecting points D, N, and A in Figure 4. This portion of the boundary corresponds to the nose of the airfoil. A blunt nose with $v = 0$ could be taken following the work in Gilbarg and Shiffman [13] for the nonlifting case, but a rounded nose is preferred. A simple choice is the linear profile $\theta = -m_u q + \pi/2$ for the arc NA, and $\theta = m_l q - \pi/2$ for the arc DN, where the slopes m_u and m_l are parameters to be chosen. The curvature at the nose is related to the choice for m_u and m_l. The curvature is zero when $m_u = m_l = 0$ and increases as the values of these slopes increase. Typical values are $m_u = m_l = 3$, but this could be left to the designer. In [21] it is found that the value of M_∞ at critical is insensitive to the choice of these parameters for the range 0 to 3 approximately.

A numerical calculation of the boundary-value problem results in $\psi(q, \theta)$ and a subsequent numerical integration of (2) around the boundary of the domain in the hodograph leads to an airfoil shape that has long sonic arcs at critical (cf. [21]). A sample airfoil obtained in this way is shown in Figure 5(a) and the behavior of the pressure coefficient C_p along the upper and lower surfaces of the airfoil is shown. The flat portions of the curves of $-C_p$ lie at the critical value $-C_p^*$ and indicate the sonic portions of the upper and lower airfoil surfaces. The critical value of M_∞ for the airfoil and its area A and lift coefficient C_l are given in the figure caption.

The lift coefficient of the airfoil shown in Figure 5(a) is small. This is due to the fact that the contribution to the lift comes mainly from the small tail portion of the airfoil where the surface velocity is no longer sonic on the opposing surfaces. To obtain a larger, more practical value for C_l, the velocity on the lower surface of the airfoil can be lowered to a value below sonic. This can be achieved in the hodograph formulation by moving the boundaries DE and EF in Figure 4 to an arc with $q < c_*$. An example of an airfoil calculated in this way is shown in Figure 5(b). In exchange for a larger value of C_l, the free-stream Mach number is reduced from a corresponding airfoil with sonic arcs on the both the upper and lower surfaces.

3 Hodograph design of shock-free slender bodies

A second problem in which hodograph methods can be used to facilitate the mathematical formulation and subsequent computation is the design of shock-free slender bodies. The discussion of this problem is organized into two basic parts. First, the mathematical formulation of the hodograph boundary-value problem and its method of solution is presented. Several shock free bodies are calculated and a discussion of these results follows in the second part of this section.

3.1 Mathematical formulation

For a slender body of revolution with thickness ratio δ, transonic small-disturbance theory can be used to simplify the equations governing steady, inviscid, potential flow. The exact potential can be expressed as an asymptotic expansion in δ and the disturbance potential $\phi(x, \tilde{r})$, $\tilde{r} = \delta r$, in an outer expansion satisfies the Karman-Guderley equation

$$(K - (\gamma + 1)\phi_x)\,\phi_{xx} + \phi_{\tilde{r}\tilde{r}} + \frac{1}{\tilde{r}}\phi_{\tilde{r}} = 0, \tag{6}$$

where $K = (1 - M_\infty^2)/\delta^2$ is the transonic similarity parameter (cf. [9]). A solution to (6) is sought in the domain $|x| < \infty$, $0 < \tilde{r} < \infty$ subject to the boundary conditions

$$\phi_x^2 + \phi_{\tilde{r}}^2 \to 0, \qquad \text{as } x^2 + \tilde{r}^2 \to \infty,$$

and

$$\phi \to S(x)\ln\tilde{r} + G(x; K) + \cdots, \qquad \text{as } \tilde{r} \to 0,\ |x| < 1. \tag{7}$$

The behavior of ϕ in (7) comes from a consideration of an inner expansion and it is found that the source strength S is given by

$$S(x) = F(x)F'(x),$$

where $r = \delta F(x)$, $\max F = 1$, defines the body shape. The function G in (7) appears in the formula for the pressure coefficient on the body

$$C_p = \delta^2 \ln\frac{1}{\delta^2}\left(2S'(x)\right) - \delta^2\left(2S'(x)\ln F(x) + 2G'(x) + F'^2(x)\right) + \cdots$$

and must be determined as part of the solution (cf. [10]).

The main problem is to find a body shape function $F(x)$, or equivalently a source function $S(x)$, and a subsonic value of K such that the solution of (6) with boundary conditions has a supersonic zone, i.e. a region in which $\phi_x > K/(\gamma + 1)$, and is free of shocks. To solve this problem it is convenient from an analytical and computational standpoint to transform it to the the hodograph plane. In particular, there is a simple check for the smoothness of the flow as will be discussed below.

The transformation of the boundary-value problem for $\phi(x,\tilde{r})$ to the hodograph plane is discussed in [11] and is outlined here. Using the variables

$$(8) \qquad w = (\gamma+1)\phi_x - K, \qquad \vartheta = (\gamma+1)\phi_{\tilde{r}}, \qquad R = \frac{\tilde{r}^2}{2}, \qquad \nu = \tilde{r}\vartheta,$$

(6) can be written in the form of a first-order system

$$(9) \qquad \left\{ \begin{array}{rcl} ww_x & = & \nu_R \\ 2Rw_R & = & \nu_x \end{array} \right\}$$

Transforming (9) to the (w,ν)-hodograph plane yields the system

$$(10) \qquad \left\{ \begin{array}{rcl} wR_\nu & = & x_w \\ 2Rx_\nu & = & R_w \end{array} \right\}$$

and then eliminating x in (10) yields the basic hodograph equation

$$(11) \qquad \left(\frac{R_w}{2R}\right)_w - wR_{\nu\nu} = 0,$$

which is to be solved for $R(w,\nu)$, an approximate Stokes streamfunction. The hodograph equation is still quasi-linear but the boundary-value problem for (11) turns out to have almost fixed boundaries which simplifies the numerical calculations. The Jacobian of the transformation is

$$J = \frac{\partial(x,R)}{\partial(w,\nu)} = x_w R_\nu - x_\nu R_w = wR_\nu^2 - \frac{R_w^2}{2R}.$$

Note that $J < 0$ in the region $w < 0$ corresponding to subsonic flow and that J may be positive or negative when $w > 0$. In order for the mapping to be smooth, it is necessary that $J < 0$ everywhere. This is the basic criterion used to detect a shock-free solution.

Figure 6 illustrates the mapping of the flow to the hodograph and indicates the boundary-value problem for (11). The boundaries of the semi-infinite strip in the hodograph plane and the behavior of $R(w,\nu)$ as $w \to \pm\infty$ are determined from the asymptotic behavior of ϕ as $\tilde{r} \to 0$. Using (7) and (8) gives

$$(12) \quad w + K = (\gamma+1)S'(x)\ln\sqrt{2R} + (\gamma+1)G'(x) + \cdots, \qquad \nu = (\gamma+1)S(x) + \cdots$$

so that as $R \to 0$ with $|x| < 1$, $w \to +\infty$ when $S'(x) < 0$ and $w \to -\infty$ when $S'(x) > 0$. A representative $S(x)$ is shown in Figure 6 which has two points, $x = x_1$ and $x = x_2$, where $S' = 0$. These points determine the boundaries $\nu_1 = (\gamma+1)S(x_1)$ and $\nu_2 = (\gamma+1)S(x_2)$ in the hodograph where $R = 0$. As $w \to \pm\infty$, (12) gives

$$R(w,\nu) = A_\pm(\nu)e^{B_\pm(\nu)w} + \cdots$$

where

$$A_\pm(\nu) = \frac{1}{2}\exp\left[B_\pm(\nu)\left(\frac{K}{\gamma+1} - G'(x_\pm(\nu))\right)\right], \qquad B_\pm(\nu) = \frac{2}{S'(x_\pm(\nu))},$$

and $x_\pm(\nu)$ is determined by inverting $\nu = (\gamma+1)S(x)$ with the plus-minus subscript referring to the two branches of the inverse function on which S' is negative ($w \to +\infty$) and positive ($w \to -\infty$), respectively.

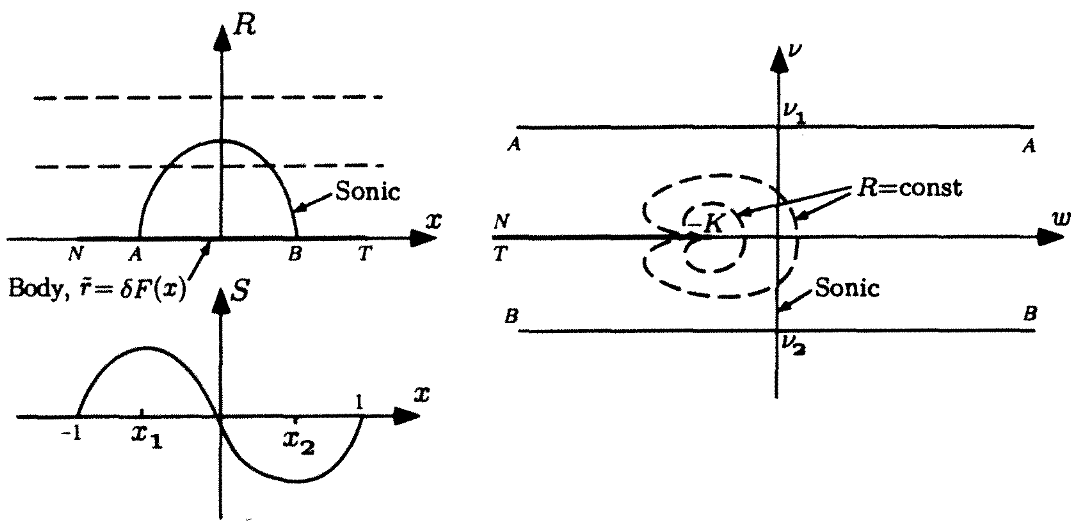

FIG. 6. *Hodograph mapping of a slender body of revolution, $\tilde{r} = \delta F(x)$, and its corresponding source function, $S(x)$.*

The far field in the physical plane maps to the singular point at $w = -K$, $\nu = 0$ in the hodograph plane. The singular behavior of $R(w,\nu)$ near $(-K,0)$ can be worked out from the far-field behavior of ϕ which for a closed body takes the form of a dipole:

$$\phi = \frac{D}{4\pi}\frac{x}{(x^2 + K\tilde{r}^2)^{3/2}} = \frac{D}{4\pi}\frac{x}{(x^2 + 2KR)^{3/2}}, \tag{13}$$

where

$$D = \pi \int_{-1}^{+1} F^2(x)\, dx + \pi(\gamma + 1) \int_{-\infty}^{\infty} \int_0^{\infty} \phi_x^2(x, \tilde{r})\tilde{r}\, d\tilde{r}\, dx \tag{14}$$

is the dipole strength (cf. [9]). Using

$$w + K = (\gamma + 1)\phi_x(x, R), \qquad \nu = (\gamma + 1)2R\phi_R(x, R)$$

where ϕ is given by (13) determines $R(w,\nu)$ implicitly near $(-K,0)$ and the double integral term in (14) can be expressed in the hodograph variables as

$$\frac{\pi}{\gamma + 1}\int_{-\infty}^{\infty}\int_{\nu_1}^{\nu_2} |J|\, (w + K)^2\, d\nu\, dw.$$

The qualitative behavior of R near $(-K,0)$ is indicated in Figure 6.

A numerical method is needed to determine a solution for (11) having the correct singular behavior near $(-K,0)$ and decay behavior as $w \to \pm\infty$ and having $J < 0$ everywhere so that the flow is shock free. One choice is discussed in [11] and this method is used to calculate a shock-free flow for a body having fore-aft symmetry. The extension of this method to general bodies is considered in [4] and several shock-free flows are found. The numerical method in [11] and in [4] is similar to a method used by Sobiezcky *et al.*[35] for planar flow. The basic numerical method is outlined here (see [11] and [4] for more details) and some results are discussed in the next part of this section.

The basic equation (11) is discretized using standard second-order finite differences and a provisional choice for K, D, and $S(x)$ for $-1 < x < x_1$ and $x_2 < x < 1$ is made. This corresponds to a choice for the free-stream Mach number, dipole strength, and body shape in the subsonic region of the flow, respectively. The choice for $S(x)$ in the subsonic region is enough to specify an approximate boundary condition

$$R_w = B_-(\nu)R, \qquad \text{at } w = -w_\infty,$$

where w_∞ is a sufficiently large value. If an additional choice for $R(w,\nu)$ along the sonic line, $w = 0$, is made, then a complete problem for (11) is defined for the subsonic (elliptic) region of the flow. The discrete equations can be solved using a combination of point relaxation and Newton's method.

The numerical solution in the supersonic (hyperbolic) region of the flow can be found by integrating (11) from the sonic line using the subsonic solution as initial conditions. As the integration proceeds, the sign of a discrete Jacobian is checked. If the Jacobian becomes positive, then the choice for $R(0,\nu)$ is adjusted and the steps are repeated. If the Jacobian remains negative, then the numerical solution represents a shock-free flow and the source function for the supersonic portion of the body is determined from

$$\frac{R_w}{R} = B_+(\nu) = \frac{2}{S'(x_+(\nu))}, \qquad \text{when } w = w_\infty.$$

In this expression, $x_+(\nu) = x(w_\infty, \nu)$ and $x(w,\nu)$ is found from $R(w,\nu)$ by integrating (10) throughout the hodograph domain. The pressure coefficient requires $G'(x)$ and this is determined by calculating $A_\pm(\nu)$ approximately at $w = \pm w_\infty$.

3.2 Results and discussion

The first shock-free axisymmetric flow was reported in Cole and Schwendeman [11] for the case of a body with fore-aft symmetry. In this case, $R(w,-\nu) = R(w,\nu)$ so that the boundary-value problem for R can be posed on a reduced hodograph domain given by $|w| < \infty$, $0 < \nu < \nu_1$ corresponding to the front portion of the flow ($x < 0$). A symmetry boundary condition, $R_\nu = 0$ when $w > -K$, is added to complete the problem. In [11] the parabolic arc $F(x) = 1 - x^2$ is used to begin the calculation. For this choice,

$$S(x) = -2x(1-x^2), \qquad x_1 = -\frac{1}{\sqrt{3}}, \qquad \nu_1 = \frac{4(\gamma+1)}{3\sqrt{3}}.$$

The transonic similarity parameter is taken to be $K = 2\nu_1 = 3.695$ for $\gamma = 1.4$ which implies that $M_\infty = 0.981$ for $\delta = 0.1$.

Figure 7 shows $F(x)$ which has a shock-free symmetric flow at $K = 3.695$. The subsonic portion of $F(x)$ at the nose (and tail) matches the parabolic arc but the supersonic portion between x_1 and 0 (and between 0 and $x_2 = -x_1$) has been changed to make the flow shock free. This has been done by adjusting the sonic line data $R(0,\nu)$ as mentioned before. Curves of constant w are approximate isobars and these curves are plotted in the physical plane (x,r), using $\delta = 0.1$, in Figure 8. The solid curves in this figure have $w > 0$ and indicate the supersonic region of the flow. The pressure coefficient C_p is shown in Figure 9.

Shock-free flows without fore-aft symmetry have been obtained by Buckmire [4]. Figure 10 shows $F(x)$ for one of the shock-free flows reported in [4] and its approximate isobars are plotted in Figure 11. The value of K for this flow is 3.919. There is a small gap in $F(x)$ at $x = 1$ in Figure 10 and this is a result of truncation error in the calculation

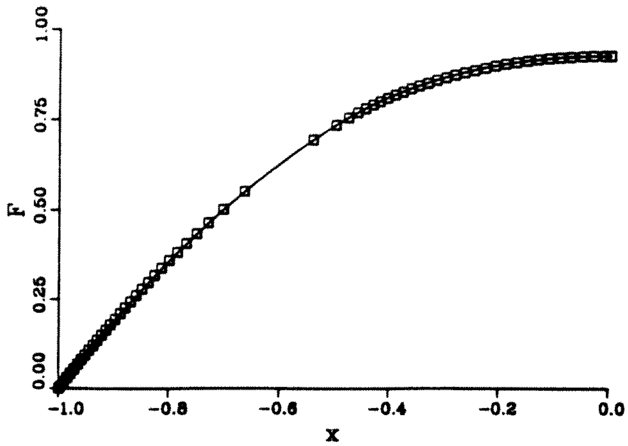

FIG. 7. *$F(x)$ for a shock-free flow with fore-aft symmetry.*

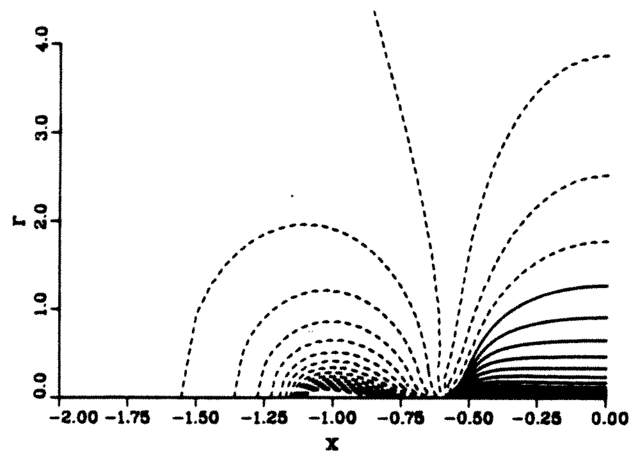

FIG. 8. *Curves of constant w (approximate isobars). Dashed curves have $w < 0$ (subsonic flow) and solid curves have $w > 0$ (supersonic flow).*

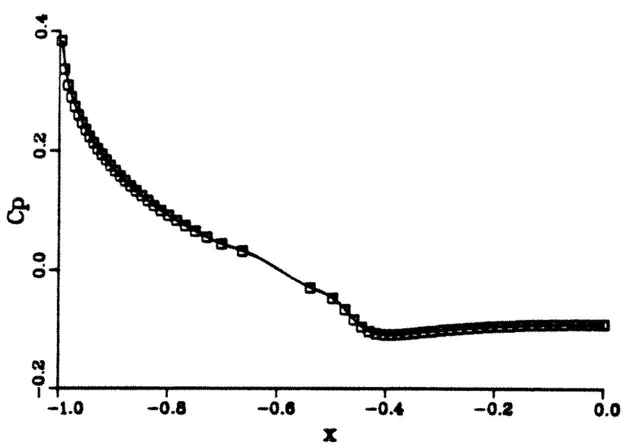

FIG. 9. *Pressure coefficient on the body.*

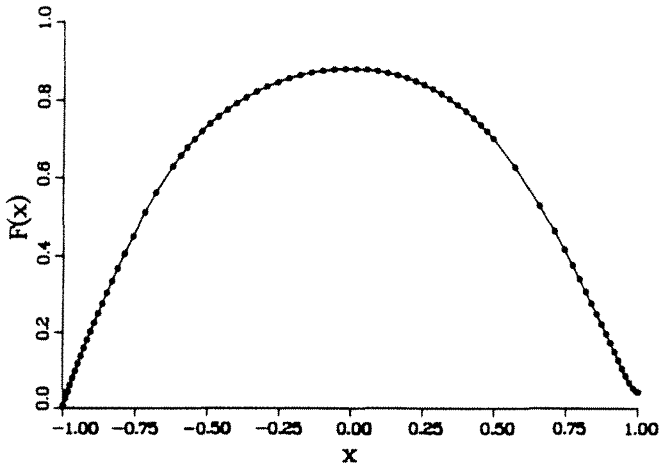

FIG. 10. *$F(x)$ for a shock-free flow without fore-aft symmetry.*

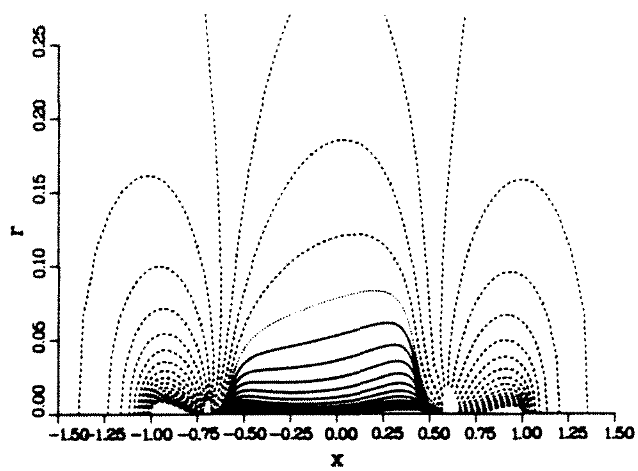

FIG. 11. *Curves of constant w (approximate isobars).*

of F from the discrete solution for $R(w, \nu)$ integrated from $x = -1$ where F is set to zero to $x = 1$. A rapid change in pressure near $x = x_1$ and $x = x_2$ is noted in the plot of the approximate isobars in Figure 11 but these are not shocks because $J < 0$ everywhere in the hodograph.

The behavior of the flow at off-design conditions can be determined by calculating the flow about a shock-free body in the physical plane at a value of K perturbed from the design value. Some results appear in [4] and an indication of these results is given in Figure 12. This figure shows the isobars for the flow about the shockfree body in Figure 10 when K is increased and decreased from the design value of 3.919. An increased K implies a decreased M_∞ (assuming δ is fixed) and this results in a smaller region of rapid change in pressure near $x = x_2$ (see Figure 12(a)). When K is decreased, M_∞ is increased and this results in a larger region of rapid change (see Figure 12(b)). This qualitative behavior is not unexpected. The main question of whether a shock develops when K is perturbed is

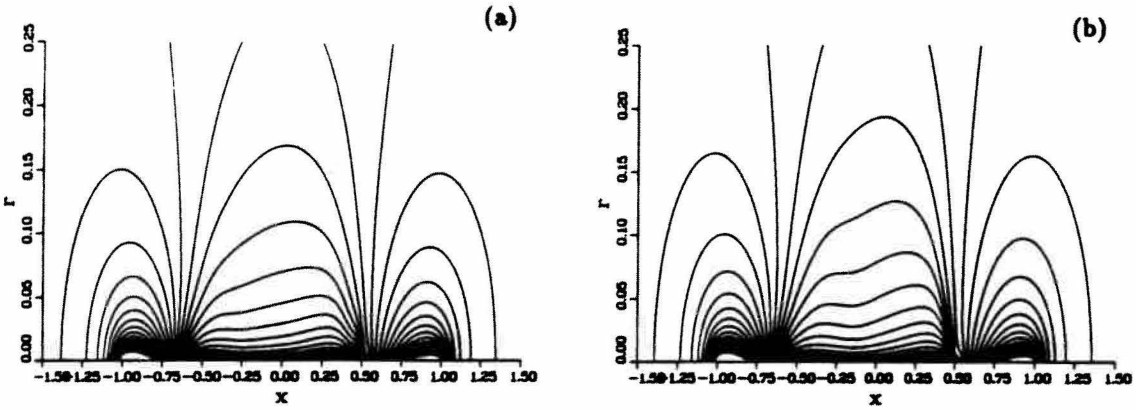

FIG. 12. *Curves of constant w at off-design conditions: (a) $K = 4.311$ and (b) $K = 3.527$.*

difficult to answer from these numerical calculations because it is impossible to distinguish between a rapid change in pressure and a smoothed-out shock. It can be stated, however, that at most a weak shock develops indicating that there is a range of free-stream Mach numbers for which the flow is essentially shock free.

Acknowledgements

I would like to thank my friend and colleague, Julian Cole, for suggesting the problems discussed in this article and for providing direction during their development. I would also like to thank my former graduate students, Mary Catherine Kropinski and Ron Buckmire, who carried out many of the calculations presented in this article.

References

[1] F. Bauer, P. Garabedian, and D. Korn, *Supercritical Wing Sections*, Lecture Notes in Economics and Mathematical Systems, No. 66, Springer-Verlag, New York, 1972.

[2] F. Bauer, P. Garabedian, and D. Korn, *Supercritical Wing Sections II*, Lecture Notes in Economics and Mathematical Systems, No. 108, Springer-Verlag, New York, 1975.

[3] F. Bauer, P. Garabedian, and D. Korn, *Supercritical Wing Sections III*, Lecture Notes in Economics and Mathematical Systems, No. 150, Springer-Verlag, New York, 1977.

[4] R. Buckmire, *The Design of Shock-Free Transonic Slender Bodies*, Ph.D. Thesis, Dept. of Mathematical Sciences, Rensselaer Polytechnic Institute, Troy, New York, June, 1994.

[5] T. M. Cherry, *Flow of a compressible fluid about a cylinder*, Proc. R. Soc. Lond. A., 192 (1947), pp. 45–79.

[6] T. M. Cherry, *Flow of a compressible fluid about a cylinder II. Flow with circulation*, Proc. R. Soc. Lond. A, 196 (1947), pp. 1–31.

[7] T. M. Cherry, *Numerical solutions for compressible flow past a cylinder*, Proc. R. Soc. Lond. A, 196 (1947), pp. 32–36.

[8] S. A. Chaplygin, *On gas jets*, Sci. Mem. Moscow Univ. Math. Phys., 21 (1902), pp. 1–121. Translated in NACA TM 1063 (1944).

[9] J. D. Cole and L. P. Cook, *Transonic Aerodynamics*, North Holland, Amsterdam, 1986.

[10] J. D. Cole and A. F. Messiter, *Expansion procedures and similarity laws for transonic flow*, ZAMP, 8 (1957), pp. 1–25.

[11] J. D. Cole and D. W. Schwendeman, *Hodograph design of transonic slender bodies*, Proc. 3rd Intl. Conference on Hyperbolic Problems, Upsala, May, 1990.

[12] D. D. Fisher, *Calculation of subsonic cavities with sonic free streamlines*, J. Math. Phys., 42 (1963), pp. 14–26.

[13] D. Gilbarg and M. Shiffman, *On bodies achieving extreme values of the critical Mach number I*, J. Rat. Mech. and Anal., 3 (1954), pp. 209–230.

[14] S. Goldstein, M. J. Lighthill, and J. W. Craggs, *On the hodograph transformation for high speed flow. I*, Qu. J. Mech. Appl. Math., 1 (1948), pp. 344–357.

[15] J. B. Helliwell and A. G. Mackie, *The flow past a closed body in a high subsonic stream*, J. Mech. Appl. Math., 12 (1959), pp. 298–313.

[16] J. J. Kacprzynski, L. H. Ohman, P. R. Garabedian, and D. G. Korn, *Analysis of the Flow Past a Shockless Lifting Airfoil in Design and Off-design Conditions*, N.R.C. of Canada Aeronautical Report LR-554, Ottawa, 1971.

[17] J. J. Kacprzynski, *Wind Tunnel Test of the Shockless Lifting Airfoil No. 1*, N.R.C. of Canada Project Report 5x5/0062, Ottawa, 1972.

[18] J. J. Kacprzynski, *Wind Tunnel Test of the Shockless Lifting Airfoil No. 2*, N.R.C. of Canada Laboratory Technical Report LTR-HA-5x5/0067, Ottawa, 1973.

[19] T. von Karman, *Compressibility effects in aerodynamics*, J. Aeronaut. Sci., 8 (1941), pp. 337–356.

[20] M. C. A. Kropinski, D. W. Schwendeman, and J. D. Cole, *Hodograph design of lifting airfoils with high critical Mach numbers*, J. Theoret. Comput. Fluid Dynamics, 7 (1995), pp. 173–188.

[21] M. C. A. Kropinski, *On the construction and calculation of lifting airfoils with high critical Mach numbers*, J. AIAA, in press.

[22] M. J. Lighthill, *On the hodograph transformation in high speed flow. II. A flow with circulation*, Qu. J. Mech. Appl. Math, 1 (1948), pp. 442–450.

[23] M. J. Lighthill, *The hodograph transformation in transonic flow. II. Auxiliary theorems on the hypergeometric functions. III. Flow around a body*, Proc. Roy. Soc. Lond. A, 191 (1947), pp. 341–369.

[24] C. S. Morawetz, *On the non-existence of continuous transonic flows past airfoils at high Reynolds numbers I*, Comm. Pure Appl. Math., 9 (1956), pp. 45–68.

[25] C. S. Morawetz, *On the non-existence of continuous transonic flows past airfoils at high Reynolds numbers II*, Comm. Pure Appl. Math., 10 (1957), pp. 107–131.

[26] C. S. Morawetz, *On the non-existence of continuous transonic flows past airfoils at high Reynolds numbers III*, Comm. Pure Appl. Math., 11 (1958), pp. 129–144.

[27] R. von Mises, *Mathematical Theory of Compressible Fluid Flow*, New York, 1958.

[28] G. Y. Nieuwland, *Transonic potential flow around a family of quasi-elliptical aerofoil sections*, NLR-TR T. 172 (1967).

[29] T. R. F. Nonweiler, *The sonic flow about some symmetric half-bodies*, J. Fluid Mech., 4 (1958), pp. 140–148.

[30] H. H. Pearcey, *The aerodynamic design of section shapes for swept wings*, Advances in Aeronautical Sciences, Vol. 3, London, 1962.

[31] D. Riabouchinsky, *On steady fluid motions with free surfaces*, Proc. London Math. Soc., Ser. 2, 19 (1920), pp. 206–215.

[32] F. Ringleb, *Exakte Lösungen der Differential-Gleichungen einer adiabatische Gasströmung*, ZAMM, 20 (1940), pp. 85–198.

[33] Z. Rusak, *The sonic flow about two-dimensional slender semi-infinite bodies*, SIAM J. Appl. Math., in press.

[34] D. W. Schwendeman, M. C. A. Kropinski, and J. D. Cole, *On the construction and calculation of optimal nonlifting critical airfoils*, ZAMP, 44 (1993), pp. 556–571.

[35] H. Sobiezcky, K.-Y. Fung, A. R. Seebass, and N. J. Yu, *A new method for designing shock-free transonic configurations*, J. AIAA, 17 (1979), pp. 722–729.

[36] N. Tollmien, *Zum Übergang von Unter- zu Überschallströmung*, ZAMM, 17 (1937), pp. 117–136.

[37] H. S. Tsien, *Two-dimensional subsonic flow of compressible fluids*, J. Aeronaut. Sci., 6 (1939), pp. 399–407.

[38] R. T. Whitcomb and L. Clark, *An Airfoil Shape for Efficient Flight at Supercritical Mach Numbers*, NASA Tech. Man. X-1109, 1965.

Non-Linear Ship Internal Waves

M. P. Tulin* P. Wang * Y. Yao * T. Miloh†

Forward *It seemed especially appropriate to discuss ship internal waves at this celebration, since they have an underlying mathematical connection with gas dynamics, a kind of dispersive gas dynamics. We are indebted to Julian Cole. He serves as an inspiration to all of us, not only for his extraordinary skill in the application of mathematics to the understanding of gas dynamics and many other subjects and in the solution of problems of engineering importance, but also for his integrity, wisdom, dedication, deep curiosity, and patience. Thank you, Julian.*

Abstract

The generation and propagation of ship internal waves in the supercritical regime are discussed with an emphasis on non-linear effects. An exact computational theory reveals the existence of quasi-solitons: fast, slowly decaying waves of depression, are generated in pycnoclines of finite thickness.

1 Introduction

Fluids with inhomogeneous density permit the propagation of internal waves, see Figure 1. They are common in large water bodies (the ocean, lakes, fjords) where normally the density variations are $\Delta\rho/\rho = O(10^{-2} \sim 10^{-3})$. Despite these small differences, internal waves of noticeable amplitude may be generated. Surface effects due to the subsurface disturbances from ships may easily be observed and their remote observation by radar, sometimes from space, has excited intense research.

The physics of internal waves has been well discussed, Lighthill (1978) or Yih (1965) for example; see Figure 2 for certain key features. It is well known, Eckart (1960), that for a given vertical stratification, $\rho = \rho(z)$, the solution of an appropriate eigenvalue problem provides a spectrum of internal waves, $\omega = \omega(\vec{k})$; certain of these are readily generated by the passage of a ship. The resulting wave patterns are governed by the densimetric Froude number, $F_h = U_s/c^*$, where U_s is the ship speed, and c^* is the (linear) speed of the fastest internal waves allowed by $\omega(\vec{k})$, which in typical ocean condition corresponds to very long shallow waves propagating horizontally, with their maximum elevation in a sharp, relatively strong, surface pycnocline of mean depth h; normally, in both the ocean and fjords, $c^* \sim 30 - 70\mathrm{cm/sec}$.

The far field (kinematical) wave patterns for ship internal waves are reasonably understood in the linear regime: Keller and Munk (1970), Yih (1990), and Tulin and Miloh

*University of California, Santa Barbara
†Tel Aviv University, Israel

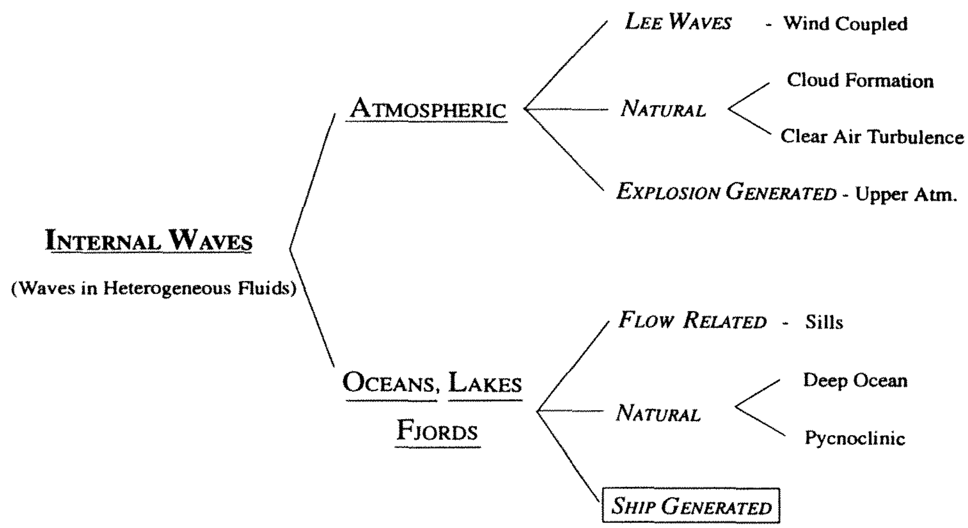
LEE WAVES - Wind Coupled
Cloud Formation
ATMOSPHERIC
NATURAL
Clear Air Turbulence
EXPLOSION GENERATED - Upper Atm.
INTERNAL WAVES
(Waves in Heterogeneous Fluids)
FLOW RELATED - Sills
Deep Ocean
OCEANS, LAKES
FJORDS
NATURAL
Pycnoclinic
SHIP GENERATED

FIG. 1.

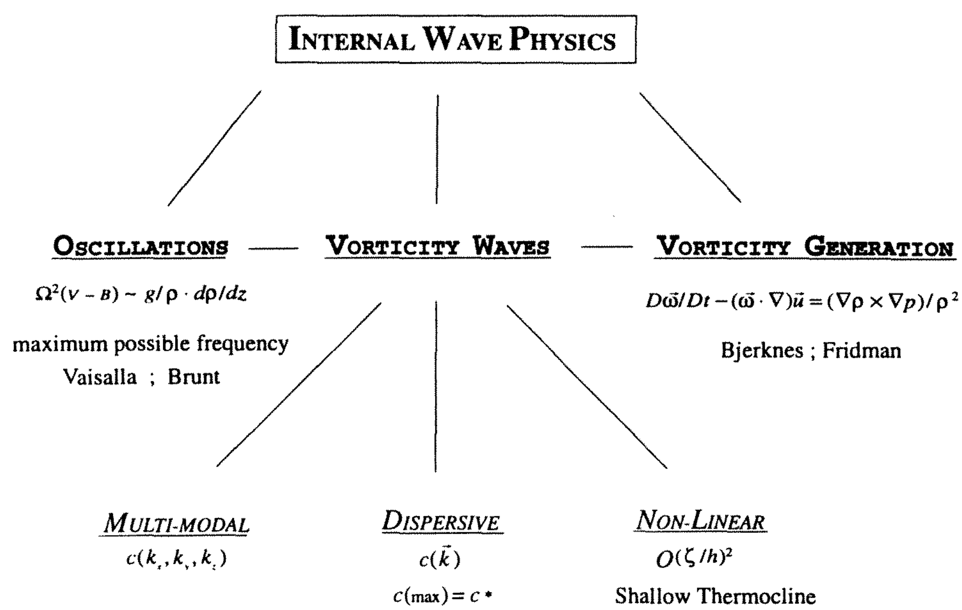
INTERNAL WAVE PHYSICS
OSCILLATIONS
VORTICITY WAVES
VORTICITY GENERATION
$\Omega^2(v - B) \sim g/\rho \cdot d\rho/dz$
maximum possible frequency
Vaisalla ; Brunt
$D\vec{\omega}/Dt - (\vec{\omega}\cdot\nabla)\vec{u} = (\nabla\rho \times \nabla p)/\rho^2$
Bjerknes ; Fridman
MULTI-MODAL
$c(k_x, k_y, k_z)$
DISPERSIVE
$c(\vec{k})$
$c(\max) = c*$
NON-LINEAR
$O(\zeta/h)^2$
Shallow Thermocline

FIG. 2.

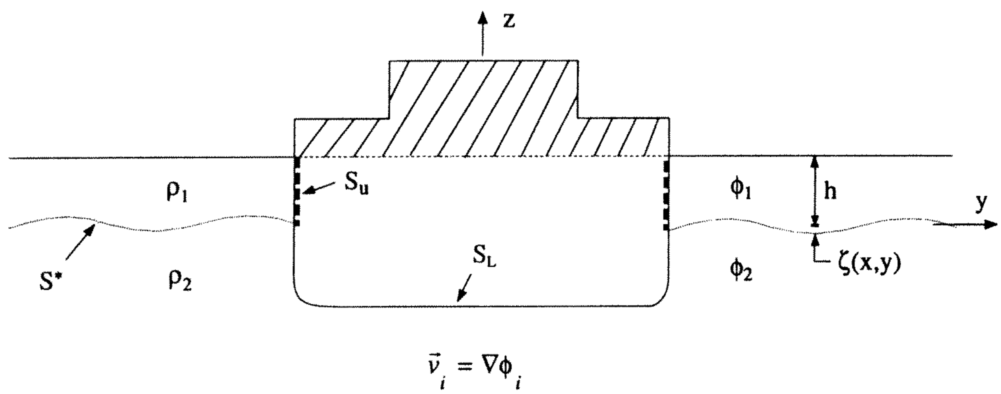

FIG. 3. *Ship Cross Section (front view) in Shallow Pycnocline (two layers).*

(1990), and have been observed in the field through their effect on the water surface, at least in part indirectly, where they both calm and intensify short wind waves. Experiments confirm the linear predictions, Ma and Tulin (1992).

Non-linear effects have received attention in the case of the transcritical or "dead water" regime, $F_h = O(1)$, Miloh and Tulin (1988; 1988a); in these same references, the possibility of soliton generation and propagation in the far field was raised. Here we present two relevant theoretical developments: (1) the asymptotic non-linear theory of long internal waves generated by ships in a two layer fluid, and (2) a more general non-linear theory for $F_h^2\, h/L >> 1$, which becomes exact in two dimensions (cross flow plane). The former leads to non-linear field equations and gives rise to the theoretical possibility of solitons. Using the latter, the existence of slowly decaying non-linear internal waves of both depression and elevation (quasi-solitons) have been discovered through numerical calculation.

2 Long Ship Waves in Two Layer Fluids (Shallow,Sharp Pycnoclines)

The ship, of draft D and length L, is slender and $\epsilon = D/L << 1$. The theory is steady in ship coordinates (x, y, z) and applies to the long wave asymptotic regime where terms,

$$O(kh)^2, \quad O(k\zeta)^2, \quad O(k\zeta^2/h) \quad \textit{are neglected} \tag{1}$$

The velocity field is $\vec{v}_i(x, y) = \nabla\phi_i = (u_i, v_i)$; the density is ρ_i, and $i = 1, 2$, above and below the pycnocline, respectively, see Figure 3.

Continuity in the upper layer requires that

$$\nabla \cdot [(h - \zeta)\nabla\phi_1] = 0\ , \qquad (kh)^2 << 1 \tag{2}$$

and Bernoulli's equation applies in each layer, so that equating the pressure on either side of the interface, S^*,

$$\frac{(\nabla\phi_1)^2}{2} + a^2 = \frac{\rho_2}{\rho_1}\frac{(\nabla\phi_2)^2}{2} - \frac{\Delta\rho}{\rho_1}\left(\frac{U_s^2}{2} - gh\right) \tag{3}$$

where $\Delta\rho$ is the density difference, $\rho_2 - \rho_1$, between the two layers, and we take,

$$a^2 = \frac{\Delta\rho}{\rho_1} g(h - \zeta) = a_0^2\left(1 - \frac{\zeta}{h}\right) \tag{4}$$

Incidentally, $''a''$ can be shown to be the non-linear, non-dispersive, long wave speed in shallow water, when $(k\zeta)(kh)^{-3} >> 1$, Mei (1983).

A field equation for ϕ_1 is then obtained by taking grad eq.(3), eliminating ∇a^2 using eq.(2), and then taking the dot product with $\nabla\phi_1$:

$$
\begin{aligned}
& (a^2 - u_1^2)(\phi_1)_{xx} + (a^2 - v_1^2)(\phi_1)_{yy} - 2u_1v_1(\phi_1)_{xy} \\
& \quad = -\frac{\rho_2}{\rho_1}\nabla\phi_1 \cdot \nabla\frac{(\nabla\phi_2)^2}{2} \qquad on\ S^* \qquad (5)
\end{aligned}
$$

where x is positive in the direction opposite to the ship, z is upwards, and y the lateral direction.

Referring to Figure 3, ϕ_1 must also satisfy the boundary condition on S_u: $\partial\phi_1/\partial n = 0$.

In the case of a single shallow layer, where $\phi_2 = 0$ on the RHS, eq.(5) leads to the well known hydraulic analogy, where ϕ_1 is then also the gas dynamic potential for $\gamma = 2$; then, in the supersonic regime, non-linear, non-dispersive waves result.

The RHS of eq.(5) arises from the contribution of both the lower hull, S_l, and the wave interface, S^*, to the velocity induced pressure on S^*.

The potential, ϕ_2, may be expressed through application of Green's formula in the lower region,

$$
\begin{aligned}
\phi_2 - U_s x &= \tilde{\phi}_2(x,y,z) \\
&= \frac{1}{4\pi}\int_{S^*+S_l}[\tilde{\phi}_2\frac{\partial G}{\partial n} - \frac{\partial\tilde{\phi}_2}{\partial n}G]dS \qquad (6)
\end{aligned}
$$

where G is a simple source, $G = r^{-1} = [(x-x')^2 + (y-y')^2 + (z-z')^2]^{-1/2}$.

Now a number of simplifications arise because we assume small slopes on $S^* + S_l$, so that terms of $O(k\zeta)^2$ may be omitted. First, the integral over S^* may be taken on the undeflected interface where: $\partial G/\partial n \equiv 0$, and $\partial\phi_2/\partial n \cong U_s\zeta_x$. Furthermore, the RHS of eq.(5) may be approximated by $(\rho_2/\rho_1)U_s^2(\tilde{\phi}_2)_{xx}$, and eq.(2) takes the form,

$$
U_s\zeta_x = h\nabla^2\phi_1 \qquad (7)
$$

Finally, the motion in the upper layer, and the shape of the interface may be defined by the forced field equation where $\tilde{\phi}_2$ represents the integration over S_l specified by eq.(6),

$$
\begin{aligned}
& \underbrace{(a^2 - u_1^2)(\phi_1)_{xx} + (a^2 - v_1^2)(\phi_1)_{yy} - 2u_1v_1(\phi_1)_{xy}}_{Exact\ Gas\ Dynamics,\ \gamma=2} \\
& \qquad \underbrace{-\frac{\rho_2}{\rho_1}U_s^2 h\frac{\partial^2}{\partial x^2}H^{(2)}\nabla^2\phi_1}_{Dispersion} \\
& \qquad = \underbrace{-\frac{\rho_2}{\rho_1}U_s^2(\tilde{\phi}_2)_{xx}}_{Forcing} \qquad (8)
\end{aligned}
$$

The two-dimensional Hilbert transform is,

$$H^2[f] = \frac{1}{2\pi}\int\limits_{S^*}[f]\frac{dx'dy'}{[x-x')^2+(y-y')^2]^{1/2} \tag{9}$$

which can be shown to be responsible for dispersive effects on wave propagation. In the linear regime, this term results in a dispersive wave train in the far field.

In the near field, in supercritical flows, $F_h^2 >> 1$, taking into account the small slenderness of the ship, the dispersive term may be shown to be $O(h/L) << 1$ in comparison to the dominant non-dispersive (gas dynamic) terms. The deflection of the pycnocline in the near field may thus be calculated in the gas dynamic approximation. A result similar to eq.(8) has been earlier obtained for the case where the ship lies above the interface, Tulin and Miloh (1990), Wang, Yao, Miloh and Tulin (1990). In this case the forcing is due to the pressure field on the interface due to the ship in the absence of the interface and is readily calculated for a given ship form. Omitting the dispersion term, the deflection of the pycnocline has been calculated using the method of characteristics. The results have some remarkable features, which might have been expected in view of eq.(8): (1) the data tend to collapse when the longitudinal (x) and transverse (y) dimensions and the wave amplitude are scaled appropriately, eq.(10) below; (2) the ship at first depresses the interface; (3) the depression rebounds along the ship track to create an upwelling at the scaled distances $\hat{x} \cong 0.3$; (4) this upwelling is accompanied by troughs on either side, to create a "triple-lobe" pattern; (5) this pattern then propagates sidewards as two non-linear acoustic waves; (6) the pattern is slender.

The empirical quasi-similarity takes the form, see Figure 4,

$$\hat{\zeta} \approx \hat{\zeta}(\hat{x}, \hat{y}) \tag{10}$$

where $\hat{\zeta} = \zeta/\zeta_p$; $\hat{x} = (x/L)F_h^{-1/2}$; $\hat{y} = (y/L)F_h^{1/2}$; and the scaling amplitude $\eta_p(F_h)$ may be taken as the peak elevation in the upwelling at $\hat{x} \approx 0.3$; $\zeta_p \sim F_h^{-1/2}$ for $2.5 \leq F_h \leq 15$. In this case $h/L = 0.1$; the pattern may change for other values of this parameter.

Subsequent to the creation of the triple lobe behind the ship and accompanying its relaxation, dispersive effects become significant, see Tulin, Wang and Yao (1993), and a dispersive wave train is generated in the linear case, in the form described by kinematical (ray) theory. The amplitude of the waves in this pattern is given by the very same amplitude function, $A(k)$, describing the spectral content of the elevation in the triple lobe pattern, Tulin and Miloh (1990), Tulin *et al* (1993). It is in the triple lobe pattern, therefore, where the matching between inner and outer flows occurs. For sufficiently large amplitudes, can non-linear waves, including solitons, be generated from the initial values provided by the triple lobe? The answer is, "in principle, yes." This was shown in a study of solitons generated in a two layer fluid by Miloh, Prestin, Shtilman and Tulin (1993), where the initial conditions were inspired by the post triple lobe patterns of Figure 4. The generation of solitons is governed by the so-called Benjamin-Ono evolution equation,

$$\hat{\zeta}_t + \hat{\zeta}\,\hat{\zeta}_\eta + \frac{\beta}{\pi}\int\limits_{-\infty}^{+\infty}\frac{\hat{\zeta}_{\eta'\eta'}}{(\eta'-\eta)}\,d\eta' = 0 \tag{11}$$

where $\hat{\zeta}$ is a scaled elevation; η and t are the scaled characteristic variable and time, respectively; for large F_h, $\eta \approx y$.

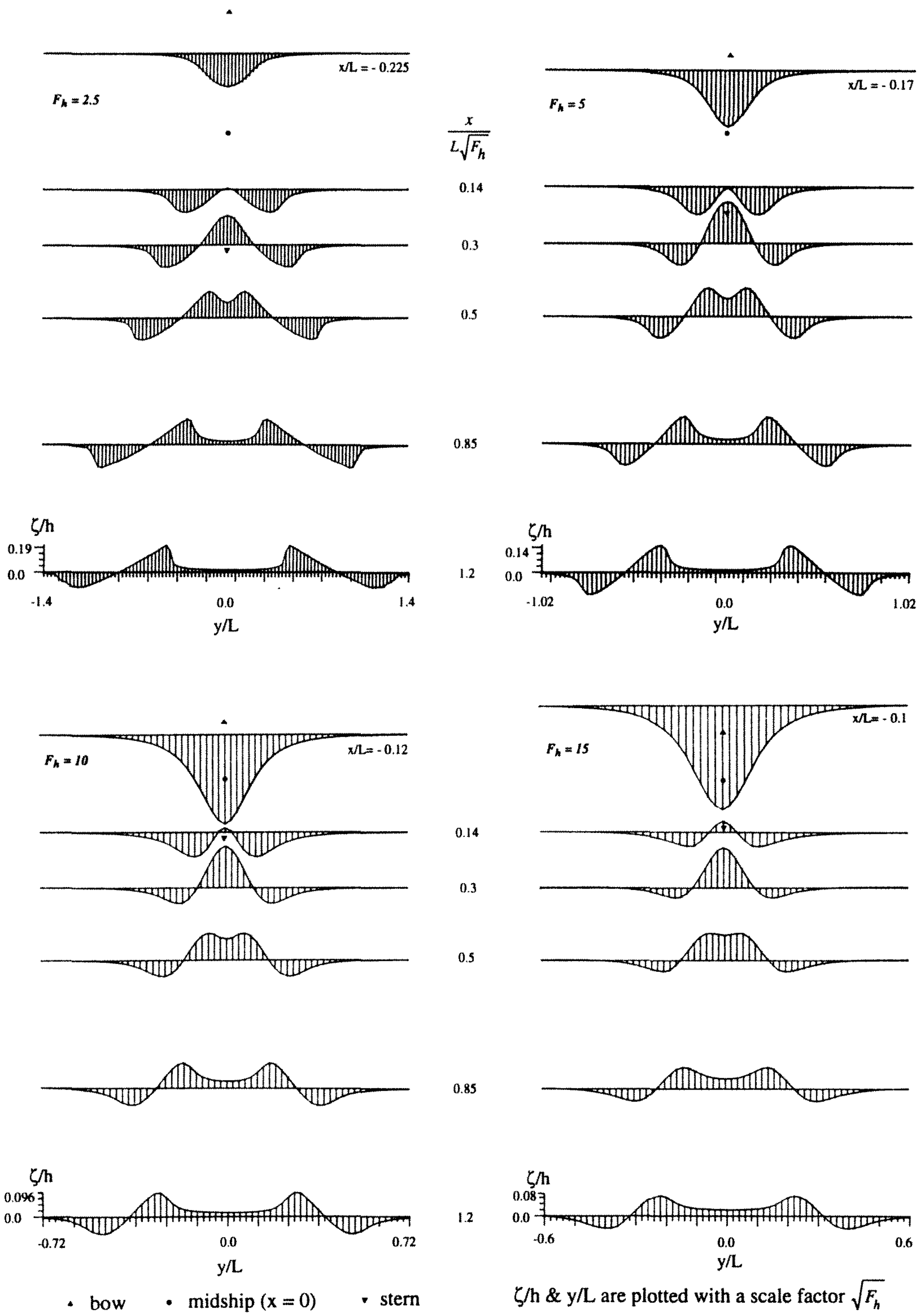

FIG. 4. *Interface elevation, ζ, vs. transverse distance, y, for various distances, x, behind the ship and for a range of densimetric Froude numbers, F_h; h/L=0.1. The similarity of the patterns is shown as well as the creation of triple lobe patterns. The calculations are non-dispersive.*

This evolution equation can be derived as an asymptotic result from the unforced field equation (8) under the assumptions: $F_h^2 >> 1$; terms of $O(\zeta/h)^3$ are omitted; the far field solution is of simple wave form, {i.e., $\gamma\,\partial/\partial y = -\,\partial/\partial x$, where γ is the slope y_x of one of the characteristics (η) of the gas dynamic part of eq.(8)}. The quantity β is a measure of the relative importance of dispersive vs. non-linear effects. For large β, i.e., small initial disturbance, eq.(11) may be linearized and its solution is the two layer equivalent of the more general far field dispersive wave solution found by Tulin and Miloh (1990). The entire wave system then lies inside the leading linearized characteristics, $dy/dx = \gamma = \pm\sqrt{F_h^2 - 1}$.

Starting with the two-lobe acoustic disturbance which emerges from the triple lobe pattern for $\hat{x} > 0.3$, Figure 4, a continual evolution may be calculated numerically from eq.(11), and this has been done by Miloh *et al* (1993). They showed that the number of solitons which emerge as the disturbance progresses is given by, N, the integer less than, but closest to N^*,

$$N^* = \frac{A_d}{A^*}\;; \qquad A^* = \frac{4}{3}\pi h^2 \frac{\rho_2}{\rho_1} \tag{12}$$

where A^* is the area of the depression of the Benjamin (1967) soliton, a constant independent of its amplitude, and A_d is the area in one of the depression lobes in the triple lobe pattern. Since solitons move faster than the long wave speed, a_0, they will be found in advance of the leading characteristics. The areas of the depression lobes shown in Figure 4 are, however, insufficient to create solitons, according to the criterion, eq.(12). But the theory is inadequate in many respects, and needs improvement: actual pycnoclines are not sharp (their thickness is $O(h)$); the energy of internal waves generated by actual triple lobe patterns are concentrated in wavenumbers, $kh = O(1)$, in violation of the asymptotic condition, $(kh)^2 << 1$; the weakly non-linear theory of internal waves is itself suspect because of its failure to agree with soliton experiments. A computational non-linear theory suggests itself.

3 An Exact Computational Theory for the Generation and Propagation of 2D Internal Waves

For $F_h^2 >> 1$, the propagation of internal waves behind a triple lobe pattern are primarily in the lateral direction (y) normal to the ship track (x), and can be well approximated as two-dimensional, but unsteady. In the horizontal (y) and vertical (z) directions the velocity components are v and w, respectively; the density ρ varies in the vertical direction. The stream function, $\psi(y,z;t)$ describes the velocity field, $\vec{u}(v,w)$: $v = \psi_z$; $w = -\,\psi_y$. It is generated by the vorticity: $\omega = w_y - v_z$,

$$\frac{\partial^2\psi}{\partial y^2} + \frac{\partial^2\psi}{\partial z^2} = -\,\omega(y,z;t) \tag{13}$$

where it is sufficient to take $\psi = 0$ on the free surface.

The vorticity is generated by tilting of the isopycnics according to the Bjerknes relation, and the pressure gradient through Euler's equation,

$$\frac{d\omega}{dt} = -\,\rho^2(\nabla\rho \times \nabla p)\;; \qquad \nabla p = \rho\left(\frac{d\vec{u}}{dt} - g\,\vec{i}_z\right) \tag{14}$$

where $\vec{i}_z$ is a unit vector in the z direction.

Combining eqs. (13) and (14),

$$\omega(x,y;t) = \int_{(x_0,y_0;0)}^{(x,y;t)} \rho^{-1}\left[\rho_z\,\vec{u}_p\cdot\nabla v_p \;-\; \rho_y\left(\vec{u}_p\cdot\nabla w_p - g\right)\right]dt \tag{15}$$

where the integration follows the particle $(x, y; t)$ in time, so that particle paths must also be traced in time, using,

$$y_p - y_0 = \int_0^t v_p\,dt\ ; \qquad z_p - z_0 = \int_0^t w_p\,dt \tag{16}$$

The system of eqs. (13), (15) and (16) define the motion exactly, and can be decoupled simply by separating their individual calculation by an infinitesimal time interval, forward marching. A numerical FEM procedure has been implemented, employing four node cubic Hermite elements, where the derivatives of ψ are obtained directly from the solution of eq.(13), preserving the continuity of $\vec{u}$ across the boundary elements. Convergence tests have been performed. For details see Tulin *et al* (1993).

In the absence of exact general soliton solutions, the implemented code, *InternalWave*, has been used to predict solitons generated in the density distribution shown in Figure 5 for $h/\epsilon = 1.25$, which is representative of thick pycnocline conditions. Benjamin (1967) has given the first mode soliton solution in the Boussinesq approximation, for a similar but slightly different pycnocline. In that case, the area of the soliton depression is $8h^2/\pi$, and the shape of the isopycnic at the bottom of the top mixed layer is identical to the two layer soliton: $\zeta = \zeta_M\lambda^2/y^2 + \lambda^2$; the speed of the soliton is $c \approx [2\sqrt{h/\epsilon}/\pi]\cdot a_0\cdot[1+\zeta_M/h]^{1/2}$.

The area of the initial depression, S_0, Figure 5, is taken as 1.04 times the value given by Benjamin, $S_s = 8h^2/\pi$. A soliton of depression quickly forms followed by a train of dispersive waves; it seems to approach a steady form by $t/T = 230$, Figure 5, where $T = h/a_0$. The shape of the soliton is approximated by Benjamin's result, but with apparent differences.

When an initial elevation of the same area is composed, a strong dispersive wavetrain forms, Figure 6 (upper), where the leading wave is entirely elevated. This leading elevation decays very slowly, as $t^{-1/6}$, in comparison with the prediction of asymptotic linear theory, $t^{-1/2}$, Tulin and Miloh (1990). This elevation is also slower, $0.685\,a_0$, than the theoretical infinitesimal value, $0.713\,a_0$. It is thus apparent that very strong non-linear effects can occur even for waves of elevation.

For an initial disturbance of the same width as shown in Figure 5 (Depression I), but smaller area, $S_0/S_s = 0.52$, a disturbance with soliton speed, but with an extremely small decay, as $t^{-1/14}$, was found, Figure 7. We call this disturbance a quasi-soliton. As the initial depression is further reduced in area below S_s, soliton-like behavior slowly disappears; see Figure 8 where a series of calculations is made for an initial disturbance (II) with half the width of (I). Even for initial areas as small as $S_s/10$, the decay exponent is less than half of the linear value. These results show that the asymptotic range of linear theory is very small. In fact, the speed of the quasi-solitons is shown to be close to the predictions of non-linear (Boussinesq) theory for a substantial range of initial volumes.

Another important finding here is the relatively slow development of the wave patterns. The parameter t/T may be given meaning in the case of a ship, through the relation: $x = U_s\,t$, or $x/L = (U_s\,/a_0)(h/L)\cdot t/T$. For $F \approx 10$, and $h/L \approx 10^{-1}$, $x/L \approx t/T$, the times of development shown in Figure 5-7 correspond, therefore, to very great distances.

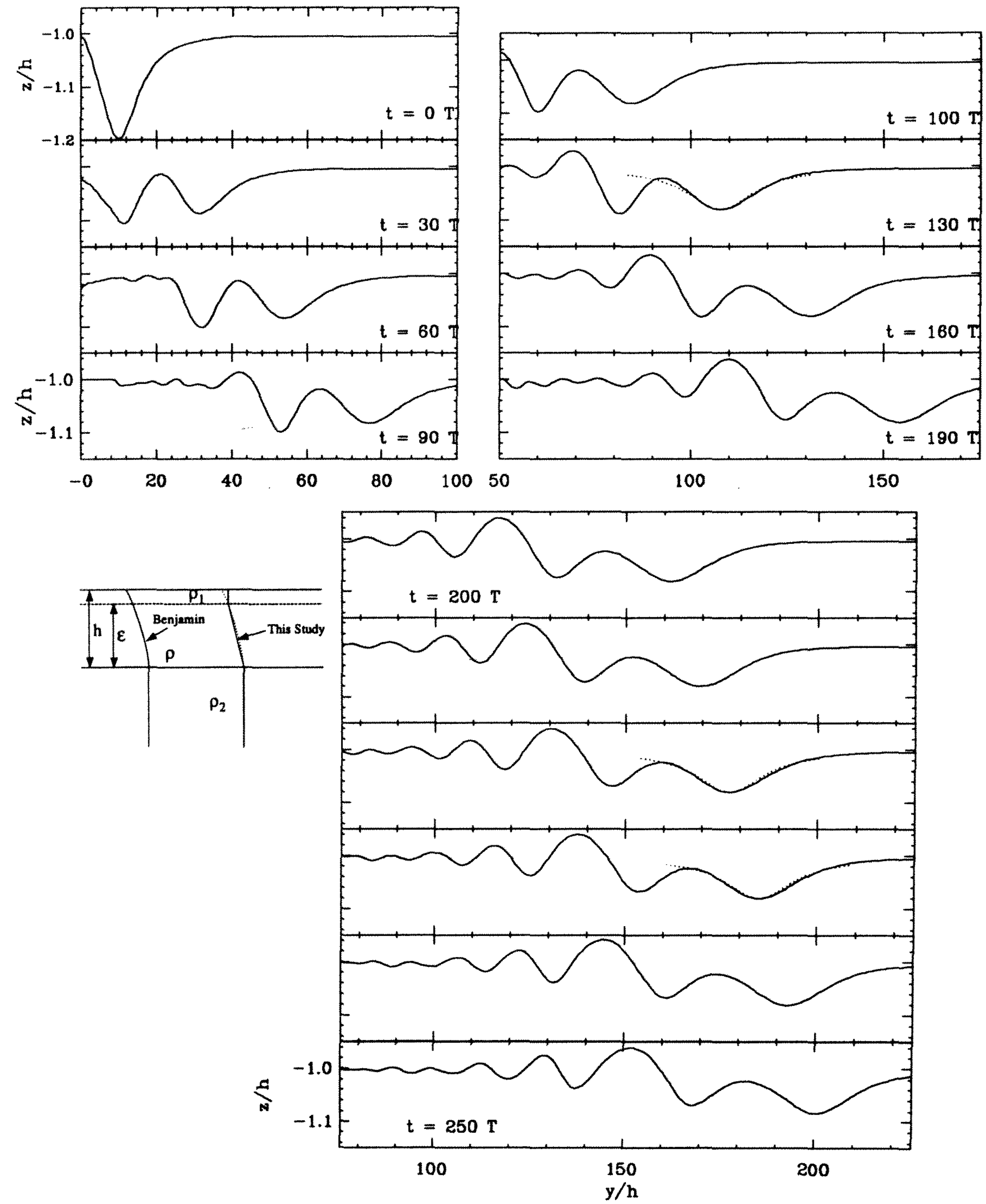

FIG. 5. *Wave trains generated by an initial depression,* $S_0/S_s = 1.04$*; the dotted line is the exact algebraic soliton shape. The leading depression is non-decaying.*

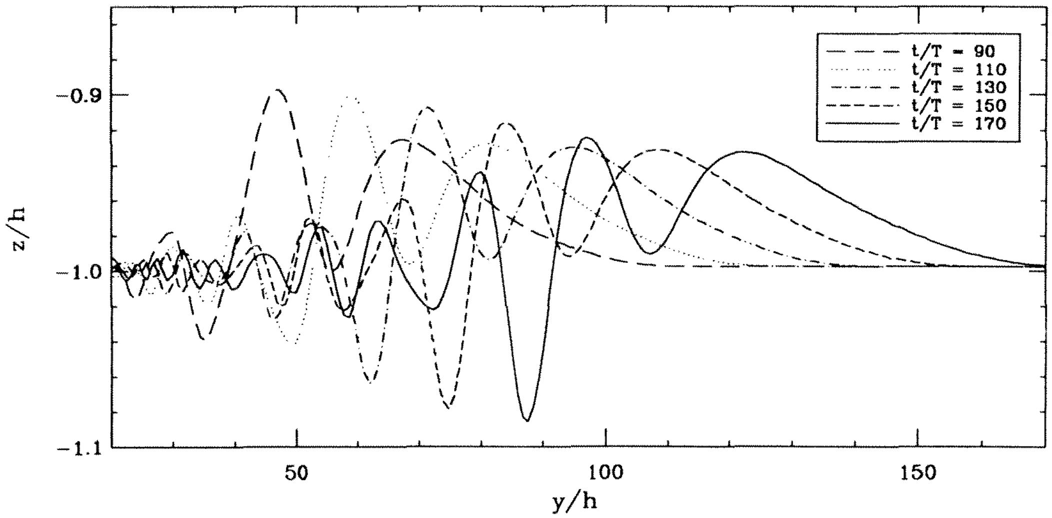

FIG. 6. *Wave trains generated by an initial elevation,* $S_0/S_s = 1.04$. *The decay of the initial elevation is slowed due to non-linear effects.*

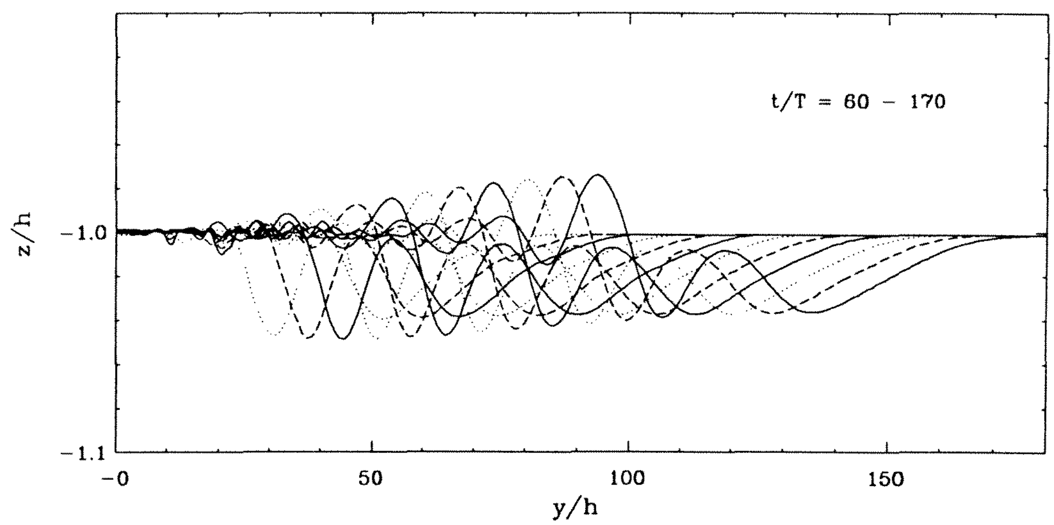

FIG. 7. *Wave trains generated by an initial depression,* $S_0/S_s = 0.52$. *The disturbance has a soliton's speed and decays very slowly.*

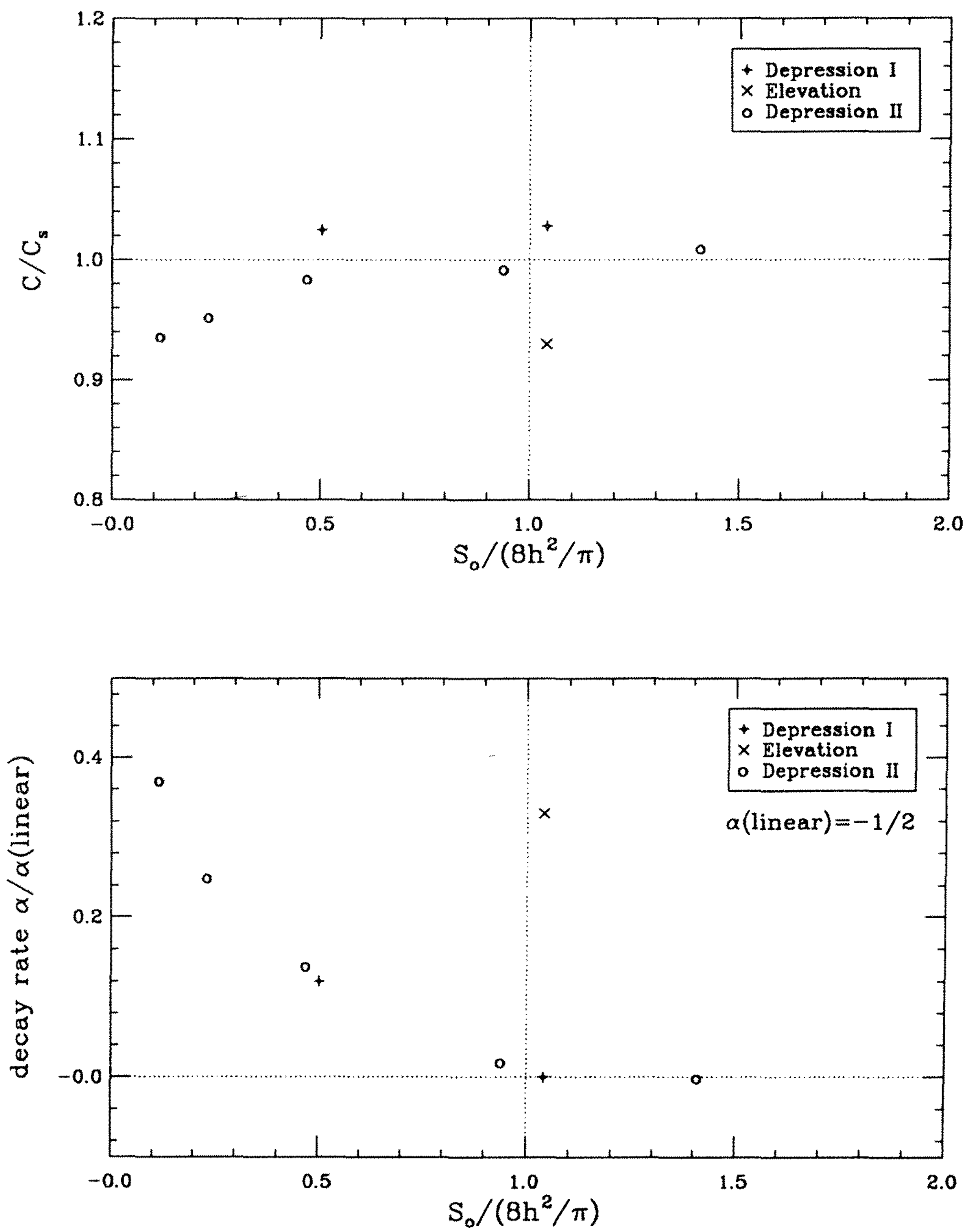

FIG. 8. *The speed of large leading disturbances, relative to soliton speed, vs. the initial area of the disturbances [upper]. The peak depression decay rate, α, of the maximum depression (elevation) vs. initial disturbance area [lower]. These results show the quasi-soliton behavior of large disturbances of depression, for $S_0 < S_s$.*

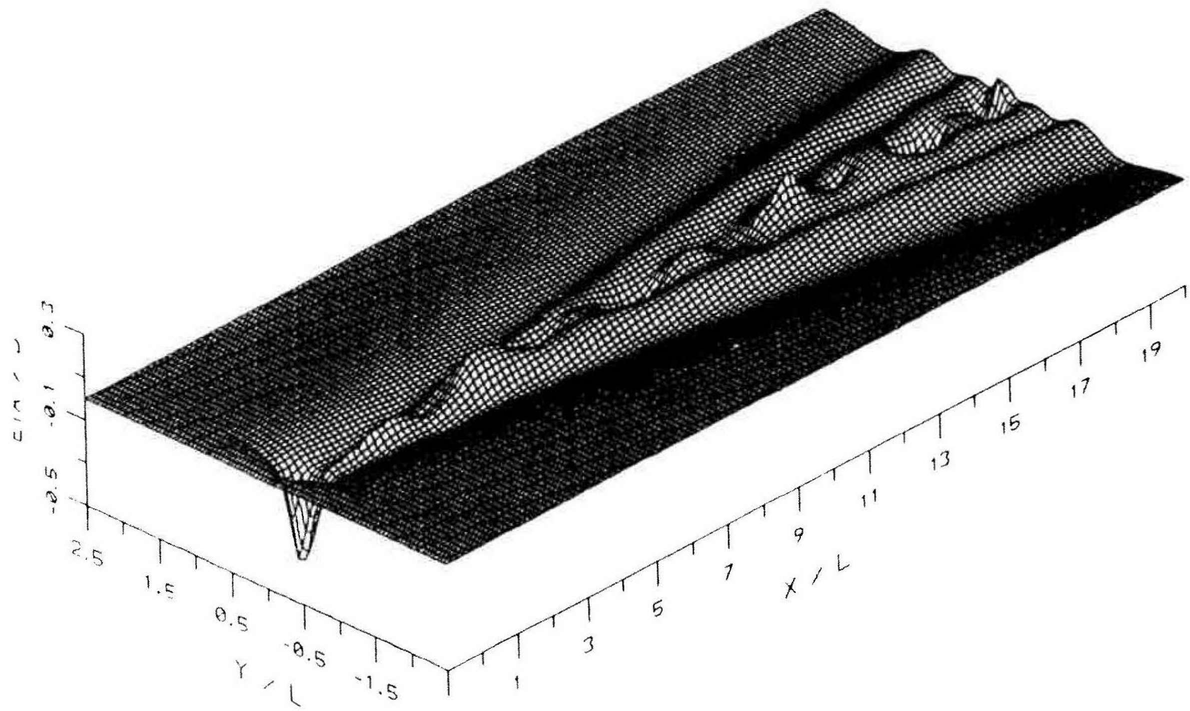

FIG. 9. *Internal wake pattern generated by triple lobe with $S_0/S_s \approx 0.22$. The strong leading waves are decaying as $t^{-1/8}$ and extend much further than shown. The resulting surface disturbances are about 10 times larger than in the linear case.*

The exact $2d + t$ theory shown here, can be extended to the asymptotic prediction of the near field, including the triple lobe pattern, in the region: $\epsilon << 1$; $F_h^2 h/L >> 1$, see Tulin *et al*(1993). In this non-linear cross flow theory, the near field densimetric flow may be considered a perturbation to the homogeneous flow and the densimetric flow pattern may be considered slender, as shown in Figure 4. Near field flows in a variety of cases have been computed numerically for the passage of a semi-submerged slender spheroid ($D/L = 0.1$). In certain cases, the hull suppresses the upwelling in the near field, resulting in triple lobe patterns with deep depressions, $S_0/S_s \approx 0.22$, and in strong, weakly decaying, leading waves, Figure 9.

This computational result shows the importance of including non-linear effects (both hull effect on upwelling and finite amplitudes on quasi-soliton propagation) in the estimation of subsurface disturbances in the wake of a ship.

Acknowledgement

The authors are grateful for the support of this work by the Ocean Technology Program of the Office of Naval Research (Dr. Tom Swean, Jr), and by the Ocean Imaging Program of the Lawrence Livermore National Laboratory (Dr. Rick Twogood).

References

[1] Benjamin, T. B. (1967) Internal waves in fluids of great depth. *J. Fluid Mech.* **29**, 559-592.

[2] Eckart, C. (1960) *Hydrodynamics of Oceans and Atmospheres* London, Pergamon Press.

[3] Ekman, V. W. (1904) *On Dead Water: The Norwegian North Polar Expedition 1893-1896* **V**, Ch. XV, Christiania.

[4] Keller, J. B. and Munk, W. H. (1970) Internal wave wakes of a body in a stratified fluid. *Physics of Fluids* **13**, 1425-1431.

[5] Lighthill, M. J. (1978) *Waves in Fluids* Cambridge University Press.

[6] Ma, H. and Tulin, M. P. (1992) Experimental study of ship internal waves: the supersonic case. *Journal of OMAE* **115**, No. 1, 16-22.

[7] Mei, C. C. (1983) *The Applied Dynamics of Ocean Surface Waves* New York: Wiley.

[8] Miloh, T. and Tulin, M. P. (1988) A theory of dead water phenomena. *Proceedings of the 17th Symposium on Naval Hydrodynamics* National Academy Press.

[9] Miloh, T. and Tulin, M. P. (1988a) Dead water phenomena: a non-linear theory of wave disturbances due to a ship in a shallow thermocline. *UCSB Ocean Engr. Lab. Tech. Rpt.* 88-31.

[10] Miloh, T., Prestin, M., Shtilman, L. and Tulin, M. P. (1993) A note on the numerical and N-soliton solutions of the Benjamin-Ono evolution equation. *Wave Motion* **17**, 1-10.

[11] Tulin, M. P. and Miloh, T. (1990) Ship internal waves in a shallow thermocline: the supersonic case. *Proceedings of the 18th Symposium on Naval Hydrodynamics* National Academy Press.

[12] Tulin, M. P., Wang, P. and Yao, Y. (1993) Numerical prediction of ship generated internal waves in a stratified ocean at supercritical Froude numbers. *Proc. of the 6th Intl. Conf. on Numerical Ship Hydrodynamics* National Academy Press.

[13] Wang, P., Yao, Y., Miloh, T. and Tulin, M. P. (1990) Near field internal waves, $F_h >> 1$: two layer asymptotic theory and characteristic calculations. *UCSB Ocean Engr. Lab. Tech. Rpt.* 90-54-1.

[14] Yih, C. S. (1965) *Dynamics of Nonhomogenous Fluids* New York: MacMillan.

[15] Yih, C. S. (1990) Patterns of ship waves. *Engineering Science- Fluid Dynamics* World Scientific Publishers.

On modeling nonlinear long waves [1]

by Theodore Yaotsu Wu and Jin E. Zhang
California Institute of Technology, Pasadena, CA 91125

Abstract

Three sets of new model equations, valid up to the third order which is higher by one order than Boussinesq's model, are derived for modeling nonlinear and dispersive long gravity waves traveling in two horizontal directions on shallow water of uniform depth. They differ in adopting different representative horizontal velocities, one being the depth-mean averaged over the vertical water column, another being at the channel bottom and the third pertaining to the water surface, with each joining the water surface elevation to constitute the unknown variables. Comparative studies of these models cover results for the wave velocity, standard wave profiles and their underlying Hamiltonian structures.

1 Introduction

Long waves in shallow water is a subject of broad interest and has a long colorful history. Physically, it has a rich variety of phenomenological manifestation, especially the existence of waves permanent in form and robust in maintaining their entities through mutual interactions and collisions as well as the remarkable property of exhibiting reccurrences of initial data when circumstances should prevail. These characteristics are due to the intimate interplay between the roles of nonlinearity and dispersion. Mathematically, it has been noted that validity of theoretical models critically depends on the domain of underlying key parameters which characterize the specific motions to be modeled. In this regard, it is so well said by Julian Cole (1968) that theories can be sought to show how different expansions based on different parametric regimes lead to different approximate equations.

The two key parameters characterizing long waves in shallow water are

$$\epsilon = h/\lambda \ , \qquad \alpha = a/h, \tag{1}$$

for waves of typical length λ, amplitude a in water of undisturbed depth h. Explanations have been provided with clarity by Cole (1968) as to how the various regimes of these parameters can be found to derive equations for approximating Airy's nonlinear long waves, linear long waves, or the class of weakly nonlinear and weakly dispersive long waves associated with the names of Boussinesq, Korteweg and De Vries. Along

[1] For the special volume "Mathematics is for solving problems: A Volume in honor of Julian Cole on his 70th birthday," to be published by SIAM.

Keywords: nonlinear wave modeling, third order soliton models.

this direction, other attempts have been made to obtain model equations for further extended premises, such as the third order approximations, for two-dimensional surface waves progressing in non-uniform media or in water of variable finite depth. Recent developments in these new areas have been achieved by Choi (1995) and Choi & Camassa (1996) who also gave a survey of relevant literatures.

In this study we shall explore, from a different approach, the role played by various different variables representing a certain unknown, even very slightly different as they may be, in developing approximate equations for modeling nonlinear waves characterized by a *fixed* parametric regime. In other words, the problem may be regarded as to enquire if there exists an optimum representative variable which can yield the best results over other alternatives, somehow in analogy to the query of seeking optimum coordinates for facilitating certain approximations to a given exact formulation. More specifically for the problem concerning long water waves, we note that in addition to the water surface elevation, we may have choices of different representative horizontal fluid velocities to constitute a pair of unkown variables. Indeed, we have at our disposal three or more candidates, one being the mean horizontal velocity averaged over the vertical water column, another being the bottom velocity, and the third pertaining to the water surface. Still, there is a fourth related to the so-called 'optimum depth' which may have effects on modifying the dispersion relationship.

All these sets of variables have of course been used in previous studies, but a comprehensive comparative study of them seems to be lacking. Historically, the bottom velocity is primarily the leading order variable used in deriving Airy's wave, Rayleigh's solution for the solitary wave, Lin and Clark's (1959) theory, and others. The mean velocity is used as the leading order variable in Boussinesq (1872), Green and Naghdi (1976), Wu (1979, 1981) and others. Use of the set consisted of the surface velocity and surface elevation is relatively more recent. Its underlying significance was first brought forth by Zakharov (1968) in that this is a natural set of canonical variables for considering the Hamiltonian structures of the model system.

In this study, we first present in §2 and §3 three sets of new model equations, valid up to the third order, based on the three sets of unknown variables just stated for modeling evolution of nonlinear dispersive waves on shallow water progressing in two horizontal directions. Of central interest is their predictions of solitary waves of the Boussinesq class, especially in regard to the differences in values for the dispersion relation, wave velocity, and wave profile; these topics are delineated and discussed in §5 and §6. Their underlying Hamiltonian structures are examined in §7.

2 The basic equations

Let us consider the class of three-dimensional long waves on a layer of water of undisturbed depth h, which is uniform. The fluid moving with velocity $(\boldsymbol{u}, w) = (u, v, w)$ occupies the flow field in $-h \leq z \leq \zeta(\boldsymbol{r}, t)$, where $z = -h$ is a rigid horizontal bottom, $\zeta(\boldsymbol{r}, t)$ is the water surface elevation from the undisturbed plane at $z = 0$, measured at the horizontal position vector $\boldsymbol{r} = (x, y, 0)$ at time t, and $\boldsymbol{r}$ is unbounded, $|\boldsymbol{r}| < \infty$. Assuming the fluid incompressible, the velocity field irrotational, so the motion satisfies the Euler equations of continuity, horizontal and vertical momentum:

$$\begin{aligned} \nabla \cdot \boldsymbol{u} + w_z &= 0, & (2)\\ \frac{d\boldsymbol{u}}{dt} = \boldsymbol{u}_t + \boldsymbol{u} \cdot \nabla \boldsymbol{u} + w\boldsymbol{u}_z &= -\frac{1}{\rho}\nabla p, & (3)\\ \frac{dw}{dt} = w_t + \boldsymbol{u} \cdot \nabla w + w w_z &= -\frac{1}{\rho} p_z - g, & (4) \end{aligned}$$

where $\nabla = (\partial_x, \partial_y, 0)$, ($\partial_x = \partial/\partial x$, etc.) is the horizontal projection of the vector gradient operator, p is the pressure, ρ the density and g the gravitational acceleration. Here, the subscripts t and z denote differentiation. The boundary conditions are

$$\begin{aligned} w &= \frac{d\zeta}{dt} & & (z = \zeta(\boldsymbol{r}, t)), & (5)\\ p &= p_a(\boldsymbol{r}, t) & & (z = \zeta(\boldsymbol{r}, t)), & (6)\\ w &= 0 & & (z = -h), & (7) \end{aligned}$$

where $p_a(\boldsymbol{r}, t)$ is a given external pressure disturbance gaged over the constant basic pressure. Here the capillary effect is not considered.

To adopt the depth-mean velocity as a dependent variable, we make use of the depth-mean equations obtained by averaging (2)-(4) over the water column $-h < z < \zeta$ under the kinematic boundary conditions (5) and (7) (Wu, 1979, 1981),

$$\begin{aligned} \eta_t + \nabla \cdot (\eta \overline{\boldsymbol{u}}) &= 0, & (8)\\ (\eta \overline{\boldsymbol{u}})_t + \nabla \cdot (\eta \overline{\boldsymbol{u}\boldsymbol{u}}) &= -\eta \overline{\nabla p}, & (9)\\ (\eta \overline{w})_t + \nabla \cdot (\eta \overline{\boldsymbol{u}w}) &= -g\eta - (p_a - p_h), & (10) \end{aligned}$$

where the quantities with an overhead bar denote their depth-mean,

$$\overline{f}(\boldsymbol{r}, t) = \frac{1}{\eta} \int_{-h}^{\zeta} f(\boldsymbol{r}, z, t)\,dz \qquad (\eta = h + \zeta), \tag{11}$$

and $\overline{\boldsymbol{u}\boldsymbol{u}}$ is the depth mean of the dyad $\boldsymbol{u}\boldsymbol{u}$ whose horizontal divergence is $\nabla \cdot (\boldsymbol{u}\boldsymbol{u}) = (\nabla \cdot \boldsymbol{u})\boldsymbol{u}$. This system of depth-mean equations is of course unclosed because there are more unknown variables than the number of equations. Closure of the system for the class of long waves can be proceeded as shown for the family of Boussinesq equations by Wu (1981).

Here we shall derive the model equations up to the third order in validity, which is higher by one order than the Boussinesq family.

3 Nonlinear dispersive long wave models

For weakly nonlinear and weakly dispersive waves, the parameter α in (1) is assumed small and $\alpha = O(\epsilon^2)$ for the Boussinesq family, which is here assumed for the present study. Thus, with the vertical length scaled by h, horizontal length by λ, the three-dimensional Laplace equation satisfied by the velocity potential ϕ involves the parameter ϵ

$$\phi_{zz} + \epsilon^2 \nabla^2 \phi = 0 \qquad (-1 \le z \le \zeta). \tag{12}$$

Further, with ϕ scaled by $c\lambda$, where $c = \sqrt{gh}$ is the linear wave speed, ϕ satisfying (12) may assume an expansion of the form

$$\phi(\boldsymbol{r}, z, t; \alpha, \epsilon) = \alpha \sum_{n=0}^{\infty} \epsilon^{2n} \Phi_n(\boldsymbol{r}, z, t) = \alpha \sum_{n=0}^{\infty} \frac{(-1)^n}{(2n)!} \left[\epsilon(1+z)\right]^{2n} \nabla^{2n} \phi_0(\boldsymbol{r}, t; \epsilon). \tag{13}$$

Here, ϕ, jointly with the horizontal velocity $\boldsymbol{u}$ (scaled by c) and the elevation ζ (scaled by h) are of order α as assumed. The function $\phi_0(\boldsymbol{r}, z, t; \epsilon)$, which is the only unknown involved in ϕ, may depend on the parameter ϵ resulting from appropriate regroupings of the complimentary solutions of the higher-order equations such that $\phi_0(\boldsymbol{r}, z, t; \epsilon) = O(1)$ as $\epsilon \to 0$. This regrouping is admissible provided the medium is uniform (h =const.) and unbounded, in the absence of any boundary effects of specific order in magnitude. From this expansion of ϕ, we deduce the horizontal and vertical velocity components, $\boldsymbol{u}$ and w, both scaled by c, from $\boldsymbol{u} = \nabla\phi$, $w = \epsilon^{-1}\partial\phi/\partial z$, giving

$$\boldsymbol{u} = \alpha \sum_{n=0}^{\infty} \epsilon^{2n} \boldsymbol{u}_n = \alpha \sum_{n=0}^{\infty} \frac{(-1)^n}{(2n)!} \left[\epsilon(1+z)\right]^{2n} \nabla^{2n+1} \phi_0(\boldsymbol{r}, t; \epsilon), \tag{14}$$

$$w = \alpha \sum_{n=1}^{\infty} \epsilon^{2n-1} w_n = \alpha \sum_{n=1}^{\infty} \frac{(-1)^n}{(2n-1)!} \left[\epsilon(1+z)\right]^{2n-1} \nabla^{2n} \phi_0(\boldsymbol{r}, t; \epsilon), \tag{15}$$

where $\boldsymbol{u}_0(\boldsymbol{r}, t) = \nabla\phi_0$. Now, the horizontal velocity at the bottom plane is simply

$$\alpha \boldsymbol{u}_0 = \alpha \nabla \phi_0. \tag{16}$$

We further have the depth-mean velocity $\overline{\boldsymbol{u}}$ and at-surface velocity $\hat{\boldsymbol{u}}$ as

$$\overline{\boldsymbol{u}} = \alpha \sum_{n=0}^{\infty} \frac{(-1)^n}{(2n+1)!} \left[\epsilon(1+\zeta)\right]^{2n} \nabla^{2n} \boldsymbol{u}_0, \tag{17}$$

$$\hat{\boldsymbol{u}} = \alpha \sum_{n=0}^{\infty} \frac{(-1)^n}{(2n)!} \left[\epsilon(1+\zeta)\right]^{2n} \nabla^{2n} \boldsymbol{u}_0. \tag{18}$$

Also, from (14), we readly see that

$$\overline{\boldsymbol{u}\boldsymbol{u}} = \overline{\boldsymbol{u}}\,\overline{\boldsymbol{u}} + O(\alpha^2 \epsilon^4). \tag{19}$$

Whence the left-hand side of (9) becomes, upon using equation (8),

$$(\eta \overline{\boldsymbol{u}})_t + \nabla \cdot (\eta \overline{\boldsymbol{u}\boldsymbol{u}}) = \eta \left[\overline{\boldsymbol{u}}_t + \overline{\boldsymbol{u}} \cdot \nabla \overline{\boldsymbol{u}}\right] + O(\epsilon^9). \tag{20}$$

To achieve the closure of the system of equations, we now apply the Bernoulli equation (properly scaled) in order to relate $\overline{\nabla p}$ in (9) to veocity, namely,

$$\begin{aligned} p + z &= -\phi_t - \frac{1}{2}(\boldsymbol{u}^2 + w^2) \\ &= -\alpha\left[\dot{\phi}_0 + \epsilon^2\dot{\Phi}_1 + \epsilon^4\dot{\Phi}_2 + \frac{\alpha}{2}\boldsymbol{u}_0^2 + \alpha\epsilon^2(\boldsymbol{u}_0 \cdot \boldsymbol{u}_1 + \frac{1}{2}w_1^2)\right] + O(\epsilon^8), \quad (21) \end{aligned}$$

which gives on the free surface another relation,

$$p_a + \zeta = -\alpha\left[\dot{\phi}_0 + \epsilon^2\hat{\dot{\Phi}}_1 + \epsilon^4\hat{\dot{\Phi}}_2 + \frac{\alpha}{2}\boldsymbol{u}_0^2 + \alpha\epsilon^2(\boldsymbol{u}_0 \cdot \hat{\boldsymbol{u}}_1 + \frac{1}{2}\hat{w}_1^2)\right] + O(\epsilon^8), \qquad (22)$$

where the symbol $\hat{(\cdot)}$ denotes the value of $(\cdot)$ at $z = \zeta(\boldsymbol{r}, t)$. From this we deduce that

$$\begin{aligned} \overline{\nabla p} - \nabla\zeta - \nabla p_a &= \alpha\epsilon^2[\nabla\hat{\dot{\Phi}}_1 - \overline{\nabla\dot{\Phi}_1} + \epsilon^2(\nabla\hat{\dot{\Phi}}_2 - \overline{\nabla\dot{\Phi}_2}) + \alpha\nabla(\boldsymbol{u}_0 \cdot \hat{\boldsymbol{u}}_1) \\ &\quad -\alpha\overline{\nabla(\boldsymbol{u}_0 \cdot \boldsymbol{u}_1)} + \frac{\alpha}{2}(\nabla\hat{w}_1^2 - \overline{\nabla w_1^2})] + O(\epsilon^9). \qquad (23) \end{aligned}$$

Substituting the resulting expressions for Φ_1, Φ_2, $\boldsymbol{u}_1$ and w_1 given in (13)-(15) into the above equation and using (9) and (20), we obtain, after some straightforward calculation, the model equations for
(A) the $\{\zeta, \overline{\boldsymbol{u}}\}$ system, —— *on the mean velocity basis*, as

$$\begin{aligned} \zeta_t + \nabla \cdot [(1+\zeta)\overline{\boldsymbol{u}}] &= 0, \qquad (24) \\ \overline{\boldsymbol{u}}_t + \overline{\boldsymbol{u}} \cdot \nabla\overline{\boldsymbol{u}} + \nabla\zeta &= \frac{1}{3}(1+\zeta)^2\nabla^2\overline{\boldsymbol{u}}_t + \frac{1}{45}\nabla^4\overline{\boldsymbol{u}}_t + (\nabla\zeta)\nabla \cdot \overline{\boldsymbol{u}}_t \\ &\quad + \frac{1}{3}\nabla\left[\overline{\boldsymbol{u}} \cdot \nabla^2\overline{\boldsymbol{u}} - (\nabla \cdot \overline{\boldsymbol{u}})^2\right] - \nabla p_a. \qquad (25) \end{aligned}$$

In (25), the third term on the right-hand side with $\nabla\zeta$ involves using the leading-term equation of (24), and (24) repeats (8). We remark that in this final form of (24) and (25), the scale factor α has been absorbed into ζ and $\overline{\boldsymbol{u}}$, and ϵ is absorbed by rescaling *both* the vertical and horizontal lengths by h as well as for the other quantities. We further note that the continuity equation (24) is exact whereas the horizontal momentum equation is accurate up to $O(\epsilon^7)$, with an error estimate of $O(\epsilon^9)$, provided of course all the derivatives involved are smooth.

Next, to convert the variable basis from $\{\zeta, \overline{\boldsymbol{u}}\}$ to $\{\zeta, \boldsymbol{u}_0\}$ we substitute the expansion (17) into (24) and (25), giving the model equations for
(B) the $\{\zeta, \boldsymbol{u}_0\}$ system, —— *on the bottom variable basis*, as

$$\begin{aligned} \zeta_t + \nabla \cdot [(1+\zeta)\boldsymbol{u}_0] &= \nabla \cdot \left[\frac{1}{6}(1+\zeta)^3\nabla^2\boldsymbol{u}_0 - \frac{1}{5!}\nabla^4\boldsymbol{u}_0\right], \qquad (26) \\ \boldsymbol{u}_{0t} + \boldsymbol{u}_0 \cdot \nabla\boldsymbol{u}_0 + \nabla\zeta &= \frac{1}{2}(1+\zeta)^2\nabla^2\boldsymbol{u}_{0t} - \frac{1}{4!}\nabla^4\boldsymbol{u}_{0t} + (\nabla\zeta)\nabla \cdot \boldsymbol{u}_{0t} \\ &\quad + \frac{1}{2}\nabla\left[\boldsymbol{u}_0 \cdot \nabla^2\boldsymbol{u}_0 - (\nabla \cdot \boldsymbol{u}_0)^2\right] - \nabla p_a. \qquad (27) \end{aligned}$$

The third conversion of variable basis is from $\{\zeta, \overline{\boldsymbol{u}}\}$ to $\{\zeta, \hat{\boldsymbol{u}}\}$; and this can be constructed by using the relationship

$$\overline{\boldsymbol{u}} = \hat{\boldsymbol{u}} + \frac{1}{3}\epsilon^2(1+\zeta)^2\nabla^2\hat{\boldsymbol{u}} + \frac{2}{15}\epsilon^4(1+\zeta)^4\nabla^4\hat{\boldsymbol{u}} + O(\epsilon^6) , \tag{28}$$

which can be deduced by eliminating $\boldsymbol{u}_0$ between (17) and (18). Substituting (28) into (24) and (25) yields the model equation for
(C) the $\{\zeta, \hat{\boldsymbol{u}}\}$ system, —— *on the surface variable basis*, as

$$\zeta_t + \nabla\cdot[(1+\zeta)\hat{\boldsymbol{u}}] = -\nabla\cdot\left[\frac{1}{3}(1+\zeta)^3\nabla^2\hat{\boldsymbol{u}} + \frac{2}{15}\nabla^4\hat{\boldsymbol{u}}\right], \tag{29}$$

$$\hat{\boldsymbol{u}}_t + \hat{\boldsymbol{u}}\cdot\nabla\hat{\boldsymbol{u}} + \nabla\zeta = (\nabla\zeta)\nabla\cdot\hat{\boldsymbol{u}}_t - \nabla p_a. \tag{30}$$

Thus we have derived three sets of model equations for evaluating weakly nonlinear and weakly dispersive three-dimensional long waves based on different variable bases. They are otherwise equivalent to each other, at least in principle, since these equations are all valid up to $O(\epsilon^7)$, with an error estimate of $O(\epsilon^9)$ except for (24) which is exact. For the general case of nonlinear three-dimensional waves, these theoretical models, accurate to the third order, are believed new. For three-dimensional wave motions of Boussinesq's family (to which these new models reduce if all the terms of $O(\epsilon^7)$ are neglected), there have been other models in existence, including the generalized Boussinesq (Wu, 1979, 1981), the Green-Naghdi equation applied by Ertekin, Webster & Wehausen (1984), and the KP (Kadomtsev-Petviashvili, 1970) equation. These models are classified as three-dimensional since after the solution is obtained in terms of any one representative basis over the domain $(\boldsymbol{r}, t)$, the local three-dimensional flow field can be readily deduced from the basic expansions (13)-(15) over the region $(\boldsymbol{r}, z, t)$. In this category of Boussinesq's family, some specific cases will be discussed in our comparative study given later.

4 Nonlinear, dispersive long waves in plane motion

For the case of plane motion taking place in a region of (x, z, t), equations (24)-(25) of medel (A) become

$$\zeta_t + [(1+\zeta)\overline{u}]_x = 0, \tag{31}$$

$$\overline{u}_t + \overline{u}\,\overline{u}_x + \zeta_x = \frac{1}{3}(1+\zeta)^2\overline{u}_{xxt} + \frac{1}{45}\overline{u}_{xxxxt} + \zeta_x\overline{u}_{xt} + \frac{1}{3}\left[\overline{u}\ \ \overline{u}_{xx} - \overline{u}_x^2\right]_x - (p_a)_x. \tag{32}$$

Similar equations can be written down for models (B) and (C). In this connection, the one-space-dimensional Green-Naghdi (or GN) equations consist of the same continuity equation as (31) but a different momentum equation (see Green & Naghdi (1976), Miles & Salmon (1985), Camassa & Holm (1993), Choi & Camassa (1995)) which reads

$$\overline{u}_t + \overline{u}\,\overline{u}_x + \zeta_x = \frac{1}{1+\zeta}\frac{\partial}{\partial x}\left[\frac{1}{3}(1+\zeta)^3(\overline{u}_{xt} + \overline{u}\,\overline{u}_{xx} - (\overline{u}_x)^2)\right]. \tag{33}$$

These GN equations have been adopted by Ertekin et al (1984) with numerical results compared with the corresponding results from Wu's (1981) gB equations, which are one order lower in accuracy, with some discrepancies.

However, it is noted that compared with the present new model, the second term on the right-hand side of (32), namely $\frac{1}{45}\overline{u}_{xxxxt}$, is missing in the GN equation (33). It remains to be of interest to find how the relevant results will fair with the missing term restored.

5 Dispersion relationship

The dispersion relation associated with the linearized version of the three models is of basic interest since they not only indicate how small long waves will propagate, but, because of their approximate forms, may also bear inference on whether their numerical solutions are apt to be stable and convergent, or not, when solutions are sought by computational methods for reasons to be seen below. Following the procedure of testing a progressive one-dimensional wave solution, $u = a\ \exp[i(kx - \omega t)]$, we readly obtain the following results.

(A) the $\{\zeta, \overline{\boldsymbol{u}}\}$ system, —— For this model, the linearized equation of (24) and (25),

$$\partial_t^2\left[1 - \frac{1}{3}\partial_x^2 - \frac{1}{45}\partial_x^4\right]\overline{u} - \overline{u}_{xx} = 0, \tag{34}$$

is found to have the dispersion relation as

$$\omega^2 = \frac{k^2}{1 + \frac{1}{3}k^2 - \frac{1}{45}k^4}. \tag{35}$$

(B) the $\{\zeta, \boldsymbol{u}_0\}$ system, —— From the linearized equation of (26) and (27),

$$\partial_t^2\left[1 - \frac{1}{2}\partial_x^2 + \frac{1}{4!}\partial_x^4\right]u_0 - \partial_x^2\left[1 - \frac{1}{3!}\partial_x^2 + \frac{1}{5!}\partial_x^4\right]u_0 = 0, \tag{36}$$

it follows that

$$\omega^2 = k^2\frac{1 + \frac{1}{3!}k^2 + \frac{1}{5!}k^4}{1 + \frac{1}{2!}k^2 + \frac{1}{4!}k^4}. \tag{37}$$

(C) the $\{\zeta, \hat{u}\}$ system, —— In this case, the linearized equation of (29) and (30),

$$\partial_t^2 \hat{u} - \partial_x^2 \left[1 + \frac{1}{3}\partial_x^2 + \frac{2}{15}\partial_x^4\right] \hat{u} = 0, \tag{38}$$

gives the dispersion relation

$$\omega^2 = k^2 \left[1 - \frac{1}{3}k^2 + \frac{2}{15}k^4\right]. \tag{39}$$

We thus see that these models have their dispersion relations expressed in terms of different rational functions of k. If all the waves that can possibly arise in the model flow field are long, the wave number k will indeed always remain small. In this event, both relations (35) and (37) agree with the finite expansion (39) which is the leading-term expansion of the dispersion relation on linear theory taking k small, i.e.,

$$\omega^2 = k \tanh k = k^2 \left[1 - \frac{1}{3}k^2 + \frac{2}{15}k^4 + O(k^6)\right], \tag{40}$$

up to the order meant for their validity.

However, when numerical solutions are sought, it is often difficult to avoid numerical errors of the grid size which correspond to large errors in the wavenumber k. Such errors would become greater, the smaller the grids, unless effective remedies be duly administered to suppress such error growth. Viewed in this light, models (A) and (B) are expected to be more robust than (C) in regard to numerical stability and convergence. Such difficulties could be curtailed with recourse to securing an algorithm effective for computation or to an appropriate modification of certain terms of the highest order (retained) in ways consistent with the first-order approximation of the original equation. The latter recourse is in much the same approach as in introducing the 'regularized KdV' equation by Benjamin et al (1972) for facilitating computation of the Korteweg-de Vries equation.

6 Solitary waves of the Boussinesq class

A point of central interest is to examine and compare the solitary wave solutions given by the various different models. Here we shall confine our investigation to the solitary waves of the Boussinesq class. In this premise, the three sets of model equations reduce, in the absence of external forcing, to the following equations:

(A) the $\{\zeta, \overline{u}\}$ system —

$$\zeta_t + [(1+\zeta)\overline{u}]_x = 0, \tag{41}$$

$$\overline{u}_t + \overline{u}\,\overline{u}_x + \zeta_x = \frac{1}{3}\overline{u}_{xxt}. \tag{42}$$

(B) the $\{\zeta, u_0\}$ system —

$$\zeta_t + [(1+\zeta)u_0]_x = \frac{1}{6}u_{0xxx}, \tag{43}$$

$$\overline{u}_t + u_0 u_{0x} + \zeta_x = \frac{1}{2}u_{0xxt}. \tag{44}$$

(C) the $\{\zeta, \hat{u}\}$ system —

$$\zeta_t + [(1+\zeta)\hat{u}]_x = -\frac{1}{3}\hat{u}_{xxx}, \tag{45}$$

$$\hat{u}_t + \hat{u}\hat{u}_x + \zeta_x = 0. \tag{46}$$

In practice, solitary wave solutions to these sets of model equations are known to have been sought with some modification of various terms of the highest order in consistency with the first-order approximation of the original equations, especially when solutions are sought in closed form. But there are two first order equations in each set, and there are several terms of the highest order that can be candidates for modification. These varieties of variations may lead to differing solutions but should not alter their error estimate, at least in principle. However, it has been found, e.g. by Yates (1995) that numerically, these different solutions can have considerable deviations in value from one another. To establish a concrete basis for the present comparative study, we shall regard the above sets of model equations as fixed standard to which we pursue their exact solution, with numerical assistence, if necessary.

For system (A), which is the original Boussinesq two-equation model, an exact solution of (41) and (42) for the solitary wave has been obtained by Teng and Wu (1992). A solitary wave of amplitude a is found to propagate with phase velocity

$$c = \left[\frac{6(1+a)^2}{a^2(3+2a)}\{(1+a)\ln(1+a) - a\}\right]^{1/2}. \tag{47}$$

This result for the phase velocity c, as shown in figure 1, is numerically slower than $c = \sqrt{1+a}$ which was first found analytically by Rayleigh (1876) and empirically by Russell (1845), which is in turn slower than $c = 1 + a/2$ found by Korteweg & de Vries (1895), but is found to be in good agreement with the experimental results of Daily & Stephan (1952). The wave profile, as shown in figures 2 - 4, is also found in broad agreement with the experimental measurement of Daily & Stephan over the amplitude range covered.

To evaluate the solitary wave solution in system (B), we set $\zeta = \zeta(s)$ and $u_0 = u_0(s)$, where $s = x - ct$ and c is the undetermined wave speed. Substituting these relations into (43) and (44) and integrating the resulting equations once under the regularity condition at infinity, we obtain

$$-c\zeta + (1+\zeta)u_0 = \frac{1}{6}u_{0ss}, \tag{48}$$

$$-cu_0 + \frac{1}{2}u_0^2 + \zeta = -\frac{1}{2}cu_{0ss}. \tag{49}$$

Eliminating u_{0ss} between these equations yields

$$\zeta = \frac{4cu_0 + u_0^2}{6c(b-u_0)} \equiv Z(u_0;c) \quad (b = c - \frac{1}{3c}). \tag{50}$$

Then substituting (50) in (49) leads to the following first integral,

$$u_s^2 = -\frac{2}{3c}u_0^3 + (2+\frac{1}{3c^2})u_0^2 + \frac{2}{3c}(5-\frac{1}{3c^2})[u_0 + b\ln(1-\frac{u_0}{b})] \equiv G(u_0;c). \tag{51}$$

$G(u_0;c)$ has a double zero as $u_0 \to 0$, so as to have u_0 fall off exponentially at infinity, and a simple zero at $u_0 = u_c$ say, at the wave crest where $\zeta = a$. The wave speed $c = c(a)$ is therefore given implicitly by

$$G(u_c,c) = 0 \quad \text{and} \quad Z(u_c,c) = a. \tag{52}$$

The velocity $u_0 = u_0(s)$ is then given by quadrature,

$$s = \pm \int_{u_c}^{u_0} \frac{du}{[G(u;c)]^{1/2}}, \tag{53}$$

and the wave profile $\zeta = \zeta(s)$ by (50). The final numerical results are shown in figures 1 - 4.

Similarly, for the solitary wave solution in system (Ç), $\zeta = \zeta(s)$ and $\hat{u} = \hat{u}(s)$ $(s = x - ct)$, the first integral of (45) and (46) reads

$$-c\zeta + (1+\zeta)\hat{u} = \frac{1}{3}\hat{u}_{ss}, \tag{54}$$

$$c\hat{u} - \frac{1}{2}\hat{u}^2 - \zeta = 0. \tag{55}$$

After eliminating ζ from these equations and integrating once more, there results

$$\hat{u}_s^2 = \frac{3}{4}\hat{u}^2(2c+2-\hat{u})(2c-2-\hat{u}). \tag{56}$$

This equation has a solitary wave solution in implicit form as

$$\left(\frac{1}{u} - \frac{1}{2(c+1)}\right)^{1/2} + \left(\frac{1}{u} - \frac{1}{2(c-1)}\right)^{1/2} = \frac{1}{\sqrt{(c^2-1)}}\exp\left(\sqrt{\frac{3}{4}(c^2-1)}|x-ct|\right). \tag{57}$$

The wave speed of the wave of amplitude a is found from (55) and (56) to be

$$c = 1 + \frac{a}{2}\,. \tag{58}$$

These results are shown in figures 1 - 4 together with that of systems (A) and (B) for comparison with the experimental data available.

7 The Hamiltonian structures

In making analysis of nonlinear evolution equations, determination of their Hamiltonian structures is of fundamental importance because these structures are intimately related to the question and answer concerning the integrability of the system. (For a discourse on recent development in the general theory, reference may be made to Olver, 1986.)

Of the three model systems at hand, only the surface-variable (C)- system is known to have a Hamiltonian structure. Indeed, we have the important discovery by Kaup (1975) and Kupershmidt (1985) that the system of equations (45) and (46) has not only a Hamiltonian structure but a tri-Hamiltonian one. In other words, this system has the remarkable property that it can be written in Hamiltonian form in not just one, but three distinct ways. For the sake of making subsequent discussions on the other two systems as well, we cite the result below.

First, by a uniform scaling change in x and t, the coefficient $(1/3)$ of the term u_{xxx} in (45) can be written as $(1/4)$ without altering (46). Then by the transformation

$$u = -v, \qquad 1 + \zeta = w - \frac{1}{2}v_x, \tag{59}$$

(45) and (46) are converted to

$$v_t = \partial(v^2 + 2w - v_x)/2, \tag{60a}$$

$$w_t = \partial(vw + \frac{1}{2}w_x), \tag{60b}$$

where $\partial = \partial/\partial x$. This system of equations can be written in the following tri-Hamiltonian form:

$$V_t = B_1\delta H_3 = B_2\delta H_2 = B_3\delta H_1, \tag{61a}$$

$$V = \begin{bmatrix} v \\ w \end{bmatrix}, \quad B_1 = \begin{bmatrix} 0 & \partial \\ \partial & 0 \end{bmatrix}, \quad B_2 = \begin{bmatrix} 2\partial & \partial v - \partial^2 \\ v\partial + \partial^2 & w\partial + \partial w \end{bmatrix}, \tag{61b}$$

$$B_3 = \begin{bmatrix} 2v\partial + 2\partial v & 2w\partial + 2\partial w + \partial(v-\partial)^2 \\ 2w\partial + 2\partial w + (v+\partial)^2\partial & (v+\partial)(w\partial + \partial w) + (w\partial + \partial w)(v - \partial) \end{bmatrix}, \tag{61c}$$

$$H_1 = \int \frac{1}{2}w\,dx, \quad H_2 = \int \frac{1}{2}wv\,dx, \quad H_3 = \int \left(\frac{1}{2}wv^2 + \frac{1}{2}w^2 + \frac{1}{2}vw_x\right)dx, \tag{61d}$$

where

$$\delta H = \begin{bmatrix} \delta H/\delta v \\ \delta H/\delta w \end{bmatrix}$$

denotes the vector of variational differentials and again, $\partial = \partial/\partial x$.

With this remarkable result, it then follows from the general theorem (e.g., Olver 1986) that the system is completely integrable, possesses infinite number of conservation laws, and integrals can be obtained by application of inverse scattering techniques. Further, the system can support solitary waves, and interactions between solitary waves will always be elastic and remain clean. These results, of course, have the root stemmed from the general theorem founded by Zakharov (1968).

In contrast to this conclusive result for system (C), no such findings are known for the systems (A) and (B). In this respect, we should note that finding the Hamiltonian structure of an evolution system can be a very difficult task. However, for practical purposes, recourse could be made to finding an approximate transformation that leaves merely slight modifications only to some terms of the highest order in the equations of the system so that the modified system can have a Hamiltonian structure that can be of use.

In the case at hand, it is relatively easy if we take the adventage of the relations (17) and (18) between the basic variables of the three systems. More specifically, by using the transformations

$$\hat{u} = u_0 - \frac{1}{2} u_{0xx}, \tag{64a}$$

$$\hat{u} = \overline{u} - \frac{1}{3} \overline{u}_{xx}, \tag{64b}$$

for system (A) and (B), respectively, the Hamiltonian equations given above for system (C) can be transformed into the variables of system (A) and (B) as useful approximations. The basic question, however, is nevertheless still left open.

8 Discussion and conclusion

Three sets of new model equations of the third order in accuracy are derived for modeling nonlinear and dispersive three-dimensional long gravity waves on shallow water. The present comparative study of these models is directed to explore the intrinsic properties in physical and mathematical terms that these models possess. The preliminary resutls can be summarized as follows.

In physical terms, the present study extends the scope of the work by Teng and Wu (1992) who compared the KdV model and Boussinesq's equations (which is the present A system to second order) with experiment for solitary waves taken as a standard reference. Here, the solitary wave solutions of the three models are further assessed by comparision with the experiments of Daily and Stephan (1952) and Weidman and Maxworthy (1968). In regard to wave velocity predicted by the three models, the mean-variable system (A) appears in the best agreement with experiments, especially for the higher range of $\alpha = a/h > 0.3$ to 0.6, as can be seen from figure 1. In comparison, the prediction by the bottom- variable system (B) is slightly lower than that by (A), whereas the surface-variable system (C) joins the KdV equation to give the value $c = 1 + \frac{1}{2}\alpha$, in a greater departure from the experiments. Although the exeprimental data have some scatter in the range below $\alpha = 0.3$, these experiments are recognized to have been accomplished with great care, especially in making necessary corrections for the effects of viscous dissipation.

With respect to wave profile shapes, Teng & Wu's (1992) finding remains to be true that the Boussinesq (the present system A) gives the most consistent agreement with experiments over the range tested. In comparison, the surface-variable system (C) gives a profile little too broad in the upper part and too narrow around the base of the wave profile, whereas the bottom-variable system (B) exhibits a very slight deviation from experimental data in the opposite sense.

In the mathematical context, the surface-variable system (C) is outstanding in possessing a tri-Hamiltonian structure from which follows the distinguished properties as stated above. Although the other two systems are not known to have an exact Hamiltonian structure, approximate Hamiltonian structures can be constructed by making a consistent transformation of variables between the systems without altering the order of the original error estimate.

In conclusion, we point out with emphasis that while the three new models are valid to third order, the present comparative study in exploring the differences between theory and experiment has been limited by the circumstance only to the second order. It would be of great interest to determine the potential effects due to the higher order corrections now gained for the three model systems on such interesting issues as their predictions of wave properties, bidirectional wave interactions as studied by Wu (1994, 1995) and Yih & Wu (1995), wave propagation in non-homogeneous media as considered by Teng & Wu (1994), their Hamiltonian structures, and other related topics, which are being pursued.

Acknowledgement: We take pleasure in expressing our appreciation for having the opportunity of taking part in this distinguished Conference and joining all the other colleagues and friends to pay our sincere tribute to Julian Cole. Especially, TYW is most grateful to Julian for valuable benefits received from dedicated studies of his outstanding writings, inspirational teaching and enlightening examples of learning that stimulate emulation.

We also acknowledge with appreciation having the support to this study from NSF Grant CMS-9503620.

References

[1] Benjamin, T. B., Bona, J. L. & Mahony, J. J. 1972 Model equations for long waves in nonlinear dispersive systems. *Phil. Trans. Roy. Soc.* A **272**, 47-78.

[2] Boussinesq, J. 1872 Theorie des ondes et des remous qui se propagent le long d'un canal rectangulaire horizontal, en communiquant au liquide contenu dans ce canal des vitesses sensiblement pareilles de la surface au fond. *J. Math. Pures Appl. Ser. 2*, **17**, 55-108.

[3] Camassa, R. & Holm, D. D. 1993 An integrable shallow water equation with peaked solitons. *Phy. Rev. Lett.* **71**, 1661-1664.

[4] Choi, W. 1995 Nonlinear evolution equations for two-dimensional surface surface waves in a fluid of finite depth. *J. Fluid Mech.* **295**, 381-394.

[5] Choi, W. & Camassa, R. 1996 Weakly nonlinear internal waves in a two-fluid system. *J. Fluid Mech.* (to be published).

[6] Cole, J. D. 1968 *Perturbation methods in applied mathematics*, Blaisdell Pub. Co..

[7] Daily, J. W. & Stephan, S. C. 1952 The solitary wave. In *Proc. Third Conf. on Coastal Engineering*, pp. 13-30.

[8] Ertekin, R. C., Webster, W. C. & Wehausen, J. V. 1984 Ship-generated solitons. In *Proc. 15th Symp. Naval Hydrodynamics.* National Academy of Sciences. Washington, D. C..

[9] Green, A. E. & Naghdi, P. M. 1976 A derivation of equations for wave propagation in water of variable depth. *J. Fluid Mech.* **78**, 237-246.

[10] Kadomtsev, B. B. & Petviashvili, V. I. 1970 On the stability of solitary waves in weakly dispersing media. *Sov. Phys. Dokl.* **15**, 539-541.

[11] Kaup, D. J. 1975 A higher-order water-wave equation and the method for solving it. *Prog. Theor. Phys.* **54**, 396-408.

[12] Kupershmidt, B. A. 1985 Mathematics of dispersive water waves. *Comm. Math. Phys.* **99**, 51-73.

[13] Korteweg, D. J. de Vries, G. 1895 On the change of form of long waves advancing in a rectangular canal, and on a new type of long stationary waves. *Phil. Mag.* **39**, 422-443.

[14] Lin, C. C. & Clark, A. 1959 On the theory of shallow water waves. *Tsing Hua J. of Chinese Studies*, Special **1**, 54-82. [*Selected Papers*, **1**, 352-360.]

[15] Miles, J. & Salmon, R. 1985 Weakly dispersive nonlinear gravity waves. *J. Fluid Mech.* **157**, 519-531.

[16] Olver, P.J. 1993 *Applications of Lie Group to Differential Equations* Springer-Verlag, 433-466.

[17] Rayleigh, L. 1876 On waves. *Phil. Mag.* **1**, 257-279; Scientific papers, vol.1, pp. 251-271.

[18] Russell, J. S. 1845 Report on waves. *Rep. Meet. Brit. Assoc. Adv. Sci., 14th, York*, 1844, pp. 311-390. London: John Murray.

[19] Teng, M.H. and Wu, T.Y. 1992 Nonlinear water waves in channels of arbitrary shape. *J. Fluid Mech.* **242**, 211-233.

[20] Teng, M.H. and Wu, T.Y. 1994 Evolution of long water waves in variable channels. *J. Fluid Mech.* **266**, 303-317.

[21] Weidman, P. D. & Maxworthy, T. 1978 Experiments on strong interactions between solitary waves. *J. Fluid Mech.* **85**, 417-431.

[22] Wu, T. Y. 1979 *Tsunamis – Proc. National Science Foundation Workshop*, May 7-9, 1979, pp. 110-149, Pasadena: Tetra Tech. Inc.

[23] Wu, T. Y. 1981 Long waves in ocean and coastal waters. *J. Engng Mech. Div. ASCE* **107**, 501-522.

[24] Wu, T.Y. 1994 A bidirectional long-wave model. *Meth. & Appl. of Anal.* **1**(1) 108-117.

[25] Wu, T. Y. 1995 Bidirectional soliton street. *ACTA Mech. Sinica* **11**(4), 289-306.

[26] Yates, G. 1995 Various Boussinesq solitary wave solutions. In *Proc. Fifth International Offshore and Polar Eng. Conf.*, June 11-16, 1995, pp. 70-76, The Hague, The Netherlands.

[27] Yih, C.S. & Wu, T.Y. 1995 General solution for interaction of solitary waves including head-on collisions. *ACTA Mech. Sinica* **11**(3), 193-199.

[28] Zakharov, V.E. 1968 Stability of periodic waves of finite amplitude on the surface of a deep fluid. *Z. Prik. Mek. Tekh. Fiziki*, **9**, 86-94.

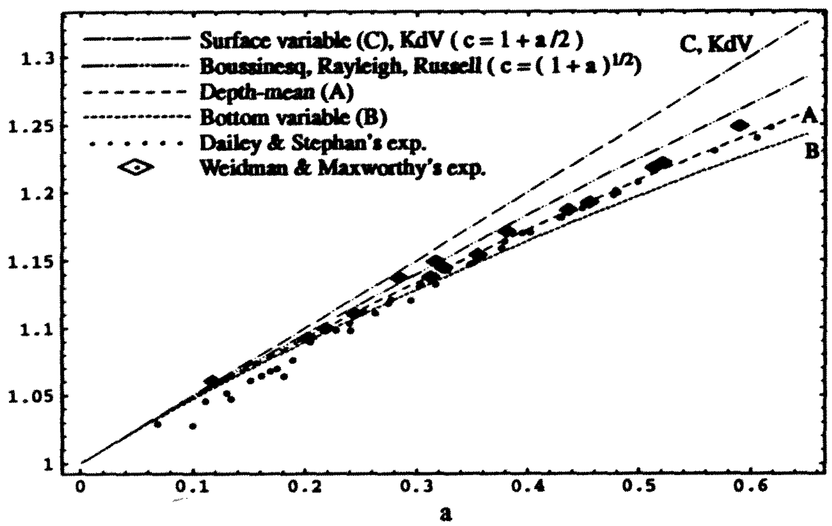

Figure 1: Comparison between theory and experiment for wave speed c versus wave amplitude a of solitary waves predicted by the different models.

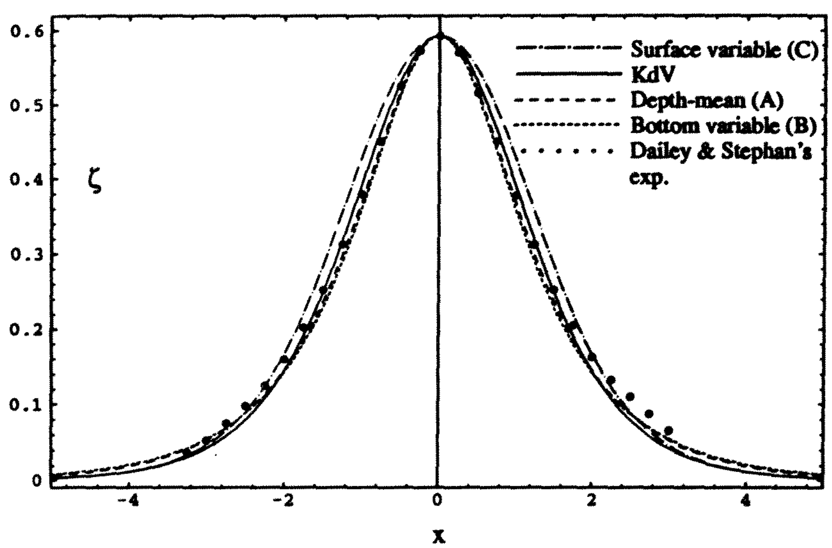

Figure 2: Comparison between theory and experiment for the profiles of solitary waves predicted by the different models, $a = 0.593$. (There is a misprint in figure 9 in Daily & Stephan's paper (1952), amplitude 0.61 should be 0.593).

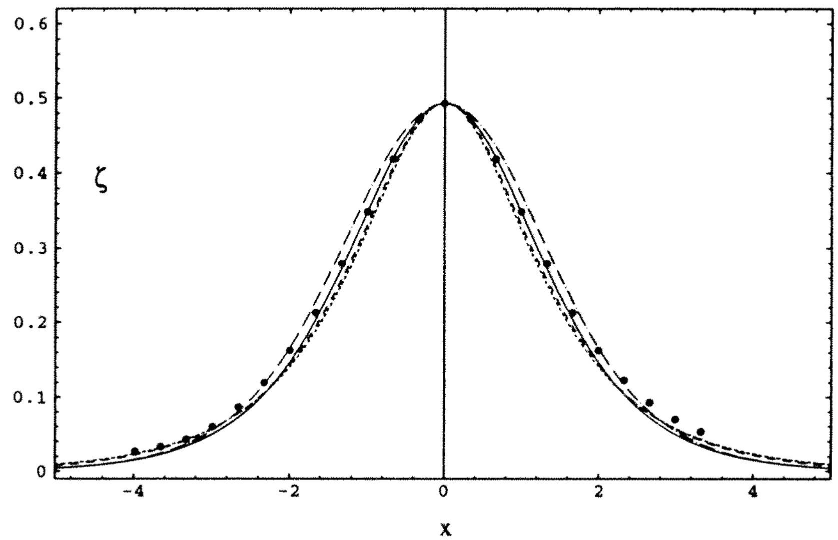

Figure 3: Comparison between theory and experiment for the profiles of solitary waves predicted by the different models, as in figure 2, here with $a = 0.493$.

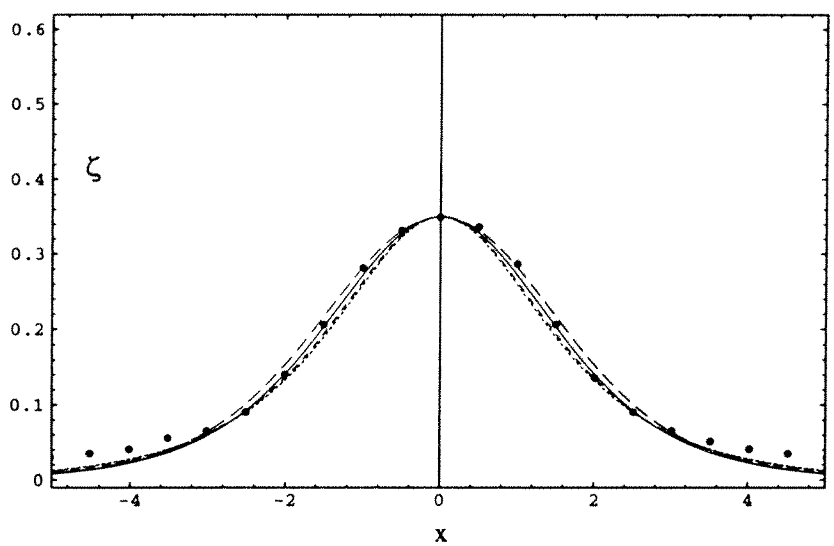

Figure 4: Comparison between theory and experiment for the profiles of solitary waves predicted by the different models, as in figure 2, here with $a = 0.350$.